

Sparse Array Signal Processing: New Array Geometries, Parameter Estimation, and Theoretical Analysis

Thesis by
Chun-Lin Liu

In Partial Fulfillment of the Requirements for the
degree of
Doctor of Philosophy

The logo for the California Institute of Technology (Caltech), featuring the word "Caltech" in a bold, orange, sans-serif font.

CALIFORNIA INSTITUTE OF TECHNOLOGY
Pasadena, California

2018
Defended May 14th, 2018

© 2018

Chun-Lin Liu

ORCID: 0000-0003-3135-9684

All rights reserved

ACKNOWLEDGEMENTS

First of all, I would like to express my deepest gratitude to my advisor, Professor P. P. Vaidyanathan, for his advice, guidance, patience, and encouragements, during the years of my PhD study at Caltech. He is an incredibly inspiring scholar and an excellent teacher. His unique insights into fundamental problems have broadened my horizons of scientific research. He taught me to explore various research topics in array signal processing, to ask influential and fundamental questions, and to think differently and creatively. Another valuable skill I learned from him is to write papers and to make presentations. I am also very thankful for his generous support whenever I faced difficulties. I am so fortunate to be advised by Professor P. P. Vaidyanathan during my PhD.

I would like to thank the members of my defense and candidacy committees: Professor Yaser Abu-Mostafa, Professor Shuki Bruck, Professor Victoria Kostina, Professor Babak Hassibi, and Professor Venkat Chandrasekaran. I learned a lot from their courses and valuable comments on my research.

Generous support from the Office of Naval Research (ONR), the National Science Foundation (NSF), California Institute of Technology, and Taiwan/Caltech Ministry of Education Fellowship is gratefully acknowledged.

I would like to thank the past and present members of my group, Professor See-May Phoong, Professor Yuan-Pei Lin, Professor Borching Su, Professor Piya Pal, Srikanth Tenneti, and Oguzhan Teke, for their generous support and valuable discussions. I would like to thank Caroline Murphy, Tanya Owen, and Carol Sosnowski for their administrative assistance. I am also very thankful to the colleagues working in signal processing, communications, physics, and mathematics for their inspiring work.

Many thanks to Kuan-Chang Chen, Yu-Hung Lai, Albert Chern, Lucas Peng, all my friends, and their associates in Association of Caltech Taiwanese for their company during my PhD. I am very thankful to Tui Tsai for his kind support, especially in my first year at Caltech. I would like to thank my friends in Taiwan, in the United States, and in Europe for their friendships.

I would like to express my deepest gratitude to the following composers: Ludwig van Beethoven, Wolfgang Amadeus Mozart, Franz Schubert, Anton Bruckner, and Philip Glass. Their musical compositions enriched my life and helped me cope with difficulties. I am also thankful to all the contributors of the computer software that I used in my research, such as Debian GNU/Linux, MATE Desktop Environment, MATLAB, L^AT_EX, and PGF/TikZ. These tools made it possible for me to experiment

with research ideas, to organize experimental results, to write papers, and to make slides as well as posters.

Finally, I would like to express my sincere gratitude to my father Hsi-Chin Liu and my mother Pi-Chu Kao, for their unconditional love and support in my life. Without their sacrifice, I would not have had opportunities to pursue my PhD at Caltech. I am very thankful to my brother Chun-Chih Liu, for taking care of my parents for me in Taiwan. I would like to thank my relatives for their kind support and wish my family good health and happiness.

ABSTRACT

Array signal processing focuses on an array of sensors receiving the incoming waveforms in the environment, from which source information, such as directions of arrival (DOA), signal power, amplitude, polarization, and velocity, can be estimated. This topic finds ubiquitous applications in radar, astronomy, tomography, imaging, and communications. In these applications, sparse arrays have recently attracted considerable attention, since they are capable of resolving $\mathcal{O}(N^2)$ uncorrelated source directions with N physical sensors. This is unlike the uniform linear arrays (ULA), which identify at most $N - 1$ uncorrelated sources with N sensors. These sparse arrays include minimum redundancy arrays (MRA), nested arrays, and coprime arrays. All these arrays have an $\mathcal{O}(N^2)$ -long central ULA segment in the difference coarray, which is defined as the set of differences between sensor locations. This $\mathcal{O}(N^2)$ property makes it possible to resolve $\mathcal{O}(N^2)$ uncorrelated sources, using only N physical sensors.

The main contribution of this thesis is to provide a new direction for array geometry and performance analysis of sparse arrays in the presence of nonidealities. The first part of this thesis focuses on designing novel array geometries that are robust to effects of mutual coupling. It is known that, mutual coupling between sensors has an adverse effect on the estimation of DOA. While there are methods to counteract this through appropriate modeling and calibration, they are usually computationally expensive, and sensitive to model mismatch. On the other hand, sparse arrays, such as MRA, nested arrays, and coprime arrays, have reduced mutual coupling compared to ULA, but all of these have their own disadvantages. This thesis introduces a new array called the super nested array, which has many of the good properties of the nested array, and at the same time achieves reduced mutual coupling. Many theoretical properties are proved and simulations are included to demonstrate the superior performance of super nested arrays in the presence of mutual coupling.

Two-dimensional planar sparse arrays with large difference coarrays have also been known for a long time. These include billboard arrays, open box arrays (OBA), and 2D nested arrays. However, all of them have considerable mutual coupling. This thesis proposes new planar sparse arrays with the same large difference coarrays as the OBA, but with reduced mutual coupling. The new arrays include half open box arrays (HOBA), half open box arrays with two layers (HOBA-2), and hourglass arrays. Among these, simulations show that hourglass arrays have the best estimation performance in presence of mutual coupling.

The second part of this thesis analyzes the performance of sparse arrays from a the-

oretical perspective. We first study the Cramér-Rao bound (CRB) for sparse arrays, which poses a lower bound on the variances of unbiased DOA estimators. While there exist landmark papers on the study of the CRB in the context of array processing, the closed-form expressions available in the literature are not applicable in the context of sparse arrays for which the number of identifiable sources exceeds the number of sensors. This thesis derives a new expression for the CRB to fill this gap. Based on the proposed CRB expression, it is possible to prove the previously known experimental observation that, when there are more sources than sensors, the CRB stagnates to a constant value as the SNR tends to infinity. It is also possible to precisely specify the relation between the number of sensors and the number of uncorrelated sources such that these sources could be resolved.

Recently, it has been shown that correlation subspaces, which reveal the structure of the covariance matrix, help to improve some existing DOA estimators. However, the bases, the dimension, and other theoretical properties of correlation subspaces remain to be investigated. This thesis proposes generalized correlation subspaces in one and multiple dimensions. This leads to new insights into correlation subspaces and DOA estimation with prior knowledge. First, it is shown that the bases and the dimension of correlation subspaces are fundamentally related to difference coarrays, which were previously found to be important in the study of sparse arrays. Furthermore, generalized correlation subspaces can handle certain forms of prior knowledge about source directions. These results allow one to derive a broad class of DOA estimators with improved performance.

It is empirically known that the coarray structure is susceptible to sensor failures, and the reliability of sparse arrays remains a significant but challenging topic for investigation. This thesis advances a general theory for quantifying such robustness, by studying the effect of sensor failure on the difference coarray. We first present the (k -)essentialness property, which characterizes the combinations of the faulty sensors that shrink the difference coarray. Based on this, the notion of (k -)fragility is proposed to quantify the reliability of sparse arrays with faulty sensors, along with comprehensive studies of their properties. These novel concepts provide quite a few insights into the interplay between the array geometry and its robustness. For instance, for the same number of sensors, it can be proved that ULA is more robust than the coprime array, and the coprime array is more robust than the nested array. Rigorous development of these ideas leads to expressions for the probability of coarray failure, as a function of the probability of sensor failure.

The thesis concludes with some remarks on future directions and open problems.

PUBLISHED CONTENT AND CONTRIBUTIONS

- [1] C.-L. Liu and P. P. Vaidyanathan, "Remarks on the spatial smoothing step in coarray MUSIC," *IEEE Signal Process. Lett.*, vol. 22, no. 9, pp. 1438–1442, Sep. 2015. doi: 10.1109/LSP.2015.2409153,
The content of this paper is the preliminary version of Chapter 2.
- [2] C.-L. Liu and P. P. Vaidyanathan, "Super nested arrays: Linear sparse arrays with reduced mutual coupling—Part I: Fundamentals," *IEEE Trans. Signal Process.*, vol. 64, no. 15, pp. 3997–4012, Aug. 2016, issn: 1053-587X. doi: 10.1109/TSP.2016.2558159,
The content of this paper is described in Chapter 3.
- [3] C.-L. Liu and P. P. Vaidyanathan, "Super nested arrays: Sparse arrays with less mutual coupling than nested arrays," in *Proc. IEEE Int. Conf. Acoust., Speech, and Sig. Proc.*, Shanghai, China, Mar. 2016, pp. 2976–2980. doi: 10.1109/ICASSP.2016.7472223,
The content of this paper is the preliminary version of Chapter 3.
- [4] C.-L. Liu and P. P. Vaidyanathan, "Super nested arrays: Linear sparse arrays with reduced mutual coupling—Part II: High-order extensions," *IEEE Trans. Signal Process.*, vol. 64, no. 16, pp. 4203–4217, Aug. 2016, issn: 1053-587X. doi: 10.1109/TSP.2016.2558167,
The content of this paper is described in Chapter 4.
- [5] C.-L. Liu and P. P. Vaidyanathan, "High order super nested arrays," in *Proc. IEEE Sensor Array and Multichannel Signal Process. Workshop*, Jul. 2016, pp. 1–5. doi: 10.1109/SAM.2016.7569621,
The content of this paper is the preliminary version of Chapter 4.
- [6] C.-L. Liu and P. P. Vaidyanathan, "Hourglass arrays and other novel 2-D sparse arrays with reduced mutual coupling," *IEEE Trans. Signal Process.*, vol. 65, no. 13, pp. 3369–3383, Jul. 2017, issn: 1053-587X. doi: 10.1109/TSP.2017.2690390,
The content of this paper is described in Chapter 5.
- [7] C.-L. Liu and P. P. Vaidyanathan, "Two-dimensional sparse arrays with hole-free coarray and reduced mutual coupling," in *Proc. IEEE Asil. Conf. on Sig., Sys., and Comp.*, Nov. 2016, pp. 1508–1512. doi: 10.1109/ACSSC.2016.7869629,
The content of this paper is the preliminary version of Chapter 5.
- [8] C.-L. Liu and P. P. Vaidyanathan, "Cramér-Rao bounds for coprime and other sparse arrays, which find more sources than sensors," *Digit. Signal Process.*, vol. 61, pp. 43–61, Feb. 2017, Special Issue on Coprime Sampling and Arrays, issn: 1051-2004. doi: 10.1016/j.dsp.2016.04.011,
The content of this paper is described in Chapter 6.
- [9] C.-L. Liu and P. P. Vaidyanathan, "New Cramér-Rao bound expressions for coprime and other sparse arrays," in *Proc. IEEE Sensor Array and Multichannel Signal Process. Workshop*, Jul. 2016, pp. 1–5. doi: 10.1109/SAM.2016.7569620,
The content of this paper is the preliminary version of Chapter 6.

- [10] C.-L. Liu and P. P. Vaidyanathan, "Correlation subspaces: Generalizations and connection to difference coarrays," *IEEE Trans. Signal Process.*, vol. 65, no. 19, pp. 5006–5020, Oct. 2017, ISSN: 1053-587X. DOI: 10.1109/TSP.2017.2721915,
The content of this paper is described in Chapter 7.
- [11] C.-L. Liu and P. P. Vaidyanathan, "The role of difference coarrays in correlation subspaces," in *Proc. IEEE Asil. Conf. on Sig., Sys., and Comp.*, Oct. 2017, pp. 1173–1177. DOI: 10.1109/ACSSC.2017.8335536,
The content of this paper is the preliminary version of Chapter 7.
- [12] C.-L. Liu and P. P. Vaidyanathan, "Robustness of coarrays of sparse arrays to sensor failures," in *Proc. IEEE Int. Conf. Acoust., Speech, and Sig. Proc.*, Apr. 2018,
The content of this paper is the preliminary version of Chapter 8.
- [13] C.-L. Liu and P. P. Vaidyanathan, "Maximally economic sparse arrays and Cantor arrays," in *Proc. IEEE Int. Workshop on Comput. Advances in Multi-Sensor Adaptive Process.*, Dec. 2017, pp. 1–5. DOI: 10.1109/CAMSAP.2017.8313139,
The content of this paper is the preliminary version of Chapter 9.

Contributions

All the above papers resulted from research carried out by C.-L. Liu and Professor P. P. Vaidyanathan. C.-L. Liu was the primary contributor of these papers. He proposed the main results, proved theorems and lemmas, conducted experimental validations, wrote papers, and corresponded with editors, reviewers, as well as readers. Professor P. P. Vaidyanathan applied for research grants, supervised research projects, discussed research topics with C.-L. Liu, and reviewed the main results, paper drafts, as well as the correspondences with reviewers.

TABLE OF CONTENTS

| | |
|--|-----|
| Acknowledgements | iii |
| Abstract | v |
| Published Content and Contributions | vii |
| Table of Contents | ix |
| List of Illustrations | xii |
| List of Tables | xxi |
| Chapter I: Introduction | 1 |
| 1.1 Review of Array Equation | 2 |
| 1.2 The Role of Array Geometry in DOA Estimation | 6 |
| 1.3 Scope and Outline of the Thesis | 9 |
| 1.4 Notations | 13 |
| Chapter II: Coarray MUSIC and Spatial Smoothing | 16 |
| 2.1 Introduction | 16 |
| 2.2 Review of Sparse Arrays | 17 |
| 2.3 Review of MUSIC and Spatial Smoothing MUSIC | 23 |
| 2.4 Coarray MUSIC without Spatial Smoothing | 29 |
| 2.5 Discussions | 31 |
| 2.6 Concluding Remarks | 35 |
| Chapter III: Super Nested Arrays: Linear Sparse Arrays with Reduced Mutual Coupling: Fundamentals | 36 |
| 3.1 Introduction | 36 |
| 3.2 Review of Mutual Coupling | 39 |
| 3.3 Mutual Coupling in Sparse Arrays: A Motivating Example | 41 |
| 3.4 Second-Order Super Nested Arrays | 45 |
| 3.5 Coarray of Second-Order Super Nested Arrays | 49 |
| 3.6 Numerical Examples | 55 |
| 3.7 Concluding Remarks | 63 |
| Chapter IV: High Order Super Nested Arrays | 65 |
| 4.1 Introduction | 65 |
| 4.2 General Guidelines for the Construction of Super Nested Arrays | 66 |
| 4.3 Q th-Order Super Nested Arrays, N_1 is Odd | 69 |
| 4.4 Q th-Order Super-Nested Arrays, N_1 is Even | 75 |
| 4.5 Proof of Theorem 4.3.1 | 80 |
| 4.6 Proof of Theorem 4.4.1 | 88 |
| 4.7 Numerical Examples | 92 |
| 4.8 Concluding Remarks | 98 |
| Chapter V: Hourglass Arrays, and Other Novel 2D Sparse Arrays with Re- duced Mutual Coupling | 99 |
| 5.1 Introduction | 99 |
| 5.2 Preliminaries | 101 |
| 5.3 Generalization of \mathbb{G}_1 in OBA | 104 |

| | | |
|---|---|-----|
| 5.4 | Reorganization of \mathbb{H}_1 and \mathbb{H}_2 in OBA | 108 |
| 5.5 | Half Open Box Arrays with Two Layers (HOBA-2) | 110 |
| 5.6 | Hourglass Arrays | 112 |
| 5.7 | Weight Functions | 115 |
| 5.8 | Numerical Examples | 121 |
| 5.9 | Concluding Remarks | 125 |
| 5.A | Proof of Lemma 5.3.1 | 125 |
| 5.B | Proof of Lemma 5.3.2 | 125 |
| 5.C | Proof of Theorem 5.3.1 | 126 |
| 5.D | Proof of Theorem 5.4.1 | 128 |
| 5.E | Proof of Theorem 5.6.1 | 131 |
| Chapter VI: Cramér-Rao Bounds for Sparse Arrays, which Find More Source Directions than Sensors | | |
| 6.1 | Introduction | 134 |
| 6.2 | The Data Model and Sparse Arrays | 137 |
| 6.3 | Review of Cramér-Rao Bounds | 139 |
| 6.4 | New Expressions for CRB, Applicable for Sparse Arrays with More Sources than Sensors | 143 |
| 6.5 | Conclusions which Follow from Theorem 6.4.2 | 149 |
| 6.6 | Connection to the ULA Part of the Coarray | 152 |
| 6.7 | Numerical Examples | 153 |
| 6.8 | Concluding Remarks | 161 |
| 6.A | Derivation to the Proposed CRB Expression | 162 |
| 6.B | Definition of \mathbf{J} | 165 |
| 6.C | Proof of the Asymptotic CRB Expression for Large SNR | 167 |
| 6.D | Proof of Theorem 6.6.1 | 170 |
| Chapter VII: Correlation Subspaces: Generalizations and Connection to Dif- ference Coarrays | | |
| 7.1 | Introduction | 173 |
| 7.2 | Review of Correlation Subspaces | 174 |
| 7.3 | Generalized Correlation Subspaces | 178 |
| 7.4 | Properties of Generalized Correlation Subspaces | 179 |
| 7.5 | Connections with Existing Methods | 190 |
| 7.6 | Generalized Correlation Subspaces in Multiple Dimensions | 193 |
| 7.7 | Numerical Examples | 196 |
| 7.8 | Concluding Remarks | 201 |
| 7.A | Proof of the Equivalence of (7.5) and Definition 7.2.1 | 201 |
| 7.B | Proof of Lemma 7.3.1 | 202 |
| 7.C | Properties of Weight Functions | 202 |
| 7.D | Numerical Examples for Section 7.6 | 204 |
| 7.E | Derivation of (7.63) | 206 |
| Chapter VIII: Robustness of Difference Coarrays of Sparse Arrays to Sensor Failures – A General Theory | | |
| 8.1 | Introduction | 209 |
| 8.2 | The Essentialness Property | 211 |
| 8.3 | The k -Fragility | 223 |
| 8.4 | The k -Essential Sperner Family | 225 |
| 8.5 | Robustness Analysis for Random Sensor Failures | 231 |

| | |
|---|-----|
| 8.6 Concluding Remarks | 235 |
| Chapter IX: Robustness of Difference Coarrays of Sparse Arrays to Sensor Fail- ures – Array Geometries | 238 |
| 9.1 Introduction | 238 |
| 9.2 Maximally Economic Sparse Arrays | 239 |
| 9.3 Uniform Linear Arrays | 247 |
| 9.4 Coprime Arrays | 253 |
| 9.5 Numerical Examples | 264 |
| 9.6 Concluding Remarks | 266 |
| Chapter X: Conclusions and Future Directions | 267 |
| Bibliography | 269 |

LIST OF ILLUSTRATIONS

| <i>Number</i> | <i>Page</i> |
|--|-------------|
| 1.1 A basic model for array signal processing. | 3 |
| 1.2 Conversion from the physical sensor locations to the normalized sensor locations. | 4 |
| 1.3 DOA estimation using uniform linear arrays (left) and sparse arrays (right). Here red dots denote physical sensors and crosses represent empty space. | 7 |
| 1.4 The physical arrays (a) \mathbb{S}_1 , (c) \mathbb{S}_2 , (e) \mathbb{S}_3 , and their difference coarrays (b) \mathbb{D}_1 , (d) \mathbb{D}_2 , (f) \mathbb{D}_3 . In these figures, dots denote elements in a set while crosses represent the empty space. | 8 |
| 2.1 An illustration of the sets \mathbb{S} , \mathbb{D} , \mathbb{U} , \mathbb{V} , and the weight function $w(m)$. Here we consider a coprime array with $M = 3$ and $N = 5$, as defined in (2.8). | 19 |
| 2.2 The array geometries \mathbb{S} , the difference coarrays \mathbb{D} , and the weight functions $w(m)$ of (a) the MRA with 6 sensors, (b) the MHA with 6 sensors, (c) the nested array with $N_1 = N_2 = 3$, and (d) the coprime array with $M = 2$, $N = 3$. All these arrays have 6 physical sensors. In \mathbb{S} and \mathbb{D} , dots denote elements and crosses represent empty locations. | 20 |
| 2.3 A schematic diagram of the MUSIC algorithm. | 24 |
| 2.4 The conversion from the $\tilde{\mathbf{R}}_{\mathbb{S}}$ to the autocorrelation vector $\tilde{\mathbf{x}}_{\mathbb{D}}$ | 28 |
| 2.5 The MUSIC spectrum based on an $M = 5$, $N = 7$ coprime array, 0 dB SNR, $K = 500$ snapshots, and the Hermitian Toeplitz matrix $\tilde{\mathbf{R}}$. $D = 35$ sources are placed uniformly over $\bar{\theta} \in [-0.49, 0.49]$. The number of sensors is $N + 2M - 1 = 16$ | 34 |
| 3.1 The concept of 2D representations of linear arrays. The top of this figure shows the 1D representation of a nested array with $N_1 = N_2 = 5$, where bullets denote sensors and crosses indicate empty locations. In the 1D representation of this example, the array aperture is divided into $N_2 = 5$ layers of size $N_1 + 1 = 6$. These layers are stacked into the associated 2D representation, as marked by arrows. Notice that in this chapter, 2D representations denote linear arrays, <i>not planar arrays</i> . They are introduced to simplify the discussion in the future development. | 37 |

- 3.2 The 1D and 2D representations of a second-order super nested array with $N_1 = N_2 = 5$. It will be proved in this chapter that super nested arrays possess the same number of sensors, the same physical aperture, and the same hole-free coarray as their parent nested arrays. Furthermore, super nested arrays alleviate the mutual coupling effect. In this example, there is only one pair of sensors with separation 1, located at 29 and 30. However, for the parent nested array in Fig. 3.1, locations 1 through 6 are crowded with sensors, leading to more severe mutual coupling effect. 37
- 3.3 Comparison among ULAs, MRAs, nested arrays, coprime arrays and their MUSIC spectra $P(\bar{\theta})$ in the presence of mutual coupling. It can be observed that higher uniform DOF and smaller weight functions $w(1), w(2), w(3)$ tend to decrease the RMSE. 42
- 3.4 1D representations of second-order super nested arrays with (a) $N_1 = 10, N_2 = 4$, and (b) $N_1 = N_2 = 7$. Bullets stand for physical sensors and crosses represent empty space. Both configurations consist of 14 physical sensors but (b) leads to larger total aperture and a sparser pattern. It will be proved that the uniform DOF of (a) and (b) are $2N_2(N_1 + 1) - 1$, which are 87 and 111, respectively. 45
- 3.5 2D representations of (a) the parent nested array, and (b) the corresponding second-order super nested array, $\mathbb{S}^{(2)}$, where $N_1 = N_2 = 13$. Bullets denote sensor locations while crosses indicate empty locations. Thin arrows illustrate how sensors migrate from nested arrays to second-order super nested arrays. The dense ULA in nested arrays is split into four sets: $\mathbb{X}_1^{(2)}, \mathbb{Y}_1^{(2)}, \mathbb{X}_2^{(2)}$, and $\mathbb{Y}_2^{(2)}$ in second-order super nested arrays. The sensor located at $N_1 + 1$, belonging to the sparse ULA of nested arrays, is moved to location $N_2(N_1 + 1) - 1$ in second-order super nested arrays. 47
- 3.6 Comparison among ULA, nested array, coprime array, second-order super nested array, and third-order super nested array in the presence of mutual coupling. The coupling leakage L is defined as $\|\mathbf{C} - \text{diag}(\mathbf{C})\|_F / \|\mathbf{C}\|_F$, where $[\text{diag}(\mathbf{C})]_{i,j} = [\mathbf{C}]_{i,j} \delta_{i,j}$ 56

- 3.7 The MUSIC spectra $P(\bar{\theta})$ for ULA, MRA, nested arrays, coprime arrays, second-order super nested arrays, and third-order super nested arrays when $D = 10$ sources are located at $\bar{\theta}_i = -0.1 + 0.2(i - 1)/9$, $i = 1, 2, \dots, 10$, as depicted by ticks and vertical lines. The SNR is 0 dB while the number of snapshots is $K = 500$. Note that the number of sources 10 is less than the number of sensors 14. The mutual coupling is based on (3.3) with $c_1 = 0.3 \exp(j\pi/3)$, $B = 100$, and $c_\ell = c_1 \exp(-j(\ell - 1)\pi/8) / \ell$ for $2 \leq \ell \leq B$ 59
- 3.8 The MUSIC spectra $P(\bar{\theta})$ for MRA, nested arrays, coprime arrays, second-order super nested arrays, and third-order super nested arrays when $D = 20$ sources are located at $\bar{\theta}_i = -0.2 + 0.4(i - 1)/19$, $i = 1, 2, \dots, 20$, as depicted by ticks and vertical lines. The SNR is 0 dB while the number of snapshots is $K = 500$. Note that the number of sources 20 is greater than the number of sensors 14. The mutual coupling is based on (3.3) with $c_1 = 0.3 \exp(j\pi/3)$, $B = 100$, and $c_\ell = c_1 \exp(-j(\ell - 1)\pi/8) / \ell$ for $2 \leq \ell \leq B$ 60
- 3.9 The MUSIC spectra $P(\bar{\theta})$ for MRA, nested arrays, coprime arrays, second-order super nested arrays, and third-order super nested arrays when $D = 20$ sources are located at $\bar{\theta}_i = -0.4 + 0.8(i - 1)/19$, $i = 1, 2, \dots, 20$, as depicted by ticks and vertical lines. The SNR is 0 dB while the number of snapshots is $K = 500$. The mutual coupling is based on (3.3) with $c_1 = 0.3 \exp(j\pi/3)$, $B = 100$, and $c_\ell = c_1 \exp(-j(\ell - 1)\pi/8) / \ell$ for $2 \leq \ell \leq B$ 62
- 3.10 Based on the practical mutual coupling model (3.2), the MUSIC spectra $P(\bar{\theta})$ are listed for MRA, nested arrays, coprime arrays, second-order super nested arrays, and third-order super nested arrays, where $D = 20$ sources are located at $\bar{\theta}_i = -0.4 + 0.8(i - 1)/19$, $i = 1, 2, \dots, 20$. The SNR is 0 dB while the number of snapshots is $K = 500$. The parameters in (3.2) are given by $Z_A = Z_L = 50$ ohms and $l = \lambda/2$ 64
- 4.1 Hierarchy of nested arrays, second-order super nested arrays $\mathbb{S}^{(2)}$, and Q th-order super nested arrays $\mathbb{S}^{(Q)}$. Arrows indicate the origin of the given sets. For instance, $\mathbb{X}_2^{(4)}$ originates from $\mathbb{X}_2^{(3)}$ while $\mathbb{Y}_3^{(3)}$ is split into $\mathbb{Y}_3^{(4)}$ and $\mathbb{Y}_4^{(4)}$. It can be observed that the sets $\mathbb{X}_q^{(Q)}$ and $\mathbb{Y}_q^{(Q)}$ result from the dense ULA part of nested arrays. The sparse ULA portion of nested arrays is rearranged into the sets $\mathbb{Z}_1^{(Q)}$ and $\mathbb{Z}_2^{(Q)}$ 67
- 4.2 1D representations of (a) second-order super nested arrays, $\mathbb{S}^{(2)}$, and (b) third-order super nested arrays, $\mathbb{S}^{(3)}$, where $N_1 = 13$ and $N_2 = 6$. Bullets denote sensor locations while crosses indicate empty locations. 67

4.3 2D representations of (a) second-order super nested arrays, $\mathbb{S}^{(2)}$, and (b) third-order super nested arrays, $\mathbb{S}^{(3)}$, where $N_1 = 13$ and $N_2 = 6$. Bullets denote sensor locations while crosses indicate empty locations. The dashed rectangles mark the sets $\mathbb{X}_q^{(Q)}$, $\mathbb{Y}_q^{(Q)}$, $\mathbb{Z}_1^{(Q)}$, and $\mathbb{Z}_2^{(Q)}$ for $1 \leq q \leq Q$. Thin arrows illustrate how sensors migrate from $\mathbb{S}^{(Q-1)}$ to $\mathbb{S}^{(Q)}$ 69

4.4 An example to show that $N_1 \geq 3 \cdot 2^Q - 1$ is not necessary in order to make the coarray of $\mathbb{S}^{(Q)}$ hole free. Here we consider the indicator function of $w(m) > 0$ for the super nested array with (a) $N_1 = 31, N_2 = 7, Q = 5$ and (b) $N_1 = 33, N_2 = 7, Q = 5$. It can be inferred that (a) is a restricted array, because $w(m) > 0$ for $-223 \leq m \leq 223$. However, (b) is not a restricted array since $w(78) = w(-78) = 0$ 73

4.5 2D representations of (a) the second-order super nested array $\mathbb{S}^{(2)}$ and (b) the third-order super nested array $\mathbb{S}^{(3)}$, where $N_1 = 16$ (even) and $N_2 = 5$. Bullets represent physical sensors while crosses denote empty space. Thin arrows illustrate the recursive rules (Rule 2 and Rule 3) in Fig. 4.1. 76

4.6 Estimation error as a function of source spacing $\Delta\bar{\theta}$ between two sources. The parameters are SNR = 0dB, $K = 500$. The sources have equal power and their normalized DOA are $\bar{\theta}_1 = \bar{\theta}_0 + \Delta\bar{\theta}/2$ and $\bar{\theta}_2 = \bar{\theta}_0 - \Delta\bar{\theta}/2$, where $\bar{\theta}_0 = 0.2$. Each point is an average over 1000 runs. 94

4.7 Estimation error as a function of (a) SNR, (b) the number of snapshots K , and (c) the number of sources D . The parameters are (a) $K = 500, D = 20$, (b) SNR = 0dB, $D = 20$, and (c) SNR = 0dB, $K = 500$. The sources have equal power and normalized DOA $\bar{\theta}_i = -0.45 + 0.9(i - 1)/(D - 1)$ for $1 \leq i \leq D$. Each point is an average over 1000 runs. 96

4.8 Estimation error as a function of mutual coupling coefficient c_1 (see Eq. (3.3)). The parameters are SNR = 0dB, $K = 500$, and the number of sources (a) $D = 10$, (b) $D = 20$, and (c) $D = 40$. The sources have equal power and are located at $\bar{\theta}_i = -0.45 + 0.9(i - 1)/(D - 1)$ for $1 \leq i \leq D$. The mutual coupling coefficients satisfy $|c_\ell/c_k| = k/\ell$ while the phases are randomly chosen from their domain. Each point is an average over 1000 runs. 97

5.1 The array geometry of (a) open box arrays (OBA) and (b) hourglass arrays, in units of half of the wavelength ($\lambda/2$). Definitions 5.2.3 and 5.6.1 give the formal description. The parameters are $N_x = 13$ and $N_y = 19$. Red and blue bullets represent physical sensors while crosses denote empty space. 99

| | | |
|-----|---|-----|
| 5.2 | Examples of 2D arrays with $N = 36$ elements. Bullets denote physical sensors and crosses represent empty space. The minimum separation between sensors is $\lambda/2$ | 103 |
| 5.3 | Examples of POBA with $N_x = 16$ and $N_y = 11$. (a) $\mathbf{g}_1 = \{1, 2, 3, 5, 6, 7, 9, 13\}$, $\mathbf{g}_2 = \{1, 3, 4, 5, 7, 11\}$, and (b) $\mathbf{g}_1 = \mathbf{g}_2 = \{1, 3, 5, 7, 9, 11, 13\}$. In both cases, \mathbf{g}_2 satisfies Theorem 5.3.1. | 106 |
| 5.4 | Examples of POBA- L . $N_x = 16$, $N_y = 11$, $\mathbf{g}_1 = \mathbf{g}_2 = \{1, 3, 5, 7, 9, 11, 13\}$. (a) $\mathbf{h}_{1,1} = \{1, 3, 5, 7, 9\}$, $\mathbf{h}_{1,2} = \{2, 4, 6, 8\}$, $L = 2$, and (b) $\mathbf{h}_{1,1} = \{1, 2, 4, 6, 8, 9\}$, $\mathbf{h}_{1,2} = \{3, 7\}$, $\mathbf{h}_{1,3} = \{5\}$, $L = 3$ | 108 |
| 5.5 | Examples of HOBA-2. (a) $N_x = 16$, $N_y = 11$ and (b) $N_x = 16$, $N_y = 12$. | 111 |
| 5.6 | Hourglass arrays with (a) $N_x = 15$, $N_y = 27$ and (b) $N_x = 15$, $N_y = 26$. The total number of sensors for (a) and (b) are 67 and 65, respectively. | 114 |
| 5.7 | The normalized source directions, as shown in circles, for the examples in Section 5.8. Here the number of sources D is assumed to be a perfect square, i.e., \sqrt{D} is an integer. The sources are uniformly located in the shaded region, over which there are \sqrt{D} equally-spaced sources in one way and \sqrt{D} equally-spaced sources in the other. . . . | 121 |
| 5.8 | The RMSE as a function of (a) SNR and (b) the number of snapshots K . The number of sensors is 81 for all arrays. The parameters are (a) $K = 200$, the number of sources $D = 9$ and (b) 0dB SNR, $D = 9$. The sources directions are depicted in Fig. 5.7. Each point is averaged from 1000 runs. | 123 |
| 5.9 | The RMSE as a function of the mutual coupling model for (a) the number of sources $D = 9$ and (b) $D = 36$. The number of sensors is 81 for all arrays. The parameters are 0dB SNR and $K = 200$. The sources directions are depicted in Fig. 5.7. The mutual coupling model is characterized by $B = 5$ and $c(\ell) = c(1) \exp [j\pi(\ell - 1)/4] / \ell$. Each point is averaged from 1000 runs. | 124 |
| 6.1 | The dependence of the proposed CRB expression on snapshots for various numbers of sources D . The array configuration is the nested array with $N_1 = N_2 = 2$ so that the sensor locations are $\mathbb{S} = \{1, 2, 3, 6\}$. The equal-power sources are located at $\bar{\theta}_i = -0.49 + 0.9(i - 1)/D$ for $i = 1, 2, \dots, D$. SNR is 20 dB. | 153 |
| 6.2 | The dependence of the proposed CRB expression on SNR for (a) $D < \mathbb{S} = 4$ and (b) $D \geq \mathbb{S} = 4$. The array configuration is the nested array with $N_1 = N_2 = 2$ so that the sensor locations are $\mathbb{S} = \{1, 2, 3, 6\}$. The equal-power sources are located at $\bar{\theta}_i = -0.49 + 0.9(i - 1)/D$ for $i = 1, 2, \dots, D$. The number of snapshots K is 500. | 154 |

| | | |
|-----|--|-----|
| 6.3 | The dependence of the proposed CRB on (a) snapshots and (b) SNR for ULA, MRA, nested arrays, coprime arrays, and super nested arrays. The total number of sensors is 10 and the sensor locations are given in (6.56) to (6.59). The number of sources is $D = 3$ (fewer sources than sensors) and the sources are located at $\bar{\theta}_i = -0.49 + 0.99(i-1)/D$ for $i = 1, 2, \dots, D$. For (a), the SNR is 20 dB while for (b) the number of snapshots K is 500. | 156 |
| 6.4 | The dependence of the proposed CRB on (a) snapshots and (b) SNR for MRA, nested arrays, coprime arrays, and super nested arrays. The total number of sensors is 10 and the sensor locations are given in (6.56) to (6.59). The number of sources is $D = 17$ (more sources than sensors) and the sources are located at $\bar{\theta}_i = -0.49 + 0.99(i-1)/D$ for $i = 1, 2, \dots, D$. For (a), the SNR is 20 dB while for (b) the number of snapshots K is 500. | 157 |
| 6.5 | The dependence of the proposed CRB on the number of sources D for various array configurations. The equal-power sources are located at $\bar{\theta}_i = -0.49 + 0.99(i-1)/D$ for $i = 1, 2, \dots, D$. The number of snapshots K is 500 and SNR is 20 dB. | 159 |
| 6.6 | The CRB expressions versus the number of sources D for a coprime array. (a) The stochastic CRB expression [167], (b) the CRB which is evaluated numerically by Abramovich et al. [1], (c) Jansson et al.'s CRB expression [66], and (d) the proposed CRB expression, as in Theorem 6.4.2. The coprime array with $M = 3, N = 5$ has sensor locations as in (6.59) and the difference coarray as in (6.64). The number of sensors $ \mathbb{S} = 10$. The equal-power sources are located at $\bar{\theta}_i = -0.48 + (i-1)/D$ for $i = 1, 2, \dots, D$. The number of snapshots K is 500 and SNR is 20 dB. | 160 |
| 7.1 | The density function in (7.16) (red), and the constant density function in Section 7.4 (blue). | 178 |
| 7.2 | The sensor locations \mathbb{S} and the nonnegative part of the difference coarrays \mathbb{D}^+ for (a) ULA with 10 sensors, (b) the nested array with $N_1 = N_2 = 5$, (c) the coprime array with $M = 3, N = 5$, and (d) the super nested array with $N_1 = N_2 = 5, Q = 2$. Here bullets denote elements in \mathbb{S} or \mathbb{D}^+ while crosses represent empty space. | 185 |
| 7.3 | (a) The eigenvalues and (b) the first four eigenvectors of the generalized correlation subspace matrix $\mathbf{S}(\mathbf{1}_{[-\alpha/2, \alpha/2]})$ in Example 7.4.3. Here the difference coarray $\mathbb{D} = \{-29, \dots, 29\}$ and α is 0.1. | 186 |
| 7.4 | The dependence of the relative error $E(\ell)$ on the parameter ℓ , where $E(\ell)$ is defined in (7.46) and the eigenvalues are shown in Fig. 7.3(a). | 189 |

- 7.5 The geometric interpretation of sample covariance matrix denoising using generalized correlation subspaces (Problem (P2)). The sample covariance matrix is denoted by $\tilde{\mathbf{R}}_S$. The vectors \mathbf{p}_1^* and \mathbf{p}_2^* are the orthogonal projections of $\text{vec}(\tilde{\mathbf{R}}_S)$ onto $\mathcal{CS} + \mathcal{I}$ and onto a subspace that approximates $\mathcal{GCS}(\mathbf{1}_{[-\alpha/2, \alpha/2]}) + \mathcal{I}$, respectively. Here $\mathcal{I} = \text{span}(\text{vec}(\mathbf{I}))$ and the sum between subspaces \mathcal{A} and \mathcal{B} is defined as $\mathcal{A} + \mathcal{B} = \{a + b : a \in \mathcal{A}, b \in \mathcal{B}\}$ 190
- 7.6 The visible region (shaded) of (a) angle-Doppler, (b) 2D DOA, (c) 2D DOA with $\theta_{\min} \leq \theta \leq \theta_{\max}$, and (d) 2D DOA with $\phi_{\min} \leq \phi \leq \phi_{\max}$. . . 194
- 7.7 The eigenvalues of the matrix $\tilde{\mathbf{S}}(\rho)$ (left) and the weight functions (right) for (a), (b) the ULA with 10 sensors ($|\mathbb{D}| = 19$), (c), (d) the nested array with $N_1 = N_2 = 5$ (10 sensors, $|\mathbb{D}| = 59$), (e), (f) the coprime array with $M = 3, N = 5$ (10 sensors, $|\mathbb{D}| = 43$), and (g), (h) the super nested array with $N_1 = N_2 = 5, Q = 2$ (10 sensors, $|\mathbb{D}| = 59$). Here the matrices $\tilde{\mathbf{S}}(\rho)$ are given by (7.64) and the eigenvalues of $\tilde{\mathbf{S}}(\rho)$ are obtained numerically. The red dashed curves in Figs. (a), (c), (e), and (g) correspond to $\rho_1(\bar{\theta}) = 2(1 - (2\bar{\theta})^2)^{-1/2} \mathbf{1}_{[-1/2, 1/2]}(\bar{\theta})$ while the blue curves in Figs. (a), (c), (e), and (g) are associated with $\rho_2(\bar{\theta}) = \mathbf{1}_{[-1/2, 1/2]}(\bar{\theta})$ 197
- 7.8 The dependence of root mean-squared errors (RMSE) on (a) SNR and (b) the number of snapshots for the optimization problems (P1) and (P2) with generalized correlation subspaces $\mathcal{GCS}(\mathbf{1}_{[-\alpha/2, \alpha/2]})$. There are $D = 3$ equal-power and uncorrelated sources at normalized DOAs $-0.045, 0$, and 0.045 . The array configuration is the nested array with $N_1 = N_2 = 5$ (10 sensors), as depicted in Fig. 7.2(b). The parameters are (a) 100 snapshots and (b) 0dB SNR. Each data point is averaged from 1000 Monte-Carlo runs. 199
- 7.9 (a) The physical array and (b) its difference coarray. 204
- 7.10 Plots for the sinc function $\text{sinc}(x)$ and the jinc function $\text{jinc}(x)$ 207
- 8.1 An illustration of the essentialness property. \mathbb{S}_i and \mathbb{D}_i represent the physical array and the difference coarray of the i th array, respectively. Elements are marked by dots while empty space is depicted by crosses. It can be observed that removing the sensor at 1 from Array #1 changes the difference coarray ($\mathbb{D}_2 \neq \mathbb{D}_1$). However, in Array #3, which is obtained by removing the sensor at 2 from Array #1, the difference coarray remains the same ($\mathbb{D}_3 = \mathbb{D}_1$). We say that the sensor at 1 is essential with respect to Array #1 while the sensor at 2 is inessential with respect to Array #1. 210

| | | |
|------|---|-----|
| 8.2 | An example of MESA. (a) The original array and its difference coarray. The array configurations and the difference coarrays after the deletion of (b) the sensor at 0, (c) the sensor at 1, (d) the sensor at 4, or (e) the sensor at 6, from the original array in (a). Here the sensors are denoted by dots while crosses denote empty space. | 213 |
| 8.3 | Array configurations and the difference coarrays for (a) the ULA with 9 sensors, and the arrays after the removal of (b) 1, (c) 2, (d) 7, (e) $\{1, 2\}$, and (f) $\{1, 7\}$ from (a). | 214 |
| 8.4 | The ULA with 6 physical sensors, where the essential sensors and the inessential sensors are denoted by diamonds and rectangles, respectively. The k -essential subarrays are also listed. | 216 |
| 8.5 | The array geometries and the weight functions for (a) the ULA with 6 sensors, (b) the MRA with 6 sensors, and (c) the MHA with 6 sensors. The sensors are depicted in dots while the empty space is shown in crosses. The definition of M_q in Theorem 8.2.1.3 leads to $M_1 = 2, M_2 = 2$ for (a), $M_1 = 22, M_2 = 4$ for (b), and $M_1 = 30, M_2 = 0$ for (c). | 217 |
| 8.6 | An illustration for the main idea of the proof of Theorem 8.2.1.1. Here the array is the ULA with 6 sensors and the k -essential family \mathcal{E}_1 and \mathcal{E}_2 are depicted in Fig. 8.4. | 221 |
| 8.7 | The directed graph \mathcal{G} in the proof of (8.15), for (a) the ULA with 6 sensors, (b) the MRA with 6 sensors, and (c) the MHA with 6 sensors. The number of directed edges is (a) $M_1 = 2$, (b) $M_1 = 22$, and (c) $M_1 = 30$ | 223 |
| 8.8 | The array geometries (top) and the k -fragility F_k (bottom) for (a) the ULA with 16 sensors, (b) the nested array with $N_1 = N_2 = 8$, and (c) the coprime array with $M = 4$ and $N = 9$ | 225 |
| 8.9 | An example of the underlying structure of k -essential family \mathcal{E}_k . Here the ULA with 7 sensors, $\mathbb{S} = \{0, 1, \dots, 6\}$, is considered while the numbers in each small box denote a subarray. For instance, “0, 1, 2” represents the subarray $\{0, 1, 2\}$ | 226 |
| 8.10 | The relation between $\mathcal{E}_k = \mathcal{S}_k$ and $\mathcal{E}'_k = \emptyset$. Here solid arrows represent logical implication while arrows with red crosses mean that one condition does not necessarily imply the other. | 230 |
| 8.11 | The probability that the difference coarray changes P_c and its lower bounds and upper bounds for the ULA with 12 sensors. | 234 |

| | | |
|------|--|-----|
| 8.12 | The dependence of the probability that the difference coarray changes P_c on the probability of single sensor failure p for (a) the ULA with 12 sensors, (b) the nested array with $N_1 = N_2 = 6$, and (c) the coprime array with $M = 4$ and $N = 5$. Here the essential sensors (diamonds) and the inessential sensors (squares) are depicted on the top of this figure. Experimental data points (Exp.) are averaged from 10^7 Monte-Carlo runs. The approximations of P_c are valid for $p \ll 1/12$ due to (8.36). | 236 |
| 9.1 | The array geometry (\mathbb{S} , in diamonds) and the nonnegative part of the weight function ($w(m)$, in dots) for (a) the MRA with 8 elements, (b) the MHA with 8 elements, (c) the nested array with $N_1 = N_2 = 4$ (8 elements), and (d) the Cantor array with 8 elements. Here crosses denote empty space. | 241 |
| 9.2 | The ULA with $N = 10$ elements and the k -essential Sperner family $\mathcal{E}'_1, \mathcal{E}'_2$, and \mathcal{E}'_3 | 248 |
| 9.3 | (a) The ULA with 10 physical elements \mathbb{S}_{ULA} and its difference coarray. The physical array (left) and the difference coarray (right) after removing (b) $\{7, 8, 9\}$, (c) $\{1, 2, 8\}$, and (d) $\{3, 5, 8\}$, from \mathbb{S}_{ULA} , respectively. Here bullets denote elements and crosses represent empty space. It can be observed that the difference coarrays of (b), (c), and (d) contain $\{0, \pm 1, \dots, \pm 6\}$ | 251 |
| 9.4 | An illustration for the k -essential Sperner family of the coprime arrays with (a) $M = 4, N = 5$ and (b) $M = 5, N = 4$. In these figures, the coprime arrays are split into two sparse ULAs for clarity. | 254 |
| 9.5 | (a) the coprime array $\mathbb{S}_{\text{coprime}}$ with $M = 7, N = 8$ and the nonnegative part of the difference coarray \mathbb{D} . (b) The array $\bar{\mathbb{S}}$, where the elements in $\mathbb{A} = \{16, 32, 56\}$ are removed from $\mathbb{S}_{\text{coprime}}$, and the nonnegative part of its difference coarray $\bar{\mathbb{D}}$ | 259 |
| 9.6 | The array configurations for (a) ULA with 10 elements, (b) the coprime array with $M = 3, N = 5$, (c) the nested array with $N_1 = N_2 = 5$, and (d) the MRA with 10 elements. | 264 |
| 9.7 | The dependence of RMSE on the element failure p with respect to the array configurations in Fig. 9.6. The number of snapshots is 100, SNR is 0dB, and the only one source has $\bar{\theta}_1 = 0.25$ | 265 |

LIST OF TABLES

| <i>Number</i> | <i>Page</i> |
|---|-------------|
| 2.1 Some terminologies related to sparse arrays | 21 |
| 3.1 Ranges of \mathbb{P}_1 and \mathbb{P}_2 | 51 |
| 3.2 Ranges of $\mathbb{X}_1^{(2)} \cup (\mathbb{X}_1^{(2)} + 1)$ and $\mathbb{Y}_1^{(2)} \cup (\mathbb{Y}_1^{(2)} + 1)$ | 52 |
| 4.1 27 cases in the proof of Theorem 4.3.1 | 81 |
| 4.2 Array profiles for the example in Section 4.7 | 93 |
| 5.1 Summary on the weight functions | 116 |
| 5.2 Sensor pairs for $w(1, 1)$ with odd N_x | 119 |
| 5.3 12 cases in the proof of Theorem 5.3.1 | 127 |
| 5.4 19 cases in the proof of Theorem 5.4.1 | 128 |
| 6.1 Summary of several related CRB expressions for DOA estimation . . . | 142 |
| 6.2 Identifiable/non-identifiable regions for coarray MUSIC. | 158 |
| 7.1 Generalized correlation subspaces with known source intervals . . . | 184 |
| 7.2 CPU time in seconds and RMSE for several cases | 200 |

Chapter 1

INTRODUCTION

The heart of modern technology is the widespread use of sensors, which produce sensor outputs to sense the surroundings. Studying these outputs finds enormous and potential applications in *communications* (5G, massive MIMO systems, mmWave communications) [6], [80], [143], *biomedical engineering* (medical imaging, bioinformatics, wearable technology) [170], *remote sensing* (satellite navigation, environmental sensing) [43], and so forth. Among all these applications, manipulating these data under limited physical resources such as bandwidth, power, and the number of sensors is a major challenge even today. Recently, due to inexpensive computation, this challenge has been addressed in the framework of *sparse sensing*. The key idea of sparse sensing is that, by exploiting *prior knowledge* about signals, only a small portion of high-dimensional big data is delivered to *signal processing algorithms* to recover the *low-dimensional information of interest*. This paradigm makes it possible to achieve the above-mentioned applications with limited physical resources.

Sparse sampling and *information inference* are two main pillars of sparse sensing. According to the prior knowledge and the information of interest, the former collects representative, low-dimensional, and *sparse samples* among big data while the latter infers the information of interest from sparse samples efficiently. For instance, in applications depending on sparse representation, *compressed sensing* has been demonstrated to be able to recover the original signal from sparse samples under certain conditions [26], [42]. Other state-of-the-art sparse sensing schemes, such as nested sampling [124], coprime sampling [186], power spectrum sensing [7], and quadratic sampling [33], demonstrate ubiquitous applications in source localization, cognitive radio, and optical imaging, with reduced data rate but performance comparable to classical approaches. However, this is just the beginning of the field since various forms of prior knowledge remain to be studied for diverse applications. Among these, the following fundamental questions are frequently raised. First, how does prior knowledge determine sparse sampling schemes (possibly nonuniform sampling) that capture the information of interest efficiently? Second, for these sampling patterns, how is the information of interest inferred from sparse samples, between theory and practice? Finally, what are the performance limits of these sampling schemes?

This thesis aims at answering the above fundamental and insightful questions, in the context of source localization in array signal processing, since it plays a central role in communication, radar, medical imaging, and radio astronomy [22], [82], [157], [170], [188]. Here sparse sampling is equivalent to *sparse sensor array configuration* while the information inference corresponds to the estimation of *direction-of-arrival (DOA)*, signal power, amplitude, polarization, and velocity of the sources. Furthermore, the estimation performance can be analyzed and explained through *the Cramér-Rao bounds*, *the generalized correlation subspace*, and *the essentialness property*. The main contributions of this thesis can be summarized as follows:

1. *Sparse sampling* (sparse array design): We proposed several one-dimensional and two-dimensional sparse array configurations that take advantage of the statistics of the source profile and the interference among sensors (mutual coupling) [89], [92]–[95], [98]. For the proposed arrays, it is possible to resolve *more uncorrelated sources than sensors* with improved resolution, in the presence of mutual coupling.
2. *Information inference* (Parameter estimation with sparse arrays): We developed new and practical algorithms that estimate more uncorrelated sources than sensors from the sparse array [86]–[88], [104].
3. *Theoretical analysis* (Cramér-Rao bounds, generalized correlation subspace, and robustness analysis): Here we studied the expressions of *the Cramér-Rao bounds* for sparse arrays, which are theoretical limits for the estimation performance of unbiased estimators [91], [97]. The proposed expressions explain why more uncorrelated sources than sensors can be identified using sparse arrays. We also show that DOA estimators can be explained through the theory of the *generalized correlation subspace*, which further provides insights to the optimal estimators [96], [102]. Furthermore, we also propose a general theory of analyzing the robustness of the difference coarray with respect to sensor failures [103].

The chapter outline is as follows. Section 1.1 reviews the data model commonly used in array signal processing. Section 1.2 discusses the interplay between array geometry and DOA estimation. Section 1.3 gives the outline and the scope of this thesis while Section 1.4 defines the notation used in this thesis.

1.1 Review of Array Equation

This section reviews the one-dimensional array equation (1.5), which is the foundation of sparse array design, DOA estimators, and theoretical analysis. The notations

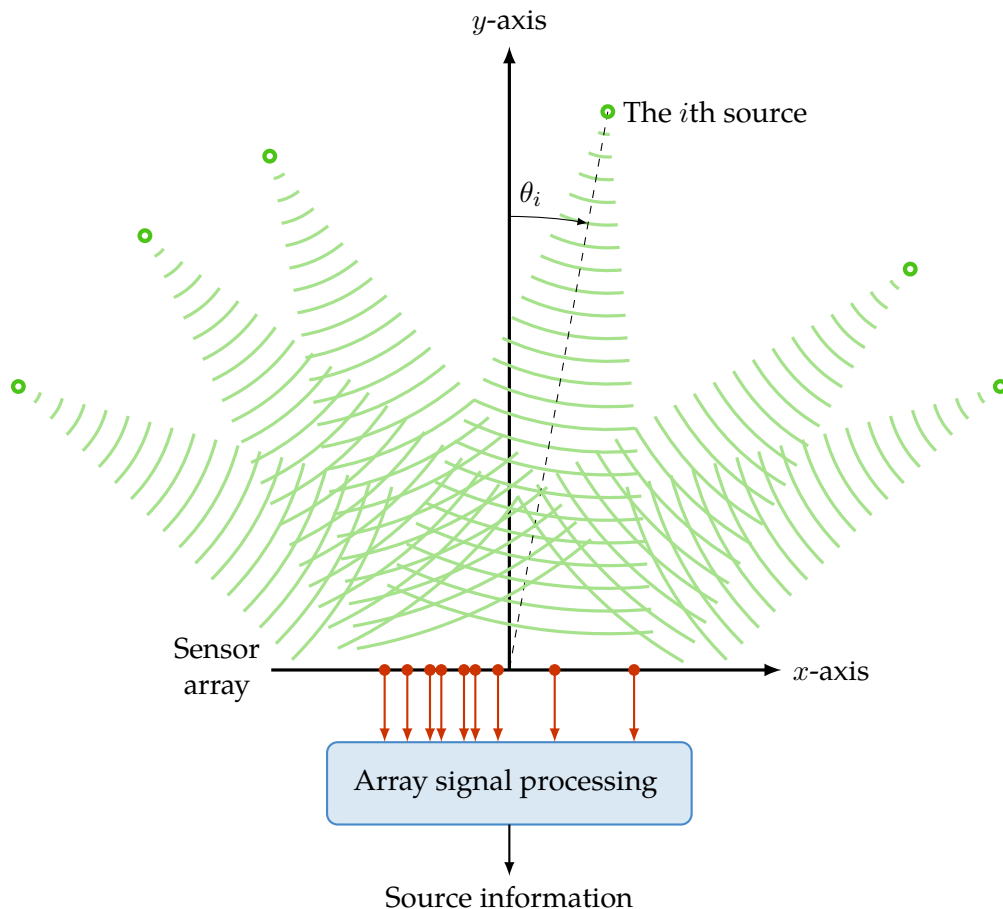


Figure 1.1: A basic model for array signal processing.

and assumptions in (1.5) will be explained comprehensively in the following development.

Fig. 1.1 illustrates a basic model of array signal processing. Here multiple *sources* emit *propagating waves*, which are received by a *sensor array*. The output of the sensor array is processed by *array signal processing algorithms*, which infer the source information, such as the distance between the source and the array, the source directions, the source powers, polarization of the incoming waves, or the velocity of the moving sources. The sources are shown in green empty circles and the wavefronts of the propagating waves are shown in green curves. The physical sensors are depicted in red solid circles. Fig. 1.1 assumes that the sensors are placed on the x -axis and the sources reside in the first or the second quadrant of the xy -plane.

In this thesis, we are interested in the *direction of arrival (DOA)* of the source. It is defined as the angle between the broadside of the array (the y -axis in Fig. 1.1) and the line segment between the source and the center of the array (the dashed line in Fig. 1.1). For example, in Fig. 1.1, the DOA of the i th source is denoted by θ_i . If the

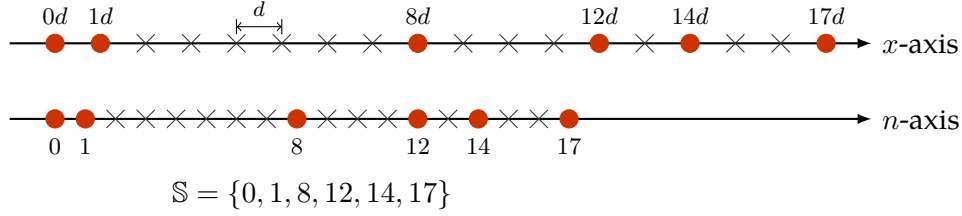


Figure 1.2: Conversion from the physical sensor locations to the normalized sensor locations.

source resides in the first quadrant, namely, the x -coordinate and the y -coordinate are both positive, then $\theta_i > 0$. By definition, the DOA of the i th source satisfies

$$-\frac{\pi}{2} \leq \theta_i \leq \frac{\pi}{2}. \quad (1.1)$$

We begin by deriving the expressions for the sensor output signals induced by the sources. It is first assumed that all the sources are *monochromatic* and all the propagating waves share the same frequency f , hence the same wavelength λ . Furthermore, each source is concentrated at a *point* in the *far-field* region [188]. Therefore, the distances between the sources and the sensors are sufficiently large so that the wavefronts can be approximated by *plane waves*. It is also assumed that the propagating medium is homogeneous and lossless [68].

Next let us assume that the sensor locations belong to a uniform grid of step size d on the x -axis. Namely, the sensor locations can be specified by nd , where n belongs to an integer set \mathbb{S} . The indices n are called normalized sensor locations, which are represented by an integer set \mathbb{S} . In this thesis, unless stated separately, the normalized sensor locations, indicated by the set \mathbb{S} , are used to characterize the array geometry. As an example, Fig. 1.2 demonstrates the conversion from the sensor locations defined on the x -axis to those defined on the integer set \mathbb{S} . Here the sensors are depicted in red solid circles and the empty space is illustrated using crosses. The physical sensors are located at $0d$, $1d$, $8d$, $12d$, $14d$, and $17d$ on the x -axis. After normalizing by d , we obtain the normalized sensor locations $\mathbb{S} = \{0, 1, 8, 12, 14, 17\}$.

Based on the above-mentioned assumptions, the signal received by the sensor at nd can be expressed as [68], [188]

$$\sum_{i=1}^D A_i \exp [j2\pi\bar{\theta}_i n] + w(n), \quad (1.2)$$

where $j \triangleq \sqrt{-1}$, $w(n)$ is the noise term, A_i is the complex amplitude of the i th source, and $\bar{\theta}_i$ is the normalized DOA of the i th source, defined as

$$\bar{\theta}_i \triangleq \frac{d \sin \theta_i}{\lambda}. \quad (1.3)$$

The model in (1.2) can be regarded as a linear combination of complex exponentials. Furthermore, the index n can be regarded as *spatial sample point* while the normalized DOA $\bar{\theta}_i$ can be interpreted as *spatial frequency*. Based on this interpretation, the step size d cannot exceed $\lambda/2$, otherwise spatial ambiguity arises. Here spatial ambiguity is analogous to aliasing in the sampling theorem [68], [188]. In particular, if $d > \lambda/2$, then there exist multiple DOAs corresponding to the same array output, so that these DOAs become indistinguishable from the array output. Due to these, in this thesis, the step size d is set to be

$$d = \frac{\lambda}{2}. \quad (1.4)$$

Finally, Eq. (1.2) can be expressed as the following vector model:

$$\mathbf{x}_{\mathbb{S}} = \sum_{i=1}^D A_i \mathbf{v}_{\mathbb{S}}(\bar{\theta}_i) + \mathbf{n}_{\mathbb{S}}, \quad (1.5)$$

where the column vector $\mathbf{x}_{\mathbb{S}} \in \mathbb{C}^{|\mathbb{S}|}$ denotes the output of the overall sensor array and $\mathbf{n}_{\mathbb{S}}$ is the additive noise term. The *steering vector* $\mathbf{v}_{\mathbb{S}}(\bar{\theta}_i)$ is defined as $\mathbf{v}_{\mathbb{S}}(\bar{\theta}_i) = [\exp(j2\pi\bar{\theta}_i n)]_{n \in \mathbb{S}}$. In this thesis, the entries in $\mathbf{x}_{\mathbb{S}}$, $\mathbf{v}_{\mathbb{S}}(\bar{\theta}_i)$, and $\mathbf{n}_{\mathbb{S}}$ are sorted in the ascending order of $n \in \mathbb{S}$. That is, the first entry of $\mathbf{x}_{\mathbb{S}}$ corresponds to output of the leftmost sensor in the array while the last entry of $\mathbf{x}_{\mathbb{S}}$ is associated with the rightmost sensor.

Example 1.1.1. Let us consider the array geometry in Fig. 1.2. Due to (1.5), the column vectors $\mathbf{x}_{\mathbb{S}}$, $\mathbf{v}_{\mathbb{S}}(\bar{\theta}_i)$, and $\mathbf{n}_{\mathbb{S}}$ can be expressed as

$$\underbrace{\begin{bmatrix} \text{Output at } n = 0 \\ \text{Output at } n = 1 \\ \text{Output at } n = 8 \\ \text{Output at } n = 12 \\ \text{Output at } n = 14 \\ \text{Output at } n = 17 \end{bmatrix}}_{\mathbf{x}_{\mathbb{S}}} = \sum_{i=1}^D A_i \underbrace{\begin{bmatrix} \exp[j2\pi\bar{\theta}_i \cdot 0] \\ \exp[j2\pi\bar{\theta}_i \cdot 1] \\ \exp[j2\pi\bar{\theta}_i \cdot 8] \\ \exp[j2\pi\bar{\theta}_i \cdot 12] \\ \exp[j2\pi\bar{\theta}_i \cdot 14] \\ \exp[j2\pi\bar{\theta}_i \cdot 17] \end{bmatrix}}_{\mathbf{v}_{\mathbb{S}}(\bar{\theta}_i)} + \underbrace{\begin{bmatrix} \text{Noise at } n = 0 \\ \text{Noise at } n = 1 \\ \text{Noise at } n = 8 \\ \text{Noise at } n = 12 \\ \text{Noise at } n = 14 \\ \text{Noise at } n = 17 \end{bmatrix}}_{\mathbf{n}_{\mathbb{S}}}. \quad (1.6)$$

In practice, the array output (1.5) is repeated K times, denoted by $\mathbf{x}_{\mathbb{S}}(k)$ for $k = 1, 2, \dots, K$, to reduce the variation of the estimates. These vectors $\mathbf{x}_{\mathbb{S}}(k)$ are called *snapshots* of (1.5). In particular, $\mathbf{x}_{\mathbb{S}}(k)$ can be modeled as

$$\mathbf{x}_{\mathbb{S}}(k) = \sum_{i=1}^D A_i(k) \mathbf{v}_{\mathbb{S}}(\bar{\theta}_i) + \mathbf{n}_{\mathbb{S}}(k), \quad k = 1, 2, \dots, K. \quad (1.7)$$

Here the notations $A_i(k)$ and $\mathbf{n}_{\mathbb{S}}(k)$ indicate that the complex amplitude and the noise term change with snapshots. The task of array signal processing algorithms

is to infer the information of interest, such as the DOA, source power, and so forth, based on the snapshots $\mathbf{x}_S(k)$. More discussions on the snapshot model can be found in Chapter 2, Chapter 6, [188, Chapter 5], [68, Section 4.9], and the references therein.

As a remark, (1.5) assumes that the sources reside in the first and the second quadrant of the xy -plane and the sensors are located on the x -axis. This scenario will be considered in most of the chapters, except for Chapter 5. Chapter 5 is based on *two-dimensional array processing*, where the sources are in the first four octants ($z > 0$) in the three-dimensional space and the sensors are restricted to the xy -plane. In this case, the DOA of the source has two parameters: azimuth and elevation. All these details will be discussed in Chapter 5.

1.2 The Role of Array Geometry in DOA Estimation

Based on the array equation in (1.5), *DOA estimation* has been a popular research field in array processing for many decades and has found ubiquitous applications in radio astronomy, radar, imaging, communications, and so forth [22], [58], [68], [77], [157], [165], [188]. In particular, DOA estimation aims to infer the source directions, i.e., θ_i for $i = 1, 2, \dots, D$, from the array output \mathbf{x}_S . This task can be divided into two stages:

Stage 1 *Array geometry*: According to the prior knowledge of the received signal, the goal here is to design an array geometry \mathbb{S} (or sensor placement) that captures the information of interest efficiently.

Stage 2 *Estimation*: Given the array geometry \mathbb{S} , this stage develops *DOA estimators* that infer the DOAs $\{\theta_1, \theta_2, \dots, \theta_D\}$ based on the array output \mathbf{x}_S .

Uniform Linear Arrays (ULA)

The diagram on the left of Fig. 1.3 considers *uniform linear arrays (ULA)*, where the sensors are placed along a straight line and sensors are uniformly placed with separation $\lambda/2$ (We shall come to the diagram on the right shortly). Then the DOA is estimated based on the output of ULA. This scheme has been popular in array signal processing for decades [58], [68], [188]. Furthermore, a great amount of literature in this topic focuses on developing DOA estimators that resolve the sources with high resolution and finite snapshots of array outputs [58], [68], [188]. DOA estimators such as the Barlett beamformer [14], the Capon beamformer [28], the Pisarenko harmonic decomposition [134], the minimum-norm method [78], MUltiple Signal Classification (MUSIC) [17], [150], Estimation of Signal Parameters via Rotational Invariance Techniques (ESPRIT) [147], maximum likelihood estimator [166], [167],

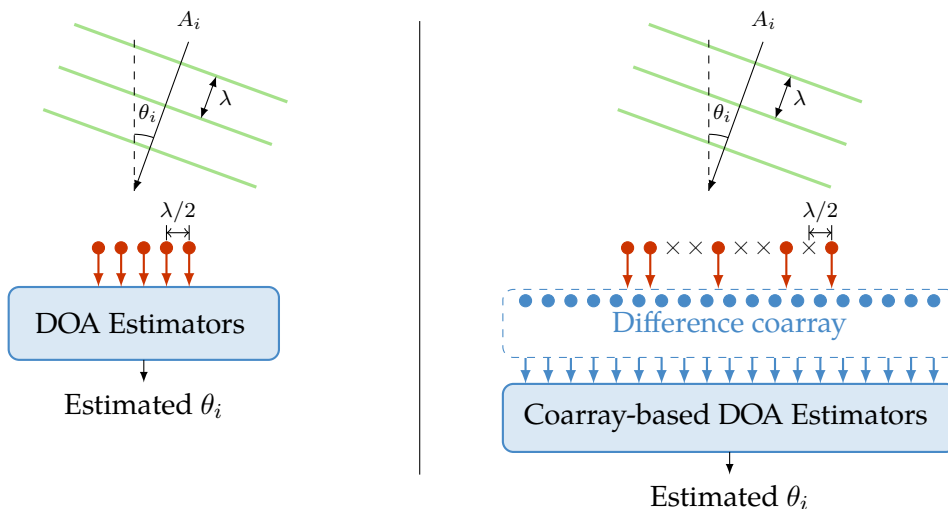


Figure 1.3: DOA estimation using uniform linear arrays (left) and sparse arrays (right). Here red dots denote physical sensors and crosses represent empty space.

Methods Of DOA Estimation (MODE) [162], and SParse Iterative Covariance-based Estimation (SPICE) [161], to name a few, have been developed for this purpose.

Sparse Arrays

It is known that ULA can resolve at most $N - 1$ sources with N physical sensors, regardless of the choice of algorithms [188]. However, recent development shows that, under mild assumptions, it is possible to identify more sources than sensors using *sparse arrays*. This result is possible because multiple time-domain snapshots are involved, as we will elaborate in Chapter 2.

The diagram on the right of Fig. 1.3 depicts DOA estimation based on sparse arrays, where the sensors do not have uniform spacing $\lambda/2$. Under mild assumptions, the array output of sparse arrays can be converted to the samples on the *difference coarray* (See Chapter 2 for more details). In particular, the difference coarray \mathbb{D} for an array \mathbb{S} (regardless of ULA or sparse arrays) is defined as the set of differences between sensor locations:

$$\mathbb{D} \triangleq \{n_1 - n_2 : n_1, n_2 \in \mathbb{S}\}, \quad (1.8)$$

where the integer \mathbb{S} denotes the normalized sensor locations of an array. Based on the structure of the difference coarray, coarray-based DOA estimators have been developed in the past few decades, including the augmented covariance matrix [132], [133], Toeplitz completion [1], [2], coarray MUSIC or spatial smoothing MUSIC [87], [124], [125], coarray interpolation [104], [137], [179], and Khatri-Rao methods [107], [108], [127], [200]. Some of the above-mentioned algorithms are also applicable to ULA, as long as the structure of the difference coarray satisfies the requirements of

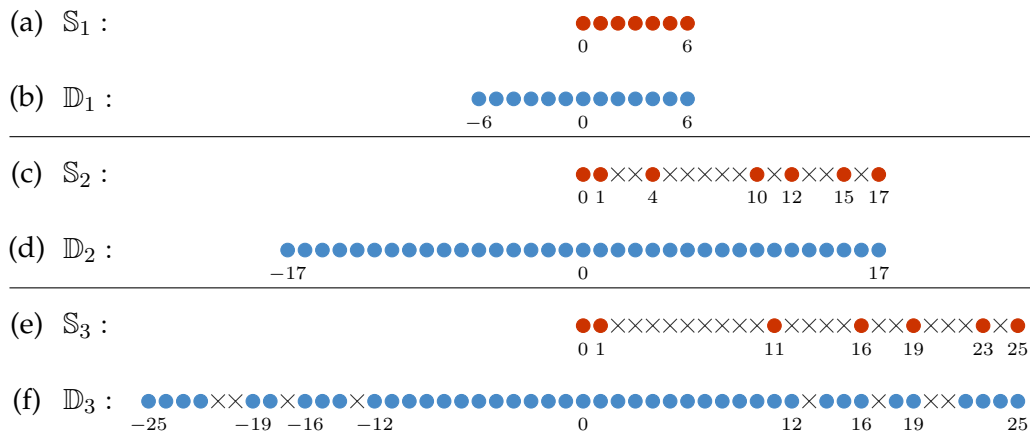


Figure 1.4: The physical arrays (a) \mathbb{S}_1 , (c) \mathbb{S}_2 , (e) \mathbb{S}_3 , and their difference coarrays (b) \mathbb{D}_1 , (d) \mathbb{D}_2 , (f) \mathbb{D}_3 . In these figures, dots denote elements in a set while crosses represent the empty space.

these algorithms. In particular, the details of coarray MUSIC will be elaborated in Chapter 2.

The main advantage of sparse arrays over ULA is the ability to resolve more uncorrelated sources than sensors [1], [2], [113], [124], [186]. Furthermore, for sufficient amount of data, sparse arrays typically enjoy better estimation performance and resolution than ULA [1], [2], [124], [186]. These advantages are due to the structure of the difference coarray, as described next.

The Difference Coarray

In what follows, the $\mathcal{O}(N^2)$ property and the hole-free property on the difference coarray will be demonstrated through examples. Formal definitions and comprehensive discussions can be found in Chapters 2 and 6.

Example 1.2.1. Fig. 1.4(a) shows the ULA with 7 sensors, i.e., $\mathbb{S}_1 = \{0, 1, 2, 3, 4, 5, 6\}$. It can be observed that these sensors are equally spaced with separation 1. As another example, Fig. 1.4(c) depicts a sparse array whose normalized sensor locations are 0, 1, 4, 10, 12, 15, 17. Therefore the differences between adjacent sensors, from left to right, are 1, 3, 6, 2, 3, 2.

It can be observed that, for the same number of sensors, sparse arrays occupy larger aperture (from 0 to 17 in Fig. 1.4(c)) than ULA (from 0 to 6 in Fig. 1.4(a)). Due to this observation, if the sensor locations are designed properly, sparse arrays may be able to capture the information of interest from large aperture using small number of sensors [113], [188].

Next we will review some useful properties of the array geometry and the difference coarray using several examples. These properties will be developed comprehensively later in Chapter 2. Fig. 1.4 illustrates three array geometries \mathbb{S}_1 , \mathbb{S}_2 , and \mathbb{S}_3 , whose difference coarrays are denoted by \mathbb{D}_1 , \mathbb{D}_2 , and \mathbb{D}_3 , respectively. Specifically, \mathbb{S}_1 is the ULA, \mathbb{S}_2 is the minimum redundancy array [113], and \mathbb{S}_3 is the minimum hole array [177], where \mathbb{S}_2 and \mathbb{S}_3 are sparse arrays. All of these arrays have 7 physical sensors.

Example 1.2.2 (The $\mathcal{O}(N^2)$ property). It can be seen from Figs. 1.4(b), (d), and (f) that the sizes of the difference coarrays are given by $|\mathbb{D}_1| = 13$, $|\mathbb{D}_2| = 35$, and $|\mathbb{D}_3| = 43$, where $|\cdot|$ denotes the cardinality of a set. Namely, the size of the difference coarray for ULA ($|\mathbb{D}_1|$) is approximately twice of the number of sensors while the size of the difference coarray for sparse arrays can be much larger than the number of sensors. In particular, ULA has only $|\mathbb{D}| = \mathcal{O}(N)$ [188], where $\mathcal{O}(\cdot)$ denotes the order of a function and N is the number of sensors. By contrast, it was shown in [59], [92], [113], [124], [139], [177], [186] that, for some sparse arrays like minimum redundancy arrays and minimum hole arrays, the size of the difference coarray achieves $|\mathbb{D}| = \mathcal{O}(N^2)$.

Example 1.2.3 (The hole-free property). Let us focus on the arrays \mathbb{S}_2 and \mathbb{S}_3 in Fig. 1.4. Even though \mathbb{S}_2 and \mathbb{S}_3 are both sparse arrays, the structures of their difference coarrays \mathbb{D}_2 and \mathbb{D}_3 are quite different. \mathbb{D}_2 is composed of consecutive integers from -17 to 17 . On the other hand, \mathbb{D}_3 contains a central ULA segment from -12 to 12 but some numbers are missing in \mathbb{D}_3 , such as 13 , 17 , 20 , and so forth. These missing numbers are also called *holes* in the difference coarray [186]. Based on this, the difference coarray \mathbb{D}_2 is called *hole-free* since there are no holes in \mathbb{D}_2 [186]. It can be seen that \mathbb{D}_1 is also hole-free.

If a sparse array satisfies the $\mathcal{O}(N^2)$ property and the hole-free property, then there are several advantages in the DOA estimation stage (Stage 2). First, it can be shown that such array is capable of resolving $\mathcal{O}(N^2)$ uncorrelated sources [73], [97], [192], implying that more sources than sensors can be identified. But the ULA can only find fewer sources than sensors [188]. Second, there exist coarray-based DOA estimators, such as coarray MUSIC [87], [124], [125], [186], that successfully identify more sources than sensors. These advantages will be elaborated in Chapters 2 and 6 later.

1.3 Scope and Outline of the Thesis

This thesis consists of two major parts. After presenting the implementation of the coarray MUSIC algorithm (Chapter 2), the first part of the thesis (Chapters 3, 4, and 5) proposes new sparse array geometries, including super nested arrays, half

open box arrays, half open box arrays with two layers, and hourglass arrays. These arrays enjoys the $\mathcal{O}(N^2)$ property and the hole-free property and they are robust to mutual coupling effects. The second part of the thesis (Chapters 6, 7, 8, and 9) analyzes the performance of sparse arrays, from the viewpoint of Cramér-Rao bounds, generalized correlation subspace, and robustness to sensor failures. In this section, the scope of each chapter will be briefly introduced.

Coarray MUSIC (Chapter 2)

The first part of Chapter 2 reviews the basics of sparse arrays and the MUSIC algorithm. The second part discusses the details of implementing the MUSIC algorithm with the difference coarray. Previously, a technique called spatial smoothing was utilized in order to successfully perform MUSIC in the difference coarray [124], [125]. Chapter 2 shows that the spatial smoothing step is not necessary in the sense that the effect achieved by that step can be obtained more directly. In particular, with $\tilde{\mathbf{R}}_{ss}$ denoting the spatial smoothed matrix with finite snapshots, it is shown here that the noise eigenspace of this matrix can be directly obtained from another matrix $\tilde{\mathbf{R}}$ which is much easier to compute from data.

Super Nested Arrays (Chapters 3 and 4)

In array processing, mutual coupling between sensors has an adverse effect on the estimation of parameters (e.g., DOA). While there are methods to counteract this through appropriate modeling and calibration, they are usually computationally expensive, and sensitive to model mismatch. On the other hand, sparse arrays, such as nested arrays, coprime arrays, and minimum redundancy arrays (MRAs), have reduced mutual coupling compared to ULA. But these well-known sparse arrays have disadvantages: MRAs do not have simple closed-form expressions for the array geometry; coprime arrays have holes in the coarray; and nested arrays contain a dense ULA in the physical array, resulting in significantly higher mutual coupling than coprime arrays and MRAs. Chapter 3 introduces a new array called the (second-order) super nested array, which has all the good properties of the nested array, and at the same time achieves reduced mutual coupling. There is a systematic procedure to determine sensor locations. For a fixed number of sensors N , the super nested array has the same physical aperture, and the same hole-free coarray as does the nested array. But the number of sensor pairs with small separations ($\lambda/2, 2 \times \lambda/2$, etc.) is significantly reduced. In Chapter 4, a generalization of super nested arrays is introduced, called the Q th-order super nested array. This has all the properties of the second-order super nested array with the additional advantage that mutual coupling effects are further reduced for $Q > 2$. Many theoretical properties are proved and simulations are included to demonstrate the superior

performance of these arrays.

Hourglass Arrays (Chapter 5)

Linear (1D) sparse arrays such as nested arrays and minimum redundancy arrays have hole-free difference coarrays with $\mathcal{O}(N^2)$ virtual sensor elements, where N is the number of physical sensors. The hole-free property makes it easier to perform beamforming and DOA estimation in the difference coarray domain which behaves like an uniform linear array. The $\mathcal{O}(N^2)$ property implies that $\mathcal{O}(N^2)$ uncorrelated sources can be identified. For the 2D case, planar sparse arrays with hole-free difference coarrays having $\mathcal{O}(N^2)$ elements have also been known for a long time. These include billboard arrays, open box arrays (OBA), and 2D nested arrays. Their merits are similar to those of the 1D sparse arrays mentioned above, although identifiability claims regarding $\mathcal{O}(N^2)$ sources have to be handled with more care in 2D. Chapter 5 introduces new planar sparse arrays with hole-free difference coarrays having $\mathcal{O}(N^2)$ elements just like the OBA, with the additional property that the number of sensor pairs with small spacings such as $\lambda/2$ decreases, reducing the effect of mutual coupling. The new arrays include half open box arrays (HOBA), half open box arrays with two layers (HOBA-2), and hourglass arrays. Among these, simulations show that hourglass arrays have the best estimation performance in presence of mutual coupling.

Cramér-Rao Bounds for Sparse Arrays (Chapter 6)

The Cramér-Rao bound (CRB) offers a lower bound on the variances of unbiased estimates of parameters, e.g., directions of arrival (DOA) in array processing. While there exist landmark papers on the study of the CRB in the context of array processing, the closed-form expressions available in the literature are not easy to use in the context of sparse arrays (such as minimum redundancy arrays (MRAs), nested arrays, or coprime arrays) for which the number of identifiable sources D exceeds the number of sensors N . Under such situations, the existing literature does not spell out the conditions under which the Fisher information matrix is nonsingular, or the condition under which specific closed-form expressions for the CRB remain valid. Chapter 6 derives a new expression for the CRB to fill this gap. The conditions for validity of this expression are expressed as the rank condition of a matrix called the augmented coarray manifold matrix, which is defined based on the difference coarray. The rank condition and the closed-form expression lead to a number of new insights. For example, it is possible to prove the previously known experimental observation that, when there are more sources than sensors, the CRB stagnates to a constant value as the SNR tends to infinity. It is also possible to precisely specify the relation between the number of sensors and the number of uncorrelated sources

such that these conditions are valid. In particular, for nested arrays, coprime arrays, and MRAs, the new expressions remain valid for $D = \mathcal{O}(N^2)$, the precise detail depending on the specific array geometry.

Generalized Correlation Subspace (Chapter 7)

Recently, it has been shown that *correlation subspaces*, which reveal the structure of the covariance matrix, help to improve some existing DOA estimators. However, the bases, the dimension, and other theoretical properties of correlation subspaces were not investigated. Chapter 7 fills this gap by proposing *generalized correlation subspaces* in one and multiple dimensions. This leads to new insights into correlation subspaces and DOA estimation with prior knowledge. First, it is shown that the bases and the dimension of correlation subspaces are fundamentally related to *difference coarrays*, which were previously found to be important in the study of sparse arrays. Furthermore, generalized correlation subspaces can handle certain forms of prior knowledge about source directions. These results allow one to derive a broad class of DOA estimators with improved performance. It is demonstrated through examples that using sparse arrays and generalized correlation subspaces, DOA estimators with source priors exhibit better estimation performance than those without priors, in extreme cases like low SNR and limited snapshots.

Robustness of Sparse Arrays (Chapters 8 and 9)

It is empirically known that the coarray structure is susceptible to sensor failures, and the reliability of sparse arrays remains a significant but challenging topic for investigation. Broadly speaking, the ULA whose difference coarray only has $\mathcal{O}(N)$ sensors, is more robust than sparse arrays with $\mathcal{O}(N^2)$ coarray sizes. Chapter 8 advances a general theory for quantifying such robustness, by studying the effect of sensor failure on the difference coarray. This is done by introducing the concepts of essentialness and k -essentialness of sensors in the array. A related quantity, called fragility is also developed systematically. The k -essential family characterizes the patterns of k faulty sensors that shrink the difference coarray. This concept leads to the notion of the k -fragility, which assesses the robustness of array geometries quantitatively. However, the large size of the k -essential family usually complicates the theory. It will be shown that the k -essential family can be compactly represented by the so-called k -essential Sperner family, named after the mathematician Sperner for reasons explained in Chapter 8. Finally, the proposed framework is used to study the probability of change of the difference coarray, as a function of the sensor failure probability and array geometry. Chapter 9 derives closed-form characterizations of the k -essential Sperner family for ULA, minimum redundancy arrays, minimum holes arrays, Cantor arrays, nested arrays, and coprime arrays. These results lead

to many insights into the relative importance of each sensor, the robustness of these arrays, and the estimation performance in the presence of sensor failure.

1.4 Notations

The notations used in this thesis are defined in this section. Scalars are denoted by lower-case letters (such as a). The ceiling function $\lceil x \rceil$ is the least integer that is greater than or equal to x , while the floor function $\lfloor x \rfloor$ denotes the greatest integer that is smaller than or equal to x . Two integers M and N are said to be coprime if and only if the greatest common divisor of M and N is 1. The nonnegative part of a real number x is denoted by $(x)^+ = \max\{x, 0\}$. We use e^x and $\exp(x)$ interchangeably to represent the natural exponential function. The imaginary unit is given by $j = \sqrt{-1}$.

Sets are represented by blackboard boldface (such as \mathbb{A}). The cardinality of a set \mathbb{A} is denoted by $|\mathbb{A}|$. The intersection and the union of two sets \mathbb{A} and \mathbb{B} are denoted by $\mathbb{A} \cap \mathbb{B}$ and $\mathbb{A} \cup \mathbb{B}$, respectively. The relative complement of a set \mathbb{A} with respect to a set \mathbb{B} is written as

$$\mathbb{B} \setminus \mathbb{A} \triangleq \{x \in \mathbb{B} : x \notin \mathbb{A}\}. \quad (1.9)$$

The notation $\mathbb{A} \subseteq \mathbb{B}$ denotes that a set \mathbb{A} is a subset of a set \mathbb{B} . A set \mathbb{A} is said to be a proper subset, or a strict subset of \mathbb{B} , denoted by $\mathbb{A} \subset \mathbb{B}$, if $\mathbb{A} \subseteq \mathbb{B}$ and $\mathbb{A} \neq \mathbb{B}$. The notations $\mathbb{A} \supseteq \mathbb{B}$ and $\mathbb{A} \supset \mathbb{B}$ represent that \mathbb{A} is a superset, or a proper superset of \mathbb{B} , respectively. The nonnegative part of a set \mathbb{S} of real-valued quantities is defined as

$$\mathbb{S}^+ \triangleq \{s \in \mathbb{S} : s \geq 0\}. \quad (1.10)$$

The empty set is denoted by \emptyset . The notations \mathbb{Z} , \mathbb{R} , and \mathbb{C} represent the set of integers, the set of real numbers, and the set of complex numbers. The notation $\mathbb{S}^{M \times N}$ denotes the set of matrices of size $M \times N$, where each entry in the matrix belongs to the set \mathbb{S} .

Two sets \mathbb{A} and \mathbb{B} are said to be disjoint if $\mathbb{A} \cap \mathbb{B} = \emptyset$. A family of sets $\{\mathbb{A}_1, \mathbb{A}_2, \dots, \mathbb{A}_K\}$ is said to be a partition of a set \mathbb{B} if 1) \mathbb{A}_p and \mathbb{A}_q are disjoint for all $1 \leq p < q \leq K$ and 2) the union of $\mathbb{A}_1, \mathbb{A}_2, \dots, \mathbb{A}_K$ is \mathbb{B} .

Vectors and matrices are denoted by lower-case letters in bold face (such as \mathbf{a}) and upper-case letters in bold face (such as \mathbf{A}), respectively. $[\mathbf{a}]_i$ denotes the i th coordinate of \mathbf{a} while $[\mathbf{A}]_{i,j}$ indicates the (i, j) th entry of \mathbf{A} . The complex conjugate, the transpose, and the complex conjugate transpose of \mathbf{A} are \mathbf{A}^* , \mathbf{A}^T , and \mathbf{A}^H , respectively. Letting $\mathbf{A} \in \mathbb{C}^{M \times N}$, the Kronecker product between \mathbf{A} and \mathbf{B} is defined

as

$$\mathbf{A} \otimes \mathbf{B} = \begin{bmatrix} [\mathbf{A}]_{1,1}\mathbf{B} & [\mathbf{A}]_{1,2}\mathbf{B} & \dots & [\mathbf{A}]_{1,N}\mathbf{B} \\ [\mathbf{A}]_{2,1}\mathbf{B} & [\mathbf{A}]_{2,2}\mathbf{B} & \dots & [\mathbf{A}]_{2,N}\mathbf{B} \\ \vdots & \vdots & \ddots & \vdots \\ [\mathbf{A}]_{M,1}\mathbf{B} & [\mathbf{A}]_{M,2}\mathbf{B} & \dots & [\mathbf{A}]_{M,N}\mathbf{B} \end{bmatrix}. \quad (1.11)$$

The Hadamard product between \mathbf{A} and \mathbf{B} of the same size is $\mathbf{A} \odot \mathbf{B}$ such that $[\mathbf{A} \odot \mathbf{B}]_{i,j} = [\mathbf{A}]_{i,j}[\mathbf{B}]_{i,j}$. The Khatri-Rao matrix product between two matrices is defined as the column-wise Kronecker product:

$$\begin{aligned} & \begin{bmatrix} \mathbf{a}_1 & \mathbf{a}_2 & \dots & \mathbf{a}_N \end{bmatrix} \circ \begin{bmatrix} \mathbf{b}_1 & \mathbf{b}_2 & \dots & \mathbf{b}_N \end{bmatrix} \\ &= \begin{bmatrix} \mathbf{a}_1 \otimes \mathbf{b}_1 & \mathbf{a}_2 \otimes \mathbf{b}_2 & \dots & \mathbf{a}_N \otimes \mathbf{b}_N \end{bmatrix}. \end{aligned} \quad (1.12)$$

For a full column rank matrix \mathbf{A} , the matrices

$$\mathbf{\Pi}_{\mathbf{A}} = \mathbf{A}(\mathbf{A}^H \mathbf{A})^{-1} \mathbf{A}^H, \quad (1.13)$$

$$\mathbf{\Pi}_{\mathbf{A}}^\perp = \mathbf{I} - \mathbf{A}(\mathbf{A}^H \mathbf{A})^{-1} \mathbf{A}^H, \quad (1.14)$$

denote the orthogonal projection onto the column space of \mathbf{A} , and to the null space of \mathbf{A}^H , respectively. $\text{diag}(a_1, \dots, a_n)$ is a diagonal matrix with diagonal entries a_1, \dots, a_n . For a real set $\mathbb{A} = \{a_1, \dots, a_n\}$ such that $a_1 < \dots < a_n$, $\text{diag}(\mathbb{A}) \triangleq \text{diag}(a_1, \dots, a_n)$. The notation $\text{rank}(\mathbf{A})$ is the rank of \mathbf{A} . The notation $\text{tr}(\mathbf{A})$ denotes the trace of \mathbf{A} , which is the sum of diagonal entries. The vectorization operation is defined as

$$\text{vec} \left(\begin{bmatrix} \mathbf{a}_1 & \mathbf{a}_2 & \dots & \mathbf{a}_N \end{bmatrix} \right) = \begin{bmatrix} \mathbf{a}_1 \\ \mathbf{a}_2 \\ \vdots \\ \mathbf{a}_N \end{bmatrix}. \quad (1.15)$$

The notation $\Pr [\mathfrak{A}]$ represents the probability of the event \mathfrak{A} . The expectation operator is denoted by $\mathbb{E}[\cdot]$. $\mathcal{N}(\boldsymbol{\mu}, \mathbf{C})$ is a multivariate real-valued normal distribution with mean $\boldsymbol{\mu}$ and covariance \mathbf{C} . $\mathcal{CN}(\mathbf{m}, \boldsymbol{\Sigma})$ is a circularly-symmetric complex normal distribution with mean \mathbf{m} and covariance matrix $\boldsymbol{\Sigma}$.

The Bracket Notation

Let \mathbb{S} be an integer set and let the signal defined over \mathbb{S} denoted by a column vector $\mathbf{x}_{\mathbb{S}}$. The square bracket notation $[\mathbf{x}_{\mathbb{S}}]_i$ represents the i th component of $\mathbf{x}_{\mathbb{S}}$. The triangular bracket notation $\langle \mathbf{x}_{\mathbb{S}} \rangle_n$ denotes the signal value on the support $n \in \mathbb{S}$ and is very useful for nonuniform arrays. For instance, if $\mathbb{S} = \{0, 2, 5\}$ and $\mathbf{x}_{\mathbb{S}} = [-1, 1, 4]^T$,

then

$$[\mathbf{x}_S]_1 = -1, \quad [\mathbf{x}_S]_2 = 1, \quad [\mathbf{x}_S]_3 = 4, \quad (1.16)$$

$$\langle \mathbf{x}_S \rangle_0 = -1, \quad \langle \mathbf{x}_S \rangle_2 = 1, \quad \langle \mathbf{x}_S \rangle_5 = 4. \quad (1.17)$$

The bracket notation also applies to matrices. If $\mathbf{A} = \mathbf{x}_S \mathbf{x}_S^T$, then $[\mathbf{A}]_{i,j} = [\mathbf{x}_S]_i [\mathbf{x}_S]_j$ and $\langle \mathbf{A} \rangle_{n_1, n_2} = \langle \mathbf{x}_S \rangle_{n_1} \langle \mathbf{x}_S \rangle_{n_2}$.

COARRAY MUSIC AND SPATIAL SMOOTHING

2.1 Introduction

Sparse arrays open a new approach to sensor array processing because of the high degrees of freedom offered in the difference-coarray domain. Nested arrays [124] and coprime arrays [186] are examples of sparse arrays obtained from a union of two uniform linear arrays (ULAs) with different interelement spacings. The increased freedom has been used to identify $\mathcal{O}(N^2)$ sources (DOAs) from only N sensors [124], [186]. Sparse arrays can be used in various applications, including DOA estimation [124], [186], [200], [201], line spectrum estimation using MUSIC algorithms [125], super resolution [175], [176], two dimensional array design [121], [122], [183], beamforming, and coprime spatial filter bank design [3], [4], [85].

In DOA estimation using the MUSIC algorithm [125] or any gridless algorithm [123], a technique called spatial smoothing [152] is sometimes used to construct a positive definite matrix on which MUSIC operates. For sparse arrays which use the MUSIC algorithm in the difference-coarray domain, it was proved in [124], [125] that the spatially smoothed matrix \mathbf{R}_{ss} in the coarray domain is a perfect square of a positive definite matrix $\hat{\mathbf{R}}$ which contains noise-subspace information. Using this fact it was possible to separate the signal subspace and the noise subspace based on the eigenvalues of \mathbf{R}_{ss} . This leads to a successful implementation of MUSIC in the coarray domain. It should be mentioned herein that when DOA estimation based on coarray domain is performed by formulating a dictionary based approach [119], spatial smoothing is not necessary. It has been used in the past only when the MUSIC algorithm or other gridless algorithms [123] is to be employed in the coarray domain.

In this chapter, we will show that spatial smoothing is not needed even to implement the MUSIC algorithm in the coarray domain. The performance reported in [124], [125] can be achieved without it. This is done as follows: based on the snapshot-based covariance estimate of the data, a new matrix $\tilde{\mathbf{R}}$ is introduced which can be directly used to find the noise eigenspace associated with $\tilde{\mathbf{R}}_{ss}$ (the finite-snapshot version of \mathbf{R}_{ss} of [124], [125]). Even with finite number of snapshots, these matrices are related as $\tilde{\mathbf{R}}_{ss} = \tilde{\mathbf{R}}^2/L$, where L is a constant factor, unlike [124], [125] where such a relation is proved only for the ideal infinite snapshot scenario. The MUSIC spectrum which is usually computed based on $\tilde{\mathbf{R}}_{ss}$ can therefore be directly computed based on $\tilde{\mathbf{R}}$. The construction of $\tilde{\mathbf{R}}$ is much simpler than that of $\tilde{\mathbf{R}}_{ss}$ while the

performance is guaranteed to be exactly the same for a fixed number of snapshots. So the complexity of the algorithm is less than that of [124], [125]. It turns out that the intermediate matrix $\tilde{\mathbf{R}}$ is *indefinite* (although Hermitian), but we show that this is of no consequence.

While computational reduction is an advantage, the insight provided by the simplification is perhaps more important, as it might lead to considerable theoretical simplification in the case of multidimensional arrays [122], [183], multiple level nested arrays [120], and other future developments of coarray applications.

The chapter outline is as follows: Basic ideas from sparse arrays are reviewed in Section 2.2. Section 2.3 reviews the MUSIC algorithm and the spatial smoothing MUSIC algorithm. The new matrix $\tilde{\mathbf{R}}$ is introduced in Section 2.4, and it is shown how coarray MUSIC can be successfully performed from certain eigenspaces computed from this matrix. The reduction in computational complexity is also discussed. In Section 2.5, the results are further discussed, before Section 2.6 concludes the chapter.

2.2 Review of Sparse Arrays

In this section, we will first review the difference coarray and its properties. Then several sparse array geometries, such as minimum redundancy arrays [113], minimum hole arrays [177], [190], nested arrays [124], and coprime arrays [186], will be reviewed in detail.

We begin by defining the difference coarray of an array geometry:

Definition 2.2.1 (Difference coarray \mathbb{D}). Let \mathbb{S} be an integer set defining the sensor locations. The difference coarray is defined as

$$\mathbb{D} \triangleq \{n_1 - n_2 : n_1, n_2 \in \mathbb{S}\}. \quad (2.1)$$

The difference coarray is symmetric, i.e., if $m \in \mathbb{D}$, then $-m \in \mathbb{D}$, so we often show the nonnegative part only. It is also useful to characterize the central ULA segment of the difference coarray, denoted as \mathbb{U} , which is utilized in some coarray-based DOA estimators [87], [125]:

Definition 2.2.2 (\mathbb{U} , the central ULA segment). Let \mathbb{D} be the difference coarray of \mathbb{S} and let m be the largest integer such that $\{0, \pm 1, \dots, \pm m\} \subseteq \mathbb{D}$. Then $\mathbb{U} \triangleq \{0, \pm 1, \dots, \pm m\}$ is called the central ULA segment of \mathbb{D} .

Some DOA estimators utilize coarray interpolation to increase the number of usable samples in the difference coarray [2], [104], [137], [179]. These algorithms depend on the smallest ULA containing the difference coarray, denoted by \mathbb{V} , and the *holes*,

which are the missing elements in the difference coarray. These quantities are defined as

Definition 2.2.3 (\mathbb{V} , the smallest ULA containing \mathbb{D}). Let \mathbb{D} be the difference coarray of a sensor array \mathbb{S} . The smallest ULA containing \mathbb{D} is defined as $\mathbb{V} \triangleq \{m \in \mathbb{Z} : \min(\mathbb{D}) \leq m \leq \max(\mathbb{D})\}$.

Definition 2.2.4 (\mathbb{H} , the holes in the difference coarray). Let \mathbb{D} be the difference coarray of \mathbb{S} . The number h is said to be a hole in \mathbb{D} if $h \in \mathbb{V}$ but $h \notin \mathbb{D}$. Furthermore, the set of holes is denoted by $\mathbb{H} \triangleq \mathbb{V} \setminus \mathbb{D} = \{h \in \mathbb{V} : h \notin \mathbb{D}\}$.

According to \mathbb{D} and \mathbb{U} , we define the following terminologies:

Definition 2.2.5 (Degrees of freedom). The number of degrees of freedom (DOF) of a sparse array \mathbb{S} is the cardinality of its difference coarray \mathbb{D} .

Definition 2.2.6 (Uniform DOF). Given an array \mathbb{S} , let \mathbb{U} denote the central ULA segment of its difference coarray. The number of elements in \mathbb{U} is called the number of uniform degrees of freedom or “uniform DOF” of \mathbb{S} .

If the uniform DOF is \mathfrak{F} , then the number of uncorrelated sources that can be identified by using coarray MUSIC is $(\mathfrak{F} - 1)/2$ [124], [125].

Definition 2.2.7 (Restricted arrays [113]). A restricted array is an array whose difference coarray \mathbb{D} is a ULA with adjacent elements separated by 1, i.e., $\mathbb{D} = \mathbb{U}$. In other words, there are no holes in the coarray domain ($\mathbb{H} = \emptyset$). Thus the phrase “restricted array” is equivalent to “array with hole-free difference coarray.”

Definition 2.2.8 (General arrays [113]). If the difference coarray \mathbb{D} of a sparse array \mathbb{S} is not a ULA with inter-element spacing 1, i.e., \mathbb{S} is not a restricted array, then \mathbb{S} is a general array.

Next, we will review the weight function, defined as

Definition 2.2.9 ($w(m)$, the weight function). Let \mathbb{S} be a sensor array and \mathbb{D} be its difference coarray. The weight function is the number of sensor pairs with separation m , defined as

$$w(m) = |\mathbb{M}(m)|, \quad (2.2)$$

$$\mathbb{M}(m) = \{(n_1, n_2) \in \mathbb{S}^2 : n_1 - n_2 = m\}. \quad (2.3)$$

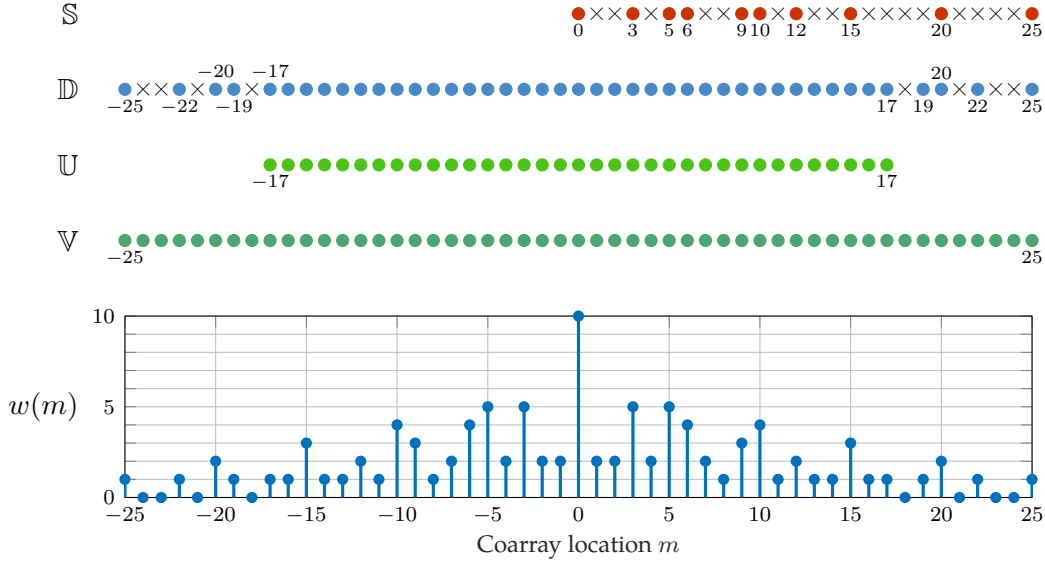


Figure 2.1: An illustration of the sets \mathbb{S} , \mathbb{D} , \mathbb{U} , \mathbb{V} , and the weight function $w(m)$. Here we consider a coprime array with $M = 3$ and $N = 5$, as defined in (2.8).

Note that the weight function $w(m)$ for any linear array with N sensors satisfies the following properties:

$$w(0) = N, \quad \sum_{m \in \mathbb{D}} w(m) = N^2, \quad w(m) = w(-m). \quad (2.4)$$

Furthermore, according to Definitions 2.2.1 and 2.2.9, the difference coarray can also be expressed as the support of the weight function.

Example 2.2.1. Fig. 2.1 illustrates an example of the sensor array \mathbb{S} , the difference coarray \mathbb{D} , the central ULA segment of the difference coarray \mathbb{U} , the smallest ULA containing \mathbb{D} , denoted by \mathbb{V} , and the weight function $w(m)$. The size of the difference coarray is $|\mathbb{D}| = 43$, which is larger than the number of physical sensors $|\mathbb{S}| = 10$. It can be observed that the difference coarray is symmetric to zero, and contains a central ULA segment from -17 to 17 . The set \mathbb{V} is composed of consecutive integers from -25 to 25 . Based on these, the set of holes is given by $\mathbb{H} = \{\pm 18, \pm 21, \pm 23, \pm 24\}$. The weight function $w(m)$ is also given in Fig. 2.1. It can be deduced that the weight function $w(m)$ satisfies $w(0) = 10$, $w(\pm 1) = w(\pm 2) = 2$. These results are consistent with (2.4).

Next we will review some existing sparse arrays, including minimum redundancy arrays [113], minimum hole arrays [177], [190], nested arrays [124], and coprime arrays [186]. Furthermore, Table 2.1 summarizes some commonly used terminologies regarding these sparse arrays.

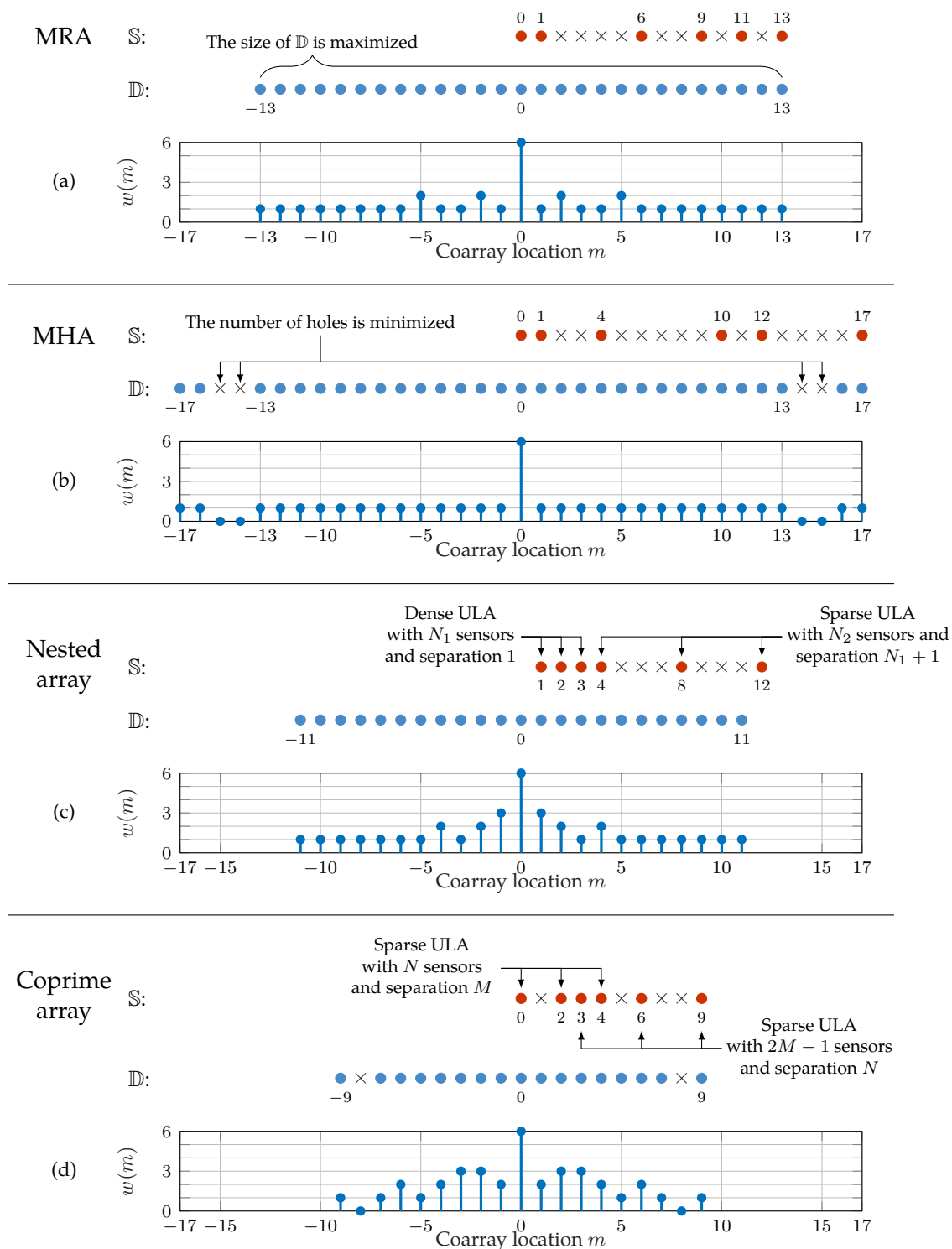


Figure 2.2: The array geometries \mathbb{S} , the difference coarrays \mathbb{D} , and the weight functions $w(m)$ of (a) the MRA with 6 sensors, (b) the MHA with 6 sensors, (c) the nested array with $N_1 = N_2 = 3$, and (d) the coprime array with $M = 2$, $N = 3$. All these arrays have 6 physical sensors. In \mathbb{S} and \mathbb{D} , dots denote elements and crosses represent empty locations.

Table 2.1: Some terminologies related to sparse arrays

| This thesis | Alternative names |
|----------------------------------|---|
| Restricted arrays[113] | Fully augmentable arrays [1] |
| General arrays [113] | Partially augmentable arrays [2] |
| Minimum redundancy arrays (MRAs) | Restricted MRAs [113] |
| Minimum hole arrays (MHAs) | Golomb arrays [177], Minimum-gap arrays [2] |

Minimum redundancy arrays (MRA) [113] maximize the size of the difference coarray under the constraint that the difference coarray is hole-free¹. If the number of sensors N is given, then the formal definition can be expressed as

Definition 2.2.10. The MRA with N physical elements can be defined as

$$\mathbb{S}_{\text{MRA}} \triangleq \arg \max_{\mathbb{S}} |\mathbb{D}| \text{ subject to } |\mathbb{S}| = N, \mathbb{D} = \mathbb{U}. \quad (2.5)$$

As an example, Fig. 2.2(a) illustrates a 6-sensor MRA, its difference coarray \mathbb{D} , and the associated weight functions. It can be seen that these sensors are placed non-uniformly along a straight line while the difference coarray contains consecutive integers from -13 to 13 . The size of the difference coarray is 27, which is much larger than the number of sensors, 6. In particular, it was shown that the size of the difference coarray achieves $|\mathbb{D}| = \mathcal{O}(N^2)$ [45], [81], [113], [145], [156]. The main drawback of MRA is that the sensor locations cannot be expressed in closed forms for large N and can only be evaluated by searching algorithms [65], [81], [84], [149].

Minimum hole arrays (MHA) [177], [190], which are also named as *Golomb arrays* or *minimum gap arrays*, minimize the number of holes, such that each nonzero element in the difference coarray results from a unique sensor pair. Formally:

Definition 2.2.11. The MHA with N physical elements can be defined as [177]

$$\begin{aligned} \mathbb{S}_{\text{MHA}} &\triangleq \arg \min_{\mathbb{S}} |\mathbb{H}| \\ &\text{subject to } |\mathbb{S}| = N, w(m) = 1 \text{ for } m \in \mathbb{D} \setminus \{0\}, \end{aligned} \quad (2.6)$$

where the set of holes \mathbb{H} is defined in Definition 2.2.4.

Note that $w(m) = 1$ means that the difference m occurs exactly once. Thus the constraint (2.6) ensures that no difference m occurs more than once. For instance, Fig.

¹ This array configuration was denoted as *restricted MRA* in [113].

2.2(b) depicts the physical array and the difference coarray of a 6-sensor MHA. It can be seen that in this case, $\mathbb{S} = \{0, 1, 4, 10, 12, 17\}$ and \mathbb{D} is $\{0, \pm 1, \dots, \pm 13, \pm 16, \pm 17\}$. The set of holes is $\{\pm 14, \pm 15\}$. It can be verified that the weight function $w(m)$ in Fig. 2.2(b) satisfies the constraint (2.6). Due to Definition 2.2.11, it can be shown that, for MHA, the size of the difference coarray is $|\mathbb{D}| = N^2 - N + 1$ [177]. Like MRA, the main issue for the MHA is that, there are no closed-form expressions for sensor locations [10], [40], [79], [146], [174], [177]. For further discussions, please see [2] and the references therein.

Nested and coprime arrays [124], [186] are sparse arrays with simple geometries having closed-form expressions. Both have $\mathcal{O}(N^2)$ distinct elements in the difference coarray domain, although they do not optimize the parameters that MRA or MHA seek to optimize. *Nested arrays* are composed of a dense ULA with sensor separation 1, and a sparse ULA with sensor separation $(N_1 + 1)$. The closed-form sensor locations are given by [124]:

$$\mathbb{S}_{\text{nested}} \triangleq \{1, 2, \dots, N_1, (N_1 + 1), 2(N_1 + 1), \dots, N_2(N_1 + 1)\}, \quad (2.7)$$

where N_1 and N_2 are positive integers. Fig. 2.2(c) demonstrates a nested array with $N_1 = N_2 = 3$. In this example, the number of physical sensors is 6 while the difference coarray consists of integers from -11 to 11 . In particular, it was proved in [124] that, if N_1 is approximately N_2 , then with $\mathcal{O}(N)$ physical sensors, the size of the difference coarray is $\mathcal{O}(N^2)$, which has the same order as MRA and MHA [113], [177]. One advantage of nested arrays is the simplicity of design equations for large number of elements [124], which cannot be achieved in MRA or MHA. Another advantage of nested arrays is that, the difference coarray consists of contiguous integers from $-N_2(N_1 + 1) + 1$ to $N_2(N_1 + 1) - 1$ and there are no holes. This property makes it possible to utilize the complete autocorrelation information in spatial smoothing MUSIC [124].

Coprime arrays are another family of sparse arrays that enjoys long difference coarray and closed-form sensor locations [186]. They are composed of two sparse ULAs with sensor separations M and N , respectively. The sensor locations for the coprime array are defined as follows:

$$\mathbb{S}_{\text{coprime}} \triangleq \{0, M, 2M, \dots, (N - 1)M, N, 2N, \dots, (2M - 1)N\}, \quad (2.8)$$

where M and N are a coprime pair of integers and $M < N$. Fig. 2.2(d) shows a coprime array with $M = 2$ and $N = 3$, as an example. The number of sensors is 6 and the difference coarray consists of consecutive integers from -7 to 7 but the lags ± 8 are missing. It was shown in [125], [186] that the difference coarray of coprime arrays, $\mathbb{D}_{\text{coprime}}$, contains consecutive integers from $-MN$ to MN and there are

holes outside this region. It was further proved in [139], [201] that the maximum central contiguous ULA section of $\mathbb{D}_{\text{coprime}}$, is actually from $-(MN + M - 1)$ to $MN + M - 1$. In other words, the size of the ULA segment in difference coarray for coprime arrays is $\mathcal{O}(MN)$, given $\mathcal{O}(M + N)$ physical sensors. The advantages of coprime arrays include, first, simple and closed-form sensor locations, as indicated in (2.8). Second, it was shown in [92], [125], [186] that, compared to nested arrays, coprime arrays reduce the mutual coupling effect, which originates from the non-ideal interference between adjacent sensor outputs.

2.3 Review of MUSIC and Spatial Smoothing MUSIC

The MUSIC Algorithm

First let us review the covariance matrix of the array output, on which the MUSIC algorithm operates. According to the details in Section 1.1, the received signal vector $\mathbf{x}_{\mathbb{S}}$ is modeled as $\mathbf{x}_{\mathbb{S}} = \sum_{i=1}^D A_i \mathbf{v}_{\mathbb{S}}(\bar{\theta}_i) + \mathbf{n}_{\mathbb{S}}$, as in (1.5). Here the set \mathbb{S} denotes the array geometry, D is the number of monochromatic sources, $\bar{\theta}_i \in [-1/2, 1/2]$ and $A_i \in \mathbb{C}$ are the normalized DOA and the complex amplitude of the i th source, $\mathbf{v}_{\mathbb{S}}(\bar{\theta}_i) \in \mathbb{C}^{|\mathbb{S}|}$ is the steering vector, and $\mathbf{n}_{\mathbb{S}}$ is the additive noise term. In this thesis, the following statistical assumptions are also considered:

- (A1) The number of sources D is known and fixed.
- (A2) The normalized DOAs $\{\bar{\theta}_1, \bar{\theta}_2, \dots, \bar{\theta}_D\}$ are unknown but fixed.
- (A3) The complex amplitude A_i and the noise term $\mathbf{n}_{\mathbb{S}}$ are zero-mean and uncorrelated random variables/vectors. In particular, the power of the i th source is denoted by p_i and the noise power is p_n at each sensor. These relations can be expressed as

$$\mathbb{E}[\mathbf{s}] = \mathbf{0}, \quad \mathbb{E}[\mathbf{s}\mathbf{s}^H] = \begin{bmatrix} p_1 & 0 & \dots & 0 & \mathbf{0} \\ 0 & p_2 & \dots & 0 & \mathbf{0} \\ \vdots & \vdots & \ddots & \vdots & \vdots \\ 0 & 0 & \dots & p_D & \mathbf{0} \\ \mathbf{0} & \mathbf{0} & \dots & \mathbf{0} & p_n \mathbf{I} \end{bmatrix}, \quad (2.9)$$

where $\mathbf{s} \triangleq [A_1, A_2, \dots, A_D, \mathbf{n}_{\mathbb{S}}^T]^T$.

Next let us derive the expression of the covariance matrix of $\mathbf{x}_{\mathbb{S}}$, denoted by $\mathbf{R}_{\mathbb{S}}$. Here the subscript \mathbb{S} in $\mathbf{R}_{\mathbb{S}}$ indicates that the covariance matrix is with respect to \mathbb{S} .

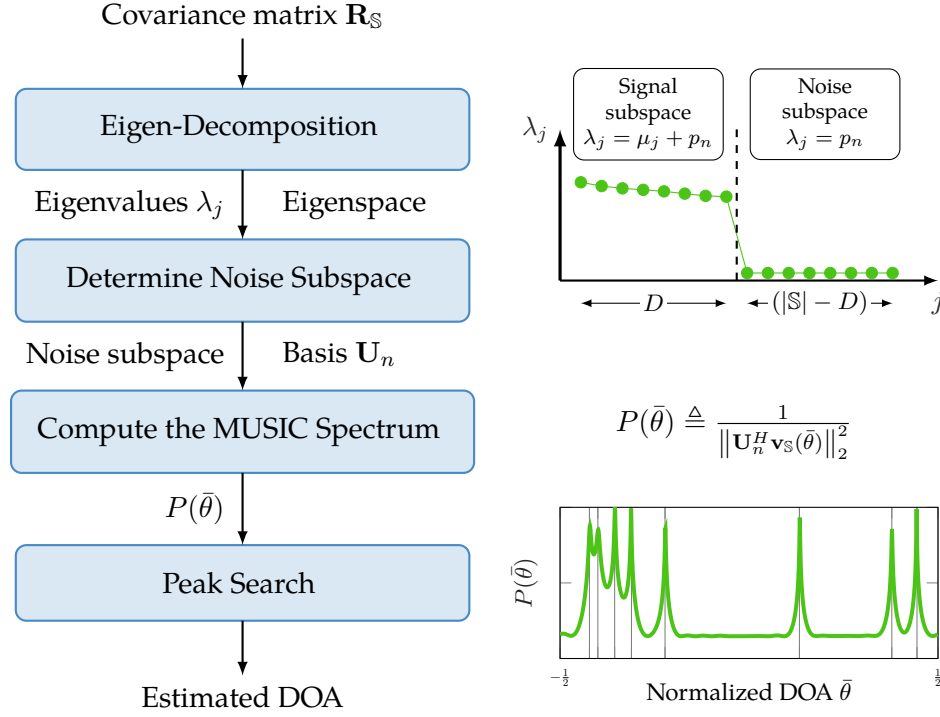


Figure 2.3: A schematic diagram of the MUSIC algorithm.

Under assumptions **(A1)** to **(A3)**, we obtain

$$\begin{aligned}
 \mathbf{R}_S &= \mathbb{E} [\mathbf{x}_S \mathbf{x}_S^H] \\
 &= \sum_{i=1}^D \sum_{j=1}^D \underbrace{\mathbb{E} [A_i A_j^*]}_{p_i \delta_{i,j}} \mathbf{v}_S(\bar{\theta}_i) \mathbf{v}_S^H(\bar{\theta}_j) + \sum_{i=1}^D \mathbf{v}_S(\bar{\theta}_i) \underbrace{\mathbb{E} [A_i \mathbf{n}_S^H]}_{\mathbf{0}} \\
 &\quad + \sum_{j=1}^D \underbrace{\mathbb{E} [\mathbf{n}_S A_j^*]}_{\mathbf{0}} \mathbf{v}_S^H(\bar{\theta}_j) + \underbrace{\mathbb{E} [\mathbf{n}_S \mathbf{n}_S^H]}_{p_n \mathbf{I}} \\
 &= \sum_{i=1}^D p_i \mathbf{v}_S(\bar{\theta}_i) \mathbf{v}_S^H(\bar{\theta}_i) + p_n \mathbf{I}.
 \end{aligned} \tag{2.10}$$

Based on the covariance matrix of \mathbf{x}_S , the *MUSIC algorithm* aims to estimate the source directions, i.e., the normalized DOAs $\{\bar{\theta}_1, \dots, \bar{\theta}_D\}$ [150], [188]. In what follows, the details of the MUSIC algorithm will be reviewed using a schematic diagram in Fig. 2.3. Note that the following development is based on the covariance matrix \mathbf{R}_S . The extension of finite snapshots will be discussed in the last subsection of Section 2.3.

We begin by decomposing the first term of (2.10), namely the signal term, into the

eigenvalues μ_j and the eigenvectors \mathbf{u}_j :

$$\sum_{i=1}^D p_i \mathbf{v}_S(\bar{\theta}_i) \mathbf{v}_S^H(\bar{\theta}_i) = \sum_{j=1}^D \mu_j \mathbf{u}_j \mathbf{u}_j^H. \quad (2.11)$$

It is assumed that the signal term has rank $D < |\mathbb{S}|$, the eigenvalues satisfy $\mu_1 \geq \mu_2 \geq \dots \geq \mu_D > 0$, and the eigenvectors are orthonormal. Under these assumptions, the eigen-decomposition of the matrix \mathbf{R}_S can be expressed as

$$\mathbf{R}_S = \sum_{j=1}^D (\mu_j + p_n) \mathbf{u}_j \mathbf{u}_j^H + \sum_{j=D+1}^{|\mathbb{S}|} p_n \mathbf{u}_j \mathbf{u}_j^H, \quad (2.12)$$

where $\mathbf{u}_1, \mathbf{u}_2, \dots, \mathbf{u}_{|\mathbb{S}|}$ form a set of orthonormal basis vectors of $\mathbb{C}^{|\mathbb{S}|}$. It can be observed that the eigenvalues of \mathbf{R}_S , denoted by λ_j , are $\mu_j + p_n$ if $j \leq D$ and are p_n otherwise. For instance, Fig. 2.3 shows a typical distribution of the eigenvalues λ_j . Due to (2.12), the first D eigenvalues are generally larger than the remaining eigenvalues, while the last $|\mathbb{S}| - D$ eigenvalues are fixed to be p_n . Based on this property, it is possible to split the space $\mathbb{C}^{|\mathbb{S}|}$ into the *signal subspace*, which corresponds to the subspace due to the signal term in (2.11), and the *noise subspace*, which is associated with the second term in (2.12). In particular, the bases of the signal subspace and the noise subspace are denoted by

$$\mathbf{U}_s = \begin{bmatrix} \mathbf{u}_1 & \mathbf{u}_2 & \dots & \mathbf{u}_D \end{bmatrix} \in \mathbb{C}^{|\mathbb{S}| \times D} \quad \text{for the signal subspace,} \quad (2.13)$$

$$\mathbf{U}_n = \begin{bmatrix} \mathbf{u}_{D+1} & \mathbf{u}_{D+2} & \dots & \mathbf{u}_{|\mathbb{S}|} \end{bmatrix} \in \mathbb{C}^{|\mathbb{S}| \times (|\mathbb{S}| - D)} \quad \text{for the noise subspace.} \quad (2.14)$$

Furthermore, Eqs. (2.11) and (2.12) imply that *the projection of the steering vectors corresponding to the true normalized DOAs onto the noise subspace is zero, i.e.,*

$$\mathbf{U}_n^H \mathbf{v}_S(\bar{\theta}_i) = \mathbf{0}, \quad (2.15)$$

for $i = 1, 2, \dots, D$. Based on (2.15), we can define the MUSIC spectrum $P(\bar{\theta})$ as follows:

$$P(\bar{\theta}) \triangleq \frac{1}{\|\mathbf{U}_n^H \mathbf{v}_S(\bar{\theta})\|_2^2}, \quad -\frac{1}{2} \leq \bar{\theta} \leq \frac{1}{2}. \quad (2.16)$$

It can be deduced from (2.15) and (2.16) that $P(\bar{\theta})$ becomes infinite as the normalized DOA $\bar{\theta}$ matches the true normalized DOA $\bar{\theta}_i$. For instance, Fig. 2.3 illustrates an example of the MUSIC spectrum $P(\bar{\theta})$, where the true normalized DOAs are shown in vertical lines. In practice, we first search the peak locations $\hat{\bar{\theta}}_i$ in $P(\bar{\theta})$, and then use the relation $\hat{\theta}_i = \sin(\hat{\bar{\theta}}_i)/2$ to estimate the DOAs $\hat{\theta}_i$. Note that the MUSIC spectrum $P(\bar{\theta})$ is related to the projection of $\mathbf{v}_S(\bar{\theta})$ onto the noise subspace, which is conceptually different from the spatial power spectrum [14] and the source

powers. Generally speaking, for the same array output, the MUSIC spectrum owns sharper peaks and better estimation performance than the spatial power spectrum [68], [150], [188].

One disadvantage of the MUSIC spectrum is the high complexity in the peak search step of Fig. 2.3, which may require a dense grid search in $\bar{\theta}$. For some array geometries like ULA, the peak search step can be avoided in some variants of the MUSIC algorithm, such as root MUSIC [12], ESPRIT [147], and matrix-pencil methods [62]. In this thesis, unless stated separately, the MUSIC spectrum is computed based on (2.16) and the maximum of $P(\bar{\theta})$ is normalized to 1. The numerical estimation error is evaluated using the root MUSIC algorithm, to reduce the overall computational complexity. For more details of the MUSIC algorithm, interested readers are referred to [68], [110], [165], [188] and the references therein.

The Spatial Smoothing MUSIC Algorithm

In this subsection, we will review the spatial smoothing MUSIC algorithm. This algorithm performs the MUSIC algorithm on the spatially smoothed matrix \mathbf{R}_{ss} , which is related to the difference coarray of sparse arrays, as we will elaborate next.

According to (2.10), the entry of $\mathbf{R}_{\mathbb{S}}$ associated with the $n_1, n_2 \in \mathbb{S}$ can be expressed as

$$\begin{aligned} \langle \mathbf{R}_{\mathbb{S}} \rangle_{n_1, n_2} &= \sum_{i=1}^D p_i \langle \mathbf{v}_{\mathbb{S}}(\bar{\theta}_i) \rangle_{n_1} \langle \mathbf{v}_{\mathbb{S}}(\bar{\theta}_i) \rangle_{n_2}^* + p_n \langle \mathbf{I} \rangle_{n_1, n_2} \\ &= \sum_{i=1}^D p_i \exp [j2\pi\bar{\theta}_i(n_1 - n_2)] + p_n \delta_{n_1 - n_2, 0}, \end{aligned} \quad (2.17)$$

where the delta function $\delta_{p,q}$ is 1 if $p = q$ and is 0 otherwise. It can be observed that the right-hand side of (2.17) depends purely on the differences between sensor locations, i.e., $n_1 - n_2$. Therefore, (2.17) can be reshaped into the autocorrelation vector defined on the difference coarray [87], [107], [108], [124], [125]

$$\mathbf{x}_{\mathbb{D}} = \sum_{i=1}^D p_i \mathbf{v}_{\mathbb{D}}(\bar{\theta}_i) + p_n \mathbf{e}_0, \quad (2.18)$$

where \mathbf{e}_0 is a column vector satisfying $\langle \mathbf{e}_0 \rangle_m = \delta_{m,0}$. Based on the relations between \mathbb{D} and \mathbb{U} , the autocorrelation vector over \mathbb{U} is then constructed to be

$$\mathbf{x}_{\mathbb{U}} = \sum_{i=1}^D p_i \mathbf{v}_{\mathbb{U}}(\bar{\theta}_i) + p_n \mathbf{e}'_0, \quad (2.19)$$

where $\langle \mathbf{e}'_0 \rangle_m = \delta_{m,0}$ for $m \in \mathbb{U}$.

Note that (2.18) can be regarded as the output defined on the difference coarray, instead of that on the physical array (1.5). If sensor locations are designed properly,

like those in Section 2.2, the size of the difference coarray can be much larger than the size of the physical array. In particular, $|\mathbb{D}| = \mathcal{O}(|\mathbb{S}|^2)$. This property makes it possible to develop coarray-based DOA estimators that resolve more source directions than sensors and achieve better spatial resolution [1], [87], [124], [186]. Furthermore, after resolving the source directions, it is possible to estimate the source powers p_i and the noise power p_n , as we will elaborate in Section 2.5.

In what follows, we will review the *spatial smoothing MUSIC algorithm* [124], [125]. To estimate the normalized DOAs $\{\bar{\theta}_i\}_{i=1}^D$, previous works perform (forward) spatial smoothing on $\mathbf{x}_{\mathbb{U}}$ to obtain a spatial smoothed matrix \mathbf{R}_{ss} and then apply the MUSIC algorithm [124], [125]. \mathbf{R}_{ss} is defined as

$$\mathbf{R}_{ss} \triangleq \frac{1}{L} \sum_{p=0}^{L-1} \mathbf{Q}_p \mathbf{x}_{\mathbb{U}} \mathbf{x}_{\mathbb{U}}^H \mathbf{Q}_p^H, \quad (2.20)$$

where \mathbf{Q}_p is a selection matrix defined as

$$\mathbf{Q}_p \triangleq \begin{bmatrix} \mathbf{0}_{L \times (L-1-p)} & \mathbf{I}_{L \times L} & \mathbf{0}_{L \times p} \end{bmatrix} \in \{0, 1\}^{L \times (2L-1)}, \quad (2.21)$$

and

$$L \triangleq \frac{|\mathbb{U}| + 1}{2}. \quad (2.22)$$

\mathbf{R}_{ss} is a positive semidefinite matrix [124], [125]. Hence, \mathbf{R}_{ss} is suitable for the MUSIC algorithm, where we can separate signal/noise subspaces and then define a valid MUSIC spectrum.

DOA Estimation with Finite Snapshots

In practice, the signal vector measured at sparse arrays is denoted by $\tilde{\mathbf{x}}_{\mathbb{S}}$, where the tilde notation, throughout this thesis, stands for observed or measured quantities. These vectors can be measured K times, denote by $\tilde{\mathbf{x}}_{\mathbb{S}}(k)$ for $k = 1, 2, \dots, K$. In the literature, $\tilde{\mathbf{x}}_{\mathbb{S}}(k)$ are also called *snapshots* of $\tilde{\mathbf{x}}_{\mathbb{S}}$. Note that, in this thesis, $\mathbf{x}_{\mathbb{S}}(k)$ represent snapshots that follow from the model in (1.7) while $\tilde{\mathbf{x}}_{\mathbb{S}}(k)$ can be regarded as the realization of the snapshot model in (1.7). More details of the snapshot model can be found in Chapter 6, [188, Chapter 5], [68, Section 4.9], and the references therein. Based on the K snapshots $\tilde{\mathbf{x}}_{\mathbb{S}}(k)$, the covariance matrix of the array output can be estimated as

$$\tilde{\mathbf{R}}_{\mathbb{S}} \triangleq \frac{1}{K} \sum_{k=1}^K \tilde{\mathbf{x}}_{\mathbb{S}}(k) \tilde{\mathbf{x}}_{\mathbb{S}}^H(k). \quad (2.23)$$

Then, the estimated covariance matrix $\tilde{\mathbf{R}}_{\mathbb{S}}$ can be utilized in DOA estimators, such as the MUSIC algorithm, as in Fig. 2.3. Furthermore, if we start from $\tilde{\mathbf{R}}_{\mathbb{S}}$ instead of \mathbf{R}_{ss} , then the quantities $\mathbf{x}_{\mathbb{D}}$, $\mathbf{x}_{\mathbb{U}}$, and \mathbf{R}_{ss} are replaced with the finite snapshot versions

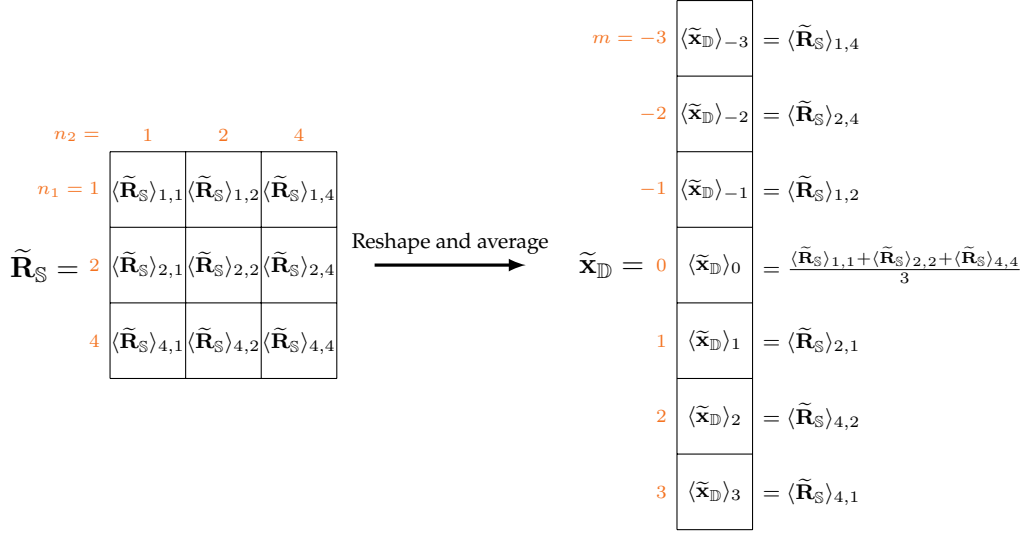


Figure 2.4: The conversion from the $\tilde{\mathbf{R}}_{\mathbb{S}}$ to the autocorrelation vector $\tilde{\mathbf{x}}_{\mathbb{D}}$.

$\tilde{\mathbf{x}}_{\mathbb{D}}$, $\tilde{\mathbf{x}}_{\mathbb{U}}$, and $\tilde{\mathbf{R}}_{ss}$, which are used in the following developments. In particular, $\tilde{\mathbf{x}}_{\mathbb{D}}$ can be determined from $\tilde{\mathbf{R}}_{\mathbb{S}}$ as follows [132]:

Definition 2.3.1. The measurement vector (or the autocorrelation vector) $\tilde{\mathbf{x}}_{\mathbb{D}}$ is defined as

$$\langle \tilde{\mathbf{x}}_{\mathbb{D}} \rangle_m \triangleq \frac{1}{w(m)} \sum_{(n_1, n_2) \in \mathbb{M}(m)} \langle \tilde{\mathbf{R}}_{\mathbb{S}} \rangle_{n_1, n_2}, \quad (2.24)$$

for all $m \in \mathbb{D}$. The weight function $w(m)$ and the set $\mathbb{M}(m)$ are defined in Definition 2.2.9. Similarly, the measurement vector over \mathbb{U} is

$$\langle \tilde{\mathbf{x}}_{\mathbb{U}} \rangle_m \triangleq \frac{1}{w(m)} \sum_{(n_1, n_2) \in \mathbb{M}(m)} \langle \tilde{\mathbf{R}}_{\mathbb{S}} \rangle_{n_1, n_2}, \quad (2.25)$$

for all $m \in \mathbb{U}$.

Note that the expressions in (2.24) and (2.25) are also called *redundancy averaging* in the literature [1], [2], [132].

According to (2.20), the measured spatial smoothed matrix $\tilde{\mathbf{R}}_{ss}$ is computed from $\tilde{\mathbf{x}}_{\mathbb{U}}$ and then the MUSIC algorithm can be applied to obtain line spectrum or DOA estimates.

Example 2.3.1. Fig. 2.4 shows an example of the conversion from $\tilde{\mathbf{R}}_{\mathbb{S}}$ to $\tilde{\mathbf{x}}_{\mathbb{D}}$ with $\mathbb{S} = \{1, 2, 4\}$. The entries in $\tilde{\mathbf{R}}_{\mathbb{S}}$ correspond to the normalized sensor locations n_1 and n_2 , as marked in Fig. 2.4. First, according to Definition 2.2.1, the difference coarray becomes $\mathbb{D} = \{-3, -2, -1, 0, 1, 2, 3\}$, and the autorrelation vector $\tilde{\mathbf{x}}_{\mathbb{D}}$ is depicted on

the right of Fig. 2.4. Next, the autocorrelation vector $\tilde{\mathbf{x}}_{\mathbb{D}}$ is constructed according to the mapping from \mathbb{S} to \mathbb{D} . For instance, the entry $\langle \tilde{\mathbf{x}}_{\mathbb{D}} \rangle_0$ is averaged from the entries $\langle \tilde{\mathbf{R}}_{\mathbb{S}} \rangle_{1,1}$, $\langle \tilde{\mathbf{R}}_{\mathbb{S}} \rangle_{2,2}$, and $\langle \tilde{\mathbf{R}}_{\mathbb{S}} \rangle_{4,4}$, since they are associated with $n_1 - n_2 = 0$.

2.4 Coarray MUSIC without Spatial Smoothing

In this section, we will propose a new matrix $\tilde{\mathbf{R}}$ such that it produces exactly the same MUSIC spectra as [124], [125] without implementing spatial smoothing.

Lemma 2.4.1. $\tilde{\mathbf{x}}_{\mathbb{D}}$ is Hermitian symmetric. That is, $\tilde{\mathbf{x}}_{\mathbb{D}} = \mathbf{Q}\tilde{\mathbf{x}}_{\mathbb{D}}^*$, where \mathbf{Q} is the anti-identity matrix that has ones along its anti-diagonal entries and zeros elsewhere.

Proof. Hermitian symmetry is equivalent to $\langle \tilde{\mathbf{x}}_{\mathbb{D}} \rangle_m = \langle \tilde{\mathbf{x}}_{\mathbb{D}} \rangle_{-m}^*$ for $m \in \mathbb{D}$. Starting with Definition 2.3.1, we obtain

$$\langle \tilde{\mathbf{x}}_{\mathbb{D}} \rangle_m = \frac{1}{|\mathbb{M}(-m)|} \sum_{(n_2, n_1) \in \mathbb{M}(-m)} \langle \tilde{\mathbf{R}}_{\mathbb{S}}^H \rangle_{n_1, n_2},$$

which is based on these properties: $|\mathbb{M}(m)| = |\mathbb{M}(-m)|$, $(n_1, n_2) \in \mathbb{M}(m)$ if and only if $(n_2, n_1) \in \mathbb{M}(-m)$, and $\tilde{\mathbf{R}}_{\mathbb{S}}$ is a Hermitian matrix. Pulling out the complex conjugate yields

$$\langle \tilde{\mathbf{x}}_{\mathbb{D}} \rangle_m = \left(\frac{1}{|\mathbb{M}(-m)|} \sum_{(n_2, n_1) \in \mathbb{M}(-m)} \langle \tilde{\mathbf{R}}_{\mathbb{S}} \rangle_{n_2, n_1} \right)^*.$$

Therefore, we obtain $\langle \tilde{\mathbf{x}}_{\mathbb{D}} \rangle_m = \langle \tilde{\mathbf{x}}_{\mathbb{D}} \rangle_{-m}^*$, which completes the proof. \square

Theorem 2.4.1. Let $\tilde{\mathbf{R}}$ be the following Toeplitz matrix,

$$\tilde{\mathbf{R}} = \begin{bmatrix} [\tilde{\mathbf{x}}_{\mathbb{U}}]_L & [\tilde{\mathbf{x}}_{\mathbb{U}}]_{L-1} & \cdots & [\tilde{\mathbf{x}}_{\mathbb{U}}]_1 \\ [\tilde{\mathbf{x}}_{\mathbb{U}}]_{L+1} & [\tilde{\mathbf{x}}_{\mathbb{U}}]_L & \cdots & [\tilde{\mathbf{x}}_{\mathbb{U}}]_2 \\ \vdots & \vdots & \ddots & \vdots \\ [\tilde{\mathbf{x}}_{\mathbb{U}}]_{2L-1} & [\tilde{\mathbf{x}}_{\mathbb{U}}]_{2L-2} & \cdots & [\tilde{\mathbf{x}}_{\mathbb{U}}]_L \end{bmatrix},$$

where L is defined in (2.22). Then $\tilde{\mathbf{R}}$ is Hermitian and $\tilde{\mathbf{R}}_{ss} = \tilde{\mathbf{R}}^2/L$.

Proof. It was proved in Lemma 2.4.1 that $\tilde{\mathbf{x}}_{\mathbb{D}}$ follows the Hermitian symmetric property. The same property also holds true for $\tilde{\mathbf{x}}_{\mathbb{U}}$ by replacing \mathbb{D} with \mathbb{U} in the proof. The Hermitian of $\tilde{\mathbf{R}}$ is, by definition,

$$\tilde{\mathbf{R}}^H = \begin{bmatrix} [\tilde{\mathbf{x}}_{\mathbb{U}}]_L^* & [\tilde{\mathbf{x}}_{\mathbb{U}}]_{L+1}^* & \cdots & [\tilde{\mathbf{x}}_{\mathbb{U}}]_{2L-1}^* \\ [\tilde{\mathbf{x}}_{\mathbb{U}}]_{L-1}^* & [\tilde{\mathbf{x}}_{\mathbb{U}}]_L^* & \cdots & [\tilde{\mathbf{x}}_{\mathbb{U}}]_{2L-2}^* \\ \vdots & \vdots & \ddots & \vdots \\ [\tilde{\mathbf{x}}_{\mathbb{U}}]_1^* & [\tilde{\mathbf{x}}_{\mathbb{U}}]_2^* & \cdots & [\tilde{\mathbf{x}}_{\mathbb{U}}]_L^* \end{bmatrix}.$$

Since $\tilde{\mathbf{x}}_{\mathbb{U}} = \mathbf{Q}\tilde{\mathbf{x}}_{\mathbb{U}}^*$, each entry in $\tilde{\mathbf{R}}^H$ is replaced with one term in $\tilde{\mathbf{x}}_{\mathbb{U}}$. We obtain $\tilde{\mathbf{R}}^H = \tilde{\mathbf{R}}$, implying $\tilde{\mathbf{R}}$ is Hermitian.

The next part involves the expression of $\tilde{\mathbf{R}}$ in terms of \mathbf{Q}_p , which is defined in (2.21). Since $\tilde{\mathbf{x}}_{\mathbb{U}}$ is the ULA part in the coarray domain, $\mathbf{Q}_0\tilde{\mathbf{x}}_{\mathbb{U}}$ extracts the responses on $0, 1, \dots, \max(\mathbb{U})$. According to the definition of $\tilde{\mathbf{R}}$, we obtain

$$\tilde{\mathbf{R}} = \begin{bmatrix} \mathbf{Q}_0\tilde{\mathbf{x}}_{\mathbb{U}} & \mathbf{Q}_1\tilde{\mathbf{x}}_{\mathbb{U}} & \dots & \mathbf{Q}_{L-1}\tilde{\mathbf{x}}_{\mathbb{U}} \end{bmatrix}.$$

The square of $\tilde{\mathbf{R}}$ is then evaluated as

$$\begin{aligned} \tilde{\mathbf{R}}^2 &= \tilde{\mathbf{R}}\tilde{\mathbf{R}}^H \\ &= \mathbf{Q}_0\tilde{\mathbf{x}}_{\mathbb{U}}(\mathbf{Q}_0\tilde{\mathbf{x}}_{\mathbb{U}})^H + \mathbf{Q}_1\tilde{\mathbf{x}}_{\mathbb{U}}(\mathbf{Q}_1\tilde{\mathbf{x}}_{\mathbb{U}})^H \\ &\quad + \dots + \mathbf{Q}_{L-1}\tilde{\mathbf{x}}_{\mathbb{U}}(\mathbf{Q}_{L-1}\tilde{\mathbf{x}}_{\mathbb{U}})^H \\ &= L\tilde{\mathbf{R}}_{ss}, \end{aligned}$$

which is equivalent to $\tilde{\mathbf{R}}_{ss} = \tilde{\mathbf{R}}^2/L$. \square

The importance of Theorem 2.4.1 is that the MUSIC spectrum can be computed directly from $\tilde{\mathbf{R}}$, rather than the spatially smoothed matrix $\tilde{\mathbf{R}}_{ss}$. It is a direct consequence of $\tilde{\mathbf{R}}_{ss} = \tilde{\mathbf{R}}^2/L$ that (i) eigenvalues of $\tilde{\mathbf{R}}_{ss}$ are proportional to the square of eigenvalues of $\tilde{\mathbf{R}}$, and (ii) $\tilde{\mathbf{R}}_{ss}$ and $\tilde{\mathbf{R}}$ share the same eigenspace. These claims lead to the following corollary:

Corollary 2.4.1. MUSIC spectra based on either $\tilde{\mathbf{R}}_{ss}$ or $\tilde{\mathbf{R}}$ are identical if the signal and noise subspaces of $\tilde{\mathbf{R}}$ are determined by magnitudes of its eigenvalues.

Computational Complexity Analysis

Our proposed method reduces the complexity of the existing approaches [124], [125]. Here, a more detailed comparison on the number of multipliers will be made to demonstrate the computational savings. The DOA estimation over sparse arrays can be divided into the following three stages:

1. *Construct $\tilde{\mathbf{x}}_{\mathbb{U}}$ from $\tilde{\mathbf{x}}_{\mathbb{S}}$.* Once the sensor array collects K snapshots, $\tilde{\mathbf{R}}_{\mathbb{S}}$ is estimated from (2.23), taking $\mathcal{O}(K|\mathbb{S}|^2)$ operations. Based on Definition 2.3.1, $|\mathbb{U}|$ multipliers are involved. Using (2.22) and the fact that $\mathcal{O}(|\mathbb{S}|^2) = \mathcal{O}(|\mathbb{U}|)$, as proved in [124], [125], we see that the total complexity is $\mathcal{O}(KL)$.
2. *Establish $\tilde{\mathbf{R}}_{ss}$ or $\tilde{\mathbf{R}}$.* In [124], [125], $\tilde{\mathbf{R}}_{ss}$ is implemented according to (2.20), where $\mathbf{J}_p\mathbf{x}_{\mathbb{U}}$ is of size L . Since each term takes $\mathcal{O}(L^2)$ multiplications, the cost for $\tilde{\mathbf{R}}_{ss}$ is $\mathcal{O}(L^3)^2$. On the contrary, to evaluate $\tilde{\mathbf{R}}$, *no multiplication* is needed,

²Note that there are some matrix multiplication algorithms with complexity $\mathcal{O}(L^\alpha)$, $\alpha < 3$ [36], [169] but it still takes some resources to do so.

since from Theorem 2.4.1, $\tilde{\mathbf{x}}_{\cup}$ is reshaped into a Toeplitz matrix $\tilde{\mathbf{R}}$ without further arithmetic operations.

3. *MUSIC spectra*. This step is dominated by the eigen-decomposition of an $L \times L$ Hermitian matrix, which can be either $\tilde{\mathbf{R}}_{ss}$ or $\tilde{\mathbf{R}}$. It is known that eigen-decomposition requires around $\mathcal{O}(L^3)$ operations [128].

Thus, the computational complexity for the two approaches are

$$\begin{array}{ll} \text{Conventional } (\tilde{\mathbf{R}}_{ss}) : & \mathcal{O}(KL + L^3 + L^3), \\ \text{Proposed } (\tilde{\mathbf{R}}) : & \mathcal{O}(KL + L^3). \end{array}$$

As we can see, our proposed method saves $\mathcal{O}(L^3)$ operations. However, the overall complexity is still dominated by the eigen-decomposition in both methods, which requires $\mathcal{O}(L^3)$ computations.

Nevertheless, the computational reduction can become more prominent when we go for multidimensional arrays [121], [183] or higher order statistics [120]. For instance, in a $2q$ -level nested array [121], the ULA segment is of length $\mathcal{O}(|\mathbb{S}|^{2q}) = \mathcal{O}(L^q)$ so that the corresponding spatially smoothed matrix has dimension $\mathcal{O}(L^q) \times \mathcal{O}(L^q)$. Following the same analysis as in this subsection, the complexity for $2q$ -level nested array becomes $\mathcal{O}(KL^q + L^{3q} + L^{3q})$ while the proposed method has complexity $\mathcal{O}(KL^q + L^{3q})$. It can be seen that $\mathcal{O}(L^{3q})$ operations will be deducted using the proposed method, which is not negligible especially for large q . But still, eigen-decomposition ($\mathcal{O}(L^{3q})$) governs the overall complexity.

2.5 Discussions

1. Note that $\tilde{\mathbf{R}}$ is an indefinite square root of $\tilde{\mathbf{R}}_{ss}$. The finite snapshot square root matrix implicitly appears in [126]. While it is not obvious, it can be shown that this matrix in [126] is the same as the matrix $\tilde{\mathbf{R}}$ in Theorem 1. This matrix has been used in [126] for the convenience of analysis of root-MUSIC in coarray domain. However, the fact that coarray MUSIC can be obtained directly from an eigen computation of the data-based matrix $\tilde{\mathbf{R}}$ has not been observed in the past. Instead of this matrix, the spatially smoothed matrix $\tilde{\mathbf{R}}_{ss}$ has been used in all recent works [124] and [125] for obtaining MUSIC spectrum.
2. Our approach is applicable to any sparse array that has a central ULA section in the coarray domain. For instance, the minimum-redundancy arrays [113] satisfy such conditions. However, these arrays do not have a simple formulation on the sensor locations, which can only be obtained from table look-up [113], [177].

3. In [2], the authors proposed to construct a positive-definite Toeplitz matrix $\widehat{\mathbf{T}}$, based on the estimated covariance matrices. The way that [2] establishes $\widehat{\mathbf{T}}$ is identical to Definition 2.3.1 in this chapter. However, in [2], $\widehat{\mathbf{T}}$ is restricted to positive-definite Toeplitz matrices, but here $\widetilde{\mathbf{R}}$ is an *indefinite* Toeplitz matrix. In addition, the goal of [2] is to fill missing lags in $\widehat{\mathbf{T}}$. Nevertheless, in our work, all entries of $\widetilde{\mathbf{R}}$ are known.
4. Our results are derived for finite snapshots. However, in the proofs of [124], [125], infinite snapshots are assumed in making the argument $\mathbf{R}_{ss} = \widehat{\mathbf{R}}^2$. Hence the statements here are stronger than [124], [125]. For instance, Theorem 2.4.1 serves as a finite-snapshot generalization of Theorem 2 in [124] as well as Theorem 1 in [125]. To show that our proposed method is consistent with [124], [125] under the infinite snapshot assumption, taking $K \rightarrow \infty$ yields $\lim_{K \rightarrow \infty} \widetilde{\mathbf{R}}_{\mathbb{S}} = \mathbf{R}_{\mathbb{S}}$ and $\lim_{K \rightarrow \infty} \widetilde{\mathbf{x}}_{\mathbb{U}} = \mathbf{x}_{\mathbb{U}}$. According to Theorem 2.4.1, the limit of $\widetilde{\mathbf{R}}$ becomes

$$\lim_{K \rightarrow \infty} \widetilde{\mathbf{R}} = \mathbf{A}_{11} \mathbf{\Lambda} \mathbf{A}_{11}^H + \sigma^2 \mathbf{I}_{L \times L},$$

where \mathbf{A}_{11} , $\mathbf{\Lambda}$, and σ follow the definitions in [124], [125]. Note that $\lim_{K \rightarrow \infty} \widetilde{\mathbf{R}}$ is proportional to $\widehat{\mathbf{R}}$ in [124], [125].

5. The source powers p_i and the noise power p_n can also be estimated from the autocorrelation vector $\widetilde{\mathbf{x}}_{\mathbb{D}}$, after the estimation of source directions. The details will be elaborated in the following development.

Let $\widehat{\theta}_i$ be the estimated normalized DOA for $i = 1, 2, \dots, D$. According (2.18), the autocorrelation vector $\widetilde{\mathbf{x}}_{\mathbb{D}}$ can be approximated by

$$\widetilde{\mathbf{x}}_{\mathbb{D}} \approx \underbrace{\begin{bmatrix} \mathbf{v}_{\mathbb{D}}(\widehat{\theta}_1) & \mathbf{v}_{\mathbb{D}}(\widehat{\theta}_2) & \dots & \mathbf{v}_{\mathbb{D}}(\widehat{\theta}_D) & \mathbf{e}_0 \end{bmatrix}}_{\mathbf{W}_{\mathbb{D}}} \begin{bmatrix} p_1 \\ p_2 \\ \vdots \\ p_D \\ p_n \end{bmatrix}. \quad (2.26)$$

Note that the matrix $\mathbf{W}_{\mathbb{D}}$ has size $|\mathbb{D}| \times (D + 1)$. As long as $\widehat{\theta}_i$ are known (i.e., $\mathbf{W}_{\mathbb{D}}$ is known), the estimation of the powers $p_1, p_2, \dots, p_D, p_n$ can be regarded as solving the linear system in (2.26).

Next we will present the following proposition:

Proposition 2.5.1. Let \mathbb{U} be the central ULA segment of the difference coarray \mathbb{D} , as defined in Definition 2.2.2. Let the estimated normalized DOAs $\widehat{\theta}_i$ for $i = 1, 2, \dots, D$ be distinct. If $|\mathbb{U}| \geq 2D + 1$, then $\mathbf{W}_{\mathbb{D}}$ has full column rank.

Proof. Let $\alpha_i = e^{j2\pi\hat{\theta}_i}$ and the matrix \mathbf{S} be

$$\mathbf{S} \triangleq \begin{bmatrix} 1 & 1 & 1 & \dots & 1 & 1 \\ \alpha_1 & \alpha_2 & \alpha_3 & \dots & \alpha_D & 0 \\ \alpha_1^2 & \alpha_2^2 & \alpha_3^2 & \dots & \alpha_D^2 & 0 \\ \vdots & \vdots & \vdots & \ddots & \vdots & \vdots \\ \alpha_1^D & \alpha_2^D & \alpha_3^D & \dots & \alpha_D^D & 0 \end{bmatrix} \in \mathbb{C}^{(D+1) \times (D+1)}. \quad (2.27)$$

Since $|\mathbb{U}| \geq 2D + 1$, the matrix \mathbf{S} is a submatrix of $\mathbf{W}_{\mathbb{D}}$. Next we will show that \mathbf{S} has full column rank. Assume that there exists a column vector $\mathbf{c} = [c_1, c_2, \dots, c_{D+1}]^T \neq \mathbf{0}$ such that $\mathbf{S}\mathbf{c} = \mathbf{0}$. Due to (2.27), the equality $\mathbf{S}\mathbf{c} = \mathbf{0}$ can be rewritten as

$$c_1 + c_2 + \dots + c_D + c_{D+1} = 0, \quad (2.28)$$

$$\underbrace{\begin{bmatrix} 1 & 1 & \dots & 1 \\ \alpha_1 & \alpha_2 & \dots & \alpha_D \\ \vdots & \vdots & \ddots & \vdots \\ \alpha_1^{D-1} & \alpha_2^{D-1} & \dots & \alpha_D^{D-1} \end{bmatrix}}_{\mathbf{V}} \begin{bmatrix} \alpha_1 c_1 \\ \alpha_2 c_2 \\ \vdots \\ \alpha_D c_D \end{bmatrix} = \begin{bmatrix} 0 \\ 0 \\ \vdots \\ 0 \end{bmatrix}. \quad (2.29)$$

Since the estimated normalized DOAs $\hat{\theta}_i$ are distinct, the parameters α_i are distinct, implying that the Vandermonde matrix \mathbf{V} is nonsingular. Therefore, the solution to (2.29) becomes $\alpha_i c_i = 0$, for all $i = 1, 2, \dots, D$, that is, $c_i = 0$. Substituting $c_1 = c_2 = \dots = c_D = 0$ into (2.28) leads to $c_{D+1} = 0$, which contradicts the assumption $\mathbf{c} \neq \mathbf{0}$. Thus, \mathbf{S} has full column rank, so does the matrix $\mathbf{W}_{\mathbb{D}}$. \square

The full rankness of $\mathbf{W}_{\mathbb{D}}$ implies the uniqueness of the solution of powers to $\tilde{\mathbf{x}}_{\mathbb{D}} = \mathbf{W}_{\mathbb{D}}[p_1, p_2, \dots, p_D, p_n]^T$, if such solution exists. As a result, the source powers and the noise power may be simply estimated by $\mathbf{W}_{\mathbb{D}}^\dagger \tilde{\mathbf{x}}_{\mathbb{D}}$, where $(\cdot)^\dagger$ denotes the pseudo-inverse of a matrix.

By definition, source powers p_i and noise power p_n are positive quantities. However, in the finite snapshot scenario, the vector $\mathbf{W}_{\mathbb{D}}^\dagger \tilde{\mathbf{x}}_{\mathbb{D}}$ might contain negative entries. In the literature, this issue was mainly addressed by casting an optimization problem based on (2.26) and the positiveness of the powers. Interested readers are referred to [1], [2] and the references therein.

As an example, consider a nested array with $N_1 = N_2 = 8$ and a coprime array with $M = 5$ and $N = 7$. The total number of sensors is then 16, as defined in (2.7) and (2.8). SNR is chosen to be 0dB and there are $K = 500$ snapshots. $D = 35$ sources

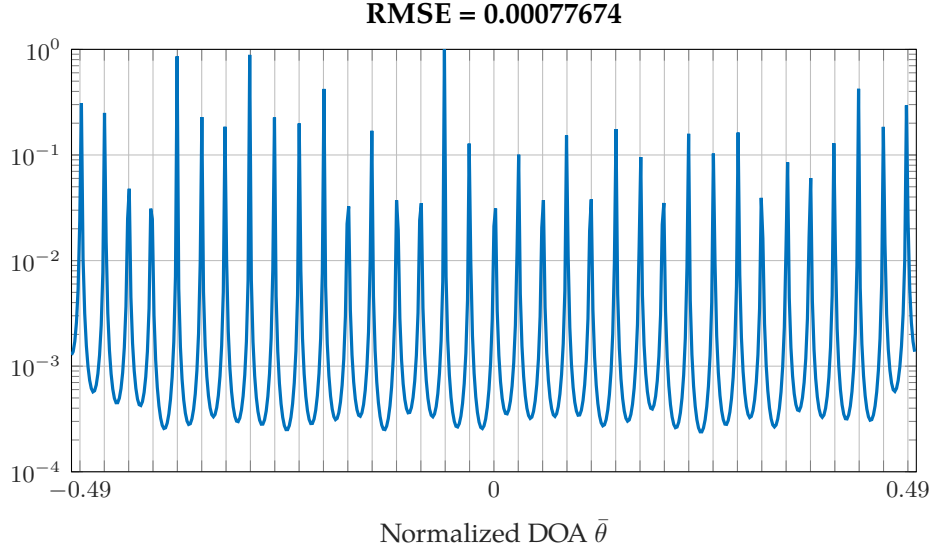


Figure 2.5: The MUSIC spectrum based on an $M = 5$, $N = 7$ coprime array, 0 dB SNR, $K = 500$ snapshots, and the Hermitian Toeplitz matrix $\tilde{\mathbf{R}}$. $D = 35$ sources are placed uniformly over $\bar{\theta} \in [-0.49, 0.49]$. The number of sensors is $N + 2M - 1 = 16$.

are selected uniformly over $\bar{\theta} = [-0.49, 0.49]$ in our first experiment. As seen in Fig. 2.5, there are 35 distinguishable peaks even though D is greater than the number of sensors, $|\mathbb{S}| = 16$. These 35 peaks match with the ideal peaks, which are marked by ticks on the $\bar{\theta}$ axis. The estimation error is quantified by the root-mean-squared error, defined as

$$\text{RMSE} = \sqrt{\frac{1}{D} \sum_{i=1}^D (\hat{\theta}_i - \bar{\theta}_i)^2}, \quad (2.30)$$

where $\hat{\theta}_i$ and $\bar{\theta}_i$ are the estimated/true normalized DOA of the i th source, respectively. In this example, the RMSE is given by 0.00077674.

The same configuration with 1000 runs is conducted for both $\tilde{\mathbf{R}}_{ss}$ (spatial smoothing) and $\tilde{\mathbf{R}}$ (no spatial smoothing). On a Ubuntu 12.04 workstation with a Intel Core™ i7-2600 3.40GHz processor and 8GB RAM, conventional approaches take 417.59 seconds for nested arrays and 85.73 seconds for coprime arrays. Nevertheless, our new method spends 399.07 seconds (4.4% reduction) for nested arrays and 75.02 seconds (12.5% less) for coprime arrays. We see that the computational reduction is rather minor. This is because the computation time is dominated by the eigenspace computation in the MUSIC stage. So, the computational advantage obtained by replacing the spatial smoothing step with the matrix $\tilde{\mathbf{R}}$ is minor. However, the insight provided by the fact that spatial smoothing can be avoided is more fundamental, and might have theoretical impact in future developments. The matrix

$\tilde{\mathbf{R}}$ also makes the performance analysis more tractable (as compared to the use of the spatial smoothing matrix), as seen from [126]. This is because $\tilde{\mathbf{R}}_{ss}$ requires 4th order statistics, whereas $\tilde{\mathbf{R}}$ is in terms of 2nd order statistics (correlations).

2.6 Concluding Remarks

We have shown that coarray MUSIC, which is used for sparse arrays such as nested and coprime arrays, can be performed without the use of spatial smoothing. While there are some computational advantages, the insight provided by the simplification is also important, as it might lead to theoretical simplification in future work.

SUPER NESTED ARRAYS: LINEAR SPARSE ARRAYS WITH REDUCED MUTUAL COUPLING: FUNDAMENTALS

3.1 Introduction

In array signal processing, electromagnetic characteristics cause *mutual coupling* between sensors, making the sensor responses interfere with each other [11], [157]. This has an adverse effect on the estimation of parameters (e.g., DOA, source power, amplitude, and so forth). Past methods in the literature aim to *decouple* (or “remove”) the effect of mutual coupling from the received data by using *proper* mutual coupling models [38], [49], [63], [64], [83], [129], [151], [172], [173], [199]. Such methods are usually computationally expensive, and sensitive to model mismatch.

An altogether different approach to reduce the effect of mutual coupling is to use sparse arrays, in which the number of sensor pairs with small separations (small multiples of $\lambda/2$) is much fewer than in uniform linear arrays (ULAs). This chapter is based on this theme. Sparse arrays such as nested arrays, coprime arrays [4], [124], [139], [175], [186], minimum redundancy arrays (MRAs) [113] and minimum hole arrays (MHAs) [177], [190] have reduced mutual coupling compared to ULAs. The definitions and the properties of these array geometries are described in Section 2.2 comprehensively.

In practice, these well-known sparse arrays have some shortcomings: MRAs and MHAs do not have simple closed-form expressions for the array geometry, and the sensor locations are usually found from tabulated entries [81], [113], [177], [190]. Coprime arrays have holes in the coarray, so that the ULA part of the coarray is smaller than those of the nested array and the MRA [186]. Finally nested arrays, by definition, contain a dense ULA in the physical array, resulting in significantly higher mutual coupling than coprime arrays and MRAs [124].

The main aim of this chapter is to introduce a new array configuration called the *super nested array*, which has all the good properties of the nested array, and at the same time achieves reduced mutual coupling by redistributing the elements of the dense ULA part of the nested array. There is a systematic procedure to do this. We will show how to determine the appropriate sensor locations for any N . For fixed N (number of sensors), the super nested array has the same physical aperture as the parent nested array. Furthermore, its difference coarray is exactly identical to that of the nested array and is, in particular, free from holes. However, unlike the nested array, the number of sensor pairs with small separations ($\lambda/2$, λ , $3\lambda/2$, etc.)

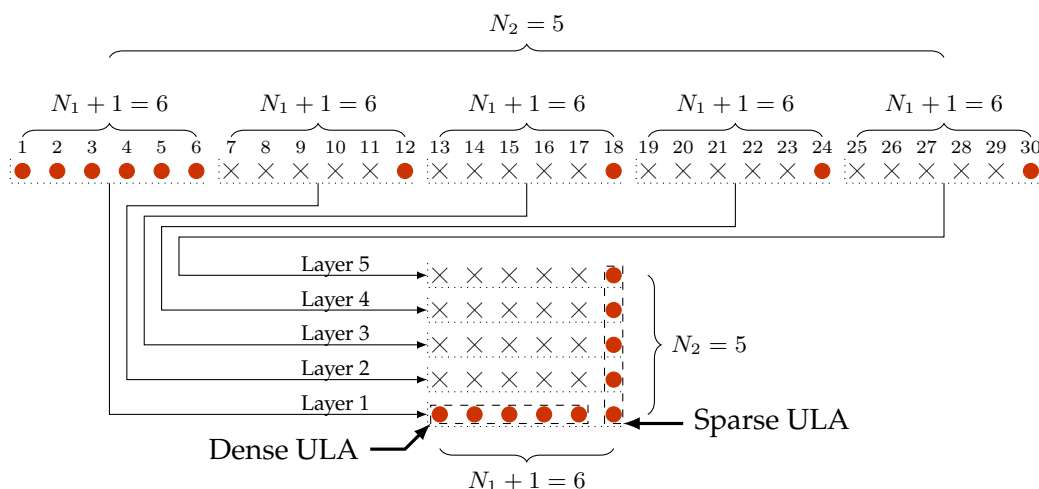


Figure 3.1: The concept of 2D representations of linear arrays. The top of this figure shows the 1D representation of a nested array with $N_1 = N_2 = 5$, where bullets denote sensors and crosses indicate empty locations. In the 1D representation of this example, the array aperture is divided into $N_2 = 5$ layers of size $N_1 + 1 = 6$. These layers are stacked into the associated 2D representation, as marked by arrows. Notice that in this chapter, 2D representations denote linear arrays, *not planar arrays*. They are introduced to simplify the discussion in the future development.

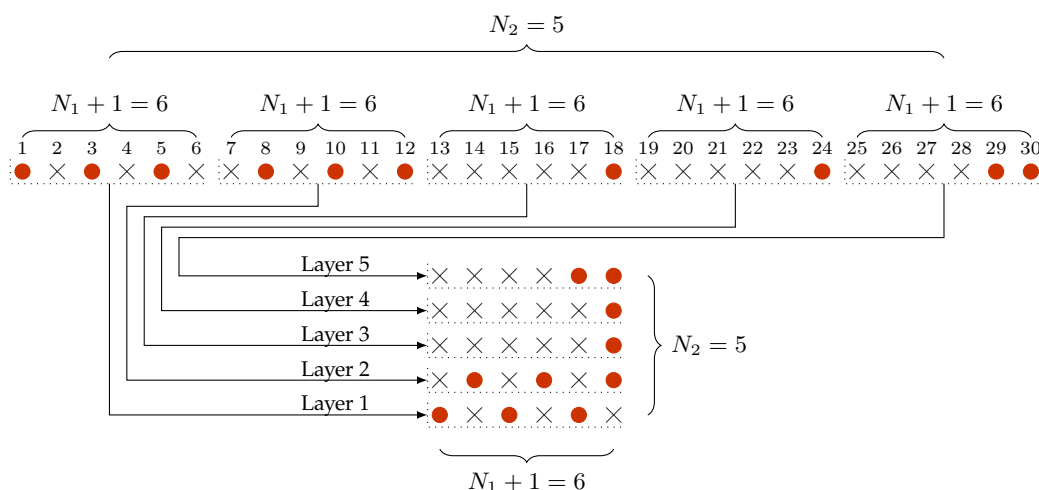


Figure 3.2: The 1D and 2D representations of a second-order super nested array with $N_1 = N_2 = 5$. It will be proved in this chapter that super nested arrays possess the same number of sensors, the same physical aperture, and the same hole-free coarray as their parent nested arrays. Furthermore, super nested arrays alleviate the mutual coupling effect. In this example, there is only one pair of sensors with separation 1, located at 29 and 30. However, for the parent nested array in Fig. 3.1, locations 1 through 6 are crowded with sensors, leading to more severe mutual coupling effect.

is significantly reduced. More quantitative statements of these properties will be given in this chapter based on the weight function $w(m)$ of the sparse array, where $w(m)$ is the number of pairs of elements with element-spacing $m\lambda/2$, as defined earlier in Definition 2.2.9. Several other properties of the new array geometry will also be established.

To explain how the super nested array is obtained from a nested array, it is first convenient to develop a two-dimensional (2D) representation of linear arrays. This is demonstrated in Fig. 3.1 which shows the traditional (1D) and the corresponding 2D representations of a nested array with $N_1 = N_2 = 5$ (N_1 and N_2 have the same meaning as in [124]; also see Fig. 2.2(c)). The top of Fig. 3.1 depicts this array configuration along an 1D axis, where bullets are physical sensors and crosses stand for empty space. *Layer 1* is defined as the locations from 1 to $N_1 + 1 = 6$ while *Layer 2* begins with $N_1 + 2 = 7$ and ends with $2(N_1 + 1) = 12$. The *2D representation* establishes a 2D topology by stacking all these layers, as illustrated in the bottom of Fig. 3.1. Then, the dense ULA and the sparse ULA structure of a nested array can be readily visualized. Note that in this chapter, 2D representations denote linear arrays, *not planar arrays*.

Next, Fig. 3.2 provides a first glance at a second-order super nested array with parameters $N_1 = N_2 = 5$. These parameters are the same as those in Fig. 3.1. Hence, the array in Fig. 3.1 is said to be the *parent nested array* of the array in Fig. 3.2. It can be seen from this example that this super nested array is sparser than its parent nested array (for the same physical aperture) in the sense that the number of element pairs with small spacing (spacings of 1, 2, and 3) are reduced. In this super nested array, there is only one pair of sensors with separation 1, but in its parent nested array, five sensor pairs of separation 1 exist. We will see that such rearrangements will significantly reduce the adverse effects of mutual coupling in DOA estimation. Later on, it will be shown in Fig. 3.7 that, with mutual coupling, the DOA estimation error for the (third-order) super nested array is as small as 2% of that for its parent nested array, which is truly remarkable.

Even though the 1D representation of super nested arrays seems irregular, their 2D representation provides a geometrical point of view, as shown in Fig. 3.2. It can be noticed that Fig. 3.2 resembles Fig. 3.1, except for few sensor locations. In this example, we start with the parent nested array in Fig. 3.1 and then relocate some sensors, from location 2 to 8, 4 to 10, and 6 to 29, yielding the super nested array in Fig. 3.2. The systematic construction of super nested arrays from nested arrays for arbitrary N_1 and N_2 will be described more rigorously in Section 3.4.

Chapter outline

Section 3.2 reviews mutual coupling models. In Section 3.3, we present a motivating example which compares the performances of well-known sparse arrays in the presence of mutual coupling. Super nested arrays are then introduced in Section 3.4, and some of their basic properties are proved (Lemma 3.4.1 and Lemma 3.4.2). In Section 3.5, we study the difference coarray of the super nested array in detail. It will be proved that super nested arrays have the same hole-free coarray as their parent nested arrays (Theorem 3.5.1, and Corollary 3.5.1). Furthermore, a closed-form expression for the weight function $w(m)$ of the super nested array is provided in Theorem 3.5.2. The first three weights (which dominate the effects of mutual coupling) are shown to be always smaller for the super nested array, compared to the parent nested array ($w(1)$ and $w(3)$ being *significantly* smaller). The improved performance of super nested arrays under mutual coupling will be demonstrated through examples in Section 3.6. Section 3.7 concludes this chapter.

A MATLAB code to generate the sensor locations of the super nested array can be found in [90]. This code takes N_1 and N_2 (which are defined by the parent nested array as in Fig. 2.2(c)) as the inputs and returns the sensor locations as the output.

The arrays introduced in this chapter will be called *second-order* super nested arrays, for reasons that will become clear soon. In Chapter 4, a further extension called the Q th-order super nested array is developed, which further reduces mutual coupling.

3.2 Review of Mutual Coupling

The array equation (1.5) assumes that the sensors do not interfere with each other. In practice, any sensor output is influenced by its neighboring elements, which is called mutual coupling. In this section, we will review mutual coupling models on sensor arrays.

Mutual coupling can be incorporated into (1.5) as follows:

$$\mathbf{x}_S = \sum_{i=1}^D A_i \mathbf{C} \mathbf{v}_S(\bar{\theta}_i) + \mathbf{n}_S, \quad (3.1)$$

where \mathbf{C} is a mutual coupling matrix that can be obtained from electromagnetics. Closed-form expressions for \mathbf{C} have been investigated for decades. If the sensor array is a linear dipole array, \mathbf{C} can be written as [70], [83], [171]–[173]

$$\mathbf{C} = (Z_A + Z_L)(\mathbf{Z} + Z_L \mathbf{I})^{-1}, \quad (3.2)$$

where Z_A and Z_L are the element/load impedance, respectively. $\langle \mathbf{Z} \rangle_{n_1, n_2}$ is given

by

$$\begin{cases} \frac{\eta_0}{4\pi} (0.5772 + \ln(2\beta l) - \text{Ci}(2\beta l) + j\text{Si}(2\beta l)), & \text{if } n_1 = n_2, \\ \frac{\eta_0}{4\pi} (\langle \mathfrak{R} \rangle_{n_1, n_2} + j \langle \mathfrak{X} \rangle_{n_1, n_2}), & \text{if } n_1 \neq n_2. \end{cases}$$

Here $\eta_0 = \sqrt{\mu_0/\epsilon_0} \approx 120\pi$ is the intrinsic impedance. $\beta = 2\pi/\lambda$ is the wavenumber, where λ is the wavelength. l is the length of dipole antennas. \mathfrak{R} and \mathfrak{X} are

$$\begin{aligned} \langle \mathfrak{R} \rangle_{n_1, n_2} &= \sin(\beta l) (-\text{Si}(u_0) + \text{Si}(v_0) + 2\text{Si}(u_1) - 2\text{Si}(v_1)) \\ &\quad + \cos(\beta l) (\text{Ci}(u_0) + \text{Ci}(v_0) - 2\text{Ci}(u_1) - 2\text{Ci}(v_1) \\ &\quad + 2\text{Ci}(\beta d_{n_1, n_2})) - (2\text{Ci}(u_1) + 2\text{Ci}(v_1) - 4\text{Ci}(\beta d_{n_1, n_2})), \\ \langle \mathfrak{X} \rangle_{n_1, n_2} &= \sin(\beta l) (-\text{Ci}(u_0) + \text{Ci}(v_0) + 2\text{Ci}(u_1) - 2\text{Ci}(v_1)) \\ &\quad + \cos(\beta l) (-\text{Si}(u_0) - \text{Si}(v_0) + 2\text{Si}(u_1) + 2\text{Si}(v_1) \\ &\quad - 2\text{Si}(\beta d_{n_1, n_2})) + (2\text{Si}(u_1) + 2\text{Si}(v_1) - 4\text{Si}(\beta d_{n_1, n_2})), \end{aligned}$$

where $d_{n_1, n_2} = |n_1 - n_2| \lambda/2$ is the distance between sensors. The parameters u_0 , v_0 , u_1 , and v_1 are

$$\begin{aligned} u_0 &= \beta \left(\sqrt{d_{n_1, n_2}^2 + l^2} - l \right), \quad v_0 = \beta \left(\sqrt{d_{n_1, n_2}^2 + l^2} + l \right), \\ u_1 &= \beta \left(\sqrt{d_{n_1, n_2}^2 + 0.25l^2} - 0.5l \right), \\ v_1 &= \beta \left(\sqrt{d_{n_1, n_2}^2 + 0.25l^2} + 0.5l \right). \end{aligned}$$

$\text{Si}(u)$ and $\text{Ci}(u)$ are sine/cosine integrals, defined as

$$\text{Si}(u) = \int_0^u \frac{\sin t}{t} dt, \quad \text{Ci}(u) = \int_\infty^u \frac{\cos t}{t} dt.$$

Eq. (3.2) quantifies the mutual coupling effect of linear dipole antenna arrays. Note that \mathbf{C} relies on the dipole length l and the sensor element spacing d_{n_1, n_2} , which are geometric parameters.

However, (3.2) is too complicated to analyze. It is desirable to establish a simple mutual coupling model. The mutual coupling matrix \mathbf{C} can be approximated by a B -banded symmetric Toeplitz matrix in the ULA configuration [49], [171], [173]. It is empirically observed that the entries of \mathbf{C} behave like functions of sensor separations only. In other words, we can write \mathbf{C} as

$$\langle \mathbf{C} \rangle_{n_1, n_2} = \begin{cases} c_{|n_1 - n_2|}, & \text{if } |n_1 - n_2| \leq B, \\ 0, & \text{otherwise,} \end{cases} \quad (3.3)$$

where $n_1, n_2 \in \mathbb{S}$ and coupling coefficients c_0, c_1, \dots, c_B satisfy $1 = c_0 > |c_1| > |c_2| > \dots > |c_B|$. It is assumed that the magnitudes of coupling coefficients are inversely proportional to their sensor separations [49], i.e. $|c_k/c_\ell| = \ell/k$.

The mutual coupling models such as (3.2) and (3.3) are based on certain assumptions [20], [49], [63], [64], [83], [105], [129], [151], [172], [173], [199]. The actual mutual coupling matrix \mathbf{C} is unknown to the user. If the mutual coupling effect is completely omitted in our estimators, the performance degrades [48]. Another approach is to estimate mutual coupling and source profiles based on particular mutual coupling models [20], [49], [83], [129], [151], [173], [199]. For instance, BouDaher *et al.* considered DOA estimation with coprime arrays in the presence of mutual coupling [20]. Their algorithm jointly estimated the mutual coupling matrix \mathbf{C} , the source power, and the DOA under certain optimization criterion. At the expense of some extra computations, this approach estimates the true DOA satisfactorily. In principle, all of the above decoupling methods are applicable with the super nested arrays to be developed in this chapter, and can only improve the performance further.

3.3 Mutual Coupling in Sparse Arrays: A Motivating Example

In this section, we provide an example of DOA estimation in the presence of mutual coupling for several array configurations. It will be observed that uniform DOF and weight functions of sensor arrays play a crucial role. This observation provides some insights to design sensor arrays that reduce the mutual coupling effect.

In Fig. 3.3, we evaluate the performance of ULAs, MRAs [113], nested arrays [124], and coprime arrays [125], [186] in the presence of mutual coupling. The number of sensors is 6 for each array. Then, the sensor locations are given by (2.7) with $N_1 = N_2 = 3$ for nested arrays and (2.8) with $M = 2$ and $N = 3$ for coprime arrays. The sensor locations are listed on the first row of Fig. 3.3. The number of sources $D = 4$ and the DOA profiles are $\bar{\theta}_1 = 0$, $\bar{\theta}_2 = 0.1$, $\bar{\theta}_3 = 0.2$, and $\bar{\theta}_4 = 0.3$. The SNR is 0 dB and the number of snapshots K is 1000. The mutual coupling matrix \mathbf{C} is based on (3.3), where $c_0 = 1$, $c_1 = 0.5 \exp(j\pi/4)$, $c_2 = 0.5 \exp(j0.7\pi)/2$, $c_3 = 0.5 \exp(j0.7\pi)/3$, and $B = 3$. The measurement with mutual coupling can be expressed as in Eq. (3.1). The DOAs are estimated from the measurement vectors without any decoupling algorithms [20], [49], [83], [129], [151], [173], [199].

The second row of Fig. 3.3 shows weight functions of different array geometries. The coarray of ULA has consecutive integers from -5 to 5 , the coarray of MRA ranges from -13 to 13 , the nested array owns coarray aperture from -11 to 11 , and the coprime array has the maximum contiguous ULA section in its coarray domain from -7 to 7 . Then, the uniform DOF, as defined in Definition 2.2.6, for ULA, MRA,

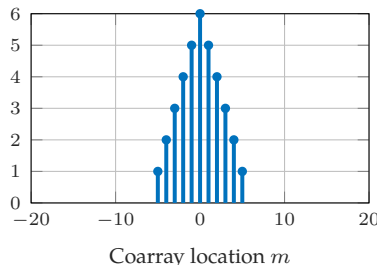
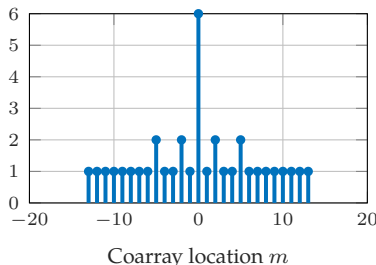
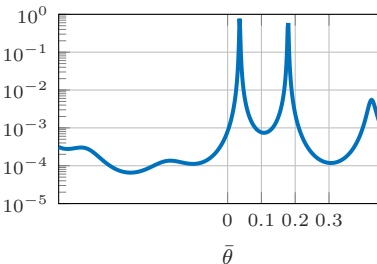
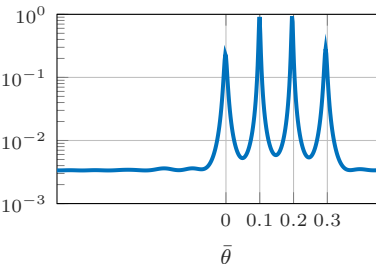
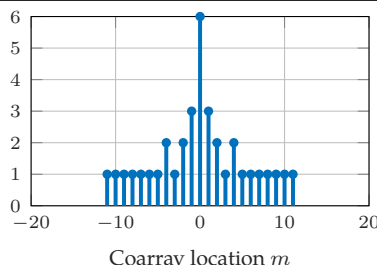
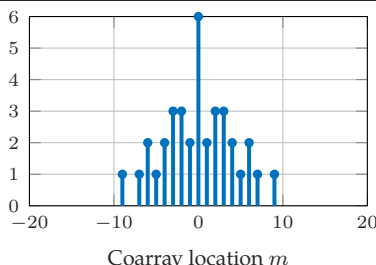
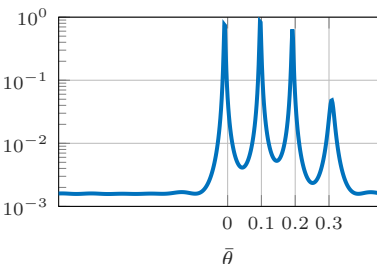
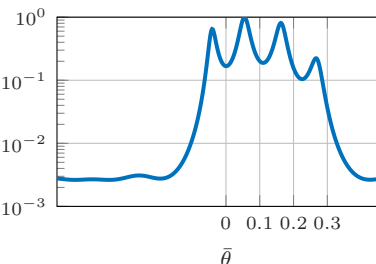
| Array | ULA | MRA |
|-------------------|---|--|
| \mathcal{S} | $\{0, 1, 2, 3, 4, 5\}$ | $\{0, 1, 6, 9, 11, 13\}$ |
| $w(m)$ |  |  |
| $P(\bar{\theta})$ |  |  |
| E | 0.22112 | 0.0033328 |
| Array | Nestd array | Coprime array |
| \mathcal{S} | $\{1, 2, 3, 4, 8, 12\}$ | $\{0, 2, 4, 3, 6, 9\}$ |
| $w(m)$ |  |  |
| $P(\bar{\theta})$ |  |  |
| E | 0.0073736 | 0.038956 |

Figure 3.3: Comparison among ULAs, MRAs, nested arrays, coprime arrays and their MUSIC spectra $P(\bar{\theta})$ in the presence of mutual coupling. It can be observed that higher uniform DOF and smaller weight functions $w(1)$, $w(2)$, $w(3)$ tend to decrease the RMSE.

the nested array, the coprime array are 11, 27, 23, and 15, respectively. Therefore, the maximum number of detectable sources for ULA, MRA, nested array, and coprime array is 5, 13, 11, and 7, respectively [124], [125]. The MUSIC algorithm is performed for ULA while the coarray MUSIC (SS MUSIC) is used in all the sparse arrays. In addition, the weight functions $w(m)$ also exhibit different distributions for different arrays. If we consider $w(1)$ among all these arrays, we obtain $w(1) = 5, 1, 3, 2$ for ULA, MRA, nested arrays, and coprime arrays, respectively. When $w(1)$ becomes smaller, there are fewer sensor pairs with separation 1 so, qualitatively, we obtain a sparser array configuration.

The associated MUSIC spectra $P(\bar{\theta})$ and the root-mean-squared error (RMSE), are shown on the third row and the fourth row of Fig. 3.3, respectively. The RMSE (E) is defined as

$$E = \sqrt{\frac{1}{D} \sum_{i=1}^D (\hat{\theta}_i - \bar{\theta}_i)^2}, \quad (3.4)$$

where $\hat{\theta}_i$ denotes the estimated normalized DOA of the i th source, according to the root MUSIC algorithm, and $\bar{\theta}_i$ is the true normalized DOA. It can be observed that ULA fails to identify four sources accurately in this example, while MRA has the best estimation performance. In nested arrays and coprime arrays, four peaks can be seen but they have more estimation error. These spectra conclude the estimation performance: MRA is the best one, followed by nested arrays and then coprime arrays. ULA has the worst performance. In the example of Section 3.6 (Fig. 3.7) we will see that super nested arrays can achieve significantly smaller error than MRAs in the presence of mutual coupling.

Fig. 3.3 provides some insightful *qualitative* statements. First, as the uniform DOF increases, the corresponding RMSE decreases. The size of this virtual ULA, or equivalently the uniform DOF, is 27 for MRA, 23 for the nested array, 15 for the coprime array, and 11 for ULA. This explains why the RMSE is the least for the MRA, followed by the nested array, coprime array and lastly the ULA.

Second, the RMSE also tends to decrease as the weight functions $w(1)$, $w(2)$, and $w(3)$ decrease. However, this qualitative argument cannot be concluded from Fig. 3.3 directly, since these examples have different uniform DOFs and weight functions. For a meaningful comparison, let us look at the nested array and the super nested array. As presented in Section 3.5, the uniform DOF of the super nested array is identical to that of the nested array while the weight functions $w(1)$, $w(2)$, and $w(3)$ of the super nested array are smaller than those of the nested array. It is observed from Fig. 3.7 to 3.10 that the RMSE of the super nested array are less than those of the nested array. This phenomenon can be elaborated as follows: de-

creasing these weights reduces the number of sensor pairs with significant mutual coupling. Less mutual coupling implies the mutual coupling matrix \mathbf{C} is closer to the identity matrix, which makes the RMSE likely to decrease.

Based on these observations, the MRA seems to be the best array with minimum mutual coupling since it owns the maximum DOF as well as the smallest $w(1)$, $w(2)$, and $w(3)$. However, it is quite intricate to determine the MRA configuration. First, the sensor locations of MRA can only be found using combinatorial search or table lookup [65], [113]. This is neither scalable nor practical if our design budget is a large number of sensors, say, 100 physical sensors. On the other hand, if our design budget is a fixed array aperture, which exists in applications such as airplane, submarine, or mobile devices, MRA might not be optimal. For instance, provided the available space being $11d$, we cannot use the MRA in Fig. 3.3 since its total aperture is $13d$. If we apply MRA with 5 sensors, we obtain $\mathbb{S} = \{0, 1, 4, 7, 9\}$ but the maximum number of distinguishable sources decreases to 9. The space is not fully utilized.

Like MRA, nested and coprime arrays also have $\mathcal{O}(N^2)$ uniform DOF given $\mathcal{O}(N)$ sensors but they have closed-form expressions for sensor locations for any N . Even though their uniform DOF are less than those of MRA, they offer simple design equations. These equations admit simple calculations and regular array geometries. In some situations, the nested arrays can be superior to MRAs. For example, under the constraint that the available aperture is $11d$, the nested array with $N_1 = 3$ and $N_2 = 3$ is an acceptable design, and it resolves 11 sources. The MRA with 5 sensors can only resolve 9 sources.

According to Fig. 3.3, it is tempting to conclude that nested arrays are superior to coprime arrays but this is not always true. The estimation performance depends heavily on the mutual coupling coefficients. If mutual coupling is negligible, the performance is governed by the uniform DOF, implying nested arrays are superior [124], [186]. However, as mutual coupling becomes severe, the performance of nested arrays worsens much more than that of coprime arrays, as we shall see in Section 3.6 later. This is because nested arrays contain a dense ULA part, while coprime arrays have only two pairs of sensors with separation one [186].

Presented with these issues, we are motivated to find a sparse array configuration that satisfies the following three criteria:

1. The sensor locations should be describable using *simple rules or closed forms* as in the case of nested and coprime arrays.

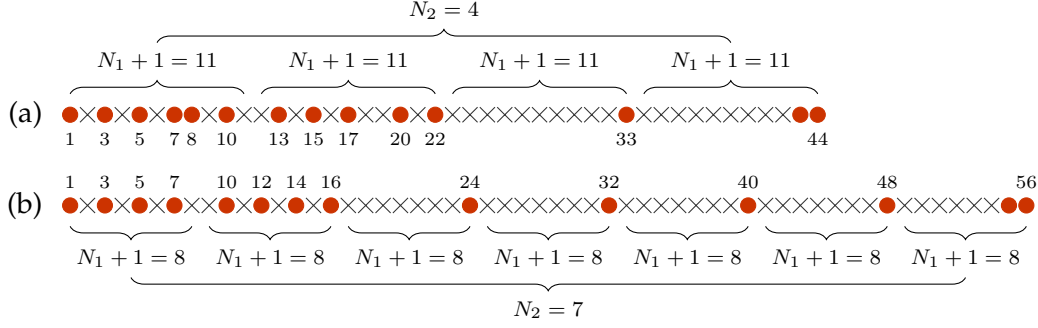


Figure 3.4: 1D representations of second-order super nested arrays with (a) $N_1 = 10$, $N_2 = 4$, and (b) $N_1 = N_2 = 7$. Bullets stand for physical sensors and crosses represent empty space. Both configurations consist of 14 physical sensors but (b) leads to larger total aperture and a sparser pattern. It will be proved that the uniform DOF of (a) and (b) are $2N_2(N_1 + 1) - 1$, which are 87 and 111, respectively.

2. The coarray of the sparse array should have a *large contiguous ULA section*. In fact we will aim for sparse arrays whose coarrays are ULAs (i.e., hole free) of the same size as coarrays of nested arrays.
3. The weight functions $w(1)$, $w(2)$, and $w(3)$ have to be *small*. It is preferable to achieve $w(1) \leq w_{\text{coprime}}(1) = 2$, so that mutual coupling can be mitigated in the new array configuration.

3.4 Second-Order Super Nested Arrays

In this section, we develop second-order super nested arrays. For fixed number of sensors, these have the same physical aperture and the same difference coarray enjoyed by nested arrays (in particular there are no holes in coarray). But they have reduced mutual coupling because of smaller values of the crucial weights $w(1)$, $w(2)$, and $w(3)$.

Nested arrays are parametrized by integers N_1 and N_2 , which denote the number of sensors in the dense ULA part and the sparse ULA part, respectively. To alleviate mutual coupling, we need to remove some sensors in the first layer (dense ULA part) and relocate them appropriately, keeping in mind the three criteria at the end of the preceding section. Note that there are many rearrangements to nested arrays that satisfy our design criteria. We will show that the following array geometry is a valid solution:

Definition 3.4.1 (Second-order super nested arrays). Assume N_1 and N_2 are integers satisfying $N_1 \geq 4$ and $N_2 \geq 3$. Second-order super nested arrays are specified by the integer set $\mathbb{S}^{(2)}$, defined by

$$\mathbb{S}^{(2)} = \mathbb{X}_1^{(2)} \cup \mathbb{Y}_1^{(2)} \cup \mathbb{X}_2^{(2)} \cup \mathbb{Y}_2^{(2)} \cup \mathbb{Z}_1^{(2)} \cup \mathbb{Z}_2^{(2)},$$

where

$$\begin{aligned}
\mathbb{X}_1^{(2)} &= \{1 + 2\ell : 0 \leq \ell \leq A_1\}, \\
\mathbb{Y}_1^{(2)} &= \{(N_1 + 1) - (1 + 2\ell) : 0 \leq \ell \leq B_1\}, \\
\mathbb{X}_2^{(2)} &= \{(N_1 + 1) + (2 + 2\ell) : 0 \leq \ell \leq A_2\}, \\
\mathbb{Y}_2^{(2)} &= \{2(N_1 + 1) - (2 + 2\ell) : 0 \leq \ell \leq B_2\}, \\
\mathbb{Z}_1^{(2)} &= \{\ell(N_1 + 1) : 2 \leq \ell \leq N_2\}, \\
\mathbb{Z}_2^{(2)} &= \{N_2(N_1 + 1) - 1\}.
\end{aligned}$$

The parameters $A_1, B_1, A_2,$ and B_2 are defined as

$$(A_1, B_1, A_2, B_2) = \begin{cases} (r, r-1, r-1, r-2), & \text{if } N_1 = 4r, \\ (r, r-1, r-1, r-1), & \text{if } N_1 = 4r + 1, \\ (r+1, r-1, r, r-2), & \text{if } N_1 = 4r + 2, \\ (r, r, r, r-1), & \text{if } N_1 = 4r + 3, \end{cases}$$

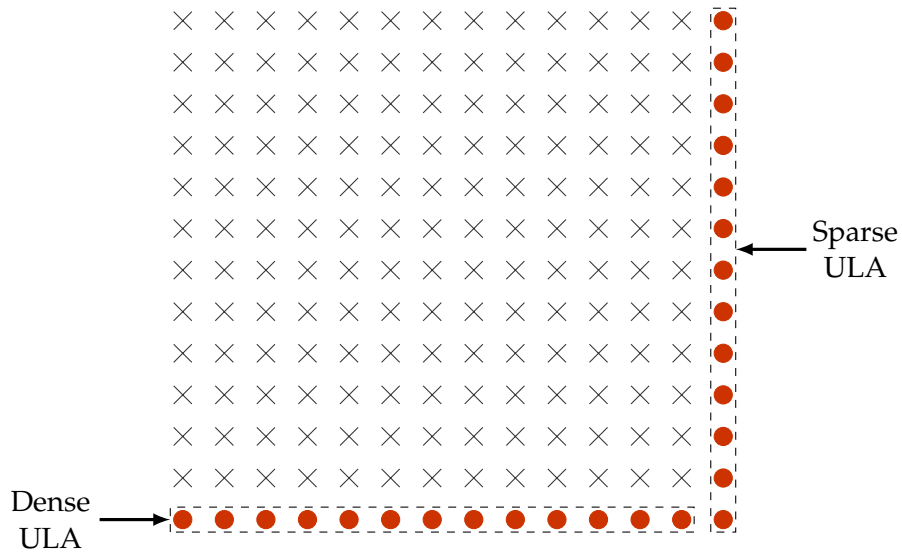
where r is an integer.

A MATLAB code for generating super nested arrays can be found in [90]. The function `super_nested.m` takes N_1 and N_2 as inputs and returns the set $\mathbb{S}^{(2)}$. (The parameter Q should be set to 2; higher Q produces higher order super nested arrays described in Chapter 4). In addition, `interactive_interface.m` offers an interactive panel where users can design their array configurations over 2D representations and visualize the associated weight functions easily.

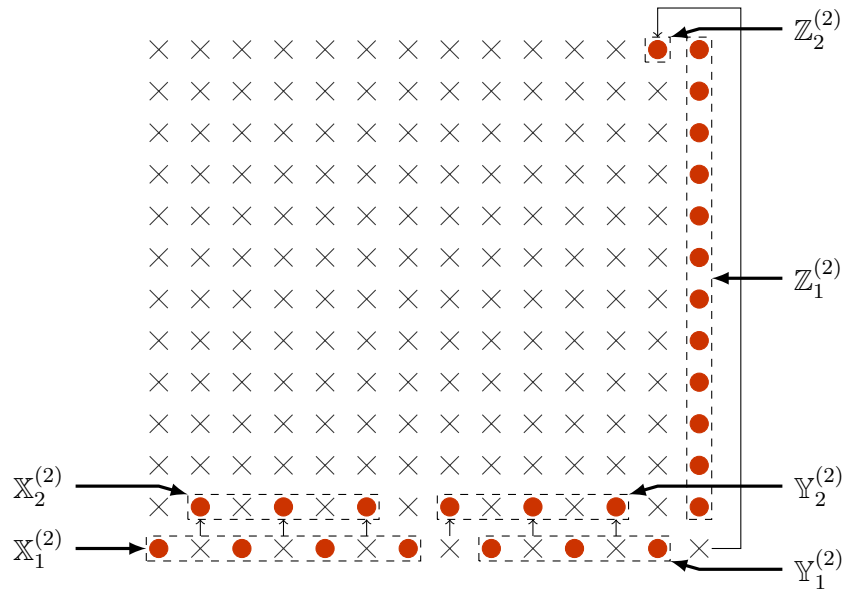
Note that Definition 3.4.1 is applicable to $N_1 \geq 4$. In particular, if $N_1 = 4$ or 6, then the sets $\mathbb{X}_1^{(2)}$, $\mathbb{Y}_1^{(2)}$, and $\mathbb{X}_2^{(2)}$ are non-empty but the set $\mathbb{Y}_2^{(2)}$ becomes the empty set, since the parameter $B_2 = -1$. Otherwise, if N_1 is 5, or greater than 6, the sets $\mathbb{X}_1^{(2)}$, $\mathbb{Y}_1^{(2)}$, $\mathbb{X}_2^{(2)}$, and $\mathbb{Y}_2^{(2)}$ are non-empty.

As an example, let us consider second-order super nested arrays with various combinations of N_1 and N_2 . In Fig. 3.4(a), $N_1 = 10$ and $N_2 = 4$ while in Fig. 3.4(b), $N_1 = N_2 = 7$. It can be observed that there are $N_1 + N_2 = 14$ sensors in each configuration. The total aperture becomes 43 and 55 in parts (a) and (b), respectively. The difference coarray for (a) and (b) comprises consecutive integers from -43 to 43, and -55 to 55, respectively.

Next, the relationship between nested arrays and second-order super nested arrays is elaborated in Fig. 3.5(a) and (b) for $N_1 = N_2 = 13$. These *linear arrays* are shown in terms of their 2D representations, as defined in Fig. 3.1. The dashed rectangles mark the support of dense ULA, sparse ULA, $\mathbb{X}_1^{(2)}$, $\mathbb{Y}_1^{(2)}$, $\mathbb{X}_2^{(2)}$, $\mathbb{Y}_2^{(2)}$, $\mathbb{Z}_1^{(2)}$, and $\mathbb{Z}_2^{(2)}$, respectively. It can be seen from Fig. 3.5(a) and (b) that second-order super nested arrays



(a)



(b)

Figure 3.5: 2D representations of (a) the parent nested array, and (b) the corresponding second-order super nested array, $\mathbb{S}^{(2)}$, where $N_1 = N_2 = 13$. Bullets denote sensor locations while crosses indicate empty locations. Thin arrows illustrate how sensors migrate from nested arrays to second-order super nested arrays. The dense ULA in nested arrays is split into four sets: $\mathbb{X}_1^{(2)}$, $\mathbb{Y}_1^{(2)}$, $\mathbb{X}_2^{(2)}$, and $\mathbb{Y}_2^{(2)}$ in second-order super nested arrays. The sensor located at $N_1 + 1$, belonging to the sparse ULA of nested arrays, is moved to location $N_2(N_1 + 1) - 1$ in second-order super nested arrays.

modify nested arrays in two ways. First, the sensors in the dense ULA part of nested arrays are broken into four ULA sections $\mathbb{X}_1^{(2)}$, $\mathbb{Y}_1^{(2)}$, $\mathbb{X}_2^{(2)}$, and $\mathbb{Y}_2^{(2)}$ in second-order super nested arrays. Each of them possesses inter-element spacing 2. In addition, the sensor at location $N_1 + 1$ is moved to $N_2(N_1 + 1) - 1$. The weight function $w(1)$ for nested arrays and second-order super nested arrays are 13 and 1, respectively. Second-order super nested arrays significantly decrease the number of sensor pairs with separation 1. As a result, second-order super nested arrays are qualitatively sparser than nested arrays and mutual coupling effect could alleviate.

In the following development, as a shorthand notation, the addition between a set and a scalar is defined as

$$\mathbb{A} \pm c = \{a \pm c : \forall a \in \mathbb{A}\}.$$

Provided with two sets \mathbb{A} and \mathbb{B} , the difference set between \mathbb{A} and \mathbb{B} is given by

$$\text{diff}(\mathbb{A}, \mathbb{B}) = \{a - b : a \in \mathbb{A}, b \in \mathbb{B}\}.$$

It can be seen that $\text{diff}(\mathbb{A}, \mathbb{B})$ does not necessarily equal to $\text{diff}(\mathbb{B}, \mathbb{A})$. Next, some simple properties of second-order super nested arrays are proved. More advanced properties pertaining to the difference coarray will be proved in Section 3.5.

Lemma 3.4.1 (Relation to the dense ULA of the parent nested array). Let $\mathbb{X}_1^{(2)}$, $\mathbb{Y}_1^{(2)}$, $\mathbb{X}_2^{(2)}$, and $\mathbb{Y}_2^{(2)}$ be given in Definition 3.4.1. Then

$$\begin{aligned} & \mathbb{X}_1^{(2)} \cup \mathbb{Y}_1^{(2)} \cup (\mathbb{X}_2^{(2)} - (N_1 + 1)) \cup (\mathbb{Y}_2^{(2)} - (N_1 + 1)) \\ & = \{1, 2, \dots, N_1\}. \end{aligned}$$

Proof. According to Definition 3.4.1, $\mathbb{X}_1^{(2)}$ collects all the odd numbers from 1 to $1 + 2A_1$ while $\mathbb{X}_2^{(2)} - (N_1 + 1)$ includes all the even numbers ranging from 2 to $2 + 2A_2$. As a result, we have

$$\begin{aligned} & \mathbb{X}_1^{(2)} \cup (\mathbb{X}_2^{(2)} - (N_1 + 1)) \\ & \supseteq \{1, 2, \dots, \min(1 + 2A_1, 2 + 2A_2) + 1\}. \end{aligned} \tag{3.5}$$

Furthermore, it can be shown that $|\max(\mathbb{X}_1^{(2)}) - \max(\mathbb{X}_2^{(2)} - (N_1 + 1))| = |(1 + 2A_1) - (2 + 2A_2)| = 1$. Therefore, we can replace the inclusion (\supseteq) in (3.5) with equality

(=) and obtain

$$\begin{aligned}
& \mathbb{X}_1^{(2)} \cup (\mathbb{X}_2^{(2)} - (N_1 + 1)) \\
&= \{1, 2, \dots, \min(1 + 2A_1, 2 + 2A_2) + 1\} \\
&= \begin{cases} \{1, 2, \dots, 2r + 1\}, & \text{if } N_1 = 4r, \\ \{1, 2, \dots, 2r + 1\}, & \text{if } N_1 = 4r + 1, \\ \{1, 2, \dots, 2r + 3\}, & \text{if } N_1 = 4r + 2, \\ \{1, 2, \dots, 2r + 2\}, & \text{if } N_1 = 4r + 3. \end{cases}
\end{aligned}$$

Similarly, $\mathbb{Y}_1^{(2)}$ and $\mathbb{Y}_2^{(2)} - (N_1 + 1)$ give

$$\begin{aligned}
& \mathbb{Y}_1^{(2)} \cup (\mathbb{Y}_2^{(2)} - (N_1 + 1)) \\
&= \{\max(N_1 - 2B_1, N_1 - 1 - 2B_2) - 1, \dots, N_1\} \\
&= \begin{cases} \{2r + 2, \dots, N_1\}, & \text{if } N_1 = 4r, \\ \{2r + 2, \dots, N_1\}, & \text{if } N_1 = 4r + 1, \\ \{2r + 4, \dots, N_1\}, & \text{if } N_1 = 4r + 2, \\ \{2r + 3, \dots, N_1\}, & \text{if } N_1 = 4r + 3. \end{cases}
\end{aligned}$$

Whichever N_1 is, the union of these four sets covers all the integers from 1 to N_1 . \square

Lemma 3.4.2 (Total number of sensors). The number of elements in $\mathbb{S}^{(2)}$ is $N_1 + N_2$.

Proof. Firstly, $\mathbb{X}_1^{(2)}$, $\mathbb{Y}_1^{(2)}$, $\mathbb{X}_2^{(2)}$, $\mathbb{Y}_2^{(2)}$, $\mathbb{Z}_1^{(2)}$, and $\mathbb{Z}_2^{(2)}$ are disjoint, which can be easily checked from Definition 3.4.1. Thus, the cardinality of $\mathbb{S}^{(2)}$ is the same as the sum of the cardinality of the individual set. We obtain

$$\begin{aligned}
|\mathbb{S}^{(2)}| &= \left(\sum_{q=1}^2 |\mathbb{X}_q^{(2)}| + |\mathbb{Y}_q^{(2)}| \right) + |\mathbb{Z}_1^{(2)}| + |\mathbb{Z}_2^{(2)}| \\
&= \left(\sum_{q=1}^2 (A_q + 1)_+ + (B_q + 1)_+ \right) + (N_2 - 1) + 1 \\
&= N_1 + N_2,
\end{aligned}$$

where $(x)_+ = \max(x, 0)$ denotes the nonnegative part of x . Therefore, there are $N_1 + N_2$ sensor in second-order super nested arrays. \square

3.5 Coarray of Second-Order Super Nested Arrays

In this section, we will show that super nested arrays are restricted arrays, that is, the coarray does not have holes. This property enables us to apply algorithms such as MUSIC in the coarray domain conveniently, as in the case of nested arrays and

MRAs. We will also derive the expressions for the first few weight functions $w(m)$ of the super nested array.

Theorem 3.5.1. Second-order super nested arrays are restricted arrays, i.e., they have hole-free difference coarrays.

Proof. The statement that a second-order super nested array is a restricted array, is equivalent to the following argument: For every m ranging from $-(N_2(N_1 + 1) - 1)$ to $N_2(N_1 + 1) - 1$, there exists at least one pair of physical sensors with sensor separation m . Nevertheless, we do not need to check all possible m 's according to the following properties:

1. If m is in the coarray, $-m$ also belongs to the same coarray.
2. $m = 0$ is included in any coarray.

Therefore, it suffices to check that for $1 \leq m \leq N_2(N_1 + 1) - 1$, we can identify at least one pair $(n_1, n_2) \in (\mathbb{S}^{(2)})^2$ such that $n_1 - n_2 = m$.

If $m = 1$, the sensors on $N_2(N_1 + 1) - 1 \in \mathbb{Z}_2^{(2)}$ and $N_2(N_1 + 1) \in \mathbb{Z}_1^{(2)}$ contribute to $w(1)$.

When $2 \leq m \leq N_1$, we turn to evaluate the following sets:

$$\begin{aligned} & \text{diff}(\{2(N_1 + 1)\}, \mathbb{X}_2^{(2)} \cup \mathbb{Y}_2^{(2)}) \\ &= \{N_1 - 1 - 2\ell : 0 \leq \ell \leq A_2\} \cup \{2 + 2\ell : 0 \leq \ell \leq B_2\}, \\ & \text{diff}(\{N_1 + 3\}, \mathbb{X}_1^{(2)} \cup \mathbb{Y}_1^{(2)}) \\ &= \{N_1 + 2 - 2\ell : 0 \leq \ell \leq A_1\} \cup \{3 + 2\ell : 0 \leq \ell \leq B_1\}. \end{aligned}$$

It is clear that these sets are contained in the difference coarray since $2(N_1 + 1) \in \mathbb{Z}_1^{(2)}$ and $N_1 + 3 \in \mathbb{X}_2^{(2)}$. Note that the set $\{2 + 2\ell : 0 \leq \ell \leq B_2\}$ includes all the even numbers starting from 2 to $2 + 2B_2$ while $\{3 + 2\ell : 0 \leq \ell \leq B_1\}$ collects all the odd numbers from 3 to $3 + 2B_1$. This observation is summarized into

$$\begin{aligned} \mathbb{P}_1 &= \{m : 2 \leq m \leq \min(3 + 2B_1, 2 + 2B_2) + 1\} \\ &\subseteq \{2 + 2\ell : 0 \leq \ell \leq B_2\} \cup \{3 + 2\ell : 0 \leq \ell \leq B_1\}, \end{aligned}$$

which indicates that the contiguous integers from 2 to $\min(3 + 2B_1, 2 + 2B_2) + 1$, denoted by \mathbb{P}_1 , are contained in the coarray of second-order super nested arrays. A similar result for $\{N_1 - 1 - 2\ell : 0 \leq \ell \leq A_2\}$ and $\{N_1 + 2 - 2\ell : 0 \leq \ell \leq A_1\}$ is given by the set \mathbb{P}_2 :

$$\begin{aligned} \mathbb{P}_2 &= \{m : \max(N_1 + 2 - 2A_1, N_1 - 1 - 2A_2) - 1 \leq m \leq N_1\} \\ &\subseteq \{N_1 - 1 - 2\ell : 0 \leq \ell \leq A_2\} \cup \{N_1 + 2 - 2\ell : 0 \leq \ell \leq A_1\}. \end{aligned}$$

Table 3.1: Ranges of \mathbb{P}_1 and \mathbb{P}_2

| N_1 | $4r$ | $4r + 1$ | $4r + 2$ | $4r + 3$ |
|---|----------|----------|----------|------------------|
| $3 + 2B_1$ | $2r + 1$ | $2r + 1$ | $2r + 1$ | $2r + 3$ |
| $2 + 2B_2$ | $2r - 2$ | $2r$ | $2r - 2$ | $2r$ |
| $\max(\mathbb{P}_1)$ | $2r - 1$ | $2r + 1$ | $2r - 1$ | $2r + 1$ |
| $N_1 + 2 - 2A_1$ | $2r + 2$ | $2r + 3$ | $2r + 2$ | $2r + 5$ |
| $N_1 - 1 - 2A_2$ | $2r + 1$ | $2r + 2$ | $2r + 1$ | $2r + 2$ |
| $\min(\mathbb{P}_2)$ | $2r + 1$ | $2r + 2$ | $2r + 1$ | $2r + 4$ |
| Holes in $\mathbb{P}_1 \cup \mathbb{P}_2$ | $2r$ | – | $2r$ | $2r + 2, 2r + 3$ |

It can be verified in Table 3.1 that $\mathbb{P}_1 \cup \mathbb{P}_2$ contains all the differences within $2 \leq m \leq N_1$, except for $N_1 = 4r, 4r + 2$, and $4r + 3$. In the case of $N_1 = 4r$, the coarray index $2r$ can be found in the pair of sensors on $1 \in \mathbb{X}_1^{(2)}$ and $1 + 2A_1 \in \mathbb{X}_1^{(2)}$. When $N_1 = 4r + 2$, the pair of sensors on $(N_1 + 1) + 2 \in \mathbb{X}_2^{(2)}$ and $(N_1 + 1) + (2 + 2A_2) \in \mathbb{X}_2^{(2)}$ leads to coarray index $2r$. If $N_1 = 4r + 3$, the differences $2r + 2$ and $2r + 3$ are exactly $N_1 - 1 - 2A_2$ and $3 + 2B_1$, respectively, as shown in Table 3.1. Thus, $2 \leq m \leq N_1$ is included in the difference coarray.

For the coarray index $q(N_1 + 1) \leq m \leq (q + 1)(N_1 + 1)$, where $1 \leq q \leq N_2 - 2$, we consider the differences

$$\begin{aligned}
& \text{diff}(\{(q + 1)(N_1 + 1)\}, \mathbb{X}_1^{(2)} \cup \mathbb{Y}_1^{(2)}) \\
&= \text{diff}(\{N_1 + 1\}, \mathbb{X}_1^{(2)} \cup \mathbb{Y}_1^{(2)}) + q(N_1 + 1), \\
& \text{diff}(\{(q + 2)(N_1 + 1)\}, \mathbb{X}_2^{(2)} \cup \mathbb{Y}_2^{(2)}) \\
&= \text{diff}(\{N_1 + 1\}, (\mathbb{X}_2^{(2)} - (N_1 + 1)) \cup (\mathbb{Y}_2^{(2)} - (N_1 + 1))) \\
& \quad + q(N_1 + 1).
\end{aligned}$$

According to Lemma 3.4.1, the union of $\text{diff}(\{N_1 + 1\}, \mathbb{X}_1^{(2)} \cup \mathbb{Y}_1^{(2)})$ and $\text{diff}(\{N_1 + 1\}, (\mathbb{X}_2^{(2)} - (N_1 + 1)) \cup (\mathbb{Y}_2^{(2)} - (N_1 + 1)))$ covers all the consecutive integers from 1 to N_1 . In other words, the coarray index $q(N_1 + 1) < m < (q + 1)(N_1 + 1)$ can be found in the difference sets among $\mathbb{X}_1^{(2)}$, $\mathbb{Y}_1^{(2)}$, $\mathbb{X}_2^{(2)}$, $\mathbb{Y}_2^{(2)}$, and $\mathbb{Z}_1^{(2)}$. It is obvious that the differences $q(N_1 + 1)$ are contained in the self-difference of $\mathbb{Z}_1^{(2)}$.

The last part of the proof considers $(N_2 - 1)(N_1 + 1) \leq m \leq N_2(N_1 + 1) - 1$. In this case, we take the following four sets: $\text{diff}(\{N_2(N_1 + 1)\}, \mathbb{X}_1^{(2)})$, $\text{diff}(\{N_2(N_1 + 1) - 1\}, \mathbb{X}_1^{(2)})$, $\text{diff}(\{N_2(N_1 + 1) - 2\}, \mathbb{X}_1^{(2)})$, and $\text{diff}(\{N_2(N_1 + 1) - 3\}, \mathbb{X}_1^{(2)})$.

Table 3.2: Ranges of $\mathbb{X}_1^{(2)} \cup (\mathbb{X}_1^{(2)} + 1)$ and $\mathbb{Y}_1^{(2)} \cup (\mathbb{Y}_1^{(2)} + 1)$

| N_1 | $4r$ | $4r + 1$ | $4r + 2$ | $4r + 3$ |
|---|----------|----------|----------|----------|
| $\max(\mathbb{X}_1^{(2)} \cup (\mathbb{X}_1^{(2)} + 1)) = 2 + 2A_1$ | $2r + 2$ | $2r + 2$ | $2r + 4$ | $2r + 2$ |
| $\min(\mathbb{Y}_1^{(2)} \cup (\mathbb{Y}_1^{(2)} + 1)) = (N_1 + 1) - (1 + 2B_1)$ | $2r + 2$ | $2r + 3$ | $2r + 4$ | $2r + 3$ |

$1\}$, $\mathbb{Y}_1^{(2)}$, and

$$\begin{aligned} \text{diff}(\{N_2(N_1 + 1) - 1\}, \mathbb{X}_1^{(2)}) &= \text{diff}(\{N_2(N_1 + 1)\}, \mathbb{X}_1^{(2)} + 1), \\ \text{diff}(\{N_2(N_1 + 1) - 1\}, \mathbb{Y}_1^{(2)}) &= \text{diff}(\{N_2(N_1 + 1)\}, \mathbb{Y}_1^{(2)} + 1). \end{aligned}$$

To prove these difference sets cover $(N_2 - 1)(N_1 + 1) \leq m \leq N_2(N_1 + 1) - 1$, it suffices to show that $\mathbb{X}_1^{(2)} \cup \mathbb{Y}_1^{(2)} \cup (\mathbb{X}_1^{(2)} + 1) \cup (\mathbb{Y}_1^{(2)} + 1)$ contains contiguous integers from 1 to $N_1 + 1$. Note that $\mathbb{X}_1^{(2)} \cup (\mathbb{X}_1^{(2)} + 1)$ is $\{1, \dots, 2 + 2A_1\}$ and $\mathbb{Y}_1^{(2)} \cup (\mathbb{Y}_1^{(2)} + 1)$ is $\{(N_1 + 1) - (1 + 2B_1), \dots, N_1 + 1\}$. Table 3.2 shows the maximum element in $\mathbb{X}_1^{(2)} \cup (\mathbb{X}_1^{(2)} + 1)$ and the minimum element in $\mathbb{Y}_1^{(2)} \cup (\mathbb{Y}_1^{(2)} + 1)$. It is evident that there are no holes in $\mathbb{X}_1^{(2)} \cup \mathbb{Y}_1^{(2)} \cup (\mathbb{X}_1^{(2)} + 1) \cup (\mathbb{Y}_1^{(2)} + 1)$. This completes the proof. \square

Corollary 3.5.1. Second-order super nested arrays have the same coarray as their parent nested arrays.

Proof. According Definition 3.4.1, second-order super nested arrays share the same boundary points, located at 1 and $N_2(N_1 + 1)$, as their parent nested arrays. In addition, both of them are restricted arrays (Theorem 3.5.1). Therefore, they possess the same coarray. \square

Theorem 3.5.2. Let $\mathbb{S}^{(2)}$ be a second-order super nested array with $N_1 \geq 4$, $N_2 \geq 3$. Its weight function $w(m)$ at $m = 1, 2, 3$ is

$$\begin{aligned} w(1) &= \begin{cases} 2, & \text{if } N_1 \text{ is even,} \\ 1, & \text{if } N_1 \text{ is odd,} \end{cases} \\ w(2) &= \begin{cases} N_1 - 3, & \text{if } N_1 \text{ is even,} \\ N_1 - 1, & \text{if } N_1 \text{ is odd,} \end{cases} \\ w(3) &= \begin{cases} 3, & \text{if } N_1 = 4, 6, \\ 4, & \text{if } N_1 \text{ is even, } N_1 \geq 8, \\ 1, & \text{if } N_1 \text{ is odd.} \end{cases} \end{aligned}$$

For comparison, the first three weight functions for nested arrays [124] and coprime arrays [125], [186] are

$$\text{Nested: } w(1) = N_1, w(2) = N_1 - 1, w(3) = N_1 - 2, \quad (3.6)$$

$$\text{Coprime: } w(1) = w(2) = w(3) = 2, \quad (3.7)$$

where N_1, N_2 for nested arrays and M, N for coprime arrays are sufficiently large. As a result, $w(1)$ and $w(3)$ for second-order super nested arrays are notably smaller than those for their parent nested array, and comparable to those for coprime arrays. The proof of Theorem 3.5.2 is as follows:

Proof. First, we analyze the structure of the positive part of the difference coarray. It is known that, if the array configuration $\mathbb{S} = \mathbb{A} \cup \mathbb{B}$, then the difference coarray \mathbb{D} can be divided into *self differences*, like $\text{diff}(\mathbb{A}, \mathbb{A})$, $\text{diff}(\mathbb{B}, \mathbb{B})$, and *cross differences*, such as $\text{diff}(\mathbb{A}, \mathbb{B})$, $\text{diff}(\mathbb{B}, \mathbb{A})$ [186]. We will use this approach to prove Theorem 3.5.2.

The self differences are discussed as follows: According to Definition 3.4.1, since $\mathbb{X}_1^{(2)}$, $\mathbb{Y}_1^{(2)}$, $\mathbb{X}_2^{(2)}$, and $\mathbb{Y}_2^{(2)}$ are ULAs with separation 2, their self differences contain $0, \pm 2, \pm 4, \pm 6$, and so on. We obtain

$$(A_1)_+ + (B_1)_+ + (A_2)_+ + (B_2)_+ \quad (3.8)$$

pairs of sensors with separation 2, where $(x)_+ = \max(x, 0)$ is the positive part of a real number x . Next, it can be shown that the self differences of $\mathbb{Z}_1^{(2)}$ include $0, \pm(N_1 + 1), \pm 2(N_1 + 1), \pm 3(N_1 + 1)$, up to $\pm(N_2 - 2)(N_1 + 1)$. Since $N_1 \geq 4$, the self differences of $\mathbb{Z}_1^{(2)}$ do not contain 1, 2, and 3. The self difference of $\mathbb{Z}_2^{(2)}$ is exactly zero because there is only one element in $\mathbb{Z}_2^{(2)}$.

For the cross differences, it suffices to consider the sets of interest: $\text{diff}(\mathbb{Y}_1^{(2)}, \mathbb{X}_1^{(2)})$, $\text{diff}(\mathbb{X}_2^{(2)}, \mathbb{Y}_1^{(2)})$, $\text{diff}(\mathbb{Y}_2^{(2)}, \mathbb{X}_2^{(2)})$, $\text{diff}(\{2(N_1 + 1)\}, \mathbb{Y}_2^{(2)})$, and $\text{diff}(\{N_2(N_1 + 1)\}, \mathbb{Z}_2^{(2)})$, since the remaining choices of cross differences, like $\text{diff}(\mathbb{X}_2^{(2)}, \mathbb{X}_1^{(2)})$, $\text{diff}(\mathbb{Z}_1^{(2)}, \mathbb{X}_1^{(2)})$, and so on, do not include 1, 2, and 3. Evaluating the minimum elements of the sets

of interest leads to

$$\begin{aligned}
\min \text{diff}(\mathbb{Y}_1^{(2)}, \mathbb{X}_1^{(2)}) &= (N_1 + 1) - (1 + 2B_1) - (1 + 2A_1) \\
&= \begin{cases} 4r - 1 - 2(r - 1 + r), & \text{if } N_1 = 4r, \\ 4r + 1 - 1 - 2(r - 1 + r), & \text{if } N_1 = 4r + 1, \\ 4r + 2 - 1 - 2(r - 1 + r + 1), & \text{if } N_1 = 4r + 2, \\ 4r + 3 - 1 - 2(r + r), & \text{if } N_1 = 4r + 3. \end{cases} \\
&= \begin{cases} 1, & \text{if } N_1 \text{ is even,} \\ 2, & \text{if } N_1 \text{ is odd,} \end{cases} \tag{3.9}
\end{aligned}$$

$$\min \text{diff}(\mathbb{X}_2^{(2)}, \mathbb{Y}_1^{(2)}) = (N_1 + 3) - (N_1) = 3, \tag{3.10}$$

$$\begin{aligned}
\min \text{diff}(\mathbb{Y}_2^{(2)}, \mathbb{X}_2^{(2)}) &= (2(N_1 + 1) - (2 + 2B_2)) - ((N_1 + 1) + (2 + 2A_2)) \\
&= \begin{cases} 3, & \text{if } N_1 \text{ is even,} \\ 2, & \text{if } N_1 \text{ is odd,} \end{cases} \tag{3.11}
\end{aligned}$$

$$\begin{aligned}
\min \text{diff}(\{2(N_1 + 1)\}, \mathbb{Y}_2^{(2)}) &= 2(N_1 + 1) - (2(N_1 + 1) - 2) = 2, \tag{3.12}
\end{aligned}$$

$$\text{diff}(\{N_2(N_1 + 1)\}, \mathbb{Z}_2^{(2)}) = 1. \tag{3.13}$$

Furthermore, since the sets $\mathbb{X}_1^{(2)}$, $\mathbb{Y}_1^{(2)}$, $\mathbb{X}_2^{(2)}$, and $\mathbb{Y}_2^{(2)}$ are ULAs with sensor separation 2, their cross differences are also ULAs with separation 2. Applying this property to (3.9) gives

$$\begin{aligned}
&\text{The second smallest element of } \text{diff}(\mathbb{Y}_1^{(2)}, \mathbb{X}_1^{(2)}), \text{ if exists,} \\
&= \begin{cases} 3, & \text{if } N_1 \text{ is even,} \\ 4, & \text{if } N_1 \text{ is odd.} \end{cases} \tag{3.14}
\end{aligned}$$

Now it is clear to determine the weight functions $w(m)$ for $m = 1, 2, 3$, based on (3.8) to (3.14). For $m = 1$, the sensor pairs of separation 1 only occur at (3.9) and (3.13), while (3.8), (3.10), (3.11), (3.12), and (3.14) do not contribute to $w(1)$. This argument proves the $w(1)$ part. When $m = 2$, the associated sensor pairs can be found in (3.8), (3.9), (3.11), and (3.12). Therefore, $w(2)$ can be expressed as

$$\begin{aligned}
w(2) &= \begin{cases} 1 + \sum_{q=1}^2 (A_q)_+ + (B_q)_+ & \text{if } N_1 \text{ is even,} \\ 3 + \sum_{q=1}^2 (A_q)_+ + (B_q)_+ & \text{if } N_1 \text{ is odd.} \end{cases} \\
&= \begin{cases} N_1 - 3, & \text{if } N_1 \text{ is even,} \\ N_1 - 1, & \text{if } N_1 \text{ is odd.} \end{cases}
\end{aligned}$$

If $m = 3$, we first consider the case when N_1 is even. When $N_1 = 4$, we obtain the following sets

$$\mathbb{X}_1^{(2)} = \{1, 3\}, \mathbb{Y}_1^{(2)} = \{4\}, \mathbb{X}_2^{(2)} = \{7\}, \mathbb{Y}_2^{(2)} = \emptyset,$$

where \emptyset denotes the empty set. Besides, the minimum element in $\mathbb{Z}_1^{(2)}$ is $2(N_1 + 1) = 10$. Counting these differences directly gives $w(3) = 3$. When $N_1 = 6$, these sets become

$$\mathbb{X}_1^{(2)} = \{1, 3, 5\}, \mathbb{Y}_1^{(2)} = \{6\}, \mathbb{X}_2^{(2)} = \{9, 11\}, \mathbb{Y}_2^{(2)} = \emptyset,$$

and $2(N_1 + 1) = 14$ so $w(3) = 3$.

If $N_1 \geq 8$ and N_1 is an even number, then $\mathbb{X}_1^{(2)}$ has at least three elements, $\mathbb{Y}_1^{(2)}$ has at least two elements, and $\mathbb{Y}_2^{(2)}$ is non-empty. In this case, the sensor pairs with separation 3 can be found in (3.10) and (3.11). Furthermore, the sensor pairs with separation 3 in (3.14) are

$$\text{Pair \#1 : } ((N_1 + 1) - (1 + 2B_1)) - (1 + 2(A_1 - 1)) = 3,$$

$$\text{Pair \#2 : } ((N_1 + 1) - (1 + 2(B_1 - 1))) - (1 + 2A_1) = 3.$$

Therefore $w(3) = 4$ if $N_1 \geq 8$ and N_1 is even.

When N_1 is odd, the only sensor pair leading to $w(3)$ is shown in (3.10), which completes the proof. \square

Summarizing this section, super nested arrays are generalizations of nested arrays. First of all, there is a simple closed-form expression for sensor locations, as in the case of nested and coprime arrays (and unlike MRAs). Second, for a fixed number of sensors, the physical aperture and the difference coarray are exactly identical to those of nested arrays, so that the DOF for DOA estimation remains unchanged. In particular, there are no holes in the coarray unlike coprime arrays. Finally, as in coprime arrays, the mutual coupling effects are much less severe than in nested arrays, because the sensors in the dense ULA part of the nested array have now been redistributed. In short, the super nested array combines the best features of nested and coprime arrays.

3.6 Numerical Examples

In this section, we select six array configurations: ULA, MRA, nested arrays, coprime arrays, second-order super nested arrays, as well as third-order super nested arrays¹, and then compare their performance in the presence of mutual coupling.

¹ Higher order super nested arrays will be introduced in Chapter 4, and have even better performance. Here we include an example just for completeness of comparison.

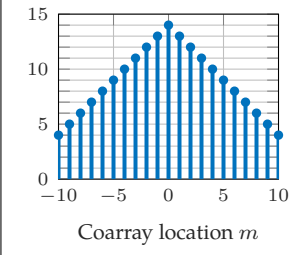
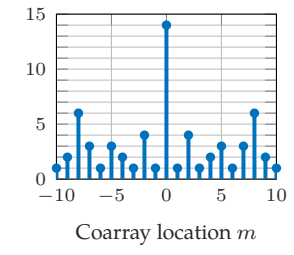
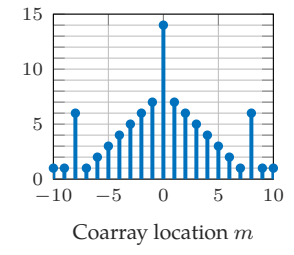
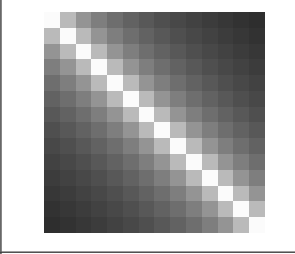
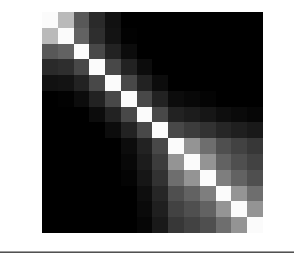
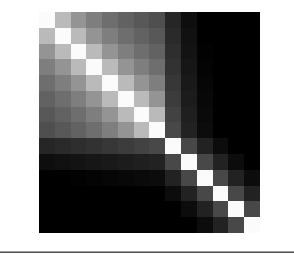
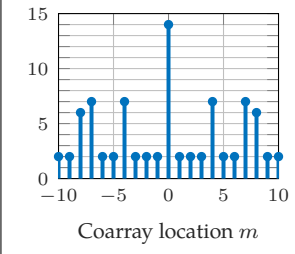
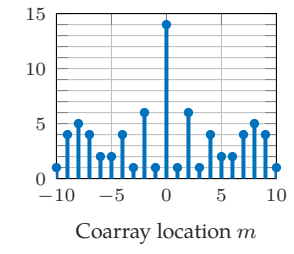
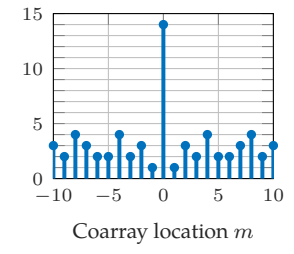
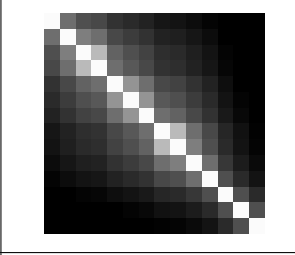
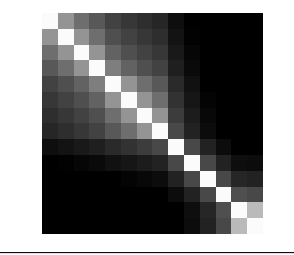
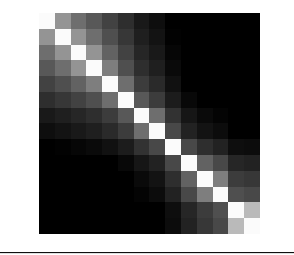
| Array | ULA | MRA | Nested |
|--------------|---|--|---|
| $w(m)$ |  |  |  |
| \mathbf{C} |  |  |  |
| L | 0.44132 | 0.18243 | 0.33327 |
| Array | Coprime | Second-order super nested | Third-order super nested |
| $w(m)$ |  |  |  |
| \mathbf{C} |  |  |  |
| L | 0.21426 | 0.20295 | 0.18203 |

Figure 3.6: Comparison among ULA, nested array, coprime array, second-order super nested array, and third-order super nested array in the presence of mutual coupling. The coupling leakage L is defined as $\|\mathbf{C} - \text{diag}(\mathbf{C})\|_F / \|\mathbf{C}\|_F$, where $[\text{diag}(\mathbf{C})]_{i,j} = [\mathbf{C}]_{i,j} \delta_{i,j}$.

The number of sensors is fixed to be 14. The sensor locations for MRA are given by [65]²

$$\mathbb{S}_{\text{MRA}} = \{0, 1, 6, 14, 22, 30, 38, 46, 54, 56, 58, 61, 63, 65\}.$$

For nested arrays and super nested arrays, we set $N_1 = N_2 = 7$. For coprime arrays, we choose $M = 4$ and $N = 7$. The sensor locations are given by (2.7), (2.8) and Definition 3.4.1 so that there are $N_1 + N_2 = 14$ sensors for nested arrays as well as super nested arrays and $N + 2M - 1 = 14$ sensors for coprime arrays. If the central ULA part of the difference coarray of an array has $2P + 1$ elements, i.e., the uniform DOF is $2P + 1$, then P sources can be identified using the coarray MUSIC (SS-MUSIC) algorithm [124], [125]. In our case the nested and super nested arrays have a ULA for the coarray and the coprime array has a central ULA part and then some holes. It is readily verified that the number of identifiable sources in each case is as follows:

$$\text{ULA: 13 sources.} \quad (3.15)$$

$$\text{MRA: 65 sources.} \quad (3.16)$$

$$\text{Coprime array: } MN + M - 1 = 31 \text{ sources.} \quad (3.17)$$

$$\text{(Super) Nested array: } N_2(N_1 + 1) - 1 = 55 \text{ sources.} \quad (3.18)$$

It is well-known that the array aperture affects the estimation performance [30], [166], [184]. Larger array aperture tends to have finer spatial resolution and smaller estimation error. However, it suffices to consider the uniform DOF rather than the array aperture, since the uniform DOF is approximately twice the array aperture for restricted arrays. For instance, consider a physical array whose sensors are located at 0, 1, 4, 6, in units of $\lambda/2$. Then, the array aperture is 6 and the difference coarray $\mathbb{D} = \{-6, \dots, 6\}$. The uniform DOF is $13 = 2 \times 6 + 1$, which is about twice the array aperture 6. Therefore, in what follows, we focus on the uniform DOF, rather than the array aperture, to explain the overall estimation performance.

Weight Functions and Mutual Coupling Matrices

The first example compares weight functions and the associated mutual coupling matrix (3.3). We choose $c_1 = 0.3 \exp(j\pi/3)$ and $B = 100$. The remaining coupling coefficients are given by $c_\ell = c_1 \exp(-j(\ell - 1)\pi/8) / \ell$ for $2 \leq \ell \leq B$. The first row of Fig. 3.6 shows the weight functions $w(m)$. In nested arrays, the associated weight function possesses a triangular region in the center, due to the dense ULA part. This triangular region breaks into smaller ones in the second-order super nested

² Strictly speaking, this array only gets close to the minimum redundancy (or equivalently maximum uniform DOF), rather than achieving the optimal one. However, it is still called MRA in [65].

array ($w(1) = 1, w(2) = 6, w(3) = 1$, as in Theorem 3.5.2) and the third-order super nested array ($w(1) = 1, w(2) = 3, w(3) = 2$). Coprime arrays exhibit smaller weight functions ($w(1) = w(2) = w(3) = 2$, as in (3.7)) than those of nested arrays ($w(1) = 7, w(2) = 6, w(3) = 5$, as in (3.6)).

The quantity $|\mathbf{C}]_{i,j}|^2$, where \mathbf{C} is the mutual coupling matrix, is shown in log-scale on the second row of Fig. 3.6. The darker region indicates less energy in the corresponding entry. It can be seen that all these \mathbf{C} matrices are nearly-diagonal. In particular, \mathbf{C} is a symmetric Toeplitz matrix for ULA. Note that if \mathbf{C} is a diagonal matrix, sensor responses do not interfere with each other so it is free from mutual coupling. Hence, the energy of the off-diagonal components characterizes the amount of mutual coupling. We define the *coupling leakage* L as

$$L = \frac{\|\mathbf{C} - \text{diag}(\mathbf{C})\|_F}{\|\mathbf{C}\|_F},$$

where $[\text{diag}(\mathbf{C})]_{i,j} = [\mathbf{C}]_{i,j} \delta_{i,j}$ and $\|\cdot\|_F$ denotes the Frobenius norm of a matrix. It is clear that $0 \leq L \leq 1$. Conceptually speaking, the smaller L is, the less the mutual coupling is. According to the third row of Fig. 3.6, the ULA suffers from the most severe mutual coupling effect. The third-order super nested array possesses the least L , suggesting it might have the least mutual coupling effect. In addition, high-order super nested arrays reduce the mutual coupling effect of their parent nested arrays, which can be inferred from the coupling leakage L among the nested array, the second-order super nested array, and the third-order one.

MUSIC Spectra in the Presence of Mutual Coupling

The second part of the simulation investigates the associated MUSIC spectra under various array configurations. The number of snapshots is 500 while the SNR is 0 dB. The measurement vector \mathbf{x}_S is contaminated by the mutual coupling matrix \mathbf{C} and the MUSIC spectrum $P(\bar{\theta})$ is evaluated directly from \mathbf{x}_S *without using any decoupling algorithms*. Note that these results can be further improved by a variety of decoupling algorithms [20], [49], [83], [151], [173]. Our setting provides a baseline performance for different arrays. We will show that, even without decoupling, super nested arrays are still able to perform DOA estimation within reasonable amount of error.

Fig. 3.7 shows the MUSIC spectra when $D = 10$ sources are located at $\bar{\theta}_i = -0.1 + 0.2(i - 1)/9$ for $i = 1, 2, \dots, 10$, as indicated by the ticks and the vertical lines. This example examines the performance when the number of sources ($D = 10$) is less than the number of sensors 14. It is deduced from Fig. 3.7 that the ULA and the coprime array have false peaks, the nested array displays 11 peaks, while the MRA and the super nested arrays can resolve 10 true peaks. In terms of the estimation

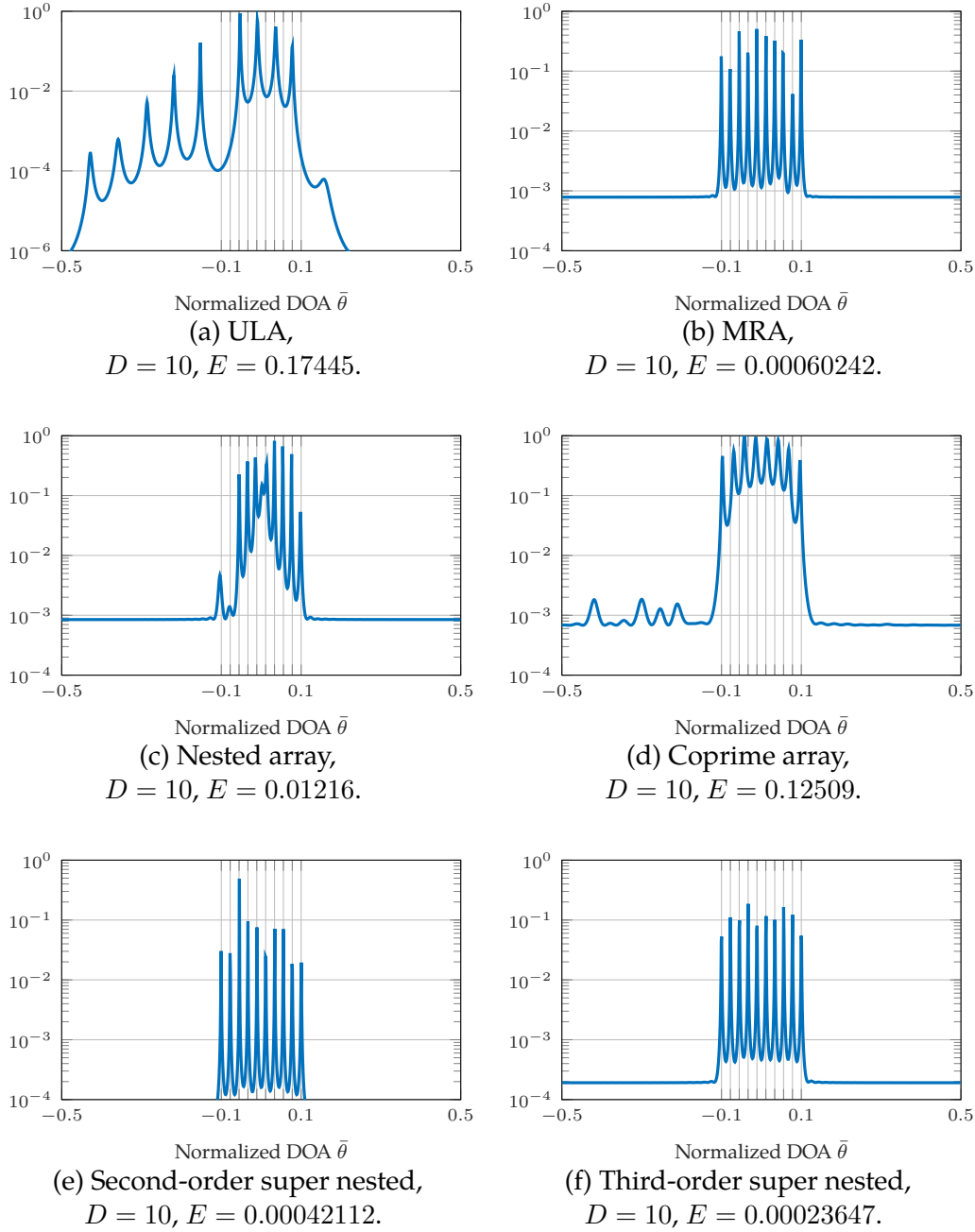


Figure 3.7: The MUSIC spectra $P(\bar{\theta})$ for ULA, MRA, nested arrays, coprime arrays, second-order super nested arrays, and third-order super nested arrays when $D = 10$ sources are located at $\bar{\theta}_i = -0.1 + 0.2(i - 1)/9$, $i = 1, 2, \dots, 10$, as depicted by ticks and vertical lines. The SNR is 0 dB while the number of snapshots is $K = 500$. Note that the number of sources 10 is less than the number of sensors 14. The mutual coupling is based on (3.3) with $c_1 = 0.3 \exp(j\pi/3)$, $B = 100$, and $c_\ell = c_1 \exp(-j(\ell - 1)\pi/8) / \ell$ for $2 \leq \ell \leq B$.

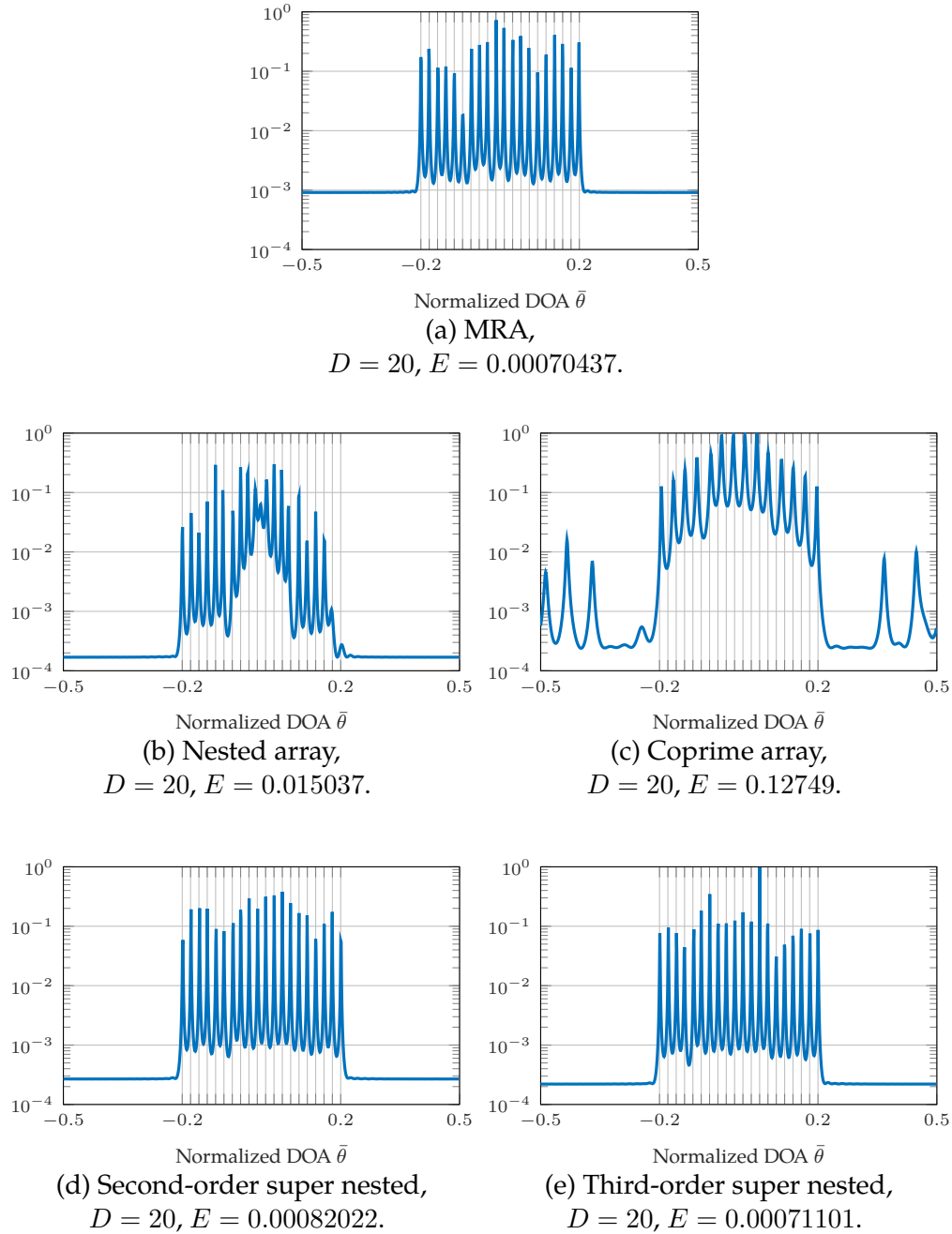


Figure 3.8: The MUSIC spectra $P(\bar{\theta})$ for MRA, nested arrays, coprime arrays, second-order super nested arrays, and third-order super nested arrays when $D = 20$ sources are located at $\bar{\theta}_i = -0.2 + 0.4(i - 1)/19$, $i = 1, 2, \dots, 20$, as depicted by ticks and vertical lines. The SNR is 0 dB while the number of snapshots is $K = 500$. Note that the number of sources 20 is greater than the number of sensors 14. The mutual coupling is based on (3.3) with $c_1 = 0.3 \exp(j\pi/3)$, $B = 100$, and $c_\ell = c_1 \exp(-j(\ell - 1)\pi/8) / \ell$ for $2 \leq \ell \leq B$.

error E defined in (3.4), the best performance is exhibited by the third-order super nested array ($E = 0.00023647$), followed by the second-order super nested array ($E = 0.00042112$), then the MRA ($E = 0.00060242$), then the nested array ($E = 0.01216$), then the coprime array ($E = 0.12509$), and finally the ULA ($E = 0.17445$). It is noteworthy that the estimation error for the second-order super nested array is approximately 70% of that for the MRA, 3.5% of that for the nested array, and 0.3% of that for the coprime array. On the other hand, the RMSE for the third-order super nested array is roughly 40% of that for the MRA, only 2% of that for the nested array, and only 0.2% of that for the coprime array. To evaluate the RMSE, we use the root MUSIC algorithm [188] on the noise subspace to estimate DOAs. In the root MUSIC algorithm, suppose the roots on or inside the unit circle are denoted by $r_1, r_2, \dots, r_D, r_{D+1}, \dots, r_P$ such that $1 \geq |r_1| \geq |r_2| \geq \dots \geq |r_D| \geq |r_{D+1}| \geq \dots \geq |r_P|$. These DOAs are obtained from the phases of r_1, r_2, \dots, r_D , which lead to D DOAs.

Fig. 3.8 lists another experiment with $D = 20$ sources, where D exceeds the number of sensors 14. These sources are located at $\bar{\theta}_i = -0.2 + 0.4(i - 1)/19$, where $i = 1, 2, \dots, 20$. The ULA fails to distinguish 20 sources due to (3.15). The MRA and the super nested arrays are capable of distinguishing 20 sources while the nested array (21 peaks) and the coprime array (with false peaks) are not. Among those resolving true DOAs, the best performance is exhibited by MRA ($E = 0.00070437$), followed by the third-order super nested array ($E = 0.00071101$), and then the second-order super nested array ($E = 0.00082022$).

The reason why the ranking is different for large D is this: when D is small, the performance depends mostly on the mutual coupling, so the super nested arrays perform better than MRA. But as D gradually increases and gets closer to the upper limit of super nested arrays (55, as in (3.18)), which is smaller than the upper limit for MRA (65, as in (3.16)), this degrades the performance of super nested arrays before it begins to affect MRA.

Fig. 3.9 plots the MUSIC spectra for $D = 20$ equal-power, uncorrelated sources. These sources are more widely separated, compared to those in Fig. 3.8. The true normalized DOAs are $\bar{\theta}_i = -0.4 + 0.8(i - 1)/19$, $i = 1, 2, \dots, 20$. Hence, based on Section 3.3, the mutual coupling (or the weight functions) becomes more significant than the uniform DOF (or the spatial resolution). The least RMSE is now enjoyed by the third-order super nested array ($E = 0.00073657$), followed by the second-order super nested array ($E = 0.0011955$), then the MRA ($E = 0.0012123$), then the coprime array ($E = 0.027151$), and finally the nested array ($E = 0.04245$). It can be observed that the coprime array, in this example, is more satisfactory than the nested array. There is only one spurious peak in the coprime array, as in Fig.

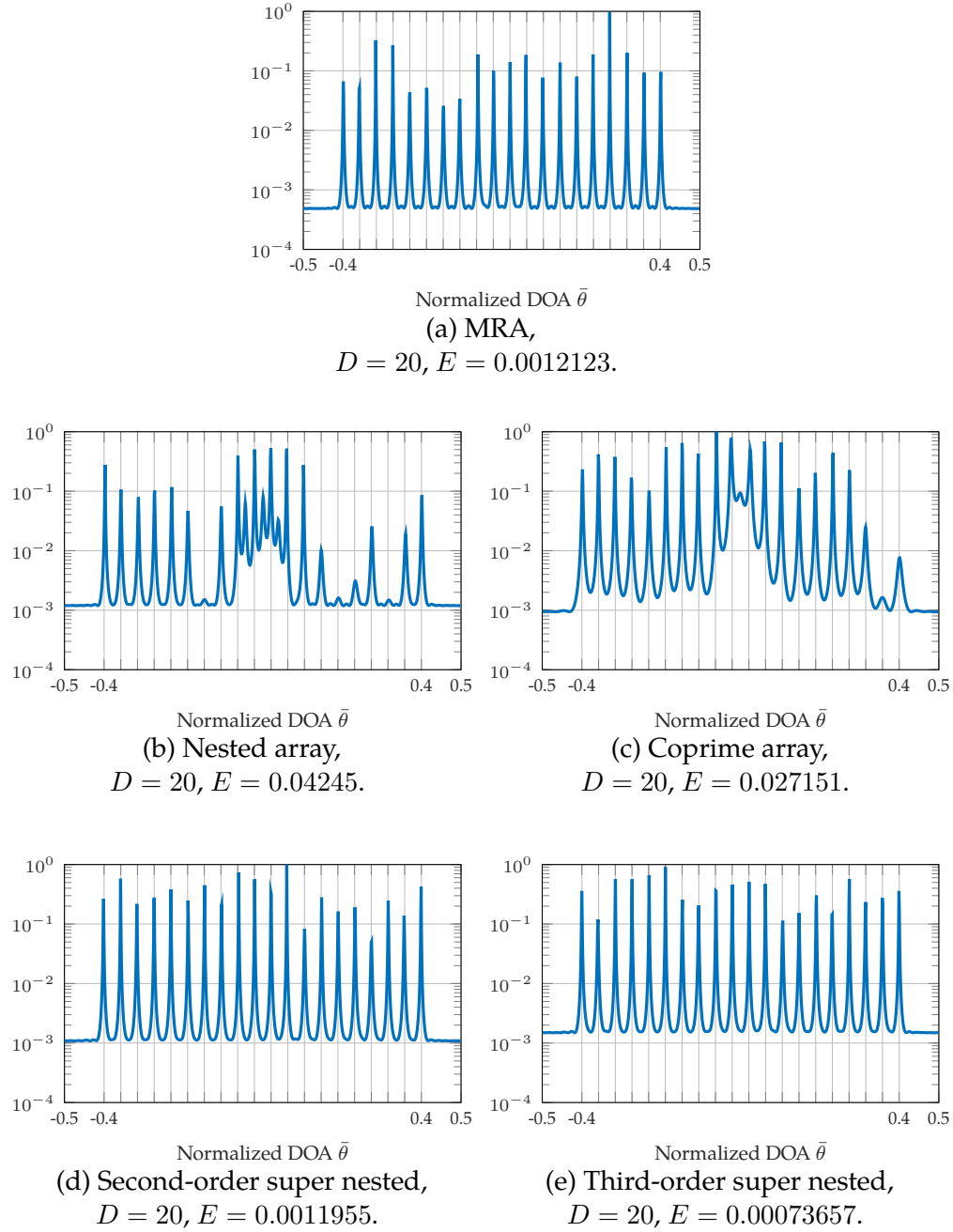


Figure 3.9: The MUSIC spectra $P(\bar{\theta})$ for MRA, nested arrays, coprime arrays, second-order super nested arrays, and third-order super nested arrays when $D = 20$ sources are located at $\bar{\theta}_i = -0.4 + 0.8(i-1)/19, i = 1, 2, \dots, 20$, as depicted by ticks and vertical lines. The SNR is 0 dB while the number of snapshots is $K = 500$. The mutual coupling is based on (3.3) with $c_1 = 0.3 \exp(j\pi/3)$, $B = 100$, and $c_\ell = c_1 \exp(-j(\ell-1)\pi/8) / \ell$ for $2 \leq \ell \leq B$.

3.9(c), while many spurious peaks and missing targets exist in the nested array, as shown in Fig. 3.9(b). It is because the coprime array has reduced mutual coupling ($w(1) = w(2) = w(3) = 2$, as in (3.7)), in comparison of the nested array ($w(1) = 7, w(2) = 6, w(3) = 5$, as in (3.6)), even though the uniform DOF of the coprime array is smaller than that of the nested array.

Fig. 3.10 considers the MUSIC spectra under the linear dipole model for mutual coupling, (3.2), which is more practical than (3.3). For the mutual coupling model (3.2), the parameters Z_A and Z_L are 50 ohms while the dipole length $l = \lambda/2$. The source locations are identical to those in Fig. 3.9. In this scenario, the best estimation performance is exhibited by the third-order super nested array ($E = 0.00083662$), followed by the MRA ($E = 0.00091204$), then the second-order super nested array ($E = 0.0010173$), then the coprime array ($E = 0.0014204$), and finally the nested array ($E = 0.0017399$). It can be observed that all these sparse arrays are capable of identifying 20 sources. This phenomenon is due to the following: First, the sources are widely separated and $D = 20$ is less than the maximum number of identifiable sources, as shown in (3.16) to (3.18). Second, the estimation performance depends on the mutual coupling model and the choice of parameters. In this specific example, the mutual coupling effect in Fig. 3.10 is less severe than that in Fig. 3.9 so that all these sparse arrays are able to resolve the sources correctly.

3.7 Concluding Remarks

In this chapter, we introduced super nested arrays. These share many of the good properties of nested arrays but at the same time, have reduced mutual coupling effects. For a fixed number of sensors, the super nested array has the same aperture and the same coarray as the parent nested array. Therefore, the DOF for DOA estimation is unchanged, while at the same time the effects of mutual coupling are reduced. One future direction for further improvement would be to use these arrays in conjunction with techniques which decouple or compensate the effect of mutual coupling such as the ones in [20], [38], [49], [83], [129], [151], [172], [173], [199].

Notice from Theorem 3.5.2 that, while the weights $w(1)$ and $w(3)$ are significantly smaller than that of the parent nested array, the weight $w(2)$ is only slightly improved. How can we modify the array configuration further so that $w(2)$ is also decreased significantly without noticeably penalizing $w(1)$ and $w(3)$? The answer lies in the Q th-order super nested array which is introduced and studied in considerable detail in Chapter 4.

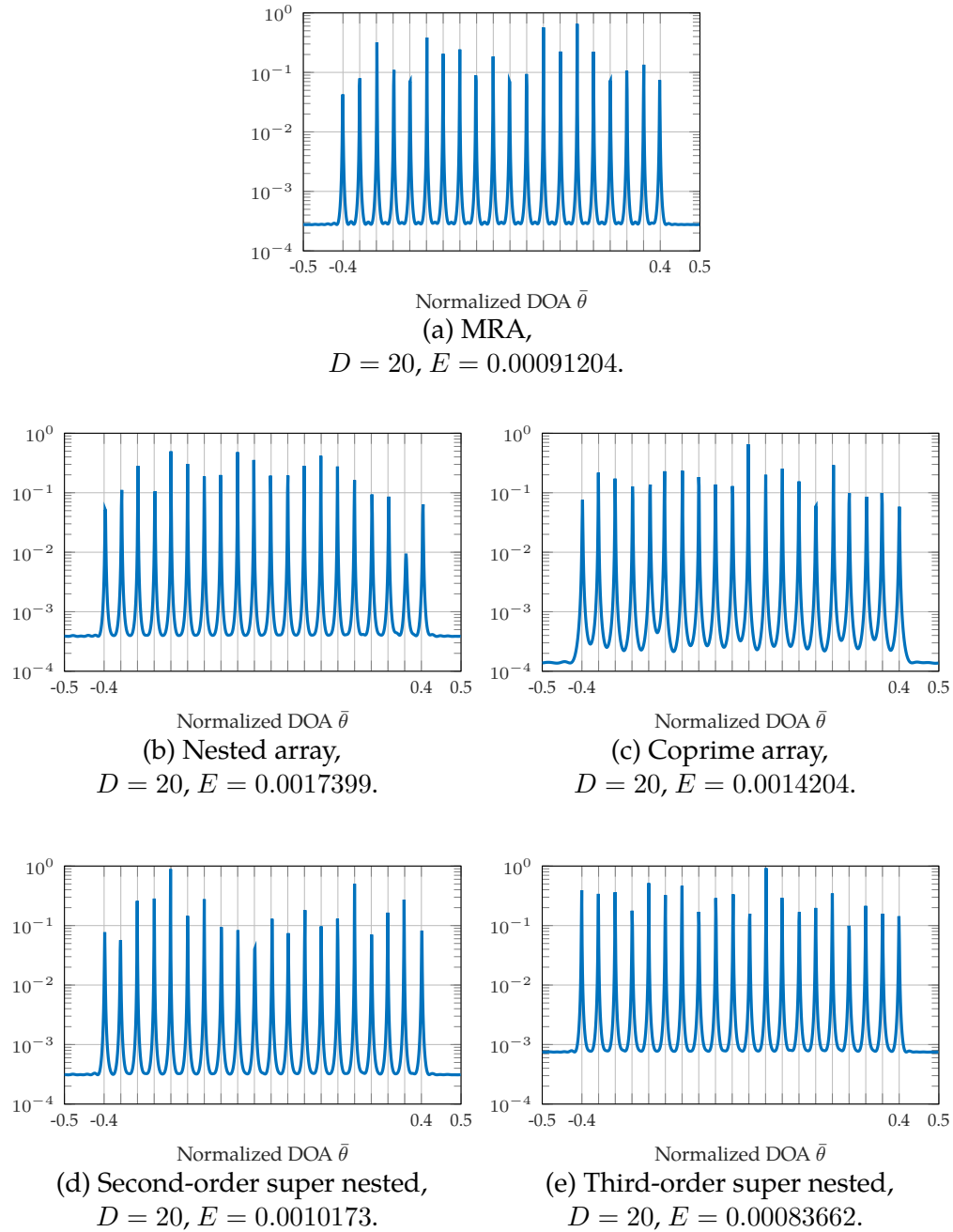


Figure 3.10: Based on the practical mutual coupling model (3.2), the MUSIC spectra $P(\bar{\theta})$ are listed for MRA, nested arrays, coprime arrays, second-order super nested arrays, and third-order super nested arrays, where $D = 20$ sources are located at $\bar{\theta}_i = -0.4 + 0.8(i - 1)/19$, $i = 1, 2, \dots, 20$. The SNR is 0 dB while the number of snapshots is $K = 500$. The parameters in (3.2) are given by $Z_A = Z_L = 50$ ohms and $l = \lambda/2$.

Chapter 4

HIGH ORDER SUPER NESTED ARRAYS

4.1 Introduction

In Chapter 3, a sparse array configuration called the (second-order) super nested array was introduced, which has many of the advantages of these sparse arrays, while removing some of the disadvantages. Namely, the sensor locations are well-defined and readily computed for any N (unlike MRAs), and the difference coarray is exactly that of a nested array, and therefore hole-free. At the same time, the mutual coupling is reduced compared to nested arrays. Super nested arrays were designed by rearranging the dense ULA part of a nested array in such a way that the coarray remains unchanged, but mutual coupling is reduced by reducing the number of elements with small inter-element spacings. Quantitatively, this is described in terms of the weight function $w(m)$, which is equal to the number of sensor pairs whose inter-element spacing is $m\lambda/2$. It was shown in Chapter 3 that the first three weight functions of second-order super nested arrays are

$$w(1) = \begin{cases} 2, & \text{if } N_1 \text{ is even,} \\ 1, & \text{if } N_1 \text{ is odd,} \end{cases} \quad (4.1)$$

$$w(2) = \begin{cases} N_1 - 3, & \text{if } N_1 \text{ is even,} \\ N_1 - 1, & \text{if } N_1 \text{ is odd,} \end{cases} \quad (4.2)$$

$$w(3) = \begin{cases} 3, & \text{if } N_1 = 4, 6, \\ 4, & \text{if } N_1 \text{ is even, } N_1 \geq 8, \\ 1, & \text{if } N_1 \text{ is odd.} \end{cases} \quad (4.3)$$

Contrast this with the nested array which has $w(1) = N_1$, $w(2) = N_1 - 1$ and $w(3) = N_1 - 2$. While $w(1)$ and $w(3)$ are significantly better in (4.1) and (4.3), there is plenty of room for improving $w(2)$, and possibly $w(m)$, $m > 3$.

In this chapter, a generalization of super nested arrays is introduced and called the *Qth-order super nested array*. It has all the good properties of the second-order super nested array with the additional advantage that mutual coupling effects are further reduced for $Q > 2$. For a given number of physical array elements N , Q th-order super nested arrays have the following properties: (a) the sensor locations can be defined using a simple algorithm, (b) the physical array has the same aperture as the nested array, (c) the difference coarray is exactly identical to that of the nested array

(hence hole free), and (d) the weight functions are further improved, compared even to second-order super nested arrays.

Like the parent nested array, the physical sensor locations of Q th-order super nested arrays are related to two integers N_1 and N_2 , as in Fig. 2.2(c). The detailed description of Q th-order super nested arrays depends on whether N_1 is even or odd. For odd N_1 , there is a simple closed-form expression for the sensor locations, but for even N_1 , the locations have to be defined recursively as we shall elaborate. A MATLAB code to find the sensor locations of Q th-order super nested arrays is given in [90]. The proof that Q th-order super nested arrays have a coarray identical to the parent nested array is rather involved, and one of the main goals of this chapter is to establish this very important result for both N_1 odd and N_1 even. We also analyze the weight functions $w(m)$ in great depth (again, quite involved in its detail because of the intricate definition of the array geometry). The good news is that it is possible to improve the crucial weights $w(1)$, $w(2)$, and $w(3)$, compared to nested arrays (see Theorem 4.3.2 and Theorem 4.4.2). In particular, $w(2)$ is only about half that of second-order super nested arrays.

Chapter Outline

Section 4.2 introduces Q th-order super nested arrays in terms of the parent nested array. The construction is based on some recursive rules to rearrange the sensors of nested arrays through successive systematic stages. In Section 4.3, we formally define Q th-order super nested arrays for odd N_1 . Many properties of these arrays are given, the highlights being (a) the result that the difference coarray is identical to that of the parent nested array (Theorem 4.3.1 and Corollary 4.3.1), and (b) that the weight functions (hence mutual coupling effects) are significantly reduced (Theorem 4.3.2). Since the details are considerably different for even N_1 , Section 4.4 is dedicated to a presentation of this case. Detailed proofs of some of the claims of Section 4.3 and 4.4 are relegated to Section 4.5 and 4.6, for ease of flow. Section 4.7 presents simulation results and detailed comparison of performances, demonstrating clearly that Q th-order super nested arrays with $Q > 2$ outperform other arrays in the presence of mutual coupling.

4.2 General Guidelines for the Construction of Super Nested Arrays

Fig. 4.1 summarizes the hierarchy among nested arrays, as in (2.7), second-order super nested arrays as in Definition 3.4.1, and Q th-order super nested arrays. It has been mentioned in Chapter 3 that the sets $\mathbb{X}_1^{(2)}$, $\mathbb{Y}_1^{(2)}$, $\mathbb{X}_2^{(2)}$, and $\mathbb{Y}_2^{(2)}$ are obtained by rearranging the dense ULA part of parent nested arrays, as in Lemma 3.4.1. The sparse ULA part of parent nested arrays is reorganized into $\mathbb{Z}_1^{(2)}$ and $\mathbb{Z}_2^{(2)}$ of second-order super nested arrays.

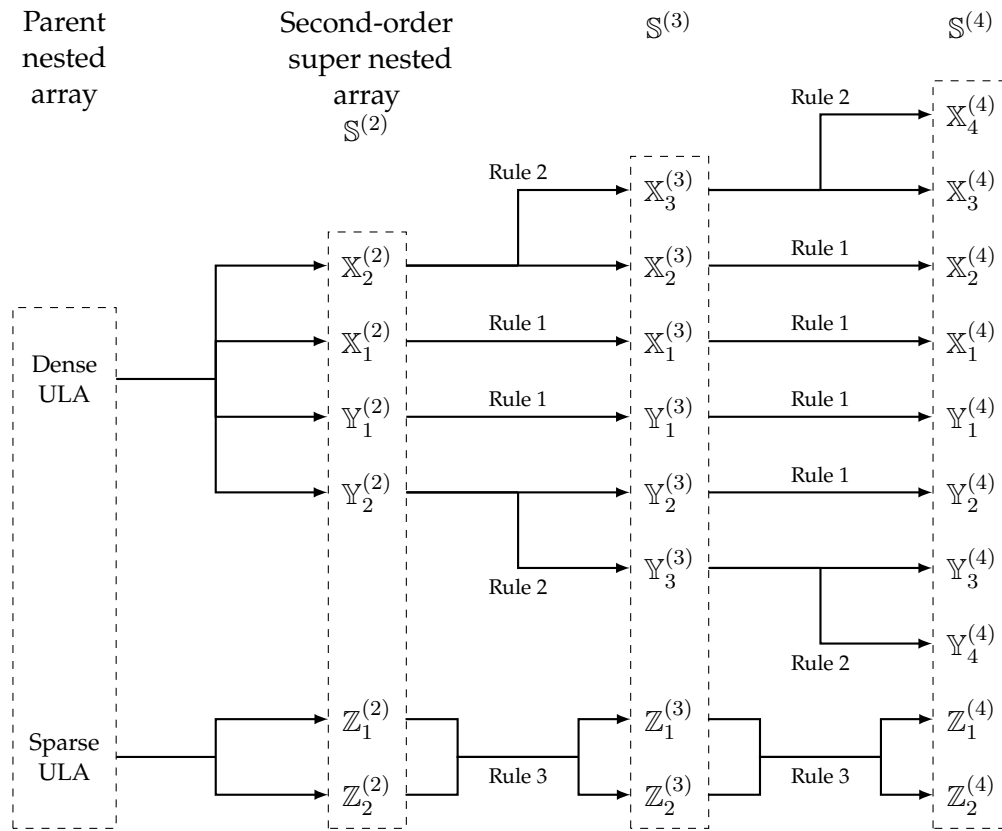


Figure 4.1: Hierarchy of nested arrays, second-order super nested arrays $\mathbb{S}^{(2)}$, and Q th-order super nested arrays $\mathbb{S}^{(Q)}$. Arrows indicate the origin of the given sets. For instance, $\mathbb{X}_2^{(4)}$ originates from $\mathbb{X}_2^{(3)}$ while $\mathbb{Y}_3^{(3)}$ is split into $\mathbb{Y}_3^{(4)}$ and $\mathbb{Y}_4^{(4)}$. It can be observed that the sets $\mathbb{X}_q^{(Q)}$ and $\mathbb{Y}_q^{(Q)}$ result from the dense ULA part of nested arrays. The sparse ULA portion of nested arrays is rearranged into the sets $\mathbb{Z}_1^{(Q)}$ and $\mathbb{Z}_2^{(Q)}$.

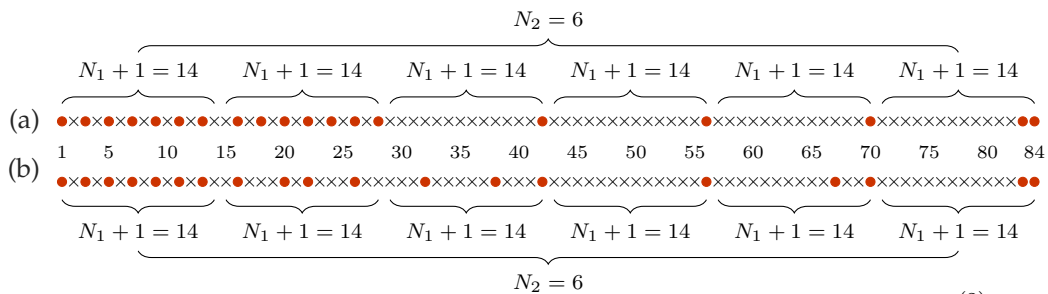


Figure 4.2: 1D representations of (a) second-order super nested arrays, $\mathbb{S}^{(2)}$, and (b) third-order super nested arrays, $\mathbb{S}^{(3)}$, where $N_1 = 13$ and $N_2 = 6$. Bullets denote sensor locations while crosses indicate empty locations.

The formal definition of Q th-order nested arrays will be given in the next section. To develop some feeling for it, first consider $Q = 3$. Third-order super nested arrays, as specified by the integer set $\mathbb{S}^{(3)}$, consist of eight sets as follows: $\mathbb{X}_1^{(3)}$, $\mathbb{Y}_1^{(3)}$, $\mathbb{X}_2^{(3)}$, $\mathbb{Y}_2^{(3)}$, $\mathbb{X}_3^{(3)}$, $\mathbb{Y}_3^{(3)}$, $\mathbb{Z}_1^{(3)}$, and $\mathbb{Z}_2^{(3)}$, which can be recursively generated from the sets $\mathbb{X}_1^{(2)}$, $\mathbb{Y}_1^{(2)}$, $\mathbb{X}_2^{(2)}$, $\mathbb{Y}_2^{(2)}$, $\mathbb{Z}_1^{(2)}$, and $\mathbb{Z}_2^{(2)}$ in second-order super nested arrays. For instance, $\mathbb{X}_1^{(3)}$ is identical to $\mathbb{X}_1^{(2)}$. $\mathbb{X}_2^{(2)}$ is split into two sets $\mathbb{X}_2^{(3)}$ and $\mathbb{X}_3^{(3)}$. The same connections also apply to $\mathbb{Y}_1^{(2)}$, $\mathbb{Y}_2^{(2)}$, $\mathbb{Y}_1^{(3)}$, $\mathbb{Y}_2^{(3)}$, and $\mathbb{Y}_3^{(3)}$. Finally, the elements in $\mathbb{Z}_1^{(2)}$ and $\mathbb{Z}_2^{(2)}$ are rearranged into $\mathbb{Z}_1^{(3)}$ and $\mathbb{Z}_2^{(3)}$. Hence, it can be interpreted that the sets $\mathbb{X}_q^{(3)}$ and $\mathbb{Y}_q^{(3)}$ for $q = 1, 2, 3$ originate from the dense ULA of parent nested arrays while $\mathbb{Z}_1^{(3)}$ and $\mathbb{Z}_2^{(3)}$ emanate from the sparse ULA of parent nested arrays.

Fourth-order super nested arrays (or super nested arrays with $Q = 4$) generalize third-order super nested arrays further. It can be deduced from Fig. 4.1 that $\mathbb{X}_3^{(3)}$ and $\mathbb{Y}_3^{(3)}$ are divided into $\mathbb{X}_3^{(4)}$, $\mathbb{X}_4^{(4)}$ and $\mathbb{Y}_3^{(4)}$, $\mathbb{Y}_4^{(4)}$, respectively. Similarly, $\mathbb{Z}_1^{(3)}$ and $\mathbb{Z}_2^{(3)}$ are rearranged into $\mathbb{Z}_1^{(4)}$ and $\mathbb{Z}_2^{(4)}$. The remaining sets of fourth-order super nested arrays are the same as their correspondences in third-order super nested arrays. To be more specific, the defining rules to go from $(Q - 1)$ th-order super nested arrays to Q th-order super nested arrays are

Rule 1: $\mathbb{X}_q^{(Q)}$ and $\mathbb{Y}_q^{(Q)}$ replicate $\mathbb{X}_q^{(Q-1)}$ and $\mathbb{Y}_q^{(Q-1)}$, respectively, for $1 \leq q \leq Q - 2$.

That is, we simply copy these portions from the $(Q - 1)$ th-order super nested array to the Q th-order super nested array.

Rule 2: $\mathbb{X}_{Q-1}^{(Q-1)}$ and $\mathbb{Y}_{Q-1}^{(Q-1)}$ are split into $\mathbb{X}_{Q-1}^{(Q)}$, $\mathbb{X}_Q^{(Q)}$ and $\mathbb{Y}_{Q-1}^{(Q)}$, $\mathbb{Y}_Q^{(Q)}$, respectively, according to rules to be specified in Sections 4.3 and 4.4.

Rule 3: $\mathbb{Z}_1^{(Q-1)}$ and $\mathbb{Z}_2^{(Q-1)}$ are reorganized into $\mathbb{Z}_1^{(Q)}$ and $\mathbb{Z}_2^{(Q)}$, using appropriate rules.

Next, we give a concrete example of how Q th-order super nested arrays are obtained from $(Q - 1)$ th-order super nested arrays. Figs. 4.2 and 4.3 depict the 1D/2D representations of the second-order super nested array (in parts (a)) and the third-order one (in parts (b)), respectively, where the details of 2D representations can be found in Fig. 3.1. In this example, it is obvious that $\mathbb{X}_1^{(2)} = \mathbb{X}_1^{(3)}$ and $\mathbb{Y}_1^{(2)} = \mathbb{Y}_1^{(3)}$, which satisfy Rule 1. To explain Rule 2, we consider the following sets in Fig. 4.3:

$$\mathbb{X}_2^{(2)} = \{16, 18, 20\}, \quad \mathbb{X}_2^{(3)} = \{16, 20\}, \quad \mathbb{X}_3^{(3)} = \{32\}. \quad (4.4)$$

The middle element of $\mathbb{X}_2^{(2)}$, which is the element 18 in this case, is selected and relocated to the third layer of 2D representations. It becomes the element 32 in $\mathbb{X}_3^{(3)}$. The remaining elements in $\mathbb{X}_2^{(2)}$, which correspond to sensor locations 16 and 20,

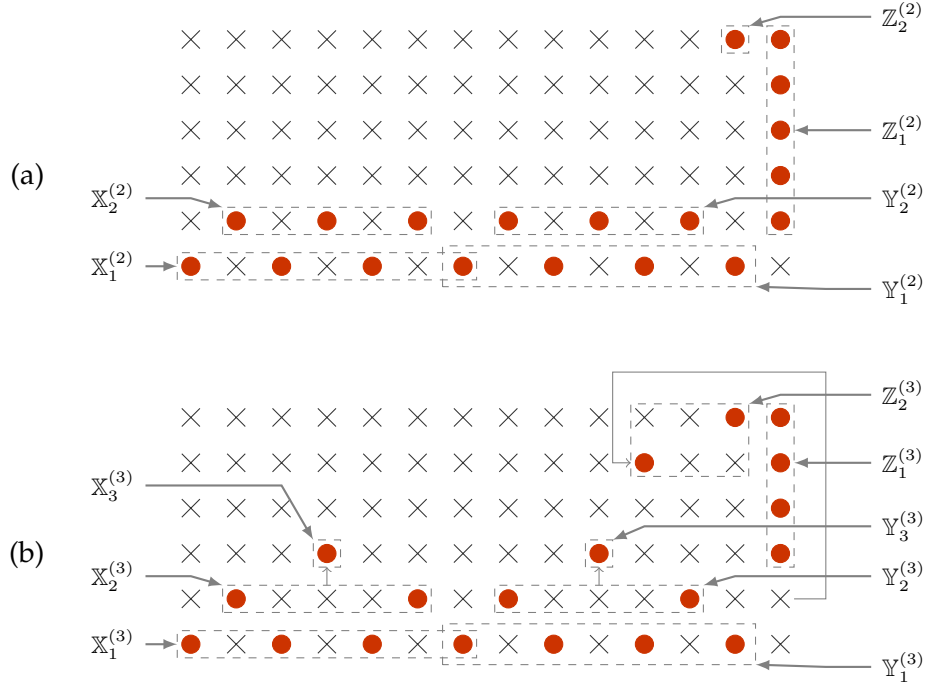


Figure 4.3: 2D representations of (a) second-order super nested arrays, $\mathbb{S}^{(2)}$, and (b) third-order super nested arrays, $\mathbb{S}^{(3)}$, where $N_1 = 13$ and $N_2 = 6$. Bullets denote sensor locations while crosses indicate empty locations. The dashed rectangles mark the sets $\mathbb{X}_q^{(Q)}$, $\mathbb{Y}_q^{(Q)}$, $\mathbb{Z}_1^{(Q)}$, and $\mathbb{Z}_2^{(Q)}$ for $1 \leq q \leq Q$. Thin arrows illustrate how sensors migrate from $\mathbb{S}^{(Q-1)}$ to $\mathbb{S}^{(Q)}$.

constitute $\mathbb{X}_2^{(3)}$. Finally, Rule 3 can also be clarified using Fig. 4.3. In the second-order super nested array, we consider the sensor located at $2(N_1 + 1) = 28$, which is the leftmost element of $\mathbb{Z}_1^{(2)}$. However, this sensor is removed from $\mathbb{S}^{(2)}$ and inserted to $\mathbb{S}^{(3)}$ at location 67, as indicated by a thin arrow in Fig. 4.3(b). This new sensor location is included in $\mathbb{Z}_2^{(3)} = \{67, 83\}$, which explains Rule 3. Furthermore, after all these operations, the first layer in 2D representations does not change while only some elements (18, 24, and 28 in Fig. 4.3) in the second layer are rearranged to somewhere else.

Summarizing, Q th-order super nested arrays can be recursively generated from $(Q - 1)$ th-order super nested arrays, as elaborated in Fig. 4.1. In the following two sections, based on the parameter N_1 , we will give formal definitions for super nested arrays, which are consistent with Rule 1, 2, and 3. These definitions also enable us to determine the sensor locations explicitly.

4.3 Q th-Order Super Nested Arrays, N_1 is Odd

Here is the formal definition of Q th-order super nested arrays if N_1 is an odd number:

Definition 4.3.1 (Q th-order super nested arrays, N_1 is odd). Let N_1 be an odd number, $N_2 \geq 2Q - 1$, and $Q \geq 1$. Q th-order super nested arrays are characterized by the integer set $\mathbb{S}^{(Q)}$, defined by

$$\mathbb{S}^{(Q)} = \left(\bigcup_{q=1}^Q \mathbb{X}_q^{(Q)} \cup \mathbb{Y}_q^{(Q)} \right) \cup \mathbb{Z}_1^{(Q)} \cup \mathbb{Z}_2^{(Q)}.$$

For a positive integer q satisfying $1 \leq q \leq Q$, $\mathbb{X}_q^{(Q)}$ and $\mathbb{Y}_q^{(Q)}$ are defined as

$$\begin{aligned} \mathbb{X}_q^{(Q)} &= \left\{ (q-1)(N_1+1) + 2^{q-1} + d_q^{(Q)}\ell : 0 \leq \ell \leq L_q^{(Q)} \right\}, \\ \mathbb{Y}_q^{(Q)} &= \left\{ q(N_1+1) - 2^{q-1} - d_q^{(Q)}\ell : 0 \leq \ell \leq L_q^{(Q)} \right\}, \\ d_q^{(Q)} &= \begin{cases} 2^q, & \text{if } q = 1, 2, \dots, Q-1, \\ 2^{Q-1}, & \text{if } q = Q, \end{cases} \\ L_q^{(Q)} &= \begin{cases} \lfloor \frac{1}{2} \left(\frac{N_1+1}{2^q} - 1 \right) \rfloor, & \text{if } q = 1, 2, \dots, Q-1, \\ \lfloor \frac{N_1+1}{2^Q} - 1 \rfloor, & \text{if } q = Q, \end{cases} \end{aligned}$$

where $\lfloor \cdot \rfloor$ is the floor function. $\mathbb{Z}_1^{(Q)}$ and $\mathbb{Z}_2^{(Q)}$ are given by

$$\begin{aligned} \mathbb{Z}_1^{(Q)} &= \{ \ell(N_1+1) : Q \leq \ell \leq N_2 \}, \\ \mathbb{Z}_2^{(Q)} &= \{ (N_2+1-q)(N_1+1) - 2^q + 1 : 1 \leq q \leq Q-1 \}. \end{aligned}$$

For convenience of the reader, here is a MATLAB code for Q th-order super nested arrays [90]. In particular, `super_nested.m` returns the set $\mathbb{S}^{(Q)}$ given the array parameters N_1 , N_2 , and Q .

If $Q = 1$, the corresponding array configuration degenerates to nested arrays with parameter N_1 and N_2 . Putting $Q = 2$ in Definition 4.3.1 gives us Definition 3.4.1¹. For any pair of N_1 , N_2 , and Q satisfying the assumption of Definition 4.3.1, super nested arrays can be characterized in a closed-form and scalable fashion.

It can be inferred from Definition 4.3.1 that the inter-element spacing of $\mathbb{X}_q^{(Q)}$, $\mathbb{Y}_q^{(Q)}$, and $\mathbb{Z}_1^{(Q)}$ are $d_q^{(Q)}$, $d_q^{(Q)}$, N_1+1 , respectively. For instance, in Fig. 4.3(b), it can be seen that $\mathbb{X}_1^{(3)}$ and $\mathbb{Y}_1^{(3)}$ are ULA with sensor separation 2. The sensor separation for $\mathbb{X}_2^{(3)}$ and $\mathbb{Y}_2^{(3)}$ is $d_2^{(3)} = 4$. $\mathbb{Z}_1^{(3)}$ is a ULA of sensor separation $N_1+1 = 14$. This property is very similar to second-order super nested arrays. Notice from Fig. 4.3(a) that $\mathbb{S}^{(2)}$ consists of a set of ULAs $\mathbb{X}_1^{(2)}$, $\mathbb{X}_2^{(2)}$, $\mathbb{Y}_1^{(2)}$, and $\mathbb{Y}_2^{(2)}$, each with sensor separation 2, another ULA $\mathbb{Z}_1^{(2)}$ with sensor separation $N_1+1 = 14$, and finally a singleton $\mathbb{Z}_2^{(2)}$.

¹ Here $\mathbb{X}_q^{(2)}$ and $\mathbb{Y}_q^{(2)}$ for $q = 1, 2$, could be slightly different across Definitions 3.4.1 and 4.3.1. In Definition 3.4.1, these sets are disjoint while in Definition 4.3.1, they might not be disjoint. Even so, both definitions lead to the same $\mathbb{S}^{(2)}$ but the latter one possesses the symmetric property: $|\mathbb{X}_q^{(2)}| = |\mathbb{Y}_q^{(2)}|$, which will be more useful in the following development.

Now we show that if an array is constructed according to Definition 4.3.1, then it satisfies Rule 1, 2, and 3 in Section 4.2. This statement is obviously true for Rule 1. For Rule 2 and 3, the details can be clarified by the following two lemmas:

Lemma 4.3.1. Let N_1 be an odd number and $\mathbb{S}^{(Q)}$ be a super nested array with order Q , as defined in Definition 4.3.1. Then $\mathbb{X}_{Q-1}^{(Q)}$ is composed of even terms (related to even ℓ) of $\mathbb{X}_{Q-1}^{(Q-1)}$ and $\mathbb{X}_Q^{(Q)} - (N_1 + 1)$ consists of odd terms (related to odd ℓ) of $\mathbb{X}_{Q-1}^{(Q-1)}$. These properties also hold true for $\mathbb{Y}_{Q-1}^{(Q-1)}$, $\mathbb{Y}_{Q-1}^{(Q)}$, and $\mathbb{Y}_Q^{(Q)}$.

Proof. According to Definition 4.3.1, any element in $\mathbb{X}_{Q-1}^{(Q-1)}$ can be written as $(Q - 2)(N_1 + 1) + 2^{Q-2} + 2^{Q-2}\ell$ where $0 \leq \ell \leq L_{Q-1}^{(Q-1)}$. If $\ell = 2k$ is an even number, we obtain

$$\begin{aligned} & (Q - 2)(N_1 + 1) + 2^{Q-2} + 2^{Q-1}k \\ &= (Q - 2)(N_1 + 1) + 2^{Q-2} + d_{Q-1}^{(Q)}k, \end{aligned}$$

where $0 \leq k \leq \frac{1}{2}L_{Q-1}^{(Q-1)}$. Since k is an integer and $\lfloor x \rfloor \leq \frac{1}{2} \lfloor 2x \rfloor < \lfloor x \rfloor + 1$, $0 \leq k \leq \frac{1}{2}L_{Q-1}^{(Q-1)}$ is equivalent to $0 \leq k \leq L_{Q-1}^{(Q)}$. That is, even terms of $\mathbb{X}_{Q-1}^{(Q-1)}$ are exactly $\mathbb{X}_{Q-1}^{(Q)}$.

If $\ell = 2k + 1$ is an odd number, the elements are

$$\begin{aligned} & (Q - 2)(N_1 + 1) + 2^{Q-2} + 2^{Q-2}(2k + 1) \\ &= \left[(Q - 1)(N_1 + 1) + 2^{Q-1} + d_Q^{(Q)}k \right] - (N_1 + 1), \end{aligned}$$

where k is a nonnegative integer with $0 \leq 2k + 1 \leq L_{Q-1}^{(Q-1)}$. The range of k can be rearranged to be $0 \leq k \leq L_Q^{(Q)}$ because $\lfloor x \rfloor \leq \frac{1}{2} \lfloor 2x \rfloor < \lfloor x \rfloor + 1$. It can be deduced that odd terms in $\mathbb{X}_{Q-1}^{(Q-1)}$ are exactly $\mathbb{X}_Q^{(Q)} - (N_1 + 1)$. The proof for $\mathbb{Y}_{Q-1}^{(Q-1)}$, $\mathbb{Y}_{Q-1}^{(Q)}$, and $\mathbb{Y}_Q^{(Q)}$ is similar. \square

Lemma 4.3.2. Let N_1 be an odd number. Assume that $\mathbb{Z}_1^{(Q)}$ and $\mathbb{Z}_2^{(Q)}$ satisfy Definition 4.3.1. Then

$$\begin{aligned} \mathbb{Z}_1^{(Q)} &= \mathbb{Z}_1^{(Q-1)} \setminus \{(Q-1)(N_1+1)\}, \\ \mathbb{Z}_2^{(Q)} &= \mathbb{Z}_2^{(Q-1)} \cup \{(N_2+1-(Q-1))(N_1+1)-2^{Q-1}+1\}, \end{aligned}$$

where $\mathbb{A} \setminus \mathbb{B}$ denotes the relative complement of \mathbb{B} in \mathbb{A} .

Proof. This proof follows from Definition 4.3.1 directly. \square

We now prove that the $\mathbb{X}_q^{(Q)}$ and the $\mathbb{Y}_q^{(Q)}$ parts of the super nested array, reduced modulo $N_1 + 1$ are exactly equal to the dense part of the parent nested array:

Lemma 4.3.3 (Relation to dense ULA of nested array). Let $\mathbb{X}_q^{(Q)}$ and $\mathbb{Y}_q^{(Q)}$ for $q = 1, 2, \dots, Q$ be defined in Definition 4.3.1. Define the sets $\mathbb{A}_q^{(Q)} = \mathbb{X}_q^{(Q)} - (q-1)(N_1+1)$ and $\mathbb{B}_q^{(Q)} = \mathbb{Y}_q^{(Q)} - (q-1)(N_1+1)$. Then

$$\bigcup_{q=1}^Q \mathbb{A}_q^{(Q)} \cup \mathbb{B}_q^{(Q)} = \{1, 2, \dots, N_1\}.$$

Proof. This lemma is proved using induction on Q since when $Q = 2$, Lemma 3.4.1 holds true. Assuming Lemma 4.3.3 holds for $Q - 1$, the case of Q becomes

$$\begin{aligned} \bigcup_{q=1}^Q \mathbb{A}_q^{(Q)} \cup \mathbb{B}_q^{(Q)} &= \bigcup_{q=1}^{Q-2} \mathbb{A}_q^{(Q)} \cup \mathbb{B}_q^{(Q)} \\ &\cup \left((\mathbb{X}_{Q-1}^{(Q)} \cup (\mathbb{X}_Q^{(Q)} - (N_1+1))) - (Q-2)(N_1+1) \right) \\ &\cup \left((\mathbb{Y}_{Q-1}^{(Q)} \cup (\mathbb{Y}_Q^{(Q)} - (N_1+1))) - (Q-2)(N_1+1) \right) \\ &= \left(\bigcup_{q=1}^{Q-2} \mathbb{A}_q^{(Q-1)} \cup \mathbb{B}_q^{(Q-1)} \right) \cup (\mathbb{X}_{Q-1}^{(Q-1)} - (Q-2)(N_1+1)) \\ &\cup (\mathbb{Y}_{Q-1}^{(Q-1)} - (Q-2)(N_1+1)) \\ &= \bigcup_{q=1}^{Q-1} \mathbb{A}_q^{(Q-1)} \cup \mathbb{B}_q^{(Q-1)} = \{1, 2, \dots, N_1\}. \end{aligned} \quad (4.5)$$

Here Rule 1 and Lemma 4.3.1 are utilized. \square

Lemma 4.3.4 (Total number of sensors). If N_1 is an odd number, the number of elements in $\mathbb{S}^{(Q)}$, as defined in Definition 4.3.1, is $N_1 + N_2$.

Proof. The proof is given by induction on Q . According to Lemma 3.4.2, the cardinality of $\mathbb{S}^{(2)}$ is $N_1 + N_2$. If $\mathbb{S}^{(Q-1)}$ has cardinality $N_1 + N_2$, we will show that $\mathbb{S}^{(Q)}$ also has cardinality $N_1 + N_2$. According to Rule 1, the number of elements in $\mathbb{X}_q^{(Q)}$ and $\mathbb{Y}_q^{(Q)}$ for $1 \leq q \leq Q - 2$ remains unchanged in $\mathbb{S}^{(Q-1)}$ and $\mathbb{S}^{(Q)}$. Lemma 4.3.1 does not alter the total number of elements since $\mathbb{X}_{Q-1}^{(Q)}$ and $\mathbb{X}_Q^{(Q)} - (N_1+1)$ correspond to the even and odd terms in $\mathbb{X}_{Q-1}^{(Q-1)}$, respectively. It is also evident that Lemma 4.3.2 preserves the total number of sensors. By induction, $|\mathbb{S}^{(Q)}| = |\mathbb{S}^{(Q-1)}| = N_1 + N_2$ for $Q \geq 2$. \square

One of the most striking properties of the Q th-order super nested array is that the coarray is exactly identical to that of the parent nested array. This is proved in the following theorem and the corollary:

Theorem 4.3.1. If $N_1 \geq 3 \cdot 2^Q - 1$ is an odd number, $N_2 \geq 3Q - 4$, and $Q \geq 3$, then Q th-order super nested arrays are restricted arrays, i.e., the difference coarray is hole-free.

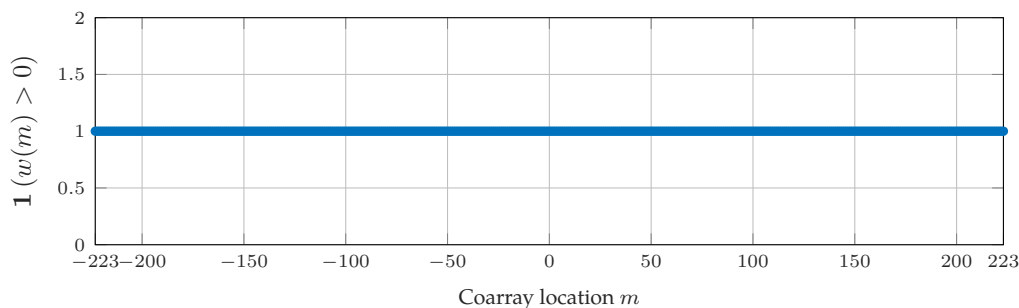
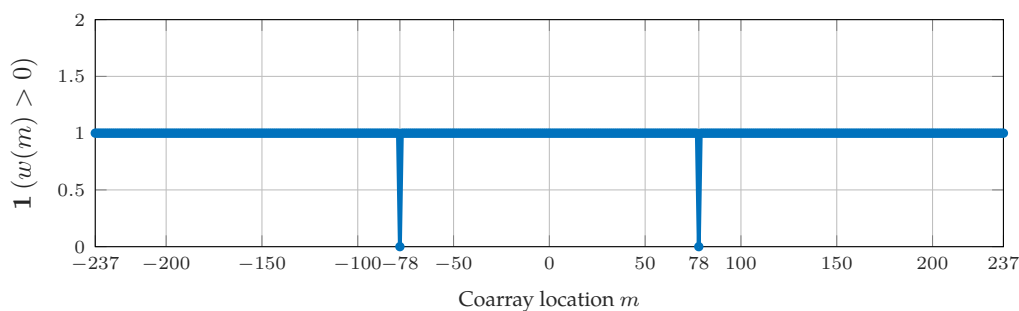
(a) $N_1 = 31, N_2 = 7, Q = 5$.(b) $N_1 = 33, N_2 = 7, Q = 5$.

Figure 4.4: An example to show that $N_1 \geq 3 \cdot 2^Q - 1$ is not necessary in order to make the coarray of $\mathbb{S}^{(Q)}$ hole free. Here we consider the indicator function of $w(m) > 0$ for the super nested array with (a) $N_1 = 31, N_2 = 7, Q = 5$ and (b) $N_1 = 33, N_2 = 7, Q = 5$. It can be inferred that (a) is a restricted array, because $w(m) > 0$ for $-223 \leq m \leq 223$. However, (b) is not a restricted array since $w(78) = w(-78) = 0$.

Proof. This proof is based on induction on Q . Beginning with Theorem 3.5.1, we know $\mathbb{S}^{(2)}$ are restricted arrays. If $(Q - 1)$ th-order super nested arrays are restricted arrays, it can be inferred that Q th-order super nested arrays are still restricted arrays. The details are quite involved, and can be found in Section 4.5. \square

Corollary 4.3.1. If $N_1 \geq 3 \cdot 2^Q - 1$ is an odd number, $N_2 \geq 3Q - 4$, and $Q \geq 3$, then Q th-order super nested arrays have the same coarray as their parent nested array.

Proof. Due to Theorem 4.3.1, applying the chain of arguments in Corollary 3.5.1 proves this corollary. \square

The *sufficient* conditions on N_1, N_2 , and Q in Theorem 4.3.1 guarantee that such array configuration is a restricted array. However, these conditions are not necessary. For instance, Fig. 4.4 examines the coarray of Q th-order super nested arrays if (a) $N_1 = 31, N_2 = 7, Q = 5$ and (b) $N_1 = 33, N_2 = 7, Q = 5$, where the indicator

function $\mathbf{1}(P)$ is 1 if the statement P is true and 0 if P is false. Theorem 4.3.1 requires N_1 to be at least $3 \cdot 2^Q - 1 = 95$. In Fig. 4.4(a) ($N_1 = 31 < 95$), it can be inferred that $w(m) > 0$ for $-223 \leq m \leq 223$ so this array configuration is a restricted array. On the other hand, the array in Fig. 4.4(b) ($N_1 = 33 < 95$) is not a restricted array since $w(78) = w(-78) = 0$.

Recall that the weight function $w(2)$ of the second-order super nested array was as in Eq. (4.2). The next theorem shows that the super nested array for $Q > 2$ has significantly improved weight function $w(2)$, which is crucial to reducing the mutual coupling effects.

Theorem 4.3.2. Assume that $N_1 \geq 3 \cdot 2^Q - 1$ is an odd number, $N_2 \geq 3Q - 4$, and $Q \geq 3$. The weight function $w(m)$ of Q th-order super nested arrays satisfies

$$w(1) = 1, \quad w(2) = 2 \left\lfloor \frac{N_1}{4} \right\rfloor + 1, \quad w(3) = 2.$$

Proof. For $m = 1$, the sensors located at $N_2(N_1 + 1) - 1$ and $N_2(N_1 + 1)$ contribute to $w(1)$. We need to show other combinations do not result in $w(1)$. It is obvious that the self-differences among $\mathbb{X}_q^{(Q)}$, $\mathbb{Y}_q^{(Q)}$, $\mathbb{Z}_1^{(Q)}$, and $\mathbb{Z}_2^{(Q)}$ have sensor separation at least 2. Since these sets are defined in the increasing order, it suffices to show that the difference between the maximum element in one set and the minimum element in the succeeding set, is strictly greater than 1. Assume $\mathbb{X}_q^{(Q)}$ and $\mathbb{Y}_q^{(Q)}$ satisfies $\min(\mathbb{Y}_q^{(Q)}) - \max(\mathbb{X}_q^{(Q)}) = 1$. We have $L_q^{(Q)} = (N_1 - 2^q)/(2d_q^{(Q)})$. This is a contradiction since $L_q^{(Q)}$ is an integer but $(N_1 - 2^q)/(2d_q^{(Q)})$ is not, if N_1 is an odd number. On the other hand, it is obvious that $\mathbb{Y}_q^{(Q)}$ and $\mathbb{X}_{q+1}^{(Q)}$ do not cause $w(1)$.

Next, $w(2)$ results from the self difference in $\mathbb{X}_1^{(Q)} \cup \mathbb{Y}_1^{(Q)}$. First, we check the difference between $\min(\mathbb{Y}_1^{(Q)})$ and $\max(\mathbb{X}_1^{(Q)})$:

$$\min(\mathbb{Y}_1^{(Q)}) - \max(\mathbb{X}_1^{(Q)}) = \begin{cases} 0, & \text{if } N_1 = 4r + 1, \\ 2, & \text{if } N_1 = 4r + 3. \end{cases} \quad (4.6)$$

Besides, consider the sensor pair located at $(q - 1)(N_1 + 1) + 2L_1^{(Q)} \in \mathbb{X}_q^{(Q)}$ and $q(N_1 + 1) - 2L_1^{(Q)} \in \mathbb{Y}_q^{(Q)}$ for some $2 \leq q \leq Q$. The exact value of q can be uniquely solved from the definitions of $\mathbb{X}_q^{(Q)}$ and $\mathbb{Y}_q^{(Q)}$. Their difference becomes

$$\begin{aligned} & (q(N_1 + 1) - 2L_1^{(Q)}) - ((q - 1)(N_1 + 1) + 2L_1^{(Q)}) \\ &= \begin{cases} 2, & \text{if } N_1 = 4r + 1, \\ 4, & \text{if } N_1 = 4r + 3. \end{cases} \end{aligned} \quad (4.7)$$

If $N_1 = 4r + 1$, there are $L_1^{(Q)}$ pairs in $\mathbb{X}_1^{(Q)}$ and $L_1^{(Q)}$ in $\mathbb{Y}_1^{(Q)}$ with separation 2. One more pair can be found in (4.7). In this case, $w(2)$ becomes

$$w(2) = 2L_1^{(Q)} + 1 = 2r + 1 = 2 \left\lfloor \frac{N_1}{4} \right\rfloor + 1.$$

On the other hand, according to (4.6), if $N_1 = 4r + 3$, $w(2)$ can be written as

$$w(2) = 2L_1^{(Q)} + 1 = 2r + 1 = 2 \left\lfloor \frac{N_1}{4} \right\rfloor + 1.$$

When $m = 3$, $w(3)$ results from the following two pairs:

1. $\min(\mathbb{X}_2^{(Q)})$ and $\max(\mathbb{Y}_1^{(Q)})$. The difference is

$$[(N_1 + 1) + 2] - [(N_1 + 1) - 1] = 3.$$

2. $\mathbb{Z}_1^{(Q)}$ and $\mathbb{Z}_2^{(Q)}$. We obtain

$$(N_2 - 1)(N_1 + 1) - [(N_2 - 1)(N_1 + 1) - 3] = 3,$$

which completes the proof. □

4.4 Q th-Order Super-Nested Arrays, N_1 is Even

For odd N_1 , we presented three recursive rules between $\mathbb{S}^{(Q)}$ and $\mathbb{S}^{(Q-1)}$, as described in Fig. 4.3, Lemma 4.3.1, and Lemma 4.3.2. For even N_1 , the framework in Fig. 4.1 still holds true but the details in Rule 2 are different from Lemma 4.3.1.

As an example, Fig. 4.5 displays 2D representations of super nested arrays with $N_1 = 16$ and $N_2 = 5$. The recursive rules are depicted by thin arrows in Fig. 4.5(b). First, the following sets are considered:

$$\mathbb{X}_2^{(2)} = \{19, 21, 23, 25\}, \mathbb{X}_2^{(3)} = \{19, 23, 25\}, \mathbb{X}_3^{(3)} = \{38\}. \quad (4.8)$$

It is clear that (4.8) justifies Rule 2 in Fig. 4.1. However, (4.8) does not satisfy Lemma 4.3.1 since $\mathbb{X}_2^{(3)}$ contains an odd term, which is the element 25 in this example. On the other hand, Fig. 4.5 gives $\mathbb{Z}_1^{(2)} = \{34, 51, 68, 85\}$, $\mathbb{Z}_2^{(2)} = \{84\}$, $\mathbb{Z}_1^{(3)} = \{51, 68, 85\}$, and $\mathbb{Z}_2^{(3)} = \{65, 84\}$. It can be readily shown that these sets satisfy Rule 3 and Lemma 4.3.2 precisely.

Hence, it can be inferred from Fig. 4.5 that for even N_1 , $\mathbb{S}^{(Q)}$ can be still generated from $\mathbb{S}^{(Q-1)}$ using three recursive rules. Rule 1 and Rule 3 can be utilized directly but Rule 2 needs further development. The formal definition of super nested arrays when N_1 is even is now given in a recursive manner as follows:

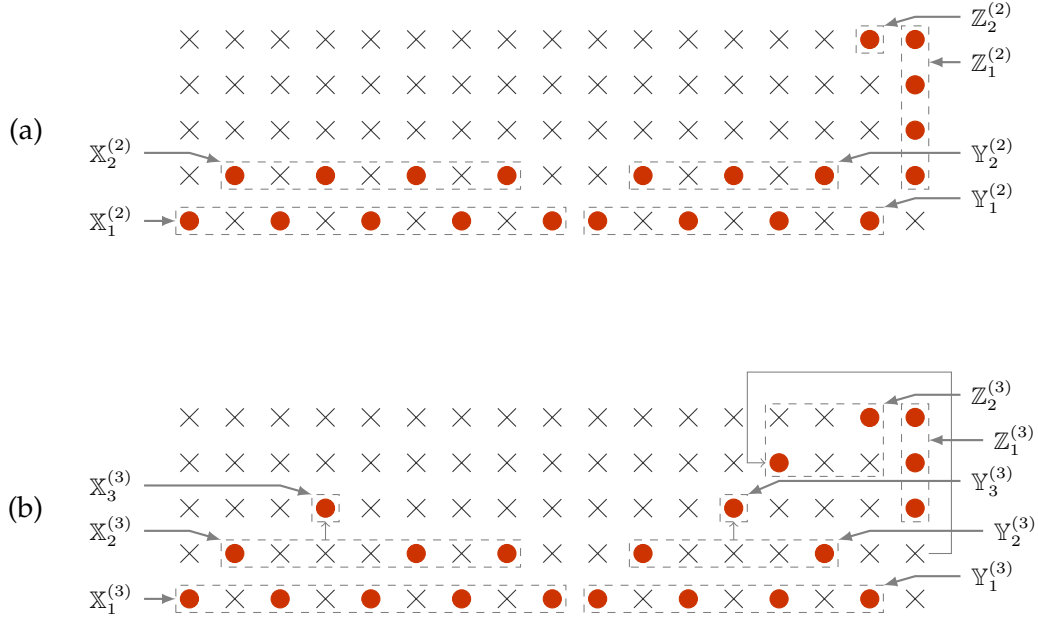


Figure 4.5: 2D representations of (a) the second-order super nested array $\mathbb{S}^{(2)}$ and (b) the third-order super nested array $\mathbb{S}^{(3)}$, where $N_1 = 16$ (even) and $N_2 = 5$. Bullets represent physical sensors while crosses denote empty space. Thin arrows illustrate the recursive rules (Rule 2 and Rule 3) in Fig. 4.1.

Definition 4.4.1 (Q th-order super nested arrays, N_1 is even). Let N_1 be an even number, $N_2 \geq 2Q$, and $Q \geq 3$. A Q th-order super nested array is specified by the integer set $\mathbb{S}^{(Q)}$,

$$\mathbb{S}^{(Q)} = \left(\bigcup_{q=1}^Q \mathbb{X}_q^{(Q)} \cup \mathbb{Y}_q^{(Q)} \right) \cup \mathbb{Z}_1^{(Q)} \cup \mathbb{Z}_2^{(Q)}.$$

These nonempty subsets $\mathbb{X}_q^{(Q)}$, $\mathbb{Y}_q^{(Q)}$, $\mathbb{Z}_1^{(Q)}$, and $\mathbb{Z}_2^{(Q)}$ satisfy

1. **(Rule 1)** For $1 \leq q \leq Q - 2$, $\mathbb{X}_q^{(Q)} = \mathbb{X}_q^{(Q-1)}$.
2. **(Rule 2)** $\mathbb{X}_{Q-1}^{(Q)}$ and $\mathbb{X}_Q^{(Q)}$ can be obtained from $\mathbb{X}_{Q-1}^{(Q-1)}$ by
 - a) If the cardinality of $\mathbb{X}_{Q-1}^{(Q-1)}$ is odd, then

$$\begin{aligned} \mathbb{X}_{Q-1}^{(Q)} &= \{\text{Even terms of } \mathbb{X}_{Q-1}^{(Q-1)}\}, \\ \mathbb{X}_Q^{(Q)} &= \{(\text{Odd terms of } \mathbb{X}_{Q-1}^{(Q-1)}) + (N_1 + 1)\}, \end{aligned}$$

where the definition of even/odd terms are consistent with Lemma 4.3.1.

b) Otherwise, we call the last element in $\mathbb{X}_{Q-1}^{(Q-1)}$ as the **extra term**. Then

$$\begin{aligned}\mathbb{X}_{Q-1}^{(Q)} &= \{\text{Even terms of } \mathbb{X}_{Q-1}^{(Q-1)}\} \cup \{\text{the extra term}\}, \\ \mathbb{X}_Q^{(Q)} &= \{(\text{Odd terms of } \mathbb{X}_{Q-1}^{(Q-1)}, \text{ except the extra term}) \\ &\quad + (N_1 + 1)\}.\end{aligned}$$

$\mathbb{Y}_q^{(Q)}$ share similar properties as $\mathbb{X}_q^{(Q)}$ in Rule 1 and 2.

3. **(Rule 3)** The sets $\mathbb{Z}_1^{(Q)}$ and $\mathbb{Z}_2^{(Q)}$ are given by

$$\begin{aligned}\mathbb{Z}_1^{(Q)} &= \{\ell(N_1 + 1) : Q \leq \ell \leq N_2\}, \\ \mathbb{Z}_2^{(Q)} &= \{(N_2 + 1 - q)(N_1 + 1) - 2^q + 1 : 1 \leq q \leq Q - 1\},\end{aligned}$$

which is equivalent to the recursive formula in Lemma 4.3.2.

A MATLAB code for Definition 4.4.1 is included in `super_nested.m` [90], where the input parameters are N_1 , N_2 , and Q and the sensor locations $\mathbb{S}^{(Q)}$ are delivered as output. This function first takes second-order super nested arrays $\mathbb{S}^{(2)}$ as an initial condition, then applies Definition 4.4.1 multiple times to obtain $\mathbb{S}^{(3)}$, $\mathbb{S}^{(4)}$, up to $\mathbb{S}^{(Q)}$.

Next, we will clarify Rule 2 in Definition 4.4.1 using Fig. 4.5. According to (4.8), the cardinality of $\mathbb{X}_2^{(2)}$ is 4 so Rule 2b is applicable. For $\mathbb{X}_2^{(2)}$, the extra term is 25, the even terms are 19 and 23, and the odd terms are 21 and 25. Using the expressions in Rule 2b of Definition 4.4.1, we obtain $\mathbb{X}_2^{(3)}$ and $\mathbb{X}_3^{(3)}$, which are identical to (4.8). On the other hand, if we consider $\mathbb{Y}_2^{(2)} = \{28, 30, 32\}$ in Fig. 4.5, then the cardinality of $\mathbb{Y}_2^{(2)}$ becomes 3, implying Rule 2a is applicable. The even terms and odd terms of $\mathbb{Y}_2^{(2)}$ are 28, 32 and 30, respectively. As a result, $\mathbb{Y}_2^{(3)} = \{28, 32\}$ and $\mathbb{Y}_3^{(3)} = \{47\}$, which are consistent with Fig. 4.5.

In short, for even N_1 , super nested arrays are defined in a recursive fashion (Definition 4.4.1). The only dissimilarity from the odd N_1 case is that, sometimes the extra terms need to be considered (Rule 2b of Definition 4.4.1).

Next we will prove some important properties which result from Definition 4.4.1 of the super nested array.

Lemma 4.4.1 (Relation to dense ULA of nested array). Let $\mathbb{S}^{(Q)}$ be a super nested array, as defined in Definition 4.4.1, when N_1 is an even number. Let $\mathbb{A}_q^{(Q)} = \mathbb{X}_q^{(Q)} - (q - 1)(N_1 + 1)$ and $\mathbb{B}_q^{(Q)} = \mathbb{Y}_q^{(Q)} - (q - 1)(N_1 + 1)$ for $q = 1, 2, \dots, Q$. Then

$$\bigcup_{q=1}^Q \mathbb{A}_q^{(Q)} \cup \mathbb{B}_q^{(Q)} = \{1, 2, \dots, N_1\}.$$

Proof. First by Lemma 3.4.1, we know this lemma is true for $Q = 2$. Then we use proof by induction. Based on Rule 2 of Definition 4.4.1, $\mathbb{X}_{Q-1}^{(Q)} \cup (\mathbb{X}_Q^{(Q)} - (N_1 + 1)) = \mathbb{X}_{Q-1}^{(Q-1)}$ and $\mathbb{Y}_{Q-1}^{(Q)} \cup (\mathbb{Y}_Q^{(Q)} - (N_1 + 1)) = \mathbb{Y}_{Q-1}^{(Q-1)}$. Therefore, the argument in the proof of Lemma 4.3.3 can be applied. \square

Lemma 4.4.2 (Total number of sensors). Let $\mathbb{S}^{(Q)}$ be a Q th-order super nested array defined by Definition 4.4.1. Then $|\mathbb{S}^{(Q)}| = N_1 + N_2$.

Proof. The proof is the same as that of Lemma 4.3.4. \square

The coarray of the Q th-order super nested array is identical to that of the parent nested array. This was proved earlier for odd N_1 . The same is true for even N_1 , as shown by the theorem and corollary below.

Theorem 4.4.1. If $N_1 \geq 2 \cdot 2^Q + 2$ is an even number, $N_2 \geq 3Q - 4$, $Q \geq 3$, then Q th-order super nested arrays are restricted arrays. That is, their coarray is hole-free.

Proof. The proof is similar to that of Theorem 4.3.1. The details are quite involved, and are presented in Section 4.6. \square

Corollary 4.4.1. If $N_1 \geq 2 \cdot 2^Q + 2$ is an even number, $N_2 \geq 3Q - 4$, $Q \geq 3$, then Q th-order super nested arrays have the same coarray as the parent nested arrays.

Proof. This proof is identical to that of Corollary 4.3.1. \square

The next theorem shows that the super nested array for $Q > 2$ has significantly improved weight function $w(2)$, which is crucial to reducing the mutual coupling effects.

Theorem 4.4.2. Assume that $N_1 \geq 2 \cdot 2^Q + 2$ is an even number, $N_2 \geq 3Q - 4$, and $Q \geq 3$. Then, the weight function $w(m)$ of Q th-order super nested arrays satisfies

$$\begin{aligned} w(1) &= 2, \\ w(2) &= \begin{cases} \frac{N_1}{2} + 1, & \text{if } N_1 = 8k - 2, \\ \frac{N_1}{2} - 1, & \text{if } N_1 = 8k + 2, \\ \frac{N_1}{2}, & \text{otherwise,} \end{cases} \\ w(3) &= 5, \end{aligned}$$

where k is an integer.

Proof. The proof is quite similar to that of Theorem 3.5.2 and Theorem 4.3.2. The parameters A_1, B_1, A_2, B_2 follow Definition 3.4.1. For $w(1)$, the two sensor pairs are identical to those in the second-order ones, which have been identified in the proof of Theorem 3.5.2.

For the weight function $w(2)$, there are some cases:

1. The self-differences of $\mathbb{X}_1^{(Q)}$ and $\mathbb{Y}_1^{(Q)}$ contribute to $(A_1)_+ + (B_1)_+$ pairs, which is $N_1/2 - 1$.
2. If $N_1 = 4r$, then $A_2 = r - 1$ and $B_2 = r - 2$. If $A_2 + 1$ is even, there is an extra term in $\mathbb{X}_2^{(Q)}$. Note that the maximum ULA element in $\mathbb{X}_2^{(Q)}$ is less than the extra term by 2, as indicated in Lemma 4.6.1-3. The similar conclusion applies to $\mathbb{Y}_2^{(Q)}$. Hence, depending on the even/odd properties of A_2 and B_2 , there is exactly one pair of sensors with sensor separation 2, in $\mathbb{X}_2^{(Q)} \cup \mathbb{Y}_2^{(Q)}$ when $N_1 = 4r$.
3. When $N_1 = 4r + 2$, $A_2 = r$, $B_2 = r - 2$. If $r = 2k - 1$ is an odd number, $A_2 + 1$ and $B_2 + 1$ are both even numbers. One extra term exists in $\mathbb{X}_2^{(Q)}$ and another one can be found in $\mathbb{Y}_2^{(Q)}$. There are two pairs of sensor separation 2. If $r = 2k$ is an even number, $A_2 + 1$ and $B_2 + 1$ are odd numbers. There is no extra term in $\mathbb{X}_2^{(Q)}$ and $\mathbb{Y}_2^{(Q)}$.

Hence, $w(2)$ is given by

$$w(2) = \begin{cases} \frac{N_1}{2}, & \text{if } N_1 = 4r, \\ \frac{N_1}{2} + 1, & \text{if } N_1 = 4(2k - 1) + 2, \\ \frac{N_1}{2} - 1, & \text{if } N_1 = 4(2k) + 2, \end{cases}$$

which proves the $w(2)$ part.

$w(3)$ can be found in these sensor pairs:

1. Four sensor pairs have been identified in the proof of Theorem 3.5.2. It is applicable because $\mathbb{X}_1^{(Q)} = \mathbb{X}_1^{(2)}$, $\mathbb{Y}_1^{(Q)} = \mathbb{Y}_1^{(2)}$, $\min(\mathbb{X}_2^{(Q)}) = \min(\mathbb{X}_2^{(2)})$, and $\max(\mathbb{Y}_2^{(Q)}) = \max(\mathbb{Y}_2^{(2)})$.
2. One more pair exists between $\mathbb{Z}_1^{(Q)}$ and $\mathbb{Z}_2^{(Q)}$. They are $(N_2 - 1)(N_1 + 1) \in \mathbb{Z}_1^{(Q)}$ and $(N_2 - 1)(N_1 + 1) - 3 \in \mathbb{Z}_2^{(Q)}$.

Then the proof is complete. □

Remarks based on Theorem 4.3.2 and 4.4.2

It seems that the super nested arrays with odd N_1 is superior to those with even N_1 in terms of the weight functions $w(1)$, $w(2)$, and $w(3)$. However, in some scenarios, the super nested arrays with even N_1 is preferred. For instance, suppose that we want to design super nested arrays with $N = 41$ physical sensors such that the number of identifiable sources is maximized. It was proved in [124] that the optimal N_1 is given by $N_1 = (N - 1)/2 = 20$, which is an even number.

Another remark is that, $w(1)$, $w(2)$, and $w(3)$ remain unchanged for $Q \geq 3$. However, this phenomenon does *not* imply that super nested arrays for $Q \geq 3$ have the same performance in the presence of mutual coupling. Instead, super nested arrays for $Q > 3$ could reduce the mutual coupling further. It is because the overall performance depends on the mutual coupling models, which are functions of the array geometry, as mentioned in (3.2) and (3.3). Super nested arrays with $Q > 3$ tend to make array geometries *more sparse*, as discussed extensively in Section 4.3 and 4.4. It can be shown that the weight functions like $w(4)$, $w(5)$, and so on, decrease as Q increases. Hence, qualitatively, mutual coupling could be reduced for super nested arrays with $Q > 3$.

Furthermore, the judgement of the estimation error based on the weight functions $w(1)$, $w(2)$, and $w(3)$, is *qualitative* and does not always lead to right conclusions, as in Chapter 3. For example, Fig. 4.6 shows that for source spacing $\Delta\bar{\theta} = 0.001$, the super nested array with $Q = 2$, $N_1 = N_2 = 17$ ($w(2) = 16$) outperforms the super nested array with $Q = 3$, $N_1 = N_2 = 17$ ($w(2) = 9$).

4.5 Proof of Theorem 4.3.1

According to Theorem 3.5.1, second-order super nested arrays are restricted arrays. To prove the same for Q th-order nested arrays with $Q > 2$, we use induction. Thus, assume that $\mathbb{S}^{(Q-1)}$ are restricted arrays. We need to show that $\mathbb{S}^{(Q)}$ are also restricted arrays under certain sufficient conditions. In the following development, we use $\mathbb{D}^{(Q)}$ to denote the difference set of Q th-order super nested arrays, $\mathbb{S}^{(Q)}$.

The main concept of the proof works as follows. Let $n_1 \in \mathbb{S}^{(Q-1)} \setminus \mathbb{S}^{(Q)}$ and $n_2 \in \mathbb{S}^{(Q-1)}$. It is obvious that $n_1 - n_2$ belongs to $\mathbb{D}^{(Q-1)}$. We need to show that there exist some $n'_1, n'_2 \in \mathbb{S}^{(Q)}$ such that $n'_1 - n'_2 = n_1 - n_2$. If the above statement holds true for every $n_1 \in \mathbb{S}^{(Q-1)} \setminus \mathbb{S}^{(Q)}$ and $n_2 \in \mathbb{S}^{(Q-1)}$, it is equivalent to saying that $\mathbb{S}^{(Q)}$ is a restricted array.

Table 4.1 lists 27 combinations, where $n_1 \in \mathbb{S}^{(Q-1)} \setminus \mathbb{S}^{(Q)}$ is divided into 3 subsets in each column and $n_2 \in \mathbb{S}^{(Q-1)}$ is partitioned into 9 categories in each row. In every case, given n_1 and n_2 , we need to identify the associated n'_1 and n'_2 such that (a) $n'_1, n'_2 \in \mathbb{S}^{(Q)}$, which will be elaborated on in detail, and (b) $n'_1 - n'_2 = n_1 - n_2$,

Table 4.1: 27 cases in the proof of Theorem 4.3.1

| $n_2 \setminus n_1$ | $\mathbb{X}_Q^{(Q)} - (N_1 + 1)$ | $\mathbb{Y}_Q^{(Q)} - (N_1 + 1)$ | $(Q-1)(N_1+1)$ |
|--|----------------------------------|----------------------------------|----------------|
| $\mathbb{X}_q^{(Q-1)},$ $1 \leq q \leq Q-2$ | Case 1 | Case 10 | Case 19 |
| $\mathbb{X}_{Q-1}^{(Q)}$ | Case 2 | Case 11 | Case 20 |
| $\mathbb{X}_Q^{(Q)} - (N_1 + 1)$ | Case 3 | Case 12 | Case 21 |
| $\mathbb{Y}_q^{(Q-1)},$ $1 \leq q \leq Q-2$ | Case 4 | Case 13 | Case 22 |
| $\mathbb{Y}_{Q-1}^{(Q)}$ | Case 5 | Case 14 | Case 23 |
| $\mathbb{Y}_Q^{(Q)} - (N_1 + 1)$ | Case 6 | Case 15 | Case 24 |
| $\mathbb{Z}_1^{(Q)}$ | Case 7 | Case 16 | Case 25 |
| $(Q-1)(N_1+1)$ | Case 8 | Case 17 | Case 26 |
| $\mathbb{Z}_2^{(Q-1)}$ | Case 9 | Case 18 | Case 27 |

which is simple to check.

(Case 1) Any n_1 and n_2 in this case can be written as

$$\begin{cases} n_1 = (Q-2)(N_1+1) + 2^{Q-1} + 2^{Q-1}\ell_1, \\ n_2 = (q-1)(N_1+1) + 2^{q-1} + 2^q\ell_2, \end{cases}$$

where $0 \leq \ell_1 \leq L_Q^{(Q)}$ and $0 \leq \ell_2 \leq L_q^{(Q)}$. According to Definition 4.3.1, $L_Q^{(Q)} \leq L_{Q-1}^{(Q)}$, and we have these cases:

1. $L_Q^{(Q)} < L_{Q-1}^{(Q)}$: The corresponding n'_1 and n'_2 can be expressed into two ways. They are

$$\begin{cases} n'_1 = (Q-2)(N_1+1) + 2^{Q-2} + 2^{Q-1}\ell_1, \\ n'_2 = (q-1)(N_1+1) + 2^{q-1} + 2^q(\ell_2 - 2^{Q-q-2}), \end{cases} \quad (4.9)$$

$$\begin{cases} n'_1 = (Q-2)(N_1+1) + 2^{Q-2} + 2^{Q-1}(\ell_1+1), \\ n'_2 = (q-1)(N_1+1) + 2^{q-1} + 2^q(\ell_2 + 2^{Q-q-2}). \end{cases} \quad (4.10)$$

The membership of n'_1 and n'_2 can be derived as follows. Since $L_Q^{(Q)} < L_{Q-1}^{(Q)}$, we have $n'_1 \in \mathbb{X}_{Q-1}^{(Q)}$ in (4.9) and (4.10). Next, n'_2 in (4.9) belongs to $\mathbb{X}_q^{(Q)}$ if $0 \leq \ell_2 - 2^{Q-q-2} \leq L_q^{(Q)}$. If $0 \leq \ell_2 + 2^{Q-q-2} \leq L_q^{(Q)}$, then n'_2 in (4.10) belongs to $\mathbb{X}_q^{(Q)}$. That is, if

$$2^{Q-q-2} \leq L_q^{(Q)} - 2^{Q-q-2}, \quad 1 \leq q \leq Q-2, \quad (4.11)$$

then we can find $n'_1, n'_2 \in \mathbb{S}^{(Q)}$ using either (4.9) or (4.10). Solving (4.11) leads to another sufficient condition $N_1 \geq \frac{7}{4} \cdot 2^Q - 1$.

2. $L_Q^{(Q)} = L_{Q-1}^{(Q)}$ and $0 \leq \ell_1 \leq L_Q^{(Q)} - 1$: The argument is the same as Case 1-1.
3. $L_Q^{(Q)} = L_{Q-1}^{(Q)}$ and $\ell_1 = L_Q^{(Q)}$: Depending on ℓ_2 , we obtain two more cases,
 - a) $2^{Q-q-2} \leq \ell_2 \leq L_q^{(Q)}$: Under this condition, (4.9) is still applicable. We obtain $\ell_1 = L_Q^{(Q)} \leq L_{Q-1}^{(Q)}$, implying $n'_1 \in \mathbb{X}_{Q-1}^{(Q)}$. In addition, the maximum value of $\ell_2 - 2^{Q-q-2}$ is $L_q^{(Q)} - 2^{Q-q-2}$, which is less than or equal to $L_q^{(Q)}$. This property proves $n'_2 \in \mathbb{X}_q^{(Q)}$.
 - b) $0 \leq \ell_2 \leq 2^{Q-q-2} - 1$: The associated n'_1 and n'_2 are

$$\begin{cases} n'_1 = (Q-1)(N_1+1) + 2^{Q-1} + 2^{Q-1}(\ell_1-1), \\ n'_2 = q(N_1+1) - 2^{q-1} - 2^q(2^{Q-q-1} - \ell_2 - 1). \end{cases} \quad (4.12)$$

It can be seen that $n'_1 \in \mathbb{X}_Q^{(Q)}$, since $\ell_1 - 1 \leq L_Q^{(Q)}$. We need to show that $n'_2 \in \mathbb{Y}_q^{(Q)}$ under some sufficient conditions. Since $0 \leq \ell_2 \leq 2^{Q-q-2} - 1$, we obtain $2^{Q-q-2} \leq 2^{Q-q-1} - \ell_2 - 1 \leq 2^{Q-q-1} - 1$. If $2^{Q-q-1} - 1 \leq L_q^{(Q)}$, it can be inferred that n'_2 belongs to $\mathbb{Y}_q^{(Q)}$. Therefore, the associated sufficient condition becomes $N_1 \geq \frac{5}{4} \cdot 2^Q - 1$.

(Case 2, 5, 11, 14) In Case 2, n_1, n_2, n'_1, n'_2 are

$$\begin{cases} n_1 = (Q-2)(N_1+1) + 2^{Q-1} + 2^{Q-1}\ell_1, \\ n_2 = (Q-2)(N_1+1) + 2^{Q-2} + 2^{Q-1}\ell_2, \end{cases} \quad (4.13)$$

$$\begin{cases} n'_1 = 1 + 2(2^{Q-2} + 2^{Q-2}\ell_1 - 1), \\ n'_2 = 1 + 2(2^{Q-3} + 2^{Q-2}\ell_2 - 1), \end{cases} \quad (4.14)$$

where $0 \leq \ell_1 \leq L_Q^{(Q)}$ and $0 \leq \ell_2 \leq L_{Q-1}^{(Q)}$. It can be concluded that $n'_1, n'_2 \in \mathbb{X}_1^{(Q)}$ since

$$\begin{aligned} & 2^{Q-2} + 2^{Q-2}\ell_1 - 1 \\ & \leq \left\lfloor 2^{Q-2} + 2^{Q-2} \left(\frac{N_1+1}{2^Q} - 1 \right) - 1 \right\rfloor \leq L_1^{(Q)}, \\ & 2^{Q-3} + 2^{Q-2}\ell_2 - 1 \\ & \leq \left\lfloor 2^{Q-3} + \frac{2^{Q-2}}{2} \left(\frac{N_1+1}{2^{Q-1}} - 1 \right) - 1 \right\rfloor \leq L_1^{(Q)}. \end{aligned}$$

Here we apply some properties of the floor function: $\lfloor 2x \rfloor \geq 2\lfloor x \rfloor$ and $\lfloor x + n \rfloor = \lfloor x \rfloor + n$ for integer n . Note that in Case 5, 11, 14, we can relate n'_1 and n'_2 with either $\mathbb{X}_1^{(Q)}$ or $\mathbb{Y}_1^{(Q)}$.

(Case 3, 6, 8, 12, 15, 17, 21, 24, 26) For any n_1 and n_2 in this combination, the corresponding $n'_1 = n_1 + (N_1 + 1)$ and $n'_2 = n_2 + (N_1 + 1)$. We have

$$n'_1, n'_2 \in \mathbb{X}_Q^{(Q)} \cup \mathbb{Y}_Q^{(Q)} \cup \{Q(N_1 + 1)\} \subset \mathbb{S}^{(Q)}.$$

(Case 4, 10) Let us consider Case 4 first. The associated n_1 and n_2 are given by

$$\begin{cases} n_1 = (Q - 2)(N_1 + 1) + 2^{Q-1} + 2^{Q-1}\ell_1, \\ n_2 = q(N_1 + 1) - 2^{q-1} - 2^q\ell_2, \end{cases}$$

where $0 \leq \ell_1 \leq L_Q^{(Q)}$ and $0 \leq \ell_2 \leq L_q^{(Q)}$. According to ℓ_1 , we have

1. $L_Q^{(Q)} < L_{Q-1}^{(Q)}$: n'_1 and n'_2 can be written as

$$\begin{cases} n'_1 = (Q - 2)(N_1 + 1) + 2^{Q-2} + 2^{Q-1}\ell_1, \\ n'_2 = q(N_1 + 1) - 2^{q-1} - 2^q(\ell_2 + 2^{Q-q-2}), \end{cases} \quad (4.15)$$

$$\begin{cases} n'_1 = (Q - 2)(N_1 + 1) + 2^{Q-2} + 2^{Q-1}(\ell_1 + 1), \\ n'_2 = q(N_1 + 1) - 2^{q-1} - 2^q(\ell_2 - 2^{Q-q-2}). \end{cases} \quad (4.16)$$

Following Case 1-1, if $N_1 \geq \frac{7}{4} \cdot 2^Q - 1$, then $n'_1 \in \mathbb{X}_{Q-1}^{(Q)}$ and $n'_2 \in \mathbb{Y}_q^{(Q)}$ in either (4.15) or (4.16).

2. $L_Q^{(Q)} = L_{Q-1}^{(Q)}$ and $0 \leq \ell_1 \leq L_Q^{(Q)} - 1$: Case 4-1 applies.
3. $L_Q^{(Q)} = L_{Q-1}^{(Q)}$ and $\ell_1 = L_Q^{(Q)}$:

a) $0 \leq \ell_2 \leq L_q^{(Q)} - 2^{Q-q-2}$: (4.15) can be applied to this case. It can be shown that $n'_1 \in \mathbb{X}_{Q-1}^{(Q)}$ and $n'_2 \in \mathbb{Y}_q^{(Q)}$.

b) $L_q^{(Q)} - 2^{Q-q-2} + 1 \leq \ell_2 \leq L_q^{(Q)}$: To identify n'_1 and n'_2 in this case, we first introduce the *remainder* $R = (Q - q - 1)(N_1 + 1) - n_1 + n_2$, which is rewritten as

$$R = (N_1 + 1) - 2^{Q-1} - 2^{Q-1}L_Q^{(Q)} - 2^{q-1} - 2^q\ell_2. \quad (4.17)$$

Corollary 4.5.1. $1 \leq R < 2^{Q-1}$.

Proof. If x is a real number, we obtain $x - 1 < [x] \leq x$. This property implies

$$\frac{N_1 + 1}{2} - 2^{Q-1} < 2^{Q-1} + 2^{Q-1}L_Q^{(Q)} \leq \frac{N_1 + 1}{2}, \quad (4.18)$$

$$\frac{N_1 + 1}{2} - 2^{Q-2} < 2^{Q-1} + 2^{Q-1}L_{Q-1}^{(Q)} \leq \frac{N_1 + 1}{2} + 2^{Q-2}, \quad (4.19)$$

$$\frac{N_1 + 1}{2} - 2^{Q-2} < 2^{q-1} + 2^q\ell_2 \leq \frac{N_1 + 1}{2}. \quad (4.20)$$

Combining (4.18) to (4.20) and $L_Q^{(Q)} = L_{Q-1}^{(Q)}$ gives $0 \leq R < 2^{Q-1}$. However, if $R = 0$, both (4.18) and (4.20) achieve their upper bound. The condition that (4.18) being equal is $N_1 + 1$ is a multiple of 2^Q , which contradicts with the condition that (4.20) being the equal. Hence, $1 \leq R < 2^{Q-1}$. \square

Next, according to R , we can identify n'_1 and n'_2 . Let us consider the *binary expansion* of R , which is

$$R = \sum_{r=0}^{Q-2} a_r 2^r, \quad a_r \in \{0, 1\}. \quad (4.21)$$

Then we define P satisfying

$$a_0 = a_1 = \cdots = a_{P-1} = 0, \quad a_P = 1. \quad (4.22)$$

It can be deduced that (a) P is unique for a given R , and (b) $0 \leq P \leq Q-2$. Here we have three more cases, where q is consistent with Case 4 in Table 4.1:

- i. $q = 1$: In this case, the proof technique in (4.15) is applicable. $n'_1 \in \mathbb{X}_{Q-1}^{(Q)}$ and n'_2 is an odd number less than $N_1 + 1$ so $n'_2 \in \mathbb{X}_1^{(Q)} \cup \mathbb{Y}_1^{(Q)}$.
- ii. $P \leq q, q \geq 2$: Since $q \geq 2$, R is an even number and $P \geq 1$. n'_1 and n'_2 become

$$\begin{cases} n'_1 = (Q+P-q-1)(N_1+1) + 2^{Q+P-q-1}, \\ n'_2 = P(N_1+1) + R + 2^{Q+P-q-1}. \end{cases} \quad (4.23)$$

It will be shown that $n'_1 \in \mathbb{X}_{Q-P-q}^{(Q)}$ and $n'_2 \in \mathbb{X}_{P+1}^{(Q)}$ under some sufficient conditions. It is obvious that n'_1 is the minimum element in $\mathbb{X}_{Q-P-q}^{(Q)}$. $n'_2 \in \mathbb{X}_{P+1}^{(Q)}$ is equivalent to

$$R + 2^{Q+P-q-1} = 2^P + 2^{P+1}\ell_3, \quad (4.24)$$

for some integer ℓ_3 satisfying $0 \leq \ell_3 \leq L_{P+1}^{(Q)}$. According to the definition of P , in (4.22), the left-hand side of (4.24) is a multiple of 2^P and ℓ_3 is an integer.

Next, we need to show $2^P < R + 2^{Q+P-q-1} \leq 2^P + 2^{P+1}L_{P+1}^{(Q)}$ under some sufficient conditions. According to (4.22) and the range of P and q , we have $R \geq 2^P$ and $2^{Q+P-q-1} \geq 1$, yielding the lower bound. A sufficient condition for the upper bound is given by

$$2^{Q-1} + 2^{Q+P-q-1} \leq 2^P + 2^{P+1}L_{P+1}^{(Q)}. \quad (4.25)$$

Using $x - 1 < \lfloor x \rfloor$, $P \leq q$, and $1 \leq q \leq Q - 2$, (4.25) becomes $N_1 \geq 3 \cdot 2^Q - 1$.

iii. $P \geq q + 1, q \geq 2$: n'_1 and n'_2 in this case are

$$\begin{cases} n'_1 = (Q + P - q - 1)(N_1 + 1), \\ n'_2 = P(N_1 + 1) + R. \end{cases} \quad (4.26)$$

A sufficient condition for n'_1 belonging to $\mathbb{Z}_1^{(Q)}$ is $Q \leq Q + P - q - 1 \leq N_2$, implying $N_2 \geq 2Q - 5$. On the other hand, n'_2 lives in $\mathbb{X}_{P+1}^{(Q)}$ when there exists some ℓ_3 satisfying $0 \leq \ell_3 \leq L_{P+1}^{(Q)}$ and $R = 2^P + 2^{P+1}\ell_3$. It suffices to solve $2^{Q-1} \leq 2^P + 2^{P+1}L_{P+1}^{(Q)}$, which gives another sufficient condition $N_1 \geq 2 \cdot 2^Q - 1$.

The proof for Case 10 is similar to Case 4.

(Case 7, 16) First we consider Case 7, where n_1 and n_2 are given by

$$\begin{cases} n_1 = (Q - 2)(N_1 + 1) + 2^{Q-1} + 2^{Q-1}\ell_1, \\ n_2 = \ell_2(N_1 + 1). \end{cases} \quad (4.27)$$

Here $0 \leq \ell_1 \leq L_Q^{(Q)}$ and $Q \leq \ell_2 \leq N_2$. According to ℓ_2 , we obtain

1. $Q \leq \ell_2 \leq N_2 - 1$: n'_1 and n'_2 can be written as

$$\begin{cases} n'_1 = (Q - 1)(N_1 + 1) + 2^{Q-1} + 2^{Q-1}\ell_1, \\ n'_2 = (\ell_2 + 1)(N_1 + 1). \end{cases} \quad (4.28)$$

It is trivial that $n'_1 \in \mathbb{X}_Q^{(Q)}$ and $n'_2 \in \mathbb{Z}_1^{(Q)}$.

2. $\ell_2 = N_2$: We obtain n'_1 and n'_2 to be

$$\begin{cases} n'_1 = 1 + 2^{Q-1}\ell_1, \\ n'_2 = (N_2 + 2 - Q)(N_1 + 1) - 2^{Q-1} + 1. \end{cases} \quad (4.29)$$

It can be seen from (4.29) that $n'_1 \in \mathbb{X}_1^{(Q)}$ and $n'_2 \in \mathbb{Z}_2^{(Q)}$.

The proof for Case 16 follows the same argument for Case 7.

(Case 9, 18) For Case 9, n_1 and n_2 are given by

$$\begin{cases} n_1 = (Q - 2)(N_1 + 1) + 2^{Q-1} + 2^{Q-1}\ell_1, \\ n_2 = (N_2 + 1 - q)(N_1 + 1) - 2^q + 1. \end{cases} \quad (4.30)$$

where $0 \leq \ell_1 \leq L_Q^{(Q)}$ and $1 \leq q \leq Q - 2$. Rewriting (4.30) gives n'_1 and n'_2

$$\begin{cases} n'_1 = 2^q - 1 + 2^{Q-1} + 2^{Q-1}\ell_1, \\ n'_2 = (N_2 + 3 - Q - q)(N_1 + 1). \end{cases} \quad (4.31)$$

We need to show that $n'_1 \in \mathbb{X}_1^{(Q)} \cup \mathbb{Y}_1^{(Q)}$ and $n'_2 \in \mathbb{Z}_1^{(Q)}$. If $Q \leq N_2 + 3 - Q - q \leq N_2$, then $n'_2 \in \mathbb{Z}_1^{(Q)}$, which leads to a sufficient condition $N_2 \geq 3Q - 5$. The membership of n'_1 can be verified as follows. It is trivial that n'_1 is an odd number. In addition, $n'_1 \leq 2^{Q-2} - 1 + 2^{Q-1} + 2^{Q-1}L_Q^{(Q)} \leq N_1 + 1$. We obtain $n'_1 \in \mathbb{X}_1^{(Q)} \cup \mathbb{Y}_1^{(Q)}$. Case 18 has the same proof as Case 9.

(Case 13) In this case, n_1, n_2 are given by

$$\begin{cases} n_1 = (Q-1)(N_1+1) - 2^{Q-1} - 2^{Q-1}\ell_1, \\ n_2 = q(N_1+1) - 2^{q-1} - 2^q\ell_2, \end{cases} \quad (4.32)$$

where $0 \leq \ell_1 \leq L_Q^{(Q)}$ and $0 \leq \ell_2 \leq L_q^{(Q)}$. According to ℓ_1 , we have two sub-cases

1. $L_Q^{(Q)} < L_{Q-1}^{(Q)}$: The pair n'_1 and n'_2 can be written as

$$\begin{cases} n'_1 = (Q-1)(N_1+1) - 2^{Q-2} - 2^{Q-1}\ell_1, \\ n'_2 = q(N_1+1) - 2^{q-1} - 2^q(\ell_2 - 2^{Q-q-2}), \end{cases} \quad (4.33)$$

$$\begin{cases} n'_1 = (Q-1)(N_1+1) - 2^{Q-2} - 2^{Q-1}(\ell_1+1), \\ n'_2 = q(N_1+1) - 2^{q-1} - 2^q(\ell_2 + 2^{Q-q-2}). \end{cases} \quad (4.34)$$

Following the same discussion as Case 1-1, we obtain a sufficient condition $N_1 \geq \frac{7}{4} \cdot 2^Q - 1$.

2. $L_Q^{(Q)} = L_{Q-1}^{(Q)}$ and $0 \leq \ell_1 < L_Q^{(Q)} - 1$: This case is the same as Case 13-1.

3. $L_Q^{(Q)} = L_{Q-1}^{(Q)}$ and $\ell_1 = L_Q^{(Q)}$:

a) $2^{Q-q-2} \leq \ell_2 \leq L_q^{(Q)}$: It can be shown that $n'_1 \in \mathbb{Y}_{Q-1}^{(Q)}$ and $n'_2 \in \mathbb{Y}_q^{(Q)}$ due to the same reason in Case 1-3a.

b) $0 \leq \ell_2 \leq 2^{Q-q-2} - 1$, $q = Q - 2$, and $Q = 3$: In this case n'_1 and n'_2 are given by

$$\begin{cases} n'_1 = N_1 + 3, \\ n'_2 = 1 + 4(L_3^{(3)} + 1). \end{cases} \quad (4.35)$$

We know that $n'_1 \in \mathbb{X}_2^{(3)}$, which is trivial, and $n'_2 \in \mathbb{X}_1^{(3)} \cup \mathbb{Y}_1^{(3)}$, since n'_2 is an odd number less than $N_1 + 1$.

c) $0 \leq \ell_2 \leq 2^{Q-q-2} - 1$, $q = Q - 2$, and $Q \geq 4$: n'_1 and n'_2 can be written as

$$\begin{cases} n'_1 = (N_1 + 2) - 2^{Q-1} \\ \quad - 2^{Q-1}L_Q^{(Q)} + 2^{Q-3} + 2^{Q-2}\ell_2, \\ n'_2 = 1. \end{cases} \quad (4.36)$$

It can be inferred that n'_1 is an odd number less than $N_1 + 1$. Therefore, $n'_1, n'_2 \in \mathbb{X}_1^{(Q)} \cup \mathbb{Y}_1^{(Q)}$.

d) $0 \leq \ell_2 \leq 2^{Q-q-2} - 1$ and $1 \leq q \leq Q - 3$: We found that n'_1 and n'_2 can be expressed as

$$\begin{cases} n'_1 = (Q-2)(N_1+1) - 2^{Q-3} - 2^{Q-1}L_Q^{(Q)}, \\ n'_2 = (q-1)(N_1+1) + 2^{q-1} \\ \quad + 2^q(2^{Q-q-2} + 2^{Q-q-3} - \ell_2 - 1), \end{cases} \quad (4.37)$$

which satisfies $n'_1 \in \mathbb{Y}_{Q-2}^{(Q)}$ and $n'_2 \in \mathbb{X}_q^{(Q)}$ under the sufficient conditions $2L_{Q-2}^{(Q)} \leq L_{Q-2}^{(Q)}$ and $0 \leq 2^{Q-q-2} + 2^{Q-q-3} - \ell_2 - 1 \leq L_q^{(Q)}$. We obtain a sufficient condition $N_1 \geq \frac{7}{8} \cdot 2^Q - 1$.

(Case 19, 22) In Case 19, n_1, n_2, n'_1 , and n'_2 can be written as

$$\begin{cases} n_1 = (Q-1)(N_1+1), \\ n_2 = (q-1)(N_1+1) + 2^{q-1} + 2^q\ell_2, \end{cases} \quad (4.38)$$

$$\begin{cases} n'_1 = (Q-1)(N_1+1) + 2^{Q-1}, \\ n'_2 = (q-1)(N_1+1) + 2^{q-1} + 2^q(\ell_2 + 2^{Q-q-1}), \end{cases} \quad (4.39)$$

$$\begin{cases} n'_1 = (Q-1)(N_1+1) - 2^{Q-2}, \\ n'_2 = (q-1)(N_1+1) + 2^{q-1} + 2^q(\ell_2 - 2^{Q-q-2}), \end{cases} \quad (4.40)$$

where $0 \leq \ell_2 \leq L_q^{(Q)}$. The next argument is similar to that in Case 1-1. A sufficient condition for $n'_1 \in \mathbb{X}_Q^{(Q)}, n'_2 \in \mathbb{X}_q^{(Q)}$ or $n'_1 \in \mathbb{Y}_{Q-1}^{(Q)}, n'_2 \in \mathbb{X}_q^{(Q)}$ is that

$$2^{Q-q-2} \leq L_q^{(Q)} - 2^{Q-q-1},$$

which leads to another sufficient condition $N_1 \geq \frac{9}{4} \cdot 2^Q - 1$. Case 22 is the same as Case 19.

(Case 20, 23) In Case 20, n_1, n_2, n'_1 , and n'_2 become

$$\begin{cases} n_1 = (Q-1)(N_1+1), \\ n_2 = (Q-2)(N_1+1) + 2^{Q-2} + 2^{Q-1}\ell_2, \end{cases} \quad (4.41)$$

$$\begin{cases} n'_1 = (N_1+1) - 1, \\ n'_2 = 1 + 2(-1 + 2^{Q-3} + 2^{Q-2}\ell_2), \end{cases} \quad (4.42)$$

where $0 \leq \ell_2 \leq L_{Q-1}^{(Q)}$. It is trivial that $n'_1 \in \mathbb{Y}_1^{(Q)}$. Besides, $n'_2 \in \mathbb{X}_1^{(Q)}$ since

$$-1 + 2^{Q-3} + 2^{Q-2}\ell_1 \leq -1 + 2^{Q-3} + 2^{Q-2}L_{Q-1}^{(Q)} \leq L_1^{(Q)}.$$

(Case 25) We can write n_1 and n_2 as

$$\begin{cases} n_1 = (Q-1)(N_1+1), \\ n_2 = q(N_1+1), \end{cases} \quad (4.43)$$

where $Q \leq q \leq N_2$. Based on q , n'_1 and n'_2 are given by the following.

1. $Q \leq q \leq N_2 - 1$: In this case $n'_1 = Q(N_1 + 1)$ and $n'_2 = (q + 1)(N_1 + 1)$. It is evident that $n'_1, n'_2 \in \mathbb{Z}_1^{(Q)}$.
2. $q = N_2$: We obtain

$$\begin{cases} n'_1 = (N_1 + 1) - 1 - 2(2^{Q-2} - 1), \\ n'_2 = (N_2 - Q + 2)(N_1 + 1) - 2^{Q-1} + 1. \end{cases} \quad (4.44)$$

It can be seen that n'_2 is contained in $\mathbb{Z}_2^{(Q)}$. The sufficient condition for n'_1 in $\mathbb{Y}_1^{(Q)}$ is $2^{Q-2} - 1 \leq L_1^{(Q)}$. We obtain $N_1 \geq 2^Q + 1$.

(Case 27) In this case, we have

$$\begin{cases} n_1 = (Q-1)(N_1+1), \\ n_2 = (N_2+1-q)(N_1+1) - 2^q + 1, \end{cases} \quad (4.45)$$

$$\begin{cases} n'_1 = 2^q - 1, \\ n'_2 = (N_2+2-Q-q)(N_1+1), \end{cases} \quad (4.46)$$

where $1 \leq q \leq Q - 2$. If $2^q - 1 \leq N_1$ and $Q \leq N_2 + 2 - Q - q \leq N_2$, n'_1 and n'_2 belong to $\mathbb{X}_1^{(Q)} \cup \mathbb{Y}_1^{(Q)}$ and $\mathbb{Z}_1^{(Q)}$, respectively. Solving these inequalities leads to the following sufficient conditions for Q th-order super nested arrays: $N_1 \geq \frac{1}{4} \cdot 2^Q - 1$ and $N_2 \geq 3Q - 4$.

The last step in the proof is to take the intersection of all these sufficient conditions. We obtain $N_1 \geq 3 \cdot 2^Q - 1$ and $N_2 \geq 3Q - 4$. Then all the (n'_1, n'_2) pairs in those 27 cases exist simultaneously, implying this array configuration is a restricted array. \square

4.6 Proof of Theorem 4.4.1

This proof follows the same strategy as that of Theorem 4.3.1, where induction on Q is applied. First of all, it is essential to characterize some properties of $\mathbb{X}_q^{(Q)}$ as well as $\mathbb{Y}_q^{(Q)}$ before the induction step.

Lemma 4.6.1 (Properties on $\mathbb{X}_q^{(Q)}$ when N_1 is even). Suppose that $2 \leq q \leq Q$, N_1 is an even number and $\mathbb{S}^{(Q)}$ is defined as Definition 4.4.1. Then $\mathbb{X}_q^{(Q)}$ possess the following properties:

1. $\mathbb{X}_Q^{(Q)}$ is a ULA with inter-element spacing 2^{Q-1} . The first element is $(Q - 1)(N_1 + 1) + 2^{Q-1}$.
2. For $2 \leq q \leq Q - 1$, $\mathbb{X}_q^{(Q)}$ has a ULA portion with inter-element spacing 2^q . The minimum (or leftmost) element of ULA in $\mathbb{X}_q^{(Q)}$ is $(q - 1)(N_1 + 1) + 2^{q-1}$.
3. If there is an extra term in $\mathbb{X}_q^{(Q)}$, it is the maximum (rightmost) element of $\mathbb{X}_q^{(Q)}$ and it is 2^{q-1} larger than the maximum element in the ULA section of $\mathbb{X}_q^{(Q)}$.
4. If $n \in \mathbb{X}_Q^{(Q)}$, then $n - (N_1 + 1) \pm 2^{Q-2} \in \mathbb{X}_{Q-1}^{(Q)}$.

Proof. 1. We can prove this property by induction. When $Q = 2$, the closed-form expression is given by Definition 3.4.1, which satisfies Lemma 4.6.1-1. Suppose $\mathbb{X}_{Q-1}^{(Q-1)}$ is an ULA with sensor separation 2^{Q-2} and first element $(Q - 2)(N_1 + 1) + 2^{Q-2}$. According to Rule 2 of Definition 4.4.1, $\mathbb{X}_Q^{(Q)}$ is derived from odd terms in $\mathbb{X}_{Q-1}^{(Q-1)}$. Therefore, the first element of $\mathbb{X}_Q^{(Q)}$ is $(Q - 1)(N_1 + 1) + 2^{Q-1}$ and the inter-element spacing is 2^{Q-1} .

2. According to Rule 1 of Definition 4.4.1, we have $\mathbb{X}_q^{(Q)} = \mathbb{X}_q^{(q+1)}$. Following Rule 2, $\mathbb{X}_q^{(q+1)}$ has at least all the the even terms of $\mathbb{X}_q^{(q)}$, which constitute the ULA portion. Based on Lemma 4.6.1-1, $\mathbb{X}_q^{(q)}$ is a ULA of separation 2^{q-1} and its minimum element is $(q - 1)(N_1 + 1) + 2^{q-1}$. Therefore, the ULA part in $\mathbb{X}_q^{(q+1)}$ owns sensor separation 2^q . The minimum element in $\mathbb{X}_q^{(Q)}$ is then given by $(q - 1)(N_1 + 1) + 2^{q-1}$.

3. In this case, Rule 2b of Definition 4.4.1 indicates that the extra term is the largest one of $\mathbb{X}_q^{(q)}$ while the last term of the ULA section of $\mathbb{X}_q^{(Q)}$ is the second largest one in $\mathbb{X}_q^{(q)}$. Based on Lemma 4.6.1-1, their difference is 2^{q-1} .

4. If $n \in \mathbb{X}_Q^{(Q)}$, then $n - (N_1 + 1)$ is an odd term of $\mathbb{X}_{Q-1}^{(Q-1)}$. Based on Rule 2 of Definition 4.4.1 and Lemma 4.6.1-1, $n - (N_1 + 1) \pm 2^{Q-2}$ are even terms of $\mathbb{X}_{Q-1}^{(Q-1)}$, which is contained in $\mathbb{X}_{Q-1}^{(Q)}$.

This completes the proof. □

Next, assuming $\mathbb{S}^{(Q-1)}$ is a restricted array, we need to show that $\mathbb{S}^{(Q)}$ is also a restricted array. Similarly, there are 27 cases, as listed in Table 4.1.

(Case 1, 13) Given n_1 and n_2 in this case, we have

1. n_2 belongs to the ULA portion of $\mathbb{X}_q^{(Q)}$: This case is the same as Case 1-1 in the proof of Theorem 4.3.1. n'_1 and n'_2 can be written in two ways:

$$n'_1 = n_1 - 2^{Q-2}, \quad n'_2 = n_2 - 2^{Q-2}, \quad (4.47)$$

$$n'_1 = n_1 + 2^{Q-2}, \quad n'_2 = n_2 + 2^{Q-2}, \quad (4.48)$$

where (4.47) and (4.48) resemble (4.9) and (4.10), respectively. According to Lemma 4.6.1-4, n'_1 lives in $\mathbb{X}_{Q-1}^{(Q)}$. In addition, at least one of the n'_2 in (4.47) or (4.48) belongs to $\mathbb{X}_q^{(Q)}$. If neither $n_2 + 2^{Q-2}$ nor $n_2 - 2^{Q-2}$ belongs to $\mathbb{X}_q^{(Q)}$, then the ULA part of $\mathbb{X}_q^{(Q)}$ has aperture less than 2^{Q-1} . On the other hand, n'_1 in (4.47) and (4.48) implies $\mathbb{X}_{Q-1}^{(Q)}$ has aperture at least 2^{Q-1} . This is a contradiction since $\mathbb{X}_q^{(Q)}$ must have larger aperture than $\mathbb{X}_{Q-1}^{(Q)}$.

2. n_2 is an extra term in $\mathbb{X}_q^{(Q)}$: In this case, we only need to consider $2 \leq q \leq Q-2$ because when $q = 1$, there is no extra term, by definition. Based on (4.48) and Lemma 4.6.1-4, we know that $n_1 + 2^{Q-2}$ belongs to $\mathbb{X}_{Q-1}^{(Q)}$ and $n_1 + 2^{Q-2} - (N_1 + 1) + 2^{Q-3}$ is contained in $\mathbb{X}_{Q-2}^{(Q)}$. Applying these rules multiple times yields,

$$\begin{cases} n'_1 = n_1 - (q-1)(N_1 + 1) + \sum_{p=Q-q-1}^{Q-2} 2^p, \\ n'_2 = n_2 - (q-1)(N_1 + 1) + \sum_{p=Q-q-1}^{Q-2} 2^p. \end{cases} \quad (4.49)$$

It ensures that n'_1 lives in $\mathbb{X}_{Q-q}^{(Q)}$. We need to show that $n'_2 \in \mathbb{Y}_1^{(Q)}$. According to Rule 2 in Definition 4.4.1, n'_2 is an even number. Its minimum value is attained when all the sets $\mathbb{X}_1^{(Q)}, \mathbb{X}_2^{(Q)}, \dots, \mathbb{X}_{q-1}^{(Q)}$ own extra terms, implying

$$n_2 - (q-1)(N_1 + 1) \geq (1 + 2A_1) - \left(1 + \sum_{p=2}^q 2^p\right),$$

where A_1 is given by Definition 3.4.1. Therefore, n'_2 is lower-bounded by

$$(1 + 2A_1) - \left(1 + \sum_{p=2}^q 2^p\right) + \sum_{p=Q-q-1}^{Q-2} 2^p > 1 + 2A_1.$$

Thus, n'_2 belongs to $\mathbb{Y}_1^{(Q)}$.

(Case 4, 10) Let us consider Case 4. According to n_2 , we obtain two cases:

1. If n_2 belongs to the ULA part of $\mathbb{Y}_q^{(Q)}$, it is the same as Case 1-1.
2. If n_2 is an extra term in $\mathbb{Y}_q^{(Q)}$, following the idea of Case 1-2, we can write

$$\begin{cases} n'_1 = n_1 - (q-1)(N_1 + 1) - \sum_{p=Q-q-1}^{Q-2} 2^p, \\ n'_2 = n_2 - (q-1)(N_1 + 1) - \sum_{p=Q-q-1}^{Q-2} 2^p. \end{cases} \quad (4.50)$$

Here n'_1 belongs to $\mathbb{X}_{Q-q}^{(Q)}$ and n'_2 is an odd number. Next we will show that n'_2 belongs to $\mathbb{X}_1^{(Q)}$. Similar to Case 1-2, $n_2 - (q-1)(N_1+1)$ is upper-bounded by

$$\begin{aligned} & n_2 - (q-1)(N_1+1) \\ & \leq (N_1+1) - (1+2B_1) + \left(1 + \sum_{p=2}^q 2^p\right). \end{aligned}$$

Therefore, n'_2 has an upper bound

$$\begin{aligned} & (N_1+1) - (1+2B_1) + \left(1 + \sum_{p=2}^q 2^p\right) - \sum_{p=Q-q-1}^{Q-2} 2^p \\ & < (N_1+1) - (1+2B_1), \end{aligned}$$

which proves that n'_2 belongs to $\mathbb{X}_1^{(Q)}$. The proof for Case 10 is similar to Case 4.

(Case 19, 22) Let $n_1 = (Q-1)(N_1+1)$ and $n_2 \in \mathbb{X}_q^{(Q)}$. Based on n_2 , we have two cases:

1. n_2 belongs to the ULA portion of $\mathbb{X}_q^{(Q)}$: Following the steps of Case 19, 22 in Section 4.5, we obtain

$$\begin{cases} n'_1 = (Q-1)(N_1+1) + 2^{Q-1}, \\ n'_2 = n_2 + 2^{Q-1}, \end{cases} \quad (4.51)$$

$$\begin{cases} n'_1 = (Q-1)(N_1+1) - 2^{Q-2}, \\ n'_2 = n_2 - 2^{Q-2}. \end{cases} \quad (4.52)$$

Then, n'_1 can be either in $\mathbb{X}_Q^{(Q)}$ or $\mathbb{Y}_{Q-1}^{(Q)}$, according to (4.51) or (4.52). It is trivial that n'_2 belongs to $\mathbb{X}_q^{(Q)}$.

2. n_2 is an extra term in $\mathbb{X}_q^{(Q)}$: n'_1 and n'_2 are given by

$$\begin{cases} n'_1 = (Q-q)(N_1+1) + 2^{Q-q} + 2^{Q-1}, \\ n'_2 = n_2 - (q-1)(N_1+1) + 2^{Q-q} + 2^{Q-1}. \end{cases} \quad (4.53)$$

It can be seen from (4.53) that n'_1 belongs to $\mathbb{X}_{Q-q+1}^{(Q)}$ and n'_2 is contained in $\mathbb{Y}_1^{(Q)}$. It can be proved by checking the lower bound of n'_2 , which is

$$\begin{aligned} & n_2 - (q-1)(N_1+1) + 2^{Q-q} + 2^{Q-1} \\ & \geq (1+2A_1) - \left(1 + \sum_{p=2}^q 2^p\right) + 2^{Q-q} + 2^{Q-1} \\ & = (1+2A_1) + (2^{Q-1} - 2^{q+1}) + (2^{Q-q} + 3) \\ & > 1 + 2A_1. \end{aligned}$$

for $1 \leq q \leq Q-2$.

(Other Cases) Proofs are the same as those in Section 4.5.

Next we discuss the sufficient conditions of $\mathbb{S}^{(Q)}$ being a restricted array. According to Definition 4.4.1, $\mathbb{X}_q^{(Q)}$ and $\mathbb{Y}_q^{(Q)}$ are not empty. Suppose there is only one element in $\mathbb{X}_Q^{(Q)}$, Lemma 4.6.1-4 implies there are at least 2 elements in $\mathbb{X}_{Q-1}^{(Q)}$. Applying this argument many times yields that $\mathbb{X}_q^{(Q)}$ has at least 2^{Q-q} elements. The same property holds for $\mathbb{Y}_q^{(Q)}$. In addition, if $N_1 = 4r+2$, the number of elements between $\mathbb{X}_1^{(Q)}$ and $\mathbb{Y}_1^{(Q)}$ differs by 2. Hence, to guarantee this proof is valid, we need

$$N_1 \geq 2 \sum_{q=1}^Q 2^{Q-q} + 4 = 2 \cdot 2^Q + 2.$$

Besides, the sufficient condition for N_2 is $N_2 \geq 3Q-4$, following the same argument in the proof of Theorem 4.3.1. \square

4.7 Numerical Examples

In this section, we make a comparison among ULA, MRA, nested arrays, coprime arrays, and super nested arrays when the mutual coupling effect is present. The total number of sensors is 34 for each array configuration. The sensor locations for MRA cannot be found in the literature, so instead we select the approximate MRA with $n = 18$ and $p = 13$ (Reference L, Table 6 of [65])². The nested array has parameter $N_1 = N_2 = 17$. We choose $M = 9, N = 17$ in coprime arrays. For super nested arrays, there are three different cases: 1) the super nested array with $Q = 2, N_1 = N_2 = 17$, 2) the super nested array with $Q = 3, N_1 = N_2 = 17$, and 3) the super nested array with $Q = 3, N_1 = 16, N_2 = 18$. The sensor locations for these arrays are given by (2.7) for the nested array, (2.8) for the coprime array, Definition 3.4.1 for the super nested array with $Q = 2$, Definition 4.3.1 for the super nested

² The sensor locations for the approximate MRA are 0, 1, 14, 30, 46, 62, 78, 94, 110, 126, 142, 158, 174, 190, 206, 222, 238, 254, 270, 286, 302, 304, 306, 308, 310, 312, 314, 317, 319, 321, 323, 325, 327, and 329.

Table 4.2: Array profiles for the example in Section 4.7

| Array | ULA | MRA | Nested array, $N_1 = N_2 = 17$ | Coprime array, $M = 9, N = 17$ |
|----------------------|---|---|--|-----------------------------------|
| Aperture | 33 | 329 | 305 | 289 |
| DOF | 67 | 659 | 611 | 451 |
| Uniform DOF | 67 | 659 | 611 | 323 |
| Restricted arrays | Yes | Yes | Yes | No |
| Max. sources | 33 | 329 | 305 | 161 |
| $w(1)$ | 33 | 1 | 17 | 2 |
| $w(2)$ | 32 | 12 | 16 | 2 |
| $w(3)$ | 31 | 1 | 15 | 2 |
| Array | $\mathbb{S}^{(2)},$ $N_1 = N_2 = 17$ | $\mathbb{S}^{(3)},$ $N_1 = N_2 = 17$ | $\mathbb{S}^{(3)}, N_1 = 16, N_2 = 18$ | |
| Aperture | 305 | 305 | 305 | |
| DOF | 611 | 611 | 611 | |
| Uniform DOF | 611 | 611 | 611 | |
| Restricted arrays | Yes | Yes | Yes | |
| Max. sources | 305 | 305 | 305 | |
| $w(1)$ | 1 | 1 | 2 | |
| $w(2)$ | 16 | 9 | 8 | |
| $w(3)$ | 1 | 2 | 5 | |

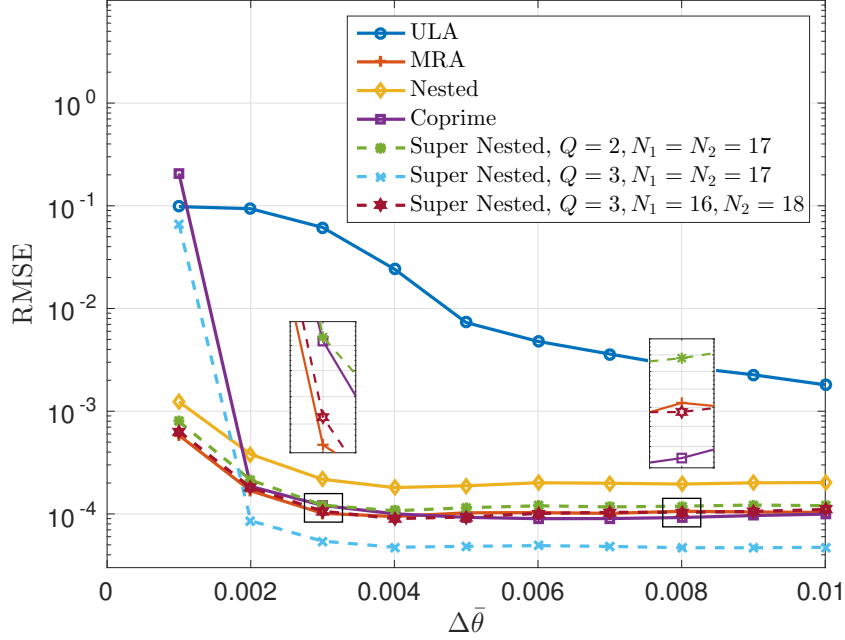


Figure 4.6: Estimation error as a function of source spacing $\Delta\bar{\theta}$ between two sources. The parameters are SNR = 0dB, $K = 500$. The sources have equal power and their normalized DOA are $\bar{\theta}_1 = \bar{\theta}_0 + \Delta\bar{\theta}/2$ and $\bar{\theta}_2 = \bar{\theta}_0 - \Delta\bar{\theta}/2$, where $\bar{\theta}_0 = 0.2$. Each point is an average over 1000 runs.

array with $Q = 3, N_1 = N_2 = 17$, and Definition 4.4.1 for the super nested array with $Q = 3, N_1 = 16, N_2 = 18$. More details on these arrays are listed in Table 4.2.

The experiments in this section are conducted as in Chapter 3. Sensor measurements are generated from the model with mutual coupling, as in (3.1). Then, for ULA, the MUSIC algorithm [150] is applied while for sparse arrays, the spatially smoothed MUSIC algorithm [87], [124], [125] is utilized to estimate the source directions. Note that *no decoupling algorithms* are involved. The parameters to be estimated are the normalized DOA: $\bar{\theta}_i = (d/\lambda) \sin \theta_i$, where $d = \lambda/2$ is the minimum sensor separation, λ is the wavelength, and $-\pi/2 \leq \theta_i \leq \pi/2$ is the DOA for the i th source. To compare the result quantitatively, the root-mean-squared error (RMSE) is defined as $E = (\sum_{i=1}^D (\hat{\theta}_i - \bar{\theta}_i)^2 / D)^{1/2}$, where $\hat{\theta}_i$ is the estimated normalized DOA of the i th source, calculated from the root MUSIC algorithm, and $\bar{\theta}_i$ is the true normalized DOA.

Two Closely-Spaced Sources

In this example, two closely-spaced sources with equal power are presented. The parameters are 0 dB SNR, and $K = 500$ snapshots. The mutual coupling matrix is based on linear dipole antennas, as in (3.2). We choose the carrier frequency $f = 2.4$ GHz so $\lambda = 0.1249$ m. The dipole length $l = \lambda/2$. The impedance $Z_A = Z_L = 50$

ohms. Two sources are located at $\bar{\theta}_1 = \bar{\theta}_0 + \Delta\bar{\theta}/2$ and $\bar{\theta}_2 = \bar{\theta}_0 - \Delta\bar{\theta}/2$, where $\bar{\theta}_0 = 0.2$. This experiment is repeated for 1000 runs, yielding 1000 instances of RMSE. In Fig. 4.6(a), the relationship between the source separation $\Delta\bar{\theta}$ and its RMSE, which is the sample mean of 1000 RMSE instances, is plotted. Some observations can be made from Fig. 4.6. First, all sparse arrays show a significant error reduction in almost all $\Delta\bar{\theta}$, compared to ULA. It can also be deduced from Fig. 4.6(a) that, as $\Delta\bar{\theta}$ increases, the coprime array becomes slightly better than the second-order super nested array and the third-order super nested array with even N_1 . The third-order super nested arrays with odd N_1 shows the best performance over $0.002 \leq \Delta\bar{\theta} \leq 0.01$ in Fig. 4.6, among all these array configurations.

Performance Evaluation under Various Parameters

The next simulation considers the performance over various SNR, number of snapshots, number of sources, and the mutual coupling matrices. The default parameter setting is 0 dB SNR, $K = 500$ snapshots, and $D = 20$ sources with equal power. The sources are located at $\bar{\theta}_i = -0.45 + 0.9(i - 1)/(D - 1)$ for $1 \leq i \leq D$. It will be observed from the simulations that the coprime array outperforms the other array configurations if the number of sources is small and the mutual coupling is small. The super nested array with $Q = 3$ and odd N_1 exhibits the best performance when there are many sources and mutual coupling is severe.

In Fig. 4.7(a), the RMSE is plotted as a function of SNR. We see that the super nested arrays with $Q = 3$ are the best and ULA is the worst. Fig. 4.7(b) shows the RMSE versus the number of snapshots K , where the super nested arrays with $Q = 3$ demonstrate a significant reduction on RMSE. The coprime array becomes more accurate as the number of snapshots increases, and it works better than the second-order super nested array when K is above 200.

The relationship between the RMSE and the number of sources D is plotted in Fig. 4.7(c). The coprime array works the best if the number of sources is small. As D increases, the super nested arrays with $Q = 3$ own the minimum RMSE. The reason is, coprime arrays might own the least mutual coupling effect while third-order super nested arrays possess larger uniform DOF. If D is small, mutual coupling might be more important than uniform DOF. On the other hand, as the number of sources gets closer to the theoretical limit, as shown in Table 4.2, the performance worsens for any array. This phenomenon happens sooner in the coprime array (around $D = 30$) than in the third-order super nested arrays (around $D = 50$), since the coprime array detects at most 161 sources while the third-order super nested arrays can resolve up to 305 sources.

Fig. 4.8 examines the RMSE of various arrays under various amount of mutual cou-

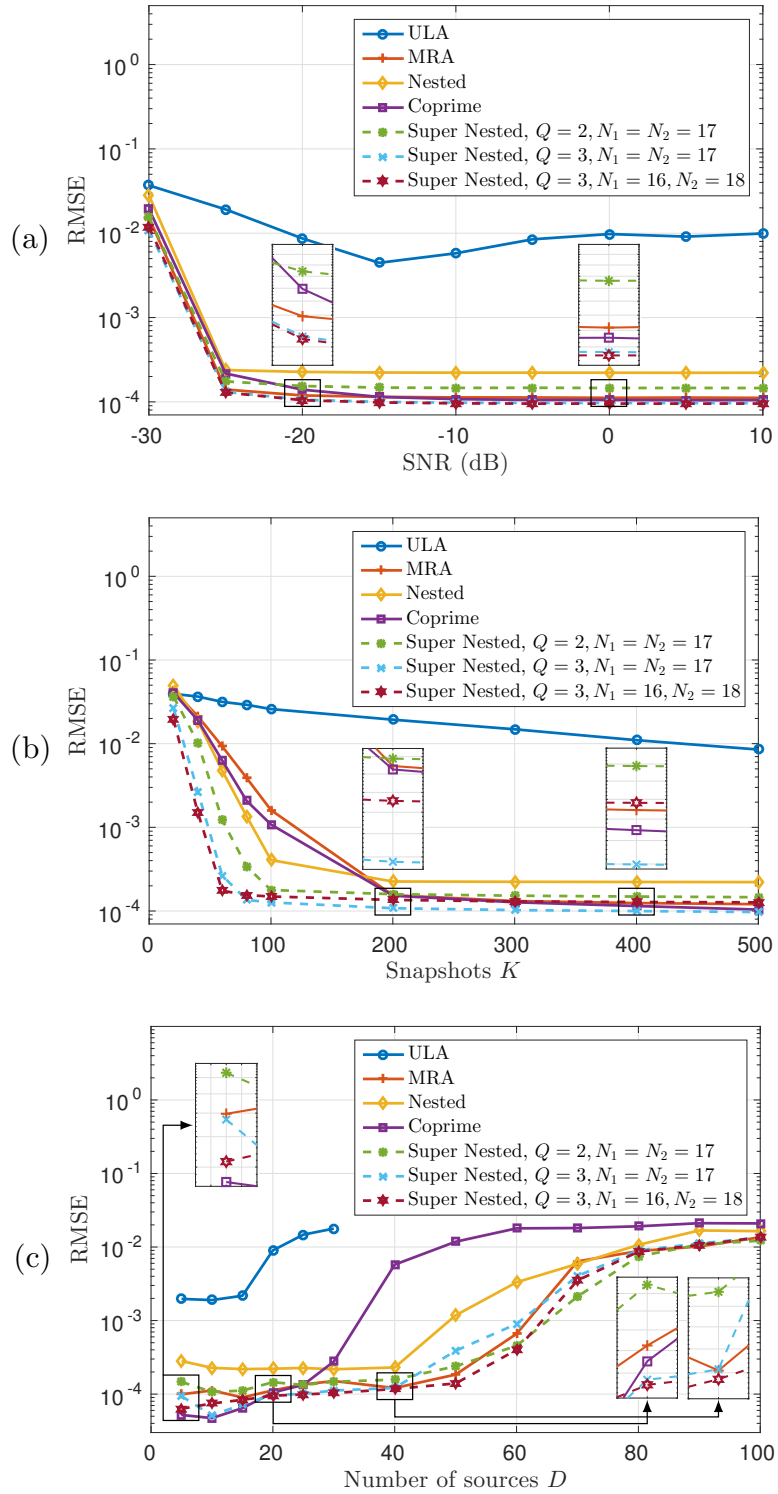


Figure 4.7: Estimation error as a function of (a) SNR, (b) the number of snapshots K , and (c) the number of sources D . The parameters are (a) $K = 500$, $D = 20$, (b) SNR = 0dB, $D = 20$, and (c) SNR = 0dB, $K = 500$. The sources have equal power and normalized DOA $\hat{\theta}_i = -0.45 + 0.9(i - 1)/(D - 1)$ for $1 \leq i \leq D$. Each point is an average over 1000 runs.

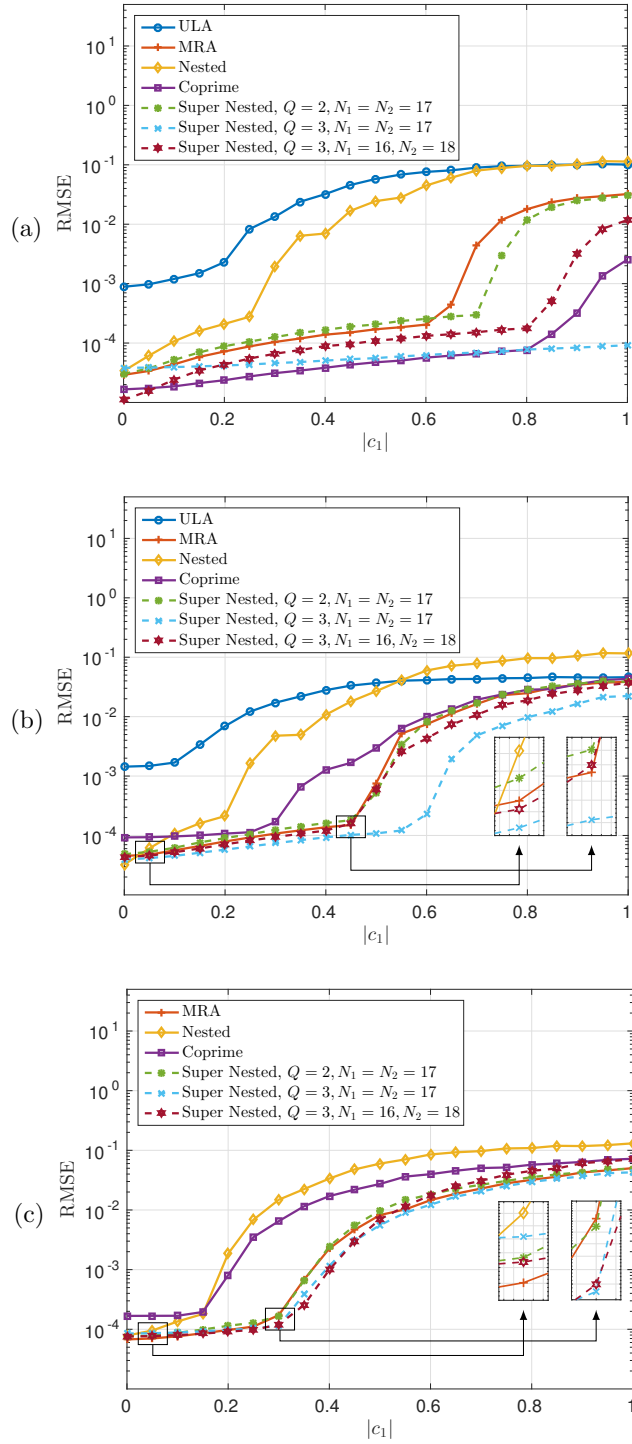


Figure 4.8: Estimation error as a function of mutual coupling coefficient c_1 (see Eq. (3.3)). The parameters are SNR = 0dB, $K = 500$, and the number of sources (a) $D = 10$, (b) $D = 20$, and (c) $D = 40$. The sources have equal power and are located at $\bar{\theta}_i = -0.45 + 0.9(i - 1)/(D - 1)$ for $1 \leq i \leq D$. The mutual coupling coefficients satisfy $|c_\ell/c_k| = k/\ell$ while the phases are randomly chosen from their domain. Each point is an average over 1000 runs.

pling effect and different number of sources $D = 10, 20,$ and 40 . Note that the total number of sensors is 34 , so $D = 40$ exceeds the resolution limit of ULA, as listed in Table 4.2. Here Eq. (3.3) is selected to be our mutual coupling model with $B = 3$. Notice that the larger the magnitudes of the mutual coupling coefficients c_1, c_2, \dots, c_B are, the more severe mutual coupling is. In this simulation, we first parametrize $|c_1|$ and then $|c_2|, \dots, |c_B|$ are obtained from the assumption that the magnitude of mutual coupling coefficients is inversely proportional to the sensor separation. In each run, the phases of c_1, c_2, \dots, c_B are randomly drawn from $[-\pi, \pi)$, the root MUSIC algorithm is used to estimate the DOA of D sources, located at $\bar{\theta}_i = -0.45 + 0.9(i - 1)/(D - 1)$ for $1 \leq i \leq D$. Finally the RMSE is evaluated. Each data point in Fig. 4.8 is the sample mean of 1000 runs.

Some observations can be drawn from Fig. 4.8. First, for any array geometry, as $|c_1|$ increases, the associated RMSE increases. This is reasonable since larger $|c_1|$ introduces more severe mutual coupling effect. Second, array configurations seem to have a direct impact on the robustness under mutual coupling. Most curves have turning points, or thresholds, such that the performance starts to become much worse. Hence larger thresholds imply the associated arrays are more tolerant to severe mutual coupling. Note that this threshold depends on the number of sources D . For instance, in coprime arrays, the thresholds in $|c_1|$ are $0.8, 0.3,$ and 0.15 for $D = 10, D = 20,$ and $D = 40,$ respectively. In the super nested array with $Q = 2,$ the threshold moves from $0.7,$ to $0.45,$ to $0.35,$ as D goes from $10,$ to $20,$ to $40.$ An interesting observation is that, the super nested array with $Q = 3$ and odd N_1 are quite robust in the case of severe mutual coupling and many sources.

Another way to interpret Fig. 4.8 is to consider a fixed D and a fixed $|c_1|$. In most cases, the super nested array with $Q = 3$ and odd N_1 give the minimum RMSE. The exception occurs in Fig. 4.8(a) when $D = 10$ and $0.1 < |c_1| < 0.8,$ where coprime arrays become the best. This result is consistent with that in Fig. 4.7(c), where coprime arrays work slightly better if the number of sources is small.

4.8 Concluding Remarks

In this chapter, we presented an extension of super nested arrays, called the Q th-order super nested arrays. These arrays preserve all the properties of nested arrays, while significantly reducing the effects of mutual coupling between sensors, by decreasing the number of sensor pairs with small separation. In the future, it will be of interest to apply to these arrays the decoupling algorithms developed in earlier literature for mitigating mutual coupling effects [20], [38], [49], [83], [151], [172], [199]. This will further improve the detection and estimation performance of these arrays. Another direction is the extension of linear super nested arrays to the case of planar arrays, as we will elaborate in Chapter 5.

HOURGLASS ARRAYS, AND OTHER NOVEL 2D SPARSE ARRAYS WITH REDUCED MUTUAL COUPLING

5.1 Introduction

Planar (2D) arrays find useful applications in beamforming, radar, imaging, and communications [58], [157], [188]. They can jointly estimate the azimuth and elevation of sources [188]. Some well-known 2D array geometries include uniform rectangular arrays (URA), uniform circular arrays (UCA), and hexagonal arrays, in which elements are placed uniformly on regular contours [188]. However, these array configurations usually suffer from significant mutual coupling, resulting in considerable interferences between sensor outputs [11], [49]. In Chapters 3 and 4, we proposed the super nested array in 1D, which has many of the good properties of the nested array, and at the same time achieves reduced mutual coupling. In this chapter, we will propose several planar arrays with large hole-free difference coarrays and reduced mutual coupling.

Planar arrays with hole-free difference coarrays (that is, coarrays that are URAs), are important for several reasons. First, if the coarrays have $\mathcal{O}(N^2)$ elements, then

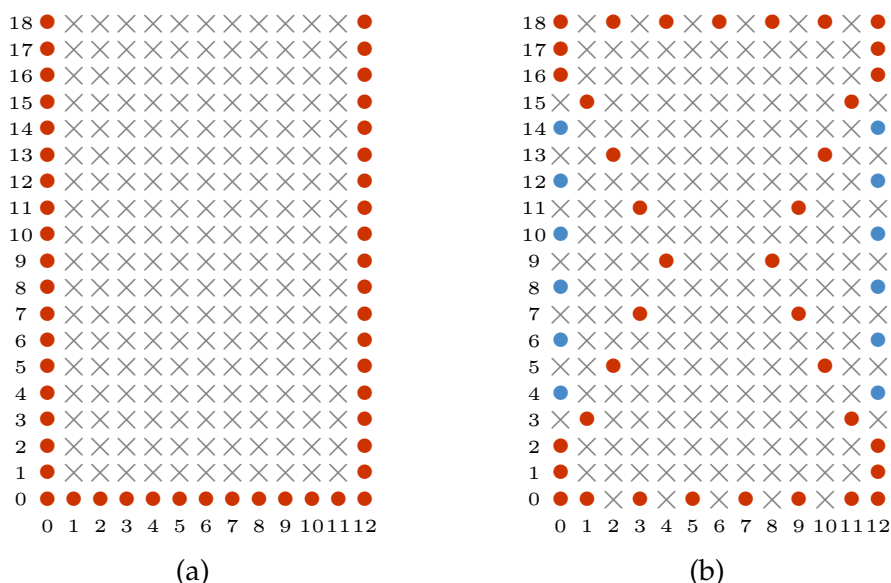


Figure 5.1: The array geometry of (a) open box arrays (OBA) and (b) hourglass arrays, in units of half of the wavelength ($\lambda/2$). Definitions 5.2.3 and 5.6.1 give the formal description. The parameters are $N_x = 13$ and $N_y = 19$. Red and blue bullets represent physical sensors while crosses denote empty space.

$\mathcal{O}(N^2)$ uncorrelated DOAs can be identified under some restrictions on the DOA locations [122]¹. Second, there is evidence from the literature on 2D arrays [56], [59] that sparse arrays with hole-free coarrays produce better responses in beam-forming applications. Finally, when DOA estimation algorithms such as MUSIC and ESPRIT are used directly on the sparse array, they do not work well, as they create ambiguities [109], [184]. However, if these algorithms are used on the ULA or URA part of the coarray domain (e.g., using spatial smoothing), they work very well [122], [124], [125], [139], [153], [175], [186]. For these reasons, we focus on the design of 2D sparse arrays with coarrays which are URAs with $\mathcal{O}(N^2)$ elements.

For 2D arrays, it is desirable to have closed-form sensor locations, large and hole-free difference coarrays, and less mutual coupling, like 1D super nested arrays. However, such 2D arrays are not fully explored in the literature. Some existing designs enjoy closed-form sensor locations with hole-free coarrays, including billboard arrays, 2D nested arrays, and open box arrays (OBA) [51], [56], [59], [121]. Hence, inspired by [67], one can expect that these 2D sparse arrays could distinguish more sources than sensors almost surely. Nevertheless, none of them takes the mutual coupling issue into account.

In this chapter, we will develop some new 2D sparse arrays that decrease mutual coupling effects in OBA. These novel array configurations include *half open box arrays (HOBA)*, *half open box arrays with two layers (HOBA-2)*, and *hourglass arrays*. By redistributing the sensors in OBA systematically, these arrays are guaranteed to have the same number of sensors as OBA, and to possess hole-free coarrays with enhanced degrees of freedom (Theorem 5.3.1, 5.4.1, 5.5.1, and 5.6.1), which makes it possible to detect more sources than sensors. Moreover, it will be shown that the number of sensor pairs with small spacing ($\lambda/2$ and $\sqrt{2}\lambda/2$) decreases considerably (Table 5.1), indicating that mutual coupling effect decreases significantly.

Fig. 5.1 offers a first glance of (a) OBA and (b) hourglass arrays. The array geometry for OBA resembles the side view of a box with an open top. The sensor locations for hourglass arrays resemble an hourglass with two pillars on both sides. The closed-form sensor locations for these arrays will be shown in Definitions 5.2.3 and 5.6.1, respectively.

In this example, it can be shown that both arrays have 49 physical sensors and hole-free coarrays. However, in OBA, there are 12 sensor pairs with separation $(\lambda/2, 0)$ and 36 pairs with separation $(0, \lambda/2)$. On the other hand, in hourglass arrays, there are only 2 sensor pairs with separation $(\lambda/2, 0)$ and 8 pairs with spacing $(0, \lambda/2)$, which are much smaller than those in OBA. This property makes hourglass arrays

¹ For arbitrary source locations, the $\mathcal{O}(N^2)$ result is not as strong as in the 1D case because identifiability in 2D can only be guaranteed in an almost sure sense [67].

more robust to mutual coupling effects, as demonstrated in Section 5.8. All these properties will be given in depth later.

The chapter outline is as follows. Section 5.2 reviews the data model and several well-known 2D arrays, like URA, billboard arrays, 2D nested arrays, and OBA. In Section 5.3, the horizontal segment in OBA is generalized into partially open box arrays (POBA) and half open box arrays (HOBA). Section 5.4 extends POBA to POBA with L layers (POBA- L) by designing the vertical segments in POBA properly. Section 5.5 and 5.6 propose HOBA with two layers (HOBA-2), and hourglass arrays, respectively, based on the theory developed in Section 5.4. For all these 2D arrays, the expression for the weight functions with small separations are listed in Section 5.7 with detailed derivation. Section 5.8 demonstrates the superior performance of the proposed arrays in the presence of mutual coupling while Section 5.9 concludes this chapter.

For the reader's convenience, [99] provides a MATLAB function `POBA_L.m`, which takes some descriptive parameters of the array as inputs and returns the sensor locations as outputs. Furthermore, `interactive_interface.m` offers an interactive panel where users can readily design their array geometries and visualize the weight functions.

5.2 Preliminaries

The Data Model

Suppose D uncorrelated sources impinge on a 2D array, whose sensors are located at $\mathbf{n}d$. Here $\mathbf{n} = (n_x, n_y) \in \mathbb{Z}^2$ is an integer-valued vector and $d = \lambda/2$ is the minimum separation between sensors. The sensor locations \mathbf{n} form a set \mathbb{S} . The i th source has complex amplitude $A_i \in \mathbb{C}$, azimuth $\phi_i \in [0, 2\pi]$, and elevation $\theta_i \in [0, \pi]$. If mutual coupling is absent, the sensor output on \mathbb{S} can be modeled as

$$\mathbf{x}_{\mathbb{S}} = \sum_{i=1}^D A_i \mathbf{v}_{\mathbb{S}}(\bar{\theta}_i, \bar{\phi}_i) + \mathbf{n}_{\mathbb{S}}, \quad (5.1)$$

where $\bar{\theta}_i = (d/\lambda) \sin \theta_i \cos \phi_i$ and $\bar{\phi}_i = (d/\lambda) \sin \theta_i \sin \phi_i$ are the normalized DOA. The element of the steering vector $\mathbf{v}_{\mathbb{S}}(\bar{\theta}_i, \bar{\phi}_i)$ corresponding to the sensor at $(n_x, n_y) \in \mathbb{S}$ is $\exp[j2\pi(\bar{\theta}_i n_x + \bar{\phi}_i n_y)]$. Signals and noise are assumed to be zero-mean and uncorrelated. That is, $E[A_i] = 0$, $E[\mathbf{n}_{\mathbb{S}}] = \mathbf{0}$, $E[A_i A_j^*] = p_i \delta_{i,j}$, $E[\mathbf{n}_{\mathbb{S}} \mathbf{n}_{\mathbb{S}}^H] = p_n \mathbf{I}$, $E[A_i \mathbf{n}_{\mathbb{S}}^H] = \mathbf{0}$, where p_i and p_n are the i th source power and the noise power, respectively. $\delta_{p,q}$ is the Kronecker delta.

For uncorrelated sources, the covariance matrix of $\mathbf{x}_{\mathbb{S}}$ can be expressed as

$$\mathbf{R}_{\mathbb{S}} = E[\mathbf{x}_{\mathbb{S}} \mathbf{x}_{\mathbb{S}}^H] = \sum_{i=1}^D p_i \mathbf{v}_{\mathbb{S}}(\bar{\theta}_i, \bar{\phi}_i) \mathbf{v}_{\mathbb{S}}^H(\bar{\theta}_i, \bar{\phi}_i) + p_n \mathbf{I}. \quad (5.2)$$

Vectorizing (5.2) and removing duplicated entries yield the signal on the difference coarray [87], [108], [124], [125]:

$$\mathbf{x}_{\mathbb{D}} = \sum_{i=1}^D p_i \mathbf{v}_{\mathbb{D}}(\bar{\theta}_i, \bar{\phi}_i) + p_n \mathbf{e}_0, \quad (5.3)$$

where \mathbf{e}_0 is a column vector with $\langle \mathbf{e}_0 \rangle_{(n_x, n_y)} = \delta_{n_x, 0} \delta_{n_y, 0}$. The bracket notation $\langle \mathbf{x}_{\mathbb{S}} \rangle_{\mathbf{n}}$ [87] denotes the value of the signal at the support location $\mathbf{n} \in \mathbb{S}$. For instance, if $\mathbb{S} = \{(0, 0), (1, 0), (0, 1)\}$ and $\mathbf{x}_{\mathbb{S}} = [4, 5, 6]^T$, then $\langle \mathbf{x}_{\mathbb{S}} \rangle_{(0,0)} = 4$, $\langle \mathbf{x}_{\mathbb{S}} \rangle_{(1,0)} = 5$, and $\langle \mathbf{x}_{\mathbb{S}} \rangle_{(0,1)} = 6$. \mathbb{D} is the difference coarray, which is defined as

Definition 5.2.1 (Difference coarray). For a 2D array specified by \mathbb{S} , its difference coarray \mathbb{D} is defined as the differences between sensor locations:

$$\mathbb{D} = \{\mathbf{n}_1 - \mathbf{n}_2 : \mathbf{n}_1, \mathbf{n}_2 \in \mathbb{S}\}.$$

For example, if \mathbb{S} consists of $(0, 0), (1, 0), (2, 0), (0, 1), (2, 1), (0, 2), (2, 2)$, then the difference coarray \mathbb{D} is composed of integer vectors (m_x, m_y) such that $-2 \leq m_x, m_y \leq 2$. The uniform rectangular part of \mathbb{D} is denoted by \mathbb{U} . In this example, $\mathbb{D} = \mathbb{U}$, and such array is said to have a *hole-free coarray*. More generally, if the coarray is the set of all integer vectors within a parallelepiped, we can regard it as hole-free, but we shall not consider this extension here.

If mutual coupling is present, the data model (5.1) becomes

$$\mathbf{x}_{\mathbb{S}} = \sum_{i=1}^D A_i \mathbf{C} \mathbf{v}_{\mathbb{S}}(\bar{\theta}_i, \bar{\phi}_i) + \mathbf{n}_{\mathbb{S}}, \quad (5.4)$$

where \mathbf{C} is the mutual coupling matrix [21], [49], [172], [173]. In this chapter, we assume that the entries of \mathbf{C} can be characterized by [49]

$$\langle \mathbf{C} \rangle_{\mathbf{n}_1, \mathbf{n}_2} = \begin{cases} c(\|\mathbf{n}_1 - \mathbf{n}_2\|_2), & \text{if } \|\mathbf{n}_1 - \mathbf{n}_2\|_2 \leq B, \\ 0 & \text{otherwise,} \end{cases} \quad (5.5)$$

where $\mathbf{n}_1, \mathbf{n}_2 \in \mathbb{S}$ denote the sensor locations. Here $\|\cdot\|_2$ is the ℓ_2 -norm of a vector and $c(\cdot)$ are the mutual coupling coefficients. It is assumed that $c(0) = 1$ and $|c(k)/c(\ell)| = \ell/k$ for $k, \ell > 0$ [49], implying that the arrays with larger sensor separations, like sparse arrays, tend to reduce mutual coupling. To quantify mutual coupling, we first define the weight function:

Definition 5.2.2 (Weight function). Let a 2D array be specified by \mathbb{S} , and let its difference coarray be \mathbb{D} . The weight function $w(\mathbf{m})$ is the number of pairs with separation $\mathbf{m} \in \mathbb{D}$, i.e.,

$$w(\mathbf{m}) = |\{(\mathbf{n}_1, \mathbf{n}_2) \in \mathbb{S}^2 : \mathbf{n}_1 - \mathbf{n}_2 = \mathbf{m}\}|.$$

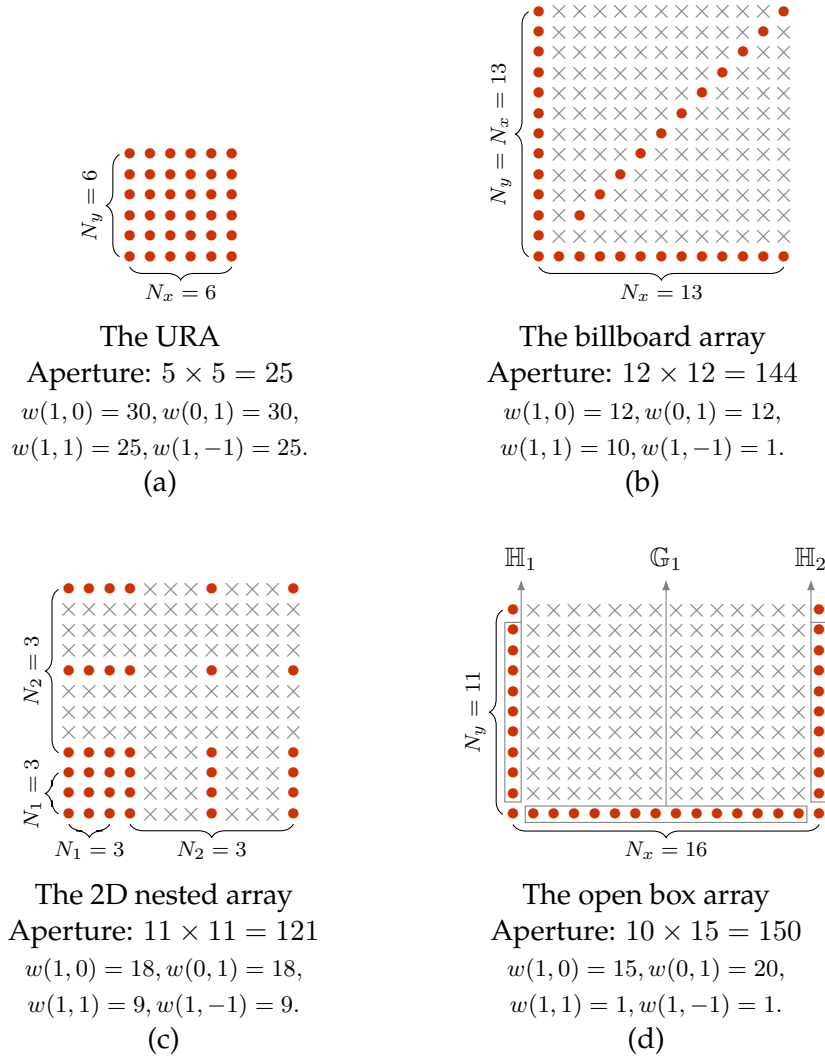


Figure 5.2: Examples of 2D arrays with $N = 36$ elements. Bullets denote physical sensors and crosses represent empty space. The minimum separation between sensors is $\lambda/2$.

We will use $w(\mathbf{m})$ and $w(m_x, m_y)$ interchangeably, where $\mathbf{m} = (m_x, m_y)$. It was shown in [92] that, qualitatively, smaller weight functions at small sensor separations reduce the effect of mutual coupling significantly.

Known Closed-Form 2D Sparse Arrays

In this subsection, we will review some known 2D arrays on rectangular grids with regular geometries, in Fig. 5.2.

The URA places $N_x N_y$ sensors on an N_y -by- N_x rectangular grid, as demonstrated in Fig. 5.2(a) for 36 sensors. The billboard array [51] consists of three ULA on a square aperture ($N_x = N_y$) and the total number of sensors is $3(N_x - 1)$, as in Fig. 5.2(b).

The 2D nested array [121] is depicted in Fig. 5.2(c). In this example, this array is the cross product of two identical 1D nested arrays with $N_1 = N_2 = 3$ (notation as in [124]) and the number of sensors is $(N_1 + N_2)^2$. Finally, the open box array [56] assigns $N_x + 2N_y - 2$ sensors on the boundaries of a rectangular aperture, as illustrated in Fig. 5.2(d). The definition of OBA is also given by²

Definition 5.2.3 (Open box arrays, OBA). Let N_x and N_y be positive integers. An open box array is characterized by the integer set \mathbb{S}_{OBA} , defined by

$$\begin{aligned} \mathbb{S}_{\text{OBA}} = & \{(0, 0), (N_x - 1, 0), (0, N_y - 1), (N_x - 1, N_y - 1)\} \\ & \cup \mathbb{G}_1 \cup \mathbb{H}_1 \cup \mathbb{H}_2, \end{aligned}$$

where $\mathbb{G}_1 = \{(n_x, 0) : n_x \in \mathfrak{g}_1\}$, $\mathbb{H}_1 = \{(0, n_y) : n_y \in \mathfrak{h}_1\}$, and $\mathbb{H}_2 = \{(N_x - 1, n_y) : n_y \in \mathfrak{h}_2\}$. Here $\mathfrak{g}_1 = \{1, 2, \dots, N_x - 2\}$ and $\mathfrak{h}_1 = \mathfrak{h}_2 = \{1, 2, \dots, N_y - 2\}$.

Fig. 5.2(d) marks the sets \mathbb{G}_1 , \mathbb{H}_1 , and \mathbb{H}_2 in rectangles on the bottom, on the left, and on the right, respectively. Furthermore, the difference coarray of OBA is given as

$$\begin{aligned} \mathbb{D}_{\text{OBA}} = & \{(m_x, m_y) \in \mathbb{Z}^2 : -N_x + 1 \leq m_x \leq N_x - 1, \\ & -N_y + 1 \leq m_y \leq N_y - 1\}, \end{aligned} \quad (5.6)$$

which is exactly a uniform rectangular region.

All of the arrays in Fig. 5.2 have 36 physical sensors and hole-free coarrays ($\mathbb{D} = \mathbb{U}$). However, the sizes of difference coarrays are different. The largest $|\mathbb{D}|$ is exhibited by the OBA (651), followed by the billboard array (625), the 2D nested array (529), and finally the URA (121). Empirically, larger $|\mathbb{D}|$ is more likely to offer better spatial resolution and more resolvable uncorrelated sources, so that in Fig. 5.2, the OBA is preferred.

Weight functions with small separations, such as $w(1, 0)$, $w(0, 1)$, $w(1, 1)$, and $w(1, -1)$, are also listed in Fig. 5.2. Notice that for the arrays mentioned herein, these weights are not small. For instance, the OBA has $w(1, 0) = 15$ and $w(0, 1) = 20$, due to the dense ULA on the boundaries. It is desirable to reduce $w(1, 0)$, $w(0, 1)$, $w(1, 1)$, and $w(1, -1)$ simultaneously, so that mutual coupling can be mitigated.

5.3 Generalization of \mathbb{G}_1 in OBA

In this section, we will develop generalizations of OBA. The reason why we start with OBA is that, based on Fig. 5.2, they have the largest aperture for the same number of sensors, leading to the best spatial resolution.

² In this chapter, the sensor locations are defined formally, as in Definition 5.2.3. This helps to develop novel array configurations systematically and to compute the sensor locations readily [99].

Partially Open Box Arrays (POBA)

The main idea of partially open box arrays (POBA) is to redistribute the elements in the dense ULA, so that the weight functions for small separations decrease. In this section, we focus on the set $\mathbb{G}_1 \cup \{(0, 0), (N_x - 1, 0)\}$, i.e., the N_x sensors on the bottom of Fig. 5.2(d). These sensors contribute to the weight function $w(1, 0)$. If we can relocate some of these sensors, it is possible to reduce $w(1, 0)$.

However, if we move these sensors arbitrarily, the difference coarray would no longer be hole-free and the estimation performance is degraded. Before we explain how to keep the difference coarray intact, we consider the following notations: Let \mathbb{S}_{OBA} be an OBA with sizes N_x and N_y , as in Definition 5.2.3, and let \mathbb{D}_{OBA} , as in (5.6), be the difference coarray. Assume we select P distinct sensors, located at $(n_p, 0) \in \mathbb{S}_{\text{OBA}}$ for $p = 1, 2, \dots, P$ and $P < N_x$. These sensors are relocated to P distinct locations, $(a_p, b_p) \notin \mathbb{S}_{\text{OBA}}$, yielding a new 2D array \mathbb{S}' and its coarray \mathbb{D}' . Then we have the following lemma:

Lemma 5.3.1. $\mathbb{D}_{\text{OBA}} = \mathbb{D}'$ only if $1 \leq a_p \leq N_x - 2$ and $1 \leq b_p \leq N_y - 1$ for all $p = 1, 2, \dots, P$, i.e., only if **the new sensor locations are inside the original array aperture**.

Proof. See Appendix 5.A. □

We can exclude $a_p = 0, N_x - 1$ or $b_p = 0$ in Lemma 5.3.1, since by assumption, $(a_p, b_p) \notin \mathbb{S}_{\text{OBA}}$.

Lemma 5.3.2. $\mathbb{D}_{\text{OBA}} = \mathbb{D}'$ only if $(0, 0) \in \mathbb{S}'$ and $(N_x - 1, 0) \in \mathbb{S}'$, where all notations are as stated before Lemma 5.3.1.

Proof. See Appendix 5.B. □

Lemma 5.3.1 and 5.3.2 indicate that for the sensors located on the bottom of OBA, only those at $(n, 0)$, where $1 \leq n \leq N_x - 2$, can be redistributed within the original aperture. For simplicity, we assume all the new sensor locations have y coordinate $N_y - 1$, i.e., $b_p = N_y - 1$ for all p in Lemma 5.3.1, which leads to the definition of POBA:

Definition 5.3.1 (Partially open box arrays, POBA). For two positive integers N_x and N_y , a partially open box array has the sensor locations defined by the integer set \mathbb{S}_{POBA} ,

$$\begin{aligned} \mathbb{S}_{\text{POBA}} = \{ & (0, 0), (N_x - 1, 0), (0, N_y - 1), (N_x - 1, N_y - 1) \} \\ & \cup \mathbb{G}_1 \cup \mathbb{G}_2 \cup \mathbb{H}_1 \cup \mathbb{H}_2, \end{aligned}$$

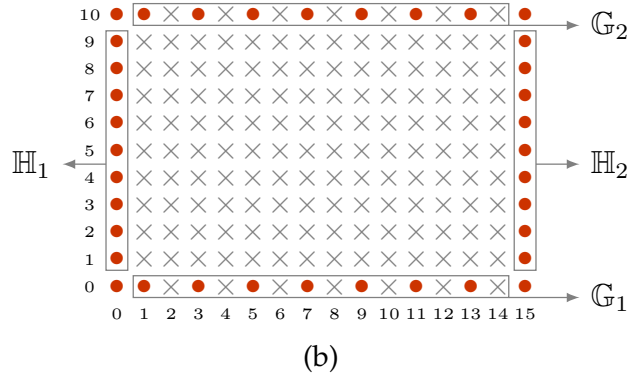
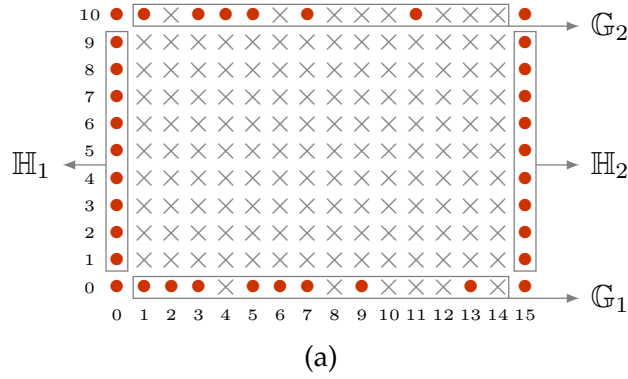


Figure 5.3: Examples of POBA with $N_x = 16$ and $N_y = 11$. (a) $\mathfrak{g}_1 = \{1, 2, 3, 5, 6, 7, 9, 13\}$, $\mathfrak{g}_2 = \{1, 3, 4, 5, 7, 11\}$, and (b) $\mathfrak{g}_1 = \mathfrak{g}_2 = \{1, 3, 5, 7, 9, 11, 13\}$. In both cases, \mathfrak{g}_2 satisfies Theorem 5.3.1.

where $\mathbb{G}_1 = \{(n_x, 0) : n_x \in \mathfrak{g}_1\}$, $\mathbb{G}_2 = \{(n_x, N_y - 1) : n_x \in \mathfrak{g}_2\}$, $\mathbb{H}_1 = \{(0, n_y) : n_y \in \mathfrak{h}_1\}$, $\mathbb{H}_2 = \{(N_x - 1, n_y) : n_y \in \mathfrak{h}_2\}$. Here \mathfrak{g}_1 , \mathfrak{g}_2 , \mathfrak{h}_1 , and \mathfrak{h}_2 satisfy

1. \mathfrak{g}_1 and \mathfrak{g}_2 are subsets of $\{1, 2, \dots, N_x - 2\}$.
2. $|\mathfrak{g}_1| + |\mathfrak{g}_2| = N_x - 2$.
3. $\mathfrak{h}_1 = \mathfrak{h}_2 = \{1, 2, \dots, N_y - 2\}$.

Note that sample MATLAB codes for POBA and all the proposed array geometries can be found in [99]. To give some feeling for POBA, let us consider two examples in Fig. 5.3, where $N_x = 16$, $N_y = 11$ and the sets \mathbb{G}_1 , \mathbb{G}_2 , \mathbb{H}_1 , and \mathbb{H}_2 are marked in rectangles. Fig. 5.3(a) illustrates the POBA with $\mathfrak{g}_1 = \{1, 2, 3, 5, 6, 7, 9, 13\}$ and $\mathfrak{g}_2 = \{1, 3, 4, 5, 7, 11\}$, which are subsets of $\{1, 2, \dots, 14\}$. Furthermore, $|\mathfrak{g}_1| + |\mathfrak{g}_2| = 8 + 6 = 14$ satisfies the second item in Definition 5.3.1. Fig. 5.3(b) also satisfies Definition 5.3.1. The missing elements (crosses) in \mathbb{G}_1 migrate to the elements (bullets) in \mathbb{G}_2 .

Next, we will develop the difference coarray of POBA. The following theorem states a necessary and sufficient condition under which OBA and POBA share the same hole-free difference coarray:

Theorem 5.3.1. Consider an open box array and a partially open box array with the same N_x and N_y , as defined in Definition 5.2.3 and 5.3.1, respectively. Then, their difference coarrays are identical if and only if $\{\mathfrak{g}_1, N_x - 1 - \mathfrak{g}_2\}$ is a partition of $\{1, 2, \dots, N_x - 2\}$, i.e., if and only if 1) $\mathfrak{g}_1 \cup (N_x - 1 - \mathfrak{g}_2) = \{1, 2, \dots, N_x - 2\}$ and 2) \mathfrak{g}_1 and $N_x - 1 - \mathfrak{g}_2$ are disjoint. Here $N_x - 1 - \mathfrak{g}_2 = \{N_x - 1 - g : \forall g \in \mathfrak{g}_2\}$.

Proof. See Appendix 5.C. □

Let us consider some examples of Theorem 5.3.1. OBA are special cases of POBA with $\mathfrak{g}_1 = \{1, 2, \dots, N_x - 2\}$ and \mathfrak{g}_2 being the empty set, which satisfy Theorem 5.3.1. For POBA in Fig. 5.3, the corresponding \mathfrak{g}_1 and \mathfrak{g}_2 also satisfy Theorem 5.3.1, so their difference coarrays are hole-free, and the same as \mathbb{D}_{OBA} .

Furthermore, Theorem 5.3.1 offers simple and straightforward design methods for POBA with hole-free difference coarrays. The first step is to choose \mathfrak{g}_1 to be a subset of $\{1, 2, \dots, N_x - 2\}$. Next, \mathfrak{g}_2 can be uniquely determined since $\{\mathfrak{g}_1, N_x - 1 - \mathfrak{g}_2\}$ is a partition of $\{1, 2, \dots, N_x - 2\}$. Finally, the closed-form sensor locations are given in Definition 5.3.1. The freedom in the choice of such \mathfrak{g}_1 can be exploited to reduce mutual coupling effects as explained next.

Half Open Box Arrays (HOBA)

In this subsection, we will study the *half open box array* (HOBA), which is a particular instance of POBA with reduced mutual coupling. This is done by setting \mathfrak{g}_1 and \mathfrak{g}_2 to be ULA with separation 2, so that the weight function $w(1, 0)$ is as small as 2. HOBA are defined as:

Definition 5.3.2 (Half open box arrays, HOBA). The half open box array with parameters N_x and N_y is a partially open box array with

$$\mathfrak{g}_1 = \{1 + 2\ell : 0 \leq \ell \leq \lfloor (N_x - 3)/2 \rfloor\}, \quad (5.7)$$

$$\mathfrak{g}_2 = \{N_x - 1 - 2\ell : 1 \leq \ell \leq \lfloor (N_x - 2)/2 \rfloor\}. \quad (5.8)$$

According to (5.7), \mathfrak{g}_1 represents an ULA whose left-most element is 1 and the interelement spacing is 2. It can be shown that (5.7) and (5.8) meet Theorem 5.3.1, so that the difference coarray of HOBA is the same as that of OBA, and hence, hole-free. The sensor positions for HOBA can also be obtained from Definition 5.3.1 and 5.3.2 readily, even for large N_x and N_y .

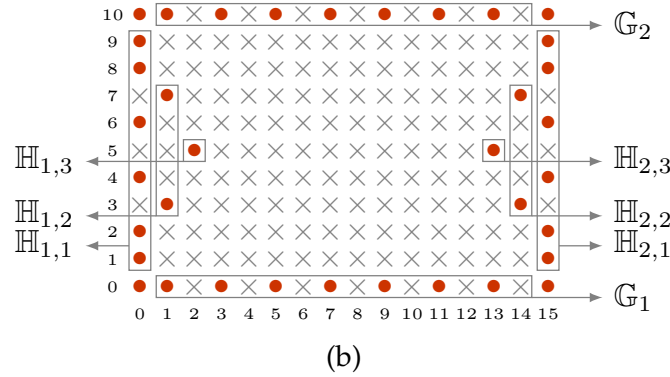
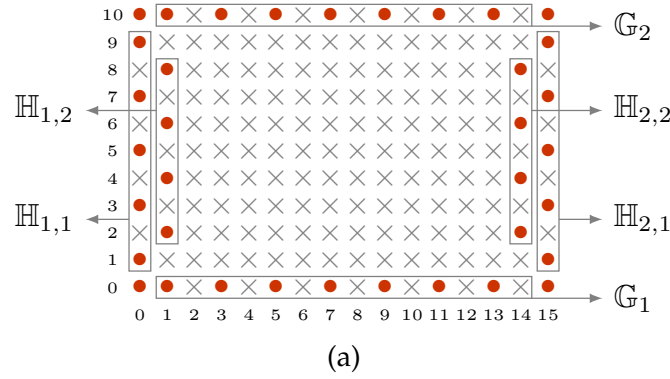


Figure 5.4: Examples of POBA- L . $N_x = 16$, $N_y = 11$, $\mathfrak{g}_1 = \mathfrak{g}_2 = \{1, 3, 5, 7, 9, 11, 13\}$. (a) $\mathfrak{h}_{1,1} = \{1, 3, 5, 7, 9\}$, $\mathfrak{h}_{1,2} = \{2, 4, 6, 8\}$, $L = 2$, and (b) $\mathfrak{h}_{1,1} = \{1, 2, 4, 6, 8, 9\}$, $\mathfrak{h}_{1,2} = \{3, 7\}$, $\mathfrak{h}_{1,3} = \{5\}$, $L = 3$.

Fig. 5.3(b) illustrates the HOBA with $N_x = 16$ and $N_y = 11$. It can be seen that, $|\mathfrak{g}_1| = |\mathfrak{g}_2| = 7$ and the weight functions for Fig. 5.3(b) are listed as follows:

$$w(1,0) = 2, \quad w(0,1) = 20, \quad w(1,1) = 1, \quad w(1,-1) = 1. \quad (5.9)$$

Compared to the OBA in Fig. 5.2(d), $w(1,0)$ decreases from 15 to 2 while $w(0,1)$, $w(1,1)$, and $w(1,-1)$ remain the same. To be more precise, the weight functions $w(1,0)$, $w(0,1)$, $w(1,1)$, $w(1,-1)$ are listed in Table 5.1 and the associated derivation can be found in Section 5.7. Therefore, the estimation performance for HOBA would be better than OBA in the presence of mutual coupling, since the weight function $w(1,0)$ for HOBA is significantly smaller.

5.4 Reorganization of \mathbb{H}_1 and \mathbb{H}_2 in OBA

In Section 5.3, the set \mathbb{G}_1 was reorganized into \mathbb{G}_1 and \mathbb{G}_2 , so that the weight function $w(1,0)$ decreases. However, the mutual coupling effect also depends on other weight functions with small separations, such as $w(0,1)$, $w(1,1)$, and $w(1,-1)$. In this section, we will develop generalizations of \mathbb{H}_1 and \mathbb{H}_2 such that the new arrays are guaranteed to have hole-free coarrays. These generalizations also provide some

insights to achieve smaller $w(0, 1)$, $w(1, 1)$, and $w(1, -1)$.

To begin with, let us consider HOBA, as shown in Fig. 5.3(b). If we redistribute the sensors in \mathbb{H}_1 and \mathbb{H}_2 , it is possible to reduce the weight function $w(0, 1)$. Fig. 5.4 depicts some extensions of HOBA. In Fig. 5.4(a), \mathbb{H}_1 is split into two layers, $\mathbb{H}_{1,1}$ and $\mathbb{H}_{1,2}$. Such rearrangement eliminates some sensor pairs with separation $(0, 1)$ in HOBA, like the sensor pair of $(0, 2)$ and $(0, 1)$. Fig. 5.4(b) extends \mathbb{H}_1 and \mathbb{H}_2 into three layers, $\mathbb{H}_{1,1}$, $\mathbb{H}_{1,2}$, $\mathbb{H}_{1,3}$, and $\mathbb{H}_{2,1}$, $\mathbb{H}_{2,2}$, $\mathbb{H}_{2,3}$, respectively. In particular, the weight functions $w(0, 1)$, $w(1, 1)$, and $w(1, -1)$ are listed as follows:

$$\begin{aligned} \text{Fig. 5.3(b):} & \quad w(0, 1) = 20, & w(1, 1) = 1, & w(1, -1) = 1, \\ \text{Fig. 5.4(a):} & \quad w(0, 1) = 4, & w(1, 1) = 9, & w(1, -1) = 9, \\ \text{Fig. 5.4(b):} & \quad w(0, 1) = 8, & w(1, 1) = 5, & w(1, -1) = 5. \end{aligned}$$

It can be deduced that the arrays in Fig. 5.4 enjoy smaller $w(0, 1)$ than that in Fig. 5.3(b). Note that smaller $w(1, 0)$ and $w(0, 1)$ are typically more important in mutual coupling models [92]. Besides, it will be shown later that the arrays in Fig. 5.4 own hole-free coarrays.

The arrays in Fig. 5.4 generalize the set \mathbb{H}_1 and \mathbb{H}_2 into multiple layers $\mathbb{H}_{1,\ell}$ and $\mathbb{H}_{2,\ell}$. This concept allows us to define *partially open box arrays with L layers* (POBA- L) as follows:

Definition 5.4.1 (Partially open box arrays with L layers, POBA- L). For two positive integers N_x and N_y and a positive integer $L \leq N_x/2$, a partially open box array with L layers has the sensor locations defined by the integer set $\mathbb{S}_{\text{POBA-}L}$,

$$\begin{aligned} \mathbb{S}_{\text{POBA-}L} = & \{(0, 0), (N_x - 1, 0), (0, N_y - 1), (N_x - 1, N_y - 1)\} \\ & \cup \mathbb{G}_1 \cup \mathbb{G}_2 \cup \left(\bigcup_{\ell=1}^L \mathbb{H}_{1,\ell} \cup \mathbb{H}_{2,\ell} \right), \end{aligned}$$

where $\mathbb{G}_1 = \{(n_x, 0) : n_x \in \mathfrak{g}_1\}$, $\mathbb{G}_2 = \{(n_x, N_y - 1) : n_x \in \mathfrak{g}_2\}$, $\mathbb{H}_{1,\ell} = \{(\ell - 1, n_y) : n_y \in \mathfrak{h}_{1,\ell}\}$, $\mathbb{H}_{2,\ell} = \{(N_x - \ell, n_y) : n_y \in \mathfrak{h}_{2,\ell}\}$. Here \mathfrak{g}_1 , \mathfrak{g}_2 , $\mathfrak{h}_{1,\ell}$, and $\mathfrak{h}_{2,\ell}$ satisfy

1. $\{\mathfrak{g}_1, N_x - 1 - \mathfrak{g}_2\}$ is a partition of $\{1, 2, \dots, N_x - 2\}$.
2. $\{\mathfrak{h}_{1,\ell}\}_{\ell=1}^L$ is a partition of $\{1, 2, \dots, N_y - 2\}$.
3. $\mathfrak{h}_{2,\ell} = N_y - 1 - \mathfrak{h}_{1,\ell}$ for $\ell = 1, \dots, L$.

The first constraint on \mathfrak{g}_1 , \mathfrak{g}_2 is due to Theorem 5.3.1. The second requirement indicates the sets $\mathbb{H}_{1,\ell}$ originate from \mathbb{H}_1 in POBA. Furthermore, the third condition enforces $\mathfrak{h}_{1,\ell}$ and $\mathfrak{h}_{2,\ell}$ to be symmetric to $N_y - 1$, which will play a crucial role in

analyzing the difference coarray. Note that, by definition, the number of sensors in POBA- L is identical to that in OBA.

Now it is clear that the arrays in Fig. 5.3 and Fig. 5.4 all satisfy Definition 5.4.1. They are characterized by different parameters L , \mathfrak{g}_1 , and $\mathfrak{h}_{1,\ell}$. For instance, the HOBA in Fig. 5.3(b) corresponds to $\mathfrak{g}_1 = \{1, 3, 5, 7, 9, 11, 13\}$, $L = 1$, and $\mathfrak{h}_{1,1} = \{1, \dots, 9\}$. The parameters for the arrays in Fig. 5.4 are listed in the caption.

Our next theorem determines a necessary and sufficient condition in terms of $\mathfrak{h}_{1,\ell}$ under which POBA- L have hole-free difference coarrays:

Theorem 5.4.1. Let N_x and N_y be positive integers. Let $\mathbb{D}_{\text{POBA-}L}$ be the difference coarray of a partially open box array with parameters N_x , N_y , and L layers. Let \mathbb{D}_{OBA} be the difference coarray of an open box array with parameters N_x and N_y . Then $\mathbb{D}_{\text{POBA-}L} = \mathbb{D}_{\text{OBA}}$ if and only if

$$\mathfrak{h}_{1,\ell} \subseteq \mathbb{P}_{\ell'} \text{ and } \mathfrak{h}_{1,\ell} \subseteq \mathbb{P}_{\ell'} - (N_y - 1), \quad (5.10)$$

where $\mathbb{P}_{\ell'} = \cup_{p+q=\ell'} \mathfrak{h}_{1,p} \oplus \mathfrak{h}_{1,q}$ for all $2 \leq \ell' \leq \ell$. Here $\mathbb{A} \oplus \mathbb{B} = \{a + b : a \in \mathbb{A}, b \in \mathbb{B}\}$ is the direct sum of \mathbb{A} and \mathbb{B} .

Proof. See Appendix 5.D. □

The importance of Theorem 5.4.1 resides in the following: Since the sets $\mathfrak{h}_{1,\ell}$ have smaller sizes than the 2D array $\mathbb{S}_{\text{POBA-}L}$, it is more tractable to verify (5.10) than to calculate $\mathbb{D}_{\text{POBA-}L}$ directly. Furthermore, if (5.10) is *not* satisfied, then all the holes in $\mathbb{D}_{\text{POBA-}L}$ can be identified from the 1D sets $\mathfrak{h}_{1,\ell}$, based on the necessity proof of Theorem 5.4.1. Another advantage is that, we can use (5.10) to design new array configurations with reduced mutual coupling. By choosing $\mathfrak{h}_{1,\ell}$ appropriately, it is possible to reduce the weight function $w(0, 1)$, $w(1, 1)$, and $w(1, -1)$ systematically.

In Section 5.5 and 5.6, we will propose half open box arrays with two layers and hourglass arrays, respectively. These arrays not only have simple, closed-form sensor locations but also satisfy Theorem 5.4.1, so that their difference coarrays are hole-free. The weight functions of these novel array configurations will be summarized in Section 5.7.

5.5 Half Open Box Arrays with Two Layers (HOBA-2)

We now introduce *the half open box array with two layers* (HOBA-2). This array is defined by choosing $\mathfrak{h}_{1,2}$ to be ULA with separation 2, so that the weight function $w(0, 1)$ decreases. The formal definition is given as follows:

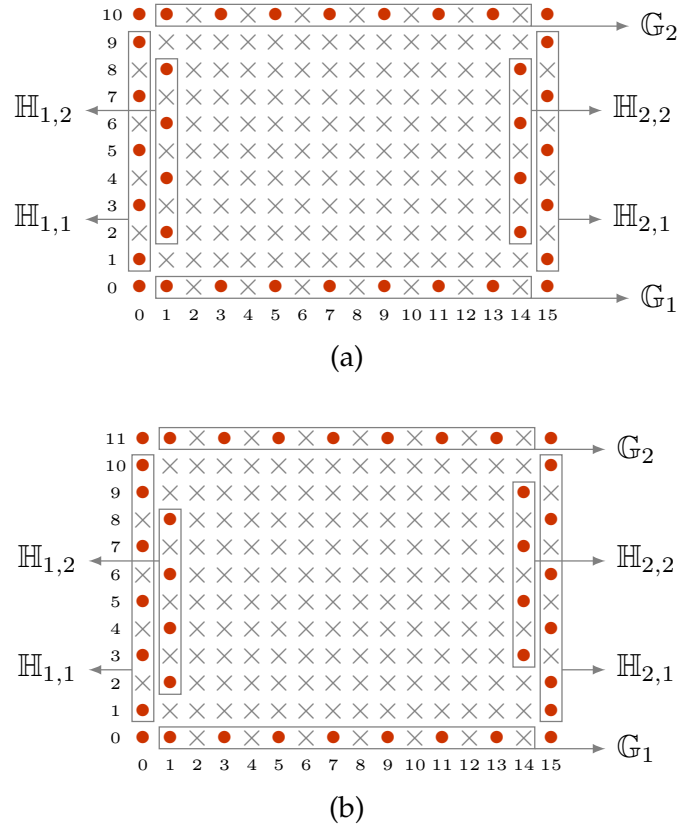


Figure 5.5: Examples of HOBA-2. (a) $N_x = 16, N_y = 11$ and (b) $N_x = 16, N_y = 12$.

Definition 5.5.1 (Half open box arrays with two layers, HOBA-2). The half open box array with two layers is a partially open box array with $L = 2$ layers, and

$$\begin{aligned} \mathfrak{g}_1 &= \{1 + 2\ell : 0 \leq \ell \leq \lfloor (N_x - 3)/2 \rfloor\}, \\ \mathfrak{g}_2 &= \{N_x - 1 - 2\ell : 1 \leq \ell \leq \lfloor (N_x - 2)/2 \rfloor\}, \\ \mathfrak{h}_{1,1} &= \{1 + 2\ell : 0 \leq \ell \leq \lfloor (N_y - 3)/2 \rfloor\} \cup \{N_y - 2\}, \\ \mathfrak{h}_{1,2} &= \{2\ell : 1 \leq \ell \leq \lfloor (N_y - 3)/2 \rfloor\}. \end{aligned}$$

The sets $\mathfrak{h}_{2,1}$ and $\mathfrak{h}_{2,2}$ satisfy Definition 5.4.1.

Fig. 5.5 depicts the array geometry of HOBA-2 for (a) $N_y = 11$ (odd) and (b) $N_y = 12$ (even). It can be observed that the weight function $w(0, 1)$ becomes smaller than HOBA with the same N_x and N_y . For instance, for HOBA with $N_x = 16$ and $N_y = 11$, $w(0, 1)$ is 20 while the weight function $w(0, 1)$ for HOBA-2, $N_x = 16$, and $N_y = 11$, as shown in Fig. 5.5(a), is as small as 4.

The difference coarray for HOBA-2 possess the same difference coarray as OBA, as indicated in the following theorem:

Theorem 5.5.1. Half open box arrays with two layers have the same difference coarray as open box arrays.

Proof. According to Theorem 5.4.1, it suffices to show that

$$\mathfrak{h}_{1,2} \subseteq \mathbb{P}_2 = \mathfrak{h}_{1,1} \oplus \mathfrak{h}_{1,1}, \quad (5.11)$$

$$\mathfrak{h}_{1,2} \subseteq \mathbb{P}_2 - (N_y - 1) = \mathfrak{h}_{1,1} \oplus \mathfrak{h}_{1,1} - (N_y - 1). \quad (5.12)$$

Eq. (5.11) can be proved as follows. Since $1 \in \mathfrak{h}_{1,1}$, we have

$$\mathfrak{h}_{1,1} \oplus \mathfrak{h}_{1,1} \supseteq \mathfrak{h}_{1,1} + 1 \supseteq \{2 + 2\ell : 0 \leq \ell \leq \lfloor (N_x - 3)/2 \rfloor\}.$$

Letting $\ell' = \ell + 1$ yields

$$\mathfrak{h}_{1,1} \oplus \mathfrak{h}_{1,1} \supseteq \{2\ell' : 1 \leq \ell' \leq \lfloor (N_x - 3)/2 \rfloor + 1\} \supset \mathfrak{h}_{1,2}.$$

Next we will prove (5.12). It can be observed that $N_y - 2 \in \mathfrak{h}_{1,1}$ whenever N_y is odd or even. Then we have

$$\begin{aligned} \mathfrak{h}_{1,1} \oplus \mathfrak{h}_{1,1} - (N_y - 1) &\supseteq \mathfrak{h}_{1,1} \oplus \{N_y - 2\} - (N_y - 1) \\ &\supseteq \{2\ell : 0 \leq \ell \leq \lfloor (N_y - 3)/2 \rfloor\} \supset \mathfrak{h}_{1,2}. \end{aligned}$$

This completes the proof. \square

The mutual coupling effect depends not only on $w(0, 1)$, but also on other weight functions at small separations, such as $w(1, 1)$ and $w(1, -1)$. For HOBA-2, even though the weight function $w(0, 1)$ becomes smaller, $w(1, 1)$ and $w(1, -1)$ increase significantly. For instance, the HOBA with $N_x = 16, N_y = 11$, as depicted in Fig. 5.3(b), enjoys $w(1, 1) = w(1, -1) = 1$ while the HOBA-2 and $N_x = 16, N_y = 11$, as illustrated in Fig. 5.5(a), owns $w(1, 1) = w(1, -1) = 9$. Therefore, for HOBA-2, the reduction in the mutual coupling effect is limited.

5.6 Hourglass Arrays

In this section, we will propose *hourglass arrays*, which look like hourglasses on the 2D plane. These novel array configurations have the same number of sensors and the same difference coarray as those in OBA. Therefore, the difference coarrays of hourglass arrays are hole-free. In addition, the sensor locations can be expressed in closed form. Most importantly, they possess small weight functions $w(1, 0)$ and $w(0, 1)$ as well as $w(1, 1)$ and $w(1, -1)$.

To develop some feeling for hourglass arrays, Fig. 5.4(b) demonstrates the hourglass array with $N_x = 16$ and $N_y = 11$. The sets \mathfrak{g}_1 and \mathfrak{g}_2 are identical to those in HOBA. There are $L = 3$ layers. The sensors in $\mathbb{H}_{1,1} \cup \mathbb{H}_{1,2} \cup \mathbb{H}_{1,3}$ can be viewed as the unions

$$\mathfrak{h}_{1,\ell} = \begin{cases} \{2p, N_y - 1 - 2p : 1 \leq p \leq \lfloor (N_y - 1)/4 \rfloor\} \cup \{1, N_y - 2\}, & \text{if } \ell = 1, \\ \{2\ell - 1, N_y - 2\ell\}, & \text{if } N_y \text{ is odd and } 2 \leq \ell \leq L, \\ \{2\ell - 1, 2\lfloor N_y/4 \rfloor - 2\ell + 3, 2\lceil N_y/4 \rceil + 2\ell - 4, N_y - 2\ell\}, & \text{if } N_y \text{ is even and } 2 \leq \ell \leq L, \end{cases} \quad (5.13)$$

of three ULAs. The first ULA contains $(0, 2), (0, 4), (0, 6), (0, 8)$, the second ULA is composed of $(0, 1), (1, 3), (2, 5)$, and the third ULA consists of $(0, 9), (1, 7), (2, 5)$. Notice that the sensor located at $(2, 5)$ is relatively far away from other sensors, since the distance from $(2, 5)$ to its nearest sensor is $\sqrt{5}$.

The hourglass arrays are formally defined as

Definition 5.6.1 (Hourglass arrays). Let N_x and N_y be positive integers. An hourglass array is a partially open box array with L layers where the sets \mathfrak{g}_1 and \mathfrak{g}_2 are given by

$$\begin{aligned} \mathfrak{g}_1 &= \{1 + 2p : 0 \leq p \leq \lfloor (N_x - 3)/2 \rfloor\}, \\ \mathfrak{g}_2 &= \{N_x - 1 - 2p : 1 \leq p \leq \lfloor (N_x - 2)/2 \rfloor\}. \end{aligned}$$

Here the number of layers L is defined as

$$L = \begin{cases} \lfloor (N_y + 1)/4 \rfloor, & \text{if } N_y \text{ is odd,} \\ \lfloor N_y/8 + 1 \rfloor, & \text{if } N_y \text{ is even.} \end{cases} \quad (5.14)$$

The sets $\mathfrak{h}_{1,\ell}$ are given in (5.13) and $\mathfrak{h}_{2,\ell} = N_y - 1 - \mathfrak{h}_{1,\ell}$.

The MATLAB function `P0BA_L.m` returns the sensor locations of hourglass arrays, by specifying the parameter N_x , N_y , and the third parameter being ‘hourglass’ [99]. Fig. 5.6 elaborates the array geometry of hourglass arrays for (a) $N_x = 15$, $N_y = 27$ and (b) $N_x = 15$, $N_y = 26$. It can be seen from Fig. 5.6(a) that, when N_y is an odd number, The array configuration, indicated by the bullets as the sensors, resembles an hourglass. The sets $\mathbb{G}_1, \mathbb{G}_2, \mathbb{H}_{1,\ell}, \mathbb{H}_{2,\ell}$ for $2 \leq \ell \leq L = 7$, constitute the two bulbs in an hourglass. The neck in this hourglass corresponds to $\mathbb{H}_{1,7}$ and $\mathbb{H}_{2,7}$. The sets $\mathbb{H}_{1,1}$ and $\mathbb{H}_{2,1}$ can be regarded as two pillars. If N_y is an even number, as shown in Fig. 5.6(b), the array geometry looks like an hourglass ($\mathbb{G}_1, \mathbb{G}_2, \mathbb{H}_{1,\ell}, \mathbb{H}_{2,\ell}$ for $2 \leq \ell \leq L = 4$) with two necks ($\mathbb{H}_{1,4}, \mathbb{H}_{2,4}$) and two pillars ($\mathbb{H}_{1,1}, \mathbb{H}_{2,1}$).

Note that the number of layers L depends on N_y . According to (5.14), L is approximately $N_y/4$ if N_y is odd while L is around $N_y/8$ when N_y is even. Furthermore,

$L \leq N_x/2$ in the definition of POBA- L (Definition 5.4.1). It can be deduced that, for large N_x and N_y , the aspect ratio N_y/N_x of hourglass arrays should be less than 2 for odd N_y and 4 for even N_y .

The next result characterizes the difference coarray of hourglass arrays:

Theorem 5.6.1. Hourglass arrays own the same difference coarray as open box arrays.

Proof. See Appendix 5.E. □

Summarizing, hourglass arrays own closed-form sensor locations and their coarrays are identical to those of OBA. Furthermore, it will be shown in the next section that, the weight functions $w(1, 0)$, $w(0, 1)$, $w(1, 1)$, and $w(1, -1)$ for hourglass arrays are sufficiently small, so that the mutual coupling effect can be significantly reduced.

5.7 Weight Functions

It is known that the weight functions at small separations are more important for mutual coupling effects [92]. It is desirable to have sufficiently small $w(1, 0)$, $w(0, 1)$, $w(1, 1)$, and $w(1, -1)$. Therefore, in this section, we will study these weight functions for URA, billboard arrays, OBA, HOBA, HOBA-2, and hourglass arrays. A summary is given in Table 5.1 for convenience. Note that some assumptions on the first row of Table 5.1 (e.g., $N_x \geq 3$ and $N_y \geq 2$ for the OBA) are not parts of the definitions for these arrays. They are introduced in order to have simple and closed-form expressions for the weight functions.

Consider the weight function $w(1, 0)$ for all these arrays. Asymptotically, $w(1, 0)$ grows linearly with $N_x N_y$ for URA. For billboard arrays and OBA, $w(1, 0)$ increases linearly with N_x . It is noteworthy that, for the proposed array configurations (HOBA, HOBA-2, and hourglass arrays), the weight function $w(1, 0)$ is fixed to be 2, even if N_x and N_y are huge.

However, mutual coupling effects also depend on $w(0, 1)$, $w(1, 1)$, and $w(1, -1)$. According to Table 5.1, hourglass arrays are the only class of arrays for which all the weight functions, such as $w(1, 0)$, $w(0, 1)$, $w(1, 1)$, and $w(1, -1)$ are significantly smaller when N_x and N_y are large. This property indicates that hourglass arrays own the least mutual coupling among all the arrays listed in Table 5.1.

Next, we will justify the expressions for some of the weight functions given in Table I.

Table 5.1: Summary on the weight functions

| Array | URA | Billboard | OBA |
|------------|----------------------|--------------------|--------------------------|
| | | $N_x = N_y \geq 4$ | $N_x \geq 3, N_y \geq 2$ |
| $w(1, 0)$ | $N_y(N_x - 1)$ | $N_x - 1$ | $N_x - 1$ |
| $w(0, 1)$ | $N_x(N_y - 1)$ | $N_y - 1$ | $2(N_y - 1)$ |
| $w(1, 1)$ | $(N_x - 1)(N_y - 1)$ | $N_x - 3$ | 1 |
| $w(1, -1)$ | $(N_x - 1)(N_y - 1)$ | 1 | 1 |

| Array | HOBA | HOBA-2 | Hourglass arrays |
|------------|--------------------------|---|---|
| | $N_x \geq 4, N_y \geq 3$ | $N_x \geq 5, N_y \geq 5$ | $N_x \geq 2L + 1, N_y \geq 7,$ L is defined in (5.14). |
| $w(1, 0)$ | 2 | 2 | 2 |
| $w(0, 1)$ | $2(N_y - 1)$ | $\begin{cases} 4, & \text{if } N_y \text{ is odd,} \\ 6, & \text{if } N_y \text{ is even.} \end{cases}$ | $\begin{cases} 8, & \text{if } N_y \text{ is odd,} \\ 10, & \text{if } N_y \text{ is even.} \end{cases}$ |
| $w(1, 1)$ | 1 | $\begin{cases} N_y - 2, & \text{if } N_y \text{ is odd,} \\ N_y - 3, & \text{if } N_y \text{ is even.} \end{cases}$ | $\begin{cases} 3, & \text{if } N_y = 7, 8, \\ 5, & \text{if } N_y = 10 \text{ or } 2r + 1, r \geq 4, \\ 7, & \text{if } N_y = 4r, r \geq 3, \\ 9, & \text{if } N_y = 4r + 2, r \geq 3. \end{cases}$ |
| $w(1, -1)$ | 1 | $\begin{cases} N_y - 2, & \text{if } N_y \text{ is odd,} \\ N_y - 3, & \text{if } N_y \text{ is even.} \end{cases}$ | $\begin{cases} 3, & \text{if } N_y = 7, 8, \\ 5, & \text{if } N_y = 10 \text{ or } 2r + 1, r \geq 4, \\ 7, & \text{if } N_y = 4r, r \geq 3, \\ 9, & \text{if } N_y = 4r + 2, r \geq 3. \end{cases}$ |

Derivation to the weight function expressions in HOBA

To evaluate $w(1, 0)$, it suffices to consider the elements whose y coordinates are either 0 or $N_y - 1$, due to Definition 5.3.1. Since $N_x \geq 4$, \mathfrak{g}_1 and \mathfrak{g}_2 are not empty. It is obvious that the sensor pair of $(1, 0)$ and $(0, 0)$ contributes to $w(1, 0)$. First consider N_x to be an odd number. According to (5.7), $N_x - 2 \in \mathfrak{g}_1$, so $(N_x - 1, 0)$ and $(N_x - 2, 0)$ also contribute to $w(1, 0)$. In this case, the smallest and the largest elements in \mathfrak{g}_2 are 2 and $N_x - 3$, respectively, implying there are no sensor pairs with separation 1 if the y coordinates are $N_y - 1$. On the other hand, if N_x is even, the only two sensor pairs contributing to $w(1, 0)$ are $(1, 0), (0, 0)$ and $(1, N_y - 1), (0, N_y - 1)$.

The weight function $w(0, 1)$ is identical to that in OBA since they share the same \mathbb{H}_1 and \mathbb{H}_2 . The weight functions $w(1, 1)$ and $w(1, -1)$ can be calculated as follows: If N_x is odd, the sensor pairs $(N_x - 1, 1), (N_x - 2, 0)$ and $(1, 0), (0, 1)$ contribute to $w(1, 1)$ and $w(1, -1)$, respectively. If N_x is even, $w(1, 1)$ and $w(1, -1)$ result from the sensor pairs $(1, N_y - 1), (0, N_y - 2)$ and $(1, 0), (0, 1)$, which completes the derivation.

Derivation to the weight function expressions in HOBA-2

The weight function $w(1, 0)$ is 2 because the sets \mathfrak{g}_1 and \mathfrak{g}_2 in HOBA-2. are exactly the same as those in HOBA.

Next we will derive the expression for $w(0, 1)$. If N_y is an odd number, it can be deduced that $1 \in \mathfrak{h}_{1,1}$, $N_y - 2 \in \mathfrak{h}_{1,1}$, and $N_y - 3 \notin \mathfrak{h}_{1,1}$. Hence, the four sensor pairs contributing to $w(0, 1)$ are $(0, 1), (0, 0); (0, N_y - 1), (0, N_y - 2); (N_x - 1, 1), (N_x - 1, 0); (N_x - 1, N_y - 1), (N_x - 1, N_y - 2)$. If N_y is an even number, we have $1 \in \mathfrak{h}_{1,1}$, $N_y - 2 \in \mathfrak{h}_{1,1}$, and $N_y - 3 \in \mathfrak{h}_{1,1}$. Apart from the four sensor pairs in the odd case, the two more pairs are $(0, N_y - 2), (0, N_y - 3)$ and $(N_x - 1, 2), (N_x - 1, 1)$. The remaining sensor pairs do not add to $w(0, 1)$ since the separations are greater than 1.

The weight function $w(1, 1)$ can be obtained as follows: For $w(1, 1)$, it suffices to consider the cross differences between $\mathbb{H}_{1,1}$ and $\mathbb{H}_{1,2}$, as well as $\mathbb{H}_{2,1}$ and $\mathbb{H}_{2,2}$. It can be inferred that the sensor pairs of $(1, 2\ell) \in \mathbb{H}_{1,2}$ and $(0, 2(\ell - 1) + 1) \in \mathbb{H}_{1,1}$ contribute to $w(1, 1)$. In this case, there are $|\mathfrak{h}_{1,2}|$ pairs. Similar arguments also apply to the sets $\mathbb{H}_{2,1}$ and $\mathbb{H}_{2,2}$. Next, if N_x is odd, the sensor pair $(N_x - 1, 1), (N_x - 2, 0)$ also has separation $(1, 1)$. On the other hand, if N_x is even, the sensor pair $(1, N_y - 1), (0, N_y - 2)$ contributes to $w(1, 1)$. Therefore, $w(1, 1)$ becomes

$$\begin{aligned} w(1, 1) &= 2|\mathfrak{h}_{1,2}| + 1 = 2\lfloor(N_y - 3)/2\rfloor + 1 \\ &= \begin{cases} N_y - 2, & \text{if } N_y \text{ is odd,} \\ N_y - 3, & \text{if } N_y \text{ is even.} \end{cases} \end{aligned}$$

The same technique can be used in finding the expression for $w(1, -1)$.

Derivation to the weight function expressions in hourglass arrays

It can be deduced that the weight function $w(1, 0)$ is also 2, since the sets \mathfrak{g}_1 and \mathfrak{g}_2 share the same expression as those in HOBA.

To derive expressions for $w(0, 1)$, consider the following chain of arguments. Since $N_y \geq 7$, we have $\lfloor(N_y - 1)/4\rfloor \geq 1$, so $2 \in \mathfrak{h}_{1,1}$ and $N_y - 3 \in \mathfrak{h}_{1,1}$. As a result, there exist eight sensor pairs:

$$(n_x, n_y + 1), (n_x, n_y), \tag{5.15}$$

where $n_x = 0, N_x - 1$, and $n_y = 0, 1, N_y - 3, N_y - 2$, contributing to the weight function $w(0, 1)$.

For other sensor pairs, the self difference of $\mathfrak{h}_{1,1}$ is first analyzed. Consider the fol-

lowing two sets,

$$\mathfrak{h}_{1,1}^+ = \{N_y - 1 - 2p : 1 \leq p \leq \lfloor (N_y - 1)/4 \rfloor\},$$

$$\mathfrak{h}_{1,1}^- = \{2p : 1 \leq p \leq \lfloor (N_y - 1)/4 \rfloor\},$$

which satisfy $\mathfrak{h}_{1,1} = \mathfrak{h}_{1,1}^+ \cup \mathfrak{h}_{1,1}^- \cup \{1, N_y - 2\}$. The self difference of $\mathfrak{h}_{1,1}$ can be decomposed into the self differences and the cross differences of $\mathfrak{h}_{1,1}^+$, $\mathfrak{h}_{1,1}^-$, and $\{1, N_y - 2\}$. Since $\mathfrak{h}_{1,1}^+$ and $\mathfrak{h}_{1,1}^-$ are ULA with spacing 2, for $w(0, 1)$, it suffices to consider the cross differences between $\mathfrak{h}_{1,1}^+$ and $\mathfrak{h}_{1,1}^-$, defined as

$$\text{diff}(\mathfrak{h}_{1,1}^+, \mathfrak{h}_{1,1}^-) = \{a - b : \forall a \in \mathfrak{h}_{1,1}^+, \forall b \in \mathfrak{h}_{1,1}^-\}.$$

The minimum element in $\text{diff}(\mathfrak{h}_{1,1}^+, \mathfrak{h}_{1,1}^-)$ is given by

$$N_y - 1 - 4\lfloor (N_y - 1)/4 \rfloor = \begin{cases} 0, & \text{if } N_y = 4r + 1, \\ 1, & \text{if } N_y = 4r + 2, \\ 2, & \text{if } N_y = 4r + 3, \\ 3, & \text{if } N_y = 4r. \end{cases} \quad (5.16)$$

Therefore, if $N_y = 4r + 2$, we have $1 \in \text{diff}(\mathfrak{h}_{1,1}, \mathfrak{h}_{1,1})$. Similarly, it can be shown that $1 \in \text{diff}(\mathfrak{h}_{2,1}, \mathfrak{h}_{2,1})$, since $\mathfrak{h}_{2,1} = N_y - 1 - \mathfrak{h}_{1,1}$.

Next we turn to the self differences of $\mathfrak{h}_{1,\ell}$ for $2 \leq \ell \leq L$. If N_y is odd, we will show that the difference $(0, 1)$ cannot be found in the self difference of $\mathfrak{h}_{1,\ell}$. This statement can be proved as follows. According to (5.13), the self difference of $\mathfrak{h}_{1,\ell}$ is

$$\text{diff}(\mathfrak{h}_{1,\ell}, \mathfrak{h}_{1,\ell}) = \{0, \pm(N_y + 1 - 4\ell)\}.$$

Since N_y is odd, all the elements in $\text{diff}(\mathfrak{h}_{1,\ell}, \mathfrak{h}_{1,\ell})$ are even numbers, so $1 \notin \text{diff}(\mathfrak{h}_{1,\ell}, \mathfrak{h}_{1,\ell})$.

If N_y is even, the self difference of $\mathfrak{h}_{1,\ell}$ becomes

$$\text{diff}(\mathfrak{h}_{1,\ell}, \mathfrak{h}_{1,\ell}) = \{0, \pm(s_2 - s_1), \pm(s_3 - s_1), \pm(s_4 - s_1), \\ \pm(s_3 - s_2), \pm(s_4 - s_2), \pm(s_4 - s_3)\},$$

where $s_1 = 2\ell - 1$, $s_2 = 2\lfloor N_y/4 \rfloor - 2\ell + 3$, $s_3 = 2\lceil N_y/4 \rceil + 2\ell - 4$, and $s_4 = N_y - 2\ell$, as indicated in (5.13). It can be shown that $s_1 < s_2 < s_3 < s_4$. Therefore, for $w(0, 1)$, it suffices to consider the differences between adjacent elements, as discussed in the following three cases:

1. $s_2 - s_1 = 2\lfloor N_y/4 \rfloor - 4\ell + 4$ is an even number, which cannot be 1.
2. $s_3 - s_2 = 2(\lceil N_y/4 \rceil - \lfloor N_y/4 \rfloor) + (4\ell - 7)$ is an odd number. If $s_3 - s_2 = 1$, then we have

$$\lceil N_y/4 \rceil - \lfloor N_y/4 \rfloor = 4 - 2\ell. \quad (5.17)$$

Table 5.2: Sensor pairs for $w(1, 1)$ with odd N_x

| | Sensor pairs $\mathbf{n}_1, \mathbf{n}_2$; |
|-------------------------------|--|
| $N_y = 7$ | $(1, 3), (0, 2); (N_x - 1, 1), (N_x - 2, 0);$ $(N_x - 1, 4), (N_x - 2, 3);$ |
| $N_y = 8$ | $(1, 3), (0, 2); (N_x - 1, 1), (N_x - 2, 0);$ $(N_x - 1, 5), (N_x - 2, 4);$ |
| $N_y = 10$ | $(1, 3), (0, 2); (1, 6), (0, 5); (N_x - 1, 1), (N_x - 2, 0);$ $(N_x - 1, 4), (N_x - 2, 3); (N_x - 1, 7), (N_x - 2, 6);$ |
| $N_y = 2r + 1,$ $r \geq 4$ | $(1, 3), (0, 2); (1, N_y - 4), (0, N_y - 5);$ $(N_x - 1, 1), (N_x - 2, 0); (N_x - 1, 4), (N_x - 2, 3);$ $(N_x - 1, N_y - 3), (N_x - 2, N_y - 4);$ |
| $N_y = 4r, r \geq 3$ | $(1, 3), (0, 2); (1, 2r - 1), (0, 2r - 2);$ $(1, N_y - 4), (0, N_y - 5); (N_x - 1, 1), (N_x - 2, 0);$ $(N_x - 1, 4), (N_x - 2, 3); (N_x - 1, 2r + 1), (N_x - 2, 2r);$ $(N_x - 1, N_y - 3), (N_x - 2, N_y - 4);$ |
| $N_y = 4r + 2,$ $r \geq 3$ | $(1, 3), (0, 2); (1, 2r - 1), (0, 2r - 2);$ $(1, 2r + 2), (0, 2r + 1); (1, N_y - 4), (0, N_y - 5);$ $(N_x - 1, 1), (N_x - 2, 0); (N_x - 1, 4), (N_x - 2, 3);$ $(N_x - 1, 2r), (N_x - 2, 2r - 1);$ $(N_x - 1, 2r + 3), (N_x - 2, 2r + 2);$ $(N_x - 1, N_y - 3), (N_x - 2, N_y - 4);$ |

Since $\lceil x \rceil - \lfloor x \rfloor$ is 0 if x is an integer and 1 otherwise, the solution to (5.17) is $\ell = 2$ and $N_y = 4r$ for some integer r . That is, if N_y is an integer multiple of 4, there exists a sensor pair in $\mathfrak{h}_{1,2}$ with separation 1.

3. $s_4 - s_3 = N_y - 2\lceil N_y/4 \rceil - 4\ell + 4$ is an even number.

Similar arguments can be applied to $\mathfrak{h}_{2,\ell}$. The expressions for $w(0, 1)$ in hourglass arrays can be obtained by combining (5.15), (5.16), and (5.17).

For $w(1, 1)$, we first consider the sensor pairs $\mathbf{n}_1, \mathbf{n}_2$ such that $\mathbf{n}_1 - \mathbf{n}_2 = (1, 1)$ for $N_y = 7, 8, 10$ and odd N_x , as listed in the first three rows of Table 5.2. Next we will focus on the remaining cases in Table 5.2.

1. $N_y = 2r + 1$ and N_x is an odd number, where $r \geq 4$ is an integer: In this case, $L \geq 2$ and $\lfloor (N_y - 1)/4 \rfloor \geq 2$. Therefore, we have

$$\{2, 4, N_y - 5, N_y - 3\} \subseteq \mathfrak{h}_{1,1}, \quad (5.18)$$

$$\{3, N_y - 4\} \subseteq \mathfrak{h}_{1,2}. \quad (5.19)$$

Due to (5.18) and (5.19), the only five sensor pairs are listed in the fourth row of Table 5.2. It can be shown that there do not exist sensor pairs with separation $(1, 1)$ within $\mathbb{H}_{1,\ell}$ and $\mathbb{H}_{2,\ell}$ for $2 \leq \ell \leq L$.

2. $N_y = 4r$ and N_x is an odd number, where $r \geq 3$ is an integer: In this case, we know that

$$L = \lfloor 4r/8 + 1 \rfloor \geq \lfloor 12/8 + 1 \rfloor = 2, \quad (5.20)$$

$$\lfloor (N_y - 1)/4 \rfloor = \lfloor (4r - 1)/4 \rfloor = r - 1 \geq 2. \quad (5.21)$$

Using (5.20) and (5.21) in (5.13) leads to

$$\{2, 4, 2r - 2, 2r + 1, N_y - 5, N_y - 3\} \subseteq \mathfrak{h}_{1,1}, \quad (5.22)$$

$$\{3, 2r - 1, 2r, N_y - 4\} \subseteq \mathfrak{h}_{1,2}. \quad (5.23)$$

As a result, the seven sensor pairs contributing to the difference $(1, 1)$ are shown in the fifth row of Table 5.2.

3. $N_y = 4r + 2$ and N_x is an odd number, where $r \geq 3$ is an integer. Similar to (5.20) and (5.21), we have $L \geq 2$ and $\lfloor (N_y - 1)/4 \rfloor = r \geq 3$, implying

$$\{2, 4, 2r - 2, 2r, 2r + 1, 2r + 3, N_y - 5, N_y - 3\} \subseteq \mathfrak{h}_{1,1}, \quad (5.24)$$

$$\{3, 2r - 1, 2r + 2, N_y - 4\} \subseteq \mathfrak{h}_{1,2}. \quad (5.25)$$

Based on (5.24) and (5.25), the nine sensor pairs can be found to be those in the last row of Table 5.2.

If N_x is an even number, it can be shown that $N_x - 2 \notin \mathfrak{g}_1$ and $1 \in \mathfrak{g}_2$. Therefore the sensor pair $(N_x - 1, 1), (N_x - 2, 0)$ does not exist. Instead, another sensor pair $(1, N_y - 1), (0, N_y - 2)$ contributes to $w(1, 1)$ for even N_x . The remaining sensor pairs are listed in Table 5.2.

For the weight function $w(1, -1)$, the associated sensor pairs can also be identified using Table 5.2. Let \mathbf{n}_1 and \mathbf{n}_2 be a sensor pair satisfying $\mathbf{n}_1 - \mathbf{n}_2 = (1, 1)$. Based on \mathbf{n}_1 and \mathbf{n}_2 , we can uniquely construct another sensor pair \mathbf{n}'_1 and \mathbf{n}'_2 such that $\mathbf{n}'_1 - \mathbf{n}'_2 = (1, -1)$, as follows:

1. If $\mathbf{n}_1 = (n_{1x}, n_{1y}) \in \mathbb{H}_{1,1}$ and $\mathbf{n}_2 = (n_{2x}, n_{2y}) \in \mathbb{H}_{1,2}$ such that $\mathbf{n}_1 - \mathbf{n}_2 = (1, 1)$, then it can be shown that the sensor pair

$$\mathbf{n}'_1 = (n_{1x}, N_y - 1 - n_{1y}), \quad \mathbf{n}'_2 = (n_{2x}, N_y - 1 - n_{2y}),$$

satisfies $\mathbf{n}'_1 \in \mathbb{H}_{1,1}$, $\mathbf{n}'_2 \in \mathbb{H}_{1,2}$, and $\mathbf{n}'_1 - \mathbf{n}'_2 = (1, -1)$. This property holds true since $\mathfrak{h}_{1,\ell}$ is symmetric. Similar arguments apply to $\mathbf{n}_1 = (n_{1x}, n_{1y}) \in \mathbb{H}_{2,1}$ and $\mathbf{n}_2 = (n_{2x}, n_{2y}) \in \mathbb{H}_{2,2}$.

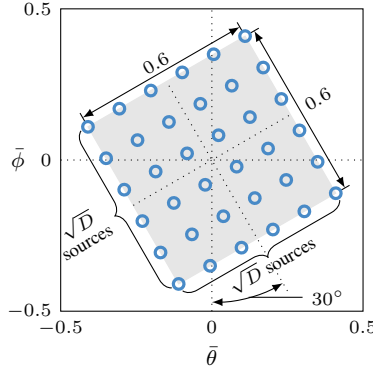


Figure 5.7: The normalized source directions, as shown in circles, for the examples in Section 5.8. Here the number of sources D is assumed to be a perfect square, i.e., \sqrt{D} is an integer. The sources are uniformly located in the shaded region, over which there are \sqrt{D} equally-spaced sources in one way and \sqrt{D} equally-spaced sources in the other.

2. For odd N_x , if $\mathbf{n}_1 = (N_x - 1, 1)$ and $\mathbf{n}_2 = (N_x - 2, 0)$, it can be proved that $\mathbf{n}'_1 = (1, 0) \in \mathbb{G}_1$, $\mathbf{n}'_2 = (0, 1) \in \mathbb{H}_{1,1}$, and $\mathbf{n}'_1 - \mathbf{n}'_2 = (1, -1)$.
3. For even N_x , if $\mathbf{n}_1 = (1, N_y - 1)$ and $\mathbf{n}_2 = (0, N_y - 2)$, then the sensor pair becomes $\mathbf{n}'_1 = (1, 0)$ and $\mathbf{n}'_2 = (0, 1)$.

Therefore, we have $w(1, -1) = w(1, 1)$ in hourglass arrays.

5.8 Numerical Examples

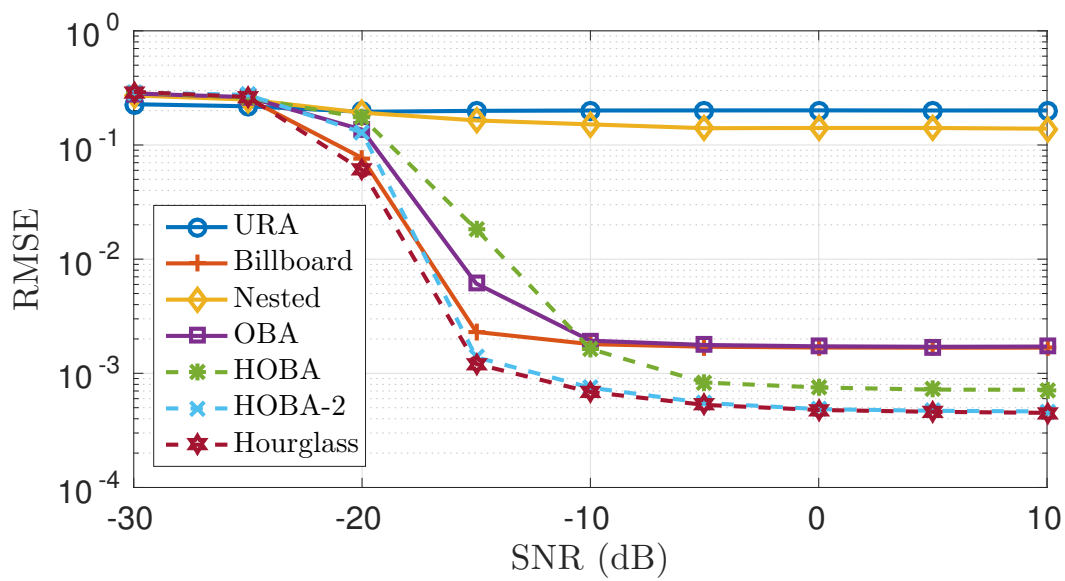
In this section, we will study the DOA estimation performance in the presence of mutual coupling, for URA, billboard arrays, 2D nested arrays, OBA, HOBA, HOBA-2, and hourglass arrays. The parameters are chosen to be $N_x = N_y = 9$ for URA, $N_x = N_y = 28$ for billboard arrays, $N_1 = 4, N_2 = 5$ for 2D nested arrays, $N_x = 29, N_y = 27$ for OBA, HOBA, HOBA-2, and hourglass arrays, where the notations are given in Fig. 5.2 to 5.6. Therefore, the number of physical sensors is fixed to be 81 for all these arrays. The aperture is 8×8 for URA, 27×27 for billboard arrays, 24×24 for 2D nested arrays, and 26×28 for OBA, HOBA, HOBA-2, as well as hourglass arrays. There are D , uncorrelated, equal-power sources with 0dB SNR. The number of snapshots K is 200, and the normalized DOAs are illustrated in Fig. 5.7, where the number of sources D is assumed to be a square number. The mutual coupling model is given in (5.5), where $c(1) = 0.3$, $B = 5$, and $c(\ell) = c(1) \exp[j\pi(\ell - 1)/4] / \ell$. The measurements are generated based on (5.4) and the DOAs are estimated using the 2D unitary ESPRIT algorithm [203] on the finite snapshot version of the signal on the difference coarray. The root-mean-squared error is defined as $\text{RMSE} = ((1/D) \sum_{i=1}^D (\hat{\theta}_i - \bar{\theta}_i)^2 + (\hat{\phi}_i - \bar{\phi}_i)^2)^{1/2}$, where $(\hat{\theta}_i, \hat{\phi}_i)$ and

$(\widehat{\theta}_i, \widehat{\phi}_i)$ are the true normalized DOA and the estimated normalized DOA of the i th source, respectively. Note that mutual coupling is present in the measurements but the 2D unitary ESPRIT algorithm does not take care of mutual coupling. This scenario offers a baseline performance for DOA estimation in the presence of mutual coupling. It will be shown that the proposed 2D sparse arrays (HOBA, HOBA-2, and hourglass arrays) are capable of estimating the DOA satisfactorily when mutual coupling is present, even if the DOA estimator does not take into account the existence of this coupling.

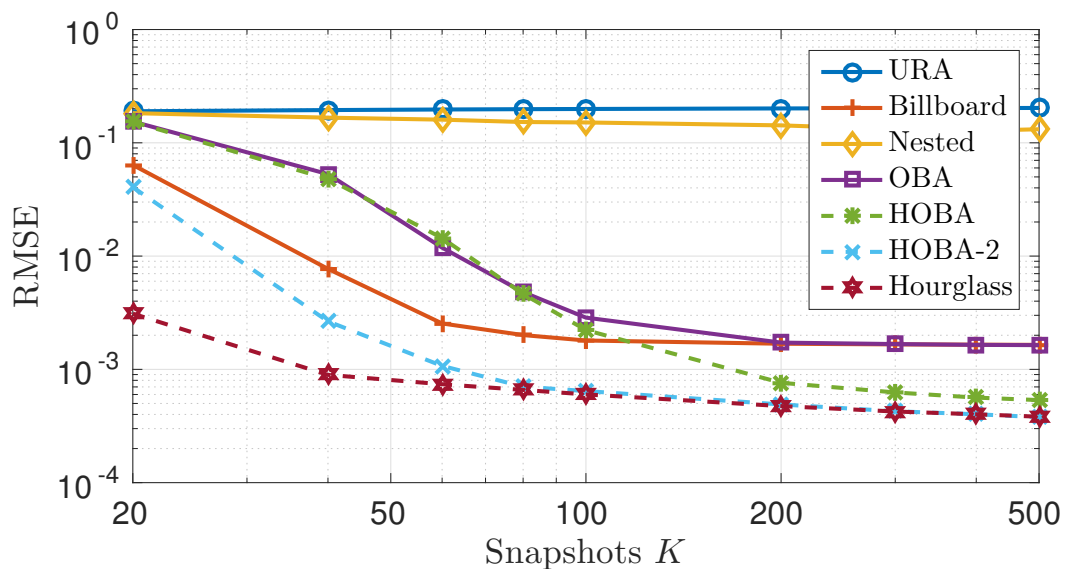
Fig. 5.8(a) shows the estimation performance as a function of SNR. Here the number of sources $D = 9$. At 0dB SNR, the least RMSE is exhibited by hourglass arrays, followed by HOBA-2, then HOBA, then billboard arrays, then OBA, then 2D nested arrays, and finally URA. Note that this result is in accordance with the associated weight functions, as listed in Table 5.1. Qualitatively, the smaller the weight functions $w(1, 0)$, $w(0, 1)$, $w(1, 1)$, $w(1, -1)$ are, the less the mutual coupling effects are. The dependence of the RMSE versus the number of snapshots K is plotted in Fig. 5.8(b). It is noteworthy that, in the presence of mutual coupling, hourglass arrays demonstrate considerable reduction on RMSE using only 40 snapshots.

Fig. 5.9 shows the dependence of the RMSE on the parameter c_1 in the mutual coupling model. It can be observed that, for any array configuration, the RMSE is small if c_1 is close to 0 (less mutual coupling), and the error starts to increase significantly above certain thresholds of c_1 . In Fig. 5.9(a), the number of sources is $D = 9$. It can be deduced that the thresholds of c_1 are approximately 0.4 for billboard arrays, 0.25 for 2D nested arrays, 0.35 for OBA, 0.3 for HOBA, 0.45 for HOBA-2, and 0.5 for hourglass arrays. This phenomenon indicates that hourglass arrays are more robust to mutual coupling effects than the others. Fig. 5.9(b) plots the RMSE versus c_1 if the number of sources $D = 36$. The thresholds of c_1 become 0.15 for billboard arrays, 0.1 for 2D nested arrays, OBA, HOBA, and 0.2 for HOBA-2 and hourglass arrays, since it is more difficult to resolve 36 sources simultaneously than to resolve 9 sources. Note that, even in the extreme case of $D = 36$ and $c_1 = 0.2$, hourglass arrays still enjoy the RMSE as small as 10^{-3} , which is much smaller than those for URA, billboard arrays, 2D nested arrays, OBA, and HOBA.

Note that the number of sources is much smaller than sensors ($9, 36 \ll 81$). It is conjectured that, 2D sparse arrays might resolve more sources than sensors almost surely, in the *absence* of mutual coupling. However, if mutual coupling is present, this is more challenging, and it will be explored in greater detail in future.



(a)



(b)

Figure 5.8: The RMSE as a function of (a) SNR and (b) the number of snapshots K . The number of sensors is 81 for all arrays. The parameters are (a) $K = 200$, the number of sources $D = 9$ and (b) 0dB SNR, $D = 9$. The sources directions are depicted in Fig. 5.7. Each point is averaged from 1000 runs.

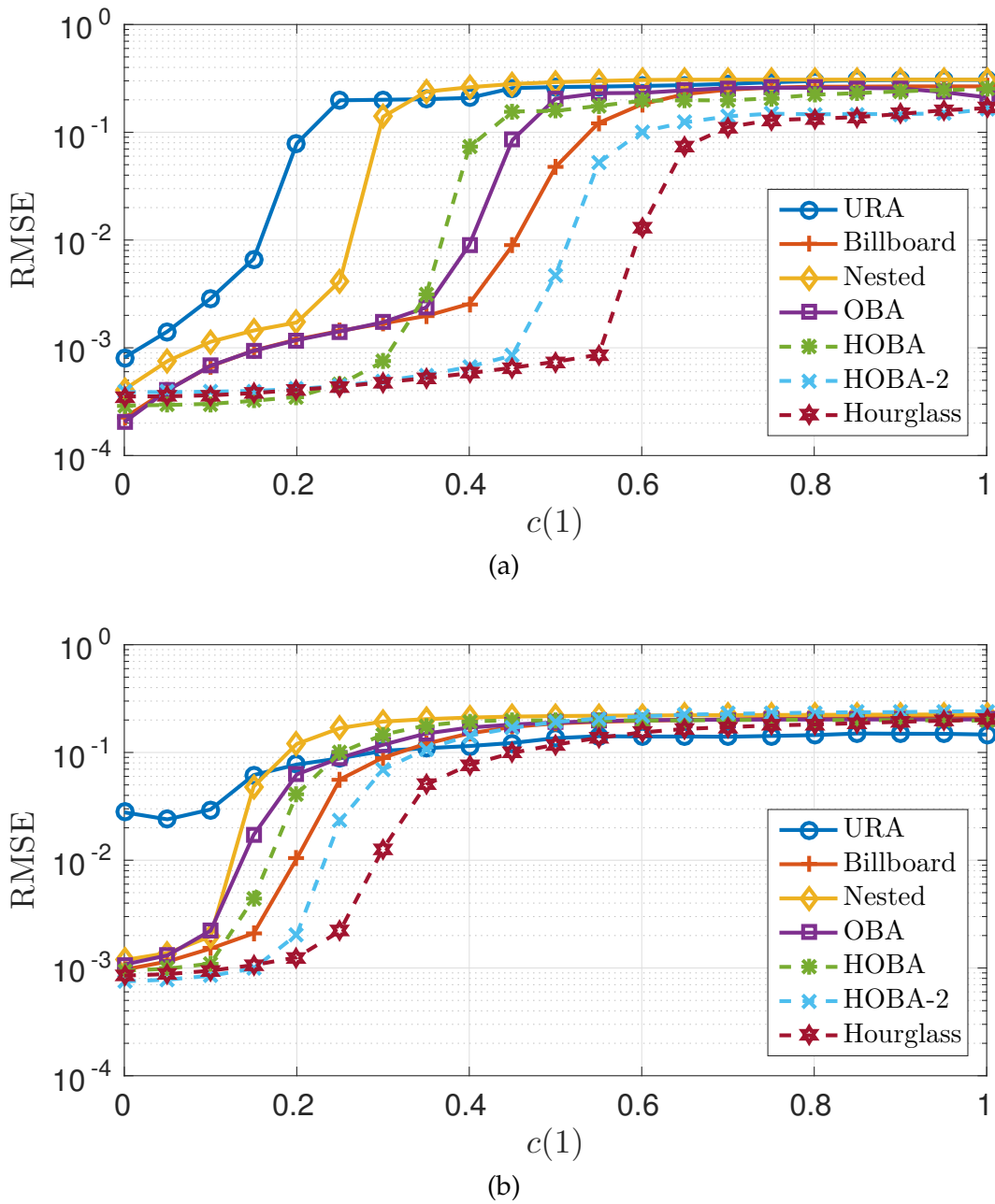


Figure 5.9: The RMSE as a function of the mutual coupling model for (a) the number of sources $D = 9$ and (b) $D = 36$. The number of sensors is 81 for all arrays. The parameters are 0dB SNR and $K = 200$. The sources directions are depicted in Fig. 5.7. The mutual coupling model is characterized by $B = 5$ and $c(\ell) = c(1) \exp [j\pi(\ell - 1)/4] / \ell$. Each point is averaged from 1000 runs.

5.9 Concluding Remarks

In this chapter, we proposed several generalizations of OBA, including POBA, HOBA, POBA- L , HOBA-2, and hourglass arrays. These arrays enjoy closed-form sensor locations, hole-free coarrays, and reduced mutual coupling effects. Our numerical examples show that, hourglass arrays perform better than the others, in the presence of mutual coupling.

Note that the hourglass array is one of the array configurations that satisfy Theorem 5.4.1. In the future, it will be of considerable interest to study the array configurations which not only satisfy Theorem 5.4.1 but also own even less mutual coupling than hourglass arrays.

Appendices

5.A Proof of Lemma 5.3.1

The proof can be divided into four cases:

1. If $a_p < 0$, consider the sensor pair in \mathcal{S}' : $(N_x - 1, N_y - 1)$ and (a_p, b_p) . Their difference is $(N_x - 1 - a_p, N_y - 1 - b_p) \notin \mathbb{D}_{\text{OBA}}$, since the first coordinate $N_x - 1 - a_p > N_x - 1$.
2. If $a_p > N_x - 1$, for the sensor pair $(a_p, b_p), (0, N_y - 1) \in \mathcal{S}'$, the difference becomes $(a_p, b_p - N_y + 1) \notin \mathbb{D}_{\text{OBA}}$ because $a_p > N_x - 1$.
3. If $b_p < 0$, we can take the sensor pair of $(0, N_y - 1)$ and (a_p, b_p) . The difference is $(-a_p, N_y - 1 - b_p) \notin \mathbb{D}_{\text{OBA}}$.
4. If $b_p > N_y - 1$, we have the following chain of arguments. Since $P < N_x$, there must exist a element $(n', 0) \in \mathcal{S}'$. Then the difference between (a_p, b_p) and $(n', 0)$ is $(a_p - n', b_p) \notin \mathbb{D}_{\text{OBA}}$, because $b_p > N_y - 1$.

These arguments show that $0 \leq a_p \leq N_x - 1$ and $0 \leq b_p \leq N_y - 1$ are necessary for $\mathbb{D}_{\text{OBA}} = \mathbb{D}'$. Furthermore, since $(a_p, b_p) \notin \mathbb{S}_{\text{OBA}}$, the necessary condition becomes $1 \leq a_p \leq N_x - 2$ and $1 \leq b_p \leq N_y - 1$, which proves this lemma.

5.B Proof of Lemma 5.3.2

Assume that $\mathbb{D}_{\text{OBA}} = \mathbb{D}'$. We obtain $(N_x - 1, N_y - 1) \in \mathbb{D}_{\text{OBA}} = \mathbb{D}'$. Due to Lemma 5.3.1, the only sensor pair with this separation is $(N_x - 1, N_y - 1)$ and $(0, 0)$, implying $(0, 0) \in \mathcal{S}'$. Similar arguments apply to the sensor pair of $(N_x - 1, 0)$ and $(0, N_y - 1)$, which proves this lemma.

5.C Proof of Theorem 5.3.1

Let \mathbb{S}_{OBA} and \mathbb{S}_{POBA} be an open box array and a partially open box array, respectively. Their difference coarrays are denoted by \mathbb{D}_{OBA} and \mathbb{D}_{POBA} . It is clear that $\mathbb{D}_{\text{POBA}} \subseteq \mathbb{D}_{\text{OBA}}$, due to (5.6) and Lemma 5.3.1.

(Sufficiency) We will show that if $\{\mathbf{g}_1, N_x - 1 - \mathbf{g}_2\}$ is a partition of $\{1, 2, \dots, N_x - 2\}$, then $\mathbb{D}_{\text{OBA}} \subseteq \mathbb{D}_{\text{POBA}}$. That is, for every $\mathbf{m} = (m_x, m_y) \in \mathbb{D}_{\text{OBA}}$, there exists at least one sensor pair $(\mathbf{n}_1, \mathbf{n}_2) \in \mathbb{S}_{\text{POBA}}^2$ such that $\mathbf{n}_1 - \mathbf{n}_2 = \mathbf{m}$. Note that we only need to check half of the elements in \mathbb{D}_{OBA} , since weight functions are symmetric, i.e., $w(\mathbf{m}) = w(-\mathbf{m})$ [124]. If $\{\mathbf{g}_1, N_x - 1 - \mathbf{g}_2\}$ is a partition of $\{1, 2, \dots, N_x - 2\}$, then $\{\mathbf{g}_2, N_x - 1 - \mathbf{g}_1\}$ is also a partition of $\{1, 2, \dots, N_x - 2\}$. Due to this property, we can identify at least one $(\mathbf{n}_1, \mathbf{n}_2)$ pair for any given difference (m_x, m_y) , as listed in Table 5.3, which proves the sufficiency.

(Necessity) If $\{\mathbf{g}_1, N_x - 1 - \mathbf{g}_2\}$ is not a partition of $\{1, 2, \dots, N_x - 2\}$, then $\mathbf{g}_1 \cup (N_x - 1 - \mathbf{g}_2) \neq \{1, 2, \dots, N_x - 2\}$ or \mathbf{g}_1 and $N_x - 1 - \mathbf{g}_2$ are not disjoint. Now there are two possible cases: For the first case, if $\mathbf{g}_1 \cup (N_x - 1 - \mathbf{g}_2) \neq \{1, 2, \dots, N_x - 2\}$, there must exist $n_0 \in \{1, 2, \dots, N_x - 2\}$ such that $n_0 \notin \mathbf{g}_1$ and $n_0 \notin N_x - 1 - \mathbf{g}_2$, since \mathbf{g}_1 and \mathbf{g}_2 are subsets of $\{1, 2, \dots, N_x - 2\}$ (the first item in Definition 5.3.1). We will show that, $(N_x - 1 - n_0, 1) \notin \mathbb{D}_{\text{POBA}}$.

Suppose there exist $(\mathbf{n}_1, \mathbf{n}_2) \in \mathbb{S}_{\text{POBA}}^2$ such that $\mathbf{n}_1 - \mathbf{n}_2 = (N_x - 1 - n_0, 1)$. This means the y coordinates of \mathbf{n}_1 and \mathbf{n}_2 must differ by 1. According to Definition 5.3.1, there are only two cases of \mathbf{n}_1 and \mathbf{n}_2 :

1. If $\mathbf{n}_1 \in \mathbb{H}_2$ and $\mathbf{n}_2 \in \mathbb{G}_1$, then the difference $(N_x - 1 - n_0, 1)$ is achieved only when $\mathbf{n}_1 = (N_x - 1, 1)$ and $\mathbf{n}_2 = (n_0, 0)$. We have $\mathbf{n}_1 \in \mathbb{H}_2$ but $\mathbf{n}_2 \notin \mathbb{G}_1$, since $n_0 \notin \mathbf{g}_1$.
2. If $\mathbf{n}_1 \in \mathbb{G}_2$ and $\mathbf{n}_2 \in \mathbb{H}_1$, then $\mathbf{n}_1 = (N_x - 1 - n_0, N_y - 1)$ and $\mathbf{n}_2 = (0, N_y - 2)$. We obtain $\mathbf{n}_1 \notin \mathbb{G}_2$ since $n_0 \notin N_x - 1 - \mathbf{g}_2$.

For the second case, if \mathbf{g}_1 and $N_x - 1 - \mathbf{g}_2$ are not disjoint, then the size of $\mathbf{g}_1 \cup (N_x - 1 - \mathbf{g}_2)$ can be expressed as

$$\begin{aligned} & |\mathbf{g}_1 \cup (N_x - 1 - \mathbf{g}_2)| \\ &= |\mathbf{g}_1| + |N_x - 1 - \mathbf{g}_2| - |\mathbf{g}_1 \cap (N_x - 1 - \mathbf{g}_2)| \\ &< |\mathbf{g}_1| + |\mathbf{g}_2| = N_x - 2, \end{aligned}$$

which implies $\mathbf{g}_1 \cup (N_x - 1 - \mathbf{g}_2) \neq \{1, 2, \dots, N_x - 2\}$. These arguments complete the proof.

Table 5.3: 12 cases in the proof of Theorem 5.3.1

| Case | m_x | m_y |
|------|---|---|
| 1 | 0 | 0 |
| 2 | $\in \mathfrak{g}_1$ | |
| 3 | $\in N_x - 1 - \mathfrak{g}_2$ | |
| 4 | $N_x - 1$ | |
| 5 | 0 | $1 \leq m_y \leq N_y - 1$ |
| 6 | $\in N_x - 1 - \mathfrak{g}_1$ | |
| 7 | $\in \mathfrak{g}_2$ | |
| 8 | $N_x - 1$ | |
| 9 | 0 | $-N_y + 1 \leq m_y \leq -1$ |
| 10 | $\in \mathfrak{g}_1$ | |
| 11 | $\in N_x - 1 - \mathfrak{g}_2$ | |
| 12 | $N_x - 1$ | |
| Case | \mathbf{n}_1 | \mathbf{n}_2 |
| 1 | $(0, 0) \in \mathbb{S}_{\text{POBA}}$ | $(0, 0) \in \mathbb{S}_{\text{POBA}}$ |
| 2 | $(m_x, 0) \in \mathbb{G}_1$ | $(0, 0) \in \mathbb{S}_{\text{POBA}}$ |
| 3 | $(N_x - 1, N_y - 1) \in \mathbb{S}_{\text{POBA}}$ | $(N_x - 1 - m_x, N_y - 1) \in \mathbb{G}_2$ |
| 4 | $(N_x - 1, 0) \in \mathbb{S}_{\text{POBA}}$ | $(0, 0) \in \mathbb{S}_{\text{POBA}}$ |
| 5 | $(0, m_y) \in \mathbb{S}_{\text{POBA}}$ | $(0, 0) \in \mathbb{S}_{\text{POBA}}$ |
| 6 | $(N_x - 1, m_y) \in \mathbb{S}_{\text{POBA}}$ | $(N_x - 1 - m_x, 0) \in \mathbb{G}_1$ |
| 7 | $(m_x, N_y - 1) \in \mathbb{G}_2$ | $(0, N_y - 1 - m_y) \in \mathbb{S}_{\text{POBA}}$ |
| 8 | $(N_x - 1, m_y) \in \mathbb{S}_{\text{POBA}}$ | $(0, 0) \in \mathbb{S}_{\text{POBA}}$ |
| 9 | $(0, 0) \in \mathbb{S}_{\text{POBA}}$ | $(0, -m_y) \in \mathbb{S}_{\text{POBA}}$ |
| 10 | $(m_x, 0) \in \mathbb{G}_1$ | $(0, -m_y) \in \mathbb{S}_{\text{POBA}}$ |
| 11 | $(N_x - 1, N_y - 1 + m_y) \in \mathbb{S}_{\text{POBA}}$ | $(N_x - 1 - m_x, N_y - 1) \in \mathbb{G}_2$ |
| 12 | $(N_x - 1, N_y - 1 + m_y) \in \mathbb{S}_{\text{POBA}}$ | $(0, N_y - 1) \in \mathbb{S}_{\text{POBA}}$ |

Table 5.4: 19 cases in the proof of Theorem 5.4.1

| Case | m_x | m_y | \mathbf{n}_1 | \mathbf{n}_2 |
|------|---|-----------------------------|---|---|
| 1 | 0 | 0 | $(0, 0) \in \mathbb{S}_{\text{POBA-L}}$ | $(0, 0) \in \mathbb{S}_{\text{POBA-L}}$ |
| 2 | $\in \mathfrak{g}_1$ | 0 | $(m_x, 0) \in \mathbb{G}_1$ | $(0, 0) \in \mathbb{S}_{\text{POBA-L}}$ |
| 3 | $\in N_x - 1 - \mathfrak{g}_2$ | 0 | $(N_x - 1, N_y - 1) \in \mathbb{S}_{\text{POBA-L}}$ | $(N_x - 1 - m_x, N_y - 1) \in \mathbb{G}_2$ |
| 4 | $N_x - 1$ | 0 | $(N_x - 1, 0) \in \mathbb{S}_{\text{POBA-L}}$ | $(0, 0) \in \mathbb{S}_{\text{POBA-L}}$ |
| 5 | $-(N_x - 1)$ | $N_y - 1$ | $(0, N_y - 1) \in \mathbb{S}_{\text{POBA-L}}$ | $(N_x - 1, 0) \in \mathbb{S}_{\text{POBA-L}}$ |
| 6 | $\in -\mathfrak{g}_1$ | $N_y - 1$ | $(0, N_y - 1) \in \mathbb{S}_{\text{POBA-L}}$ | $(-m_x, 0) \in \mathbb{G}_1$ |
| 7 | $\in -(N_x - 1 - \mathfrak{g}_2)$ | $N_y - 1$ | $(N_x - 1 + m_x, N_y - 1) \in \mathbb{G}_2$ | $(N_x - 1, 0) \in \mathbb{S}_{\text{POBA-L}}$ |
| 8 | 0 | $N_y - 1$ | $(0, N_y - 1) \in \mathbb{S}_{\text{POBA-L}}$ | $(0, 0) \in \mathbb{S}_{\text{POBA-L}}$ |
| 9 | $\in N_x - 1 - \mathfrak{g}_1$ | $N_y - 1$ | $(N_x - 1, N_y - 1) \in \mathbb{S}_{\text{POBA-L}}$ | $(N_x - 1 - m_x, 0) \in \mathbb{G}_1$ |
| 10 | $\in \mathfrak{g}_2$ | $N_y - 1$ | $(m_x, N_y - 1) \in \mathbb{G}_2$ | $(0, 0) \in \mathbb{S}_{\text{POBA-L}}$ |
| 11 | $N_x - 1$ | $N_y - 1$ | $(N_x - 1, N_y - 1) \in \mathbb{S}_{\text{POBA-L}}$ | $(0, 0) \in \mathbb{S}_{\text{POBA-L}}$ |
| 12 | $0 < m_x < (N_x - 1) - (\ell - 1)$ | $\in \mathfrak{h}_{2,\ell}$ | $(N_x - \ell, m_y) \in \mathbb{H}_{2,\ell}$ | $(N_x - \ell - m_x, 0) \in \mathbb{G}_1$ |
| 13 | $0 < m_x < (N_x - 1) - (\ell - 1)$ | $\in \mathfrak{h}_{2,\ell}$ | $(m_x + \ell - 1, N_y - 1) \in \mathbb{G}_2$ | $(\ell - 1, N_y - 1 - m_y) \in \mathbb{H}_{1,\ell}$ |
| 14 | $N_x - \ell$ | $\in \mathfrak{h}_{2,\ell}$ | $(N_x - \ell, m_y) \in \mathbb{H}_{2,\ell}$ | $(0, 0) \in \mathbb{S}_{\text{POBA-L}}$ |
| 15 | $N_x - k$ for $1 \leq k \leq \ell - 1$ | $\in \mathfrak{h}_{2,\ell}$ | $(N_x - p, m_y + r) \in \mathbb{H}_{2,p}$ | $(k - p, r) \in \mathbb{H}_{1,k-p+1}$ |
| 16 | $-(N_x - 1) + (\ell - 1) < m_x < 0$ | $\in \mathfrak{h}_{1,\ell}$ | $(\ell - 1, m_y) \in \mathbb{H}_{1,\ell}$ | $(\ell - 1 - m_x, 0) \in \mathbb{G}_1$ |
| 17 | $-(N_x - 1) + (\ell - 1) < m_x < 0$ | $\in \mathfrak{h}_{1,\ell}$ | $(N_x - \ell + m_x, N_y - 1) \in \mathbb{G}_2$ | $(N_x - \ell, N_y - 1 - m_y) \in \mathbb{H}_{2,\ell}$ |
| 18 | $-(N_x - \ell)$ | $\in \mathfrak{h}_{1,\ell}$ | $(\ell - 1, m_y) \in \mathbb{H}_{1,\ell}$ | $(N_x - 1, 0) \in \mathbb{S}_{\text{POBA-L}}$ |
| 19 | $-(N_x - k)$ for $1 \leq k \leq \ell - 1$ | $\in \mathfrak{h}_{1,\ell}$ | $(p - 1, m_y + r) \in \mathbb{H}_{1,p}$ | $(N_x - (k - p + 1), r) \in \mathbb{H}_{2,k-p+1}$ |

For Cases 2, 3, 6, 7, 9, and 10, we assume that $\{\mathfrak{g}_1, N_x - 1 - \mathfrak{g}_2\}$ partitions $\{1, \dots, N_x - 2\}$.

For Cases 12 - 19, the parameter ℓ satisfies $1 \leq \ell \leq L$.

Case 12 assumes that $N_x - \ell - m_x \in \mathfrak{g}_1$.

Case 13 assumes that $m_x + \ell - 1 \in \mathfrak{g}_2$.

Case 15 assumes that $\exists p \in \{1, \dots, k\}$ and $\exists r \in \mathfrak{h}_{1,k-p+1}$ such that $m_y + r \in \mathfrak{h}_{2,p}$.

Case 16 assumes that $\ell - 1 - m_x \in \mathfrak{g}_1$.

Case 17 assumes that $N_x - \ell + m_x \in \mathfrak{g}_2$.

Case 19 assumes that $\exists p \in \{1, \dots, k\}$ and $\exists r \in \mathfrak{h}_{2,k-p+1}$ such that $m_y + r \in \mathfrak{h}_{1,p}$.

5.D Proof of Theorem 5.4.1

(Sufficiency) The proof of this theorem is similar to that of Theorem 5.3.1. We need to show that, if $\{\mathfrak{h}_{1,\ell}\}_{\ell=1}^L$ satisfies (5.10), then for every $\mathbf{m} = (m_x, m_y) \in \mathbb{D}_{\text{OBA}}$, there exist $\mathbf{n}_1, \mathbf{n}_2 \in \mathbb{S}_{\text{POBA-L}}$ such that $\mathbf{n}_1 - \mathbf{n}_2 = \mathbf{m}$. It suffices to consider $0 \leq |m_x| \leq N_x - 1$ and $0 \leq m_y \leq N_y - 1$ since the weight functions satisfy $w(\mathbf{m}) = w(-\mathbf{m})$.

For $0 \leq |m_x| \leq N_x - 1$ and $0 \leq m_y \leq N_y - 1$, the associated \mathbf{n}_1 and \mathbf{n}_2 are summarized into 19 cases in Table 5.4. In particular, some cases are elaborated as follows:

(Case 6, 7, 9, 10) In Case 6 and 7, since $\{\mathfrak{g}_1, N_x - 1 - \mathfrak{g}_2\}$ is a partition of $\{1, \dots, N_x - 2\}$, for $-(N_x - 1) < m_x < 0$ and $m_y = N_y - 1$, the pair $(\mathbf{n}_1, \mathbf{n}_2)$ can be identified using either Case 6 or 7. Similar arguments can be applied to Case 9 and 10.

(Case 12, 13, 16, 17) For $0 < m_x < (N_x - 1) - (\ell - 1)$ and $0 < m_y < N_y - 1$, it is

guaranteed that either Case 12 or 13 can be exploited to identify the sensor pair \mathbf{n}_1 and \mathbf{n}_2 . This is true because $\{\mathbf{g}_1, N_x - 1 - \mathbf{g}_2\}$ is a partition of $\{1, \dots, N_x - 2\}$, and $\{\mathfrak{h}_{2,\ell}\}_{\ell=1}^L$ is a partition of $\{1, \dots, N_y - 2\}$. Case 16 and 17 are similar to Case 12 and 13.

(Case 15) In this case, for some $p \in \{1, \dots, k\}$, if there exists $r \in \mathfrak{h}_{1,k-p+1}$ such that $m_y + r \in \mathfrak{h}_{2,p}$, then, by definition, it can be deduced that $\mathbf{n}_1 \in \mathbb{H}_{2,p}$ and $\mathbf{n}_2 \in \mathbb{H}_{1,k-p+1}$. This sufficient condition is equivalent to

$$\begin{aligned} \exists r \in \mathfrak{h}_{1,k-p+1}, \exists s \in \mathfrak{h}_{2,p}, \forall m_y \in \mathfrak{h}_{2,\ell}, \\ \text{such that } m_y + r = s. \end{aligned}$$

Letting $\tilde{s} = N_y - 1 - s$ and $\tilde{m}_y = N_y - 1 - m_y$ yields

$$\begin{aligned} \exists r \in \mathfrak{h}_{1,k-p+1}, \exists \tilde{s} \in \mathfrak{h}_{1,p}, \forall \tilde{m}_y \in \mathfrak{h}_{1,\ell} \\ \text{such that } \tilde{m}_y = \tilde{s} + r. \end{aligned} \quad (5.26)$$

Eq. (5.26) indicates that, any element in $\mathfrak{h}_{1,\ell}$ can be expressed as the sum of an element in $\mathfrak{h}_{1,p}$ and an element in $\mathfrak{h}_{1,k-p+1}$. Therefore, we obtain

$$\begin{aligned} \mathfrak{h}_{1,\ell} &\subseteq \mathfrak{h}_{1,p} \oplus \mathfrak{h}_{1,k-p+1} = (\mathfrak{h}_{1,p} \oplus \mathfrak{h}_{1,q})|_{p+q=k+1} \\ &\subseteq \bigcup_{\tilde{p}+\tilde{q}=k+1} \mathfrak{h}_{1,\tilde{p}} \oplus \mathfrak{h}_{1,\tilde{q}} = \mathbb{P}_{k+1}, \end{aligned} \quad (5.27)$$

where $2 \leq k+1 \leq \ell$. If (5.10) holds true, then (5.27) also holds true, and so does (5.26). Therefore, there exist $\mathbf{n}_1 \in \mathbb{H}_{2,p}$ and $\mathbf{n}_2 \in \mathbb{H}_{1,k-p+1}$ such that $\mathbf{n}_1 - \mathbf{n}_2 = \mathbf{m}$.

(Case 19) The proof of this case is similar to that of Case 15. For some $p \in \{1, \dots, k\}$, the sufficient condition on the last row of Table 5.4 is equivalent to this statement:

$$\begin{aligned} \exists r \in \mathfrak{h}_{2,k-p+1}, \exists s \in \mathfrak{h}_{1,p}, \forall m_y \in \mathfrak{h}_{1,\ell}, \\ \text{such that } m_y + r = s. \end{aligned}$$

Setting $\tilde{r} = N_y - 1 - r$ gives

$$\begin{aligned} \exists \tilde{r} \in \mathfrak{h}_{1,k-p+1}, \exists s \in \mathfrak{h}_{1,p}, \forall m_y \in \mathfrak{h}_{1,\ell} \\ \text{such that } m_y = s + \tilde{r} - (N_y - 1). \end{aligned}$$

Similar to (5.27), we have $\mathfrak{h}_{1,\ell} \subseteq \mathbb{P}_{k+1} - (N_y - 1)$. Hence, if (5.10) is satisfied, then $\mathbf{n}_1 \in \mathbb{H}_{1,p}$ and $\mathbf{n}_2 \in \mathbb{H}_{2,k-p+1}$.

(Necessity) This part can be proved by contradiction. If there exists $n \in \mathfrak{h}_{1,\ell}$ such that $n \notin \mathbb{P}_{\ell'}$ for some $\ell' \leq \ell$, then $\mathbf{m} = (N_x + 1 - \ell', N_y - 1 - n)$ is a hole in $\mathbb{D}_{\text{POBA-L}}$. We will show that there do not exist any sensor pairs $(\mathbf{n}_1, \mathbf{n}_2) \in \mathbb{S}_{\text{POBA-L}}^2$ such that $\mathbf{n}_1 - \mathbf{n}_2 = (N_x + 1 - \ell', N_y - 1 - n)$. Enumerating all possible combinations of $(\mathbf{n}_1, \mathbf{n}_2)$ leads to the following:

1. If $\mathbf{n}_2 = (0, 0)$, then $\mathbf{n}_1 = (N_x - (\ell' - 1), N_y - 1 - n)$. According to the x coordinate of \mathbf{n}_1 , \mathbf{n}_1 could belong to \mathbb{G}_1 , $\mathbb{H}_{2,\ell'-1}$, or \mathbb{G}_2 . However, based on the y coordinate of \mathbf{n}_1 , we have $n \in \mathfrak{h}_{1,\ell}$, and $N_x - 1 - n \in \mathfrak{h}_{2,\ell}$. Furthermore, since $\{\mathfrak{h}_{2,\ell}\}_{\ell=1}^L$ is a partition of $\{1, \dots, N_y - 2\}$, we have $\mathbf{n}_1 \in \mathbb{H}_{2,\ell}$. This is a contradiction.
2. $\mathbf{n}_2 = (N_x - 1, 0), (0, N_y - 1), (N_x - 1, N_y - 1)$ or $\mathbf{n}_2 \in \mathbb{G}_2$. It is evident that $\mathbf{n}_1 = \mathbf{n}_2 + \mathbf{m} \notin \mathbb{S}_{\text{POBA-}L}$.
3. If $\mathbf{n}_2 = (n_x, 0) \in \mathbb{G}_1$, then $\mathbf{n}_1 = (N_x - (\ell' - 1 - n_x), N_y - 1 - n)$. The y coordinate of \mathbf{n}_1 indicates that \mathbf{n}_1 belongs to $\mathbb{H}_{2,\ell}$. From the x coordinate of \mathbf{n}_1 , we have $\ell' - 1 - n_x = \ell$. By definition, $\ell' \leq \ell$ and $n_x \geq 1$ suggest that $\ell' - 1 - n_x \leq \ell - 2$, causing a contradiction.
4. If $\mathbf{n}_2 = (p - 1, r) \in \mathbb{H}_{1,p}$, then $\mathbf{n}_1 = (N_x - (\ell' - p), N_y - 1 + r - n)$. The x coordinate of \mathbf{n}_1 leads to three cases:
 - a) If $\mathbf{n}_1 \in \mathbb{G}_1$, then $N_y - 1 + r - n = 0$ so $r = n - (N_y - 1)$. Since $n \in \mathfrak{h}_{1,\ell}$, we have $1 \leq n \leq N_y - 2$ and then $-N_y + 2 \leq r \leq -1$. This statement contradicts with $r \in \mathfrak{h}_{1,p} \subseteq \{1, \dots, N_y - 2\}$.
 - b) If $\mathbf{n}_1 \in \mathbb{G}_2$, from the y coordinate of \mathbf{n}_1 , we obtain $N_y - 1 + r - n = N_y - 1$ so $r = n$. Since $\{\mathfrak{h}_{1,\ell}\}_{\ell=1}^L$ is a partition of $\{1, \dots, N_y - 2\}$, the y coordinate of $\mathbf{n}_2 = (p - 1, n)$ implies $\mathbf{n}_2 \in \mathbb{H}_{1,\ell}$. We obtain $p = \ell$. However, the x coordinate of \mathbf{n}_1 becomes $N_x - (\ell' - p) = N_x + \ell - \ell' \geq N_x + \ell - \ell = N_x$. Therefore, $\mathbf{n}_1 \notin \mathbb{G}_2$.
 - c) If $\mathbf{n}_1 \in \mathbb{H}_{2,\ell'-p}$, we obtain $N_y - 1 + r - n \in \mathfrak{h}_{2,\ell'-p}$, which is equivalent to $n - r \in \mathfrak{h}_{1,\ell'-p}$. Since $r \in \mathfrak{h}_{1,p}$, it can be concluded that
$$n \in \mathfrak{h}_{1,\ell'-p} \oplus \mathfrak{h}_{1,p} \subseteq \bigcup_{p+q=\ell'} \mathfrak{h}_{1,p} \oplus \mathfrak{h}_{1,q} = \mathbb{P}_{\ell'}$$
which contradicts with the assumption $n \notin \mathbb{P}_{\ell'}$.
5. If $\mathbf{n}_2 = (N_x - p, r) \in \mathbb{H}_{2,p}$, then $\mathbf{n}_1 = (2N_x + 1 - \ell' - p, N_y - 1 - n + r)$. Since $1 \leq \ell' \leq \ell \leq L$ and $1 \leq p \leq L$, the x coordinate of \mathbf{n}_1 ranges from $2N_x - 2L + 1$ to $2N_x - 1$. According to Definition 5.4.1, we have $L \leq N_x/2$, so the minimum value of the x coordinate in \mathbf{n}_1 is $N_x + 1$, implying $\mathbf{n}_1 \notin \mathbb{S}_{\text{POBA-}L}$.

Second, assume that there exists $n \in \mathfrak{h}_{1,\ell}$ such that $n \notin \mathbb{P}_{\ell'} - (N_y - 1)$ for some $\ell' \leq \ell$. Following the same steps in the previous case, it can be shown that $\mathbf{m} = (N_x + 1 - \ell', -n)$ is a hole in the difference coarray \mathbb{D} . As a result, the condition (5.10) is also necessary.

5.E Proof of Theorem 5.6.1

This theorem is a consequence of Theorem 5.4.1. We will first show that $\mathfrak{h}_{1,\ell} \subseteq \mathfrak{h}_{1,1} \oplus \mathfrak{h}_{1,\ell'-1} \subseteq \mathbb{P}_{\ell'}$ for every ℓ' and ℓ in $2 \leq \ell' \leq \ell \leq L$. That is, for every $h \in \mathfrak{h}_{1,\ell}$, it suffices to find $n_1 \in \mathfrak{h}_{1,1}$ and $n_2 \in \mathfrak{h}_{1,\ell'-1}$ such that $h = n_1 + n_2$. According to (5.13), h can be divided into four cases as follows:

(Case 1) If $h = 2\ell - 1$, then n_1 and n_2 are given by

$$n_1 = 2(\ell - \ell' + 1), \quad n_2 = 2(\ell' - 1) - 1.$$

It can be seen that $n_2 \in \mathfrak{h}_{1,\ell'-1}$. We need to show that $n_1 \in \mathfrak{h}_{1,1}$. Since $2 \leq \ell' \leq \ell \leq L$, we have

$$1 \leq \ell - \ell' + 1 \leq L - 1.$$

The upper bound $L - 1$ can be divided into two cases: If N_y is odd, then $L - 1 = \lfloor (N_y - 3)/4 \rfloor \leq \lfloor (N_y - 1)/4 \rfloor$. If N_y is even, we obtain $L - 1 = \lfloor N_y/8 \rfloor \leq \lfloor (N_y - 1)/4 \rfloor$. In either cases, $n_1 \in \mathfrak{h}_{1,1}$.

(Case 2) If $h = N_y - 2\ell$, it is divided into two cases based on N_y :

1. If N_y is odd, n_1 and n_2 are given by

$$n_1 = N_y - 1 - 2(\ell + \ell' - 2), \quad n_2 = 2(\ell' - 1) - 1. \quad (5.28)$$

It is obvious that n_1 is even and $n_2 \in \mathfrak{h}_{1,\ell'-1}$. Next we will prove that $n_1 \in \mathfrak{h}_{1,1}$. since $2 \leq \ell' \leq \ell \leq L$, we have $2 \leq \ell + \ell' - 2 \leq 2L - 2$. There are two subcases according to $\ell + \ell' - 2$:

- a) If $2 \leq \ell + \ell' - 2 \leq \lfloor (N_y - 1)/4 \rfloor$, it can be shown that $n_1 \in \mathfrak{h}_{1,1}$.
- b) If $\lfloor (N_y - 1)/4 \rfloor + 1 \leq \ell + \ell' - 2 \leq 2L - 2$, then the minimum of n_1 is lower bounded by

$$\begin{aligned} n_{1,\min} &= N_y - 1 - 2(2L - 2) \\ &= 4 \left(\frac{N_y + 1}{4} - \left\lfloor \frac{N_y + 1}{4} \right\rfloor \right) + 2 \geq 2. \end{aligned} \quad (5.29)$$

The maximum of n_1 becomes

$$\begin{aligned} n_{1,\max} &= N_y - 1 - 2(\lfloor (N_y - 1)/4 \rfloor + 1) \\ &= 4 \times \frac{N_y - 1}{4} - 2 \left\lfloor \frac{N_y - 1}{4} \right\rfloor - 2. \end{aligned}$$

For odd N_y , it can be shown that $(N_y - 1)/4 \leq \lfloor (N_y - 1)/4 \rfloor + 1/2$. The maximum of n_1 is upper bounded by

$$\begin{aligned} n_{1,\max} &\leq 4 \left(\left\lfloor \frac{N_y - 1}{4} \right\rfloor + \frac{1}{2} \right) - 2 \left\lfloor \frac{N_y - 1}{4} \right\rfloor - 2 \\ &= 2 \left\lfloor \frac{N_y - 1}{4} \right\rfloor. \end{aligned} \quad (5.30)$$

Hence, $n_1 \in \mathfrak{h}_{1,1}$, due to (5.13), (5.29), and (5.30).

2. If N_y is even, the pair (n_1, n_2) can be written as

$$\begin{aligned} n_1 &= N_y - 2\lceil N_y/4 \rceil - 2(\ell + \ell' - 3), \\ n_2 &= 2\lceil N_y/4 \rceil + 2(\ell' - 1) - 4. \end{aligned}$$

It is also true that $n_2 \in \mathfrak{h}_{1,\ell'-1}$. It suffices to show that $n_1 \in \mathfrak{h}_{1,1}$. Due to even N_y , the quantity n_1 is even. For $2 \leq \ell' \leq \ell \leq L$, the maximum of n_1 is upper bounded by

$$\begin{aligned} n_{1,\max} &= N_y - 2\lceil N_y/4 \rceil - 2 \leq N_y - 2 \times N_y/4 - 2 \\ &= 2 \left(\frac{N_y - 1}{4} - \frac{3}{4} \right) \leq 2 \left\lfloor \frac{N_y - 1}{4} \right\rfloor, \end{aligned}$$

where the last inequality is due to $(N_y - 1)/4 - 3/4 \leq \lfloor (N_y - 1)/4 \rfloor$ for even N_y . On the other hand, the minimum of n_1 is given by

$$\begin{aligned} n_{1,\min} &= N_y - 2\lceil N_y/4 \rceil - 2(2L - 3) \\ &= N_y - 2\lceil N_y/4 \rceil - 4\lfloor N_y/8 \rfloor + 2. \end{aligned}$$

Since $N_y/2 = \lfloor N_y/4 \rfloor + \lceil N_y/4 \rceil$ and $\lfloor 2x \rfloor \geq 2\lfloor x \rfloor$, the quantity $n_{1,\min}$ is lower bounded by

$$\begin{aligned} n_{1,\min} &= N_y - 2 \left(\frac{N_y}{2} - \left\lfloor \frac{N_y}{4} \right\rfloor \right) - 4 \left\lfloor \frac{N_y}{8} \right\rfloor + 2 \\ &\geq 2 \times 2 \left\lfloor \frac{N_y}{8} \right\rfloor - 4 \left\lfloor \frac{N_y}{8} \right\rfloor + 2 \geq 2. \end{aligned}$$

Therefore, $n_1 \in \mathfrak{h}_{1,1}$ because n_1 is an even number between 2 and $2\lfloor (N_y - 1)/4 \rfloor$.

(Case 3) If N_y is even and $h = 2\lceil N_y/4 \rceil - 2\ell + 3$, the pair (n_1, n_2) becomes

$$n_1 = 2\lceil N_y/4 \rceil - 2(\ell + \ell') + 6, \quad n_2 = 2(\ell' - 1) - 1.$$

We will again show that $n_1 \in \mathfrak{h}_{1,1}$. Note that n_1 is an even number. The maximum of n_1 is bounded by

$$n_{1,\max} = 2\lceil N_y/4 \rceil - 2 \leq 2\lfloor (N_y - 1)/4 \rfloor.$$

The minimum of n_1 is lower bounded by

$$\begin{aligned} n_{1,\min} &= 2\lfloor N_y/4 \rfloor - 2L + 6 = 2\lfloor N_y/4 \rfloor - 2\lfloor N_y/8 \rfloor + 4 \\ &\geq 2\lfloor N_y/4 \rfloor - \lfloor N_y/4 \rfloor + 4 \geq 4. \end{aligned}$$

The inequality is due to $2\lfloor x \rfloor \leq \lfloor 2x \rfloor$. Therefore, $n_1 \in \mathfrak{h}_{1,1}$.

(Case 4) If N_y is even and $h = 2\lceil N_y/4 \rceil + 2\ell - 4$, n_1 and n_2 are given by

$$n_1 = 2(\ell - \ell' + 1), \quad n_2 = 2\lceil N_y/4 \rceil + 2(\ell' - 1) - 4.$$

The membership of n_1 can be shown as follows: Since $2 \leq \ell' \leq \ell \leq L$, we have

$$1 \leq \ell - \ell' + 1 \leq L - 1 = \lfloor N_y/8 \rfloor \leq \lfloor (N_y - 1)/4 \rfloor,$$

so that $n_1 \in \mathfrak{h}_{1,1}$. For n_2 , if $\ell' \geq 3$, it is clear that $n_2 \in \mathfrak{h}_{1,\ell'-1}$. If $\ell' = 2$, then n_2 becomes

$$n_2 = 2\lceil N_y/4 \rceil - 2 = 2\lfloor (N_y - 1)/4 \rfloor.$$

The last equality can be shown by considering two cases: $N_y = 4r$ and $N_y = 4r + 2$, where r is an integer. Therefore, $n_1 \in \mathfrak{h}_{1,1}$.

So far we have proved the statement that $\mathfrak{h}_{1,\ell} \subseteq \mathbb{P}_{\ell'}$ for $2 \leq \ell' \leq \ell \leq L$. It is required to prove $\mathfrak{h}_{1,\ell} \subseteq \mathbb{P}_{\ell'} - (N_y - 1)$. Based on the definition of $\mathfrak{h}_{1,\ell}$, it is evident that these sets are symmetric. That is, for every $h \in \mathfrak{h}_{1,\ell}$, there uniquely exists $h' \in \mathfrak{h}_{1,\ell}$ such that $h = N_y - 1 - h'$. Since $h' \in \mathfrak{h}_{1,\ell}$, there must exist $n'_1 \in \mathfrak{h}_{1,1}$ and $n'_2 \in \mathfrak{h}_{1,\ell'-1}$ such that $h' = n'_1 + n'_2$. We obtain

$$\begin{aligned} h &= N_y - 1 - h' = N_y - 1 - n'_1 - n'_2 \\ &= (N_y - 1 - n'_1) + (N_y - 1 - n'_2) - (N_y - 1). \end{aligned}$$

It can be deduced that $N_y - 1 - n'_1 \in \mathfrak{h}_{1,1}$ and $N_y - 1 - n'_2 \in \mathfrak{h}_{1,\ell'-1}$, since these sets are symmetric. We have $h \in \mathbb{P}_{\ell'} - (N_y - 1)$, which proves this theorem.

CRAMÉR-RAO BOUNDS FOR SPARSE ARRAYS, WHICH FIND MORE SOURCE DIRECTIONS THAN SENSORS

6.1 Introduction

The celebrated Cramér-Rao bound (CRB), which has influenced our thinking for many decades of statistical signal processing, has found significant use in direction-of-arrival (DOA) problems, among others [37], [69], [109], [142], [188]. The DOA problem is of great importance in passive array processing [188], radar [52], [71], [157], digital communications [50], radio astronomy [58], and other applications [57], [77], [180]. The CRB offers a lower bound on the variances of unbiased estimates of the parameters (e.g., DOA). Closed-form expressions for the CRB offer insights into the dependence of the array performance with respect to various parameters such as the number of sensors N in the array, the array geometry, the number of sources D , the number of snapshots, signal to noise ratio (SNR), and so forth.

Two of the most influential papers in the DOA context are the papers by Stoica and Nehorai [166] and [167]. These papers distinguish between the deterministic CRB and the stochastic CRB (reviewed here in Section 6.3), and obtain closed-form expressions for these. In both cases, the expressions for CRB come from the inversion of the Fisher information matrix (FIM), which contains information about all the unknown parameters. An appropriate principal submatrix of this inverse reveals the CRB of the DOAs, which we denote as $\text{CRB}(\bar{\theta})$. In this chapter, we will be especially interested in the stochastic CRB because the model assumptions used therein are more appropriate in our context, namely sparse array processing using the difference coarray (Section 6.3).

The specific CRB expressions given in Eqs. (2.11) and (3.1) of [167] are valid only when $D < N$ (fewer sources than sensors). This is because the expressions are based on the inverse of the matrix $\mathbf{A}^H \mathbf{A}$ (e.g., see the equation after (2.11) in [167]), where \mathbf{A} is the so-called *array manifold matrix*. The assumption $D < N$ is however not fundamental to the existence of CRB of the DOA parameters because even when $D \geq N$, with proper prior information, the FIM can remain nonsingular (invertible) under a much broader range of conditions, as we shall prove in this chapter. So it is possible to get more useful expressions which do not involve $(\mathbf{A}^H \mathbf{A})^{-1}$.

The closed-form expressions for $\text{CRB}(\bar{\theta})$ given in Eq. (3.1) of [167] assume an arbitrary covariance matrix for the sources. For the case where it is known a priori that the sources are uncorrelated, it has been shown in a very interesting paper by

Jansson et al. [66] that the CRB is in general smaller than what one would get if one substituted a diagonal covariance in the expression (3.1) given in [167]. Closed-form expressions for $\text{CRB}(\bar{\theta})$ for the case of uncorrelated sources are also given in [66]. The authors mention that it is possible to estimate more sources than sensors in the case of certain array configurations [66], [130]. However, the detailed conditions under which this is possible are not provided in [66]. Furthermore, all the examples given in [66] are for the case of uniform linear arrays (ULAs), for which the number of identifiable sources is less than the number of sensors. Finally, the inverses of certain matrices are assumed to exist in the CRB expression (13) in [66] although the conditions under which these inverses exist are not spelt out. In fact, the appearance of $m - d$ (i.e., $N - D$ in our notation) in the denominator Eq. (14) of [66] makes this expression invalid when $N = D$.

Most importantly, suppose we are interested in the question "Given an array configuration, what is the upper limit on the number of sources D (in relation to the number of sensors) such that the expression for $\text{CRB}(\bar{\theta})$ is valid?" This is not answered in [66]. One of our contributions here is to give a precise theoretical answer to such questions. The reason why this is possible is because there are multiple ways to express the CRB in closed forms, and some of them are more revealing than others.

The reason for the renewed interest in finding more useful closed-form expressions for the CRB is the following. For a long time, **sparse arrays**, such as the minimum redundancy arrays (MRAs) have been known to be able to identify more sources than sensors ($D \geq N$) [113]. More recently, the development of sparse arrays such as the nested arrays [124], the coprime arrays [125], [186], and their extensions [92]–[94], [139], [140], have generated a new wave of interest in this topic. These new arrays have simple closed-form expressions for array geometry (compared to MRAs which do not have this advantage), which makes them more practical than MRAs. The most essential property of these successful sparse arrays is that, given N sensors, the difference coarrays of these arrays have $\mathcal{O}(N^2)$ elements, which allows them to identify $D = \mathcal{O}(N^2)$ sources using N sensors. In particular, therefore, $D \gg N$ is possible as demonstrated amply in [1], [4], [55], [59], [66], [113], [124], [132], [139], [175], [177], [186].

It is therefore of great importance to study the performance limits of these sparse arrays by using standard tools such as the CRB. If we try to do this using the existing results in the literature, we run into a road block. Either the known closed-form expressions are not valid when $D \geq N$, or the precise conditions under which they are valid are not specified. In this context, it is worth mentioning that the pioneering work by Abramovich et al. many years ago [1] discussed the performances of MRAs

by successfully plotting the CRB even for the case of $D \geq N$. The same can be done today for nested and coprime arrays. However, the theoretical conditions under which the CRB exists (for the case $D \geq N$) have not been spelt out in the past.

We now summarize the main contributions of this chapter. Starting from the Fisher information matrix for the case of stochastic CRB with uncorrelated priors, as in [66], we derive a new closed-form expression for the CRB, specifically for the case of uncorrelated sources. The new CRB expressions are valid if and only if the FIM is nonsingular. The condition for the validity of our CRB expression are here expressed explicitly in terms of the geometry of the difference coarray. Thus, with \mathbb{D} denoting the difference coarray of a linear array, let $\mathbf{V}_{\mathbb{D}}$ be the array manifold matrix defined on this difference coarray. So $\mathbf{V}_{\mathbb{D}}$ is a $|\mathbb{D}| \times D$ matrix. The number of rows is the size of difference coarray (which could be $\mathcal{O}(N^2)$), and the number of columns is the number of sources. Now consider the $|\mathbb{D}| \times (2D + 1)$ matrix

$$\mathbf{A}_c = \begin{bmatrix} \text{diag}(\mathbb{D})\mathbf{V}_{\mathbb{D}} & \mathbf{V}_{\mathbb{D}} & \mathbf{e}_0 \end{bmatrix}, \quad (6.1)$$

where $\text{diag}(\mathbb{D})$ is a diagonal matrix with \mathbb{D} on its diagonals, and \mathbf{e}_0 is an all zero vector except for one nonzero element, the location of which depends on the coarray geometry. We refer to the matrix (6.1) as the **augmented coarray manifold** matrix or **ACM** matrix. The main result is that the FIM is nonsingular if and only if the ACM matrix \mathbf{A}_c has full column rank $2D + 1$. We shall refer to this as the **rank condition**. To the best of our knowledge, the invertibility of the FIM has not in the past been characterized in terms of the difference coarray geometry. The proposed CRB expression holds under this rank condition, and is given by our Eq. (6.40) (to be proved in Theorem 6.4.2). Thus the specific CRB expression is valid whenever the FIM is invertible.

The invertibility of FIM, expressed as a rank condition on the ACM matrix, leads to a number of further insights as we shall elaborate in this chapter. In short, the rank condition depends explicitly only on the difference coarray and the DOAs, whereas the CRB itself depends also on the physical array, the number of snapshots, and the SNR (Propositions 6.5.1 and 6.5.2 of Section 6.5). We will also see that if the rank condition on the ACM matrix is satisfied, then $\text{CRB}(\bar{\boldsymbol{\theta}})$ converges to zero as the number of snapshots increases. This is true even for the case $D \geq N$ (more sources than sensors).

Rather surprisingly, the same *cannot* be said for the SNR. Thus, when the array manifold matrix $\mathbf{V}_{\mathbb{S}}$ has full row rank, implying $D \geq N$, we show that if the sources have identical powers p , then for a fixed number of snapshots, the CRB **stagnates** to a constant value as p/p_n goes to infinity, where p_n is the noise power (Theorem 6.5.2 in Section 6.5). When $\mathbf{V}_{\mathbb{S}}$ does not have full row rank, we will see that the CRB

decays to zero for large SNR, under suitable assumptions (Theorem 6.5.1 in Section 6.5). Similar behavior for $D \geq N$ and $D < N$ was first noticed by Abramovich et al. in [1] experimentally. Here we elaborate the conditions and find these to be provable consequences of the specific CRB expression we derive.

Another corollary of our results is that if the central ULA segment in the difference coarray has length L , then the rank condition on the ACM matrix is indeed satisfied as long as $D \leq (L - 1)/2$ (Theorem 6.6.1). This is very satisfying because experimentally it has indeed been observed repeatedly that, methods such as spatial-smoothing based coarray MUSIC always succeed in identifying the sources in this case [87], [124], [125], [186].

Yet another outcome of the rank condition is that it is possible to give a precise bound on the number of sources D such that the proposed CRB expression is valid. In particular, for nested arrays, coprime arrays, and MRAs, the FIM is provably invertible for $\mathcal{O}(N^2)$ uncorrelated sources (the exact number depending on the specific array used, the source locations, and so forth), and therefore the CRB expression is provably valid for this many sources. Needless to say, our results (the rank condition and the proposed CRB expression) and the conclusions derived from them are valid for any linear array, sparse or otherwise, including the redoubtable ULA.

Chapter outline. In Section 6.2, we introduce the data model and provide a brief review of sparse arrays (minimum redundancy arrays, minimum hole arrays, nested arrays, coprime arrays, and so on). In Section 6.3, we review some known results on the CRB, which are necessary for building up new results. The new CRB expression and the rank condition for its validity are presented in Section 6.4. The implications of this CRB expression are detailed in Section 6.5 and 6.6. Numerical examples are given in Section 6.7 to demonstrate the implications of the new results. Details of some of the proofs are given in Appendices 6.A to 6.D.

As a remark, it is noted that somewhat related results are also reported by Koochakzadeh and Pal [73] and by Wang and Nehorai [192].

6.2 The Data Model and Sparse Arrays

Recall that the array equation is reviewed in (1.5). In this section, to analyze the DOA estimation performance based on K independent and identically distributed snapshots of (1.5), two probability models are commonly considered:

1. The conditional or deterministic model [166]: The complex amplitude $[A_i]_{i=1}^D$ is assumed to be unknown but non-random. The noise vector \mathbf{n}_S is a complex Gaussian random vector with mean zero and covariance $p_n \mathbf{I}$.

2. The unconditional or stochastic model [167]: $[A_i]_{i=1}^D$ is assumed to be a Gaussian random vector with mean zero and covariance \mathbf{P} such that $[\mathbf{P}]_{i,j} = \mathbb{E}[A_i A_j^*]$. $\mathbf{n}_\mathbb{S}$ is a complex Gaussian random vector with mean zero and covariance $p_n \mathbf{I}$. $\mathbf{n}_\mathbb{S}$ and A_i are uncorrelated.

A more detailed description of these models can be found in [165]–[167].

Next, the details of coarray-based DOA estimators are developed as follows. It is assumed that the sources are uncorrelated and the sensor output $\mathbf{x}_\mathbb{S}$ follows the stochastic model and (1.5), with an additional constraint that the complex amplitude $[A_i]_{i=1}^D$ and the noise term $\mathbf{n}_\mathbb{S}$ have the following distribution:

$$[A_1, A_2, \dots, A_D]^T \sim \mathcal{CN}(\mathbf{0}, \text{diag}(p_1, p_2, \dots, p_D)), \quad (6.2)$$

$$\mathbf{n}_\mathbb{S} \sim \mathcal{CN}(\mathbf{0}, p_n \mathbf{I}), \quad (6.3)$$

where $p_1, p_2, \dots, p_D > 0$ are the source powers and $p_n > 0$ is the noise power. The theory of sparse arrays admits one to convert the covariance matrix $\mathbf{R}_\mathbb{S}$ into the autocorrelation vector $\mathbf{x}_\mathbb{D}$ defined on the difference coarray \mathbb{D} . Furthermore, the concept of the central ULA segment \mathbb{U} , the weight function $w(m)$, and their connections to DOA estimation are reviewed comprehensively in Sections 2.2 and 2.3.

It is known in Sections 2.2 and 2.3 that, in spatial smoothing MUSIC (SS MUSIC) and coarray MUSIC, the size and the structure of the difference coarray are crucial to the number of identifiable sources for nested arrays [124] and coprime arrays [125]. Empirically, the number of identifiable sources can be characterized by the following propositions:

Proposition 6.2.1 ([124], [125]). If the number of distinct sources $D \leq (|\mathbb{U}| - 1)/2$, then SS MUSIC is able to identify these sources for larger number of snapshots.

Proposition 6.2.2 ([120]). If $D > (|\mathbb{D}| - 1)/2$, then it is impossible to identify these sources using SS MUSIC.

Propositions 6.2.1 and 6.2.2 indicate that the size of \mathbb{D} and \mathbb{U} plays a crucial role in the number of identifiable sources. So it is motivating to design the sensor locations \mathbb{S} such that $|\mathbb{D}|$ or $|\mathbb{U}|$ is large. Several well-known solutions include minimum redundancy arrays (MRA) [113], minimum hole arrays (MHA) [177], [190], nested arrays [124], coprime arrays [186], super nested arrays [92]–[94], and many other variants [9], [15], [23], [25], [41], [61], [65], [84], [120], [139], [148], [149], [153], [154], [197]. Furthermore, the details of MRA, MHA, nested array, and coprime arrays can be found in Section 2.2.

6.3 Review of Cramér-Rao Bounds

Consider a real-valued random vector \mathbf{x} with probability density function (pdf) $p(\mathbf{x}; \boldsymbol{\alpha})$, where $\boldsymbol{\alpha}$ is a real-valued deterministic parameter vector. Assume that the pdf $p(\mathbf{x}; \boldsymbol{\alpha})$ satisfies the regularity condition $\mathbb{E}_{\mathbf{x}} [(\partial/\partial\boldsymbol{\alpha}) \log p(\mathbf{x}; \boldsymbol{\alpha})] = \mathbf{0}$, where $\mathbb{E}_{\mathbf{x}}[\cdot]$ indicates that the expectation is over \mathbf{x} . The Fisher information matrix (FIM) $\mathcal{I}(\boldsymbol{\alpha})$ is defined as

$$[\mathcal{I}(\boldsymbol{\alpha})]_{i,j} = -\mathbb{E}_{\mathbf{x}} \left[\frac{\partial^2}{\partial[\boldsymbol{\alpha}]_i \partial[\boldsymbol{\alpha}]_j} \log p(\mathbf{x}; \boldsymbol{\alpha}) \right]. \quad (6.4)$$

It can be shown that the FIM is positive semidefinite [69]. Furthermore, if the FIM is positive definite, then the FIM is invertible and the Cramér-Rao bound (CRB) is given by the inverse of the FIM:

$$\text{CRB}(\boldsymbol{\alpha}) = \mathcal{I}^{-1}(\boldsymbol{\alpha}), \quad (6.5)$$

which is also positive definite. The significance of the CRB is that the covariance of any *unbiased* estimator is lower bounded by the CRB. Namely, any unbiased estimator $\hat{\boldsymbol{\alpha}}(\mathbf{x})$ for $\boldsymbol{\alpha}$, based on the observation \mathbf{x} , satisfies the following:

$$\mathbb{E}_{\mathbf{x}} [\hat{\boldsymbol{\alpha}}(\mathbf{x})\hat{\boldsymbol{\alpha}}(\mathbf{x})^T] \succeq \text{CRB}(\boldsymbol{\alpha}), \quad (6.6)$$

where $\mathbf{A} \succeq \mathbf{B}$ is equivalent to $\mathbf{A} - \mathbf{B}$ being positive semidefinite for two Hermitian matrices \mathbf{A} and \mathbf{B} . More details on the FIM and the CRB can be found in [69], [165], [188].

For the deterministic or conditional CRB model, we use K snapshots of (1.5):

$$\mathbf{x}_{\mathbb{S}}(k) = \sum_{i=1}^D A_i(k) \mathbf{v}_{\mathbb{S}}(\bar{\theta}_i) + \mathbf{n}_{\mathbb{S}}(k), \quad k = 1, 2, \dots, K. \quad (6.7)$$

It is assumed that the noise is both spatially and temporally uncorrelated, i.e.,

$$\mathbb{E}[\mathbf{n}_{\mathbb{S}}(k_1) \mathbf{n}_{\mathbb{S}}^H(k_2)] = p_n \mathbf{I}_{\delta_{k_1, k_2}}, \quad (6.8)$$

while the source amplitudes $A_i(k)$ are deterministic. As a result, the probability model for the deterministic model with K snapshots becomes

$$\begin{bmatrix} \mathbf{x}_{\mathbb{S}}(1) \\ \mathbf{x}_{\mathbb{S}}(2) \\ \vdots \\ \mathbf{x}_{\mathbb{S}}(K) \end{bmatrix} \sim \mathcal{CN} \left(\begin{bmatrix} \sum_{i=1}^D A_i(1) \mathbf{v}_{\mathbb{S}}(\bar{\theta}_i) \\ \sum_{i=1}^D A_i(2) \mathbf{v}_{\mathbb{S}}(\bar{\theta}_i) \\ \vdots \\ \sum_{i=1}^D A_i(K) \mathbf{v}_{\mathbb{S}}(\bar{\theta}_i) \end{bmatrix}, p_n \mathbf{I} \right), \quad (6.9)$$

and the parameters to be estimated contain normalized DOAs, source amplitudes at K snapshots, and the noise power. In particular, the parameter vector $\boldsymbol{\alpha}_{\text{det}}$ for the deterministic model over K snapshots becomes

$$\boldsymbol{\alpha}_{\text{det}} = [\bar{\theta}_i, \text{Re}\{A_i(k)\}, \text{Im}\{A_i(k)\}, p_n]^T, \quad (6.10)$$

where $1 \leq i \leq D, 1 \leq k \leq K$, and the subscript “det” stands for the deterministic model. The total number of real parameters is $D + 2DK + 1$. According to (6.9), the *deterministic CRB* for $\bar{\boldsymbol{\theta}}$ can be expressed as [165], [166]

$$\text{CRB}_{\text{det}}(\bar{\boldsymbol{\theta}}) = \frac{p_n}{2K} \left\{ \text{Re} \left[\left(\mathbf{U}_{\mathbb{S}}^H \boldsymbol{\Pi}_{\mathbf{V}_{\mathbb{S}}}^{\perp} \mathbf{U}_{\mathbb{S}} \right) \odot \widehat{\mathbf{P}}^T \right] \right\}^{-1}, \quad (6.11)$$

where

$$\mathbf{V}_{\mathbb{S}} = \begin{bmatrix} \mathbf{v}_{\mathbb{S}}(\bar{\theta}_1) & \mathbf{v}_{\mathbb{S}}(\bar{\theta}_2) & \dots & \mathbf{v}_{\mathbb{S}}(\bar{\theta}_D) \end{bmatrix}, \quad (6.12)$$

$$\mathbf{U}_{\mathbb{S}} = \begin{bmatrix} \frac{\partial \mathbf{v}_{\mathbb{S}}(\bar{\theta}_1)}{\partial \theta_1} & \frac{\partial \mathbf{v}_{\mathbb{S}}(\bar{\theta}_2)}{\partial \theta_2} & \dots & \frac{\partial \mathbf{v}_{\mathbb{S}}(\bar{\theta}_D)}{\partial \theta_D} \end{bmatrix}, \quad (6.13)$$

$$\widehat{\mathbf{P}} = \frac{1}{K} \sum_{k=1}^K \begin{bmatrix} A_1(k) \\ A_2(k) \\ \vdots \\ A_D(k) \end{bmatrix} \begin{bmatrix} A_1(k) \\ A_2(k) \\ \vdots \\ A_D(k) \end{bmatrix}^H, \quad (6.14)$$

and $\boldsymbol{\Pi}_{\mathbf{A}}^{\perp}$ is as defined in (1.14). Thus $\mathbf{V}_{\mathbb{S}}$ is the array manifold matrix, and $\widehat{\mathbf{P}}$ is the sample covariance of $[A_1, A_2, \dots, A_D]^T$. Note that a nonsingular $\widehat{\mathbf{P}}$ is required for (6.11) being valid, which in turn requires that $K \geq D$.

The *stochastic CRB* model [167] also uses K snapshots as in (6.7). It is assumed that the noise is spatially and temporally uncorrelated, and, in addition, the source amplitudes are stochastic with mean zero and

$$\mathbb{E} \left[\begin{bmatrix} A_1(k_1) \\ A_2(k_1) \\ \vdots \\ A_D(k_1) \end{bmatrix} \begin{bmatrix} A_1(k_2) \\ A_2(k_2) \\ \vdots \\ A_D(k_2) \end{bmatrix}^H \right] = \mathbf{P} \delta_{k_1, k_2}, \quad (6.15)$$

where $[\mathbf{P}]_{i,j} = \mathbb{E}[A_i A_j^*]$. Thus the probability model for stochastic CRB for K snapshots is given by

$$\begin{bmatrix} \mathbf{x}_{\mathbb{S}}(1) \\ \mathbf{x}_{\mathbb{S}}(2) \\ \vdots \\ \mathbf{x}_{\mathbb{S}}(K) \end{bmatrix} \sim \mathcal{CN} \left(\mathbf{0}, \begin{bmatrix} \boldsymbol{\Sigma} & \mathbf{O} & \dots & \mathbf{O} \\ \mathbf{O} & \boldsymbol{\Sigma} & \dots & \mathbf{O} \\ \vdots & \vdots & \ddots & \vdots \\ \mathbf{O} & \mathbf{O} & \dots & \boldsymbol{\Sigma} \end{bmatrix} \right), \quad (6.16)$$

where

$$\boldsymbol{\Sigma} = \mathbf{V}_{\mathbb{S}} \mathbf{P} \mathbf{V}_{\mathbb{S}}^H + p_n \mathbf{I}. \quad (6.17)$$

In this scenario, the parameter vector $\boldsymbol{\alpha}_{\text{sto}}$ is

$$\boldsymbol{\alpha}_{\text{sto}} = [\bar{\theta}_i, [\mathbf{P}]_{i,i}, \text{Re}\{[\mathbf{P}]_{i,j}\}, \text{Im}\{[\mathbf{P}]_{i,j}\}, p_n]^T, \quad (6.18)$$

where $1 \leq i \leq D$ and $i > j$. The number of real scalar parameters becomes $D + D^2 + 1$. This does not depend on K (snapshots) unlike in the deterministic model. Using (6.16) and (6.18) yields the stochastic CRB expression for $\bar{\boldsymbol{\theta}}$:

$$\text{CRB}_{\text{sto}}(\bar{\boldsymbol{\theta}}) = \frac{p_n}{2K} \left\{ \text{Re} \left[\left(\mathbf{U}_{\mathbb{S}}^H \boldsymbol{\Pi}_{\mathbf{V}_{\mathbb{S}}}^{\perp} \mathbf{U}_{\mathbb{S}} \right) \odot \left(\mathbf{P} \mathbf{V}_{\mathbb{S}}^H \boldsymbol{\Sigma}^{-1} \mathbf{V}_{\mathbb{S}} \mathbf{P} \right)^T \right] \right\}^{-1}, \quad (6.19)$$

where $\mathbf{V}_{\mathbb{S}}$, $\mathbf{U}_{\mathbb{S}}$, \mathbf{P} , $\boldsymbol{\Sigma}$ are defined in (6.12), (6.13), (6.15), and (6.17), respectively. Note that the CRB expression (6.19) does not assume any prior information on the source covariance matrix \mathbf{P} , except that \mathbf{P} is nonsingular for the inverse in (6.19) to exist.

In DOA estimation literature, it is often assumed that the sources are uncorrelated [13], [135], [150]. In such cases, a subtle distinction should be made depending upon whether we *know* apriori the fact that the sources are uncorrelated:

1. If the sources are uncorrelated but this information is **not known a priori**, then the CRB can be evaluated from the expression (6.19) with a diagonal \mathbf{P} .
2. Otherwise, if the sources are **known a priori to be uncorrelated**, then the off-diagonal entries of \mathbf{P} are known to be zero. This prior information modifies the parameter vector $\boldsymbol{\alpha}$, the FIM $\mathcal{I}(\boldsymbol{\alpha})$, and the CRB expression. Hence, the CRB expression (6.19) cannot be applied. The closed-form CRB expression for this scenario was proposed in [66], which will be reviewed next.

The probability model for the stochastic model with uncorrelated sources and K snapshots (6.7) is given by

$$\begin{bmatrix} \mathbf{x}_{\mathbb{S}}(1) \\ \mathbf{x}_{\mathbb{S}}(2) \\ \vdots \\ \mathbf{x}_{\mathbb{S}}(K) \end{bmatrix} \sim \mathcal{CN} \left(\mathbf{0}, \begin{bmatrix} \mathbf{R}_{\mathbb{S}} & \mathbf{O} & \dots & \mathbf{O} \\ \mathbf{O} & \mathbf{R}_{\mathbb{S}} & \dots & \mathbf{O} \\ \vdots & \vdots & \ddots & \vdots \\ \mathbf{O} & \mathbf{O} & \dots & \mathbf{R}_{\mathbb{S}} \end{bmatrix} \right), \quad (6.20)$$

where $\mathbf{R}_{\mathbb{S}}$ is defined in (2.10). The parameters to be estimated are composed of normalized DOAs $\bar{\theta}_i$, source powers p_i , and noise power p_n , so that the parameter vector $\boldsymbol{\alpha}_{\text{uncor}}$ becomes

$$\boldsymbol{\alpha}_{\text{uncor}} = [\bar{\theta}_i, p_i, p_n]^T, \quad (6.21)$$

where $1 \leq i \leq D$. It can be seen that the number of real parameters is only $2D + 1$ in this case. According to [66], the CRB for $\bar{\boldsymbol{\theta}}$ can be expressed as

$$\text{CRB}_{\text{uncor}}(\bar{\boldsymbol{\theta}}) = \frac{1}{K} \left(\mathbf{P} \mathbf{D}^H \mathbf{G} \left(\mathbf{G}^H \tilde{\mathbf{C}} \mathbf{G} \right)^{-1} \mathbf{G}^H \mathbf{D} \mathbf{P} \right)^{-1}, \quad (6.22)$$

Table 6.1: Summary of several related CRB expressions for DOA estimation¹

| | Deterministic or Conditional [166] | Stochastic or Unconditional [167] | [66] and the CRB expression proposed in this chapter |
|---|--|---|---|
| Number of sources, D | Known ($D < \mathbb{S} $) | Known ($D < \mathbb{S} $) | Known ($D < \mathbb{S} $ in [66]) ($D < \mathbb{S} $ or $D \geq \mathbb{S} $ in the proposed CRB expression) |
| Normalized DOAs, $\{\bar{\theta}_i\}_{i=1}^D$ | Unknown, non-random | Unknown, non-random | Unknown, non-random |
| Complex amplitude $\{A_i\}_{i=1}^D$ | Unknown, non-random | Unknown, random, correlated, $[A_i]_{i=1}^D \sim \mathcal{CN}(\mathbf{0}, \mathbf{P})$ | Unknown, random, uncorrelated, $[A_i]_{i=1}^D \sim \mathcal{CN}(\mathbf{0}, \text{diag}(p_1, \dots, p_D))$ |
| Noise vector $\mathbf{n}_\mathbb{S}$ | Unknown, random, $\mathbf{n}_\mathbb{S} \sim \mathcal{CN}(\mathbf{0}, p_n \mathbf{I})$ | Unknown, random, $\mathbf{n}_\mathbb{S} \sim \mathcal{CN}(\mathbf{0}, p_n \mathbf{I})$ | Unknown, random, $\mathbf{n}_\mathbb{S} \sim \mathcal{CN}(\mathbf{0}, p_n \mathbf{I})$ |
| Distribution of $\mathbf{x}_\mathbb{S}$ | $\mathcal{CN}(\sum_{i=1}^D A_i \mathbf{v}_\mathbb{S}(\bar{\theta}_i), p_n \mathbf{I})$ | $\mathcal{CN}(\mathbf{0}, \mathbf{V}_\mathbb{S} \mathbf{P} \mathbf{V}_\mathbb{S}^H + p_n \mathbf{I})$ | $\mathcal{CN}(\mathbf{0}, \mathbf{R}_\mathbb{S})$ |
| Distribution of K snapshots | (6.9) | (6.16) | (6.20) |
| Unknown parameters | (6.10) | (6.18) | (6.21) |
| Number of unknown parameters | $D + 2DK + 1$ | $D + D^2 + 1$ | $2D + 1$ |
| CRB($\bar{\boldsymbol{\theta}}$) | (6.11) | (6.19) | (6.22), or the new expression proposed in Theorem 6.4.2 |

¹ $\bar{\boldsymbol{\theta}} = [\bar{\theta}_1, \dots, \bar{\theta}_D]^T$, $[\mathbf{P}]_{i,j} = E[A_i A_j^*]$, $\mathbf{V}_\mathbb{S} = [\mathbf{v}_\mathbb{S}(\bar{\theta}_1), \dots, \mathbf{v}_\mathbb{S}(\bar{\theta}_D)]$, $\mathbf{R}_\mathbb{S} = \sum_{i=1}^D p_i \mathbf{v}_\mathbb{S}(\bar{\theta}_i) \mathbf{v}_\mathbb{S}^H(\bar{\theta}_i) + p_n \mathbf{I}$.

where

$$\tilde{\mathbf{C}} = (\mathbf{R}_\mathbb{S}^T \otimes \mathbf{R}_\mathbb{S}) + \frac{p_n^2}{|\mathbb{S}| - D} \text{vec}(\mathbf{\Pi}_{\mathbf{V}_\mathbb{S}}) \text{vec}^H(\mathbf{\Pi}_{\mathbf{V}_\mathbb{S}}), \quad (6.23)$$

$$\mathbf{D} = (\mathbf{U}_\mathbb{S}^* \circ \mathbf{V}_\mathbb{S}) + (\mathbf{V}_\mathbb{S}^* \circ \mathbf{U}_\mathbb{S}), \quad (6.24)$$

\mathbf{G} is any matrix whose columns span the null space of $(\mathbf{V}_\mathbb{S}^* \circ \mathbf{V}_\mathbb{S})^H$, and the source covariance matrix is denoted by $\mathbf{P} = \text{diag}(p_1, p_2, \dots, p_D)$. $\mathbf{V}_\mathbb{S}$ and $\mathbf{U}_\mathbb{S}$ are given in (6.12) and (6.13), respectively. Eq. (6.22) will be called Jansson et al.'s CRB expression in this chapter. However, if $D = |\mathbb{S}|$, then the denominator in (6.23) becomes zero, which makes (6.23) and Jansson et al.'s CRB expression (6.22) invalid. Furthermore, if $D > |\mathbb{S}|$, then $\mathbf{\Pi}_{\mathbf{V}_\mathbb{S}}$ is not well-defined.

Table 6.1 summarizes some CRB expressions along with their model assumptions, as in [166], [167], and [66]. The deterministic CRB expression [166] and the stochastic CRB expression [167] assume less sources than the number of sensors, namely $D < |\mathbb{S}|$, while Jansson et al.'s CRB expression [66] implicitly assumes $D < |\mathbb{S}|$ so

that the expression for $\mathbf{\Pi}_{\mathbf{V}_S}$ is valid. For the complex amplitude A_i , the deterministic CRB expression [166] assumes unknown, non-random A_i , the stochastic CRB expression [167] supposes unknown, random A_i with mean zero and covariance \mathbf{P} , while Jansson et al.'s CRB expression presumes unknown, random A_i with mean zero and a diagonal covariance matrix.

The CRB for DOA estimation with sparse arrays is gaining importance due to recent developments in coarray-based DOA estimators and sparse array design. An early work by Abramovich et al. [1] demonstrated numerically that the CRB exhibits two different behaviors in the regimes $D < |\mathcal{S}|$ and $D \geq |\mathcal{S}|$. For $D < |\mathcal{S}|$, the CRB at high SNR decays to zero. For $D \geq |\mathcal{S}|$, the CRB at high SNR tends to saturate to a non-zero value as SNR increases. Among other results, we will prove both of these in this chapter (Theorems 6.5.1 and 6.5.2).

The connection between the CRB and the array geometry has been studied in previous literature. The CRB for single source with azimuth, elevation, and planar arrays was investigated in [30]. It was observed that the CRB for DOAs is inversely proportional to the array variance, under suitable assumptions. The CRB for two sources with one-dimensional DOA profiles was considered in [184], [185], based on the deterministic CRB expression, (6.11). It was noted empirically that larger array aperture helps to reduce the CRB and the array geometry influences the maximum number of identifiable sources.

Another interesting work by Koochakzadeh and Pal formulates the DOA estimation using a predefined DOA grid and sensor perturbation [75], [76]. The DOA grid is denoted by $\vartheta_1, \vartheta_2, \dots, \vartheta_{N_\vartheta}$ while the perturbation is characterized by $\boldsymbol{\delta} \in \mathbb{R}^{|\mathcal{S}|}$. In particular, the measurement $\mathbf{y}(k)$ originates from the following data model:

$$\mathbf{y}(k) = \mathbf{A}_{\text{grid}}\mathbf{x}(k) + \mathbf{w}(k) \in \mathbb{C}^{|\mathcal{S}|}, \quad k = 1, 2, \dots, K,$$

where $\mathbf{x}(k) \in \mathbb{C}^{N_\vartheta}$ is the source amplitude on the grid with source powers $\gamma_i = E[|\mathbf{x}(k)|_i|^2]$. $\mathbf{w}(k)$ is the noise term. $\mathbf{A}_{\text{grid}} \in \mathbb{C}^{|\mathcal{S}| \times N_\vartheta}$ is given by $[\mathbf{v}_S(\bar{\vartheta}_1), \mathbf{v}_S(\bar{\vartheta}_2), \dots, \mathbf{v}_S(\bar{\vartheta}_{N_\vartheta})]$. In this setting, the parameters to be estimated are the source powers γ_i and the sensor location perturbation $\boldsymbol{\delta}$. The FIM and the CRB for γ_i were also analyzed in detail.

6.4 New Expressions for CRB, Applicable for Sparse Arrays with More Sources than Sensors

Remarks on the CRB expressions [66], [166], [167]

We now argue that, among the three CRB expressions: the deterministic CRB expression [166], the stochastic CRB expression [167], and Jansson et al.'s CRB expression [66], in Section 6.3, only Jansson et al.'s CRB expression is appropriate when coarray-based methods are applicable for DOA estimation.

The deterministic CRB expression [166] is not suitable for coarray-based DOA estimators since the assumptions do not match. It is assumed in the deterministic model that the complex amplitude A_i is deterministic, as summarized in Table 6.1. Coarray-based DOA estimators operate under the condition that sources are stochastic, as mentioned in (6.2).

The stochastic CRB expression in [167] is incompatible with coarray-based DOA estimators due to the following:

1. The stochastic CRB expression in [167] is valid if $D < |\mathbb{S}|$. Hence, it is inappropriate to consider the stochastic CRB expression for the regime $D \geq |\mathbb{S}|$ where coarray based DOA estimators are usually of interest.
2. The assumptions are different. The stochastic CRB expression in [167] considers the stochastic model with source covariance \mathbf{P} . But it is not known a priori that the sources are uncorrelated. On the other hand, for coarray-based DOA estimators, it is **known a priori** that sources are uncorrelated, as stated in (6.2).

Finally, Jansson et al.'s CRB expression [66] is applicable to coarray-based DOA estimators. It is because the uncorrelated information is assumed to be known a priori, which matches the assumptions of coarray-based DOA estimators.

To demonstrate how much the uncorrelated prior helps to reduce the CRB, consider a sensor array with $\mathbb{S} = \{0, 1, 4, 6\}$. Assume there are two equal-power, uncorrelated sources with normalized DOAs $\bar{\boldsymbol{\theta}} = [-0.25, 0.25]^T$. The number of snapshots K is 500 and the SNR is 0 dB. Substituting these parameters into (6.19) and (6.22) yields

The stochastic CRB expression [167] :

$$[\text{CRB}(\bar{\boldsymbol{\theta}})]_{1,1} = [\text{CRB}(\bar{\boldsymbol{\theta}})]_{2,2} = 1.809 \times 10^{-6}, \quad (6.25)$$

Jansson et al.'s CRB expression [66]:

$$[\text{CRB}(\bar{\boldsymbol{\theta}})]_{1,1} = [\text{CRB}(\bar{\boldsymbol{\theta}})]_{2,2} = 1.696 \times 10^{-6}. \quad (6.26)$$

Thus, Jansson et al.'s CRB (with uncorrelated prior) is less than the stochastic CRB (without uncorrelated prior).

However, Jansson et al.'s CRB expression has some limitations. First of all, the precise conditions that Jansson et al.'s CRB expression is valid are not explicitly stated in [66]. From Jansson et al.'s CRB expression, it is not so easy to study the behavior of the CRB with respect to the number of snapshots K , the number of sources D , and the SNR. Furthermore, [66] considers only the ULA and it is not clear from [66] how sparse arrays, like MRA, nested arrays, and coprime arrays, influence the CRB.

Finally, for $D = |\mathbb{S}|$, Jansson et al.'s CRB expression becomes undefined, due to the appearance of $|\mathbb{S}| - D$ in the denominator of (6.23).

In Section 6.4, we will propose a CRB expression that addresses all these issues raised in the previous paragraph. First, it will be shown that a rank condition on the augmented coarray manifold (ACM) matrix is necessary and sufficient for the nonsingular FIM, which leads to a closed-form CRB expression.

The proposed Cramér-Rao bound expression

Consider a random vector \mathbf{x} with a complex normal distribution with mean zero and covariance $\Sigma(\boldsymbol{\alpha})$, where $\boldsymbol{\alpha}$ is a real-valued parameter vector. The (p, ℓ) th entry of the FIM $\mathcal{I}(\boldsymbol{\alpha})$ is given by [164], [165], [167]

$$[\mathcal{I}(\boldsymbol{\alpha})]_{p,\ell} = \text{tr} \left(\Sigma^{-1}(\boldsymbol{\alpha}) \frac{\partial \Sigma(\boldsymbol{\alpha})}{\partial [\boldsymbol{\alpha}]_p} \Sigma^{-1}(\boldsymbol{\alpha}) \frac{\partial \Sigma(\boldsymbol{\alpha})}{\partial [\boldsymbol{\alpha}]_\ell} \right). \quad (6.27)$$

Setting the probability model to be (6.20) and the parameter vector to be (6.21) results in

$$\begin{aligned} [\mathcal{I}(\boldsymbol{\alpha})]_{p,\ell} &= K \text{tr} \left(\mathbf{R}_{\mathbb{S}}^{-1} \frac{\partial \mathbf{R}_{\mathbb{S}}}{\partial [\boldsymbol{\alpha}]_p} \mathbf{R}_{\mathbb{S}}^{-1} \frac{\partial \mathbf{R}_{\mathbb{S}}}{\partial [\boldsymbol{\alpha}]_\ell} \right) \\ &= K \left[\text{vec} \left(\frac{\partial \mathbf{R}_{\mathbb{S}}}{\partial [\boldsymbol{\alpha}]_p} \right) \right]^H \left(\mathbf{R}_{\mathbb{S}}^{-T} \otimes \mathbf{R}_{\mathbb{S}}^{-1} \right) \text{vec} \left(\frac{\partial \mathbf{R}_{\mathbb{S}}}{\partial [\boldsymbol{\alpha}]_\ell} \right) \\ &= K \left[\left(\mathbf{R}_{\mathbb{S}}^T \otimes \mathbf{R}_{\mathbb{S}} \right)^{-\frac{1}{2}} \frac{\partial \mathbf{r}_{\mathbb{S}}}{\partial [\boldsymbol{\alpha}]_p} \right]^H \left[\left(\mathbf{R}_{\mathbb{S}}^T \otimes \mathbf{R}_{\mathbb{S}} \right)^{-\frac{1}{2}} \frac{\partial \mathbf{r}_{\mathbb{S}}}{\partial [\boldsymbol{\alpha}]_\ell} \right], \end{aligned} \quad (6.28)$$

since $\text{tr}(\mathbf{ABCD}) = \text{vec}(\mathbf{B}^H)^H (\mathbf{A}^T \otimes \mathbf{C}) \text{vec}(\mathbf{D})$, and $(\mathbf{A} \otimes \mathbf{B})^{-1} = \mathbf{A}^{-1} \otimes \mathbf{B}^{-1}$ for nonsingular \mathbf{A} and \mathbf{B} [106]. The vector $\mathbf{r}_{\mathbb{S}}$ is defined as

$$\mathbf{r}_{\mathbb{S}} = \text{vec}(\mathbf{R}_{\mathbb{S}}). \quad (6.29)$$

Eq. (6.28) leads to an expression for the FIM $\mathcal{I}(\boldsymbol{\alpha})$ as follows:

$$\mathcal{I}(\boldsymbol{\alpha}) = K \begin{bmatrix} \mathbf{G}^H \\ \Delta^H \end{bmatrix} \begin{bmatrix} \mathbf{G} & \Delta \end{bmatrix} \quad (6.30)$$

$$= \begin{matrix} & \xleftarrow{D} & & \xleftarrow{D+1} \\ & & & \\ \begin{matrix} D \uparrow \\ D+1 \downarrow \end{matrix} & & \begin{bmatrix} K\mathbf{G}^H\mathbf{G} & K\mathbf{G}^H\Delta \\ K\Delta^H\mathbf{G} & K\Delta^H\Delta \end{bmatrix} & \end{matrix}, \quad (6.31)$$

where

$$\mathbf{G} = (\mathbf{R}_S^T \otimes \mathbf{R}_S)^{-\frac{1}{2}} \begin{bmatrix} \frac{\partial \mathbf{r}_S}{\partial \theta_1} & \cdots & \frac{\partial \mathbf{r}_S}{\partial \theta_D} \end{bmatrix} = \underset{|\mathcal{S}|^2}{\overset{D}{\left[\begin{array}{c} \boxed{} \\ \end{array} \right]}}, \quad (6.32)$$

$$\Delta = (\mathbf{R}_S^T \otimes \mathbf{R}_S)^{-\frac{1}{2}} \begin{bmatrix} \frac{\partial \mathbf{r}_S}{\partial p_1} & \cdots & \frac{\partial \mathbf{r}_S}{\partial p_D} & \frac{\partial \mathbf{r}_S}{\partial p_n} \end{bmatrix} = \underset{|\mathcal{S}|^2}{\overset{D+1}{\left[\begin{array}{c} \boxed{} \\ \end{array} \right]}}. \quad (6.33)$$

It follows from (6.30) that the FIM is positive semidefinite. And $\Delta^H \Delta$ is obviously positive semidefinite. If the FIM $\mathcal{I}(\alpha)$ is nonsingular, then the CRB for the normalized DOAs $\bar{\theta} = [\bar{\theta}_1, \dots, \bar{\theta}_D]^T$ can be expressed as the inverse of the Schur complement of the block $\Delta^H \Delta$ of the FIM $\mathcal{I}(\alpha)$ [164]

$$\text{CRB}(\bar{\theta}) = \frac{1}{K} \left(\mathbf{G}^H \mathbf{\Pi}_\Delta^\perp \mathbf{G} \right)^{-1}, \quad (6.34)$$

where $\mathbf{\Pi}_\Delta^\perp = \mathbf{I} - \Delta(\Delta^H \Delta)^{-1} \Delta^H$ is defined as in (1.14).

An important observation here is that nonsingularity of the FIM is equivalent to nonsingularity of $\Delta^H \Delta$ and $\mathbf{G}^H \mathbf{\Pi}_\Delta^\perp \mathbf{G}$:

Lemma 6.4.1. Let \mathbf{F} be a positive semidefinite matrix of the form

$$\mathbf{F} = \begin{bmatrix} \mathbf{A} & \mathbf{B} \\ \mathbf{B}^H & \mathbf{D} \end{bmatrix} \succeq \mathbf{0},$$

where \mathbf{A} and \mathbf{D} are Hermitian matrices. Then \mathbf{F} is nonsingular (invertible) if and only if \mathbf{D} and the Schur complement of \mathbf{D} , namely, $\mathbf{A} - \mathbf{B}\mathbf{D}^{-1}\mathbf{B}^H$, are both nonsingular.

Proof. The proof can be found in 6.A. □

Lemma 6.4.1 can be applied to (6.31). Let \mathbf{F} be the FIM $\mathcal{I}(\alpha)$, which is positive semidefinite. The submatrices $\mathbf{A} = K\mathbf{G}^H \mathbf{G}$, $\mathbf{B} = K\mathbf{G}^H \Delta$, and $\mathbf{D} = K\Delta^H \Delta$ so that the Schur complement of \mathbf{D} becomes $\mathbf{A} - \mathbf{B}\mathbf{D}^{-1}\mathbf{B}^H = K\mathbf{G}^H \mathbf{\Pi}_\Delta^\perp \mathbf{G}$. Lemma 6.4.1 indicates that the FIM $\mathcal{I}(\alpha)$ is nonsingular if and only if $\Delta^H \Delta$ and $\mathbf{G}^H \mathbf{\Pi}_\Delta^\perp \mathbf{G}$ are both nonsingular.

It is of great interest to simplify the condition that $\Delta^H \Delta$ and $\mathbf{G}^H \mathbf{\Pi}_\Delta^\perp \mathbf{G}$ are both nonsingular. The following lemmas characterize the necessary and sufficient conditions that $\Delta^H \Delta$ and $\mathbf{G}^H \mathbf{\Pi}_\Delta^\perp \mathbf{G}$ are positive definite, hence nonsingular. For the following lemma, the reader should recall the triangular bracket notation from Section 1.4.

Lemma 6.4.2. Let $\mathbf{V}_{\mathbb{D}}$ be the array manifold matrix defined on the difference coarray and $\mathbf{W}_{\mathbb{D}} = [\mathbf{V}_{\mathbb{D}}, \mathbf{e}_0]$, where \mathbf{e}_0 is a column vector satisfying $\langle \mathbf{e}_0 \rangle_m = \delta_{m,0}$ for $m \in \mathbb{D}$. The triangular brackets $\langle \cdot \rangle$ are defined in Section 1.4. Therefore, $\mathbf{V}_{\mathbb{D}}$ is a $|\mathbb{D}| \times D$ matrix while $\mathbf{W}_{\mathbb{D}}$ has size $|\mathbb{D}| \times (D + 1)$. Then $\mathbf{\Delta}^H \mathbf{\Delta}$ is positive definite if and only if

$$\text{rank}(\mathbf{W}_{\mathbb{D}}) = D + 1, \quad (6.35)$$

i.e., if and only if $\mathbf{W}_{\mathbb{D}}$ has full column rank.

Proof. The proof can be found in 6.A. □

Definition 6.4.1 (ACM matrix). The augmented coarray manifold (ACM) matrix is defined as

$$\mathbf{A}_c = \begin{bmatrix} \text{diag}(\mathbb{D})\mathbf{V}_{\mathbb{D}} & \mathbf{W}_{\mathbb{D}} \end{bmatrix} \quad (6.36)$$

$$= \begin{array}{c} \xleftrightarrow{D} \quad \xleftrightarrow{D} \quad \xleftrightarrow{1} \\ |\mathbb{D}| \updownarrow \left[\begin{array}{ccc} \text{diag}(\mathbb{D})\mathbf{V}_{\mathbb{D}} & \mathbf{V}_{\mathbb{D}} & \mathbf{e}_0 \end{array} \right] \end{array}, \quad (6.37)$$

where $\text{diag}(\mathbb{D})$ is a diagonal matrix with \mathbb{D} on its diagonals, $\mathbf{V}_{\mathbb{D}}$ is the array manifold matrix defined on \mathbb{D} , and $\mathbf{W}_{\mathbb{D}} = [\mathbf{V}_{\mathbb{D}}, \mathbf{e}_0]$, where \mathbf{e}_0 is a column vector satisfying $\langle \mathbf{e}_0 \rangle_m = \delta_{m,0}$ for $m \in \mathbb{D}$. The triangular brackets $\langle \cdot \rangle$ are defined in Section 1.4.

Lemma 6.4.3. Assume that $\text{rank}(\mathbf{W}_{\mathbb{D}}) = D + 1$ and let \mathbf{A}_c be the augmented coarray manifold (ACM) matrix. Then $\mathbf{G}^H \mathbf{\Pi}_{\mathbf{\Delta}}^{\perp} \mathbf{G}$ is positive definite if and only if

$$\text{rank}(\mathbf{A}_c) = 2D + 1, \quad (6.38)$$

i.e., if and only if the ACM matrix \mathbf{A}_c has full column rank.

Proof. The proof can be found in 6.A. □

The significance of Lemma 6.4.2 and Lemma 6.4.3 is that the invertibility of $\mathbf{\Delta}^H \mathbf{\Delta}$ and $\mathbf{G}^H \mathbf{\Pi}_{\mathbf{\Delta}}^{\perp} \mathbf{G}$ can be simply characterized by (6.35) and (6.38). Furthermore, these conditions lead to a necessary and sufficient condition for nonsingular FIMs, as summarized next:

Theorem 6.4.1. Let \mathbf{A}_c be the ACM matrix, as defined in Definition 6.4.1. Then the FIM $\mathcal{I}(\alpha)$, given in (6.27), is nonsingular if and only if \mathbf{A}_c has full column rank, i.e., if and only if

$$\text{rank}(\mathbf{A}_c) = 2D + 1. \quad (6.39)$$

Proof. It follows directly from Lemma 6.4.1, 6.4.2, and 6.4.3. \square

The next result is that, if the FIM is nonsingular, then the CRB exists and the closed-form CRB expression is given by the following theorem. The quantity \mathbf{J} in this theorem is defined in Definition 6.B.1 in 6.B.

Theorem 6.4.2. Let \mathbf{A}_c be the ACM matrix, as defined in Definition 6.4.1. If $\text{rank}(\mathbf{A}_c) = 2D + 1$, then the CRB for normalized DOAs $\bar{\boldsymbol{\theta}} = [\bar{\theta}_1, \dots, \bar{\theta}_D]^T$ can be expressed as

$$\text{CRB}(\bar{\boldsymbol{\theta}}) = \frac{1}{4\pi^2 K} \left(\mathbf{G}_0^H \boldsymbol{\Pi}_{\mathbf{M}\mathbf{W}_{\mathbb{D}}}^{\perp} \mathbf{G}_0 \right)^{-1}, \quad (6.40)$$

where

$$\mathbf{G}_0 = \mathbf{M}(\text{diag}(\mathbb{D})) \times \mathbf{V}_{\mathbb{D}} \times (\text{diag}(p_1, p_2, \dots, p_D)), \quad (6.41)$$

$$\mathbf{M} = \left(\mathbf{J}^H (\mathbf{R}_{\mathbb{S}}^T \otimes \mathbf{R}_{\mathbb{S}})^{-1} \mathbf{J} \right)^{\frac{1}{2}}, \quad (6.42)$$

$$\mathbf{R}_{\mathbb{S}} = \sum_{i=1}^D p_i \mathbf{v}_{\mathbb{S}}(\bar{\theta}_i) \mathbf{v}_{\mathbb{S}}^H(\bar{\theta}_i) + p_n \mathbf{I}, \quad (6.43)$$

$$\mathbf{V}_{\mathbb{D}} = \begin{bmatrix} \mathbf{v}_{\mathbb{D}}(\bar{\theta}_1) & \mathbf{v}_{\mathbb{D}}(\bar{\theta}_2) & \dots & \mathbf{v}_{\mathbb{D}}(\bar{\theta}_D) \end{bmatrix}, \quad (6.44)$$

$$\mathbf{W}_{\mathbb{D}} = \begin{bmatrix} \mathbf{V}_{\mathbb{D}} & \mathbf{e}_0 \end{bmatrix}. \quad (6.45)$$

Here K is the number of snapshots, D is the number of sources, p_i is the i th source power, and p_n is the noise power.

Recall that, \mathbb{D} is the difference coarray, as defined in Definition 2.2.1, and \mathbf{J} is given in Definition 6.B.1 of 6.B. $\mathbf{V}_{\mathbb{D}}$ is the array manifold matrix on \mathbb{D} . \mathbf{e}_0 is defined in Lemma 6.4.2. The matrix $\boldsymbol{\Pi}_{\mathbf{A}}^{\perp} = \mathbf{I} - \mathbf{A}(\mathbf{A}^H \mathbf{A})^{-1} \mathbf{A}^H$ is defined in (1.14).

Proof. The proof of this Theorem follows from 6.A, 6.A, (6.76), and (6.34). \square

Comparison between [1], [66] and the proposed CRB expression

In this subsection, we will include more detailed discussions on the CRB expressions [1], [66] and the proposed CRB expression (Theorem 6.4.2). These expressions are equivalent under appropriate assumptions.

Abramovich et al. [1] plotted the CRB curves numerically based on the FIM of the complex normal distribution (6.27) (or (11) in [1]). It is also known a priori that sources are uncorrelated and there is no assumption on the number of sources. As a result, their CRB plots should be identical to those from Theorem 6.4.2, for any choice of parameters. However, Abramovich et al.'s CRB expressions make it difficult to explain the number of resolvable sources, the behavior of the CRB for large SNR, and the conditions under which the FIM is nonsingular.

Jansson et al.'s CRB expressions [66] were derived from (6.34) (or (38) in [66]). Then, to simplify (6.34) into (6.22), the projection matrix $\mathbf{\Pi}_{\mathbf{V}_S} = \mathbf{V}_S(\mathbf{V}_S^H \mathbf{V}_S)^{-1} \mathbf{V}_S^H$ was introduced. Note that, if $D > |\mathbb{S}|$, then $\mathbf{V}_S^H \mathbf{V}_S$ is singular, so $\mathbf{\Pi}_{\mathbf{V}_S}$ and (6.22) are undefined. However, for certain parameters, if (6.22) is well-defined, then it should agree with (6.40) in Theorem 6.4.2, since they are both derived from (6.34).

The proposed CRB expressions overcome the limitations of [1], [66], as we shall see in Section 6.5 and 6.6. Later on, all these CRB expressions will be compared through numerical examples in Section 6.7 and Fig. 6.6.

6.5 Conclusions which Follow from Theorem 6.4.2

Theorem 6.4.2 enables us to study various parameters that affect the CRB, such as the array configuration, the normalized DOAs, the number of snapshots, and the SNR, as explained next.

Proposition 6.5.1. The rank condition, (6.39), depends only on four factors: the difference coarray \mathbb{D} , the normalized DOAs $\bar{\theta}$, the number of sources D , and \mathbf{e}_0 . The following parameters are irrelevant to (6.39): The source powers p_1, \dots, p_D , the noise power p_n , and the number of snapshots K .

Proposition 6.5.2. The CRB for $\bar{\theta}$ is a function of the physical array \mathbb{S} , the normalized DOA $\bar{\theta}$, the number of sources D , the number of snapshots K , and the SNR of sources $p_1/p_n, \dots, p_D/p_n$.

The fact that the CRB depends on the SNRs and not on individual powers can be proved as follows: If we replace p_i and p_n with Cp_i and Cp_n , then \mathbf{R}_S , \mathbf{M} , and \mathbf{G}_0 change to

$$\begin{aligned} \mathbf{R}'_S &= \sum_{i=1}^D Cp_i \mathbf{v}_S(\bar{\theta}_i) \mathbf{v}_S^H(\bar{\theta}_i) + Cp_n \mathbf{I} = C\mathbf{R}_S, \\ \mathbf{M}' &= (\mathbf{J}^H ((C\mathbf{R}_S)^T \otimes (C\mathbf{R}_S))^{-1} \mathbf{J})^{\frac{1}{2}} = C^{-1} \mathbf{M}, \\ \mathbf{G}'_0 &= \mathbf{M}' (\text{diag}(\mathbb{D})) \mathbf{V}_{\mathbb{D}} (\text{diag}(Cp_1, Cp_2, \dots, Cp_D)) = \mathbf{G}_0. \end{aligned}$$

Therefore, $\mathbf{G}'_0{}^H \mathbf{\Pi}_{\mathbf{M}' \mathbf{W}_{\mathbb{D}}}^{\perp} \mathbf{G}'_0 = \mathbf{G}_0{}^H \mathbf{\Pi}_{\mathbf{M} \mathbf{W}_{\mathbb{D}}}^{\perp} \mathbf{G}_0$, implying that the CRB is unchanged if all the ratios p_i/p_n are unchanged.

Proposition 6.5.1 characterizes the parameters that affect the singularity of the FIM, due to Theorem 6.4.1. If two distinct array configurations \mathbb{S}_1 and \mathbb{S}_2 have the same difference coarray \mathbb{D} , then for the same DOAs, the ACM matrices are exactly identical.

Example 1. For instance, consider the nested array with $N_1 = N_2 = 5$ and the second-order super nested array with $N_1 = N_2 = 5$. The sensor locations are given

by [92], [124]:

$$\mathbb{S}_{\text{nested}} = \{1, 2, 3, 4, 5, 6, 12, 18, 24, 30\}, \quad (6.46)$$

$$\mathbb{S}_{\text{super nested}} = \{1, 3, 5, 8, 10, 12, 18, 24, 29, 30\}. \quad (6.47)$$

It was proved in [92] that their difference coarray are identical, i.e., $\mathbb{D}_{\text{nested}} = \mathbb{D}_{\text{super nested}} = \{-29, \dots, 29\}$. Hence,

$$(\mathbf{A}_c)_{\text{nested}} = (\mathbf{A}_c)_{\text{super nested}}.$$

The above equation indicates that for some normalized DOAs $\bar{\boldsymbol{\theta}}^*$, if the nested array (6.46) leads to a singular FIM, then the super nested array (6.47) also results in a singular FIM for the same $\bar{\boldsymbol{\theta}}^*$.

However, two distinct array configurations \mathbb{S}_1 and \mathbb{S}_2 with the same difference coarray do not necessarily imply the same CRB. This is because, as in (6.42), the matrix $\mathbf{M} = (\mathbf{J}^H (\mathbf{R}_{\mathbb{S}}^T \otimes \mathbf{R}_{\mathbb{S}})^{-1} \mathbf{J})^{\frac{1}{2}}$ depends on \mathbb{S} .

Example 2. To demonstrate, consider the nested array and the super nested array in (6.46) and (6.47). Let $\bar{\boldsymbol{\theta}} = [0.1, 0.2]^T$, $p_1 = p_2 = p_n = 1$, and $K = 500$. Evaluating (6.40) yields

Nested array:

$$[\text{CRB}(\bar{\boldsymbol{\theta}})]_{1,1} = [\text{CRB}(\bar{\boldsymbol{\theta}})]_{2,2} = 3.2648 \times 10^{-8},$$

Super nested array:

$$[\text{CRB}(\bar{\boldsymbol{\theta}})]_{1,1} = [\text{CRB}(\bar{\boldsymbol{\theta}})]_{2,2} = 2.9352 \times 10^{-8}.$$

Therefore, the CRBs are indeed different even if the difference coarrays are identical.

Proposition 6.5.3. If $\text{rank}(\mathbf{A}_c) = 2D + 1$, then as the number of snapshots K approaches infinity, $\text{CRB}(\bar{\boldsymbol{\theta}})$ converges to zero.

Proof. This follows directly from the expression (6.40). □

The following theorems investigate the asymptotic behavior of the CRB for large SNR. Assume the sources have identical power. It was experimentally noticed in [1] that for $D < |\mathbb{S}|$, the CRB decays to zero for large SNR while for $D \geq |\mathbb{S}|$, the CRB tends to converge to a non-zero value for large SNR. Here we find these phenomena to be a provable consequence of the proposed CRB expression as given in Theorem 6.4.2.

However, in this chapter, we notice that the conditions $D < |\mathbb{S}|$ and $D \geq |\mathbb{S}|$ are not fundamental to the asymptotic behavior of the CRB for large SNR. Instead, the

condition that the array manifold matrix \mathbf{V}_S has full row rank, i.e., $\text{rank}(\mathbf{V}_S) = |S|$, is more critical. In the regime $D < |S|$, \mathbf{V}_S does not have full row rank since \mathbf{V}_S is a tall matrix. Thus, the asymptotic CRB expression can be specified by the following theorem:

Theorem 6.5.1. If the D uncorrelated sources have equal SNR p/p_n , $\text{rank}(\mathbf{V}_S) < |S|$, and $\text{rank}(\mathbf{A}_c) = 2D + 1$, then for sufficiently large SNR, the CRB has the following asymptotic expression which converges to zero as SNR tends to infinity:

$$\text{CRB}(\bar{\boldsymbol{\theta}}) \Big|_{\substack{\text{large SNR} \\ \text{rank}(\mathbf{V}_S) < |S|}} = \frac{p_n}{4\pi^2 K p} \mathbf{S}^{-1}, \quad (6.48)$$

where

$$\mathbf{S} = \mathbf{G}_\infty^H \mathbf{\Pi}_{\mathbf{M}_\infty}^\perp \mathbf{M}_\infty \mathbf{W}_D \mathbf{G}_\infty + \frac{(\mathbf{G}_\infty^H \mathbf{u})(\mathbf{G}_\infty^H \mathbf{u})^H}{\|\mathbf{u}\|^2}, \quad (6.49)$$

$$\mathbf{M}_\infty = [\mathbf{J}^H [(\mathbf{U}_s \mathbf{\Lambda}^{-1} \mathbf{U}_s^H)^T \otimes (\mathbf{U}_n \mathbf{U}_n^H) + (\mathbf{U}_n \mathbf{U}_n^H)^T \otimes (\mathbf{U}_s \mathbf{\Lambda}^{-1} \mathbf{U}_s^H)] \mathbf{J}]^{\frac{1}{2}}, \quad (6.50)$$

$$\mathbf{G}_\infty = \mathbf{M}_\infty (\text{diag}(\mathbb{D})) \mathbf{V}_D, \quad (6.51)$$

$$\mathbf{u} = (\mathbf{M}_\infty \mathbf{W}_D) (\mathbf{W}_D^H \mathbf{M}_\infty^2 \mathbf{W}_D)^{-1} \mathbf{e}_{D+1}, \quad (6.52)$$

$$\mathbf{e}_{D+1} = \overbrace{[0, \dots, 0, 1]^T}^D. \quad (6.53)$$

$\mathbf{W}_D^H \mathbf{M}_\infty^2 \mathbf{W}_D$ and \mathbf{S} can be readily shown to be positive definite. The vector \mathbf{u} can be shown to be non-zero.

Here $\mathbf{V}_S \mathbf{V}_S^H$ has eigen-decomposition $\mathbf{U}_s \mathbf{\Lambda} \mathbf{U}_s^H$. \mathbf{U}_s has dimension $|S| \times \text{rank}(\mathbf{V}_S)$ with normalized eigenvectors on its columns. $\mathbf{\Lambda}$ is a $\text{rank}(\mathbf{V}_S) \times \text{rank}(\mathbf{V}_S)$ diagonal matrix with eigenvalues on its diagonals. The eigen-decomposition of \mathbf{R}_S is $\mathbf{U}_s (p \mathbf{\Lambda} + p_n \mathbf{I}) \mathbf{U}_s^H + p_n \mathbf{U}_n \mathbf{U}_n^H$, where \mathbf{U}_n is orthonormal to \mathbf{U}_s .

Proof. The proof can be found in 6.C. □

It is obvious from (6.48) that, as the SNR approaches infinity, the CRB decays to zero for $D < |S|$, which is consistent with the observation in [1].

For $D \geq |S|$ and \mathbf{V}_S being full row rank, the asymptotic CRB expression can be given by

Theorem 6.5.2. If the D uncorrelated sources have equal SNR p/p_n , $D \geq |S|$, $\text{rank}(\mathbf{V}_S) = |S|$, and $\text{rank}(\mathbf{A}_c) = 2D + 1$, then for sufficiently large SNR, the CRB has an asymptotic expression which does not decay to zero as SNR tends to infinity. Thus,

$$\text{CRB}(\bar{\boldsymbol{\theta}}) \Big|_{\substack{\text{large SNR} \\ \text{rank}(\mathbf{V}_S) = |S|}} = \frac{1}{4\pi^2 K} \mathbf{S}^{-1}, \quad (6.54)$$

where

$$\begin{aligned}\mathbf{S} &= \mathbf{G}_\infty^H \mathbf{\Pi}_{\mathbf{M}_\infty}^\perp \mathbf{W}_\mathbb{D} \mathbf{G}_\infty, \\ \mathbf{M}_\infty &= (\mathbf{J}^H ((\mathbf{V}_\mathbb{S} \mathbf{V}_\mathbb{S}^H)^{-T} \otimes (\mathbf{V}_\mathbb{S} \mathbf{V}_\mathbb{S}^H)^{-1}) \mathbf{J})^{\frac{1}{2}}, \\ \mathbf{G}_\infty &= \mathbf{M}_\infty (\text{diag}(\mathbb{D})) \mathbf{V}_\mathbb{D}.\end{aligned}$$

Here $\mathbf{W}_\mathbb{D}^H \mathbf{M}_\infty^2 \mathbf{W}_\mathbb{D}$ and \mathbf{S} can be shown to be positive definite.

Proof. The proof can be found in 6.C. □

Theorem 6.5.2 also confirms what was empirically observed in [1], for $D \geq |\mathbb{S}|$. It will be demonstrated in Section 6.7 that the proposed CRB expression (6.40) indeed comes close to the asymptotic values (6.48) and (6.54).

6.6 Connection to the ULA Part of the Coarray

It was observed from Proposition 6.5.1 that the difference coarray \mathbb{D} has a direct impact on the singularity of the FIM. In this section, it will be shown that, if the difference coarray has certain structure, then the rank condition (6.39) is guaranteed for any choice of distinct DOAs. This can be regarded as a theoretical justification of the identifiability observations empirically made in Propositions 6.2.1 and 6.2.2.

Theorem 6.6.1. Let \mathbb{U} be the central ULA segment of the difference coarray \mathbb{D} , as in Definition 2.2.2. Let \mathbf{A}_c be the ACM matrix. If $D \leq (|\mathbb{U}| - 1)/2$, then $\text{rank}(\mathbf{A}_c) = 2D + 1$, for every $\bar{\boldsymbol{\theta}} = [\bar{\theta}_1, \bar{\theta}_2, \dots, \bar{\theta}_D]^T$ such that $\bar{\theta}_i \neq \bar{\theta}_j$ for $i \neq j$.

Proof. The proof can be found in 6.D. □

Theorem 6.6.1 and Proposition 6.5.3 indicate that if $D \leq (|\mathbb{U}| - 1)/2$, then the CRB expression approaches zero for large snapshots. This result is consistent with Proposition 6.2.1.

Corollary 6.6.1. If $D > (|\mathbb{D}| - 1)/2$, then for any choice of D distinct DOAs, we have $\text{rank}(\mathbf{A}_c) < 2D + 1$, and the FIM is singular.

Proof. If $D > (|\mathbb{D}| - 1)/2$, then for any choice of $\bar{\boldsymbol{\theta}}$, the ACM matrix \mathbf{A}_c becomes a fat matrix. This proves the Corollary. □

Note that Corollary 6.6.1 explains the observation given in Proposition 6.2.2. Finally, when

$$(|\mathbb{U}| - 1)/2 < D \leq (|\mathbb{D}| - 1)/2, \tag{6.55}$$

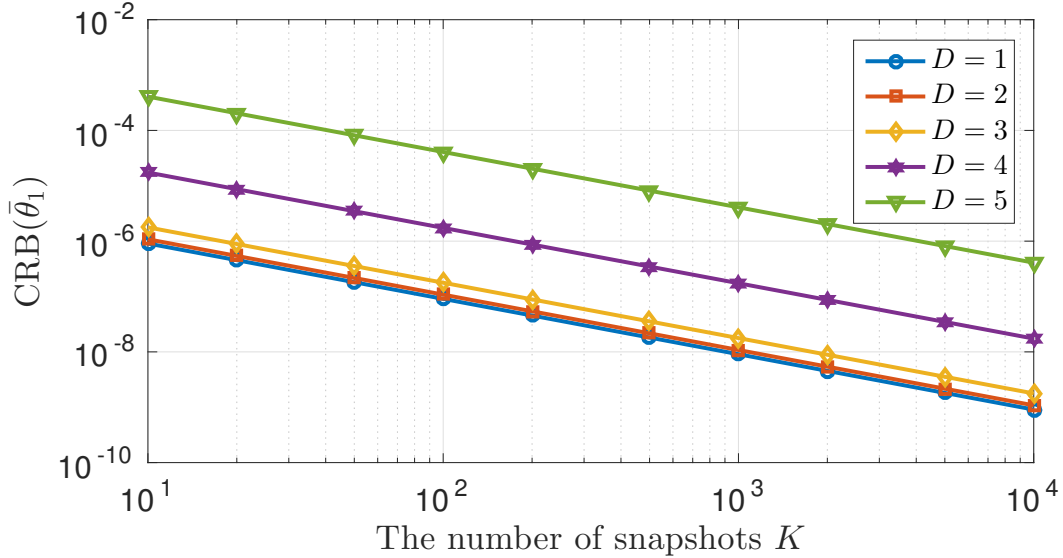


Figure 6.1: The dependence of the proposed CRB expression on snapshots for various numbers of sources D . The array configuration is the nested array with $N_1 = N_2 = 2$ so that the sensor locations are $\mathbb{S} = \{1, 2, 3, 6\}$. The equal-power sources are located at $\bar{\theta}_i = -0.49 + 0.9(i-1)/D$ for $i = 1, 2, \dots, D$. SNR is 20 dB.

it is unclear whether the rank condition (6.39) holds true or not. For some choices of the DOA values, the rank condition (6.39) holds and for some values it does not. So in the regime (6.55), whether the FIM is nonsingular and whether the CRB exists depends on the specific values of the DOA.

6.7 Numerical Examples

The proposed CRB expression versus snapshots and SNR

Our first numerical example examines Proposition 6.5.3, Theorem 6.5.1, and Theorem 6.5.2. Consider a nested array with $N_1 = N_2 = 2$, so that the sensor locations $\mathbb{S} = \{1, 2, 3, 6\}$ and the difference coarray becomes $\mathbb{D} = \{-5, \dots, 5\}$. As a result, the total number of sensors is 4 while the maximum number of identifiable sources is 5. The equal-power sources are located at $\bar{\theta}_i = -0.49 + 0.9(i-1)/D$ for $i = 1, 2, \dots, D$. It can be shown that these parameters indeed satisfy the rank condition (6.39), so that, the proposed CRB expression is valid.

Fig. 6.1 plots the proposed CRB expression for $\bar{\theta}_1$ as a function of snapshots, with 20 dB SNR. It can be observed that this expression is inversely proportional to the number of snapshots K , which verifies Proposition 6.5.3. These curves also depend on the number of sources D . In this specific example, these CRBs increase with D , which suggests that if there are more sources, it is more difficult to estimate $\bar{\theta}_1$ accurately.

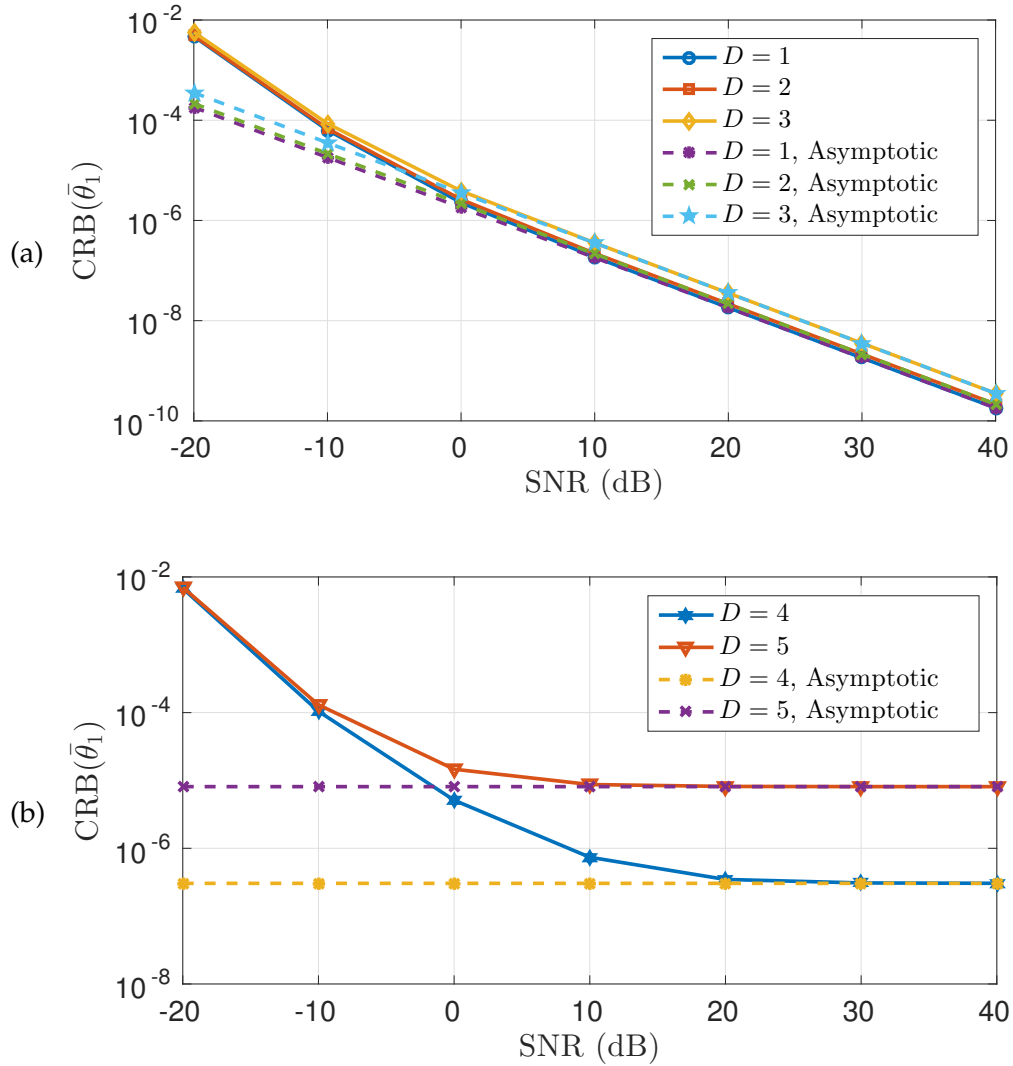


Figure 6.2: The dependence of the proposed CRB expression on SNR for (a) $D < |\mathbb{S}| = 4$ and (b) $D \geq |\mathbb{S}| = 4$. The array configuration is the nested array with $N_1 = N_2 = 2$ so that the sensor locations are $\mathbb{S} = \{1, 2, 3, 6\}$. The equal-power sources are located at $\bar{\theta}_i = -0.49 + 0.9(i - 1)/D$ for $i = 1, 2, \dots, D$. The number of snapshots K is 500.

Fig. 6.2(a) and (b) display the relationship between the proposed CRB expression and the SNR for 500 snapshots. Fig. 6.2(a) shows that if $D < |\mathbb{S}| = 4$, the CRBs decrease with the SNR. For $D \geq |\mathbb{S}| = 4$, the CRBs saturate when the SNR is over 20dB, as indicated in Fig. 6.2(b). These phenomena are consistent with what was observed experimentally in [1]. Furthermore, the dashed lines in Fig. 6.2(a) and (b) demonstrate that, for large SNR, the CRBs indeed converge to the asymptotic CRB expressions, as presented in Theorem 6.5.1 and 6.5.2.

The proposed CRB expression for ULA, MRA, nested arrays, coprime arrays, and super nested arrays

In the following simulations, consider the following five array configurations: uniform linear arrays (ULA) [188], minimum redundancy arrays (MRA) [113], as in Definition 2.2.10, nested arrays with $N_1 = N_2 = 5$ [124], as in (2.7), coprime arrays with $M = 3, N = 5$ [186], as in (2.8), and second-order super nested arrays with $N_1 = N_2 = 5$ [92], as in Definition 3.4.1. The sensor locations for these arrays are given by

$$\mathbb{S}_{\text{ULA}} = \{0, 1, 2, 3, 4, 5, 6, 7, 8, 9\}, \quad (6.56)$$

$$\mathbb{S}_{\text{MRA}} = \{0, 1, 3, 6, 13, 20, 27, 31, 35, 36\}, \quad (6.57)$$

$$\mathbb{S}_{\text{nested}} = \{1, 2, 3, 4, 5, 6, 12, 18, 24, 30\}, \quad (6.58)$$

$$\mathbb{S}_{\text{coprime}} = \{0, 3, 5, 6, 9, 10, 12, 15, 20, 25\}, \quad (6.59)$$

$$\mathbb{S}_{\text{super nested}} = \{1, 3, 5, 8, 10, 12, 18, 24, 29, 30\}. \quad (6.60)$$

In each array, the total number of sensors is 10. The difference coarray is listed as follows:

$$\mathbb{D}_{\text{ULA}} = \{0, \pm 1, \dots, \pm 9\}, \quad (6.61)$$

$$\mathbb{D}_{\text{MRA}} = \{0, \pm 1, \dots, \pm 36\}, \quad (6.62)$$

$$\mathbb{D}_{\text{nested}} = \{0, \pm 1, \dots, \pm 29\}, \quad (6.63)$$

$$\mathbb{D}_{\text{coprime}} = \{0, \pm 1, \dots, \pm 17, \pm 19, \pm 20, \pm 22, \pm 25\}, \quad (6.64)$$

$$\mathbb{D}_{\text{super nested}} = \{0, \pm 1, \dots, \pm 29\}. \quad (6.65)$$

According to Propositions 6.2.1 and 6.2.2, the identifiability capabilities of coarray MUSIC are summarized in Table 6.2.

Fig. 6.3 compares the CRB for DOA estimation over ULA, MRA, nested arrays, coprime arrays, and super nested arrays if there are fewer sources ($D = 3$) than sensors ($|\mathbb{S}| = 10$). The equal-power sources are located at $\bar{\theta}_i = -0.49 + 0.99(i - 1)/D$ for $i = 1, 2, \dots, D$, where the number of sources D is 3. According to Table 6.2, all of these arrays can identify such sources using coarray MUSIC because $D < |\mathbb{S}|$.

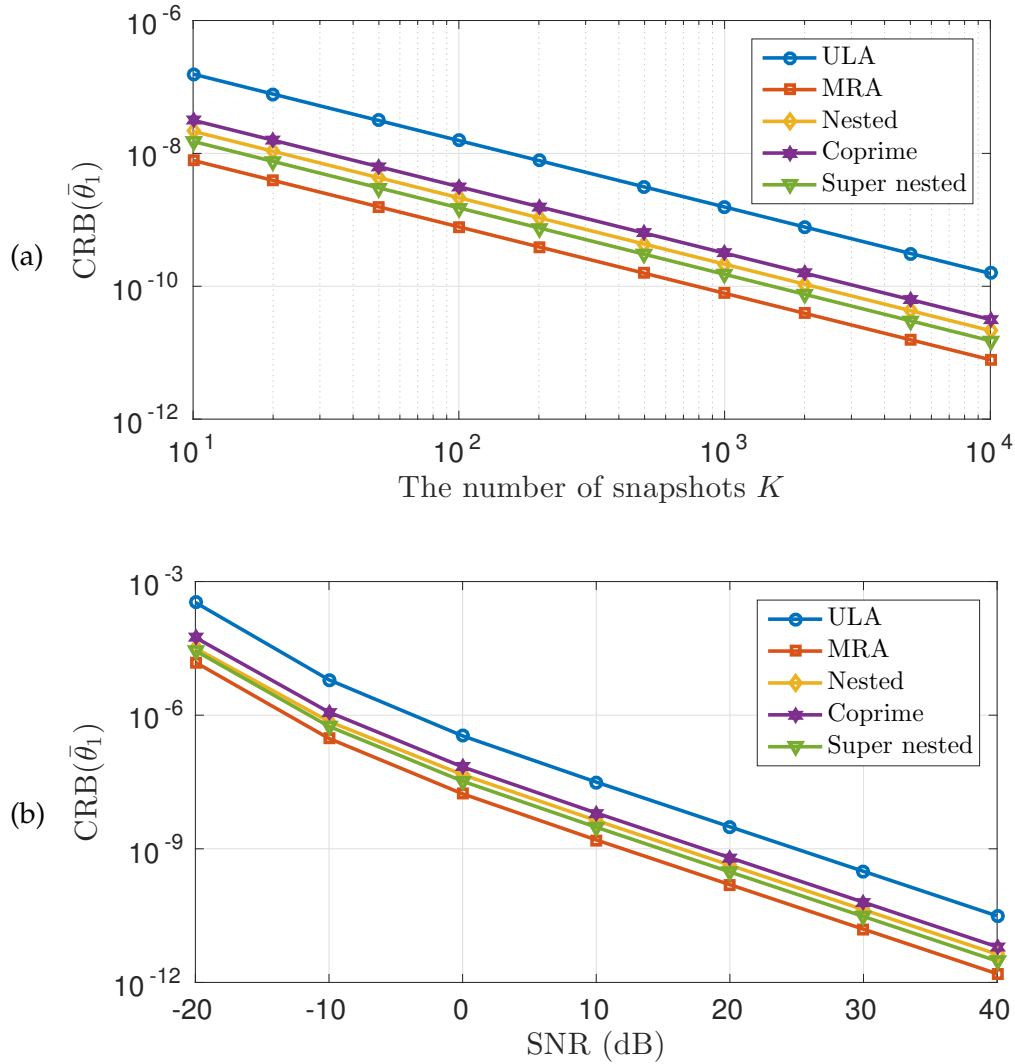


Figure 6.3: The dependence of the proposed CRB on (a) snapshots and (b) SNR for ULA, MRA, nested arrays, coprime arrays, and super nested arrays. The total number of sensors is 10 and the sensor locations are given in (6.56) to (6.59). The number of sources is $D = 3$ (fewer sources than sensors) and the sources are located at $\bar{\theta}_i = -0.49 + 0.99(i - 1)/D$ for $i = 1, 2, \dots, D$. For (a), the SNR is 20 dB while for (b) the number of snapshots K is 500.

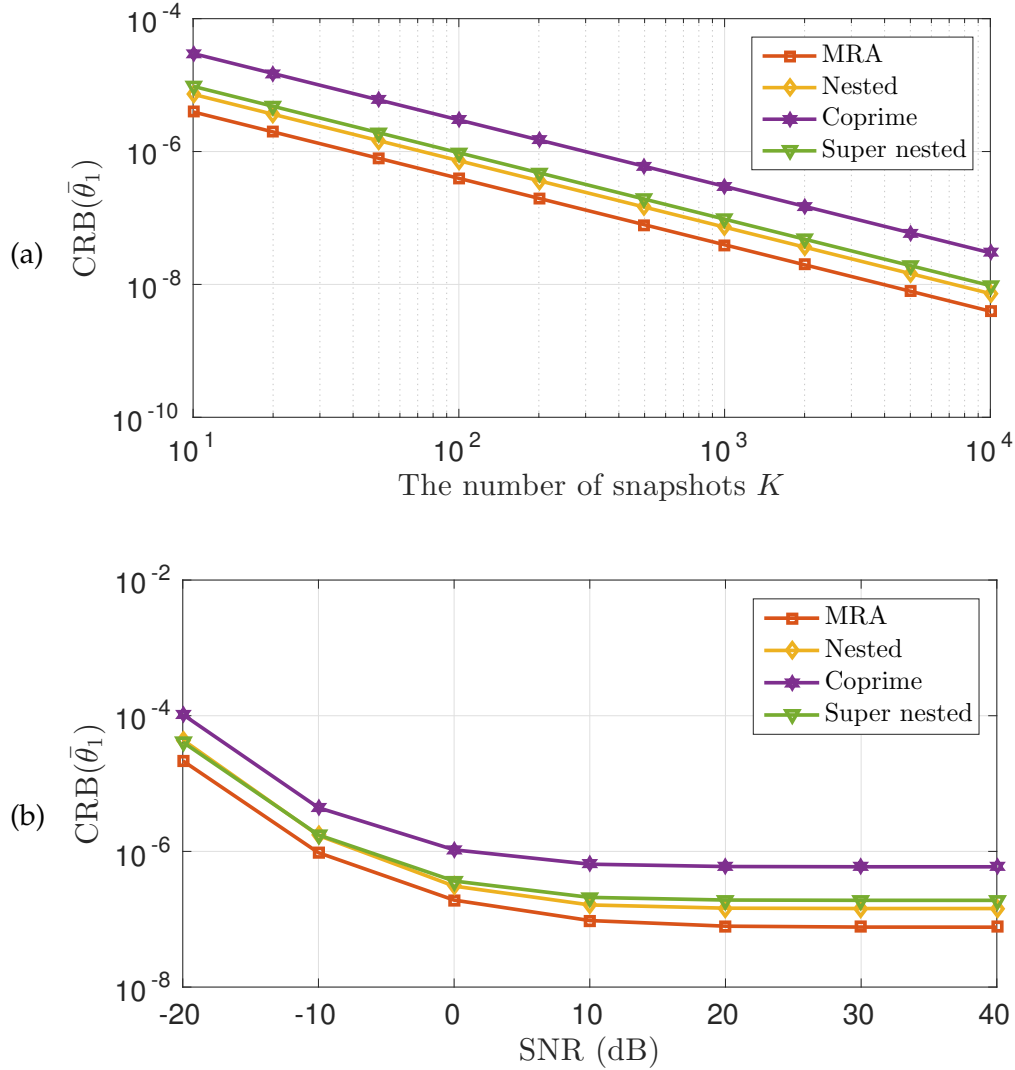


Figure 6.4: The dependence of the proposed CRB on (a) snapshots and (b) SNR for MRA, nested arrays, coprime arrays, and super nested arrays. The total number of sensors is 10 and the sensor locations are given in (6.56) to (6.59). The number of sources is $D = 17$ (more sources than sensors) and the sources are located at $\bar{\theta}_i = -0.49 + 0.99(i - 1)/D$ for $i = 1, 2, \dots, D$. For (a), the SNR is 20 dB while for (b) the number of snapshots K is 500.

Table 6.2: Identifiable/non-identifiable regions for coarray MUSIC.

| | Identifiable | Cannot judge | Non-identifiable |
|---------------------|--------------------|---------------------|------------------|
| ULA (6.56) | $1 \leq D \leq 9$ | - | $10 \leq D$ |
| MRA (6.57) | $1 \leq D \leq 36$ | - | $37 \leq D$ |
| Nested (6.58) | $1 \leq D \leq 29$ | - | $30 \leq D$ |
| Coprime (6.59) | $1 \leq D \leq 17$ | $18 \leq D \leq 21$ | $22 \leq D$ |
| Super nested (6.60) | $1 \leq D \leq 29$ | - | $30 \leq D$ |

Fig. 6.3(a) depicts the CRBs in terms of the number of snapshots K with 20 dB SNR while Fig. 6.3(b) shows the dependence of the CRBs on SNR for 500 snapshots. It can be inferred that, for fixed K and SNR, the least CRB is exhibited by MRA, followed by the super nested array, then the nested array, then the coprime array, and finally ULA. This ranking is consistent with the empirical observation that the estimation error decreases with the increasing size of the difference coarray [1], [113], [124], [125], [184]. In particular, the size of the difference coarray is 73 for MRA, 59 for the super nested array and the nested array, 43 for the coprime array, and 19 for ULA.

Fig. 6.4 illustrates the CRB for MRA, nested arrays, coprime arrays, and super nested arrays if there are more sources ($D = 17$) than sensors ($|\mathcal{S}| = 10$). The remaining parameters are identical to those in Fig. 6.3. The least CRB is now enjoyed by MRA, followed by the nested array, the super nested array, and finally the coprime array. Note that the CRB for ULA is divergent since the number of sources $D = 17$ resides in the non-identifiable regime, as indicated in Table 6.2. Another observation is that, in this example, the coprime array has the largest CRB. It is because the number of sources $D = 17$ is the upper limit of the identifiable region for the coprime array, while the number of identifiable sources for the remaining three arrays is larger than 17. Hence, the estimation performance for the coprime array is worst among the others.

The proposed CRB expression versus the number of sources

Next, the maximum number of detectable sources for ULA, MRA, nested arrays, coprime arrays, and super nested arrays is investigated. The sensor locations for these arrays are listed from (6.56) to (6.60). The normalized DOAs for D equal-power sources are $\bar{\theta}_i = -0.49 + 0.99(i - 1)/D$ for $i = 1, 2, \dots, D$. The SNR is 20dB and the number of snapshots is 500. According to Propositions 6.2.1 and 6.2.2, the identifiability capabilities of coarray MUSIC are summarized in Table 6.2.

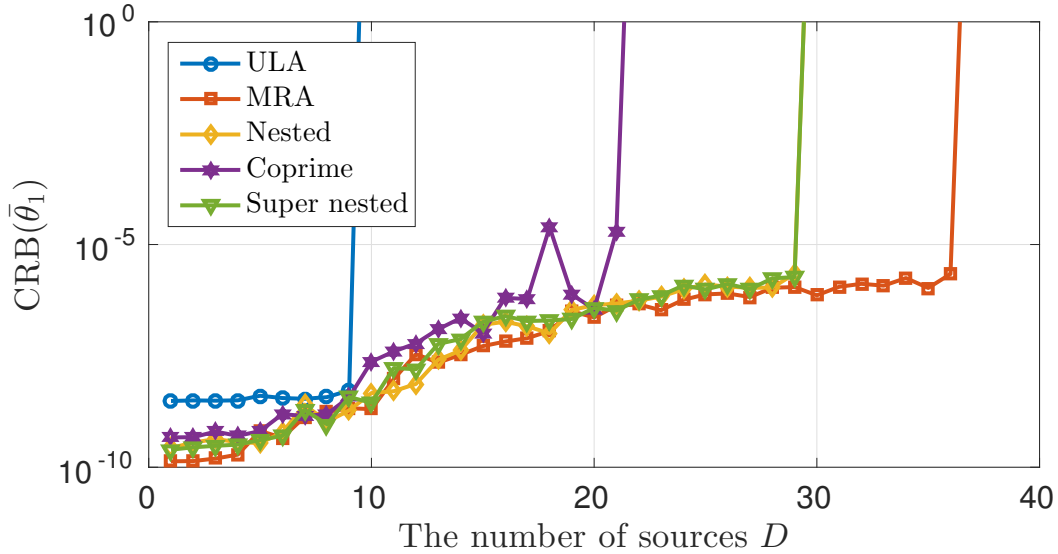


Figure 6.5: The dependence of the proposed CRB on the number of sources D for various array configurations. The equal-power sources are located at $\bar{\theta}_i = -0.49 + 0.99(i-1)/D$ for $i = 1, 2, \dots, D$. The number of snapshots K is 500 and SNR is 20 dB.

Fig. 6.5 evaluates the proposed CRB expression with respect to the number of sources D for these array configurations. It can be observed that the identifiability, as shown in Table 6.2, is actually consistent with the proposed CRB expression. Each CRB curve diverges for D greater than a certain threshold, which can be inferred from the non-identifiable regimes in Table 6.2. As an example, for the coprime array with $1 \leq D \leq 17$, the associated CRB expressions are small, which match the identifiability of coarray MUSIC in Proposition 6.2.1. On the other hand, for $D \geq 22$, the CRB expressions become divergent, which is consistent with non-identifiability of coarray MUSIC (Proposition 6.2.2). In the region $18 \leq D \leq 21$ which corresponds to the regime (6.55), the existence or otherwise of CRB is inconclusive. In this example, the CRB is small but in an example in Section 6.7, we will see that it is divergent.

Fig. 6.5 also elaborates the discussion, given earlier in Section 6.5, on the associated CRB expression for two sparse arrays \mathbb{S}_1 and \mathbb{S}_2 with the same difference coarray \mathbb{D} . Consider the CRBs for the nested array and the super nested array. It can be seen that both CRBs are convergent for $1 \leq D \leq 29$ and divergent for $D \geq 30$, even if the physical array configurations are different. This behavior is truly compatible with the discussion in Section 6.5.

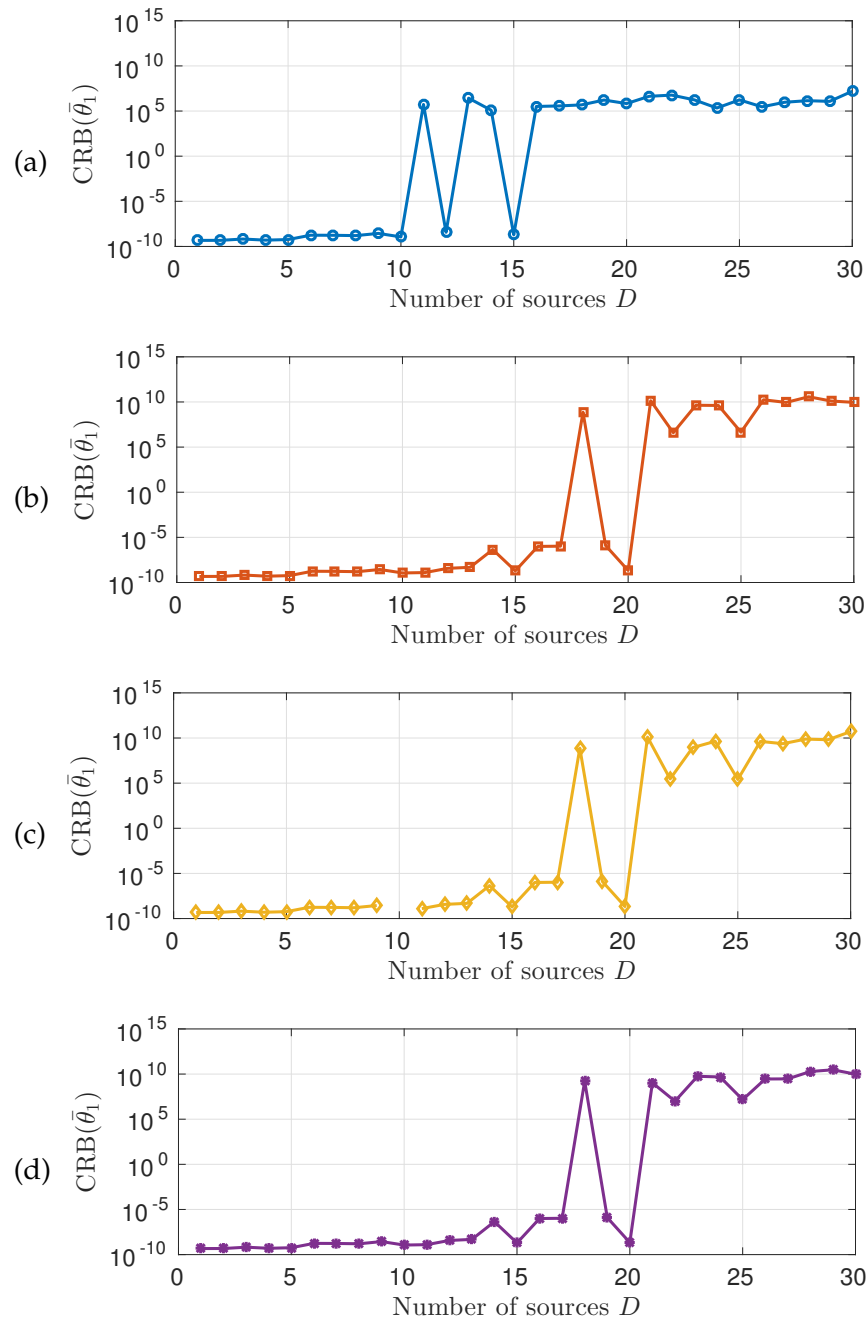


Figure 6.6: The CRB expressions versus the number of sources D for a coprime array. (a) The stochastic CRB expression [167], (b) the CRB which is evaluated numerically by Abramovich et al. [1], (c) Jansson et al.'s CRB expression [66], and (d) the proposed CRB expression, as in Theorem 6.4.2. The coprime array with $M = 3$, $N = 5$ has sensor locations as in (6.59) and the difference coarray as in (6.64). The number of sensors $|\mathcal{S}| = 10$. The equal-power sources are located at $\bar{\theta}_i = -0.48 + (i - 1)/D$ for $i = 1, 2, \dots, D$. The number of snapshots K is 500 and SNR is 20 dB.

Comparison between the well-known CRB expressions and the proposed expression

In this subsection, the coprime array with $M = 3$, $N = 5$ is considered, where the sensor locations are given in (6.59). The SNR is 20dB and the number of snapshots is $K = 500$. The sources have normalized DOAs $\bar{\theta}_i = -0.48 + (i - 1)/D$ for $i = 1, 2, \dots, D$, which is different from those in Section 6.7.

Fig. 6.6 depicts several different CRB expressions: (a) the stochastic CRB expression of [167], (b) the CRB which is evaluated numerically by Abramovich et al. [1], (c) Jansson et al.'s CRB expression [66], and (d) the proposed CRB expression, as in Theorem 6.4.2. First of all, the stochastic CRB expression of [167] is valid only when $D < |\mathbb{S}|$, as discussed in Section 6.4. Hence, it cannot be used to derive conclusions about identifiability in the regime $D \geq |\mathbb{S}|$. This is indeed seen in Fig. 6.6(a) where the CRB of [167] diverges for $D \geq |\mathbb{S}| = 10$, even though this is still an identifiable regime according to Table 6.2.

Abramovich et al.'s CRB expression, in Fig. 6.6(b), is calculated numerically from the FIM. Jansson et al.'s CRB expression, as shown in Fig. 6.6(c), is consistent with the identifiable and non-identifiable regions in Table 6.2, except for $D = |\mathbb{S}| = 10$. It is because the appearance of $|\mathbb{S}| - D$ in the denominator of (6.23) makes the whole expression invalid. Furthermore, if $D > |\mathbb{S}| = 10$, even though $\mathbf{\Pi}_{\mathbf{V}_s}$ is undefined, we still calculate Jansson et al.'s CRB expression (6.22) numerically and it resembles the plot given in Fig. 6.6(b).

Finally, the newly proposed CRB expression (6.40), as plotted in Fig. 6.6(d), fully agrees with Jansson et al.'s CRB expression for $D < |\mathbb{S}| = 10$ and Abramovich et al.'s for any D . Unlike Jansson et al.'s expression, the new expression can also be evaluated for $D = |\mathbb{S}| = 10$. Furthermore, the proposed CRB expression is in agreement with the identifiability results for every D in Table 6.2. This example also justifies the relations among Abramovich et al.'s, Jansson et al.'s, and the proposed CRB expression, as discussion in Section 6.4.

Note that in the example, the proposed CRB expression becomes divergent at $D = 18$, as seen in Fig. 6.6(d). It is because the rank of the ACM matrix is $35 < 2D + 1 = 37$, which violates the rank condition (6.39). Hence, these particular DOAs lead to a singular FIM, as stated in Theorem 6.4.1. This example also shows that, in the "unknown" region of Table 6.2, which is $18 \leq D \leq 21$, the FIM could be singular or nonsingular, depending on the DOAs.

6.8 Concluding Remarks

In this chapter, we derived a new expression for the CRB of DOA estimates using linear arrays. The expression is especially useful in the case of sparse arrays

such as nested arrays, coprime arrays, or MRAs, which can identify many more sources than the number of sensors. The conditions for validity of the expression are expressed in terms of the rank of an augmented coarray manifold matrix. The expression is valid for up to $\mathcal{O}(N^2)$ sources where N is the number of sensors. The precise details depend on the array configuration. We found that considerable insights regarding the behavior of sparse arrays can be gained from these expressions. All results were derived for uncorrelated sources, and only the estimation of source DOAs were considered, and not the source powers. In the future, it will be of interest to extend the results of this chapter to the case where source powers are also parameters of interest. Extension to correlated sources will be of future interest as well.

Appendices

6.A Derivation to the Proposed CRB Expression

Connection to the difference coarray

To simplify the CRB, it can be inferred from (6.29) that

$$\begin{aligned} \mathbf{r}_S &= \text{vec} \left(\sum_{i=1}^D p_i \mathbf{v}_S(\bar{\theta}_i) \mathbf{v}_S^H(\bar{\theta}_i) + p_n \mathbf{I} \right) \\ &= \sum_{i=1}^D p_i \text{vec} \left(\mathbf{v}_S(\bar{\theta}_i) \mathbf{v}_S^H(\bar{\theta}_i) \right) + p_n \text{vec}(\mathbf{I}) \\ &= \sum_{i=1}^D p_i \mathbf{v}_S^*(\bar{\theta}_i) \otimes \mathbf{v}_S(\bar{\theta}_i) + p_n \text{vec}(\mathbf{I}), \end{aligned} \quad (6.66)$$

since $\text{vec}(\mathbf{a}\mathbf{b}^T) = \mathbf{b} \otimes \mathbf{a}$ [106]. It is useful to express $\mathbf{v}_S^*(\bar{\theta}_i) \otimes \mathbf{v}_S(\bar{\theta}_i)$ in terms of the difference coarray manifold vector $\mathbf{v}_D(\bar{\theta}_i)$ using a matrix \mathbf{J} as follows:

$$\mathbf{v}_S^*(\bar{\theta}_i) \otimes \mathbf{v}_S(\bar{\theta}_i) = \mathbf{J} \mathbf{v}_D(\bar{\theta}_i). \quad (6.67)$$

The appropriate matrix \mathbf{J} for this is given in 6.B. It is shown in 6.B that \mathbf{J} has full column rank, which leads to the following corollary:

Corollary 6.A.1. $\mathbf{J}^H(\mathbf{R}_S^T \otimes \mathbf{R}_S)^{-1} \mathbf{J}$ is positive definite. Therefore, it has a positive definite square root $\mathbf{M} = (\mathbf{J}^H(\mathbf{R}_S^T \otimes \mathbf{R}_S)^{-1} \mathbf{J})^{\frac{1}{2}}$.

Proof. Since $p_1, \dots, p_D, p_n > 0$, \mathbf{R}_S and \mathbf{R}_S^T are both positive definite, implying $(\mathbf{R}_S^T \otimes \mathbf{R}_S)^{-1}$ is also positive definite [106]. Hence, $\mathbf{J}^H(\mathbf{R}_S^T \otimes \mathbf{R}_S)^{-1} \mathbf{J}$ is positive definite [60], [106]. \square

Proposition 6.B.2 and Corollary 6.B.1, both given later in 6.B, simplify (6.66) as

$$\mathbf{r}_S = \mathbf{J}\mathbf{x}_D = \mathbf{J}(\mathbf{V}_D\mathbf{p} + p_n\mathbf{e}_0) = \mathbf{J}\mathbf{W}_D \begin{bmatrix} \mathbf{p} \\ p_n \end{bmatrix}, \quad (6.68)$$

$$\mathbf{V}_D = [\mathbf{v}_D(\bar{\theta}_1) \quad \mathbf{v}_D(\bar{\theta}_2) \quad \dots \quad \mathbf{v}_D(\bar{\theta}_D)] = \underset{|\mathbb{D}|}{\overset{D}{\boxed{\phantom{\mathbf{V}_D}}}}, \quad (6.69)$$

$$\mathbf{W}_D = [\mathbf{V}_D \quad \mathbf{e}_0] = \underset{|\mathbb{D}|}{\overset{D+1}{\boxed{\phantom{\mathbf{W}_D}}}}, \quad (6.70)$$

and $\mathbf{p} = [p_1, p_2, \dots, p_D]^T$.

Proof of Lemma 6.4.1

(Sufficiency) If \mathbf{D} is nonsingular, \mathbf{F} can always be decomposed as [60], [106], [187] [181, Problem A.18]

$$\mathbf{F} = \begin{bmatrix} \mathbf{A} & \mathbf{B} \\ \mathbf{B}^H & \mathbf{D} \end{bmatrix} \quad (6.71)$$

$$= \begin{bmatrix} \mathbf{I} & \mathbf{B}\mathbf{D}^{-1} \\ \mathbf{0} & \mathbf{I} \end{bmatrix} \begin{bmatrix} \mathbf{A} - \mathbf{B}\mathbf{D}^{-1}\mathbf{B}^H & \mathbf{0} \\ \mathbf{0} & \mathbf{D} \end{bmatrix} \begin{bmatrix} \mathbf{I} & \mathbf{0} \\ \mathbf{D}^{-1}\mathbf{B}^H & \mathbf{I} \end{bmatrix}. \quad (6.72)$$

Taking the determinant on both sides of (6.72) leads to

$$\det(\mathbf{F}) = \det(\mathbf{A} - \mathbf{B}\mathbf{D}^{-1}\mathbf{B}^H) \det(\mathbf{D}). \quad (6.73)$$

If $\mathbf{A} - \mathbf{B}\mathbf{D}^{-1}\mathbf{B}^H$ is also nonsingular, then $\det(\mathbf{A} - \mathbf{B}\mathbf{D}^{-1}\mathbf{B}^H) \neq 0$ and $\det(\mathbf{F}) \neq 0$. Hence, \mathbf{F} is nonsingular.

(Necessity) Suppose \mathbf{D} is nonsingular and $\mathbf{A} - \mathbf{B}\mathbf{D}^{-1}\mathbf{B}^H$ is singular. Then $\det(\mathbf{A} - \mathbf{B}\mathbf{D}^{-1}\mathbf{B}^H) = 0$. Eq. (6.73) becomes $\det(\mathbf{F}) = 0$ hence \mathbf{F} is singular.

If \mathbf{D} is singular, then $\det(\mathbf{D}) = 0$. It is well-known that a Hermitian matrix is positive definite if and only if all the leading principal minors are positive [181, Fact A.6.3]. Since $\det(\mathbf{D})$ is a leading principal minor, it follows trivially that \mathbf{F} is not positive definite. This concludes the proof.

Proof of Lemma 6.4.2

(Sufficiency) According to (6.33) and (6.68), $\Delta^H \Delta = \mathbf{W}_D^H \mathbf{J}^H (\mathbf{R}_S^T \otimes \mathbf{R}_S)^{-1} \mathbf{J} \mathbf{W}_D$. Since $\text{rank}(\mathbf{W}_D) = D + 1$, it follows from Corollary 6.A.1 that $\Delta^H \Delta$ is positive definite.

(Necessity) If $\text{rank}(\mathbf{W}_D) < D + 1$, then there exists a non-zero vector \mathbf{u} such that $\mathbf{W}_D \mathbf{u} = \mathbf{0}$. It can be deduced that

$$\mathbf{u}^H (\Delta^H \Delta) \mathbf{u} = (\mathbf{W}_D \mathbf{u})^H \mathbf{J}^H (\mathbf{R}_S^T \otimes \mathbf{R}_S)^{-1} \mathbf{J} (\mathbf{W}_D \mathbf{u}) = 0,$$

implying that $\Delta^H \Delta$ is not positive definite.

$$\begin{aligned}
& \frac{\mathbf{G}^H \boldsymbol{\Pi}_{\Delta}^{\perp} \mathbf{G}}{4\pi^2} \\
&= \mathbf{P}^H \mathbf{V}_{\mathbb{D}}^H (\text{diag}(\mathbb{D}))^H \\
&\quad \times \left[\mathbf{J}^H (\mathbf{R}_{\mathbb{S}}^T \otimes \mathbf{R}_{\mathbb{S}})^{-\frac{1}{2}} \boldsymbol{\Pi}^{\perp} \right. \\
&\quad \left. (\mathbf{R}_{\mathbb{S}}^T \otimes \mathbf{R}_{\mathbb{S}})^{-\frac{1}{2}} \mathbf{J} \mathbf{W}_{\mathbb{D}} (\mathbf{R}_{\mathbb{S}}^T \otimes \mathbf{R}_{\mathbb{S}})^{-\frac{1}{2}} \mathbf{J} \right] (\text{diag}(\mathbb{D})) \mathbf{V}_{\mathbb{D}} \mathbf{P} \\
&= \mathbf{P}^H \mathbf{V}_{\mathbb{D}}^H (\text{diag}(\mathbb{D}))^H \\
&\quad \times \left[\mathbf{M}^H \mathbf{M} - \mathbf{M}^H (\mathbf{M} \mathbf{W}_{\mathbb{D}}) [(\mathbf{M} \mathbf{W}_{\mathbb{D}})^H (\mathbf{M} \mathbf{W}_{\mathbb{D}})]^{-1} (\mathbf{M} \mathbf{W}_{\mathbb{D}})^H \mathbf{M} \right] \\
&\quad \times (\text{diag}(\mathbb{D})) \mathbf{V}_{\mathbb{D}} \mathbf{P} \\
&= \mathbf{G}_0^H \boldsymbol{\Pi}_{\mathbf{M} \mathbf{W}_{\mathbb{D}}}^{\perp} \mathbf{G}_0, \quad \text{where } \mathbf{G}_0 = \mathbf{M}(\text{diag}(\mathbb{D})) \mathbf{V}_{\mathbb{D}} \mathbf{P}. \tag{6.76}
\end{aligned}$$

Proof of Lemma 6.4.3

(Sufficiency) Combining (6.68) and (6.32) yields

$$\begin{aligned}
\mathbf{G} &= (\mathbf{R}_{\mathbb{S}}^T \otimes \mathbf{R}_{\mathbb{S}})^{-\frac{1}{2}} \mathbf{J} \left[p_1 \frac{\partial \mathbf{v}_{\mathbb{D}}(\bar{\theta}_1)}{\partial \theta_1} \quad \dots \quad p_D \frac{\partial \mathbf{v}_{\mathbb{D}}(\bar{\theta}_D)}{\partial \theta_D} \right] \\
&= j2\pi (\mathbf{R}_{\mathbb{S}}^T \otimes \mathbf{R}_{\mathbb{S}})^{-\frac{1}{2}} \mathbf{J} \text{diag}(\mathbb{D}) \left[p_1 \mathbf{v}_{\mathbb{D}}(\bar{\theta}_1) \quad \dots \quad p_D \mathbf{v}_{\mathbb{D}}(\bar{\theta}_D) \right] \\
&= j2\pi (\mathbf{R}_{\mathbb{S}}^T \otimes \mathbf{R}_{\mathbb{S}})^{-\frac{1}{2}} \mathbf{J} (\text{diag}(\mathbb{D})) \mathbf{V}_{\mathbb{D}} \mathbf{P}, \tag{6.74}
\end{aligned}$$

where $\mathbf{P} = \text{diag}(p_1, p_2, \dots, p_D)$. Similarly, (6.33) and (6.68) lead to

$$\begin{aligned}
\boldsymbol{\Delta} &= (\mathbf{R}_{\mathbb{S}}^T \otimes \mathbf{R}_{\mathbb{S}})^{-\frac{1}{2}} \mathbf{J} \left[\mathbf{v}_{\mathbb{D}}(\bar{\theta}_1) \quad \dots \quad \mathbf{v}_{\mathbb{D}}(\bar{\theta}_D) \quad \mathbf{e}_0 \right] \\
&= (\mathbf{R}_{\mathbb{S}}^T \otimes \mathbf{R}_{\mathbb{S}})^{-\frac{1}{2}} \mathbf{J} \mathbf{W}_{\mathbb{D}}. \tag{6.75}
\end{aligned}$$

Substituting (6.74) and (6.75) into $\mathbf{G}^H \boldsymbol{\Pi}_{\Delta}^{\perp} \mathbf{G} / (4\pi^2)$ gives (6.76), where the matrix \mathbf{M} is defined in Corollary 6.A.1.

Let $\mathbf{u} \in \mathbb{C}^D$. Since the projection matrix $\boldsymbol{\Pi}_{\mathbf{M} \mathbf{W}_{\mathbb{D}}}^{\perp}$ is Hermitian and idempotent [60], [106], it can be deduced from (6.76) that

$$\mathbf{u}^H \left(\frac{\mathbf{G}^H \boldsymbol{\Pi}_{\Delta}^{\perp} \mathbf{G}}{4\pi^2} \right) \mathbf{u} = \left\| \boldsymbol{\Pi}_{\mathbf{M} \mathbf{W}_{\mathbb{D}}}^{\perp} \mathbf{G}_0 \mathbf{u} \right\|_2^2 \geq 0.$$

The equality holds only if $\boldsymbol{\Pi}_{\mathbf{M} \mathbf{W}_{\mathbb{D}}}^{\perp} \mathbf{G}_0 \mathbf{u} = \mathbf{0}$, i.e., only if there exists a vector $\mathbf{v} \in \mathbb{C}^{D+1}$ such that

$$\mathbf{M}(\text{diag}(\mathbb{D})) \mathbf{V}_{\mathbb{D}} \mathbf{P} \mathbf{u} = \mathbf{M} \mathbf{W}_{\mathbb{D}} \mathbf{v}. \tag{6.77}$$

Since \mathbf{M} is positive definite, (6.77) can be expressed as

$$\underbrace{\begin{bmatrix} \text{diag}(\mathbb{D}) \mathbf{V}_{\mathbb{D}} & \mathbf{W}_{\mathbb{D}} \end{bmatrix}}_{\mathbf{A}_c} \begin{bmatrix} \mathbf{P} \mathbf{u} \\ -\mathbf{v} \end{bmatrix} = \mathbf{0},$$

where \mathbf{A}_c is the ACM matrix, as defined in Definition 6.4.1. If $\text{rank}(\mathbf{A}_c) = 2D + 1$, then $\mathbf{P}\mathbf{u} = \mathbf{0}$, implying $\mathbf{u} = \mathbf{0}$. As a result, $\mathbf{G}^H \mathbf{\Pi}_\Delta^\perp \mathbf{G}$ is positive definite.

(*Necessity*) If $\text{rank}(\mathbf{A}_c) < 2D + 1$, then there exists $\mathbf{a} \in \mathbb{C}^D$ and $\mathbf{b} \in \mathbb{C}^{D+1}$ such that $[\mathbf{a}^T, \mathbf{b}^T]^T \neq \mathbf{0}$ and

$$\text{diag}(\mathbb{D})\mathbf{V}_\mathbb{D}\mathbf{a} + \mathbf{W}_\mathbb{D}\mathbf{b} = \mathbf{0}. \quad (6.78)$$

Left multiplying (6.78) by \mathbf{M} leads to an expression similar to (6.77):

$$(\mathbf{M}(\text{diag}(\mathbb{D}))\mathbf{V}_\mathbb{D}\mathbf{P})(\mathbf{P}^{-1}\mathbf{a}) = (\mathbf{M}\mathbf{W}_\mathbb{D})(-\mathbf{b}), \quad (6.79)$$

where $\mathbf{P} = \text{diag}(p_1, \dots, p_D)$ is positive definite. If $\mathbf{a} \neq \mathbf{0}$, then we have $\mathbf{P}^{-1}\mathbf{a} \neq \mathbf{0}$, $\mathbf{\Pi}_{\mathbf{M}\mathbf{W}_\mathbb{D}}^\perp \mathbf{G}_0(\mathbf{P}^{-1}\mathbf{a}) = \mathbf{0}$, and $\mathbf{G}^H \mathbf{\Pi}_\Delta^\perp \mathbf{G}$ is not positive definite. On the other hand, if $\mathbf{a} = \mathbf{0}$ and $\mathbf{b} \neq \mathbf{0}$, then (6.79) becomes $\mathbf{W}_\mathbb{D}\mathbf{b} = \mathbf{0}$, which contradicts with the assumption that $\text{rank}(\mathbf{W}_\mathbb{D}) = D + 1$. These arguments complete the proof.

6.B Definition of \mathbf{J}

Definition 6.B.1. The binary matrix \mathbf{J} has size $|\mathbb{S}|^2$ -by- $|\mathbb{D}|$ such that the column of \mathbf{J} associated with the difference m is given by

$$\langle \mathbf{J} \rangle_{:,m} = \text{vec}(\mathbf{I}(m)), \quad m \in \mathbb{D},$$

where the $|\mathbb{S}|$ -by- $|\mathbb{S}|$ matrix $\mathbf{I}(m)$ satisfies

$$\langle \mathbf{I}(m) \rangle_{n_1, n_2} = \begin{cases} 1 & \text{if } n_1 - n_2 = m, \\ 0 & \text{otherwise.} \end{cases} \quad n_1, n_2 \in \mathbb{S}. \quad (6.80)$$

As an example of \mathbf{J} , if $\mathbb{S} = \{0, 1, 4\}$, then $\mathbb{D} = \{-4, -3, -1, 0, 1, 3, 4\}$, and $\mathbf{I}(m)$ are

$$\mathbf{I}(m=0) = \begin{array}{c} n_2 = 0 \quad 1 \quad 4 \\ n_1 = 0 \\ 1 \\ 4 \end{array} \begin{bmatrix} 1 & 0 & 0 \\ 0 & 1 & 0 \\ 0 & 0 & 1 \end{bmatrix},$$

$$\mathbf{I}(m=1) = \begin{array}{c} n_2 = 0 \quad 1 \quad 4 \\ n_1 = 0 \\ 1 \\ 4 \end{array} \begin{bmatrix} 0 & 0 & 0 \\ 1 & 0 & 0 \\ 0 & 0 & 0 \end{bmatrix},$$

$$\mathbf{I}(m=3) = \begin{array}{c} n_2 = 0 \quad 1 \quad 4 \\ n_1 = 0 \\ 1 \\ 4 \end{array} \begin{bmatrix} 0 & 0 & 0 \\ 0 & 0 & 0 \\ 0 & 1 & 0 \end{bmatrix},$$

$$\mathbf{I}(m=4) = \begin{array}{c} n_2 = 0 \quad 1 \quad 4 \\ n_1 = 0 \\ 1 \\ 4 \end{array} \begin{bmatrix} 0 & 0 & 0 \\ 0 & 0 & 0 \\ 1 & 0 & 0 \end{bmatrix},$$

and $\mathbf{I}(-1) = \mathbf{I}(1)^T$, $\mathbf{I}(-3) = \mathbf{I}(3)^T$, and $\mathbf{I}(-4) = \mathbf{I}(4)^T$. As a result, \mathbf{J} is given by

$$\mathbf{J} = \begin{array}{c} m = -4 \quad -3 \quad -1 \quad 0 \quad 1 \quad 3 \quad 4 \\ \left[\begin{array}{ccccccc} 0 & 0 & 0 & 1 & 0 & 0 & 0 \\ 0 & 0 & 0 & 0 & 1 & 0 & 0 \\ 0 & 0 & 0 & 0 & 0 & 0 & 1 \\ 0 & 0 & 1 & 0 & 0 & 0 & 0 \\ 0 & 0 & 0 & 1 & 0 & 0 & 0 \\ 0 & 0 & 0 & 0 & 0 & 1 & 0 \\ 1 & 0 & 0 & 0 & 0 & 0 & 0 \\ 0 & 1 & 0 & 0 & 0 & 0 & 0 \\ 0 & 0 & 0 & 1 & 0 & 0 & 0 \end{array} \right]. \end{array}$$

The following propositions of \mathbf{J} are useful:

Proposition 6.B.1. \mathbf{J} has full column rank, i.e., $\text{rank}(\mathbf{J}) = |\mathbb{D}|$.

Proof. It suffices to prove that $\{\mathbf{I}(m)\}_{m \in \mathbb{D}}$ is a linearly independent set. Consider the linear equation $\sum_{m \in \mathbb{D}} c_m \mathbf{I}(m) = \mathbf{0}$. Suppose there exists $P \in \mathbb{D}$ such that $c_P \neq 0$.

For any $n_1, n_2 \in \mathbb{S}$ such that $n_1 - n_2 = P$, it can be deduced that

$$\begin{aligned} 0 &= \langle \mathbf{0} \rangle_{n_1, n_2} = \left\langle \sum_{m \in \mathbb{D}} c_m \mathbf{I}(m) \right\rangle_{n_1, n_2} \\ &= \sum_{m \in \mathbb{D}} c_m \langle \mathbf{I}(m) \rangle_{n_1, n_2} = c_P, \end{aligned}$$

which contradicts $c_P \neq 0$. Hence, the coefficients c_m are all zero, implying \mathbf{J} has full column rank. \square

Proposition 6.B.2. With \mathbf{J} as in Definition 6.B.1, we have $\mathbf{v}_{\mathbb{S}}^*(\bar{\theta}_i) \otimes \mathbf{v}_{\mathbb{S}}(\bar{\theta}_i) = \mathbf{J}\mathbf{v}_{\mathbb{D}}(\bar{\theta}_i)$.

Proof. Letting $\alpha_i = e^{j2\pi\bar{\theta}_i}$ and starting with the right-hand side of the equation yield

$$\mathbf{J}\mathbf{v}_{\mathbb{D}}(\bar{\theta}_i) = \sum_{m \in \mathbb{D}} \text{vec}(\mathbf{I}(m)) \alpha_i^m = \text{vec} \left(\sum_{m \in \mathbb{D}} \mathbf{I}(m) \alpha_i^m \right).$$

The (n_1, n_2) entry of $\sum_{m \in \mathbb{D}} \mathbf{I}(m) \alpha_i^m$ is

$$\left\langle \sum_{m \in \mathbb{D}} \mathbf{I}(m) \alpha_i^m \right\rangle_{n_1, n_2} = \sum_{m \in \mathbb{D}} \langle \mathbf{I}(m) \rangle_{n_1, n_2} \alpha_i^m = \alpha_i^{n_1} (\alpha_i^{n_2})^*,$$

so that $\sum_{m \in \mathbb{D}} \mathbf{I}(m) \alpha_i^m = \mathbf{v}_{\mathbb{S}}(\bar{\theta}_i) \mathbf{v}_{\mathbb{S}}^H(\bar{\theta}_i)$. Therefore, $\mathbf{J}\mathbf{v}_{\mathbb{D}}(\bar{\theta}_i) = \text{vec}(\mathbf{v}_{\mathbb{S}}(\bar{\theta}_i) \mathbf{v}_{\mathbb{S}}^H(\bar{\theta}_i)) = \mathbf{v}_{\mathbb{S}}^*(\bar{\theta}_i) \otimes \mathbf{v}_{\mathbb{S}}(\bar{\theta}_i)$, which proves the proposition. \square

Corollary 6.B.1. $\text{vec}(\mathbf{I}) = \mathbf{J}\mathbf{e}_0$, where $\mathbf{e}_0 \in \{0, 1\}^{|\mathbb{D}|}$ satisfying

$$\langle \mathbf{e}_0 \rangle_m = \begin{cases} 1, & \text{if } m = 0, \\ 0, & \text{otherwise,} \end{cases} \quad m \in \mathbb{D}.$$

6.C Proof of the Asymptotic CRB Expression for Large SNR

Proof of Theorem 6.5.1

According to Proposition 6.5.2, the CRB expression depends on the SNR p/p_n , so without loss of generality, we set $p_n = 1$. For sufficiently large SNR, p is much greater than p_n , so that $\mathbf{R}_{\mathbb{S}}$ can be approximated by $p\mathbf{U}_s\mathbf{\Lambda}\mathbf{U}_s^H + \mathbf{U}_n\mathbf{U}_n^H$ and $\mathbf{R}_{\mathbb{S}}^{-1}$ approaches $p^{-1}\mathbf{U}_s\mathbf{\Lambda}^{-1}\mathbf{U}_s^H + \mathbf{U}_n\mathbf{U}_n^H$ asymptotically. The quantity $\mathbf{R}_{\mathbb{S}}^{-T} \otimes \mathbf{R}_{\mathbb{S}}^{-1}$ can be expressed as

$$\mathbf{R}_{\mathbb{S}}^{-T} \otimes \mathbf{R}_{\mathbb{S}}^{-1} = \mathbf{A} + p^{-1}\mathbf{B} + p^{-2}\mathbf{C},$$

where \mathbf{A} , \mathbf{B} , and \mathbf{C} are defined as

$$\mathbf{A} = (\mathbf{U}_n \mathbf{U}_n^H)^T \otimes (\mathbf{U}_n \mathbf{U}_n^H), \quad (6.81)$$

$$\mathbf{B} = [(\mathbf{U}_s \mathbf{\Lambda}^{-1} \mathbf{U}_s^H)^T \otimes (\mathbf{U}_n \mathbf{U}_n^H) + (\mathbf{U}_n \mathbf{U}_n^H)^T \otimes (\mathbf{U}_s \mathbf{\Lambda}^{-1} \mathbf{U}_s^H)], \quad (6.82)$$

$$\mathbf{C} = (\mathbf{U}_s \mathbf{\Lambda}^{-1} \mathbf{U}_s^H)^T \otimes (\mathbf{U}_s \mathbf{\Lambda}^{-1} \mathbf{U}_s^H). \quad (6.83)$$

For large p , $\mathbf{R}_S^{-T} \otimes \mathbf{R}_S^{-1}$ can be approximated by

$$\mathbf{R}_S^{-T} \otimes \mathbf{R}_S^{-1} \xrightarrow{\text{large } p} \mathbf{A} + p^{-1}\mathbf{B}. \quad (6.84)$$

The following corollaries show two identities regarding \mathbf{A} :

Corollary 6.C.1. $\mathbf{A}\mathbf{J}(\text{diag}(\mathbb{D}))\mathbf{V}_\mathbb{D} = \mathbf{0}$, where \mathbf{A} and \mathbf{J} are given in (6.81) and Definition 6.B.1, respectively.

Proof. According to Definition 6.B.1, the i th column of $\mathbf{A}\mathbf{J}(\text{diag}(\mathbb{D}))\mathbf{V}_\mathbb{D}$ can be expressed as

$$\mathbf{A}\mathbf{J}(\text{diag}(\mathbb{D}))\mathbf{v}_\mathbb{D}(\bar{\theta}_i) = \mathbf{A} \text{vec} \left(\sum_{m \in \mathbb{D}} \mathbf{I}(m) m \alpha_i^m \right), \quad (6.85)$$

where $\alpha_i = e^{j2\pi\bar{\theta}_i}$. The matrix $\mathbf{I}(m)$ is defined in Definition 6.B.1. The (n_1, n_2) entry of $\sum_{m \in \mathbb{D}} \mathbf{I}(m) m \alpha_i^m$ becomes

$$\left\langle \sum_{m \in \mathbb{D}} \mathbf{I}(m) m \alpha_i^m \right\rangle_{n_1, n_2} = n_1 \alpha_i^{n_1} (\alpha_i^{n_2})^* - \alpha_i^{n_1} (\alpha_i^{n_2})^* n_2,$$

so that

$$\begin{aligned} & \sum_{m \in \mathbb{D}} \mathbf{I}(m) m \alpha_i^m \\ &= \text{diag}(\mathbb{S}) \mathbf{v}_\mathbb{S}(\bar{\theta}_i) \mathbf{v}_\mathbb{S}^H(\bar{\theta}_i) - \mathbf{v}_\mathbb{S}(\bar{\theta}_i) \mathbf{v}_\mathbb{S}^H(\bar{\theta}_i) (\text{diag}(\mathbb{S})). \end{aligned} \quad (6.86)$$

Substituting (6.86) into (6.85) yields

$$\begin{aligned} & \mathbf{A}\mathbf{J}(\text{diag}(\mathbb{D}))\mathbf{v}_\mathbb{D}(\bar{\theta}_i) \\ &= [(\mathbf{U}_n \mathbf{U}_n^H)^T \otimes (\mathbf{U}_n \mathbf{U}_n^H)] \\ & \quad \times \text{vec}(\text{diag}(\mathbb{S}) \mathbf{v}_\mathbb{S}(\bar{\theta}_i) \mathbf{v}_\mathbb{S}^H(\bar{\theta}_i) - \mathbf{v}_\mathbb{S}(\bar{\theta}_i) \mathbf{v}_\mathbb{S}^H(\bar{\theta}_i) (\text{diag}(\mathbb{S}))) \\ &= \text{vec}(\mathbf{U}_n \mathbf{U}_n^H (\text{diag}(\mathbb{S})) \mathbf{v}_\mathbb{S}(\bar{\theta}_i) \underbrace{\mathbf{v}_\mathbb{S}^H(\bar{\theta}_i) \mathbf{U}_n \mathbf{U}_n^H}_{\mathbf{0}}) \\ & \quad - \text{vec}(\mathbf{U}_n \underbrace{\mathbf{U}_n^H \mathbf{v}_\mathbb{S}(\bar{\theta}_i)}_{\mathbf{0}} \mathbf{v}_\mathbb{S}^H(\bar{\theta}_i) (\text{diag}(\mathbb{S})) \mathbf{U}_n \mathbf{U}_n^H) = \mathbf{0}, \end{aligned}$$

where the identity $(\mathbf{C}^T \otimes \mathbf{A})\text{vec}(\mathbf{B}) = \text{vec}(\mathbf{ABC})$ is utilized. Hence we have the relation $\mathbf{A}\mathbf{J}(\text{diag}(\mathbb{D}))\mathbf{V}_\mathbb{D} = \mathbf{0}$. \square

Corollary 6.C.2. $\mathbf{W}_\mathbb{D}^H \mathbf{J}^H \mathbf{A} \mathbf{J} \mathbf{W}_\mathbb{D} = (\text{rank}(\mathbf{U}_n)) \mathbf{e}_{D+1} \mathbf{e}_{D+1}^H$, where \mathbf{e}_{D+1} is defined in (6.53).

Proof. For $1 \leq i, j \leq D$, the (i, j) th entry of $\mathbf{W}_{\mathbb{D}}^H \mathbf{J}^H \mathbf{A} \mathbf{J} \mathbf{W}_{\mathbb{D}}$ can be simplified as

$$\begin{aligned}
& [\mathbf{W}_{\mathbb{D}}^H \mathbf{J}^H \mathbf{A} \mathbf{J} \mathbf{W}_{\mathbb{D}}]_{i,j} \\
&= \mathbf{v}_{\mathbb{D}}^H(\bar{\theta}_i) \mathbf{J}^H \mathbf{A} \mathbf{J} \mathbf{v}_{\mathbb{D}}(\bar{\theta}_j) \\
&= [\mathbf{v}_{\mathbb{S}}^T(\bar{\theta}_i) \otimes \mathbf{v}_{\mathbb{S}}^H(\bar{\theta}_i)] [(\mathbf{U}_n \mathbf{U}_n^H)^T \otimes (\mathbf{U}_n \mathbf{U}_n^H)] [\mathbf{v}_{\mathbb{S}}^*(\bar{\theta}_j) \otimes \mathbf{v}_{\mathbb{S}}(\bar{\theta}_j)] \\
&= (\mathbf{v}_{\mathbb{S}}^H(\bar{\theta}_j) \mathbf{U}_n \mathbf{U}_n^H \mathbf{v}_{\mathbb{S}}(\bar{\theta}_i))^T \otimes (\mathbf{v}_{\mathbb{S}}^H(\bar{\theta}_i) \mathbf{U}_n \mathbf{U}_n^H \mathbf{v}_{\mathbb{S}}(\bar{\theta}_j)) = 0.
\end{aligned}$$

The $(i, D+1)$ th entry of $\mathbf{W}_{\mathbb{D}}^H \mathbf{J}^H \mathbf{A} \mathbf{J} \mathbf{W}_{\mathbb{D}}$ becomes

$$\begin{aligned}
& [\mathbf{W}_{\mathbb{D}}^H \mathbf{J}^H \mathbf{A} \mathbf{J} \mathbf{W}_{\mathbb{D}}]_{i,D+1} \\
&= \mathbf{v}_{\mathbb{D}}^H(\bar{\theta}_i) \mathbf{J}^H \mathbf{A} \mathbf{J} \mathbf{e}_0 \\
&= [\mathbf{v}_{\mathbb{S}}^T(\bar{\theta}_i) \otimes \mathbf{v}_{\mathbb{S}}^H(\bar{\theta}_i)] [(\mathbf{U}_n \mathbf{U}_n^H)^T \otimes (\mathbf{U}_n \mathbf{U}_n^H)] \text{vec}(\mathbf{I}) \\
&= \text{vec}(\mathbf{v}_{\mathbb{S}}^H(\bar{\theta}_i) \mathbf{U}_n \mathbf{U}_n^H \mathbf{U}_n \mathbf{U}_n^H \mathbf{v}_{\mathbb{S}}(\bar{\theta}_i)) = 0.
\end{aligned}$$

Similarly, the $(D+1, j)$ th entry of $\mathbf{W}_{\mathbb{D}}^H \mathbf{J}^H \mathbf{A} \mathbf{J} \mathbf{W}_{\mathbb{D}}$ is also zero. Finally the $(D+1, D+1)$ th entry of $\mathbf{W}_{\mathbb{D}}^H \mathbf{J}^H \mathbf{A} \mathbf{J} \mathbf{W}_{\mathbb{D}}$ is given by

$$\begin{aligned}
& [\mathbf{W}_{\mathbb{D}}^H \mathbf{J}^H \mathbf{A} \mathbf{J} \mathbf{W}_{\mathbb{D}}]_{D+1,D+1} \\
&= \text{vec}(\mathbf{I})^H [(\mathbf{U}_n \mathbf{U}_n^H)^T \otimes (\mathbf{U}_n \mathbf{U}_n^H)] \text{vec}(\mathbf{I}) \\
&= \text{tr}(\mathbf{U}_n \mathbf{U}_n^H \mathbf{I} \mathbf{U}_n \mathbf{U}_n^H \mathbf{I}) = \text{rank}(\mathbf{U}_n),
\end{aligned}$$

since $\text{tr}(\mathbf{ABCD}) = \text{vec}(\mathbf{B}^H)^H (\mathbf{A}^T \otimes \mathbf{C}) \text{vec}(\mathbf{D})$ and $\text{tr}(\mathbf{AB}) = \text{tr}(\mathbf{BA})$. \square

To evaluate the asymptotic expression of the CRB, we first consider the inverse of $\mathbf{W}_{\mathbb{D}}^H \mathbf{M}^2 \mathbf{W}_{\mathbb{D}}$, based on (6.84) and Corollary 6.C.2:

$$\begin{aligned}
& (\mathbf{W}_{\mathbb{D}}^H \mathbf{M}^2 \mathbf{W}_{\mathbb{D}})^{-1} \\
& \xrightarrow{\text{large } p} (\mathbf{W}_{\mathbb{D}}^H \mathbf{J}^H \mathbf{A} \mathbf{J} \mathbf{W}_{\mathbb{D}} + p^{-1} \mathbf{W}_{\mathbb{D}}^H \mathbf{J}^H \mathbf{B} \mathbf{J} \mathbf{W}_{\mathbb{D}})^{-1} \\
&= (p^{-1} \mathbf{W}_{\mathbb{D}}^H \mathbf{J}^H \mathbf{B} \mathbf{J} \mathbf{W}_{\mathbb{D}} + \text{rank}(\mathbf{U}_n) \mathbf{e}_{D+1} \mathbf{e}_{D+1}^H)^{-1} \\
&= p (\mathbf{W}_{\mathbb{D}}^H \mathbf{M}_{\infty}^2 \mathbf{W}_{\mathbb{D}} + \text{rank}(\mathbf{U}_n) p \times \mathbf{e}_{D+1} \mathbf{e}_{D+1}^H)^{-1}, \tag{6.87}
\end{aligned}$$

where \mathbf{M}_{∞} is the positive definite squared root of $\mathbf{J}^H \mathbf{B} \mathbf{J}$, as defined in (6.50).

To be more rigorous, we need to show that $\mathbf{J}^H \mathbf{B} \mathbf{J}$ is positive semidefinite. Since $\mathbf{U}_s \mathbf{\Lambda}^{-1} \mathbf{U}_s^H$ and $\mathbf{U}_n \mathbf{U}_n^H$ are both positive semidefinite, $(\mathbf{U}_s \mathbf{\Lambda}^{-1} \mathbf{U}_s^H)^T \otimes (\mathbf{U}_n \mathbf{U}_n^H)$ and $(\mathbf{U}_n \mathbf{U}_n^H)^T \otimes (\mathbf{U}_s \mathbf{\Lambda}^{-1} \mathbf{U}_s^H)$ are also positive semidefinite [106]. Then, according to (6.82), \mathbf{B} is a sum of two positive semidefinite matrices, implying \mathbf{B} is also positive semidefinite [106]. These arguments prove the existence of \mathbf{M}_{∞} .

If $\mathbf{W}_{\mathbb{D}}^H \mathbf{M}_{\infty}^2 \mathbf{W}_{\mathbb{D}}$ has full rank, then applying the matrix inversion lemma [60] to (6.87) leads to

$$\begin{aligned} & (\mathbf{W}_{\mathbb{D}}^H \mathbf{M}^2 \mathbf{W}_{\mathbb{D}})^{-1} \\ \xrightarrow{\text{large } p} & p \left((\mathbf{W}_{\mathbb{D}}^H \mathbf{M}_{\infty}^2 \mathbf{W}_{\mathbb{D}})^{-1} - \frac{(\mathbf{W}_{\mathbb{D}}^H \mathbf{M}_{\infty}^2 \mathbf{W}_{\mathbb{D}})^{-1} \mathbf{e}_{D+1} \mathbf{e}_{D+1}^H (\mathbf{W}_{\mathbb{D}}^H \mathbf{M}_{\infty}^2 \mathbf{W}_{\mathbb{D}})^{-1}}{(\text{rank}(\mathbf{U}_n)p)^{-1} + \mathbf{e}_{D+1}^H (\mathbf{W}_{\mathbb{D}}^H \mathbf{M}_{\infty}^2 \mathbf{W}_{\mathbb{D}})^{-1} \mathbf{e}_{D+1}} \right) \\ \xrightarrow{\text{large } p} & p \left((\mathbf{W}_{\mathbb{D}}^H \mathbf{M}_{\infty}^2 \mathbf{W}_{\mathbb{D}})^{-1} - \frac{(\mathbf{W}_{\mathbb{D}}^H \mathbf{M}_{\infty}^2 \mathbf{W}_{\mathbb{D}})^{-1} \mathbf{e}_{D+1} \mathbf{e}_{D+1}^H (\mathbf{W}_{\mathbb{D}}^H \mathbf{M}_{\infty}^2 \mathbf{W}_{\mathbb{D}})^{-1}}{\mathbf{e}_{D+1}^H (\mathbf{W}_{\mathbb{D}}^H \mathbf{M}_{\infty}^2 \mathbf{W}_{\mathbb{D}})^{-1} \mathbf{e}_{D+1}} \right), \end{aligned} \quad (6.88)$$

where it is assumed that $\mathbf{e}_{D+1}^H (\mathbf{W}_{\mathbb{D}}^H \mathbf{M}_{\infty}^2 \mathbf{W}_{\mathbb{D}})^{-1} \mathbf{e}_{D+1}$ is not zero. Next, we consider the asymptotic expression of $\mathbf{G}_0^H \mathbf{G}_0$ for large SNR,

$$\begin{aligned} & \mathbf{G}_0^H \mathbf{G}_0 \\ \xrightarrow{\text{large } p} & p^2 \mathbf{V}_{\mathbb{D}}^H (\text{diag}(\mathbb{D})) \mathbf{J}^H (\mathbf{A} + p^{-1} \mathbf{B}) \mathbf{J} (\text{diag}(\mathbb{D})) \mathbf{V}_{\mathbb{D}} \\ = & p \mathbf{V}_{\mathbb{D}}^H (\text{diag}(\mathbb{D})) \mathbf{J}^H \mathbf{B} \mathbf{J} (\text{diag}(\mathbb{D})) \mathbf{V}_{\mathbb{D}} = p \mathbf{G}_{\infty}^H \mathbf{G}_{\infty}, \end{aligned} \quad (6.89)$$

due to Corollary 6.C.1. Here \mathbf{G}_{∞} is defined in (6.51). Similarly, $(\mathbf{M} \mathbf{W}_{\mathbb{D}})^H \mathbf{G}_0$ has an asymptotic expression,

$$\begin{aligned} (\mathbf{M} \mathbf{W}_{\mathbb{D}})^H \mathbf{G}_0 & \xrightarrow{\text{large } p} \mathbf{W}_{\mathbb{D}}^H \mathbf{J}^H (\mathbf{A} + p^{-1} \mathbf{B}) \mathbf{J} (\text{diag}(\mathbb{D})) \mathbf{V}_{\mathbb{D}} (p \mathbf{I}) \\ & = (\mathbf{M}_{\infty} \mathbf{W}_{\mathbb{D}})^H \mathbf{G}_{\infty}. \end{aligned} \quad (6.90)$$

Substituting (6.88), (6.89), and (6.90) into (6.40) yields (6.48).

Proof of Theorem 6.5.2

Since $\mathbf{V}_{\mathbb{S}}$ has full row rank, $\mathbf{V}_{\mathbb{S}} \mathbf{V}_{\mathbb{S}}^H$ is nonsingular. It can be inferred from (6.43) that

$$\begin{aligned} \mathbf{R}_{\mathbb{S}}^{-1} & \xrightarrow{\text{large } p} (p \mathbf{V}_{\mathbb{S}} \mathbf{V}_{\mathbb{S}}^H)^{-1}, \\ \mathbf{M} & \xrightarrow{\text{large } p} (\mathbf{J}^H ((p \mathbf{V}_{\mathbb{S}} \mathbf{V}_{\mathbb{S}}^H)^{-T} \otimes (p \mathbf{V}_{\mathbb{S}} \mathbf{V}_{\mathbb{S}}^H)^{-1}) \mathbf{J})^{\frac{1}{2}} = \frac{\mathbf{M}_{\infty}}{p}, \\ \mathbf{G} & \xrightarrow{\text{large } p} \frac{\mathbf{M}_{\infty}}{p} (\text{diag}(\mathbb{D})) \mathbf{V}_{\mathbb{D}} (p \mathbf{I}) = \mathbf{G}_{\infty}. \end{aligned}$$

Replacing \mathbf{M} and \mathbf{G}_0 with their limits in (6.40) proves this theorem.

6.D Proof of Theorem 6.6.1

To prove that $\text{rank}(\mathbf{A}_c) = 2D + 1$, it suffices to show that, there exists a $(2D + 1) \times (2D + 1)$ full rank submatrix. Since $D \leq (|\mathbb{U}| - 1)/2$, the following matrix \mathbf{S}_0 is a

submatrix of \mathbf{A}_c ,

$$\mathbf{S}_0 = \begin{bmatrix} -D\alpha_1^{-D} & \dots & -D\alpha_D^{-D} & \alpha_1^{-D} & \dots & \alpha_D^{-D} & 0 \\ \vdots & \ddots & \vdots & \vdots & \ddots & \vdots & \vdots \\ -2\alpha_1^{-2} & \dots & -2\alpha_D^{-2} & \alpha_1^{-2} & \dots & \alpha_D^{-2} & 0 \\ -\alpha_1^{-1} & \dots & -\alpha_D^{-1} & \alpha_1^{-1} & \dots & \alpha_D^{-1} & 0 \\ 0 & \dots & 0 & 1 & \dots & 1 & 1 \\ \alpha_1 & \dots & \alpha_D & \alpha_1 & \dots & \alpha_D & 0 \\ 2\alpha_1^2 & \dots & 2\alpha_D^2 & \alpha_1^2 & \dots & \alpha_D^2 & 0 \\ \vdots & \ddots & \vdots & \vdots & \ddots & \vdots & \vdots \\ D\alpha_1^D & \dots & D\alpha_D^D & \alpha_1^D & \dots & \alpha_D^D & 0 \end{bmatrix},$$

where $\alpha_i = e^{j2\pi\bar{\theta}_i}$ for $i = 1, 2, \dots, D$. It will be shown that $\text{rank}(\mathbf{S}_0) = 2D + 1$.

Consider another matrix \mathbf{S}_1 , defined as

$$\mathbf{S}_1 = \mathbf{S}_0 \underbrace{\begin{bmatrix} \mathbf{L}_{1,1} & \mathbf{0} & \mathbf{0} \\ \mathbf{L}_{2,1} & \mathbf{L}_{2,2} & \mathbf{0} \\ \mathbf{0}^T & \mathbf{0}^T & 1 \end{bmatrix}}_{\mathbf{L}}, \quad (6.91)$$

where the matrices $\mathbf{L}_{1,1}$, $\mathbf{L}_{2,1}$, and $\mathbf{L}_{2,2}$ are given by

$$\begin{aligned} \mathbf{L}_{1,1} &= \text{diag}(\alpha_1^{D-1}, \alpha_2^{D-1}, \dots, \alpha_D^{D-1}), \\ \mathbf{L}_{2,1} &= \text{diag}(D\alpha_1^{D-1}, D\alpha_2^{D-1}, \dots, D\alpha_D^{D-1}), \\ \mathbf{L}_{2,2} &= \text{diag}(\alpha_1^D, \alpha_2^D, \dots, \alpha_D^D). \end{aligned}$$

\mathbf{S}_0 , \mathbf{S}_1 , and \mathbf{L} are square matrices of size $2D + 1$. Expanding (6.91) results in

$$\mathbf{S}_1 = \begin{bmatrix} 0 & \dots & 0 & 1 & \dots & 1 & 0 \\ 1 & \dots & 1 & \alpha_1 & \dots & \alpha_D & 0 \\ 2\alpha_1 & \dots & 2\alpha_D & \alpha_1^2 & \dots & \alpha_D^2 & 0 \\ \vdots & \ddots & \vdots & \vdots & \ddots & \vdots & \vdots \\ (D-1)\alpha_1^{D-2} & \dots & (D-1)\alpha_D^{D-2} & \alpha_1^{D-1} & \dots & \alpha_D^{D-1} & 0 \\ D\alpha_1^{D-1} & \dots & D\alpha_D^{D-1} & \alpha_1^D & \dots & \alpha_D^D & 1 \\ (D+1)\alpha_1^D & \dots & (D+1)\alpha_D^D & \alpha_1^{D+1} & \dots & \alpha_D^{D+1} & 0 \\ \vdots & \ddots & \vdots & \vdots & \ddots & \vdots & \vdots \\ 2D\alpha_1^{2D-1} & \dots & 2D\alpha_D^{2D-1} & \alpha_1^{2D} & \dots & \alpha_D^{2D} & 0 \end{bmatrix}.$$

It holds true that $\text{rank}(\mathbf{S}_0) = \text{rank}(\mathbf{S}_1)$, since the lower triangular matrix \mathbf{L} has non-zero diagonal entries.

Next, it will be shown that \mathbf{S}_1 has full rank. Let $\mathbf{h} = [h_0, h_1, \dots, h_{2D}]^T$ satisfy $\mathbf{h}^T \mathbf{S}_1 = \mathbf{0}$. Define a polynomial $H(z) = \sum_{n=0}^{2D} h_n z^n$. Then $\mathbf{h}^T \mathbf{S}_1 = \mathbf{0}$ is equivalent to

$$H'(\alpha_1) = \dots = H'(\alpha_D) = 0, \quad (6.92)$$

$$H(\alpha_1) = \dots = H(\alpha_D) = 0, \quad (6.93)$$

$$h_D = 0, \quad (6.94)$$

where $H'(z) = (d/dz)H(z) = \sum_{n=0}^{2D} h_n (nz^{n-1})$. Since the DOAs are distinct, (6.92) and (6.93) indicate $H(z)$ can be expressed as

$$H(z) = K \prod_{i=1}^D (z - \alpha_i)^2 = K_0 z^D \underbrace{\prod_{i=1}^D \left(\frac{\alpha_i}{z} - 2 + \frac{z}{\alpha_i} \right)}_{G(z)}, \quad (6.95)$$

where $K_0 = K \prod_{i=1}^D \alpha_i$ for some constant K . Eqs. (6.94) and (6.95) imply

$$\begin{aligned} 0 &= K_0 \times (\text{Constant term of } G(z)) \\ &= K_0 \int_{-\frac{1}{2}}^{\frac{1}{2}} G(e^{j2\pi\bar{\theta}}) d\bar{\theta} \\ &= K_0 \int_{-\frac{1}{2}}^{\frac{1}{2}} \prod_{i=1}^D \left(e^{-j2\pi(\bar{\theta} - \bar{\theta}_i)} - 2 + e^{j2\pi(\bar{\theta} - \bar{\theta}_i)} \right) d\bar{\theta}, \end{aligned} \quad (6.96)$$

where the constant term is based on the inverse discrete-time Fourier transform of $G(e^{j2\pi\bar{\theta}})$ [181]. (6.96) can be simplified as

$$0 = K_0 (-2)^D \int_{-\frac{1}{2}}^{\frac{1}{2}} \underbrace{\left(\prod_{i=1}^D (1 - \cos 2\pi(\bar{\theta} - \bar{\theta}_i)) \right)}_{\geq 0} d\bar{\theta}.$$

Since the integrand is nonnegative, this integral is strictly positive, implying $K_0 = K = 0$ and $\mathbf{h} = \mathbf{0}$. Hence, $2D + 1 = \text{rank}(\mathbf{S}_1) = \text{rank}(\mathbf{S}_0) = \text{rank}(\mathbf{A}_c)$.

CORRELATION SUBSPACES: GENERALIZATIONS AND CONNECTION TO DIFFERENCE COARRAYS

7.1 Introduction

In Chapter 2, we discussed DOA estimation using sparse arrays. It was demonstrated that more uncorrelated sources can be resolved for some sparse arrays. More details of this property can be found in Chapter 2.

Recently, the elegant concept of *correlation subspaces* was proposed by Rahmani and Atia [141], to improve DOA estimation in a number of ways. For *any given array geometry*, the correlation subspace is uniquely determined, and imposes some implicit constraints on the structure of the covariance, as we shall see. This subspace can be utilized in denoising the sample covariance matrix. Then the source directions are estimated from the denoised covariance matrix using off-the-shelf DOA estimators, such as the MUSIC algorithm. Note that the correlation subspace depends on the array configurations and prior knowledge about the sources but is independent of the choice of DOA estimators. Hence, a broad class of DOA estimators are applicable to the denoised covariance matrix. However, the explicit expressions for the correlation subspace were not known, so its approximation was computed numerically in [141]. Furthermore, the way in which the correlation subspace is influenced by the array configuration, and by partial knowledge about sources, was not explored.

Inspired by the concept of correlation subspaces introduced in [141], this chapter makes a number of new contributions. To analyze the correlation subspace for any array configuration explicitly, we first generalize the definition in [141] to formulate what we call the *generalized correlation subspace*. This makes it possible to incorporate some types of a priori information on source locations, leading to improvements in DOA estimation. Furthermore, we show that the (generalized) correlation subspaces can be uniquely characterized in terms of the difference coarray of the original physical array. In fact we will show how to obtain simple and elegant closed form expressions for the basis vectors of the correlation subspace, in terms of the sensor geometry and the difference coarray geometry. Furthermore, if source directions belong to *a priori known intervals* [22], [31], [74], [112], [157], then it is shown that the generalized correlation subspace finds close connections to *discrete prolate spheroidal sequences* [158] defined on the difference coarrays. Similar results can be developed in multiple dimensions, and are useful in angle-Doppler estimation [8], [86], angle-delay estimation [189], angle-range estimation [138], 2D DOA estimation [188], and harmonic retrieval [53], [116]. These results not only facilitate the

implementation of the denoising framework as in [141] but also offer better understanding of several DOA estimators with prior knowledge about sources.

The original work on correlation subspaces [141] did not emphasize any knowledge about the sources except that they are uncorrelated¹. In our work, we show how to incorporate prior knowledge about source intervals with generalized correlation subspaces. Furthermore, correlation subspaces for 1D and 2D arrays were analyzed numerically in [141] while our work provides closed-form characterizations of generalized correlation subspaces for 1D and multidimensional arrays. Finally, in our work, covariance matrix denoising using the generalized correlation subspace is implemented more efficiently than that in [141].

The outline of this chapter is as follows: Section 7.2 reviews correlation subspaces. Section 7.3 proposes the generalized correlation subspaces while Section 7.4 derives their expressions for unknown and known source intervals. Section 7.5 discusses the connections with existing methods while Section 7.6 studies the generalized correlation subspace for multidimensional arrays. Section 7.7 presents several examples and numerical simulations to demonstrate the advantages of the new methods while Section 7.8 concludes this chapter.

7.2 Review of Correlation Subspaces

We begin by considering the array output equation of \mathbf{x}_S in (1.5), where the assumptions were stated in Section 1.1. Following the derivation in Section 2.3, the covariance matrix of \mathbf{x}_S can be expressed as

$$\mathbf{R}_S = E[\mathbf{x}_S \mathbf{x}_S^H] = \sum_{i=1}^D p_i \mathbf{v}_S(\bar{\theta}_i) \mathbf{v}_S^H(\bar{\theta}_i) + p_n \mathbf{I}. \quad (7.1)$$

Rearranging the elements in (7.1) leads to

$$\text{vec}(\mathbf{R}_S - p_n \mathbf{I}) = \sum_{i=1}^D p_i \mathbf{c}(\bar{\theta}_i), \quad (7.2)$$

where the correlation vectors $\mathbf{c}(\bar{\theta}_i)$ are defined as

$$\mathbf{c}(\bar{\theta}_i) \triangleq \text{vec}(\mathbf{v}_S(\bar{\theta}_i) \mathbf{v}_S^H(\bar{\theta}_i)) \in \mathbb{C}^{|\mathcal{S}|^2}. \quad (7.3)$$

The relation (7.2) implies

$$\text{vec}(\mathbf{R}_S - p_n \mathbf{I}) \in \text{span}\{\mathbf{c}(\bar{\theta}_i) : i = 1, 2, \dots, D\} \quad (7.4)$$

$$\subseteq \mathcal{CS} \triangleq \text{span}\{\mathbf{c}(\bar{\theta}) : -1/2 \leq \bar{\theta} \leq 1/2\}, \quad (7.5)$$

¹ A numerical simulation with prior knowledge about source intervals was shown in [141, Section IV-B2] but this idea was not developed further.

where the linear span in (7.5) is defined as the set of *all* vectors of the form $\sum_{p=1}^P a_p \mathbf{c}(\bar{\theta}_p)$ where $P \in \mathbb{N}$, $a_p \in \mathbb{C}$, and $-1/2 \leq \bar{\theta}_p \leq 1/2$ [60]. This subspace is called the *correlation subspace*, denoted by \mathcal{CS} . Eq. (7.5) also indicates that $\text{vec}(\mathbf{R}_S - p_n \mathbf{I})$ is constrained in a certain way by \mathcal{CS} , and these constraints can be used in designing DOA estimators for improved performance.

It is clear that \mathcal{CS} is a finite-dimensional subspace of $\mathbb{C}^{|\mathcal{S}|^2}$, due to (7.3). However, the definition of the correlation subspace in (7.5) is computationally intractable since it involves infinitely many $\mathbf{c}(\bar{\theta})$. The correlation subspace was originally computed by the following definition [141]:

Definition 7.2.1. The correlation subspace \mathcal{CS} satisfies

$$\mathcal{CS} = \text{col}(\mathbf{S}), \quad (7.6)$$

where the correlation subspace matrix \mathbf{S} is defined as

$$\mathbf{S} \triangleq \int_{-\pi/2}^{\pi/2} \mathbf{c}(\bar{\theta}) \mathbf{c}^H(\bar{\theta}) d\theta \in \mathbb{C}^{|\mathcal{S}|^2 \times |\mathcal{S}|^2}. \quad (7.7)$$

In Appendix 7.A, we show that this definition is equivalent to our revised definition given in (7.5). Note that this integral is carried out over the DOA, $\theta \in [-\pi/2, \pi/2]$ and the relation $\bar{\theta} = (\sin \theta)/2$ can be utilized to evaluate (7.7). According to (7.7), it can be shown that the correlation subspace matrix \mathbf{S} is Hermitian and positive semidefinite.

It was shown in [141] that the right-hand side of (7.6) can be simplified further, based on the eigenvectors of \mathbf{S} associated with the nonzero eigenvalues. In particular, let the eigen-decomposition of \mathbf{S} be

$$\mathbf{S} = \underbrace{\begin{bmatrix} \mathbf{Q}_{CS} & \mathbf{Q}_{CS^\perp} \end{bmatrix}}_{\mathbf{Q}} \begin{bmatrix} \Lambda_1 & \mathbf{0} \\ \mathbf{0} & \mathbf{0} \end{bmatrix} \begin{bmatrix} \mathbf{Q}_{CS} & \mathbf{Q}_{CS^\perp} \end{bmatrix}^H, \quad (7.8)$$

where the diagonal matrix Λ_1 contains the positive eigenvalues in the descending order and the columns of \mathbf{Q} consist of the orthonormal eigenvectors. Then, (7.6) and (7.8) lead to $\mathcal{CS} = \text{col}(\mathbf{Q}_{CS})$. Namely, the correlation subspace \mathcal{CS} is the column space of the matrix \mathbf{Q}_{CS} . Eqs. (7.6), (7.7), and (7.8) indicate that the matrix \mathbf{S} , its eigenvalues, its eigenvectors, and the correlation subspace *depend purely on the array configuration*.

For any array geometry, the correlation subspace is uniquely determined, and imposes some implicit constraints on the structure of the covariance matrix, as indicated in (7.5). This leads to a covariance-matrix denoising approach [141]. To begin with, consider finite snapshot sensor measurements $\tilde{\mathbf{x}}_S(k)$ for $k = 1, \dots, K$. The

sample covariance matrix $\tilde{\mathbf{R}}_{\mathcal{S}}$ can be estimated by $\tilde{\mathbf{R}}_{\mathcal{S}} = \frac{1}{K} \sum_{k=1}^K \tilde{\mathbf{x}}_{\mathcal{S}}(k) \tilde{\mathbf{x}}_{\mathcal{S}}^H(k)$, which is defined in (2.23). The algorithm in [141] first denoises the sample covariance matrix $\tilde{\mathbf{R}}_{\mathcal{S}}$ using the following convex program (P1):

$$(P1): \mathbf{R}_{\mathcal{P}1}^* \triangleq \arg \min_{\mathbf{R}} \|\tilde{\mathbf{R}}_{\mathcal{S}} - p_n \mathbf{I} - \mathbf{R}\|_2^2 \quad (7.9)$$

$$\text{subject to } (\mathbf{I} - \mathbf{Q}_{\mathcal{CS}} \mathbf{Q}_{\mathcal{CS}}^\dagger) \text{vec}(\mathbf{R}) = \mathbf{0}, \quad (7.10)$$

$$\mathbf{R} \succeq \mathbf{0}, \quad (7.11)$$

where the noise power p_n is estimated from the eigenvalues of $\tilde{\mathbf{R}}_{\mathcal{S}}$ and $\|\cdot\|_2$ denotes the spectral norm of a matrix (i.e., the largest singular value). The cost function in (7.9) suggests that the matrix $\mathbf{R}_{\mathcal{P}1}^*$ resembles $\sum_{i=1}^D p_i \mathbf{v}_{\mathcal{S}}(\bar{\theta}_i) \mathbf{v}_{\mathcal{S}}^H(\bar{\theta}_i)$ in (7.1). The constraint (7.10) ensures that $\text{vec}(\mathbf{R}_{\mathcal{P}1}^*)$ belongs to the correlation subspace while (7.11) indicates that $\mathbf{R}_{\mathcal{P}1}^*$ is positive semidefinite.

The final stage is to perform DOA estimation on $\mathbf{R}_{\mathcal{P}1}^*$. It was shown in [141] that the MUSIC algorithm on $\mathbf{R}_{\mathcal{P}1}^*$ can exhibit better estimation performance than that on $\tilde{\mathbf{R}}_{\mathcal{S}}$. It should be noted that *the DOA estimators are not restricted to the MUSIC algorithm*. Other estimators, such as ESPRIT, MODE, and SPICE, can also be exploited. This result shows that the structure of the covariance matrix, as specified by the correlation subspace, helps to improve the estimation performance.

Summarizing, the DOA estimator associated with the correlation subspace is composed of the following three steps [141]:

Step 1: Correlation subspace. For a given array geometry, *numerically* calculate the correlation subspace matrix \mathbf{S} and its eigen-decomposition, as in (7.7) and (7.8), respectively. Save the matrix $\mathbf{Q}_{\mathcal{CS}}$ for the correlation subspace.

Step 2: Denoising. Given the sensor measurements, evaluate the sample covariance matrix $\tilde{\mathbf{R}}_{\mathcal{S}}$, as in (2.23). Then solve the optimization problem (P1). Let the optimal solution be $\mathbf{R}_{\mathcal{P}1}^*$.

Step 3: DOA estimation. In the simulations of [141], the MUSIC algorithm is applied to $\mathbf{R}_{\mathcal{P}1}^*$.

Remarks on Step 1: Note that this step needs to be done only once per array. Once the matrix $\mathbf{Q}_{\mathcal{CS}}$ is obtained, it can be used repeatedly in Step 2. To calculate $\mathbf{Q}_{\mathcal{CS}}$, the numerical integration was utilized in [141]. This step is typically done by choosing a dense grid of the parameter θ , which only approximates the integral in (7.7). Furthermore, the *numerical* eigen-decomposition in (7.8) introduces perturbations on zero eigenvalues, making it challenging to determine the correlation subspace precisely. It is desirable to mitigate the negative effects caused by numerical computations. It will be shown in Theorem 7.4.1 that the correlation subspace can be fully characterized by simple, elegant, and closed-form expressions.

Remarks on Step 2: The convex optimization problem (P1) can be solved by numerical solvers. However, it requires several numerical iterations to obtain the optimal solution, which could be an issue if real-time processing is needed. To avoid high computational cost, (P1) is approximated by two sub-problems (P1a) and (P1b) in [141]:

$$(P1a): \mathbf{R}_{P1a}^* \triangleq \arg \min_{\mathbf{R}} \|\tilde{\mathbf{R}}_{\mathcal{S}} - p_n \mathbf{I} - \mathbf{R}\|_F^2 \quad (7.12)$$

$$\text{subject to } (\mathbf{I} - \mathbf{Q}_{CS} \mathbf{Q}_{CS}^\dagger) \text{vec}(\mathbf{R}) = \mathbf{0}, \quad (7.13)$$

$$(P1b): \mathbf{R}_{P1b}^* \triangleq \arg \min_{\mathbf{R}} \|\mathbf{R} - \mathbf{R}_{P1a}^*\|_2^2 \quad (7.14)$$

$$\text{subject to } \mathbf{R} \succeq \mathbf{0}. \quad (7.15)$$

In particular, we first compute the solution to (P1a) using the orthogonal projection onto the correlation subspace, $\text{vec}(\mathbf{R}_{P1a}^*) = \mathbf{Q}_{CS} \mathbf{Q}_{CS}^\dagger \text{vec}(\tilde{\mathbf{R}}_{\mathcal{S}} - p_n \mathbf{I})$. Then the solution \mathbf{R}_{P1b}^* can be obtained explicitly from the eigen-decomposition of \mathbf{R}_{P1a}^* . It was demonstrated in [141] that this two-step approach can be readily implemented with a moderate degradation in the estimation performance.

It can be seen that we need to estimate the noise power p_n first before solving either (P1) or (P1a). This extra processing is not desirable if the source directions are the only parameters of interest. In Section 7.5, we will present another optimization problem that enjoys good DOA estimation performance without estimating the noise power.

Remarks on Step 3: If $\mathbf{R}_{P1}^* \in \mathbb{C}^{|\mathcal{S}| \times |\mathcal{S}|}$, then the MUSIC algorithm on \mathbf{R}_{P1}^* can resolve at most $|\mathcal{S}| - 1$ uncorrelated sources, regardless of array configurations [188]. However, sparse arrays can identify more uncorrelated sources than sensors by using augmented covariance matrices [133], positive definite Toeplitz completion [1], [2], and spatial smoothing MUSIC (SS MUSIC) [87], [124], [125], [186]. Furthermore, these approaches usually provide better spatial resolution than the MUSIC algorithm [1], [2], [87], [124], [125], [133], [186]. Hence, we will use sparse arrays and SS MUSIC in the examples of Section 7.7.

Furthermore, it was demonstrated numerically in [141] that, prior knowledge about source directions can be embedded into the correlation subspace by changing the intervals of integration in (7.7). However, the influences of prior knowledge about the correlation subspace and the optimization problem have not been studied in detail. These above points will be addressed by generalized correlation subspaces, as we will present next.

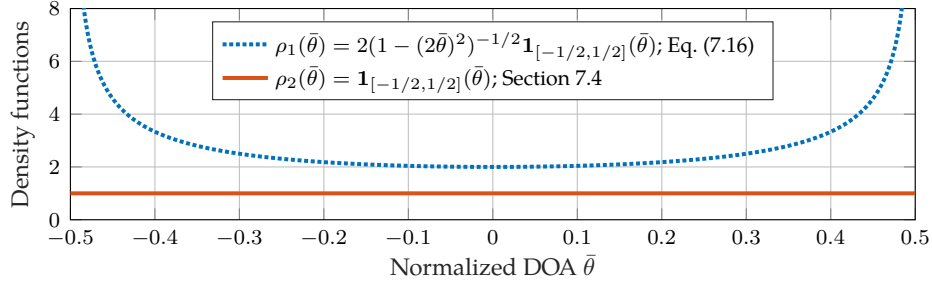


Figure 7.1: The density function in (7.16) (red), and the constant density function in Section 7.4 (blue).

7.3 Generalized Correlation Subspaces

The main difficulty in deriving the closed-form expressions for \mathcal{CS} using (7.6), (7.7), and (7.8) is as follows. Eq. (7.7) implies that the entries of \mathbf{S} are related to Bessel functions, making it complicated to obtain analytical forms of (7.8). In order to derive closed-form expressions for \mathcal{CS} , we will first propose the generalized correlation subspace $\mathcal{GCS}(\rho)$, which is parameterized by a nonnegative density function $\rho(\bar{\theta})$. Then it will be shown that $\mathcal{GCS}(\rho)$ depends only on the support of $\rho(\bar{\theta})$, and is invariant to its exact shape. Using this property, we can derive simple and closed forms for \mathcal{CS} by selecting some density functions $\rho(\bar{\theta})$ such that 1) $\mathcal{CS} = \mathcal{GCS}(\rho)$ and 2) it is straightforward to derive closed-form expressions for $\mathcal{GCS}(\rho)$.

As a motivating example, let us consider the definition of \mathbf{S} in (7.7). Since $\bar{\theta} = 0.5 \sin \theta$, we have $d\theta = 2(1 - (2\bar{\theta})^2)^{-1/2} d\bar{\theta}$. Hence, (7.7) can be rewritten as

$$\mathbf{S} = \int_{-1/2}^{1/2} \mathbf{c}(\bar{\theta}) \mathbf{c}^H(\bar{\theta}) \underbrace{\left(2(1 - (2\bar{\theta})^2)^{-1/2} \right)}_{\text{the density function}} d\bar{\theta}. \quad (7.16)$$

Note that (7.16) can be regarded as a weighted integral with the density function $2(1 - (2\bar{\theta})^2)^{-1/2}$ over $\bar{\theta} \in [-1/2, 1/2]$. Hence, we can generalize the correlation subspace matrix by varying the density function in (7.16). It is formally defined as

Definition 7.3.1. Let the correlation vector $\mathbf{c}(\bar{\theta})$ be defined as in (7.3). Let $\rho(\bar{\theta})$ be a nonnegative Lebesgue integrable function over the set $[-1/2, 1/2]$. The generalized correlation subspace matrix associated with $\rho(\bar{\theta})$ is defined as

$$\mathbf{S}(\rho) = \int_{-1/2}^{1/2} \mathbf{c}(\bar{\theta}) \mathbf{c}^H(\bar{\theta}) \rho(\bar{\theta}) d\bar{\theta}. \quad (7.17)$$

It can be seen that (7.16) is a special case of Definition 7.3.1, with $\rho(\bar{\theta}) = 2(1 - (2\bar{\theta})^2)^{-1/2} \mathbf{1}_{[-1/2, 1/2]}(\bar{\theta})$. The density function $\rho(\bar{\theta})$ quantifies the importance of the term $\mathbf{c}(\bar{\theta}) \mathbf{c}^H(\bar{\theta})$ in $\mathbf{S}(\rho)$, across different $\bar{\theta}$. This $\rho(\bar{\theta})$ is shown in the dashed curve of Fig. 7.1. Note that $\rho(\bar{\theta})$ grows rapidly as $\bar{\theta}$ approaches ± 0.5 .

Based on Definition 7.2.1, the generalized correlation subspace can be defined as follows:

Definition 7.3.2. Let $\mathbf{S}(\rho)$ be the generalized correlation subspace matrix associated with $\rho(\bar{\theta})$, as in (7.17). The generalized correlation subspace is defined as $\mathcal{GCS}(\rho) = \text{col}(\mathbf{S}(\rho))$.

It can be seen from Definition 7.3.1 and 7.3.2 that the generalized correlation subspaces are parameterized by the density function $\rho(\bar{\theta})$. For any given support of $\rho(\bar{\theta})$, the generalized correlation subspace is invariant to the exact shape of $\rho(\bar{\theta})$ under that support, as indicated by the following lemma:

Lemma 7.3.1. Let $\rho_1(\bar{\theta})$ and $\rho_2(\bar{\theta})$ be two nonnegative Lebesgue integrable functions over the set $[-1/2, 1/2]$. If $\text{supp}(\rho_1) = \text{supp}(\rho_2)$, then $\mathcal{GCS}(\rho_1) = \mathcal{GCS}(\rho_2)$.

Proof. See Appendix 7.B. □

Corollary 7.3.1. Let the density function in (7.16) be

$$\rho_1(\bar{\theta}) = 2(1 - (2\bar{\theta})^2)^{-1/2} \mathbf{1}_{[-1/2, 1/2]}(\bar{\theta}), \quad (7.18)$$

and the constant density function be

$$\rho_2(\bar{\theta}) = \mathbf{1}_{[-1/2, 1/2]}(\bar{\theta}). \quad (7.19)$$

Then $\mathcal{CS} = \mathcal{GCS}(\rho_1) = \mathcal{GCS}(\rho_2)$.

The density functions $\rho_1(\bar{\theta})$ and $\rho_2(\bar{\theta})$ are illustrated in Fig. 7.1. It can be observed that these density functions share the same support $[-1/2, 1/2]$. Furthermore, Corollary 7.3.1 also enables us to analyze the correlation subspace readily through the generalized correlation subspace $\mathcal{GCS}(\rho_2)$. The details will be developed in Section 7.4.

7.4 Properties of Generalized Correlation Subspaces

In this section, the generalized correlation subspaces for several density functions will be investigated. It will be shown that *the correlation subspace and the generalized correlation subspace depend on the difference coarray*. Furthermore, we will derive simple, explicit, and computationally tractable representations of the correlation subspace and the generalized correlation subspace in certain cases.

First, it is known from [97] that the correlation vector (7.3) can be rewritten as:

$$\mathbf{c}(\bar{\theta}_i) = \mathbf{J}\mathbf{v}_{\mathbb{D}}(\bar{\theta}_i), \quad (7.20)$$

where $\mathbf{v}_{\mathbb{D}}(\bar{\theta}_i) = [e^{j2\pi\bar{\theta}_i m}]_{m \in \mathbb{D}}$ are the steering vectors on the difference coarray. Here the difference coarray \mathbb{D} and the matrix \mathbf{J} [97] are defined as in Definitions 2.2.1 and 6.B.1, respectively.

Example 7.4.1. Assume the sensor locations are characterized by an integer set $\mathbb{S} = \{0, 2\}$. According to Definition 2.18, the difference coarray becomes $\mathbb{D} = \{-2, 0, 2\}$. Next we will evaluate the matrix \mathbf{J} , as in Definition 6.B.1. First we consider the matrices $\mathbf{I}(m)$ for $m \in \mathbb{D}$ as follows:

$$\mathbf{I}(0) = \begin{matrix} & \begin{matrix} n_2=0 & 2 \end{matrix} \\ \begin{matrix} n_1=0 \\ 2 \end{matrix} & \begin{bmatrix} 1 & 0 \\ 0 & 1 \end{bmatrix} \end{matrix}, \quad \mathbf{I}(2) = \begin{matrix} & \begin{matrix} n_2=0 & 2 \end{matrix} \\ \begin{matrix} n_1=0 \\ 2 \end{matrix} & \begin{bmatrix} 0 & 0 \\ 1 & 0 \end{bmatrix} \end{matrix},$$

where n_1 and n_2 are marked in the corresponding rows and columns. Furthermore, due to (6.80), it can be shown that $\mathbf{I}(-2) = (\mathbf{I}(2))^T$. Hence, the matrix \mathbf{J} can be written as

$$\mathbf{J} = \begin{matrix} & \begin{matrix} \text{vec}(\mathbf{I}(-2)) & \text{vec}(\mathbf{I}(0)) & \text{vec}(\mathbf{I}(2)) \end{matrix} \\ \begin{bmatrix} 0 & 1 & 0 \\ 0 & 0 & 1 \\ 1 & 0 & 0 \\ 0 & 1 & 0 \end{bmatrix} \end{matrix}, \quad (7.21)$$

where the first, the second, and the third column of \mathbf{J} correspond to the coarray index $m = -2, 0, 2$, respectively. Finally, we will verify (7.20) in this example. Starting with (7.3), the correlation vector is given by

$$\mathbf{c}(\bar{\theta}_i) = \text{vec} \left(\begin{bmatrix} 1 \\ e^{j2\pi\bar{\theta}_i \cdot 2} \end{bmatrix} \begin{bmatrix} 1 & e^{-j2\pi\bar{\theta}_i \cdot 2} \end{bmatrix} \right) = \begin{bmatrix} 1 \\ e^{j4\pi\bar{\theta}_i} \\ e^{-j4\pi\bar{\theta}_i} \\ 1 \end{bmatrix}.$$

Similarly, the quantity $\mathbf{J}\mathbf{v}_{\mathbb{D}}(\bar{\theta}_i)$ can be calculated as

$$\mathbf{J}\mathbf{v}_{\mathbb{D}}(\bar{\theta}_i) = \begin{bmatrix} 0 & 1 & 0 \\ 0 & 0 & 1 \\ 1 & 0 & 0 \\ 0 & 1 & 0 \end{bmatrix} \begin{bmatrix} e^{j2\pi\bar{\theta}_i \cdot (-2)} \\ 1 \\ e^{j2\pi\bar{\theta}_i \cdot 2} \end{bmatrix} = \begin{bmatrix} 1 \\ e^{j4\pi\bar{\theta}_i} \\ e^{-j4\pi\bar{\theta}_i} \\ 1 \end{bmatrix}.$$

This result verifies (7.20).

Using (7.20) and Definition 7.3.1, the generalized correlation subspace matrix can be expressed in terms of the difference coarray as in Lemma 7.4.1:

Lemma 7.4.1. The generalized correlation subspace matrix satisfies $\mathbf{S}(\rho) = \mathbf{J}\mathbf{S}_{\mathbb{D}}(\rho)\mathbf{J}^H$, where \mathbf{J} is defined in Definition 6.B.1 and $\mathbf{S}_{\mathbb{D}}(\rho)$ is given by

$$\mathbf{S}_{\mathbb{D}}(\rho) = \int_{-1/2}^{1/2} \mathbf{v}_{\mathbb{D}}(\bar{\theta})\mathbf{v}_{\mathbb{D}}^H(\bar{\theta})\rho(\bar{\theta})d\bar{\theta}. \quad (7.22)$$

Note that the matrix $\mathbf{S}_{\mathbb{D}}(\rho)$ depends on *the difference coarray*, rather than the physical sensor locations. This property suggests that *the generalized correlation subspace is fundamentally related to the difference coarray*. This is indeed true and we will elaborate this point later. Furthermore, Lemma 7.4.1 also allows us to readily analyze the matrix $\mathbf{S}(\rho)$ of size $|\mathbb{S}|^2$ -by- $|\mathbb{S}|^2$, by examining a smaller matrix $\mathbf{S}_{\mathbb{D}}(\rho)$ of size $|\mathbb{D}|-$ by- $|\mathbb{D}|$. Next, we will consider two simple examples of the density function as follows:

- The density function is a constant over $\bar{\theta} \in [-1/2, 1/2]$. Namely, $\rho(\bar{\theta}) = \mathbf{1}_{[-1/2, 1/2]}(\bar{\theta})$.
- The density function is a constant over some known intervals \mathbb{I} . That is, $\rho(\bar{\theta}) = \mathbf{1}_{\mathbb{I}}(\bar{\theta})$. This case corresponds to known source intervals.

In both cases, we will present the closed-form expressions of $\mathbf{S}_{\mathbb{D}}(\rho)$ and $\mathbf{S}(\rho)$, from which the generalized correlation subspaces can be analyzed systematically.

The constant density function

In this case, the entry of $\mathbf{S}_{\mathbb{D}}(\mathbf{1}_{[-1/2, 1/2]})$ associated with coarray locations $m_1, m_2 \in \mathbb{D}$ becomes

$$\langle \mathbf{S}_{\mathbb{D}}(\mathbf{1}_{[-1/2, 1/2]}) \rangle_{m_1, m_2} = \int_{-1/2}^{1/2} e^{j2\pi\bar{\theta}(m_1 - m_2)} d\bar{\theta} = \delta_{m_1, m_2}, \quad (7.23)$$

since m_1 and m_2 are integers. Substituting (7.23) into Lemma 7.4.1 gives

$$\mathbf{S}(\mathbf{1}_{[-1/2, 1/2]}) = \mathbf{J}\mathbf{J}^H. \quad (7.24)$$

In order to obtain the eigen-decomposition of $\mathbf{S}(\mathbf{1}_{[-1/2, 1/2]})$, we invoke a lemma regarding the matrix \mathbf{J} :

Lemma 7.4.2. $\mathbf{J}^H\mathbf{J} = \mathbf{W} \triangleq \text{diag}(w(m))_{m \in \mathbb{D}}$, where the weight function $w(m)$ is defined in Definition 2.2.9. Namely, \mathbf{J} has orthogonal columns and the norm of the column associated with the coarray index m is $\sqrt{w(m)}$.

Proof. It was proved in [97] that the columns of \mathbf{J} are orthogonal. It suffices to consider the norms of the individual columns of \mathbf{J} . For the coarray location $m \in \mathbb{D}$, the

norm of the associated column is

$$\begin{aligned} \|\text{vec}(\mathbf{I}(m))\|_2^2 &= \sum_{n_1, n_2 \in \mathbb{S}} |\langle \mathbf{I}(m) \rangle_{n_1, n_2}|^2 \\ &= \text{the number of ones in } \mathbf{I}(m) = w(m), \end{aligned}$$

which proves this lemma. \square

Example 7.4.2. Assume the sensor locations are given by $\mathbb{S} = \{0, 2\}$, as in Example 7.4.1. Then the weight functions $w(m)$ are given by

$$w(-2) = |\{(0, 2)\}| = 1, \quad w(0) = |\{(0, 0), (2, 2)\}| = 2, \quad w(2) = |\{(2, 0)\}| = 1.$$

Hence the matrix \mathbf{W} in Lemma 7.4.2 can be written as

$$\mathbf{W} = \text{diag}(w(-2), w(0), w(2)) = \text{diag}(1, 2, 1). \quad (7.25)$$

Then, Lemma 7.4.2 can be verified using (7.21) and \mathbf{W} .

Due to Definition 2.2.9 and Lemma 7.4.2, the generalized correlation subspace matrix $\mathbf{S}(\mathbf{1}_{[-1/2, 1/2]})$ can be expressed as

$$\mathbf{S}(\mathbf{1}_{[-1/2, 1/2]}) = (\mathbf{J}\mathbf{W}^{-1/2})\mathbf{W}(\mathbf{J}\mathbf{W}^{-1/2})^H, \quad (7.26)$$

where the sizes of these terms are $\mathbf{J}\mathbf{W}^{-1/2} \in \mathbb{C}^{|\mathbb{S}|^2 \times |\mathbb{D}|}$ and $\mathbf{W} \in \mathbb{C}^{|\mathbb{D}| \times |\mathbb{D}|}$. Eq. (7.26) also indicates that the matrix $\mathbf{J}\mathbf{W}^{-1/2}$ corresponds to the orthonormal eigenvectors while the diagonal matrix \mathbf{W} is associated with the eigenvalues. In particular, the *positive eigenvalues* and the associated eigenvectors of $\mathbf{S}(\mathbf{1}_{[-1/2, 1/2]})$ are given by

$$\text{Positive eigenvalues of } \mathbf{S}(\mathbf{1}_{[-1/2, 1/2]}) = w(m), \quad (7.27)$$

$$\text{Eigenvectors of } \mathbf{S}(\mathbf{1}_{[-1/2, 1/2]}) = \frac{\text{vec}(\mathbf{I}(m))}{\sqrt{w(m)}}, \quad (7.28)$$

where $m \in \mathbb{D}$. Note that (7.27) and (7.28) can be calculated readily from the array geometry using Definitions 2.2.9 and 6.B.1, respectively. Namely, the eigen-decomposition of $\mathbf{S}(\mathbf{1}_{[-1/2, 1/2]})$ can be evaluated without using the numerical integration in Definition 7.3.1 and the numerical eigen-decomposition on $\mathbf{S}(\mathbf{1}_{[-1/2, 1/2]})$.

Properties of $\mathbf{S}(\mathbf{1}_{[-1/2, 1/2]})$: The following list some properties regarding the eigen-structure of $\mathbf{S}(\mathbf{1}_{[-1/2, 1/2]})$. Some items are direct consequences of the properties of the weight function $w(m)$, as in Lemma 7.C.1.

1. The eigenvalues of $\mathbf{S}(\mathbf{1}_{[-1/2, 1/2]})$ are nonnegative integers, due to (7.26), (7.27), and Lemma 7.C.1.1.

2. The number of nonzero eigenvalues is $|\mathbb{D}|$, which is the size of the difference coarray. Here repeated eigenvalues are counted separately.
3. The largest eigenvalue of $\mathbf{S}(\mathbf{1}_{[-1/2, 1/2]})$ is $w(0) = |\mathbb{S}|$ with algebraic multiplicity 1. This is a direct consequence of Lemma 7.C.1.4.
4. For any nonzero eigenvalue that is not the largest, the associated algebraic multiplicity is an *even* positive integer, due to Lemma 7.C.1.2.
5. The eigenvalue zero has algebraic multiplicity $|\mathbb{S}|^2 - |\mathbb{D}|$.
6. The orthonormal eigenvectors associated with nonzero eigenvalues are given in (7.28).
7. For all the eigenvalues of $\mathbf{S}(\mathbf{1}_{[-1/2, 1/2]})$, the geometric multiplicities achieve the algebraic multiplicities.

Finally, based on (7.26), the generalized correlation subspace $\mathcal{GCS}(\mathbf{1}_{[-1/2, 1/2]})$ becomes

$$\text{col}(\mathbf{S}(\mathbf{1}_{[-1/2, 1/2]})) = \text{col}(\mathbf{J}\mathbf{W}^{-1/2}) = \text{col}(\mathbf{J}). \quad (7.29)$$

The significance of (7.29) is that, the correlation subspace in (7.5) can be characterized in closed forms, as in the following theorem:

Theorem 7.4.1. Let the matrix \mathbf{J} be defined as in Definition 6.B.1. Then the correlation subspace satisfies

$$\mathcal{CS} = \text{col}(\mathbf{J}). \quad (7.30)$$

Proof. Corollary 7.3.1 indicates that $\mathcal{CS} = \mathcal{GCS}(\rho_1) = \mathcal{GCS}(\rho_2)$. The relation $\mathcal{GCS}(\rho_2) = \text{col}(\mathbf{J})$ is due to (7.29). \square

This theorem indicates that the correlation subspace is fully characterized by the binary matrix \mathbf{J} , which can be readily computed from *sensor locations and the difference coarray* using Definition 6.B.1. Namely, to compute the correlation subspace, the numerical integration (7.7) and the eigen-decomposition (7.8) can be avoided completely. Due to Theorem 7.4.1 and Lemma 7.4.2, the dimension of the correlation subspace is given by

Corollary 7.4.1. The dimension of the correlation subspace is the size of the difference coarray, i.e., $\dim(\mathcal{CS}) = |\mathbb{D}|$.

Table 7.1: Generalized correlation subspaces with known source intervals

| |
|---|
| Input: Array configuration \mathbb{S} , source intervals \mathbb{I} , and error tolerance δ . |
| 1) Evaluate the matrix \mathbf{J} according to Definition 6.B.1. |
| 2) Based on \mathbb{I} , compute $\mathbf{S}_{\mathbb{D}}(\mathbf{1}_{\mathbb{I}})$ using either (7.32), (7.40), or (7.45). |
| 3) Numerical eigen-decomposition: $\mathbf{S}_{\mathbb{D}}(\mathbf{1}_{\mathbb{I}}) = \mathbf{\Psi}\mathbf{\Lambda}\mathbf{\Psi}^H$. |
| a) Eigenvectors: $\mathbf{\Psi} = [\psi_1, \psi_2, \dots, \psi_{ \mathbb{D} }]$; $\mathbf{\Psi}^H\mathbf{\Psi} = \mathbf{I}$. |
| b) Eigenvalues: $\mathbf{\Lambda} = \text{diag}(\lambda_1, \lambda_2, \dots, \lambda_{ \mathbb{D} })$; $\lambda_1 \geq \dots \geq \lambda_{ \mathbb{D} } \geq 0$. |
| 4) Determine a positive integer L using (7.47). |
| 5) Construct $\mathbf{\Psi}_L = [\psi_1, \psi_2, \dots, \psi_L]$. |
| Output: $\mathcal{GCS}(\mathbf{1}_{\mathbb{I}})$ is approximated by $\text{col}(\mathbf{J}\mathbf{\Psi}_L)$. |

The constant density function with known source intervals

Here we will study the generalized correlation subspace with known source intervals. This scenario arises in practical applications such as stationary radar and the diagnosis of rotating machines in industrial environments [196].

Table 7.1 summarizes the procedure for the generalized correlation subspaces with known source intervals. For a given array configuration \mathbb{S} and source intervals \mathbb{I} , we can calculate $\mathbf{S}_{\mathbb{D}}(\mathbf{1}_{\mathbb{I}})$ explicitly using either (7.32), (7.40), or (7.45), as we shall explain later. The eigen-decomposition of $\mathbf{S}_{\mathbb{D}}(\mathbf{1}_{\mathbb{I}})$ suggests that $\mathbf{S}_{\mathbb{D}}(\mathbf{1}_{\mathbb{I}})$ can be approximated by $\mathbf{\Psi}_L \cdot \text{diag}(\lambda_1, \lambda_2, \dots, \lambda_L) \cdot \mathbf{\Psi}_L^H$, where the related quantities are given in Table 7.1.² This property leads to an approximation of the generalized correlation subspace $\mathcal{GCS}(\mathbf{1}_{\mathbb{I}}) \approx \text{col}(\mathbf{J}\mathbf{\Psi}_L)$. Note that Table 7.1 is applicable to a given array \mathbb{S} and given source intervals \mathbb{I} . In the following development, we will study the generalized correlation subspaces based on these factors.

Hole-free difference coarrays and $\mathbb{I} = [-\alpha/2, \alpha/2]$

In this case, the density function is assumed to be

$$\rho(\bar{\theta}) = \mathbf{1}_{[-\alpha/2, \alpha/2]}(\bar{\theta}) = \begin{cases} 1, & \text{if } -\alpha/2 \leq \bar{\theta} \leq \alpha/2, \\ 0, & \text{otherwise,} \end{cases} \quad (7.31)$$

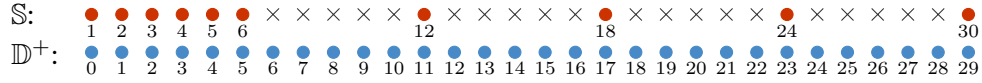
where $0 < \alpha < 1$. Now we can derive the expression for the generalized correlation subspace matrix. According to Lemma 7.4.1, the entry of $\mathbf{S}_{\mathbb{D}}(\mathbf{1}_{[-\alpha/2, \alpha/2]})$ associated

² The symbols ψ_k , $\mathbf{\Psi}_L$, and $\mathbf{\Psi}$ are reserved for the eigenvectors of the matrix $\mathbf{S}_{\mathbb{D}}(\mathbf{1}_{\mathbb{I}})$ while the notations \mathbf{v}_k and \mathbf{V}_L represent the discrete prolate spheroidal sequences.

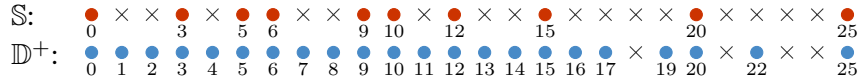
(a) ULA:



(b) Nested array:



(c) Coprime array:



(d) Super nested array:

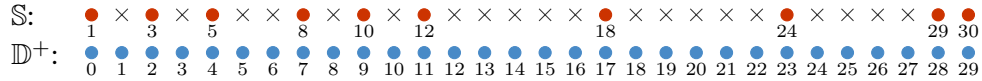


Figure 7.2: The sensor locations \mathbb{S} and the nonnegative part of the difference coarrays \mathbb{D}^+ for (a) ULA with 10 sensors, (b) the nested array with $N_1 = N_2 = 5$, (c) the coprime array with $M = 3, N = 5$, and (d) the super nested array with $N_1 = N_2 = 5, Q = 2$. Here bullets denote elements in \mathbb{S} or \mathbb{D}^+ while crosses represent empty space.

with coarray locations $m_1, m_2 \in \mathbb{D}$ is given by

$$\begin{aligned} \langle \mathbf{S}_{\mathbb{D}}(\mathbf{1}_{[-\alpha/2, \alpha/2]}) \rangle_{m_1, m_2} &= \int_{-\alpha/2}^{\alpha/2} e^{j2\pi\bar{\theta}(m_1 - m_2)} d\bar{\theta} \\ &= \alpha \cdot \text{sinc}(\alpha(m_1 - m_2)), \end{aligned} \quad (7.32)$$

where the normalized sinc function $\text{sinc}(x)$ is 1 for $x = 0$ and $\sin(\pi x)/(\pi x)$ otherwise. The eigen-decomposition of $\mathbf{S}_{\mathbb{D}}(\mathbf{1}_{[-\alpha/2, \alpha/2]})$ is assumed to be

$$\mathbf{S}_{\mathbb{D}}(\mathbf{1}_{[-\alpha/2, \alpha/2]}) = \mathbf{\Psi} \mathbf{\Lambda} \mathbf{\Psi}^H, \quad (7.33)$$

where the matrices $\mathbf{\Psi}$ and $\mathbf{\Lambda}$ are given by

$$\mathbf{\Psi} = [\boldsymbol{\psi}_1, \boldsymbol{\psi}_2, \dots, \boldsymbol{\psi}_{|\mathbb{D}|}] \quad (7.34)$$

$$\mathbf{\Lambda} = \text{diag}(\lambda_1, \lambda_2, \dots, \lambda_{|\mathbb{D}|}). \quad (7.35)$$

Here the eigenvalues satisfy $\lambda_1 \geq \lambda_2 \geq \dots \geq \lambda_{|\mathbb{D}|} \geq 0$ and $\boldsymbol{\psi}_1, \boldsymbol{\psi}_2, \dots, \boldsymbol{\psi}_{|\mathbb{D}|}$ are the associated orthonormal eigenvectors.

Note that the matrix $\mathbf{S}_{\mathbb{D}}(\mathbf{1}_{[-\alpha/2, \alpha/2]})$ depends purely on the difference coarray \mathbb{D} and the parameter α . Next we assume the difference coarray \mathbb{D} is *hole-free*. Namely, \mathbb{D} is composed of consecutive integers. For instance, Fig. 7.2 depicts array configurations like (a) ULA [188], (b) nested array [124], as in (2.7), (c) coprime array [186], as in (2.8), and (d) super nested array [92], as in Definition 3.4.1. It can be observed from

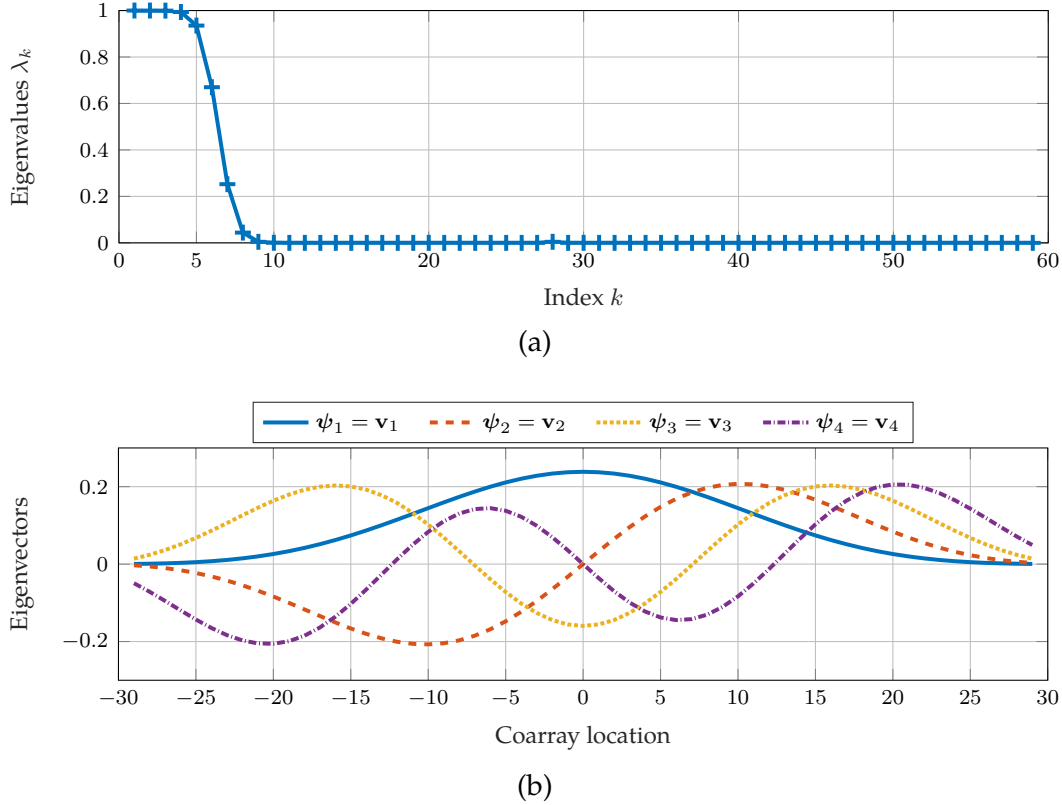


Figure 7.3: (a) The eigenvalues and (b) the first four eigenvectors of the generalized correlation subspace matrix $\mathbf{S}(\mathbf{1}_{[-\alpha/2, \alpha/2]})$ in Example 7.4.3. Here the difference coarray $\mathbb{D} = \{-29, \dots, 29\}$ and α is 0.1.

the nonnegative part of the difference coarray that (a), (b), and (d) have hole-free difference coarrays while (c) does not. These array configurations will be elaborated in Section 7.7 later.

For arrays with hole-free difference coarrays, the eigenvectors ψ_k are known to be *discrete prolate spheroidal sequences (DPSS)*. That is, the matrix $\mathbf{S}_{\mathbb{D}}(\mathbf{1}_{[-\alpha/2, \alpha/2]})$ owns

$$\text{Eigenvalues of } \mathbf{S}_{\mathbb{D}}(\mathbf{1}_{[-\alpha/2, \alpha/2]}) = \lambda_k, \quad (7.36)$$

$$\text{Eigenvectors of } \mathbf{S}_{\mathbb{D}}(\mathbf{1}_{[-\alpha/2, \alpha/2]}) \triangleq \psi_k = \mathbf{v}_k, \quad (7.37)$$

where $\mathbf{v}_1, \mathbf{v}_2, \dots, \mathbf{v}_{|\mathbb{D}|}$ denote DPSS on the difference coarray \mathbb{D} . Note that DPSS were studied comprehensively in [131], [158] and they arise in various fields such as multitapers [178], time-frequency analysis [39], eigenfilters [181], [182], and MIMO radar [32]. Here several properties of the eigenvalues λ_k and the DPSS \mathbf{v}_k are reviewed briefly using the following example:

Example 7.4.3. Consider the super nested array with $N_1 = N_2 = 5$ as in Definition 3.4.1. The sensor locations are depicted in Fig. 7.2(d). The difference coarray becomes $\mathbb{D} = \{-29, \dots, 29\}$ (hole-free) and $|\mathbb{D}| = 59$. We also choose the parameter

$\alpha = 0.1$. According to (7.36) and (7.37), the eigenvalues λ_k and the eigenvectors are illustrated in Fig. 7.3. It was shown in [158] that the eigenvalues λ_k are distinct, and the first $\lfloor \alpha|\mathbb{D}| \rfloor$ eigenvalues are close to one, but less than one, where $\lfloor \cdot \rfloor$ is the floor function. As the index k exceeds $\lfloor \alpha|\mathbb{D}| \rfloor$, the magnitude of the eigenvalues decays exponentially [158]. This property indicates that the matrix $\mathbf{S}_{\mathbb{D}}(\mathbf{1}_{[-\alpha/2, \alpha/2]})$ can be well-approximated by a matrix of rank L . Namely,

$$\mathbf{S}_{\mathbb{D}}(\mathbf{1}_{[-\alpha/2, \alpha/2]}) \approx \mathbf{V}_L \cdot \text{diag}(\lambda_1, \lambda_2, \dots, \lambda_L) \cdot \mathbf{V}_L^H, \quad (7.38)$$

where $\lfloor \alpha|\mathbb{D}| \rfloor \leq L \leq |\mathbb{D}|$ and $\mathbf{V}_L = [\mathbf{v}_1, \mathbf{v}_2, \dots, \mathbf{v}_L]$ consists of the first L DPSS. Note that the exact value of L depends on the approximation error of (7.38), which will be elaborated in (7.47) later. In this example, $\lfloor \alpha|\mathbb{D}| \rfloor = 5$. This means that the first five eigenvalues are close to one, as depicted in Fig. 7.3(a). The DPSS $\mathbf{v}_1, \mathbf{v}_2, \mathbf{v}_3$, and \mathbf{v}_4 are illustrated in Fig. 7.3(b). These DPSS can be proved to be orthogonal, real, and unique up to scale [158]. Furthermore, these DPSS satisfy $\langle \mathbf{v}_k \rangle_{-m} = (-1)^{k+1} \langle \mathbf{v}_k \rangle_m$ for $m \in \mathbb{D}$. Namely, they are either even or odd symmetric.

Substituting (7.38) into Lemma 7.4.1, the generalized correlation subspace matrix can be approximated by

$$\mathbf{S}(\mathbf{1}_{[-\alpha/2, \alpha/2]}) \approx \mathbf{J}\mathbf{V}_L \cdot \text{diag}(\lambda_1, \lambda_2, \dots, \lambda_L) \cdot (\mathbf{J}\mathbf{V}_L)^H.$$

Since the matrix $\mathbf{J}\mathbf{V}_L$ has full column rank, the generalized correlation subspace can be characterized by the following theorem:

Theorem 7.4.2. Let the density function be $\mathbf{1}_{[-\alpha/2, \alpha/2]}$ for $0 < \alpha < 1$. Assume the difference coarray \mathbb{D} is hole-free. Then we have

$$\mathcal{GCS}(\mathbf{1}_{[-\alpha/2, \alpha/2]}) \approx \text{col}(\mathbf{J}\mathbf{V}_L), \quad (7.39)$$

where the columns of \mathbf{V}_L contain the first L DPSS on \mathbb{D} . The parameter L is obtained by (7.47), for a given error tolerance δ .

The significance of Theorem 7.4.2 is that, the interval information α is embedded in the matrix \mathbf{V}_L . The approximation \mathbf{V}_L is constructed by selecting the DPSS associated with the largest L eigenvalues of $\mathbf{S}_{\mathbb{D}}(\mathbf{1}_{[-1/2, 1/2]})$. The details in choosing the parameter L will be developed in (7.46) further. Note that Theorem 7.4.2 can be utilized to denoise the sample covariance matrix, as we shall present in Section 7.5.

Hole-free difference coarrays and $\mathbb{I} = [\bar{\theta}_{\min}, \bar{\theta}_{\max}]$

Let us consider another scenario where the known interval is not centered around the origin, such as $[\bar{\theta}_{\min}, \bar{\theta}_{\max}]$ with $-0.5 < \bar{\theta}_{\min} < \bar{\theta}_{\max} < 0.5$. In this case, the

density function can be

$$\rho(\bar{\theta}) = \mathbf{1}_{[\bar{\theta}_{\min}, \bar{\theta}_{\max}]}(\bar{\theta}) = \begin{cases} 1, & \text{if } \bar{\theta}_{\min} \leq \bar{\theta} \leq \bar{\theta}_{\max}, \\ 0, & \text{otherwise.} \end{cases}$$

Then, due to Lemma 7.4.1, the entry of $\mathbf{S}_{\mathbb{D}}(\mathbf{1}_{[\bar{\theta}_{\min}, \bar{\theta}_{\max}]})$ associated with the coarray location $m_1, m_2 \in \mathbb{D}$ becomes

$$\begin{aligned} & \langle \mathbf{S}_{\mathbb{D}}(\mathbf{1}_{[\bar{\theta}_{\min}, \bar{\theta}_{\max}]}) \rangle_{m_1, m_2} \\ &= e^{j2\pi\bar{\theta}_{\text{avg}}m_1} \cdot \alpha \cdot \text{sinc}(\alpha(m_1 - m_2)) \cdot e^{-j2\pi\bar{\theta}_{\text{avg}}m_2}, \end{aligned} \quad (7.40)$$

where $\bar{\theta}_{\text{avg}} = (\bar{\theta}_{\max} + \bar{\theta}_{\min})/2$ and $\alpha = \bar{\theta}_{\max} - \bar{\theta}_{\min}$ are known. Using similar arguments in Section 7.4, the matrix $\mathbf{S}_{\mathbb{D}}(\mathbf{1}_{[\bar{\theta}_{\min}, \bar{\theta}_{\max}]})$ owns

$$\text{Eigenvalues of } \mathbf{S}_{\mathbb{D}}(\mathbf{1}_{[\bar{\theta}_{\min}, \bar{\theta}_{\max}]}) = \lambda_k, \quad (7.41)$$

$$\text{Eigenvectors of } \mathbf{S}_{\mathbb{D}}(\mathbf{1}_{[\bar{\theta}_{\min}, \bar{\theta}_{\max}]}) = \text{diag}(e^{j2\pi\bar{\theta}_{\text{avg}}m})_{m \in \mathbb{D}} \times \mathbf{v}_k, \quad (7.42)$$

where λ_k are defined in (7.33) and \mathbf{v}_k are the DPSS. These eigenvectors can be regarded as the modulated version of DPSS. Hence, following similar arguments in Example 7.4.3, the generalized correlation subspace can be approximated by

$$\mathcal{GCS}(\mathbf{1}_{[\bar{\theta}_{\min}, \bar{\theta}_{\max}]}) \approx \text{col}(\mathbf{J} \cdot \text{diag}(e^{j2\pi\bar{\theta}_{\text{avg}}m})_{m \in \mathbb{D}} \cdot \mathbf{V}_L), \quad (7.43)$$

where the matrix \mathbf{J} is defined in Definition 6.B.1. The matrix $\mathbf{V}_L = [\mathbf{v}_1, \mathbf{v}_2, \dots, \mathbf{v}_L]$ includes the first L DPSS, where L will be chosen as in (7.47).

Hole-free difference coarrays and unions of multiple source intervals

In this case, the interval information \mathbb{I} is given by

$$\mathbb{I} \triangleq \bigcup_{p=1}^P [\bar{\theta}_{\min, p}, \bar{\theta}_{\max, p}], \quad (7.44)$$

where $[\bar{\theta}_{\min, p}, \bar{\theta}_{\max, p}]$ for $p = 1, 2, \dots, P$ are non-overlapping intervals. The density function is assumed to be $\mathbf{1}_{\mathbb{I}}(\bar{\theta})$. Using (7.40) across all intervals yields

$$\begin{aligned} & \langle \mathbf{S}_{\mathbb{D}}(\mathbf{1}_{\mathbb{I}}) \rangle_{m_1, m_2} \\ &= \sum_{p=1}^P \alpha_p e^{j2\pi\bar{\theta}_{\text{avg}, p}(m_1 - m_2)} \text{sinc}(\alpha_p(m_1 - m_2)), \end{aligned} \quad (7.45)$$

where $\bar{\theta}_{\text{avg}, p} = (\bar{\theta}_{\max, p} + \bar{\theta}_{\min, p})/2$ is the centroid of the p th interval and $\alpha_p = \bar{\theta}_{\max, p} - \bar{\theta}_{\min, p}$ is the width of the p th interval. Here the indices $m_1, m_2 \in \mathbb{D}$. Although the entries of $\mathbf{S}_{\mathbb{D}}(\mathbf{1}_{\mathbb{I}})$ are sums of modulated sinc functions, the eigenvectors of $\mathbf{S}_{\mathbb{D}}(\mathbf{1}_{\mathbb{I}})$ cannot be expressed in terms of DPSS in general. In this case, the generalized correlation subspace $\mathcal{GCS}(\mathbf{1}_{\mathbb{I}})$ has to be evaluated *numerically* using Table 7.1.

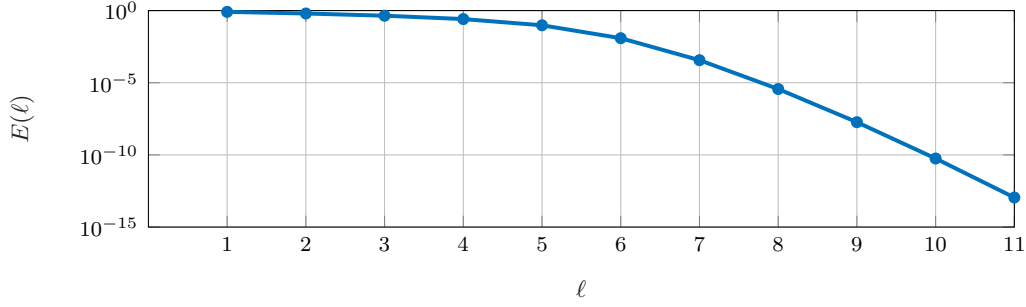


Figure 7.4: The dependence of the relative error $E(\ell)$ on the parameter ℓ , where $E(\ell)$ is defined in (7.46) and the eigenvalues are shown in Fig. 7.3(a).

Difference coarrays with holes

The results in Section 7.4 hold true for 1D arrays, regardless of the difference coarrays. However, it is assumed in Section 7.4 to 7.4 that the difference coarrays are hole-free. These arrays with hole-free difference coarrays include ULA [188], minimum redundancy arrays [113], nested arrays [124], and super nested arrays [92]. For such arrays, Eqs. (7.39) and (7.43) are applicable.

However, for arrays containing holes in the difference coarrays, such as minimum hole arrays [177], coprime arrays [186], and some generalizations of coprime arrays [139], Eqs. (7.39) and (7.43) are not applicable in general. It is because the hole-free property of the difference coarray is used to derive (7.37) and (7.42). In this case, $\mathbf{S}_{\mathbb{D}}(\mathbf{1}_{\mathbb{I}})$ can still be computed from (7.32), (7.40), and (7.45) accordingly. Then, the generalized correlation subspaces need to be calculated numerically using Table 7.1.

The choice of the parameter L : Here we will present the details on the parameter L in Section 7.4. Let $\Psi_{\ell} \mathbf{\Lambda}_{\ell} \Psi_{\ell}^H$ be the rank- ℓ approximation of $\mathbf{S}_{\mathbb{D}}(\mathbf{1}_{\mathbb{I}})$, where the notations are consistent with those in Table 7.1. Let the matrix $\mathbf{\Lambda}_{\ell}$ be $\text{diag}(\lambda_1, \dots, \lambda_{\ell})$. Then the relative error $E(\ell)$ is

$$E(\ell) \triangleq \frac{\|\Psi_{\ell} \mathbf{\Lambda}_{\ell} \Psi_{\ell}^H - \mathbf{S}_{\mathbb{D}}(\mathbf{1}_{\mathbb{I}})\|_F^2}{\|\mathbf{S}_{\mathbb{D}}(\mathbf{1}_{\mathbb{I}})\|_F^2} = \frac{\sum_{k=\ell+1}^{|\mathbb{D}|} \lambda_k^2}{\sum_{k=1}^{|\mathbb{D}|} \lambda_k^2}. \quad (7.46)$$

For a given error tolerance $0 \leq \delta \ll 1$, L is the minimum ℓ such that $E(\ell) < \delta$, i.e.,

$$L = \min_{\ell \in \mathbb{Z}, 1 \leq \ell \leq |\mathbb{D}|} \ell \quad \text{subject to} \quad E(\ell) < \delta. \quad (7.47)$$

Then this L is used in computing the generalized correlation subspace.

In particular, the smaller δ is, the larger L is. For instance, Fig. 7.4 plots the relative error $E(\ell)$, where the eigenvalues are given in Fig. 7.3(a). It can be seen that, if the error tolerance $\delta = 10^{-5}$, then the parameter $L = 8$. If $\delta = 10^{-10}$, then we have $L = 10$.

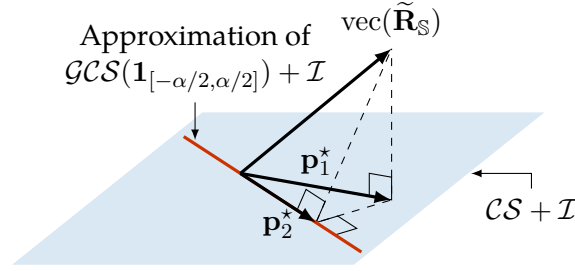


Figure 7.5: The geometric interpretation of sample covariance matrix denoising using generalized correlation subspaces (Problem (P2)). The sample covariance matrix is denoted by $\tilde{\mathbf{R}}_{\mathbb{S}}$. The vectors \mathbf{p}_1^* and \mathbf{p}_2^* are the orthogonal projections of $\text{vec}(\tilde{\mathbf{R}}_{\mathbb{S}})$ onto $\mathcal{CS} + \mathcal{I}$ and onto a subspace that approximates $\mathcal{GCS}(\mathbf{1}_{[-\alpha/2, \alpha/2]}) + \mathcal{I}$, respectively. Here $\mathcal{I} = \text{span}(\text{vec}(\mathbf{I}))$ and the sum between subspaces \mathcal{A} and \mathcal{B} is defined as $\mathcal{A} + \mathcal{B} = \{a + b : a \in \mathcal{A}, b \in \mathcal{B}\}$.

7.5 Connections with Existing Methods

In this section, we will discuss a covariance matrix denoising framework associated with the (generalized) correlation subspace. This method, denoted by problem (P2), can be regarded as a modified version of the optimization problem (P1). This problem (P2) can be solved by simple, closed-form, and computationally tractable expressions, unlike the problem (P1). We also relate it to *redundancy averaging*, which is a well-known processing technique in coarray-based DOA estimators, as shown in Example 7.5.1. This idea can be extended to the case of known source intervals, as in Example 7.5.2.

To develop some feelings for this method, Fig. 7.5 demonstrates the main idea of (P2), where the sample covariance matrix $\tilde{\mathbf{R}}_{\mathbb{S}}$ is defined in (2.23). For a given element $\text{vec}(\tilde{\mathbf{R}}_{\mathbb{S}})$, we can calculate its orthogonal projection \mathbf{p}_1^* onto the subspace $\mathcal{CS} + \mathcal{I}$, where $\mathcal{I} = \text{span}(\text{vec}(\mathbf{I}))$ and the sum of subspaces \mathcal{A} and \mathcal{B} is defined as $\mathcal{A} + \mathcal{B} = \{a + b : a \in \mathcal{A}, b \in \mathcal{B}\}$. Furthermore, if the source interval is known to be $[-\alpha/2, \alpha/2]$, then the projection can be refined as \mathbf{p}_2^* . These projections \mathbf{p}_1^* and \mathbf{p}_2^* can be matricized as indefinite Hermitian matrices, to which some existing DOA estimators can be applied.

The rationale for (P2) is based on the following chain of arguments. According to (7.5), we have $\text{vec}(\mathbf{R}_{\mathbb{S}} - p_n \mathbf{I}) \in \mathcal{CS}$. This result implies that $\text{vec}(\mathbf{R}_{\mathbb{S}})$ can be decomposed as $p_n \text{vec}(\mathbf{I})$ plus a vector in \mathcal{CS} . Namely, $\text{vec}(\mathbf{R}_{\mathbb{S}}) \in \mathcal{CS} + \mathcal{I}$, where $\mathcal{I} = \text{span}(\text{vec}(\mathbf{I}))$. Hence, in the finite snapshot scenario, we can find the vector \mathbf{p}^* in $\mathcal{CS} + \mathcal{I}$ that minimizes the Euclidean distance to $\text{vec}(\tilde{\mathbf{R}}_{\mathbb{S}})$. More generally, if the prior knowledge about sources is available, as embedded in the generalized correlation subspace $\mathcal{GCS}(\rho)$, then we have $\text{vec}(\mathbf{R}_{\mathbb{S}}) \in \mathcal{GCS}(\rho) + \mathcal{I}$. This idea leads to the

following convex program:

$$(P2): \mathbf{p}^* \triangleq \arg \min_{\mathbf{p}} \|\text{vec}(\tilde{\mathbf{R}}_{\mathcal{S}}) - \mathbf{p}\|_2^2 \quad \text{subject to} \quad (7.48)$$

$$(\mathbf{I} - \mathbf{Q}_{\mathcal{GCS}(\rho)+\mathcal{I}} \mathbf{Q}_{\mathcal{GCS}(\rho)+\mathcal{I}}^\dagger) \mathbf{p} = \mathbf{0}, \quad (7.49)$$

where the columns of $\mathbf{Q}_{\mathcal{A}}$ are the bases for the subspace \mathcal{A} . The solution to (P2) is given by

$$\mathbf{p}^* = \mathbf{Q}_{\mathcal{GCS}(\rho)+\mathcal{I}} \mathbf{Q}_{\mathcal{GCS}(\rho)+\mathcal{I}}^\dagger \text{vec}(\tilde{\mathbf{R}}_{\mathcal{S}}). \quad (7.50)$$

Note that (7.50) can be evaluated directly, given the sample covariance matrix $\tilde{\mathbf{R}}_{\mathcal{S}}$ and the generalized correlation subspace $\mathcal{GCS}(\rho)$. The computational complexity of (7.50) is much less than solving (P2) numerically. It can be observed that (7.50) shares similar expressions with the solution to (P1a). The main difference is that, estimating the noise power p_n is required in (P1a), but not in (7.50).

Next, we will demonstrate some instances of (7.50) using the generalized correlation subspaces in Section 7.4.

Example 7.5.1. First let us consider the correlation subspace. Recall that $\mathcal{CS} = \mathcal{GCS}(\mathbf{1}_{[-1/2, 1/2]}) = \text{col}(\mathbf{J})$, as in Theorem 7.4.1. The subspace $\mathcal{CS} + \mathcal{I}$ becomes

$$\mathcal{CS} + \mathcal{I} = \text{col}(\mathbf{J}) + \text{span}(\text{vec}(\mathbf{I})) = \text{col}([\mathbf{J}, \mathbf{J}\mathbf{e}_0]) = \text{col}(\mathbf{J}).$$

Here we use the property that $\text{vec}(\mathbf{I}) = \mathbf{J}\mathbf{e}_0$ [97]. The column vector $\mathbf{e}_0 \in \{0, 1\}^{|\mathbb{D}|}$ satisfies $\langle \mathbf{e}_0 \rangle_m = \delta_{m,0}$ for $m \in \mathbb{D}$. Next, according to (7.50), the orthogonal projection \mathbf{p}_1^* , as shown in Fig. 7.5, can be written as

$$\mathbf{p}_1^* = \mathbf{J}\tilde{\mathbf{x}}_{\mathbb{D}} \in \mathbb{C}^{|\mathbb{S}|^2}, \quad \tilde{\mathbf{x}}_{\mathbb{D}} \triangleq \mathbf{J}^\dagger \text{vec}(\tilde{\mathbf{R}}_{\mathcal{S}}) \in \mathbb{C}^{|\mathbb{D}|}. \quad (7.51)$$

Due to (7.51) and Lemma 7.4.2, the sample value of $\tilde{\mathbf{x}}_{\mathbb{D}}$ at the coarray location $m \in \mathbb{D}$ is given by

$$\langle \tilde{\mathbf{x}}_{\mathbb{D}} \rangle_m = \frac{1}{w(m)} \sum_{n_1 - n_2 = m} \langle \tilde{\mathbf{R}}_{\mathcal{S}} \rangle_{n_1, n_2}, \quad (7.52)$$

where $n_1, n_2 \in \mathbb{S}$. Eq. (7.52) was previously known as *redundancy averaging* [1], [2], [132] and (2.24). The vector $\tilde{\mathbf{x}}_{\mathbb{D}}$ is known to be the sample autocorrelation vector on the difference coarray, which was used extensively in DOA estimators such as the augmented covariance matrix [132] positive definite Toeplitz completion [1], [2], and SS MUSIC [87], [124]. This example shows that *redundancy averaging is closely related to (7.50), which uses the concept of the correlation subspace.*

Example 7.5.2. Eq. (7.50) can be used to derive a large class of DOA estimators with prior knowledge about source directions. According to Section 7.4, if the difference coarray is hole-free and the known source interval is $[-\alpha/2, \alpha/2]$, then the generalized correlation subspace $\mathcal{GCS}(\rho)$ can be approximated by $\text{col}(\mathbf{J}\mathbf{V}_L)$, as in Theorem 7.4.2. Hence the subspace $\mathcal{GCS}(\rho) + \mathcal{I}$ is approximated by

$$\text{col}(\mathbf{J}\mathbf{V}_L) + \text{span}(\text{vec}(\mathbf{I})) = \text{col}([\mathbf{J}\mathbf{V}_L, \mathbf{J}\mathbf{e}_0]) = \text{col}(\mathbf{J}\mathbf{U}_L),$$

where $\mathbf{U}_L \triangleq [\mathbf{V}_L, \mathbf{e}_0]$. Then the associated orthogonal projection \mathbf{p}_2^* , as illustrated in Fig. 7.5, is given by

$$\mathbf{p}_2^* = (\mathbf{J}\mathbf{U}_L)(\mathbf{J}\mathbf{U}_L)^\dagger \text{vec}(\tilde{\mathbf{R}}_{\mathcal{S}}). \quad (7.53)$$

Eq. (7.53) shows that the orthogonal projection can be evaluated using the matrix \mathbf{J} and the DPSS \mathbf{V}_L . If the matrix $\mathbf{J}\mathbf{U}_L$ has full column rank, then Eq. (7.53) can be rewritten as

$$\mathbf{p}_2^* = \mathbf{J}\tilde{\mathbf{y}}_{\mathbb{D}}, \quad (7.54)$$

where

$$\tilde{\mathbf{y}}_{\mathbb{D}} = \mathbf{U}_L((\mathbf{W}\mathbf{U}_L)^H \mathbf{U}_L)^{-1} (\mathbf{W}\mathbf{U}_L)^H \tilde{\mathbf{x}}_{\mathbb{D}}, \quad (7.55)$$

and the matrix \mathbf{W} is defined in Lemma 7.4.2. Here $\tilde{\mathbf{x}}_{\mathbb{D}}$ is given by (7.52). Note that (7.54) shares the same formulation as the first equation of (7.51). Furthermore, according to (7.55), the vector $\tilde{\mathbf{y}}_{\mathbb{D}}$ can be regarded as the denoised version of $\tilde{\mathbf{x}}_{\mathbb{D}}$, as characterized by the oblique projection operator $\mathbf{U}_L((\mathbf{W}\mathbf{U}_L)^H \mathbf{U}_L)^{-1} (\mathbf{W}\mathbf{U}_L)^H$. Eq. (7.55) can also be interpreted as *redundancy averaging with prior knowledge about sources*. Most importantly, coarray-based DOA estimators such as the augmented covariance matrix, positive definite Toeplitz completion, and SS MUSIC can work on the denoised sample autocorrelation vector $\tilde{\mathbf{y}}_{\mathbb{D}}$, without any modification.

For other cases in Section 7.4, (7.54) and (7.55) remains applicable, except that the DPSS \mathbf{V}_L have to be replaced with the eigenvectors Ψ_L .

Covariance matrix denoising using the (generalized) correlation subspace is not limited to the optimization problems presented in this chapter. The constraints imposed on the covariance matrices by the (generalized) correlation subspace can be readily applied to state-of-the-art covariance matrix denoising methods and DOA estimators such as SPICE [161], [163], [168], gridless SPICE [198], and atomic norm denoising [16], [31], [74], [112]. This idea could lead to new DOA estimators that enjoy improved performance, which could even approach the Cramér-Rao bounds for sparse arrays [73], [97], [192].

7.6 Generalized Correlation Subspaces in Multiple Dimensions

The results developed in [141] were not restricted to one dimension. Even though our discussions in this chapter were so far restricted to 1D arrays and 1D DOAs, they can also be readily generalized to multiple dimensions as we shall elaborate next. This is useful in many practical scenarios such as angle-Doppler estimation [8], [86], angle-delay estimation [189], angle-range estimation [138], 2D DOA (azimuth and elevation) estimation [188], and harmonic retrieval [53], [116].

Let us consider the data model for the R -dimensional (R -D) case. The R -D sampling locations $\mathbf{n} = (n^{(1)}, n^{(2)}, \dots, n^{(R)})$ are collected by the set $\mathbb{S} \subset \mathbb{Z}^R$ and the harmonic parameters to be estimated are denoted by

$$\bar{\boldsymbol{\mu}} = (\bar{\mu}^{(1)}, \bar{\mu}^{(2)}, \dots, \bar{\mu}^{(R)}) \in [-1/2, 1/2]^R. \quad (7.56)$$

Then we have the following data model:

$$\mathbf{x}_{\mathbb{S}} = \sum_{i=1}^D A_i \mathbf{v}_{\mathbb{S}}(\bar{\boldsymbol{\mu}}_i) + \mathbf{n}_{\mathbb{S}}, \quad (7.57)$$

where the *vectors* $\mathbf{x}_{\mathbb{S}}$, $\mathbf{v}_{\mathbb{S}}(\bar{\boldsymbol{\mu}}_i)$, and $\mathbf{n}_{\mathbb{S}}$ represent the measurement, the steering vector, and the noise term, respectively. The entry of the steering vector associated with the sample locations $\mathbf{n} \in \mathbb{S}$ is given by $e^{j2\pi\bar{\boldsymbol{\mu}}_i^T \mathbf{n}}$. The source amplitudes A_i and the noise term $\mathbf{n}_{\mathbb{S}}$ are assumed to be uncorrelated, as in Section 7.2. Then we can define the R -D difference coarray and the matrix \mathbf{J} as follows:

Definition 7.6.1 (R -D difference coarray). Let \mathbb{S} be a set of R -D sampling locations. The difference coarray is defined as $\mathbb{D} = \{\mathbf{n}_1 - \mathbf{n}_2 : \forall \mathbf{n}_1, \mathbf{n}_2 \in \mathbb{S}\}$.

Definition 7.6.2 (The matrix \mathbf{J} for R -D). Let \mathbb{S} be a set of R -D sampling locations and \mathbb{D} be the R -D difference coarray. The matrix \mathbf{J} is an $|\mathbb{S}|^2$ -by- $|\mathbb{D}|$ matrix satisfying $\langle \mathbf{J} \rangle_{:,m} = \text{vec}(\mathbf{I}(\mathbf{m}))$. The matrix $\mathbf{I}(\mathbf{m})$ is given by

$$\langle \mathbf{I}(\mathbf{m}) \rangle_{\mathbf{n}_1, \mathbf{n}_2} = \begin{cases} 1, & \text{if } \mathbf{n}_1 - \mathbf{n}_2 = \mathbf{m}, \\ 0, & \text{otherwise,} \end{cases}$$

where $\mathbf{m} \in \mathbb{D}$ and $\mathbf{n}_1, \mathbf{n}_2 \in \mathbb{S}$.

Using Definitions 7.6.1 and 7.6.2, the correlation vector can be expressed as $\mathbf{c}(\bar{\boldsymbol{\mu}}) \triangleq \text{vec}(\mathbf{v}_{\mathbb{S}}(\bar{\boldsymbol{\mu}})\mathbf{v}_{\mathbb{S}}^H(\bar{\boldsymbol{\mu}})) = \mathbf{J}\mathbf{v}_{\mathbb{D}}(\bar{\boldsymbol{\mu}})$, where $\mathbf{v}_{\mathbb{D}}(\bar{\boldsymbol{\mu}})$ is the steering vector on the difference coarray. A numerical example is demonstrated in Section 7.D for clarity. Then, the

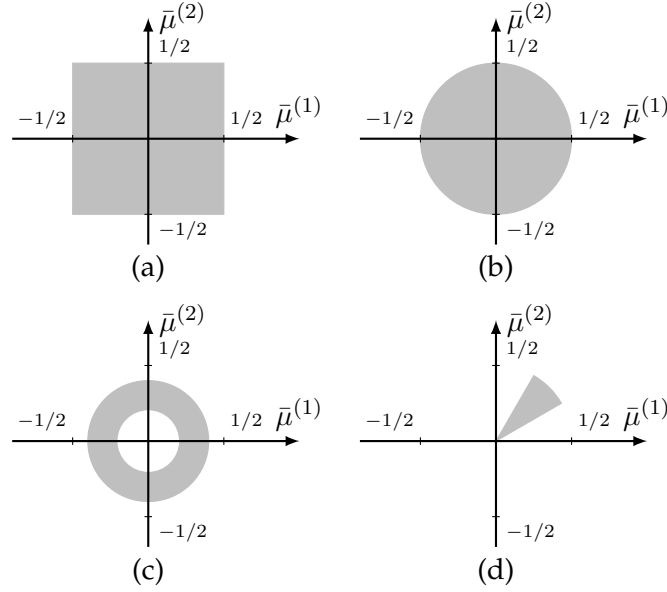


Figure 7.6: The visible region (shaded) of (a) angle-Doppler, (b) 2D DOA, (c) 2D DOA with $\theta_{\min} \leq \theta \leq \theta_{\max}$, and (d) 2D DOA with $\phi_{\min} \leq \phi \leq \phi_{\max}$.

generalized correlation subspace matrix becomes

$$\mathbf{S}(\rho) \triangleq \int_{[-1/2, 1/2]^R} \mathbf{c}(\bar{\boldsymbol{\mu}}) \mathbf{c}^H(\bar{\boldsymbol{\mu}}) \rho(\bar{\boldsymbol{\mu}}) d\bar{\boldsymbol{\mu}} \quad (7.58)$$

$$= \mathbf{J} \left(\underbrace{\int_{[-1/2, 1/2]^R} \mathbf{v}_{\mathbb{D}}(\bar{\boldsymbol{\mu}}) \mathbf{v}_{\mathbb{D}}^H(\bar{\boldsymbol{\mu}}) \rho(\bar{\boldsymbol{\mu}}) d\bar{\boldsymbol{\mu}}}_{\mathbf{S}_{\mathbb{D}}(\rho)} \right) \mathbf{J}^H. \quad (7.59)$$

Eq. (7.58) and (7.59) are analogous to Definition 7.3.1 and Lemma 7.4.1, respectively. Finally, the generalized correlation subspace $\mathcal{GCS}(\rho) \triangleq \text{col}(\mathbf{S}(\rho))$, as in Definition 7.3.2. According to (7.59), the generalized correlation subspace for R -D depends on the difference coarray, similar to Lemma 7.4.1.

Next we will consider some concrete examples in 2D. They are joint angle-Doppler estimation and 2D DOA estimation.

Example 7.6.1 (Joint angle-Doppler estimation). The joint angle-Doppler estimation [8], [86] corresponds to the data model (7.57) with $R = 2$. It aims to estimate the angle and Doppler frequency from the spatiotemporal measurements $\mathbf{x}_{\mathbb{S}}$. The harmonic parameters $\bar{\boldsymbol{\mu}} = (\bar{\mu}^{(1)}, \bar{\mu}^{(2)})$ are related to the DOA and the Doppler frequency as follows:

$$\bar{\mu}^{(1)} = (d/\lambda) \sin \theta, \quad \bar{\mu}^{(2)} = (T/\lambda) v, \quad (7.60)$$

where λ is the wavelength, $d = \lambda/2$ is the minimum sensor separation, $\theta \in [-\pi/2, \pi/2]$ is the DOA, T is the sampling interval in the temporal domain, and v is the radial

velocity of the source. $\bar{\mu}^{(1)}$ and $\bar{\mu}^{(2)}$ are called the normalized angle and normalized Doppler, respectively. If the sampling interval T is chosen properly, the parameters $(\bar{\mu}^{(1)}, \bar{\mu}^{(2)})$ belongs to $[-1/2, 1/2]^2$. This region is also depicted in Fig. 7.6(a) for clarity.

Next, suppose we choose the density function $\rho(\bar{\boldsymbol{\mu}})$ to be $\mathbf{1}_{[-1/2, 1/2]^2}(\bar{\boldsymbol{\mu}})$. The generalized correlation subspace matrix becomes

$$\mathbf{S}(\mathbf{1}_{[-1/2, 1/2]^2}) = \mathbf{J}\mathbf{J}^H = (\mathbf{J}\mathbf{W}^{-1/2})\mathbf{W}(\mathbf{J}\mathbf{W}^{-1/2})^H,$$

where $\mathbf{W} = \text{diag}(w(\mathbf{m}))_{\mathbf{m} \in \mathbb{D}}$. Here $w(\mathbf{m}) = |\{(\mathbf{n}_1, \mathbf{n}_2) \in \mathbb{S}^2 : \mathbf{n}_1 - \mathbf{n}_2 = \mathbf{m}\}|$ denotes 2D weight function. This result is analogous to that in Section 7.4. It can be inferred that the positive eigenvalues of $\mathbf{S}(\mathbf{1}_{[-1/2, 1/2]^2})$ are $w(\mathbf{m})$ and the associated eigenvectors are $\text{vec}(\mathbf{I}(\mathbf{m}))/\sqrt{w(\mathbf{m})}$. Note that the results in Example 7.6.1 can be trivially extended to the R -D case if the parameters $\bar{\boldsymbol{\mu}} \in [-1/2, 1/2]^R$.

Example 7.6.2 (2D DOA estimation). Another example of (7.57) with $R = 2$ is the 2D DOA estimation. The parameters of interest are the *azimuth* $\phi \in [0, 2\pi]$ and the *elevation* $\theta \in [0, \pi/2]$. The relation between the 2D DOA (θ, ϕ) and the harmonic parameters $\bar{\boldsymbol{\mu}} = (\bar{\mu}^{(1)}, \bar{\mu}^{(2)})$ is given by

$$\bar{\mu}^{(1)} = (d_x/\lambda) \sin \theta \cos \phi, \quad \bar{\mu}^{(2)} = (d_y/\lambda) \sin \theta \sin \phi, \quad (7.61)$$

where $d_x = d_y = \lambda/2$. According to (7.61), the visible region of $\bar{\boldsymbol{\mu}}$ becomes a disc with radius $1/2$, i.e.,

$$\mathbb{K} = \{\bar{\boldsymbol{\mu}} : \|\bar{\boldsymbol{\mu}}\|_2 \leq 1/2\}. \quad (7.62)$$

The set \mathbb{K} is also depicted in Fig. 7.6(b). Using (7.59), the generalized correlation subspace matrix with density function $\rho(\bar{\boldsymbol{\mu}}) = \mathbf{1}_{\mathbb{K}}(\bar{\boldsymbol{\mu}})$ becomes $\mathbf{S}(\mathbf{1}_{\mathbb{K}}) = \mathbf{J}\mathbf{S}_{\mathbb{D}}(\mathbf{1}_{\mathbb{K}})\mathbf{J}^H$. Here the entry of $\mathbf{S}_{\mathbb{D}}(\mathbf{1}_{\mathbb{K}})$ associated with coarray location $\mathbf{m}_1, \mathbf{m}_2 \in \mathbb{D}$ can be derived as in Section 7.E:

$$\langle \mathbf{S}_{\mathbb{D}}(\mathbf{1}_{\mathbb{K}}) \rangle_{\mathbf{m}_1, \mathbf{m}_2} = \text{jinc}(\|\mathbf{m}_1 - \mathbf{m}_2\|_2), \quad (7.63)$$

where the jinc function $\text{jinc}(x)$ is $\pi/4$ for $x = 0$ and $J_1(\pi x)/(2x)$ otherwise [24]. Here $J_1(x)$ is the first-order Bessel function of the first kind [24]. Eq. (7.63) can be regarded as an extension of (7.32) since the jinc function is analogous to the sinc function in the 2D polar coordinate [24]. The eigenvectors of $\mathbf{S}_{\mathbb{D}}(\mathbf{1}_{\mathbb{K}})$ are *2D discrete prolate spheroidal sequences (2D DPSS)*. Details about these sequences can be found in [155] and the references therein. Finally the generalized correlation subspace can be approximated by $\text{col}(\mathbf{J}\boldsymbol{\Psi}_L)$, where $\boldsymbol{\Psi}_L$ contains the first L 2D DPSS and L is defined in (7.47).

If the prior knowledge about 2D DOA is available, then the visible region could be an annulus or a circular sector. For instance, if we know a priori that the elevation $\theta_{\min} \leq \theta \leq \theta_{\max}$, then the visible region is depicted in Fig. 7.6(c). On the other hand, if the the prior knowledge is $\phi_{\min} \leq \phi \leq \phi_{\max}$, then the visible region becomes a circular sector, as illustrated in Fig. 7.6(d).

7.7 Numerical Examples

Generalized Correlation Subspaces

In this section, we will consider the following four 1D array configurations: the ULA with 10 sensors, the nested array with $N_1 = N_2 = 5$, as in (2.7), the coprime array with $M = 3, N = 5$, as in (2.8), and the super nested array with $N_1 = N_2 = 5, Q = 2$, as in Definition 3.4.1. The number of sensors is 10 for each array. The sensor locations and the nonnegative part of the difference coarrays for these arrays are depicted in Fig. 7.2. Since the difference coarray is symmetric (Lemma 7.C.1.2), the size of the difference coarray is 19 for ULA, 59 for the nested array, 43 for the coprime array, and 59 for the super nested array.

The following example aims to demonstrate Theorem 7.4.1 and (7.27). The experiment is conducted as follows. We first compute the numerical approximation of $\mathbf{S}(\rho)$, as denoted by $\tilde{\mathbf{S}}(\rho)$, as follows:

$$\tilde{\mathbf{S}}(\rho) = \sum_{\ell=-(N_{\text{pt}}-1)/2}^{(N_{\text{pt}}-1)/2} \mathbf{c}(\ell\Delta)\mathbf{c}^H(\ell\Delta)\rho(\ell\Delta) \times \Delta, \quad (7.64)$$

where the number of discrete samples is $N_{\text{pt}} = 2^{14} + 1$ and the step size is $\Delta = 1/N_{\text{pt}}$. Then the eigenvalues of $\tilde{\mathbf{S}}(\rho_1)$ and $\tilde{\mathbf{S}}(\rho_2)$ are plotted in Fig. 7.7(a), (c), (e), and (g), where $\rho_1(\bar{\theta})$ and $\rho_2(\bar{\theta})$ are given in Theorem 7.4.1. As a comparison, the weight functions for these arrays are plotted in Fig. 7.7(b), (d), (f), and (h).

The results in Fig. 7.7 show that, $\text{col}(\tilde{\mathbf{S}}(\rho_1))$ and $\text{col}(\tilde{\mathbf{S}}(\rho_2))$ have the same dimension $|\mathbb{D}|$, which is the size of the difference coarray. For example, the nested array (Fig. 7.7(c)) and the super nested array (Fig. 7.7(g)) share the same number of nonzero eigenvalues, since they own the same difference coarray, as shown in Fig. 7.2(b) and (d). Furthermore, the eigenvalues for $\tilde{\mathbf{S}}(\rho_2)$ should be close to the weight functions, as indicated in (7.27). This property can be verified, for instance, in Fig. 7.7(g) and (h), where the eigenvalues $\lambda_2 = \lambda_3 = 4$ and the weight functions $w(2) = w(-2) = 4$.

DOA Estimation with Nested Arrays and Prior Source Intervals

Fig. 7.8 shows the estimation performance as a function of SNR and the number of snapshots. The equal-power and uncorrelated sources have normalized DOAs $-0.045, 0$, and 0.045 . The number of sources D is 3. The array configuration is the nested array with $N_1 = N_2 = 5$ (10 sensors), as depicted in Fig. 7.2(b). Then the

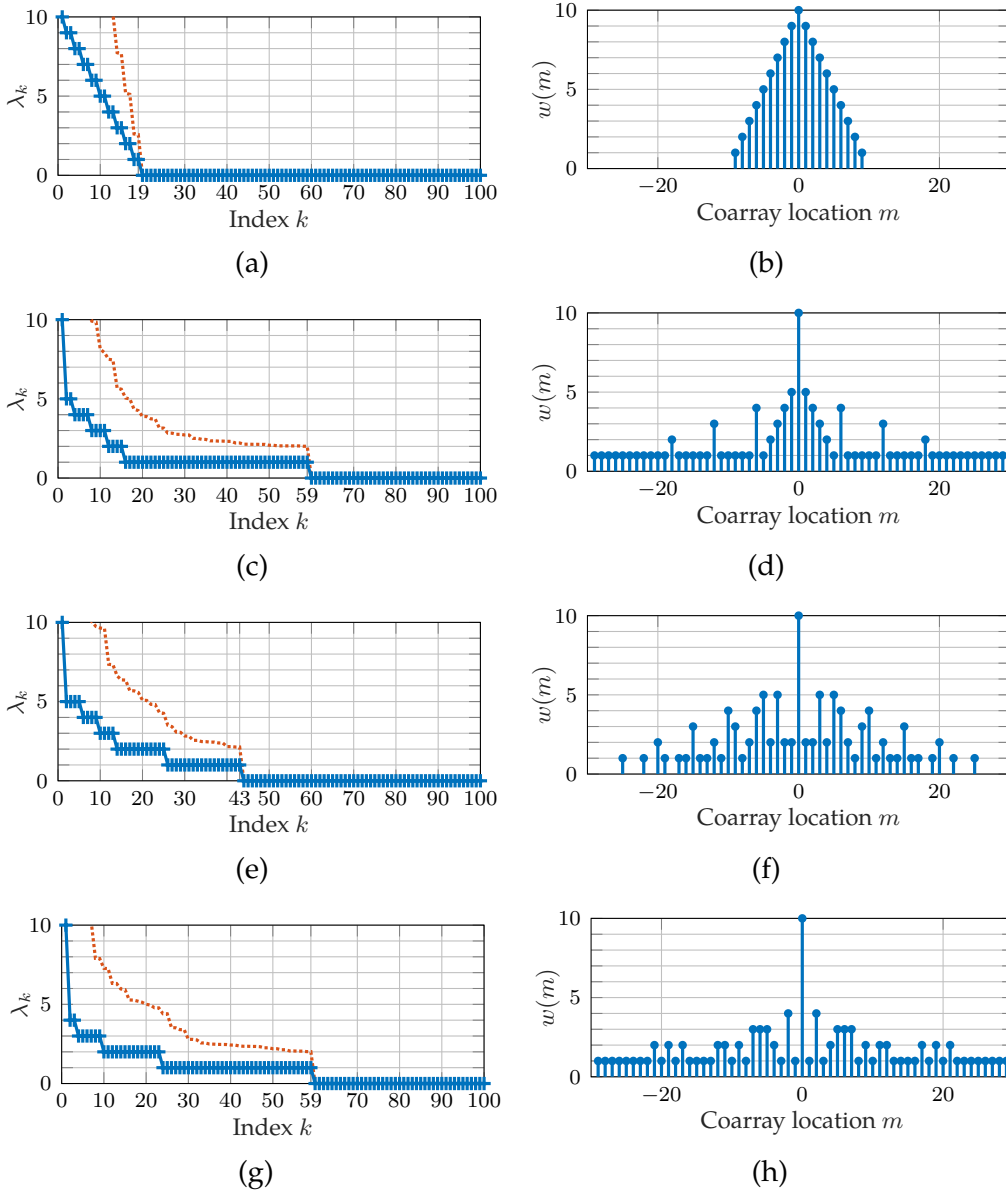


Figure 7.7: The eigenvalues of the matrix $\tilde{\mathbf{S}}(\rho)$ (left) and the weight functions (right) for (a), (b) the ULA with 10 sensors ($|\mathbb{D}| = 19$), (c), (d) the nested array with $N_1 = N_2 = 5$ (10 sensors, $|\mathbb{D}| = 59$), (e), (f) the coprime array with $M = 3, N = 5$ (10 sensors, $|\mathbb{D}| = 43$), and (g), (h) the super nested array with $N_1 = N_2 = 5, Q = 2$ (10 sensors, $|\mathbb{D}| = 59$). Here the matrices $\tilde{\mathbf{S}}(\rho)$ are given by (7.64) and the eigenvalues of $\tilde{\mathbf{S}}(\rho)$ are obtained numerically. The red dashed curves in Figs. (a), (c), (e), and (g) correspond to $\rho_1(\bar{\theta}) = 2(1 - (2\bar{\theta})^2)^{-1/2} \mathbf{1}_{[-1/2, 1/2]}(\bar{\theta})$ while the blue curves in Figs. (a), (c), (e), and (g) are associated with $\rho_2(\bar{\theta}) = \mathbf{1}_{[-1/2, 1/2]}(\bar{\theta})$.

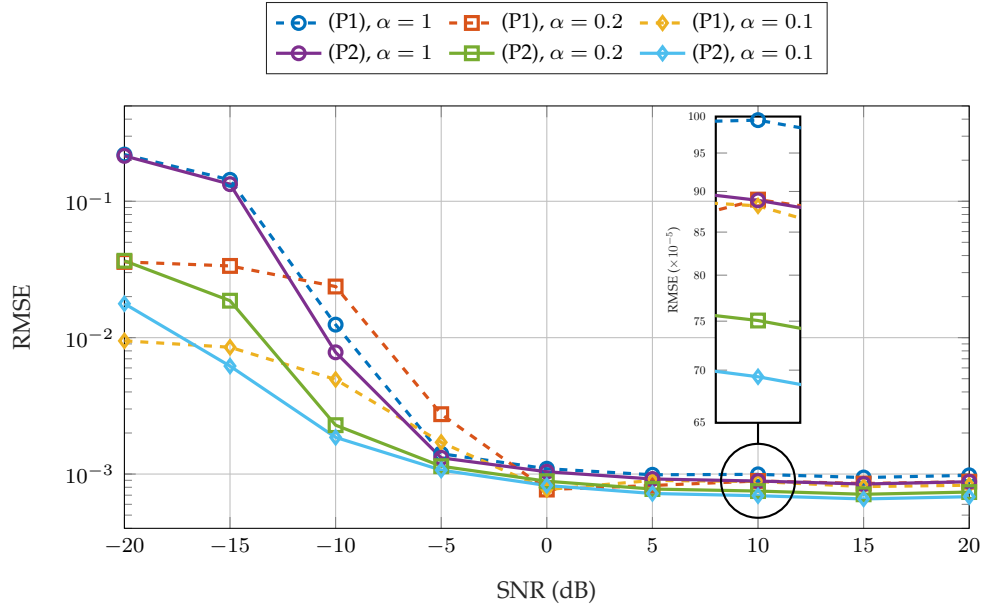
generalized correlation subspaces $\mathcal{GCS}(\mathbf{1}_{[-\alpha/2, \alpha/2]})$ can be evaluated according to Section 7.4. The error tolerance in (7.47) is $\delta = 10^{-10}$ so the parameter L becomes 10 and 17 for $\alpha = 0.1$ and 0.2 , respectively. In each run, the sensor measurements $\tilde{\mathbf{x}}_{\mathcal{S}}(k)$ for $k = 1, \dots, K$ are realized by (1.5), from which the sample covariance matrix $\tilde{\mathbf{R}}_{\mathcal{S}}$ can be determined by (2.23). Then the covariance matrices are denoised according to 1) Problem (P1) and the *cvx* package with perfect knowledge about the noise power; 2) Problem (P2) and (7.50) without knowing the noise power. Finally the source directions are estimated by the SS MUSIC algorithm [87], [124] on the denoised covariance matrices. The estimation performance is measured in terms of root mean-squared errors (RMSE), defined as

$$\text{RMSE} = \sqrt{\frac{1}{D} \sum_{i=1}^D (\hat{\theta}_i - \bar{\theta}_i)^2},$$

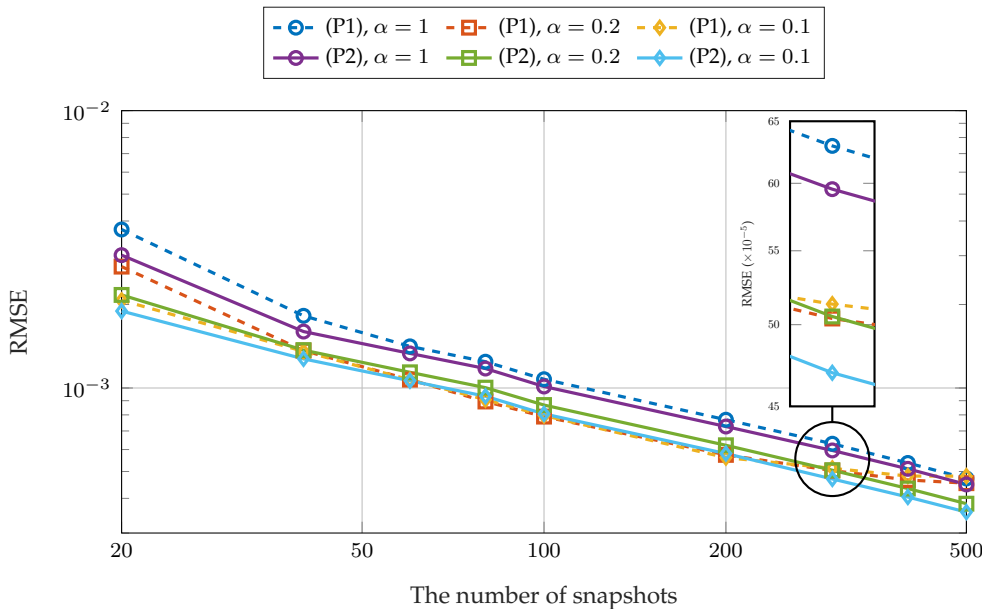
where $\hat{\theta}_i$ denotes the estimated normalized DOAs. Each sample point is averaged from 1000 Monte-Carlo runs.

It can be seen from Fig. 7.8 that if the source interval $[-\alpha/2, \alpha/2]$ is known, the RMSEs decrease except at very low SNRs. In this example, we choose $\alpha = 1, 0.2$, and 0.1 in Fig. 7.8. The following discuss the performances of these estimators:

1. In most cases, the RMSE for (P1) and (P2) decrease with α , for the same SNR and the same number of snapshots. The improvement is significant for low SNR and limited snapshots. This is because smaller source intervals $[-\alpha/2, \alpha/2]$ help to improve the estimation performances.
2. (P1) requires much more time than (P2), provided that the generalized correlation subspace is computed using the results in Section 7.4. For instance, the computational time for (P1) and $\alpha = 0.1$ in Fig. 7.8(a) is 9904.5 seconds while that for (P2) and $\alpha = 0.1$ in Fig. 7.8(a) is 53.7 seconds. The reason is that (P1) is solved numerically using the *cvx* package but (P2) can be implemented efficiently using (7.50).
3. As shown in Fig. 7.8(a), empirically, (P2) has better estimation performance than (P1) for the same α in most cases. For instance, if $\alpha = 0.1$ and $\text{SNR} = -10\text{dB}$, then the RMSE for (P1) is 4.9×10^{-3} while that for (P2) becomes 1.9×10^{-3} . If $\alpha = 0.1$ and $\text{SNR} = 10\text{dB}$, then the RMSEs for (P1) and (P2) are about 8.8×10^{-4} and 6.9×10^{-4} , respectively. These phenomena can also be observed in Fig. 7.8(b).



(a)



(b)

Figure 7.8: The dependence of root mean-squared errors (RMSE) on (a) SNR and (b) the number of snapshots for the optimization problems (P1) and (P2) with generalized correlation subspaces $\mathcal{GCS}(\mathbf{1}_{[-\alpha/2, \alpha/2]})$. There are $D = 3$ equal-power and uncorrelated sources at normalized DOAs -0.045 , 0 , and 0.045 . The array configuration is the nested array with $N_1 = N_2 = 5$ (10 sensors), as depicted in Fig. 7.2(b). The parameters are (a) 100 snapshots and (b) 0dB SNR. Each data point is averaged from 1000 Monte-Carlo runs.

Table 7.2: CPU time in seconds and RMSE for several cases

| Case | α | Step 1 (time) | Step 2 (time) | Total time (including Step 3) | RMSE |
|------|----------|-------------------------|------------------|----------------------------------|----------|
| A | 1 | Numerical (3.288s) | P1 (1.057s) | 4.351s | 0.000991 |
| B | 1 | Numerical (3.248s) | P2 (0.00008s) | 3.255s | 0.000918 |
| C | 1 | Analytical (0.0013s) | P1 (0.802s) | 0.810s | 0.000990 |
| D | 1 | Analytical (0.0013s) | P2 (0.00009s) | 0.008s | 0.000918 |
| E | 0.1 | Numerical (3.296s) | P1 (1.118s) | 4.421s | 0.000903 |
| F | 0.1 | Numerical (3.271s) | P2 (0.00008s) | 3.278s | 0.000718 |
| G | 0.1 | Analytical (0.0066s) | P1 (1.053s) | 1.067s | 0.000901 |
| H | 0.1 | Analytical (0.0066s) | P2 (0.00010s) | 0.013s | 0.000718 |

[†] “Analytical” is the new analytical method for Step 1, as in Section 7.4.

[‡] P2 is the proposed method for Step 2, as in Section 7.5.

* Step 3 took between 0.0063 to 0.0068 seconds.

Computational Complexity

Table 7.2 investigates the interplay between the computational complexity and the estimation performance by varying the parameter α and the implementation details. These cases are denoted by Cases A to H, respectively. Here Step 1, which computes the (generalized) correlation subspace, can be realized in two ways. One is the numerical integration (7.64), followed by numerical eigen-decompositions [141]. The number of grids N_{pt} in (7.64) is $2^{14} + 1$ while the density function $\rho(\bar{\theta})$ is $2(1 - (2\bar{\theta})^2)^{-1/2} \mathbf{1}_{[-\alpha/2, \alpha/2]}(\bar{\theta})$. The other is to use the proposed analytical expressions, based on Definition 6.B.1, Theorem 7.4.1, and Table 7.1. Then, in Step 2, either (P1) or (P2) is solved. Finally, Step 3 uses SS MUSIC to estimate the source directions. We assume 100 snapshots and 5dB SNR. The CPU time and the RMSEs in Table 7.2 are averaged from 1000 Monte-Carlo runs, on a Ubuntu 16.04 workstation with a Intel Core i7-2600 3.40GHz processor and 8GB RAM. The remaining parameters are given in Section 7.7.

Some observations can be drawn from Table 7.2. First, the proposed analytical expressions lead to almost the same RMSE but much less CPU time than those with numerical approximations. For instance, the CPU time for Step 1 in Case D is about

0.04% of that for Step 1 in Case B. Second, in these examples, (P2) enjoys smaller RMSE and much less computational time than (P1). As an example, the CPU time of Step 2 in Case B costs only 0.007% of that of Step 2 in Case A, while the RMSE is 0.000991 for Case A and 0.000918 for Case B, respectively. Finally, if $\alpha = 0.1$, the proposed analytical approach remains computationally tractable. It can be observed that the CPU time for Step 1 in Case H is approximately 0.2% of that for Step 1 in Case F. These observations show that, for a given α , it is preferable to use the proposed analytical expressions and problem (P2), since they lead to the least total time and the smallest RMSE.

7.8 Concluding Remarks

In this chapter, we presented generalized correlation subspaces with applications to DOA estimation for uncorrelated sources and known source intervals. Generalized correlation subspaces have closed-form characterizations in terms of array profiles such as sensor locations and difference coarrays. Furthermore, our theory provides insights to existing DOA estimators and multidimensional sparse arrays with prior knowledge about sources.

In the future, it is of considerable interest to exploit generalized correlation subspaces in other topics of array processing, like adaptive beamforming, source detection, and target tracking. Another future topic would be the performance analysis for the proposed approach using generalized correlation subspaces.

Appendices

7.A Proof of the Equivalence of (7.5) and Definition 7.2.1

To begin with, we need the following lemmas:

Lemma 7.A.1. Let $\mathbf{M} \in \mathbb{C}^{N \times N}$ be a Hermitian, positive semidefinite matrix. Assume $\mathbf{u} \in \mathbb{C}^N$. Then $\mathbf{u}^H \mathbf{M} \mathbf{u} = 0$ if and only if \mathbf{u} belongs to the null space of \mathbf{M} .

Proof. If \mathbf{u} belongs to the null space of \mathbf{M} , then $\mathbf{M} \mathbf{u} = \mathbf{0}$ and clearly $\mathbf{u}^H \mathbf{M} \mathbf{u} = 0$. Conversely, if $\mathbf{u}^H \mathbf{M} \mathbf{u} = 0$, then $(\mathbf{M}^{1/2} \mathbf{u})^H (\mathbf{M}^{1/2} \mathbf{u}) = 0$, where the matrix square root exists due to the positive semidefiniteness of \mathbf{M} . Hence, $\mathbf{M}^{1/2} \mathbf{u} = \mathbf{0}$, so $\mathbf{M} \mathbf{u} = \mathbf{0}$. □

Lemma 7.A.2. Let $f(x)$ be a real-valued Lebesgue integrable function defined over a measurable set \mathbb{A} . Assume that $f(x) \geq 0$ for $x \in \mathbb{A}$ almost everywhere (a.e.). Then $\int_{\mathbb{A}} f(x) dx = 0$ if and only if $f(x) = 0$ a.e.

Proof. See [54, Chapter V] for details. □

Next it will be first shown that $\mathcal{CS}^\perp = \text{null}(\mathbf{S}^H)$, where \mathcal{CS}^\perp denotes the orthogonal complement of \mathcal{CS} and $\text{null}(\mathbf{A})$ represents the null space of \mathbf{A} .

First consider any $\mathbf{v} \in \text{null}(\mathbf{S}^H)$. Since \mathbf{S} is a Hermitian positive semidefinite matrix, Lemma 7.A.1 implies that $\mathbf{v} \in \text{null}(\mathbf{S}^H)$ is equivalent to $\mathbf{v}^H \mathbf{S}^H \mathbf{v} = 0$. Substituting the definition of \mathbf{S} , (7.7), into $\mathbf{v}^H \mathbf{S}^H \mathbf{v} = 0$ yields

$$\int_{-\pi/2}^{\pi/2} |\mathbf{v}^H \mathbf{c}(\bar{\theta})|^2 d\theta = 0. \quad (7.65)$$

Since the nonnegative function $|\mathbf{v}^H \mathbf{c}(\bar{\theta})|^2$ is continuous in θ , Lemma 7.A.2 indicates that (7.65) is equivalent to $|\mathbf{v}^H \mathbf{c}(\bar{\theta})|^2 = 0$ for all $\theta \in [-\pi/2, \pi/2]$. Namely, $\mathbf{v} \in \mathcal{CS}^\perp$. Note that all the above arguments are both necessary and sufficient so we have $\mathcal{CS}^\perp = \text{null}(\mathbf{S}^H)$.

Finally, the correlation subspace can be obtained by $\mathcal{CS} = \mathcal{CS}^{\perp\perp} = \text{null}(\mathbf{S}^H)^\perp = \text{col}(\mathbf{S})$, which proves this observation.

7.B Proof of Lemma 7.3.1

Let $\rho_1(\bar{\theta})$ and $\rho_2(\bar{\theta})$ be two nonnegative Lebesgue integrable functions with the same support. The support of $\rho_1(\bar{\theta})$ and $\rho_2(\bar{\theta})$ satisfies $\text{supp}(\rho_1) = \text{supp}(\rho_2) = \mathbb{A} \subseteq [-1/2, 1/2]$. The corresponding generalized correlation subspace matrices are denoted by $\mathbf{S}(\rho_1)$ and $\mathbf{S}(\rho_2)$, respectively.

Consider a nonzero and finite-valued vector $\mathbf{u} \in \mathbb{C}^{|\mathbb{S}|^2}$. It will be shown that $\mathbf{u}^H \mathbf{S}(\rho_1) \mathbf{u} = 0$ if and only if $\mathbf{u}^H \mathbf{S}(\rho_2) \mathbf{u} = 0$. Based on Definition 7.3.1, the condition $\mathbf{u}^H \mathbf{S}(\rho_1) \mathbf{u} = 0$ is equivalent to the following:

$$\begin{aligned} \mathbf{u}^H \left(\int_{\mathbb{A}} \mathbf{c}(\bar{\theta}) \mathbf{c}^H(\bar{\theta}) \rho_1(\bar{\theta}) d\bar{\theta} \right) \mathbf{u} &= 0 \\ \text{if and only if } \int_{\mathbb{A}} |\mathbf{c}^H(\bar{\theta}) \mathbf{u}|^2 \rho_1(\bar{\theta}) d\bar{\theta} &= 0. \end{aligned} \quad (7.66)$$

Due to Lemma 7.A.2, Eq. (7.66) is equivalent to the statement that $|\mathbf{c}^H(\bar{\theta}) \mathbf{u}|^2 \rho_1(\bar{\theta}) = 0$ for $\bar{\theta} \in \mathbb{A}$ a.e. Since $\bar{\theta}$ belongs to the support \mathbb{A} , multiplying both sides with $\rho_2(\bar{\theta})/\rho_1(\bar{\theta})$ yields $|\mathbf{c}^H(\bar{\theta}) \mathbf{u}|^2 \rho_2(\bar{\theta}) = 0$ for $\bar{\theta} \in \mathbb{A}$ a.e. Invoking Lemma 7.A.2 again gives $\mathbf{u}^H \mathbf{S}(\rho_2) \mathbf{u} = 0$. Combining the above arguments with Lemma 7.A.1 leads to $\text{null}(\mathbf{S}(\rho_1)) = \text{null}(\mathbf{S}(\rho_2))$, where $\text{null}(\mathbf{S})$ denotes the null space of \mathbf{S} . Taking the orthogonal complement on the null spaces gives $\text{col}(\mathbf{S}(\rho_1)) = \text{col}(\mathbf{S}(\rho_2))$, which proves this theorem.

7.C Properties of Weight Functions

In this section, some useful properties of the weight function $w(m)$ are listed in Lemma 7.C.1, as follows:

Lemma 7.C.1. Let \mathbb{S} be an integer-valued sensor location set. Assume that the difference coarray \mathbb{D} and the weight function $w(m)$ are as defined in Definitions 2.18 and 2.2.9, respectively. Then the following properties are satisfied:

1. $w(m)$ is a positive integer.
2. $w(-m) = w(m)$ for $m \in \mathbb{D}$.
3. $1 \leq w(m) \leq |\mathbb{S}|$ for $m \in \mathbb{D}$.
4. $w(m) = |\mathbb{S}|$ if and only if $m = 0$.
5. $\sum_{m \in \mathbb{D}} w(m) = |\mathbb{S}|^2$.

Proof. 1) Based on Definition 2.2.9, the weight function $w(m)$ is the number of sensor pairs with separation m , which is a positive interger.

2) The quantity $w(-m)$ can be simplified as

$$\begin{aligned} w(-m) &= |\{(n_1, n_2) \in \mathbb{S}^2 : n_1 - n_2 = -m\}| \\ &= |\{(n_2, n_1) \in \mathbb{S}^2 : n_2 - n_1 = m\}| = w(m). \end{aligned}$$

3) If $w(m) = 0$, then there does not exist $(n_1, n_2) \in \mathbb{S}^2$ such that $n_1 - n_2 = m \in \mathbb{D}$, which contradicts Definition 2.18.

Next we consider the case of $w(m) > |\mathbb{S}|$. According to Definition 2.2.9, there exist *distinct* sensor pairs $(n_{1,p}, n_{2,p}) \in \mathbb{S}^2$ such that $n_{1,p} - n_{2,p} = m$, where $p = 1, 2, \dots, w(m)$. Since $w(m) > |\mathbb{S}|$ and all $n_{1,p}$'s belong to \mathbb{S} , there must exist at least two $n_{1,p}$'s that are identical. Without loss of generality, it is assumed that $n_{1,1} = n_{1,2}$. Then $n_{2,1} = n_{1,1} - m = n_{1,2} - m = n_{2,2}$ so these sensor pairs are not distinct, which contradicts the assumption. Hence we have $1 \leq w(m) \leq |\mathbb{S}|$.

4) If $w(m) = |\mathbb{S}|$, then the *distinct* sensor pairs $(n_{1,p}, n_{2,p}) \in \mathbb{S}^2$ must satisfy

$$\{n_{1,1}, n_{1,2}, \dots, n_{1,|\mathbb{S}|}\} = \mathbb{S}, \quad (7.67)$$

$$\{n_{1,1} - m, n_{1,2} - m, \dots, n_{1,|\mathbb{S}|} - m\} = \mathbb{S}, \quad (7.68)$$

where (7.68) is due to $n_{2,p} = n_{1,p} - m$ for $p = 1, 2, \dots, w(m)$. If $m = 0$, then (7.67) and (7.68) hold true simultaneously. If $m \neq 0$, then (7.67) contradicts (7.68), which can be shown as follows. Let $n_{1,\min} = \min\{n_{1,1}, n_{1,2}, \dots, n_{1,|\mathbb{S}|}\}$. Therefore the minimum of the left-hand side of (7.68) is $n_{1,\min} - m$. The right-hand sides of (7.67) and (7.68) indicate that $n_{1,\min} = n_{1,\min} - m$, which contradicts the assumption $m \neq 0$.

5) Using Definition 2.2.9, the left-hand side becomes

$$\sum_{m \in \mathbb{D}} w(m) = \sum_{m \in \mathbb{D}} |\{(n_1, n_2) \in \mathbb{S}^2 : n_1 - n_2 = m\}|.$$

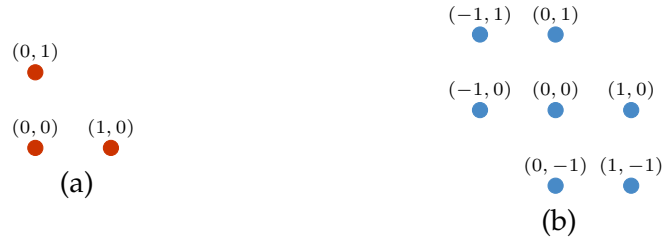


Figure 7.9: (a) The physical array and (b) its difference coarray.

Reindexing the summation by $(n_1, n_2) \in \mathbb{S}^2$ leads to $\sum_{(n_1, n_2) \in \mathbb{S}^2} 1 = |\mathbb{S}|^2$, which completes the proof. \square

7.D Numerical Examples for Section 7.6

Consider the array configuration in Fig. 7.9(a), which corresponds to the set

$$\mathbb{S} = \{(0, 0), (0, 1), (1, 0)\}. \quad (7.69)$$

The difference set \mathbb{D} is depicted in Fig. 7.9(b). Here the elements in \mathbb{D} are sorted in the ascending order, based on the first coordinate. If two elements share the same first coordinate, then they are sorted in the ascending order, based on the second coordinate, and so on. Therefore, the elements in \mathbb{D} are sorted as

$$\mathbb{D} = \{(-1, 0), (-1, 1), (0, -1), (0, 0), (0, 1), (1, -1), (1, 0)\}. \quad (7.70)$$

In the following development, the rows or the columns in the steering vectors, the matrix $\mathbf{I}(\mathbf{m})$, and the \mathbf{J} are sorted according to the order in (7.69) and (7.70).

Next we will construct the matrix \mathbf{J} , as in Definition 7.6.2. For the coarray locations

$\mathbf{m} = (0, 0), (0, 1), (1, -1), (1, 0)$, the matrices $\mathbf{I}(\mathbf{m})$ are given by

$$\mathbf{I}(\mathbf{m} = (0, 0)) = \begin{array}{c} \mathbf{n}_2=(0,0) \quad (0,1) \quad (1,0) \\ \mathbf{n}_1=(0,0) \\ (0,1) \\ (1,0) \end{array} \begin{bmatrix} 1 & 0 & 0 \\ 0 & 1 & 0 \\ 0 & 0 & 1 \end{bmatrix},$$

$$\mathbf{I}(\mathbf{m} = (0, 1)) = \begin{array}{c} \mathbf{n}_2=(0,0) \quad (0,1) \quad (1,0) \\ \mathbf{n}_1=(0,0) \\ (0,1) \\ (1,0) \end{array} \begin{bmatrix} 0 & 0 & 0 \\ 1 & 0 & 0 \\ 0 & 0 & 0 \end{bmatrix},$$

$$\mathbf{I}(\mathbf{m} = (1, -1)) = \begin{array}{c} \mathbf{n}_2=(0,0) \quad (0,1) \quad (1,0) \\ \mathbf{n}_1=(0,0) \\ (0,1) \\ (1,0) \end{array} \begin{bmatrix} 0 & 0 & 0 \\ 0 & 0 & 0 \\ 0 & 1 & 0 \end{bmatrix},$$

$$\mathbf{I}(\mathbf{m} = (1, 0)) = \begin{array}{c} \mathbf{n}_2=(0,0) \quad (0,1) \quad (1,0) \\ \mathbf{n}_1=(0,0) \\ (0,1) \\ (1,0) \end{array} \begin{bmatrix} 0 & 0 & 0 \\ 0 & 0 & 0 \\ 1 & 0 & 0 \end{bmatrix}.$$

It can be shown that $\mathbf{I}(-\mathbf{m}) = \mathbf{I}^T(\mathbf{m})$, as in the 1D case. Therefore, the matrix \mathbf{J} can be expressed as

$$\mathbf{J} = \begin{array}{c} \mathbf{m}= \\ (-1,0) \quad (-1,1) \quad (0,-1) \quad (0,0) \quad (0,1) \quad (1,-1) \quad (1,0) \end{array} \begin{bmatrix} 0 & 0 & 0 & 1 & 0 & 0 & 0 \\ 0 & 0 & 0 & 0 & 1 & 0 & 0 \\ 0 & 0 & 0 & 0 & 0 & 0 & 1 \\ 0 & 0 & 1 & 0 & 0 & 0 & 0 \\ 0 & 0 & 0 & 1 & 0 & 0 & 0 \\ 0 & 0 & 0 & 0 & 0 & 1 & 0 \\ 1 & 0 & 0 & 0 & 0 & 0 & 0 \\ 0 & 1 & 0 & 0 & 0 & 0 & 0 \\ 0 & 0 & 0 & 1 & 0 & 0 & 0 \end{bmatrix}. \quad (7.71)$$

According to Section 7.6, the 2D weight function can be computed as

$$\begin{aligned} w(\mathbf{m} = (0, 0)) &= 3, & w(\mathbf{m} = (0, 1)) &= 1, \\ w(\mathbf{m} = (1, -1)) &= 1, & w(\mathbf{m} = (1, 0)) &= 1. \end{aligned}$$

Given the matrix \mathbf{J} and the weight function, now we can verify the property $\mathbf{c}(\bar{\boldsymbol{\mu}}) = \mathbf{J}\mathbf{v}_{\mathbb{D}}(\bar{\boldsymbol{\mu}})$. To begin with, we first write the steering vector on the physical array $\mathbf{v}_{\mathbb{S}}(\bar{\boldsymbol{\mu}})$ as

$$\mathbf{v}_{\mathbb{S}}(\bar{\boldsymbol{\mu}}) = [e^{j2\pi\bar{\boldsymbol{\mu}}^T \mathbf{n}}]_{\mathbf{n} \in \mathbb{S}} = \begin{bmatrix} e^{j2\pi(\bar{\mu}^{(1)} \cdot 0 + \bar{\mu}^{(2)} \cdot 0)} \\ e^{j2\pi(\bar{\mu}^{(1)} \cdot 0 + \bar{\mu}^{(2)} \cdot 1)} \\ e^{j2\pi(\bar{\mu}^{(1)} \cdot 1 + \bar{\mu}^{(2)} \cdot 0)} \end{bmatrix} = \begin{bmatrix} 1 \\ \beta \\ \alpha \end{bmatrix},$$

where $\alpha = e^{j2\pi\bar{\mu}^{(1)}}$, $\beta = e^{j2\pi\bar{\mu}^{(2)}}$, and $\bar{\boldsymbol{\mu}} = (\bar{\mu}^{(1)}, \bar{\mu}^{(2)})$. Then the correlation vector $\mathbf{c}(\bar{\boldsymbol{\mu}})$ can be expressed as

$$\begin{aligned} \mathbf{c}(\bar{\boldsymbol{\mu}}) &\triangleq \text{vec}(\mathbf{v}_{\mathbb{S}}(\bar{\boldsymbol{\mu}})\mathbf{v}_{\mathbb{S}}^H(\bar{\boldsymbol{\mu}})) \\ &= [1, \beta, \alpha, \beta^{-1}, 1, \alpha\beta^{-1}, \alpha^{-1}, \alpha^{-1}\beta, 1]^T. \end{aligned} \quad (7.72)$$

Similarly, the steering vector on the difference coarray $\mathbf{v}_{\mathbb{D}}(\bar{\boldsymbol{\mu}})$ becomes

$$\begin{aligned} \mathbf{v}_{\mathbb{D}}(\bar{\boldsymbol{\mu}}) &= [e^{j2\pi\bar{\boldsymbol{\mu}}^T \mathbf{m}}]_{\mathbf{m} \in \mathbb{D}} \\ &= [\alpha^{-1}, \alpha^{-1}\beta, \beta^{-1}, 1, \beta, \alpha\beta^{-1}, \alpha]^T. \end{aligned} \quad (7.73)$$

It can be verified from (7.71), (7.72), and (7.73) that $\mathbf{c}(\bar{\boldsymbol{\mu}}) = \mathbf{J}\mathbf{v}_{\mathbb{D}}(\bar{\boldsymbol{\mu}})$.

7.E Derivation of (7.63)

Starting with (7.59), the entry associated with coarray locations $\mathbf{m}_1 = (m_1^{(1)}, m_1^{(2)})$ and $\mathbf{m}_2 = (m_2^{(1)}, m_2^{(2)})$ is given by

$$\langle \mathbf{S}_{\mathbb{D}} \rangle_{\mathbf{m}_1, \mathbf{m}_2} = \int_{\mathbb{K}} e^{j2\pi\bar{\boldsymbol{\mu}}^T (\mathbf{m}_1 - \mathbf{m}_2)} d\bar{\boldsymbol{\mu}}.$$

Next we express $\bar{\boldsymbol{\mu}}$ in terms of polar coordinates. Letting $\bar{\boldsymbol{\mu}} = (\bar{\mu}^{(1)}, \bar{\mu}^{(2)}) = (r \cos \phi, r \sin \phi)$ where $0 \leq r \leq 1/2$ and $0 \leq \phi \leq 2\pi$ yields

$$\langle \mathbf{S}_{\mathbb{D}} \rangle_{\mathbf{m}_1, \mathbf{m}_2} = \int_0^{1/2} \int_0^{2\pi} e^{j2\pi r(p \cos \phi + q \sin \phi)} r d\phi dr, \quad (7.74)$$

where $p = m_1^{(1)} - m_2^{(1)}$ and $q = m_1^{(2)} - m_2^{(2)}$. Based on the values of p and q , we have the following cases:

If $(p, q) = (0, 0)$, namely $\mathbf{m}_1 = \mathbf{m}_2$, then (7.74) becomes

$$\langle \mathbf{S}_{\mathbb{D}} \rangle_{\mathbf{m}_1, \mathbf{m}_2} = \int_0^{1/2} \int_0^{2\pi} r d\phi dr = \frac{\pi}{4}.$$

If $(p, q) \neq (0, 0)$, then (7.74) can be expressed as

$$\langle \mathbf{S}_{\mathbb{D}} \rangle_{\mathbf{m}_1, \mathbf{m}_2} = \int_0^{1/2} \int_0^{2\pi} e^{j2\pi r \sqrt{p^2 + q^2} \cos(\phi - \phi')} d\phi \cdot r dr, \quad (7.75)$$

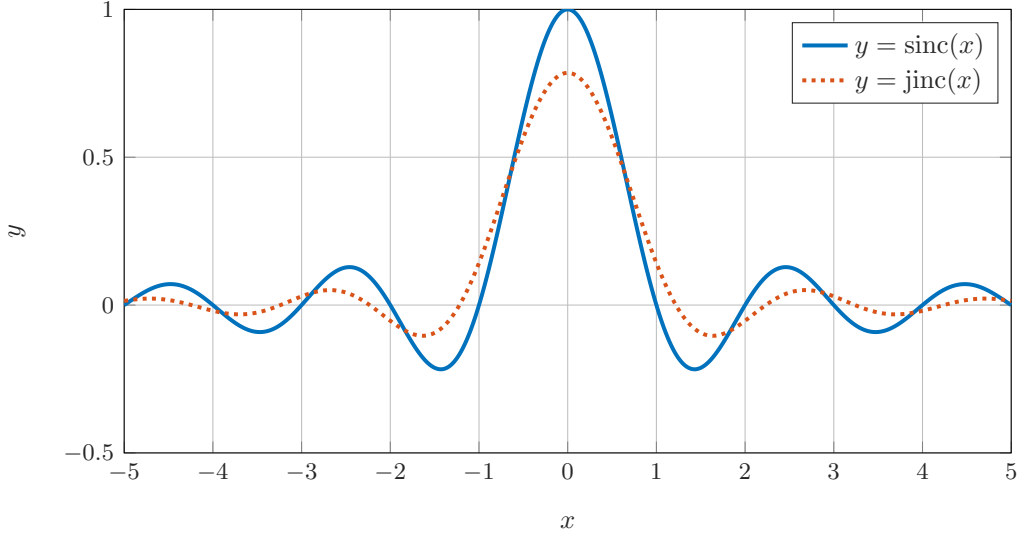


Figure 7.10: Plots for the sinc function $\text{sinc}(x)$ and the jinc function $\text{jinc}(x)$.

where the quantity ϕ' satisfies

$$\cos \phi' = \frac{p}{\sqrt{p^2 + q^2}}, \quad \sin \phi' = \frac{q}{\sqrt{p^2 + q^2}}.$$

The integral associated with ϕ can be written as the zeroth-order Bessel function of the first kind $J_0(x)$, since

$$J_0(x) = \frac{1}{2\pi} \int_{2\pi} e^{jx \cos \phi} d\phi. \quad (7.76)$$

Here $\int_{2\pi}$ denotes that the integration is carried over an interval of length 2π . Substituting (7.76) into (7.75) yields

$$\langle \mathbf{S}_{\mathbb{D}} \rangle_{\mathbf{m}_1, \mathbf{m}_2} = \int_0^{1/2} 2\pi J_0(2\pi r \sqrt{p^2 + q^2}) r dr. \quad (7.77)$$

Note that the Bessel functions satisfy

$$\int_0^R J_0(Kr) r dr = \frac{R}{K} J_1(KR), \quad (7.78)$$

where $J_1(x)$ is the first-order Bessel function of the first kind. K and R are positive numbers. Due to (7.78), Eq. (7.77) becomes

$$\langle \mathbf{S}_{\mathbb{D}} \rangle_{\mathbf{m}_1, \mathbf{m}_2} = \frac{J_1(\pi \sqrt{p^2 + q^2})}{2\sqrt{p^2 + q^2}} = \frac{J_1(\pi \|\mathbf{m}_1 - \mathbf{m}_2\|_2)}{2\|\mathbf{m}_1 - \mathbf{m}_2\|_2}, \quad (7.79)$$

which is (7.63).

Fig. 7.10 illustrates the sinc function and the jinc function, which are defined as

$$\begin{aligned}\operatorname{sinc}(x) &\triangleq \begin{cases} \frac{\sin(\pi x)}{\pi x}, & \text{if } x \neq 0, \\ 1, & \text{if } x = 0, \end{cases} \\ \operatorname{jinc}(x) &\triangleq \begin{cases} \frac{J_1(\pi x)}{2x}, & \text{if } x \neq 0, \\ \frac{\pi}{4}, & \text{if } x = 0. \end{cases}\end{aligned}$$

It can be observed that both functions attain their maxima at $x = 0$. In particular, $\operatorname{sinc}(0) = 1$ and $\operatorname{jinc}(0) = \pi/4$. Furthermore, these functions decay to zero asymptotically, as $|x|$ increases.

ROBUSTNESS OF DIFFERENCE COARRAYS OF SPARSE ARRAYS TO SENSOR FAILURES – A GENERAL THEORY

8.1 Introduction

In Chapters 2 and 6, it was shown that some sparse arrays are capable of identifying $\mathcal{O}(N^2)$ uncorrelated sources using N physical sensors, making it possible to resolve more uncorrelated source directions than sensors. More details of this result were reviewed in Sections 2.2 and 2.3.

In practice, *sensor failure* could occur randomly and may lead to the breakdown of the overall system [72], [115]. It can be *empirically* observed that, for some sparse arrays, such as MRA, faulty sensors could shrink the $\mathcal{O}(N^2)$ -long ULA segment in the difference coarray significantly. Furthermore, small ULA segments in the difference coarray typically lead to degraded performance [1], [87], [124], [192]. Due to these observations, in the past, sparse arrays were considered not to be robust to sensor failure. However, the impact of damaged sensors on sparse arrays remains to be analyzed, since these observations assume specific array configurations.

The issue of sensor failure was addressed in the literature in two aspects, including 1) developing new algorithms that are functional in the presence of sensor failure and 2) analyzing the robustness of array geometries. In the first part, various approaches have been developed, including DOA estimators based on minimal resource allocation network [191], impaired array beamforming and DOA estimation [202], array diagnosis based on Bayesian compressive sensing [117], and so on [114], [193]. However, the interplay between the array configuration and the exact condition under which these algorithms are applicable, remains to be investigated. The second aspect assesses the robustness of array configurations with faulty sensors [5], [29]. For instance, Alexiou and Manikas [5] proposed various measures to quantify the robustness of arrays while Carlin *et al.* [29] performed a statistical study on the beampattern with a given sensor failure rate. Even so, the impact of damaged sensors on the difference coarray has not yet been analyzed in a deterministic fashion, which is crucial for sparse arrays.

In this chapter, we aim to investigate the influence of faulty sensors on the difference coarray. The main focus of this chapter is not to develop new algorithms, but to analyze the robustness of arrays. A sensor is said to be *essential* if its deletion changes the difference coarray. Note that the essentialness property, which was originally introduced to study the economy of sensors [100], depends purely on the array ge-

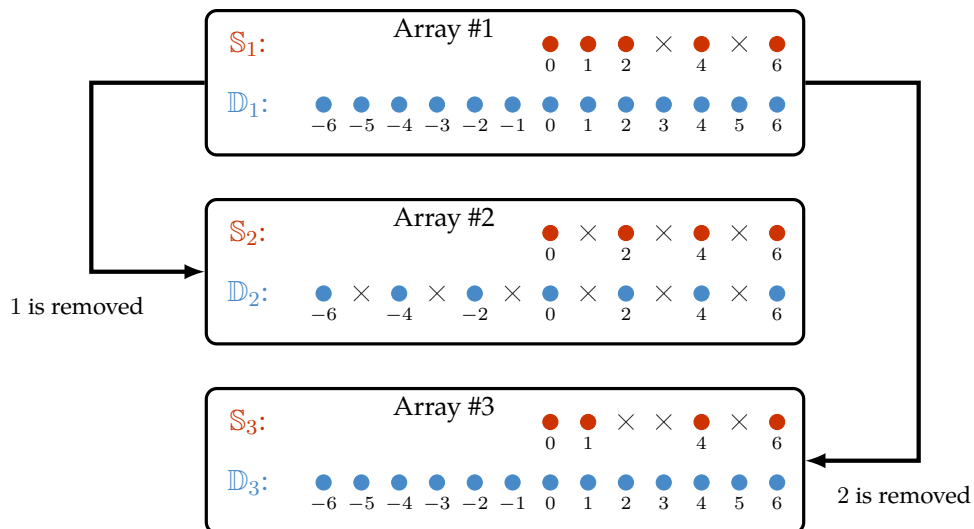


Figure 8.1: An illustration of the essentialness property. S_i and D_i represent the physical array and the difference coarray of the i th array, respectively. Elements are marked by dots while empty space is depicted by crosses. It can be observed that removing the sensor at 1 from Array #1 changes the difference coarray ($D_2 \neq D_1$). However, in Array #3, which is obtained by removing the sensor at 2 from Array #1, the difference coarray remains the same ($D_3 = D_1$). We say that the sensor at 1 is essential with respect to Array #1 while the sensor at 2 is inessential with respect to Array #1.

ometry, rather than the source parameters and the estimation algorithms. One of the main contributions of this chapter is to show that the essentialness property can be used to assess the robustness of the array geometry, in the sense of preserving the difference coarray. A generalization of this, called k -essentialness, is then developed in order to study the effect of multiple sensor failures on the difference coarray. The coarray robustness is quantified using the notion of k -fragility which is introduced later in this chapter. This quantity ranges from 0 to 1; an array is more robust if the fragility is closer to 0.

For an array with N sensors, the size of the k -essential family can be as large as $\binom{N}{k}$, which makes it challenging to analyze and to store the complete information. To address this issue, we introduce the k -essential Sperner family, which encodes the information in the k -essential family with great economy.

These proposed quantities find applications in quantifying the susceptibility of the difference coarray with respect to random sensor failures. Note that this topic is of considerable interest in reliability engineering [72], [115]. Our study offers several insights into the interplay between the overall reliability, the essentialness property, and the fragility. For instance, under mild assumptions, the system reliability decreases as the number of essential sensors increases.

As an example, Fig. 8.1 demonstrates the main idea of the essentialness property. Let us consider Array #1 and its difference coarray, as depicted on the top of Fig. 8.1. The sensor at 1 is essential since its removal from Array #1 alters the difference coarray. However, the sensor at 2 is inessential, since $\mathbb{D}_3 = \mathbb{D}_1$. This example shows that according to the sensor locations, some sensors are more important than others, as far as preserving the difference coarray is concerned. The essentialness property and its connection to the robustness of the array geometry will be developed in depth later.

Chapter outline: Section 8.2 proposes the k -essential family while Section 8.3 introduces the k -fragility. Section 8.4 presents the k -essential Sperner family. Section 8.5 offers a number of insights into the system reliability for the difference coarray while Section 8.6 concludes this chapter.

8.2 The Essentialness Property

In this section, we will present the essentialness property and the fragility, which are useful in studying the robustness of sparse arrays. These concepts are related to the difference coarray \mathbb{D} , as in Definition 2.2.1, the weight function $w(m)$, as in Definition 2.2.9, and other quantities defined in Chapter 2.

It is well-known that coarray MUSIC is applicable to the autocorrelation vector on \mathbb{U} as long as $|\mathbb{U}| > 1$ (e.g., see [87]). However, it will be demonstrated in Example 8.2.1 that \mathbb{U} is susceptible to sensor failure. For certain array geometries, even one damaged physical sensor could alter \mathbb{U} significantly and coarray MUSIC may fail.

Example 8.2.1. In Fig. 8.1, Array #1 has $\mathbb{S}_1 = \{0, 1, 2, 4, 6\}$ and $\mathbb{D}_1 = \{0, \pm 1, \dots, \pm 6\} = \mathbb{U}_1$. In this case, the coarray MUSIC algorithm may be used, since $|\mathbb{U}_1| = 13 > 1$. Now suppose the sensor located at 1 fails. The new array configuration (Array #2) and the associated difference coarray becomes $\mathbb{S}_2 = \{0, 2, 4, 6\}$ and $\mathbb{D}_2 = \{0, \pm 2, \pm 4, \pm 6\}$, respectively. So the size of the ULA segment of \mathbb{D}_2 is 1 and the coarray MUSIC algorithm is not applicable. On the other hand, if the sensor at 2 fails, we have Array #3, which has $\mathbb{S}_3 = \{0, 1, 4, 6\}$ and $\mathbb{D}_3 = \{0, \pm 1, \dots, \pm 6\}$. Since $|\mathbb{U}_3| = 13 > 1$, the coarray MUSIC algorithm may still be implemented.

Example 8.2.1 shows that, the location of the faulty sensors could modify the difference coarray, which affects the applicability of coarray MUSIC. Note that, even if the difference coarray changes, there might exist other DOA estimators, such as compressed sensing based methods [127], [200] and coarray interpolation [2], [137], that work on the new difference coarray. However, these approaches are typically computationally expensive and the exact conditions under which the method works, remain to be explored. For this reason, we only focus on coarray MUSIC and the

integrity of the difference coarray in Chapters 8 and 9. Other scenarios are left for future work.

We begin with the following definition [100]:

Definition 8.2.1. The sensor located at $n \in \mathbb{S}$ is said to be essential with respect to \mathbb{S} if the difference coarray changes when sensor at n is deleted from the array. That is, if $\bar{\mathbb{S}} = \mathbb{S} \setminus \{n\}$, then $\bar{\mathbb{D}} \neq \mathbb{D}$. Here \mathbb{D} and $\bar{\mathbb{D}}$ are the difference coarrays for \mathbb{S} and $\bar{\mathbb{S}}$, respectively.

In this chapter, Definition 8.2.1 is equivalent to the statement that the element n is essential with respect to \mathbb{S} . The element $n \in \mathbb{S}$ is said to be inessential if it is not essential. For instance, in Fig. 8.1, the sensor at 1 is essential with respect to Array #1, since the difference coarray of Array #2 is distinct from that of Array #1 ($\mathbb{D}_2 \neq \mathbb{D}_1$). However, the sensor at 2 is inessential, because Array #1 and Array #3 share the same difference coarray ($\mathbb{D}_3 = \mathbb{D}_1$).

The essentialness property was originally introduced in [100] to study symmetric arrays and Cantor arrays. The main focus in [100] was the economy of sensors.

In this chapter, we focus on the fact that the removal of (or failure of) an essential sensor makes it difficult to apply coarray MUSIC. The removal of an inessential sensor, on the other hand, does not affect the applicability of coarray MUSIC at all. Our focus in this chapter is a study of essentialness, and its generalization called k -essentialness for arbitrary array geometries. One potential use of this knowledge is that one can design essential sensors more carefully so they have smaller failure probability, although this is not the focus here.

Given an array \mathbb{S} , the essential sensors can be found by searching over all the sensors in \mathbb{S} , according to Definition 8.2.1. The knowledge of the weight function $w(m)$ also gives useful insights about this:

Lemma 8.2.1. Suppose that $w(m)$ is the weight function of \mathbb{S} . Let n_1 and n_2 belong to \mathbb{S} . If $w(n_1 - n_2) = 1$, then n_1 and n_2 are both essential [100].

Note that the condition that $w(n_1 - n_2) = 1$ is sufficient, but not necessary for the essentialness of both n_1 and n_2 . For instance, if $\mathbb{S} = \{0, 1, 2\}$, then it can be shown that $n_1 = 1$ and $n_2 = 0$ are both essential with respect to \mathbb{S} , due to Definition 8.2.1. However, the weight function satisfies $w(n_1 - n_2) = w(1) = 2$.

Proof of Lemma 8.2.1. If $w(n_1 - n_2) = 1$ for $n_1, n_2 \in \mathbb{S}$, then (n_1, n_2) is the only sensor pair with separation $m = n_1 - n_2$. If n_1 is removed from \mathbb{S} , then the element m is also removed from the difference coarray. As a result, n_1 is essential. Similarly, n_2 is also essential since $w(n_2 - n_1) = w(n_1 - n_2) = 1$. \square

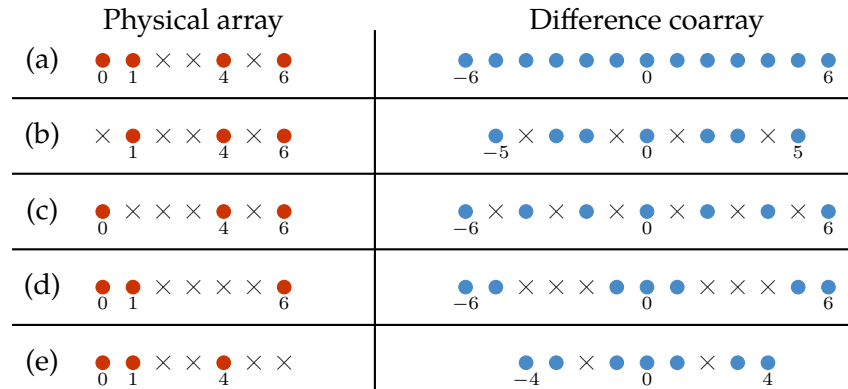


Figure 8.2: An example of MESA. (a) The original array and its difference coarray. The array configurations and the difference coarrays after the deletion of (b) the sensor at 0, (c) the sensor at 1, (d) the sensor at 4, or (e) the sensor at 6, from the original array in (a). Here the sensors are denoted by dots while crosses denote empty space.

Lemma 8.2.1 serves as a building block of many results in Chapters 8 and 9, as we will develop later.

Due to Lemma 8.2.1 and the fact that $w(\max(\mathbb{S}) - \min(\mathbb{S})) = 1$ for any \mathbb{S} , we have the following lemma:

Lemma 8.2.2. For any array \mathbb{S} , the leftmost element ($\min(\mathbb{S})$) and the rightmost element ($\max(\mathbb{S})$) are both essential.

As a result, when studying the essentialness property, it suffices to consider the elements $\min(\mathbb{S}) < n < \max(\mathbb{S})$, which simplifies the discussion.

Next we will develop the concept of maximal economy, which was first presented in [100]. It is formally defined as

Definition 8.2.2. A sensor array \mathbb{S} is said to be *maximally economic* if all the sensors in \mathbb{S} are essential [100].

These arrays are also called maximally economic sparse arrays (MESA) [100]. By definition, none of the sensors in MESA can be removed without changing the difference coarray.

Example 8.2.2. Consider the array $\mathbb{S} = \{0, 1, 4, 6\}$ in Fig. 8.2(a). This array has a hole-free difference coarray $\{0, \pm 1, \dots, \pm 6\}$. If the sensor at 0 is removed from (a), it can be observed in Fig. 8.2(b) that the difference coarray changes. Hence 0 is essential with respect to \mathbb{S} . Similarly, from Fig. 8.2(c-e), the sensors at 1, 4, and 6 are all essential. Due to Definition 8.2.2, the array \mathbb{S} is maximally economic.

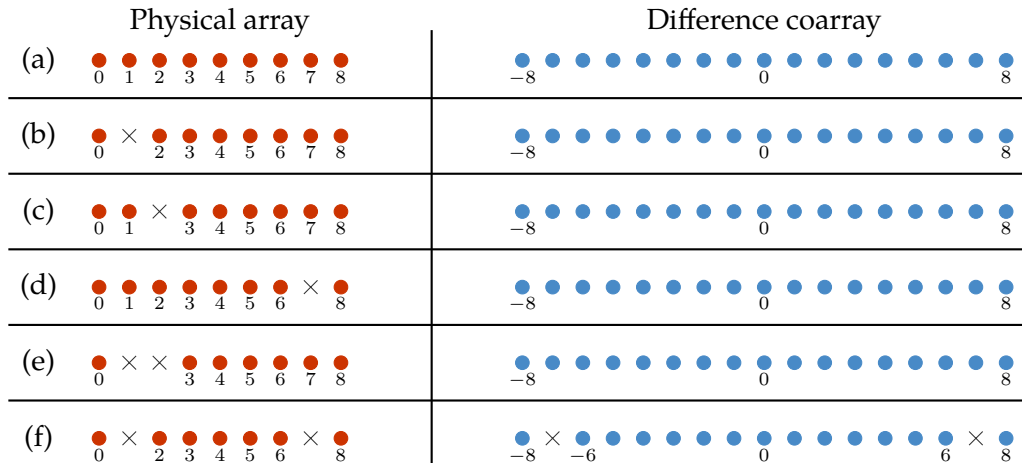


Figure 8.3: Array configurations and the difference coarrays for (a) the ULA with 9 sensors, and the arrays after the removal of (b) 1, (c) 2, (d) 7, (e) $\{1, 2\}$, and (f) $\{1, 7\}$ from (a).

Note that maximal economy is a property of the entire array, in contrast to the essentialness property, which is associated with sensors in an array, as in Definition 8.2.1. In this chapter, the general properties will be discussed while in Section 9.2, it will be proved that MESA includes MRA, MHA, nested arrays with $N_1 \geq 2$, and Cantor arrays.

The essentialness property and the maximal economy are distinct from the *redundancy* R [113], which can be expressed as $R = |\mathbb{S}|(|\mathbb{S}| - 1)/(|\mathbb{U}| - 1)$, where $|\mathbb{S}|$ is the number of sensors and \mathbb{U} is the central ULA segment of the difference coarray. The redundancy R serves as a criterion for the optimality of the difference coarray, which is not explicitly related to the importance of each physical sensor. The essentialness property and the maximal economy, on the other hand, describe the importance of each sensor with respect to the difference coarray. Furthermore, minimum redundancy (MRA) is sufficient but not necessary for maximal economy (MESA), as we will shown in Section 9.2 later.

The k -Essential Family

If there are *multiple sensor failures*, the influence of these faulty sensors on the difference coarray becomes more complicated. If two sensors are inessential, it means that either one of them can be removed without changing the coarray. But *if both sensors are removed, the difference coarray may change*. This case is demonstrated through the following example:

Example 8.2.3. Let us consider the ULA with 9 sensors, as depicted in Fig. 8.3. As seen from Figs. 8.3(b), (c), and (d), the sensors at 1, 2, and 7 are all inessential. Fig.

8.3(e) shows that removing inessential sensors at 1 and 2 at the same time preserves the difference coarray. However, removing both 1 and 7 modifies the difference coarray, as illustrated in Fig. 8.3(f). This example shows that two elements, such as 1 and 7, could be individually inessential, but together the subarray, $\{1, 7\}$, could change the difference coarray. Therefore, in general, multiple sensor failures have to be examined separately.

In the following development, the essentialness property in Definition 8.2.1 will be generalized into the k -essentialness property to handle multiple sensor failures. To begin with, let us consider the following definition:

Definition 8.2.3. The family of all subarrays of size k over an integer set \mathbb{S} is defined as

$$\mathcal{S}_k \triangleq \{\mathbb{A} \subseteq \mathbb{S} : |\mathbb{A}| = k\}. \quad (8.1)$$

Next, the k -essentialness property is defined as

Definition 8.2.4. A subarray \mathbb{A} is said to be k -essential with respect to array \mathbb{S} if 1) $\mathbb{A} \in \mathcal{S}_k$, and 2) the difference coarray changes when \mathbb{A} is removed from \mathbb{S} . Namely, $\bar{\mathbb{D}} \neq \mathbb{D}$ if $\bar{\mathbb{S}} = \mathbb{S} \setminus \mathbb{A}$. Here \mathbb{D} and $\bar{\mathbb{D}}$ are the difference coarrays of \mathbb{S} and $\bar{\mathbb{S}}$, respectively.

Note that essentialness, as defined in Definition 8.2.1, is equivalent to 1-essentialness ($k = 1$ in Definition 8.2.4). Namely, $n \in \mathbb{S}$ is essential if and only if $\{n\} \subseteq \mathbb{S}$ is 1-essential. For brevity, we will use these terms interchangeably.

Following Definition 8.2.4, in Example 8.2.3 and Fig. 8.3, we have that $\{1\}$ is not 1-essential, $\{2\}$ is not 1-essential, $\{7\}$ is not 1-essential, $\{1, 2\}$ is not 2-essential, but $\{1, 7\}$ is 2-essential.

It is useful to enumerate all the k -essential subarrays because these are the subarrays whose failure could make the coarray MUSIC fail. The collection of these subarrays is called the k -essential family:

Definition 8.2.5. The k -essential family \mathcal{E}_k with respect to a sensor array \mathbb{S} is defined as

$$\mathcal{E}_k \triangleq \{\mathbb{A} : \mathbb{A} \text{ is } k\text{-essential with respect to } \mathbb{S}\}. \quad (8.2)$$

Here $k \in \{1, 2, \dots, |\mathbb{S}|\}$.

Example 8.2.4. Consider the ULA with 6 sensors, $\mathbb{S} = \{0, 1, \dots, 5\}$, as illustrated in Fig. 8.4. Based on Definition 8.2.5, Fig. 8.2.4 depicts the k -essential family \mathcal{E}_1 and \mathcal{E}_2 . \mathcal{E}_1 just contains the end points of \mathbb{S} . Note that the size of \mathcal{E}_2 ($|\mathcal{E}_2| = 11$) is greater than the number of sensors ($|\mathbb{S}| = 6$). If more than 2 sensors are removed from the array ($k \geq 3$), then it can be shown that $\mathcal{E}_k = \mathcal{S}_k$.

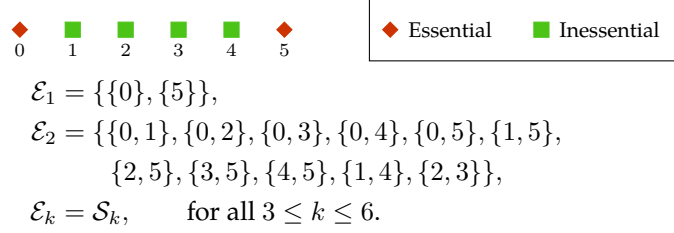


Figure 8.4: The ULA with 6 physical sensors, where the essential sensors and the inessential sensors are denoted by diamonds and rectangles, respectively. The k -essential subarrays are also listed.

The implication of the k -essential family is as follows. If an array \mathbb{S} and its k -essential family \mathcal{E}_k are given, then for any subarray \mathbb{A} of size k , it is possible to determine whether \mathbb{S} and $\mathbb{S} \setminus \mathbb{A}$ share the same difference coarray, without actually computing the difference coarray. This can be done by searching for \mathbb{A} in \mathcal{E}_k . Furthermore, the size of \mathcal{E}_k (i.e., the number of k -essential subarrays) also quantifies the robustness of the system, as we shall elaborate in Section 8.3.

In general, given an array configuration \mathbb{S} , the k -essential family \mathcal{E}_k can be uniquely determined, by examining all possible $\binom{|\mathbb{S}|}{k}$ subarrays, as in Definition 8.2.5. From the computational perspective, this task becomes intractable for large number of sensors. In addition, even if \mathcal{E}_k can be enumerated, it remains difficult to retrieve information from \mathcal{E}_k , which might have size up to the order of $\binom{|\mathbb{S}|}{k}$.

These challenges will be addressed in two respects. First, the size of the k -essential family, namely $|\mathcal{E}_k|$, can be expressed or bounded in terms of simpler things like the number of sensors, the weight function, and the number of essential sensors, as presented in Theorem 8.2.1. These results lead to the robustness analysis of array configurations, as we will develop in Section 8.3. Second, the retrieval of the information in \mathcal{E}_k could be accelerated by the k -essential Sperner family, which will be discussed in Section 8.4 in detail.

Next, some properties of \mathcal{E}_k are discussed in Theorem 8.2.1, whose proof can be found in the next subsection.

Theorem 8.2.1. Let \mathcal{E}_k be the k -essential family with respect to a nonempty integer set \mathbb{S} (set of sensors), and let the family \mathcal{S}_k be as defined in (8.1). Let $\lceil \cdot \rceil$ and $\lfloor \cdot \rfloor$ be the ceiling function and the floor function, respectively. Then the following properties hold true:

1. $(|\mathbb{S}| - k)|\mathcal{E}_k| \leq (k + 1)|\mathcal{E}_{k+1}|$ for all $1 \leq k \leq |\mathbb{S}| - 1$. The equality holds if and only if $\mathcal{E}_k = \mathcal{S}_k$.

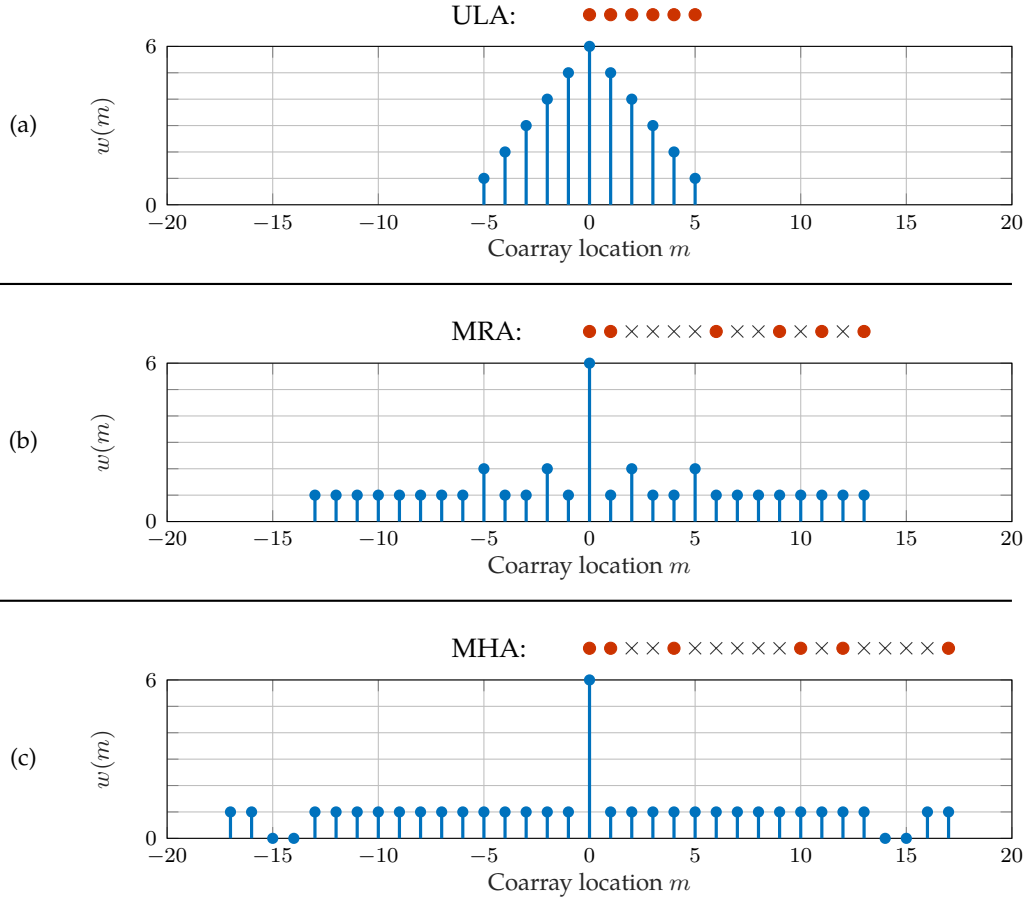


Figure 8.5: The array geometries and the weight functions for (a) the ULA with 6 sensors, (b) the MRA with 6 sensors, and (c) the MHA with 6 sensors. The sensors are depicted in dots while the empty space is shown in crosses. The definition of M_q in Theorem 8.2.1.3 leads to $M_1 = 2$, $M_2 = 2$ for (a), $M_1 = 22$, $M_2 = 4$ for (b), and $M_1 = 30$, $M_2 = 0$ for (c).

2. $\mathcal{E}_k = \mathcal{S}_k$ for all $Q \leq k \leq |\mathcal{S}|$, where $Q = \min\{Q_1, Q_2\}$. The parameters Q_1 and Q_2 are given by

$$Q_1 = |\mathcal{S}| - |\mathcal{E}_1| + 1, \quad (8.3)$$

$$Q_2 = \left\lceil |\mathcal{S}| - \frac{\sqrt{8|\mathcal{S}| - 11} + 1}{2} \right\rceil, \quad \text{for } |\mathcal{S}| \geq 2. \quad (8.4)$$

3. Let $M_q = |\{m \in \mathbb{D} : w(m) = q\}|$ be the number of elements in the difference coarray such that the associated weight function is q . If $|\mathcal{S}| \geq 2$, then

$$\left\lceil \frac{\sqrt{4M_1 + 1} + 1}{2} \right\rceil \leq |\mathcal{E}_1| \leq \min \left\{ M_1 + \left\lfloor \frac{M_2}{2} \right\rfloor, |\mathcal{S}| \right\}. \quad (8.5)$$

Example 8.2.5. Theorem 8.2.1 can be illustrated by the following concrete examples. First, the ULA in Fig. 8.4 indicates that $\mathcal{E}_1 \neq \mathcal{S}_1$, $|\mathcal{E}_1| = 2$, and $|\mathcal{E}_2| = 11$. If $k = 1$, then

we have $(|\mathbb{S}| - 1)|\mathcal{E}_1| = 10$ and $(1 + 1)|\mathcal{E}_2| = 22$, which illustrates Theorem 8.2.1.1. Second, Fig. 8.4 shows that the ULA with 6 sensors has $|\mathcal{E}_1| = 2$ and $\mathcal{E}_k = \mathcal{S}_k$ for $3 \leq k \leq 6$. This is consistent with Theorem 8.2.1.2, since we have $Q_1 = 5$, $Q_2 = 3$, and $Q = 3$ in (8.3) and (8.4). Finally, let us demonstrate Theorem 8.2.1.3 using the ULA, the MRA, and the MHA. The array geometries and the weight functions for these arrays are depicted in Fig. 8.5. Furthermore, the parameters M_1 and M_2 can be found in the caption of Fig. 8.5. Substituting M_1 and M_2 into the lower bound and the upper bound in (8.5) leads to

$$(a) \text{ ULA:} \quad \text{Lower bound} = 2, \quad \text{Upper bound} = 3, \quad (8.6)$$

$$(b) \text{ MRA:} \quad \text{Lower bound} = 6, \quad \text{Upper bound} = 6, \quad (8.7)$$

$$(c) \text{ MHA:} \quad \text{Lower bound} = 6, \quad \text{Upper bound} = 6. \quad (8.8)$$

Next let us consider the number of essential sensors ($|\mathcal{E}_1|$) for these arrays. According to Fig. 8.3, we have $|\mathcal{E}_1| = 2$ for the ULA with 6 sensors, which is in accordance with (8.6). For MRA and MHA with 6 sensors, using Definition 8.2.4, it can be numerically shown that they are maximally economic. This result is consistent with (8.7) and (8.8). Note that the maximal economy of MRA and MHA will be proved in Chapter 9.

Remarks on Theorem 8.2.1.1

Theorem 8.2.1.1 (i.e., part 1 of Theorem 8.2.1) shows that the size of \mathcal{E}_k cannot be arbitrary. In particular, if \mathcal{E}_k becomes \mathcal{S}_k , we have the following corollary:

Corollary 8.2.1. For any k in $1 \leq k \leq |\mathbb{S}| - 1$, if $\mathcal{E}_k = \mathcal{S}_k$, then $\mathcal{E}_{k+1} = \mathcal{S}_{k+1}$.

Note that Corollary 8.2.1 can be utilized to accelerate the computation of \mathcal{E}_k for all k . Due to Definition 8.2.5, \mathcal{E}_k can be evaluated numerically from $k = 1, 2$, and so on. If \mathcal{E}_k is \mathcal{S}_k for some particular k , then the algorithm stops, since it is guaranteed that $\mathcal{E}_\ell = \mathcal{S}_\ell$ for $k + 1 \leq \ell \leq |\mathbb{S}|$. Another usage of Corollary 8.2.1 is to study the k -essential family of MESA. Due to Definition 8.2.2 ($\mathcal{E}_1 = \mathcal{S}_1$) and Corollary 8.2.1, we obtain

Corollary 8.2.2. If \mathbb{S} is maximally economic, then $\mathcal{E}_k = \mathcal{S}_k$ for all $1 \leq k \leq |\mathbb{S}|$.

Implications of Theorem 8.2.1.2

If the number of faulty sensors k is sufficiently large ($\geq Q$ where Q is defined in Theorem 8.2.1.2), then the difference coarray is guaranteed to change. For instance, if $k = |\mathbb{S}|$, then all the sensors fail so the difference coarray changes from a nonempty set to the empty set. The parameter Q depends on Q_1 and Q_2 , which can be readily

computed given the array geometry. Q_1 is the number of inessential sensors plus one while Q_2 is purely a function of the number of sensors. In particular, assume that the number of sensors $|\mathbb{S}|$ is large enough. Based on (8.4), we have $Q_2 \approx |\mathbb{S}| - \sqrt{2|\mathbb{S}|}$, implying that, if the number of operational sensors is smaller than $\sqrt{2|\mathbb{S}|}$, then $\mathcal{E}_k = \mathcal{S}_k$, that is, any subset of k sensors is k -essential.

Note that the condition that $Q \leq k \leq |\mathbb{S}|$ is only sufficient but not necessary for $\mathcal{E}_k = \mathcal{S}_k$. For instance, if $\mathbb{S} = \{0, 1, \dots, 15\}$, then (8.3) and (8.4) result in $Q_1 = 15$, $Q_2 = 11$, so $Q = 11$. However, in this case, it can be numerically shown that $\mathcal{E}_{10} = \mathcal{S}_{10}$.

Theorem 8.2.1.2 can also be utilized to characterize MESA, as in the following corollary:

Corollary 8.2.3. Let \mathbb{S} be a sensor array. If $1 \leq |\mathbb{S}| \leq 3$, then \mathbb{S} is maximally economic.

Proof. If $|\mathbb{S}| = 1$, then due to Definition 8.2.1 and 8.2.2, \mathbb{S} is maximally economic. If $2 \leq |\mathbb{S}| \leq 3$, then $Q_2 = 1$ in (8.4), so $\mathcal{E}_1 = \mathcal{S}_1$, implying \mathbb{S} is maximally economic. \square

Remarks on Theorem 8.2.1.3

Eq. (8.5) is analogous to Cheeger inequalities in graph theory [35], where the Cheeger constant is bounded by the expressions based on the topology of graphs. Here in (8.5), the number of essential sensors is analogous to the Cheeger constant. The bounds in (8.5) also depend on the weight functions, which depend on the array geometry.

Proof of Theorem 8.2.1

The following results are useful in proving Theorem 8.2.1:

Proposition 8.2.1. Let \mathbb{D} and $\overline{\mathbb{D}}$ be the difference coarrays of \mathbb{S} and $\overline{\mathbb{S}}$, respectively. If $\overline{\mathbb{S}} \subseteq \mathbb{S}$, then $\overline{\mathbb{D}} \subseteq \mathbb{D}$.

Proof. Let $m \in \overline{\mathbb{D}}$. By definition, there exist $n_1, n_2 \in \overline{\mathbb{S}}$ such that $n_1 - n_2 = m$. Since $\overline{\mathbb{S}} \subseteq \mathbb{S}$, we have $n_1, n_2 \in \mathbb{S}$, implying $m \in \mathbb{D}$. This completes the proof. \square

Lemma 8.2.3. Assume that \mathbb{A} and \mathbb{B} are sets such that $\mathbb{A} \subseteq \mathbb{B} \subseteq \mathbb{S}$. If $\mathbb{A} \in \mathcal{E}_{|\mathbb{A}|}$, then $\mathbb{B} \in \mathcal{E}_{|\mathbb{B}|}$.

Proof. Assume that $\mathbb{S}_1 \triangleq \mathbb{S} \setminus \mathbb{A}$ and $\mathbb{S}_2 \triangleq \mathbb{S} \setminus \mathbb{B}$. The difference coarrays of \mathbb{S} , \mathbb{S}_1 , and \mathbb{S}_2 are denoted by \mathbb{D} , \mathbb{D}_1 , and \mathbb{D}_2 , respectively. The notation $\mathbb{X} \subset \mathbb{Y}$ denotes that \mathbb{X} is a subset of \mathbb{Y} but $\mathbb{X} \neq \mathbb{Y}$. We will show that $\mathbb{D}_2 \subseteq \mathbb{D}_1 \subset \mathbb{D}$. First, since $\mathbb{A} \subseteq \mathbb{B} \subseteq \mathbb{S}$, we have $\mathbb{S}_2 \subseteq \mathbb{S}_1$, implying $\mathbb{D}_2 \subseteq \mathbb{D}_1$ due to Proposition 8.2.1. Second, due to the definition of the k -essential family, $\mathbb{A} \in \mathcal{E}_{|\mathbb{A}|}$ is equivalent to $\mathbb{D}_1 \subset \mathbb{D}$. Hence $\mathbb{D}_2 \subset \mathbb{D}$, which means $\mathbb{B} \in \mathcal{E}_{|\mathbb{B}|}$. \square

Lemma 8.2.4. Assume that an array \mathbb{S} has difference coarray \mathbb{D} . Then \mathbb{D} satisfies $2|\mathbb{S}| - 1 \leq |\mathbb{D}| \leq |\mathbb{S}|^2 - |\mathbb{S}| + 1$.

Proof. Let \mathbb{S} be $\{s_1, s_2, \dots, s_N\}$ such that $s_1 < s_2 < \dots < s_N$, where $N = |\mathbb{S}|$ is the number of sensors. If $N = 1$, then this lemma is trivially true. Next let us consider $N \geq 2$. Since the sensor locations s_1, s_2, \dots, s_N are distinct, the differences $0, \pm(s_2 - s_1), \pm(s_3 - s_1), \dots, \pm(s_N - s_1)$ are all distinct, which proves the lower bound. For the upper bound, it is known that there are $\binom{N}{2}$ ways to choose two distinct numbers from N numbers and each choice leads to two differences. In addition, the difference 0 is obtained by choosing the same number twice. Hence $|\mathbb{D}|$ is at most $2\binom{N}{2} + 1 = N^2 - N + 1$. \square

Now let us move on to the proof of Theorem 8.2.1:

Proof of Theorem 8.2.1.1

This proof technique can be found in [44]. Let us count the number of pairs $(\mathbb{A}, \mathbb{B}) \in \mathcal{E}_k \times \mathcal{E}_{k+1}$ such that $\mathbb{A} \subset \mathbb{B}$. Let L be the number of such pairs. For every $n_1 \in \mathbb{S}$ but $n_1 \notin \mathbb{A}$, it can be shown that $\mathbb{A} \subset \mathbb{A} \cup \{n_1\} \subseteq \mathbb{S}$ and therefore $\mathbb{A} \cup \{n_1\} \in \mathcal{E}_{k+1}$, due to Lemma 8.2.3. Since $(\mathbb{A}, \mathbb{A} \cup \{n_1\})$ has $|\mathcal{E}_k| \times |\mathbb{S} \setminus \mathbb{A}|$ choices, we have

$$L = (|\mathbb{S}| - k)|\mathcal{E}_k|. \quad (8.9)$$

Similarly, it can be shown that $\mathbb{B} \setminus \{n_2\} \subset \mathbb{B} \subseteq \mathbb{S}$, for all $\mathbb{B} \in \mathcal{E}_{k+1}$ and $n_2 \in \mathbb{B}$. However, the statement that $\mathbb{B} \setminus \{n_2\} \in \mathcal{E}_k$, (the converse of Lemma 8.2.3), is not necessarily true. Therefore, by counting the number of n_2 and \mathbb{B} , we have

$$L \leq (k + 1)|\mathcal{E}_{k+1}|, \quad (8.10)$$

with equality if and only if $\mathbb{B} \setminus \{n_2\} \in \mathcal{E}_k$ for all $\mathbb{B} \in \mathcal{E}_{k+1}$ and all $n_2 \in \mathbb{B}$. Combining (8.9) and (8.10) proves the inequality. The equality holds if and only if $(\mathbb{A} \cup \{n_1\}) \setminus \{n_2\} \in \mathcal{E}_k$. Therefore $\mathcal{E}_k = \emptyset$ or \mathcal{S}_k , where \emptyset is the empty set. Since $\min(\mathbb{S})$ and $\max(\mathbb{S})$ are both essential, \mathcal{E}_k is not empty. This proves the condition for equality. \square

Example 8.2.6. For clarity, the proof of Theorem 8.2.1.1 is demonstrated using an undirected graph in Fig. 8.6. We focus on the ULA with 6 sensors and $k = 1$. The array geometry and the k -essential family \mathcal{E}_1 and \mathcal{E}_2 are depicted in Fig. 8.4. The nodes in Fig. 8.6 are grouped into Layer #1 (elements in \mathcal{E}_1), Layer #2 (elements in \mathcal{E}_2), and Layer #3 (elements in \mathcal{S}_1). The numbers in the nodes denote subarrays of the ULA. We say that the node \mathbb{A} in Layer #1 and the node \mathbb{B} in Layer #2 are connected, if and only if \mathbb{A} is a subset of \mathbb{B} . For instance, the node $\{0\}$ in Layer #1 and the

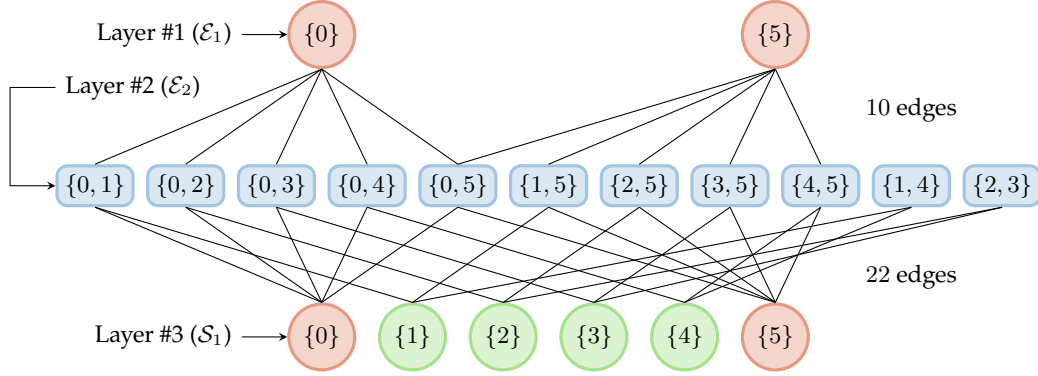


Figure 8.6: An illustration for the main idea of the proof of Theorem 8.2.1.1. Here the array is the ULA with 6 sensors and the k -essential family \mathcal{E}_1 and \mathcal{E}_2 are depicted in Fig. 8.4.

node $\{0, 1\}$ in Layer #2 are connected. By definition, the parameter L is exactly the number of edges between Layer #1 and Layer #2. Since there are $|\mathcal{E}_1| = 2$ nodes in Layer #1 and each node contributes to $|\mathbb{S}| - 1 = 5$ edges, we have $L = 2 \times 5 = 10$, which is (8.9). Next, let us consider the number of edges between Layer #2 and Layer #3. Let \mathbb{B} in Layer #2 and \mathbb{C} in Layer #3. We say that there exists an edge between \mathbb{B} and \mathbb{C} if and only if \mathbb{C} is a subset of \mathbb{B} . For example, the node $\{3, 5\}$ in Layer #2 is connected to both node $\{3\}$ and node $\{5\}$ in Layer #3. As a result, each node in Layer #2 corresponds to $k + 1 = 2$ edges. Then the number of edges between Layer #2 and #3 becomes $11 \times 2 = 22$, which is indeed greater than or equal to $L = 10$.

Proof of Theorem 8.2.1.2

Let us consider any subarray $\mathbb{A} \subseteq \mathbb{S}$ such that $|\mathbb{A}| = k \geq |\mathbb{S}| - |\mathcal{E}_1| + 1 = Q_1$. The cardinality of $\mathbb{S} \setminus \mathbb{A}$ becomes $|\mathbb{S}| - k \leq |\mathcal{E}_1| - 1 < |\mathcal{E}_1|$, implying that there is at least one essential element in \mathbb{A} . Due to Lemma 8.2.3, \mathbb{A} is k -essential, which proves the lower bound Q_1 .

The proof for the lower bound Q_2 is as follows. Let the difference coarray of an array \mathbb{S} be denoted by \mathbb{D} . Suppose that $\mathbb{A} \subseteq \mathbb{S}$ and $|\mathbb{A}| = k$. Assume that $\bar{\mathbb{S}} \triangleq \mathbb{S} \setminus \mathbb{A}$ has difference coarray $\bar{\mathbb{D}}$. Due to Lemma 8.2.4, \mathbb{D} and $\bar{\mathbb{D}}$ satisfy

$$2|\mathbb{S}| - 1 \leq |\mathbb{D}| \leq |\mathbb{S}|^2 - |\mathbb{S}| + 1, \quad (8.11)$$

$$2(|\mathbb{S}| - k) - 1 \leq |\bar{\mathbb{D}}| \leq (|\mathbb{S}| - k)^2 - (|\mathbb{S}| - k) + 1. \quad (8.12)$$

It is guaranteed that $\mathbb{D} \neq \bar{\mathbb{D}}$, if the range of $|\mathbb{D}|$ in (8.11) and that of $|\bar{\mathbb{D}}|$ in (8.12) are disjoint. Therefore, $\mathcal{E}_k = \mathcal{S}_k$ if

$$(|\mathbb{S}| - k)^2 - (|\mathbb{S}| - k) + 1 \leq (2|\mathbb{S}| - 1) - 1. \quad (8.13)$$

If $|\mathbb{S}| \geq 2$, then the sufficient condition (8.13) leads to $|\mathbb{S}| - (\sqrt{8|\mathbb{S}| - 11} + 1)/2 \leq k \leq |\mathbb{S}| + (\sqrt{8|\mathbb{S}| - 11} - 1)/2$. Since k is an integer, we have $k \geq Q_2$. \square

Proof of Theorem 8.2.1.3

Let $\mathbb{S}_q = \{n_1, n_2 : w(n_1 - n_2) = q\} \subseteq \mathbb{S}$ be the sensors such that the associated weight function is q . The set \mathbb{G}_q collects the essential sensors in \mathbb{S}_q but not in \mathbb{S}_ℓ for $1 \leq \ell \leq q - 1$. Namely,

$$\mathbb{G}_q = \{n : \{n\} \in \mathcal{E}_1, n \in \mathbb{S}_q, n \notin \mathbb{S}_\ell, 1 \leq \ell \leq q - 1\}. \quad (8.14)$$

By definition, the number of essential sensors is given by $|\mathcal{E}_1| = \sum_{q=1}^{|\mathbb{S}|} |\mathbb{G}_q|$. Next, it can be shown (see below) that the size of \mathbb{G}_q satisfies:

$$(\sqrt{4M_1 + 1} + 1)/2 \leq |\mathbb{G}_1| \leq M_1, \quad (8.15)$$

$$0 \leq |\mathbb{G}_2| \leq M_2/2, \quad (8.16)$$

$$|\mathbb{G}_q| = 0, \quad q \geq 3. \quad (8.17)$$

Since $|\mathcal{E}_1|$ is an integer, $|\mathcal{E}_1|$ is lower bounded by $\lceil (\sqrt{4M_1 + 1} + 1)/2 \rceil$ and upper bounded by $M_1 + \lfloor M_2/2 \rfloor$, which proves this theorem. \square

Proof of (8.15). Consider a simple, directed graph \mathcal{G} with vertices \mathbb{G}_1 and directed edges from n_1 to n_2 if $w(n_1 - n_2) = 1$ for all distinct $n_1, n_2 \in \mathbb{G}_1$. Due to $|\mathbb{S}| \geq 2$ and Lemma 8.2.2, both of the distinct elements $\min(\mathbb{S})$ and $\max(\mathbb{S})$ belong to \mathbb{G}_1 . Therefore $|\mathbb{G}_1| \geq 2$. By definition, M_1 is the number of directed edges in \mathcal{G} . Next the range of M_1 is discussed. Due to (8.14), each vertex in \mathcal{G} corresponds to at least one directed edge and hence $|\mathbb{G}_1| \leq M_1$. On the other hand, the maximum number of edges in \mathcal{G} is $2 \binom{|\mathbb{G}_1|}{2} = |\mathbb{G}_1|(|\mathbb{G}_1| - 1)$ [18]. Rearranging $M_1 \leq |\mathbb{G}_1|(|\mathbb{G}_1| - 1)$ proves the lower bound in (8.15). \square

Example 8.2.7. Let us consider the arrays in Fig. 8.5 to elaborate the proof of (8.15). For instance, in Figs. 8.4 and 8.5(a), the ULA has $\mathcal{E}_1 = \{\{0\}, \{5\}\}$ and $w(5 - 0) = 1$. In this case, we have $\mathbb{G}_1 = \{0, 5\}$, due to (8.14), and the number of directed edges is $M_1 = 2$, as in Fig. 8.7(a), which is in accordance with (8.15). For the MRA with 6 sensors, Example 8.2.5 and Fig. 8.5(b) show that all sensors are essential and $w(13 - 0) = w(11 - 1) = w(9 - 6) = 1$. Therefore, we obtain $\mathbb{G}_1 = \{0, 1, 6, 9, 11, 13\}$ and $M_1 = 22$, as depicted in Fig. 8.7(b). These quantities also confirm (8.15). Finally, as in Example 8.2.5 and Fig. 8.5(c), the MHA with 6 sensors has $\mathcal{E}_1 = \mathcal{S}_1$ and $w(1 - 0) = w(12 - 10) = w(17 - 4) = 1$. Hence $\mathbb{G}_1 = \{0, 1, 4, 10, 12, 17\}$ and $M_1 = 30$, which are consistent with (8.15). Note that, in this case, the associated graph \mathcal{G} is a complete directed graph, as illustrated in Fig. 8.7(c).

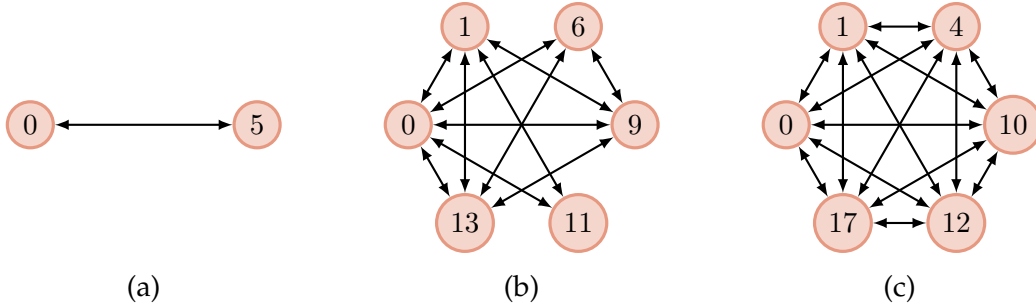


Figure 8.7: The directed graph \mathcal{G} in the proof of (8.15), for (a) the ULA with 6 sensors, (b) the MRA with 6 sensors, and (c) the MHA with 6 sensors. The number of directed edges is (a) $M_1 = 2$, (b) $M_1 = 22$, and (c) $M_1 = 30$.

Proof of (8.16). First, it will be shown that, each case of $w(m) = w(-m) = 2$ corresponds to at most one element in \mathbb{G}_2 . Then the upper bound in (8.16) can be proved since there are at most $M_2/2$ such cases.

Let $(n_1, n_2), (n'_1, n'_2) \in \mathbb{S}^2$ be the only two sensor pairs such that $(n_1, n_2) \neq (n'_1, n'_2)$ and $n_1 - n_2 = n'_1 - n'_2$. We have $w(n_1 - n_2) = w(n_2 - n_1) = 2$. Without loss of generality, the pair (n_1, n_2) is considered in the following. If $n_1 \in \mathbb{G}_2$, then the sensor failure at n_1 removes the pairs (n_1, n_2) and (n'_1, n'_2) at the same time. Since $n_1 \neq n'_1$, we have $n'_2 = n_1 \in \mathbb{G}_2$ and $n_2 + n'_1 = 2n_1$. Similarly, if $n_2 \in \mathbb{G}_2$, then $n'_1 = n_2 \in \mathbb{G}_2$ and $n_1 + n'_2 = 2n_2$. If both n_1 and n_2 belong to \mathbb{G}_2 , then $n_1 = n_2 = n'_1 = n'_2$. These arguments show that, among n_1, n_2, n'_1 , and n'_2 , there is at most one element in \mathbb{G}_2 . Therefore, each case of $w(m) = w(-m) = 2$ leads to at most one element in \mathbb{G}_2 . \square

Proof of (8.17). Let $n_1 \in \mathbb{G}_q$. Since $3 \leq q \leq |\mathbb{S}|$, there exist three distinct pairs $(n_1, n_2), (n'_1, n'_2), (n''_1, n''_2) \in \mathbb{S}^2$ such that $n_1 - n_2 = n'_1 - n'_2 = n''_1 - n''_2$. The essentialness property of n_1 indicates that, the sensor failure at n_1 removes these three pairs simultaneously. Since $n_1 \neq n'_1$ and $n_1 \neq n''_1$, we have $n_1 = n'_2 = n''_2$ so $n'_1 = n''_1$, which disagrees with the assumption of distinct pairs. Hence $|\mathbb{G}_q| = 0$. \square

8.3 The k -Fragility

After studying the general properties of the k -essential family \mathcal{E}_k , in this section, we will focus on the size of the k -essential family. Larger the size, higher is the likelihood that the difference coarray changes due to failure of k sensors. For instance, if $\mathcal{E}_k = \mathcal{S}_k$, it means that any k faulty sensors shrink the difference coarray. The notion of *fragility* is useful to capture this idea.

Definition 8.3.1. The fragility or k -fragility of a sensor array \mathbb{S} is defined as

$$F_k \triangleq \frac{|\mathcal{E}_k|}{|\mathcal{S}_k|} = \frac{|\mathcal{E}_k|}{\binom{|\mathbb{S}|}{k}}, \quad (8.18)$$

where $k = 1, 2, \dots, |\mathbb{S}|$.

F_k can also be regraded as the probability that the difference coarray changes, if all failure patterns of size k are equiprobable. *Larger F_k indicates that this array configuration is less robust, or more fragile to sensor failure, in the sense of changing the difference coarray.*

With these physical interpretations, next we will move on to some properties of the k -fragility F_k :

Theorem 8.3.1. Let \mathbb{S} be an integer set denoting the sensor locations. The k -fragility F_k with respect to \mathbb{S} has the following properties:

1. $F_k \leq F_{k+1}$ for all $1 \leq k \leq |\mathbb{S}| - 1$. The equality holds if and only if $F_k = 1$.
2. $F_k = 1$ for all k such that $Q \leq k \leq |\mathbb{S}|$, where Q is defined in Theorem 8.2.1.2.
3. $\min\{1, 2/|\mathbb{S}|\} \leq F_k \leq 1$ for all $1 \leq k \leq |\mathbb{S}|$.

Proof. Theorem 8.3.1.1 and 8.3.1.2 follow from Theorem 8.2.1.1 and 8.2.1.2, respectively. The lower bound in Theorem 8.3.1.3 is due to Definition 8.3.1, Lemma 8.2.2, and Theorem 8.3.1.1. \square

Example 8.3.1. Fig. 8.8 demonstrates the k -fragility F_k for (a) the ULA with 16 sensors, (b) the nested array with $N_1 = N_2 = 8$, as in (2.7), and (c) the coprime array with $M = 4$ and $N = 9$, (2.8). All these arrays have 16 physical sensors. The array geometries for these arrays are depicted on the top of Fig. 8.8. On the bottom of Fig. 8.8, the data points of F_k are computed numerically using Definition 8.2.5 and Definition 8.3.1. For all these arrays, the k -fragility F_k is increasing in k (Theorem 8.3.1.1) and F_k is bounded between $2/|\mathbb{S}| = 0.125$ and 1 (Theorem 8.3.1.3). As an example, the ULA has $|\mathbb{S}| = 16$, $Q_1 = 15$, $Q_2 = 11$, and $Q = \min\{Q_1, Q_2\} = 11$. Hence we obtain $F_k = 1$ for all $11 \leq k \leq 16$ (Theorem 8.3.1.2), which is consistent with Fig. 8.8.

Furthermore, smaller F_k indicates that the array configuration tends to be more robust to sensor failures. Among the arrays considered in Fig. 8.8, the most robust array in terms of F_1 , is the ULA, followed by the coprime array, and finally the nested array.

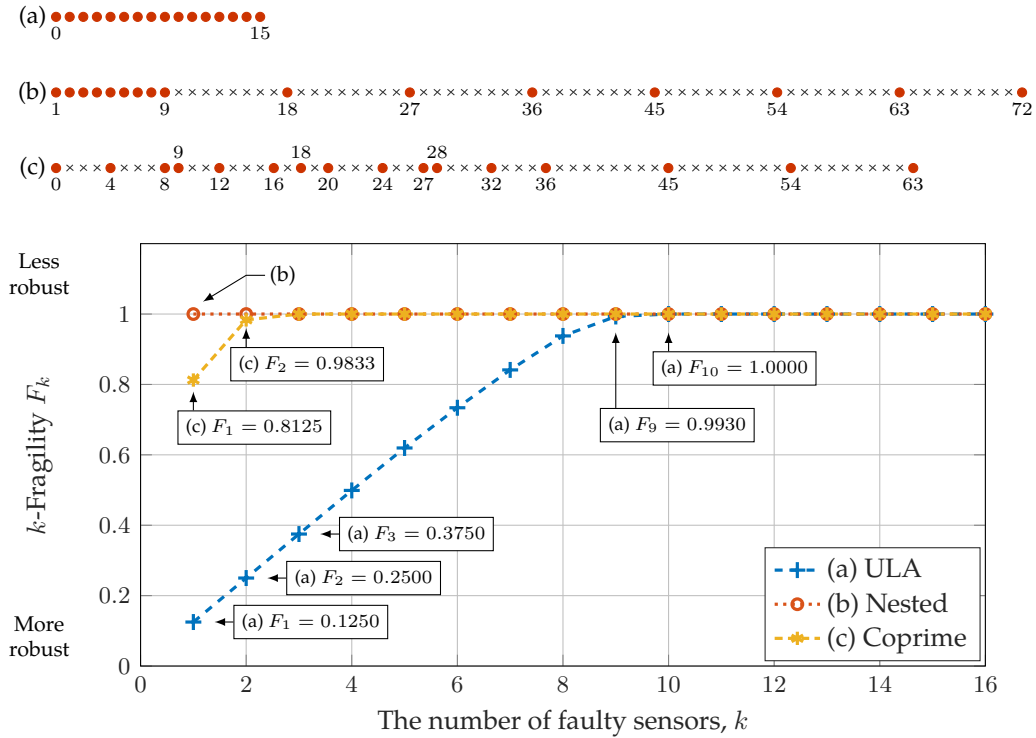


Figure 8.8: The array geometries (top) and the k -fragility F_k (bottom) for (a) the ULA with 16 sensors, (b) the nested array with $N_1 = N_2 = 8$, and (c) the coprime array with $M = 4$ and $N = 9$.

Next we will present the k -fragility for MESA. According to Definition 8.2.2, an array \mathbb{S} being a MESA is equivalent to $F_1 = 1$, implying the following corollary due to Theorem 8.3.1:

Corollary 8.3.1. If \mathbb{S} is maximally economic, then $F_k = 1$ for all $1 \leq k \leq |\mathbb{S}|$.

For instance, for the nested array with $N_1 = N_2 = 8$, the k -fragility $F_k = 1$ for all k , as shown in Fig. 8.8. This numerical result is consistent with the fact that the nested array with $N_2 \geq 2$ is a MESA, as proved in Theorem 9.2.1.

8.4 The k -Essential Sperner Family

The concept of the k -essentialness property makes it possible to investigate the failure patterns that modify the difference coarray. However the k -essential family \mathcal{E}_k may contain as many as $\binom{|\mathbb{S}|}{k}$ subarrays of size k . Hence, in general, it is challenging to retrieve information from \mathcal{E}_k , for large number of sensors and k . It will be demonstrated through the following example that there exist simple and compact representations of the k -essential family:

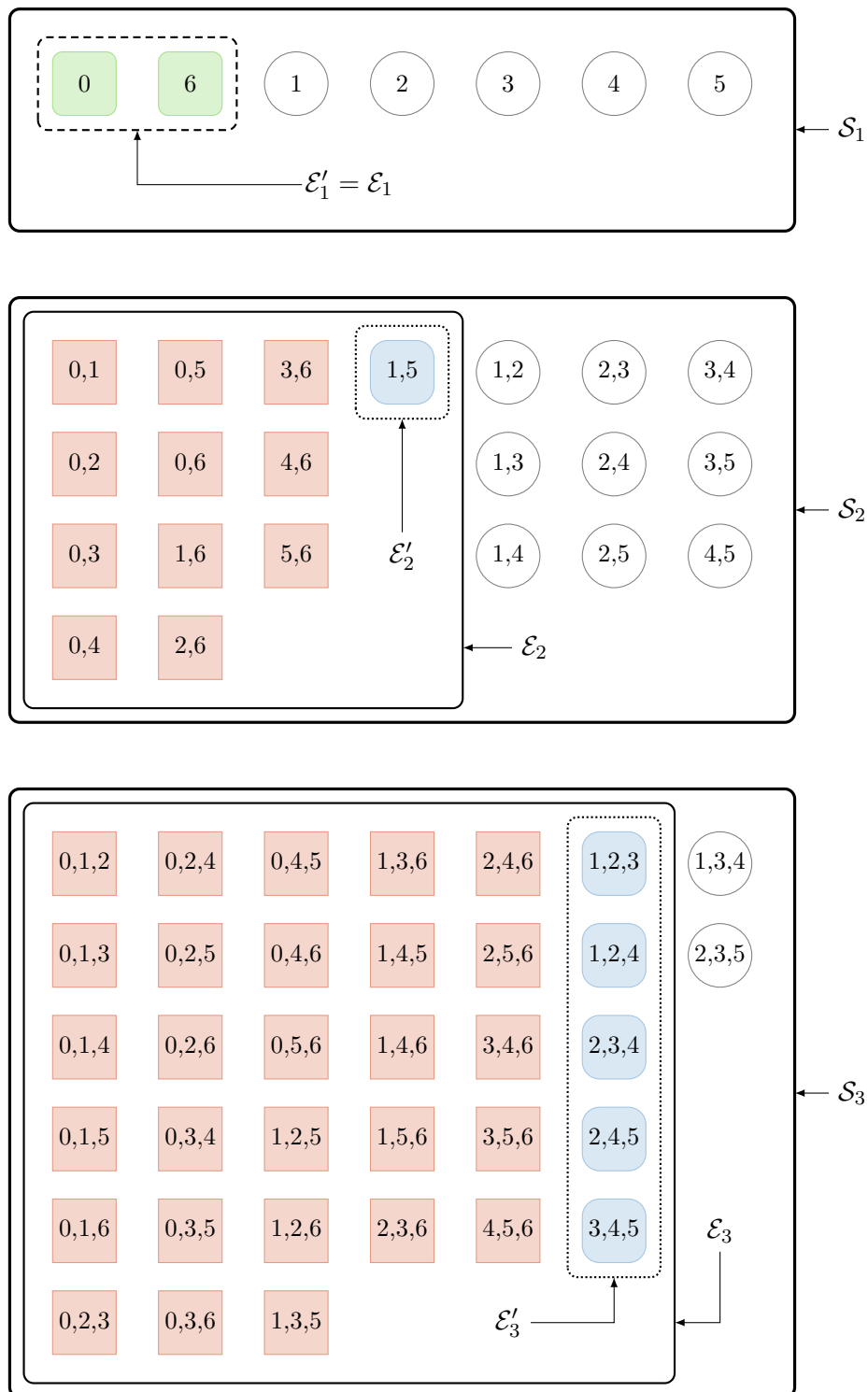


Figure 8.9: An example of the underlying structure of k -essential family \mathcal{E}_k . Here the ULA with 7 sensors, $\mathcal{S} = \{0, 1, \dots, 6\}$, is considered while the numbers in each small box denote a subarray. For instance, "0, 1, 2" represents the subarray $\{0, 1, 2\}$.

Example 8.4.1. Here we consider the ULA with 7 physical sensors $\mathbb{S} = \{0, 1, 2, 3, 4, 5, 6\}$. All of the subarrays over \mathbb{S} with size 1, 2, and 3 are depicted in small boxes in Fig. 8.9. The numbers in the small box denote the contents of the subarray. For instance, “0, 1, 2” represent the subarray $\{0, 1, 2\}$. Among these, the subarrays in \mathcal{E}_k are enumerated and shown in shaded boxes. For example, the boxes within \mathcal{S}_1 show that 0 and 6 are both essential while 1, 2, 3, 4, and 5 are all inessential. Next, let us focus on the 12 subarrays in the family \mathcal{E}_2 . It can be observed that \mathcal{E}_2 can be partitioned into two parts:

1. *Subarrays that contain essential sensors.* For instance, the subarray $\{0, 1\} \in \mathcal{E}_2$ satisfies $0 \in \{0, 1\}$, where 0 is essential. These subarrays are illustrated in light red rectangles with sharp corners.
2. *Subarrays that do not contain essential sensors.* For example, $\{1, 5\} \in \mathcal{E}_2$ but 1 and 5 are both inessential. This subarray is depicted in a light blue rectangle with rounded corners.

Furthermore, every subarray in Part 1 of \mathcal{E}_2 can be obtained by combining an essential sensor and another sensor in \mathbb{S} . For instance, $\{0, 1\}$ is constructed from the essential element 0 and the inessential element 1. As another example, the subarray $\{0, 6\} \in \mathcal{E}_2$ is composed of two essential elements 0 and 6.

The above discussion indicates that \mathcal{E}_2 can be characterized by

1. $\{0\}, \{6\} \in \mathcal{E}_1$ (essential sensors), and
2. $\{1, 5\}$ (those belonging to \mathcal{E}_2 but not containing essential sensors),

without listing all the 12 subarrays in \mathcal{E}_2 . This decomposition results in a compact representation of \mathcal{E}_2 , where only 3 subarrays ($\{0\}, \{6\}, \{1, 5\}$) are recorded.

Similarly, in Fig. 8.9, the same technique can be utilized in \mathcal{E}_3 , which is decomposed into 1) subarrays that include the elements in \mathcal{E}_2 , as depicted in light red rectangles with sharp corners, and 2) those that do not, as illustrated in light blue rectangles with rounded corners. In particular, the second part of \mathcal{E}_3 is grouped by a dashed box and denoted by the family \mathcal{E}'_3 . This second part of \mathcal{E}_k , called the *k-essential Sperner family*, is formally defined next. The name comes from Sperner theory in discrete mathematics [44], [160] as elaborated later.

Definition 8.4.1. Let \mathcal{E}_k be the *k-essential family* with respect to the array \mathbb{S} , where the integer *k* satisfies $1 \leq k \leq |\mathbb{S}|$. The *k-essential Sperner family* \mathcal{E}'_k is defined as

follows:

$$\mathcal{E}'_k \triangleq \begin{cases} \mathcal{E}_1, & \text{if } k = 1, \\ \{\mathbb{A} \in \mathcal{E}_k : \forall \mathbb{B} \in \mathcal{E}_{k-1}, \mathbb{B} \not\subseteq \mathbb{A}\}, & \text{otherwise,} \end{cases} \quad (8.19a)$$

$$(8.19b)$$

where $\mathbb{B} \not\subseteq \mathbb{A}$ denotes that \mathbb{B} is not a proper subset of \mathbb{A} .

Note that the definition $\mathcal{E}'_1 = \mathcal{E}_1$ is introduced such that \mathcal{E}'_k is well-defined for all $1 \leq k \leq |\mathbb{S}|$.

As one of the advantages, the k -essential Sperner family \mathcal{E}'_k could compress \mathcal{E}_k significantly, which would be quite useful especially when the size of \mathcal{E}_k is huge. The example in Fig. 8.9 displays the k -essential Sperner family \mathcal{E}'_1 , \mathcal{E}'_2 , and \mathcal{E}'_3 . It can be deduced that the sizes of the k -essential Sperner family $|\mathcal{E}'_1| = 2$, $|\mathcal{E}'_2| = 1$, and $|\mathcal{E}'_3| = 5$ are much smaller than those of the k -essential family $|\mathcal{E}_1| = 2$, $|\mathcal{E}_2| = 12$, and $|\mathcal{E}_3| = 33$.

Definition 9 shows that $\{\mathcal{E}'_1, \mathcal{E}'_2, \dots, \mathcal{E}'_{|\mathbb{S}|}\}$ can be uniquely determined from $\{\mathcal{E}_1, \mathcal{E}_2, \dots, \mathcal{E}_{|\mathbb{S}|}\}$. Conversely, if $\{\mathcal{E}'_1, \mathcal{E}'_2, \dots, \mathcal{E}'_{|\mathbb{S}|}\}$ is given, then $\{\mathcal{E}_1, \mathcal{E}_2, \dots, \mathcal{E}_{|\mathbb{S}|}\}$ can be perfectly reconstructed due to the following Lemma:

Lemma 8.4.1. Let \mathcal{E}'_k be the k -essential Sperner family of \mathbb{S} with $1 \leq k \leq |\mathbb{S}|$. Then the k -essential family \mathcal{E}_k satisfies

$$\mathcal{E}_k = \begin{cases} \mathcal{E}'_1, & \text{if } k = 1, \\ \{\mathbb{A} \cup \mathbb{B} : \mathbb{A} \in \mathcal{E}'_\ell, 1 \leq \ell \leq k, \\ \mathbb{B} \subseteq \mathbb{S} \setminus \mathbb{A}, |\mathbb{B}| = k - \ell\}, & \text{otherwise.} \end{cases} \quad (8.20a)$$

$$(8.20b)$$

For instance, as in Fig. 8.9, the 3-essential subarray $\{1, 2, 5\}$ can be decomposed into $\mathbb{A} \cup \mathbb{B}$, where $\mathbb{A} = \{1, 5\} \in \mathcal{E}'_2$ and $\mathbb{B} = \{2\} \subseteq \mathbb{S} \setminus \mathbb{A} = \{0, 2, 3, 4, 6\}$. Another example is $\{0, 3, 6\}$, which corresponds to either $\mathbb{A} = \{0\} \in \mathcal{E}'_1, \mathbb{B} = \{3, 6\} \subseteq \mathbb{S} \setminus \mathbb{A}$ or $\mathbb{A} = \{6\} \in \mathcal{E}'_1, \mathbb{B} = \{0, 3\} \subseteq \mathbb{S} \setminus \mathbb{A}$.

Proof of Lemma 8.4.1. Eq. (8.20a) follows from (8.19a) directly, so it suffices to prove (8.20b). Let $\mathbb{C}_0 \in \mathcal{E}_k$. If $\mathbb{C}_0 \in \mathcal{E}'_k$, then \mathbb{C}_0 is trivially included in (8.20b). If $\mathbb{C}_0 \notin \mathcal{E}'_k$, due to Definition 8.4.1, there exists $\mathbb{C}_1 \in \mathcal{E}_{k-1}$ such that $\mathbb{C}_1 \subset \mathbb{C}_0$. The same argument for \mathbb{C}_1 and \mathcal{E}_{k-1} shows that either $\mathbb{C}_1 \in \mathcal{E}'_{k-1}$ or \mathbb{C}_1 is a superset of some $\mathbb{C}_2 \in \mathcal{E}_{k-2}$. Repeating these steps show that \mathbb{C}_0 is a superset of some element in \mathcal{E}'_ℓ . Next, let us consider the right-hand side of (8.20b). Since $\mathbb{A} \subseteq \mathbb{A} \cup \mathbb{B} \subseteq \mathbb{S}$ and $\mathbb{A} \in \mathcal{E}'_\ell \subseteq \mathcal{E}_\ell$, we have $\mathbb{A} \cup \mathbb{B} \in \mathcal{E}_{|\mathbb{A} \cup \mathbb{B}|} = \mathcal{E}_k$, due to Lemma 8.2.3. \square

Another advantage of the k -essential Sperner family is that the k -essentialness property of a given subarray $\mathbb{A} \subseteq \mathbb{S}$, can be readily determined from the k -essential

Sperner family, without computing the difference coarray or searching within \mathcal{E}_k . This can be done by iterating over the elements in \mathcal{E}'_k from $k = 1$ to $k = |\mathbb{S}|$. The subarray \mathbb{A} is reported to be k -essential if there exists $\mathbb{B} \subseteq \mathbb{A}$ for some $\mathbb{B} \in \mathcal{E}'_\ell$ and $1 \leq \ell \leq k$. As an example, we know that $\{4, 5, 6\}$ in Fig. 8.9 is 3-essential since $\{0\} \not\subseteq \{4, 5, 6\}$ and $\{6\} \subseteq \{4, 5, 6\}$, where only two comparisons are needed. On the other hand, if we search for $\{4, 5, 6\}$ within the box of \mathcal{E}_3 from top to bottom and then from left to right, then 28 comparisons are required. As another example, $\{1, 3, 4\}$ can be concluded not to be 3-essential with 8 comparisons using $\mathcal{E}'_1, \mathcal{E}'_2, \mathcal{E}'_3$, but with 33 comparisons using \mathcal{E}_3 . Empirically, the reduction in the number of comparisons is huge especially for large number of sensors and large k . However, the precise analysis of the complexity is beyond the scope of this chapter and is left for future work.

The term *Sperner* originates from the Sperner theory in discrete mathematics [44], [160]. A Sperner family is a family of sets in which none of the elements is a subset of the other, which is formally defined as

Definition 8.4.2. A family of sets \mathcal{F} is a Sperner family if $\mathbb{A} \not\subseteq \mathbb{B}$ for all $\mathbb{A}, \mathbb{B} \in \mathcal{F}$ [44].

With Definition 8.4.2, we will show an explicit connection between the k -essential Sperner family and the Sperner family, as indicated in Lemma 8.4.2:

Lemma 8.4.2. The union of any selection of the k -essential Sperner family $\{\mathcal{E}'_1, \mathcal{E}'_2, \dots, \mathcal{E}'_{|\mathbb{S}|}\}$ is a Sperner family. Namely, $\bigcup_{k \in \mathbb{I}} \mathcal{E}'_k$ is a Sperner family, where $\mathbb{I} \subseteq \{1, 2, \dots, |\mathbb{S}|\}$.

Proof. Let $\mathbb{A}, \mathbb{B} \in \bigcup_{k \in \mathbb{I}} \mathcal{E}'_k$ such that $\mathbb{A} \subset \mathbb{B}$. Here $\mathbb{A} \subset \mathbb{B}$ indicates that \mathbb{A} is a subset of \mathbb{B} and $\mathbb{A} \neq \mathbb{B}$. If $\mathbb{A}, \mathbb{B} \in \mathcal{E}'_k$ for some $k \in \mathbb{I}$, then $|\mathbb{A}| = |\mathbb{B}| = k$, violating $\mathbb{A} \subset \mathbb{B}$. Assume that $\mathbb{A} \in \mathcal{E}'_{k_1}$ and $\mathbb{B} \in \mathcal{E}'_{k_2}$ for some $k_1, k_2 \in \mathbb{I}$ and $k_1 < k_2$. Let \mathbb{C} be a subset of $\mathbb{B} \setminus \mathbb{A}$ with size $|\mathbb{C}| = k_2 - k_1 - 1$. Since $\mathbb{A} \in \mathcal{E}'_{k_1} \subseteq \mathcal{E}_{k_1}$ and $\mathbb{A} \subseteq \mathbb{A} \cup \mathbb{C} \subseteq \mathbb{S}$, Lemma 8.4.1 indicates that, $\mathbb{A} \cup \mathbb{C} \in \mathcal{E}_{k_2-1}$. However $\mathbb{A} \cup \mathbb{C} \subset \mathbb{B}$, contradicting (8.19b). \square

As an example of Lemma 8.4.2, if $\mathbb{I} = \{2, 3\}$ and \mathcal{E}'_k is given in Fig. 8.9, then $\mathcal{E}'_2 \cup \mathcal{E}'_3$ contains $\{1, 5\}, \{1, 2, 3\}, \{1, 2, 4\}, \{2, 3, 4\}, \{2, 4, 5\}$, and $\{3, 4, 5\}$, where none of the elements in $\mathcal{E}'_2 \cup \mathcal{E}'_3$ is a superset of another. Hence $\mathcal{E}'_2 \cup \mathcal{E}'_3$ is a Sperner family.

Furthermore, Lemma 8.4.2 connects the essentialness property, the fragility, and the k -essential (Sperner) family, with the well-established results in Sperner theory, such as Sperner's theorem [160], and so on [44].

Similar to Corollary 8.2.1, the following show the relations between the equality $\mathcal{E}_k = \mathcal{S}_k$ and the emptiness of \mathcal{E}'_k . These results will be quite useful in studying the

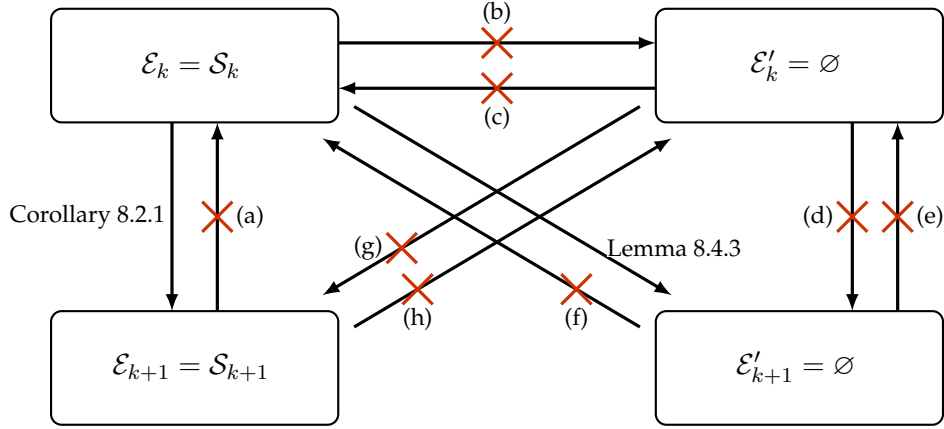


Figure 8.10: The relation between $\mathcal{E}_k = \mathcal{S}_k$ and $\mathcal{E}'_k = \emptyset$. Here solid arrows represent logical implication while arrows with red crosses mean that one condition does not necessarily imply the other.

probability that the difference coarray changes in Section 8.5 and the k -essentialness property for several array configurations in Chapter 9.

Lemma 8.4.3. Let \emptyset denote the empty set. Assume that the integer k satisfies $1 \leq k \leq |\mathbb{S}| - 1$. If $\mathcal{E}_k = \mathcal{S}_k$, then $\mathcal{E}'_{k+1} = \emptyset$.

Proof. Let $\mathbb{A} \in \mathcal{E}'_{k+1}$ and \mathbb{B} be a subset of \mathbb{A} with size $|\mathbb{B}| = k$. Since $\mathcal{E}_k = \mathcal{S}_k$, we have $\mathbb{B} \in \mathcal{E}_k$, which contradicts Definition 8.4.1. \square

Lemma 8.4.4. Let \mathcal{E}'_k be the k -essential Sperner family of an array \mathbb{S} . Then $\mathcal{E}'_k = \emptyset$ for all $Q + 1 \leq k \leq |\mathbb{S}|$, where Q is defined in Theorem 8.2.1.2.

Proof. It follows from Theorem 8.2.1.2 and Lemma 8.4.3. \square

Fig. 8.10 summarizes the logical relation between $\mathcal{E}_k = \mathcal{S}_k$ and $\mathcal{E}'_k = \emptyset$ in detail. Here Corollary 8.2.1 and Lemma 8.4.3 are denoted by solid arrows while dashed arrows (Case (a) to (h)) indicate that one condition does not imply the other. The counter examples for (a)-(h) are listed as follows. If $\mathbb{S} = \{0, 1, 3, 4, 5, 6, 7, 8, 10\}$, then the k -essential family and the k -essential Sperner family become

$$\mathcal{E}_1 \neq \mathcal{S}_1, \quad \mathcal{E}'_1 = \{\{0\}, \{1\}, \{8\}, \{10\}\} \neq \emptyset, \quad (8.21)$$

$$\mathcal{E}_2 \neq \mathcal{S}_2, \quad \mathcal{E}'_2 = \emptyset, \quad (8.22)$$

$$\mathcal{E}_3 \neq \mathcal{S}_3, \quad \mathcal{E}'_3 = \{\{3, 5, 6\}, \{4, 6, 7\}\} \neq \emptyset, \quad (8.23)$$

$$\mathcal{E}_4 = \mathcal{S}_4, \quad \mathcal{E}'_4 = \{\{3, 4, 5, 7\}\} \neq \emptyset, \quad (8.24)$$

$$\mathcal{E}_5 = \mathcal{S}_5, \quad \mathcal{E}'_5 = \emptyset. \quad (8.25)$$

Counter examples for Cases (a) to (h) can be found in (8.21) to (8.25). For instance, $\mathcal{E}_4 = \mathcal{S}_4$ but $\mathcal{E}_3 \neq \mathcal{S}_3$, which contradicts (a). Furthermore, \mathcal{E}_4 and \mathcal{E}'_4 contradicts (b); \mathcal{E}_2 and \mathcal{E}'_2 contradicts (c). The example of \mathcal{E}'_1 , \mathcal{E}'_2 , and \mathcal{E}'_3 disapproves Case (d) and (e) while \mathcal{E}_1 , \mathcal{E}'_2 , and \mathcal{E}_3 contradict Case (f) and (g). Case (h) has a counter example of \mathcal{E}'_4 and \mathcal{E}_5 . These examples confirm that Cases (a)-(h) are not necessarily true.

8.5 Robustness Analysis for Random Sensor Failures

In this section, we assume that the sensors in an array have a certain probability of failure, and derive an expression for the probability that the difference coarray will change due to this failure. We will show that the concepts introduced in this chapter, such as k -essentialness and fragility, play a crucial role in this analysis. As explained earlier, the importance of this analysis arises from the fact that the robustness of the difference coarray (to sensor failures) is crucial for the success of algorithms such as coarray MUSIC.

Assumptions

In this section, let a sensor array be \mathbb{S} and the difference coarray be \mathbb{D} . Assume that *each sensor fails independently with probability p* . After the removal of faulty sensors, the array and the difference coarray are denoted by $\bar{\mathbb{S}}$ and $\bar{\mathbb{D}}$, respectively. Then the probability that $\bar{\mathbb{D}} \neq \mathbb{D}$ is denoted by

$$P_c \triangleq \Pr[\bar{\mathbb{D}} \neq \mathbb{D}]. \quad (8.26)$$

An array is more robust, as P_c is close to 0. This property can also be used in comparing the robustness among several array configurations.

Note that P_c is different from the k -fragility F_k , even though they both correspond to the concept of probability. As presented in Section 8.3, if there are k faulty sensors in the array and all possible failure patterns are equiprobable, the k -fragility F_k can be interpreted as the probability that the difference coarray changes. On the other hand, P_c denotes the probability that the difference coarray changes, due to any possible sensor failure pattern. Furthermore, F_k depends purely on the array geometry while P_c depends on the array geometry and the failure probability of each sensor. In practice, P_c is more useful since 1) it does not require the information of the number of faulty sensors and 2) the parameter p , which determines the quality and the cost of the sensing device, can be designed based on the budget.

Next, we will present a closed-form relation between P_c and F_k . Let $\mathbb{A} \subseteq \mathbb{S}$ be the set of faulty sensors. Assume that $\bar{\mathbb{S}} \triangleq \mathbb{S} \setminus \mathbb{A}$ and the associated difference coarray $\bar{\mathbb{D}}$. Due to Definition 8.2.4, the difference coarray changes ($\bar{\mathbb{D}} \neq \mathbb{D}$) if and only if there exist $1 \leq k \leq |\mathbb{S}|$ and $\mathbb{A} \in \mathcal{E}_k$ such that 1) all the elements in $\mathbb{A} \in \mathcal{E}_k$ fail and 2) all

the elements in $\bar{\mathbb{S}}$ are operational. Summing over all possible k and \mathbb{A} leads to the following expression of P_c :

$$\begin{aligned}
P_c &= \sum_{k=1}^{|\mathbb{S}|} \sum_{\mathbb{A} \in \mathcal{E}_k} \Pr \left[\left(\bigcap_{n_1 \in \mathbb{A}} (n_1 \text{ fails}) \right) \cap \left(\bigcap_{n_2 \in \bar{\mathbb{S}}} (n_2 \text{ fails})^c \right) \right] \\
&= \sum_{k=1}^{|\mathbb{S}|} \sum_{\mathbb{A} \in \mathcal{E}_k} \left[\prod_{n_1 \in \mathbb{A}} \Pr [n_1 \text{ fails}] \right] \left[\prod_{n_2 \in \bar{\mathbb{S}}} (1 - \Pr [n_2 \text{ fails}]) \right] \\
&= \sum_{k=1}^{|\mathbb{S}|} |\mathcal{E}_k| p^k (1-p)^{|\mathbb{S}|-k}, \tag{8.27}
\end{aligned}$$

where the second equation is due to the independence of sensor failures. The complement of an event \mathfrak{F} is denoted by \mathfrak{F}^c . Substituting Definition 8.3.1 into (8.27) leads to

$$P_c = \sum_{k=1}^{|\mathbb{S}|} F_k \binom{|\mathbb{S}|}{k} p^k (1-p)^{|\mathbb{S}|-k}, \tag{8.28}$$

where F_k is the k -fragility of \mathbb{S} .

Note that (8.28) shows the explicit relation between F_k and P_c , which holds for any array configuration \mathbb{S} . Here each term in (8.28) has two contributions: F_k and $\binom{|\mathbb{S}|}{k} p^k (1-p)^{|\mathbb{S}|-k}$. F_k depends purely on the array geometry while $\binom{|\mathbb{S}|}{k} p^k (1-p)^{|\mathbb{S}|-k}$ relies on k , the number of sensors $|\mathbb{S}|$, and p . This observation means that, for a fixed number of sensors and a fixed p , it is possible to reduce P_c by designing new array geometries with reduced F_k . On the other hand, for a fixed array configuration, F_k is uniquely determined. In this case, it can be shown that P_c decreases with p , as p is sufficiently small. Namely, to reduce P_c , we can deploy sensing devices with small p .

However, the right-hand side of (8.28) is not computationally tractable. For instance, if k is approximately $|\mathbb{S}|/2$, the complexity for evaluating F_k is around $\binom{|\mathbb{S}|}{|\mathbb{S}|/2}$, which becomes computationally expensive for large $|\mathbb{S}|$. Even so, the behavior of P_c can still be analyzed based on the following theorem:

Theorem 8.5.1. The probability that the difference coarray changes satisfies $\max\{L_1, L_2\} \leq$

$P_c \leq \min\{U_1, U_2, 1\}$, where L_1, U_1, L_2 , and U_2 are given by

$$L_1 = 1 - (1-p)^{|\mathbb{S}|} - \left(1 - \frac{2}{|\mathbb{S}|}\right) \sum_{k=1}^{Q-1} \binom{|\mathbb{S}|}{k} p^k (1-p)^{|\mathbb{S}|-k}, \quad (8.29)$$

$$U_1 = 1 - (1-p)^{|\mathbb{S}|}, \quad (8.30)$$

$$L_2 = 1 - (1-p)^{|\mathcal{E}_1|}, \quad (8.31)$$

$$U_2 = 1 - (1-p)^{|\mathcal{E}_1|} + (1-p)^{|\mathcal{E}_1|} \sum_{k=2}^Q |\mathcal{E}'_k| p^k. \quad (8.32)$$

Here the parameter Q is given in Theorem 8.2.1.2. The notation \mathcal{E}_k and \mathcal{E}'_k represent the k -essential family and the k -essential Sperner family for the sensor array \mathbb{S} .

Proof. First we will show that $L_1 \leq P_c \leq U_1$. Theorem 8.3.1.3 indicates that P_c is upper bounded by $\sum_{k=1}^{|\mathbb{S}|} \binom{|\mathbb{S}|}{k} p^k (1-p)^{|\mathbb{S}|-k} = 1 - (1-p)^{|\mathbb{S}|} = U_1$, which proves the upper bound. For the lower bound, if $|\mathbb{S}| = 1$, then it can be shown that $P_c = p = L_1$. If $|\mathbb{S}| \geq 2$, then Theorem 8.3.1.3 and 8.3.1.2 imply that $F_k \geq 2/|\mathbb{S}|$ for $k = 1, 2, \dots, Q-1$ and $F_k = 1$ otherwise. Substituting these relations into (8.28) proves L_1 .

The proof of Eqs. (8.31) and (8.32) is as follows. Let the sensor array be \mathbb{S} and the k -essential Sperner family be \mathcal{E}'_k . Assume that each sensor fails independently with probability p . Let \mathbb{B} be the set of faulty sensors. Assume that $\bar{\mathbb{S}} \triangleq \mathbb{S} \setminus \mathbb{B}$ and difference coarray is denoted by $\bar{\mathbb{D}}$. Since a subarray \mathbb{B} is k -essential if and only if \mathbb{B} is a superset of some elements in \mathcal{E}'_ℓ for some $1 \leq \ell \leq k$, as in (8.20b), it suffices to consider all elements in $\mathcal{E}'_1, \mathcal{E}'_2, \dots, \mathcal{E}'_{|\mathbb{S}|}$ and the probability that $\bar{\mathbb{D}} \neq \mathbb{D}$ becomes

$$\begin{aligned} P_c &= \Pr[\bar{\mathbb{D}} \neq \mathbb{D}] = \Pr\left[\bigcup_{k=1}^{|\mathbb{S}|} \bigcup_{\mathbb{A}_k \in \mathcal{E}'_k} \mathfrak{F}(\mathbb{A}_k)\right] \\ &= \Pr\left[\underbrace{\left(\bigcup_{\mathbb{A}_1 \in \mathcal{E}'_1} \mathfrak{F}(\mathbb{A}_1)\right)}_{\text{Event } \mathfrak{G}_1} \cup \underbrace{\left(\bigcup_{k=2}^{|\mathbb{S}|} \bigcup_{\mathbb{A}_k \in \mathcal{E}'_k} \mathfrak{F}(\mathbb{A}_k)\right)}_{\text{Event } \mathfrak{G}_2}\right], \end{aligned} \quad (8.33)$$

where $\mathfrak{F}(\mathbb{A}_k) \triangleq \cap_{n \in \mathbb{A}_k} (n \text{ fails})$ denotes the event in which all the elements in \mathbb{A}_k fail. Since the event \mathfrak{G}_1 involves only the essential elements and \mathfrak{G}_2 are associated with inessential sensors, \mathfrak{G}_1 and \mathfrak{G}_2 are independent. Namely, $\Pr[\mathfrak{G}_1 \cap \mathfrak{G}_2] = \Pr[\mathfrak{G}_1] \Pr[\mathfrak{G}_2]$. Hence $\Pr[\mathfrak{G}_1 \cup \mathfrak{G}_2] = 1 - \Pr[\mathfrak{G}_1^c] + \Pr[\mathfrak{G}_1^c] \Pr[\mathfrak{G}_2]$, where \mathfrak{G}_1^c is the complement of the event \mathfrak{G}_1 . The probability $\Pr[\mathfrak{G}_1^c]$ can be simplified as

$$\Pr[\mathfrak{G}_1^c] = \Pr\left[\bigcap_{\mathbb{A}_1 \in \mathcal{E}'_1} (\mathfrak{F}(\mathbb{A}_1))^c\right] = (1-p)^{|\mathcal{E}_1|}. \quad (8.34)$$

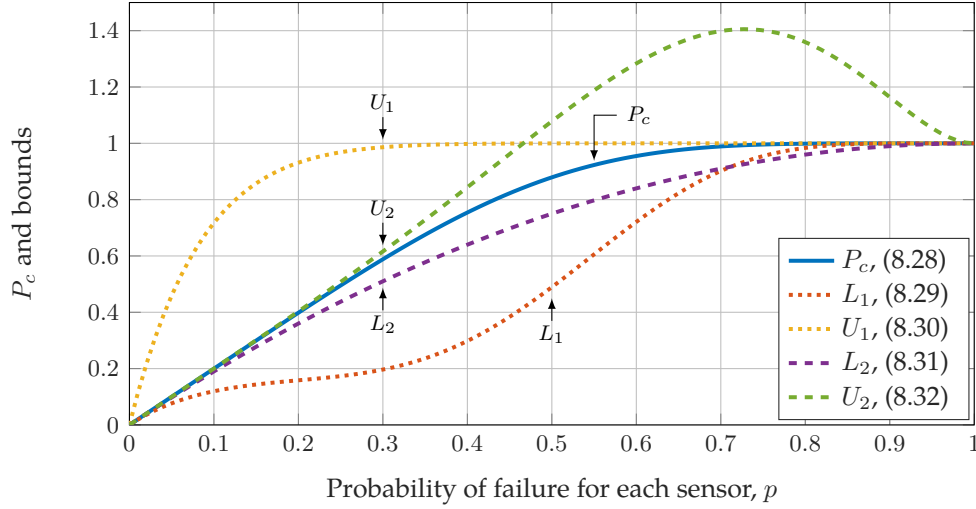


Figure 8.11: The probability that the difference coarray changes P_c and its lower bounds and upper bounds for the ULA with 12 sensors.

Applying the union bound of $\Pr[\mathfrak{G}_2]$ leads to

$$0 \leq \Pr[\mathfrak{G}_2] \leq \sum_{k=2}^{|\mathcal{S}|} \sum_{\mathbb{A}_k \in \mathcal{E}'_k} \Pr[\mathfrak{F}(\mathbb{A}_k)] = \sum_{k=2}^{|\mathcal{S}|} |\mathcal{E}'_k| p^k. \quad (8.35)$$

Substituting (8.34), (8.35), and Lemma 8.4.4 into $P_c = 1 - \Pr[\mathfrak{G}_1^c] + \Pr[\mathfrak{G}_1^c] \Pr[\mathfrak{G}_2]$ proves (8.31) and (8.32). \square

It can be observed that all these expressions (8.29) to (8.32) do not require the complete knowledge of F_k . For instance, U_1 depends only on the probability of single sensor failure p and the number of sensors, while L_2 requires p and the size of \mathcal{E}_1 . The bounds L_1 and U_2 are functions of the parameter Q , as given in Theorem 8.2.1.2. If Q is much smaller than the number of sensors, then U_2 can be evaluated efficiently with the first few \mathcal{E}'_k .

Example 8.5.1. Next we will demonstrate an example for the bounds in Theorem 8.5.1. Fig. 8.11 shows the curves of P_c , L_1 , U_1 , L_2 , and U_2 for the ULA with $N = 12$ physical sensors, as a function of p . First it can be observed that the bounds L_1 and U_1 are close to P_c for $p \geq 0.8$ while for small p , the bounds L_2 and U_2 are tighter than L_1 and U_1 . Second, in this example, the bound U_2 is greater than 1 for $p \geq 0.5$, which becomes a trivial upper bound for P_c . This is because the term $\sum_{k=2}^Q |\mathcal{E}'_k| p^k$ in (8.32) is derived from the union bound of the probability, which could be greater than 1.

The bounds in Theorem 8.5.1 also makes it possible to derive asymptotic expressions for P_c . For fixed number of sensors, if $p \ll 1/|\mathcal{S}|$, then the high order terms

$\sum_{k=2}^Q |\mathcal{E}'_k| p^k$ in (8.32) become negligible, since $|\mathcal{E}'_k| \leq \binom{|\mathbb{S}|}{k} = \mathcal{O}(|\mathbb{S}|^k)$. Then we have $L_2 \leq P_c \leq U_2 \approx L_2$. Therefore, for any array geometry \mathbb{S} and $p \ll 1/|\mathbb{S}|$, the probability that the difference coarray changes can be approximated by

$$P_c \approx L_2 = 1 - (1 - p)^{|\mathcal{E}_1|} \approx |\mathcal{E}_1| p, \quad (8.36)$$

since $(1+x)^N \approx 1+Nx$ for $|x| \ll 1$. Eq. (8.36) shows that, for small p , the probability P_c is approximately linear in p with slope $|\mathcal{E}_1|$. This result can be verified through the curve of P_c in Fig. 8.11, where the ULA has $|\mathcal{E}_1| = 2$, as proved in (9.20).

Note that (8.36) holds for any array configuration \mathbb{S} , which indicates that for the same $p \ll 1/|\mathbb{S}|$, smaller $|\mathcal{E}_1|$ leads to smaller P_c . For instance, due to (9.20), the ULA with $N \geq 4$ physical sensors always has $P_c \approx 2p$, even for large N . However this does not hold for MESA, since MESA with N sensors own $P_c \approx Np$, which grows linearly with N . Eq. (8.36) can also be expressed as $P_c \approx (|\mathbb{S}|p)F_1$. This indicates that, if the number of sensors $|\mathbb{S}|$ and the sensor failure rate p are fixed, then P_c is proportional to fragility F_1 , instead of F_k .

Example 8.5.2. Fig. 8.12 demonstrates a numerical example for P_c across various array configurations with 12 sensors, such as the ULA with 12 sensors, the nested array with $N_1 = N_2 = 6$, as in (2.7), and the coprime array with $M = 4$ and $N = 5$, as in (2.8). The probability that the difference coarray changes is first evaluated based on (8.28), as depicted in solid, dashed, and dotted curves on the bottom of Fig. 8.12. Next, these probabilities are also averaged empirically from 10^7 Monte-Carlo runs and each run corresponds to an independent realization of the array geometry with sensor failure rate p . The results based on Monte-Carlo runs are marked in either empty circles, crosses, and empty squares on the bottom of Fig. 8.12.

First, it can be deduced that the experimental results match (8.28) for all these array configurations. For the same p and the same number of physical sensors, by comparing the values of P_c , the most robust array geometry is the ULA, followed by the coprime array, and finally the nested array. Furthermore, for $p \ll 1/|\mathbb{S}| = 1/12$, the asymptotic expressions for P_c in Fig. 8.12 become $P_c \approx 2p$ for ULA, $P_c \approx 12p$ for the nested array, and $P_c \approx 9p$ for the coprime array. These results are consistent with the asymptotic expressions in (8.36).

8.6 Concluding Remarks

In this chapter, we presented a general theory to quantify the robustness of difference coarrays with respect to sensor failures. We began by defining the (k -)essentialness property and the k -essential family. Based on these, the k -fragility characterizes the likelihood that the difference coarray changes, while the k -essential Sperner family offers a compact representation of the k -essential family. Under mild assumptions,

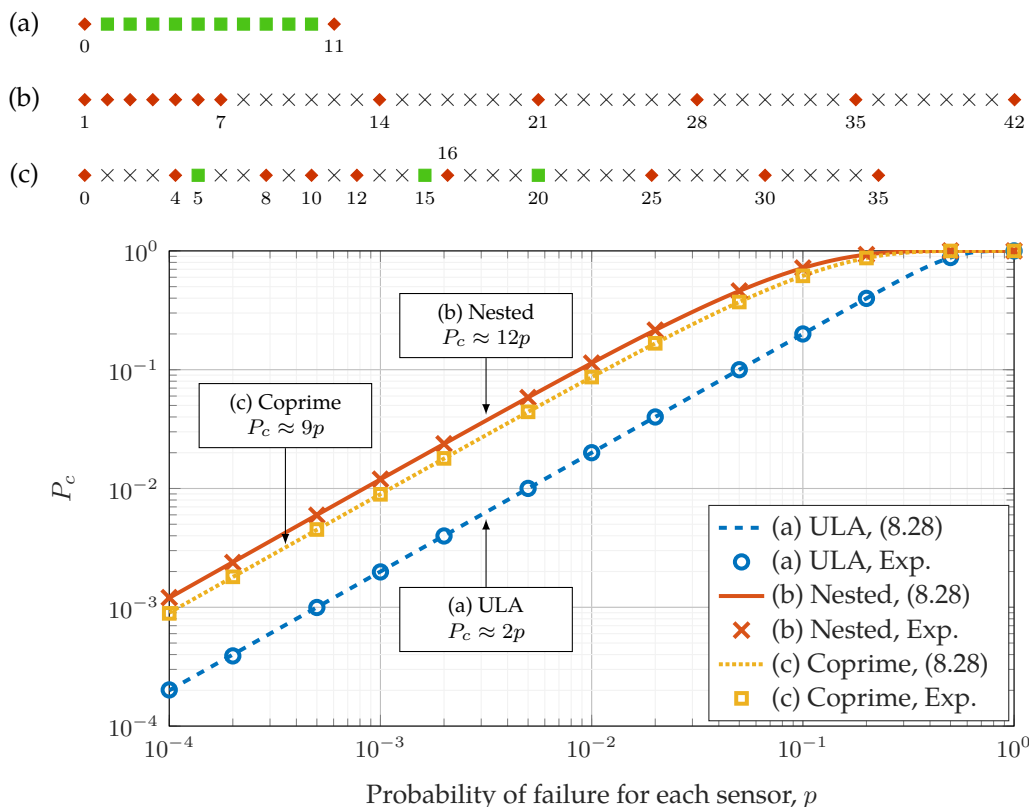


Figure 8.12: The dependence of the probability that the difference coarray changes P_c on the probability of single sensor failure p for (a) the ULA with 12 sensors, (b) the nested array with $N_1 = N_2 = 6$, and (c) the coprime array with $M = 4$ and $N = 5$. Here the essential sensors (diamonds) and the inessential sensors (squares) are depicted on the top of this figure. Experimental data points (Exp.) are averaged from 10^7 Monte-Carlo runs. The approximations of P_c are valid for $p \ll 1/12$ due to (8.36).

it was shown that the probability that the difference coarray changes, which is crucial for the functionality of coarray MUSIC, can be derived using the proposed theory.

In Chapter 9, we will concentrate on the relation between the presented theory and the array geometry. The closed-form expressions of the k -essential Sperner family for ULA, MRA, MHA, Cantor arrays, nested arrays, and coprime arrays, will be derived to provide insights into the importance of each sensor and the robustness of arrays.

In the future, it is of considerable interest to investigate the interplay between the DOA estimation performance and coarray robustness, which may find applications in practical systems using sparse arrays. Another future topic is to quantify the robustness of sparse arrays with respect to the central ULA segment in the difference

coarray, which affects the applicability of DOA estimators such as coarray MUSIC.

As a final remark, the essentialness property can be reformulated to study the robustness of sparse arrays in various problems. For instance, the performance of MIMO radar [82] depends on the sum coarray while the $2q$ th-order difference coarray [120] plays a critical role in DOA estimation with $2q$ th-order cumulants. Future directions can be conducted towards the robustness of the coarray in these scenarios.

ROBUSTNESS OF DIFFERENCE COARRAYS OF SPARSE ARRAYS TO SENSOR FAILURES – ARRAY GEOMETRIES

9.1 Introduction

In Chapter 8, the general theory of the k -essential family, the k -fragility, and the k -essential Sperner family was proposed to assess the robustness of difference coarrays of sparse arrays to sensor failures. A subarray of size k is said to be k -essential if its deletion changes the difference coarray. All these k -essential subarrays constitute the k -essential family. With this tool, the robustness can be quantified by the k -fragility, or simply *fragility*, which ranges from 0 to 1. An array is more robust or less fragile if the fragility is closer to 0. However, from the computational perspective, the size of the k -essential family can be as large as $\binom{N}{k}$, where N is the number of physical elements. This attribute makes it challenging to analyze and to store the complete information of the k -essential family. It was shown in Chapter 8 that the k -essential family can be compactly represented by the k -essential Sperner family. With these tools, the system reliability can be quantified by the probability that the difference coarray changes, P_c , under the assumption of random sensor failures. Many insights into the interplay between the proposed theory and P_c were also offered in Chapter 8.

The main contribution of this chapter is to analyze the robustness of several commonly used array configurations, like ULA [188], MRA [113], minimum hole arrays (MHA) [177], Cantor arrays [100], [136], nested arrays [124], and coprime arrays [186], based on the general theory in Chapter 8. These arrays are widely used in various topics of array signal processing, such as beamforming [4], [68], [124], [136], [188] and DOA estimation [19], [124], [139], [186]. However the robustness of the difference coarrays of these arrays to sensor failures remains an open but significant topic in this field. It will be shown in this chapter that most arrays we consider are maximally economic, namely, any sensor failure changes the difference coarray, except for ULA and coprime arrays. It can be proved that the fragility and P_c for maximally economic sparse arrays (MESA) are the largest among all arrays with a fixed number of sensors. These theoretical results confirm the empirical observation that MRA are not robust to sensor failures, in terms of the preservation of the difference coarray.

In this chapter, the closed-form expressions of the k -essential Sperner family for ULA and coprime arrays are also established with detailed derivations. These expressions lead to a number of contributions. First, it can be proved that, for suf-

ficiently large number of sensors, ULA are more robust than MESA and coprime arrays (in terms of the fragility), which is in accordance with the observation that sparse arrays are in general less robust than ULA. Furthermore, the explicit expressions of the k -essential Sperner family for the coprime array allow one to construct arrays with fewer sensors but with the same difference coarray as the coprime array. Note that this topic was previously addressed in the thinned coprime array [144], where a specific selection of sensors is removed from the coprime array. Using the proposed expressions, it can be shown that there exist other array geometries that achieve the same number of sensors and the same difference coarray, as the thinned coprime array.

It is also demonstrated through numerical examples that, the DOA estimation performance of arrays is influenced by the trade-offs between the size and the robustness of the difference coarray. It is assumed that each element in an array fails independently with probability p and the number of sensors is fixed for the ULA, the MRA, the nested array, and the coprime array. It will be deduced in the examples that, for small p , the MRA has the best DOA estimation performance, due to the largest difference coarray, while for large p , the ULA owns the best performance because of its robustness. An interesting observation is that, for moderate p , the coprime array could outperform the ULA, the MRA, and the nested array, owing to its striking a balance between the size and the robustness of the difference coarray.

Chapter outline: Section 9.2, 9.3, and 9.4 study the k -essential Sperner family for MESA, ULA, and coprime arrays, respectively, along with examples, discussions, and proofs. The performance of these arrays in the presence of sensor failure is demonstrated in Section 9.5 while Section 9.6 concludes this chapter.

9.2 Maximally Economic Sparse Arrays

The definition of the maximally economic sparse arrays (MESA), as in Definition 8.2.2, is actually equivalent to $\mathcal{E}_1 = \mathcal{S}_1$. This result leads to the following lemma:

Lemma 9.2.1. Let \mathbb{S} be a MESA, as defined in Definition 8.2.2. Then the k -essential family \mathcal{E}_k , the k -fragility F_k , and the k -essential Sperner family \mathcal{E}'_k for \mathbb{S} are given by

$$\mathcal{E}_k = \mathcal{S}_k, \quad F_k = 1, \quad k = 1, 2, \dots, |\mathbb{S}|, \quad (9.1)$$

$$\mathcal{E}'_1 = \mathcal{S}_1, \quad \mathcal{E}'_k = \emptyset, \quad k = 2, 3, \dots, |\mathbb{S}|, \quad (9.2)$$

where \mathcal{S}_k is defined in Definition 8.2.3 and \emptyset denotes the empty set.

Due to Lemma 9.2.1, MESA are the least robust arrays in terms of the k -fragility F_k , since they own the largest k -fragility F_k among all array configurations. Furthermore, according to Lemma 9.2.1, the condition that $\mathcal{E}'_k = \emptyset$ for all $2 \leq k \leq N$ is

necessary, but not sufficient for \mathbb{S} being maximally economic. As an example, the array $\mathbb{S} = \{0, 1, 2, 3, 4, 12, 14\}$ has $\mathcal{E}'_k = \emptyset$ for all $2 \leq k \leq 7$. But $\mathcal{E}'_1 = \mathcal{S}_1 \setminus \{\{2\}\}$ and \mathbb{S} is not maximally economic.

The probability that the difference coarray changes P_c can also be characterized in closed forms. Substituting Lemma 9.2.1 into (8.28) leads to

$$P_c = 1 - (1 - p)^{|\mathbb{S}|} \quad \text{for MESA.} \quad (9.3)$$

Eq. (9.3) depends only on the number of sensors in MESA, instead of the sensor locations.

It can be deduced from (9.3) and Theorem 8.5.1 that, for a fixed number of sensors, MESA has the largest P_c . This observation is in accordance with the statement that MESA are the least robust or the most fragile arrays among all possible array geometries, as seen from our earlier discussion on k -fragility.

The above discussions do not assume a specific array geometry. As one of the main contributions of this chapter, the following theorem characterizes several instances of MESA:

Theorem 9.2.1. The MESA family includes minimum redundancy arrays (MRA), minimum hole arrays (MHA), nested arrays with $N_2 \geq 2$, and Cantor arrays.

Example 9.2.1. The definitions of these arrays and the proofs can be found later in Section 9.2 to 9.2. Before presenting these details, for clarity, first let us review the geometries (depicted in diamonds) and the weight functions (shown in dots) of these arrays with 8 physical sensors through the example in Fig. 9.1. Due to the symmetry of the difference coarray, only the nonnegative portion of the weight function is depicted. By definition, the difference coarray is the support of the weight function, as in Definitions 2.2.1 and 2.2.9. It can be observed that the size of the nonnegative part of the difference coarray, as given by the number of m such that $w(m) \geq 1$ in Fig. 9.1, is 24 for the MRA, 29 for the MHA, 20 for the nested array, and finally 14 for the Cantor array. This is because Cantor arrays only have $\mathcal{O}(|\mathbb{S}|^{1.585})$ elements in the difference coarray [100] while the remaining arrays have $\mathcal{O}(|\mathbb{S}|^2)$ elements in \mathbb{D} [113], [124], [177]. Furthermore, the MHA has holes in the difference coarray. Namely, there are some missing elements, such as 26, 27, and 29 in Fig. 9.1(b), which cannot be obtained from the pairwise differences of the sensor locations. The remaining arrays have hole-free difference coarrays, i.e., the difference coarray is composed of consecutive integers ($\mathbb{D} = \mathbb{U}$). Theorem 9.2.1 indicates that none of the physical elements (as the diamonds in Fig. 9.1) in these arrays can be removed without changing the difference coarray.

In Section 9.2 to 9.2, the details of Theorem 9.2.1 will be clarified, including the definition of these arrays and the proof of their maximal economy.

Minimum Redundancy Arrays

Minimum redundancy arrays (MRA) were first proposed by Moffet [113]. These minimize the so-call *redundancy* R , defined as

$$R \triangleq \frac{\binom{|\mathbb{S}|}{2}}{(|\mathbb{U}| - 1)/2}, \quad (9.4)$$

subject to the hole-free constraint on the difference coarray. Next, the definition of the MRA is given as follows (Definition 2.2.10):

Definition 9.2.1. The MRA with N physical elements can be defined as:

$$\mathbb{S}_{\text{MRA}} \triangleq \arg \max_{\mathbb{S}} |\mathbb{D}| \text{ subject to } |\mathbb{S}| = N, \mathbb{D} = \mathbb{U}. \quad (9.5)$$

For a fixed number of sensors, it can be shown that Moffet's definition is equivalent to Definition 2.2.10, or Definition 9.2.1. However, this chapter considers Definition 2.2.10 to facilitate the proof of Theorem 9.2.1, as presented below.

Proof of the maximal economy of MRA

Definition 2.2.10 implies that the MRA has the largest hole-free difference coarray $\mathbb{D}_{\text{MRA}} \triangleq \{0, \pm 1, \pm 2, \dots, \pm (\max(\mathbb{S}_{\text{MRA}}) - \min(\mathbb{S}_{\text{MRA}}))\}$, among all array configurations with N elements. Due to Corollary 8.2.3, the MRA is maximally economic for $1 \leq N \leq 3$. If $N \geq 4$, then we have the following chain of arguments. Assume that $n \in \mathbb{S}_{\text{MRA}}$ is inessential. It can be shown that 1) $n \neq \min(\mathbb{S}_{\text{MRA}})$ as in Lemma 8.2.2, and 2) the difference coarray of $\mathbb{S}_{\text{MRA}} \setminus \{n\}$ is also \mathbb{D}_{MRA} . Now we construct a new array geometry

$$\bar{\mathbb{S}} \triangleq (\mathbb{S}_{\text{MRA}} \setminus \{n\}) \cup \{\max(\mathbb{S}_{\text{MRA}}) + 1\}, \quad (9.6)$$

which has difference coarray $\bar{\mathbb{D}}$. It can be shown that 1) $|\bar{\mathbb{S}}| = N$ and 2) $\bar{\mathbb{D}} = \mathbb{D}_{\text{MRA}} \cup \{\pm(\max(\mathbb{S}_{\text{MRA}}) - \min(\mathbb{S}_{\text{MRA}}) + 1)\}$. Hence $\bar{\mathbb{D}}$ is hole-free. However, $|\bar{\mathbb{D}}| = |\mathbb{D}_{\text{MRA}}| + 2$, which contradicts (2.5). Therefore all elements in \mathbb{S}_{MRA} are essential. \square

Minimum Hole Arrays

Minimum hole arrays (MHA) are also called Golomb arrays or minimum gap arrays [177], [190]. These arrays are defined to minimize the number of holes, such that each nonzero element in the difference coarray results from a unique sensor pair, as in Definition 2.2.11. More details on MHA can be found in [2] and the references therein. In this chapter, the main focus of MHA is to prove their maximal economy, as presented below:

Proof of the maximal economy of MHA

Let $\mathbb{S}_{\text{MHA}} = \{s_1, s_2, \dots, s_N\}$ be a MHA with N elements such that $s_1 < s_2 < \dots < s_N$. Due to Corollary 8.2.3, it suffices to consider MHA with $N \geq 4$. Next, Definition 2.2.11 indicates that the weight function of \mathbb{S}_{MHA} satisfies $w(s_2 - s_1) = w(s_3 - s_1) = \dots = w(s_N - s_1) = 1$. This relation proves the maximal economy of MHA owing to Lemma 8.2.1 and Definition 8.2.2. \square

Example 9.2.2. Consider Fig. 9.1(b), where the MHA has sensor locations $\mathbb{S}_{\text{MHA}} = \{0, 1, 4, 9, 15, 22, 32, 34\}$. It can be observed that the weight function satisfies $w(1 - 0) = w(4 - 0) = w(9 - 0) = w(15 - 0) = w(22 - 0) = w(32 - 0) = w(34 - 0) = 1$. As a result, the MHA with 8 sensors is maximally economic.

Nested Arrays with $N_2 \geq 2$

A downside for MRA and MHA is the lack of computationally efficient algorithms or closed-form solutions for the sensor locations [113], [177]. By contrast, the sensor locations of nested arrays are expressed in closed forms, as in [124], and (2.7):

Definition 9.2.2. Assume that N_1 and N_2 are positive integers. The nested array with N_1 and N_2 is specified by the set $\mathbb{S}_{\text{nested}} \triangleq \mathbb{T}_1 \cup \mathbb{T}_2$, where \mathbb{T}_1 and \mathbb{T}_2 are defined as

$$\mathbb{T}_1 = \{1, 2, \dots, N_1\}, \quad (9.7)$$

$$\mathbb{T}_2 = \{n(N_1 + 1) : n = 1, 2, \dots, N_2\}. \quad (9.8)$$

Here \mathbb{T}_1 denotes a dense ULA with interelement spacing 1 (in unit of half of the wavelength) while \mathbb{T}_2 represents a sparse ULA with spacing $N_1 + 1$. For instance, in Fig. 9.1(c), the nested array has $\mathbb{T}_1 = \{1, 2, 3, 4\}$ and $\mathbb{T}_2 = \{5, 10, 15, 20\}$.

Nested arrays possess hole-free difference coarrays [124]. Furthermore, if N_1 and N_2 are approximately $N/2$, then the size of the difference coarray of the nested array becomes $\mathcal{O}(N^2)$, which is as many as that of MRA and MHA [113], [124], [177]. For brevity, other properties of the nested array are skipped in this chapter and interested readers are referred to [124] and the references therein.

Next, as one of the contributions of this chapter, the maximal economy of nested arrays with $N_2 \geq 2$ will be proved. As a remark, if $N_2 = 1$, then the nested array becomes the ULA with $N_1 + 1$ elements, which is, in general, not maximally economic, as we will shown in Theorem 9.3.1.

Proof of the maximal economy of nested arrays with $N_1 \geq 2$

First, the weight function for $\mathbb{S}_{\text{nested}}$ is denoted by $w_{\text{nested}}(m)$. Then, we invoke the following two lemmas, whose proofs can be found at the end of this subsection.

Lemma 9.2.2. Assume that $N_2 \geq 2$. If $n_1 = N_2(N_1 + 1)$ and $n_2 \in \mathbb{T}_1$, then $w_{\text{nested}}(n_1 - n_2) = 1$.

Lemma 9.2.3. If $n_1 \in \mathbb{T}_2$ and $n_2 = 1$, then $w_{\text{nested}}(n_1 - n_2) = 1$.

Finally, combining Lemma 8.2.1, 9.2.2, 9.2.3, and Definition 8.2.2 proves the maximal economy of the nested array with $N_2 \geq 2$. \square

Example 9.2.3. Let us verify Lemma 9.2.2 and 9.2.3 using the nested array with $N_1 = N_2 = 4$ in Fig. 9.1(c). Assume that $n_1 = N_2(N_1 + 1) = 20$ and $n_2 = 3 \in \mathbb{T}_1$. Due to Fig. 9.1(c), the weight function of the nested array satisfies $w(n_1 - n_2) = w(17) = 1$, which confirms Lemma 9.2.2. Next, suppose that $n_1 = 15 \in \mathbb{T}_2$ and $n_2 = 1$. We obtain $w(n_1 - n_2) = 14$ based on Fig. 9.1(c). The above example is also consistent with Lemma 9.2.3.

Finally, the proofs of Lemma 9.2.2 and 9.2.3 are given as follows:

Proof of Lemma 9.2.2. In this case, we have $n_1 - n_2 \geq N_2(N_1 + 1) - N_1$. Assume that there exist $n'_1, n'_2 \in \mathbb{S}_{\text{nested}}$ such that the pair $(n'_1, n'_2) \neq (n_1, n_2)$ and $n'_1 - n'_2 = n_1 - n_2$. If n'_1 is not the rightmost element in $\mathbb{S}_{\text{nested}}$, namely, $n'_1 \neq N_2(N_1 + 1)$, then $n'_1 \leq (N_2 - 1)(N_1 + 1)$, because $N_2 \geq 2$. Furthermore, since $n'_2 \geq 1$, we have $n'_1 - n'_2 \leq (N_2 - 1)(N_1 + 1) - 1 = N_2(N_1 + 1) - N_1 - 2$, which disagrees with $n'_1 - n'_2 = n_1 - n_2 \geq N_2(N_1 + 1) - N_1$. Therefore $n'_1 = n_1 = N_2(N_1 + 1)$, $n'_2 = n_2$, and $w_{\text{nested}}(n_1 - n_2) = 1$. \square

Proof of Lemma 9.2.3. Since $n_1 \in \mathbb{T}_2$ and $n_2 = 1$, we have

$$n_1 - n_2 \equiv N_1 \pmod{(N_1 + 1)}, \quad (9.9)$$

$$n_1 - n_2 \geq N_1, \quad (9.10)$$

where $\text{mod } N$ denotes the modulo- N operation. Suppose that there exist $n'_1, n'_2 \in \mathbb{S}_{\text{nested}}$ such that the pair $(n_1, n_2) \neq (n'_1, n'_2)$ and $n'_1 - n'_2 = n_1 - n_2$. The parameters n'_1 and n'_2 can be divided into four cases. If $n'_1, n'_2 \in \mathbb{T}_1$, then $|n'_1 - n'_2| \leq N_1 - 1$, which contradicts (9.10). If $n'_1, n'_2 \in \mathbb{T}_2$, then $n'_1 - n'_2$ is divisible by $N_1 + 1$, which violates (9.9). If $n'_1 \in \mathbb{T}_1$ and $n'_2 \in \mathbb{T}_2$, then $n'_1 - n'_2 \leq -1$, which disagrees with (9.10). Finally, if $n'_1 \in \mathbb{T}_2$ and $n'_2 \in \mathbb{T}_1$, then we obtain

$$n'_2 = n'_1 - (n_1 - n_2) \equiv 1 \pmod{(N_1 + 1)},$$

due to (9.9) and $n'_1 \in \mathbb{T}_2$. Therefore $n'_2 = n_2 = 1$ and $n'_1 = n_1$, which proves this lemma. \square

Cantor Arrays

In this subsection, we will concentrate on *Cantor arrays*, which first appeared in the context of fractal array design [136], [194], [195]. These arrays originated from the Cantor set in fractal theory [27], [159]. Previous research on Cantor arrays was mainly conducted towards the relationships between fractal geometries and the beampatterns of the arrays [136], [194], [195]. A recent study focused on the difference coarray of Cantor arrays [100], including the weight function, the size and the structure of the difference coarray, and its maximal economy, as we will present next.

First, the definition of the Cantor array \mathbb{S}_r is parameterized by a nonnegative integer r . The translated array of \mathbb{S}_r is defined as $\mathbb{T}_r \triangleq \{n + D_r : \forall n \in \mathbb{S}_r\}$, where $D_r \triangleq 2A_r + 1$, with A_r denoting the aperture of \mathbb{S}_r , that is, $A_r \triangleq \max(\mathbb{S}_r) - \min(\mathbb{S}_r)$. With this, we are ready to define a Cantor array:

Definition 9.2.3. The Cantor array \mathbb{S}_r is defined as

$$\mathbb{S}_r \triangleq \begin{cases} \{0\} & \text{if } r = 0, \\ \mathbb{S}_{r-1} \cup \mathbb{T}_{r-1}, & \text{if } r \geq 1. \end{cases} \quad (9.11)$$

Notice that \mathbb{S}_r has $N = 2^r$ sensors. So, Cantor arrays are defined only for the case that the number of sensors is a power of two. Furthermore, it was shown in [100] that Cantor arrays are symmetric arrays, i.e. $n \in \mathbb{S}_r$ if and only if $A_r - n \in \mathbb{S}_r$.

For instance, let us consider the Cantor arrays for $r = 0, 1, 2, 3$. According to Definition 9.2.3, these arrays become

$$\mathbb{S}_0 = \{0\}, \quad A_0 = 0, \quad D_0 = 1, \quad (9.12)$$

$$\mathbb{S}_1 = \{0, 1\}, \quad A_1 = 1, \quad D_1 = 3, \quad (9.13)$$

$$\mathbb{S}_2 = \{0, 1, 3, 4\}, \quad A_2 = 4, \quad D_2 = 9 \quad (9.14)$$

$$\mathbb{S}_3 = \{0, 1, 3, 4, 9, 10, 12, 13\}, \quad A_3 = 13, \quad D_3 = 27, \quad (9.15)$$

where (9.15) is depicted in Fig. 9.1(d). It can also be deduced from Fig. 9.1(d) that \mathbb{S}_3 is symmetric.

The arrays in Definition 9.2.3 are equivalent to the Cantor array proposed in [136], [194], [195], with proper amount of translation and scaling. The Cantor arrays in [136], [194], [195] are built upon the Cantor sets in fractal theory [46], [47]. But here we start with a different definition (Definition 9.2.3), which will facilitate the discussion on its coarray properties. We begin by proving:

Lemma 9.2.4. For the Cantor array (9.11) with parameter $r \geq 1$ in Definition 9.2.3, the weight function $w_r(m)$ satisfies

$$w_r(m) = \begin{cases} 2w_{r-1}(m), & \text{if } |m| \leq A_{r-1}, \\ w_{r-1}(m \pm D_{r-1}), & \text{if } |m \pm D_{r-1}| \leq A_{r-1}, \\ 0, & \text{otherwise,} \end{cases} \quad (9.16)$$

where A_r and D_r are defined as in Definition 9.2.3.

Proof. The weight function $w_r(m)$ can be expressed as

$$\begin{aligned} w_r(m) &= |\{(n_1, n_2) \in \mathbb{S}_r^2 : n_1 - n_2 = m\}| \\ &= |\{(n_1, n_2) \in \mathbb{S}_{r-1}^2 : n_1 - n_2 = m\}| \\ &\quad + |\{(n_1, n_2) \in \mathbb{T}_{r-1}^2 : n_1 - n_2 = m\}| \\ &\quad + |\{(n_1, n_2) \in \mathbb{S}_{r-1} \times \mathbb{T}_{r-1} : n_1 - n_2 = m\}| \\ &\quad + |\{(n_1, n_2) \in \mathbb{T}_{r-1} \times \mathbb{S}_{r-1} : n_1 - n_2 = m\}|, \end{aligned} \quad (9.17)$$

which is due to $\mathbb{S}_r = \mathbb{S}_{r-1} \cup \mathbb{T}_{r-1}$ for $r \geq 1$ in Definition 9.2.3. Since every element in \mathbb{T}_{r-1} can be expressed as $n' + D_{r-1}$, where $n' \in \mathbb{S}_{r-1}$, (9.17) can be written as

$$\begin{aligned} w_r(m) &= |\{(n_1, n_2) \in \mathbb{S}_{r-1}^2 : n_1 - n_2 = m\}| \\ &\quad + |\{(n'_1, n'_2) \in \mathbb{S}_{r-1}^2 : n'_1 - n'_2 = m\}| \\ &\quad + |\{(n_1, n'_2) \in \mathbb{S}_{r-1}^2 : n_1 - n'_2 = m + D_{r-1}\}| \\ &\quad + |\{(n'_1, n_2) \in \mathbb{S}_{r-1}^2 : n'_1 - n_2 = m - D_{r-1}\}| \\ &= 2w_{r-1}(m) + w_{r-1}(m + D_{r-1}) \\ &\quad + w_{r-1}(m - D_{r-1}). \end{aligned} \quad (9.18)$$

Since the aperture of the Cantor array with parameter $r - 1$ is A_{r-1} , we have, by definition, $w_{r-1}(m) = 0$ if $|m| > A_{r-1}$. Hence, (9.18) can be simplified as (9.16). \square

Lemma 9.2.4 shows that the weight function for the Cantor array \mathbb{S}_r can be recursively constructed from the weight function for \mathbb{S}_{r-1} . To give some feelings for Lemma 9.2.4, the following numerical example is considered. Due to Lemma 9.2.4 and (9.12) to (9.15), the weight function becomes $w_3(6) = w_2(6 - D_2) = w_2(3) = w_1(3 - D_1) = 2w_0(0) = 2$, which is consistent with the weight function in Fig. 9.1(d).

Furthermore, based on Lemma 9.2.4, it can be proved that Cantor arrays have hole-free difference coarrays of size $\mathcal{O}(|\mathbb{S}|^{\log_2 3}) \approx \mathcal{O}(|\mathbb{S}|^{1.585})$. This result is distinct from the MRA (hole-free difference coarray of size $\mathcal{O}(|\mathbb{S}|^2)$) and the ULA (hole-free difference coarray of size $\mathcal{O}(|\mathbb{S}|)$). The detailed proofs are skipped here and can be found in [100].

Proof of the maximal economy of Cantor arrays

Finally the maximal economy of Cantor arrays will be proved at the end of this subsection. First we prove:

Lemma 9.2.5. Let the Cantor array with parameter r be denoted by $\mathbb{S}_r = \{s_1, s_2, \dots, s_N\}$, where $0 = s_1 < s_2 < \dots < s_N$ and $N = 2^r$. Then the weight function of \mathbb{S}_r satisfies $w_r(s_{N+1-k} - s_k) = 1$ for all $k = 1, 2, \dots, N$.

Proof. First, if $r = 0$, then $\mathbb{S}_0 = \{0\}$ and $w_0(0) = 1$, which holds trivially. Assume $w_r(s_{N+1-k} - s_k) = 1$ holds true for all $k = 1, 2, \dots, N$. Then the sensor locations for \mathbb{S}_{r+1} are given by

$$\mathbb{S}_{r+1} = \{s_1, s_2, \dots, s_N, s_1 + D_r, s_2 + D_r, \dots, s_N + D_r\}.$$

It can be shown that $s_N < s_1 + D_r < s_2 + D_r < \dots < s_N + D_r$. Due to Lemma 9.2.4, the weight function of \mathbb{S}_{r+1} satisfies $w_{r+1}((s_{N+1-k} + D_r) - s_k) = w_r(s_{N+1-k} - s_k) = 1$ for all $k = 1, 2, \dots, N$. Furthermore, the symmetry of the difference coarray shows that $w_{r+1}(s_k - (s_{N+1-k} + D_r)) = 1$. These arguments complete the proof. \square

Due to Lemma 8.2.1 and 9.2.5, s_k and s_{N+1-k} are both essential for all $k = 1, 2, \dots, N$, which proves the maximal economy of Cantor arrays. \square

For clarity, Fig. 9.1(d) demonstrates the weight function of \mathbb{S}_3 , where $w(13 - 0) = w(12 - 1) = w(10 - 3) = w(9 - 4) = 1$. Due to Lemma 8.2.1, this result implies that the sensors at 13, 0, 12, 1, 10, 3, 9, and 4 are all essential, which confirms the maximal economy of \mathbb{S}_3 .

9.3 Uniform Linear Arrays

In what follows, two commonly used array geometries, the ULA and the coprime array, will be discussed in Section 9.3 and 9.4, respectively. Among the arrays considered in this chapter, it will be shown that the most robust arrays are ULA, followed by coprime arrays, and finally MESA.

The ULA with N physical elements is defined as [188]:

$$\mathbb{S}_{\text{ULA}} \triangleq \{0, 1, \dots, N - 1\}. \quad (9.19)$$

It can be shown that the difference coarray of the ULA is $\{0, \pm 1, \dots, \pm(N - 1)\}$, whose size is $2N - 1$. This property indicates that ULA resolve at most $N - 1$ uncorrelated sources, unlike sparse arrays such as MRA or nested arrays ($\mathcal{O}(N^2)$ uncorrelated sources) [124]. However, in the past, ULA are regarded as more robust

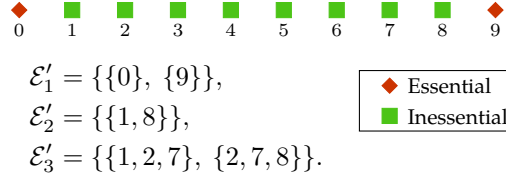


Figure 9.2: The ULA with $N = 10$ elements and the k -essential Sperner family \mathcal{E}'_1 , \mathcal{E}'_2 , and \mathcal{E}'_3 .

than sparse arrays. In this section, this observation will be confirmed using the general theory in Chapter 8. Using (9.19) and Definition 8.4.1, the k -essential Sperner family of the ULA can be shown to have the following closed-form expressions:

Theorem 9.3.1. The k -essential Sperner family of \mathbb{S}_{ULA} satisfies

$$\mathcal{E}'_1 = \begin{cases} \mathcal{S}_{1,\text{ULA}}, & \text{if } 1 \leq N \leq 3, \\ \{\{0\}, \{N-1\}\}, & \text{if } N \geq 4, \end{cases} \quad (9.20)$$

$$\mathcal{E}'_2 = \begin{cases} \emptyset, & \text{if } 1 \leq N \leq 3, \\ \{\{1, 2\}\}, & \text{if } N = 4, \\ \{\{1, 2\}, \{1, 3\}, \{2, 3\}\}, & \text{if } N = 5, \\ \{\{1, 4\}, \{2, 3\}\}, & \text{if } N = 6, \\ \{\{1, N-2\}\}, & \text{if } N \geq 7, \end{cases} \quad (9.21)$$

$$\mathcal{E}'_3 = \begin{cases} \emptyset, & \text{if } N \leq 6, \\ \{\{1, 2, 3\}, \{1, 2, 4\}, \{2, 3, 4\}, \\ \quad \{2, 4, 5\}, \{3, 4, 5\}\}, & \text{if } N = 7, \\ \{\{1, 2, 5\}, \{2, 3, 4\}, \\ \quad \{2, 5, 6\}, \{3, 4, 5\}\}, & \text{if } N = 8, \\ \{\{1, 2, 6\}, \{2, 6, 7\}, \{3, 4, 5\}\}, & \text{if } N = 9, \\ \{\{1, 2, N-3\}, \\ \quad \{2, N-3, N-2\}\}, & \text{if } N \geq 10. \end{cases} \quad (9.22)$$

Here $\mathcal{S}_{1,\text{ULA}} \triangleq \{\{n\} : n \in \mathbb{S}_{\text{ULA}}\}$ denotes all the subarrays of size 1 over \mathbb{S}_{ULA} .

The derivation of the expressions in Theorem 9.3.1 is quite involved, and it can be found in Section 9.3. Next the expressions in Theorem 9.3.1 are demonstrated through the following numerical example:

Example 9.3.1. Consider the ULA with $N = 10$ elements. Fig. 9.2 depicts the k -essential Sperner family \mathcal{E}'_1 , \mathcal{E}'_2 , and \mathcal{E}'_3 . Since $N \geq 3k + 1$ for $k = 1, 2, 3$, the last

equations in (9.20) to (9.22) are used. First, some of the subarrays in \mathcal{E}'_k are mirror images of each other, with respect to the center of \mathbb{S}_{ULA} , like $\{1, 2, 7\}$ and $\{2, 7, 8\}$. This phenomenon is because the difference coarray is invariant to the reversal of the array configuration [100]. Second, using Fig. 9.2, given any subarray of size $k \leq 3$, its k -essentialness property can be readily examined by the contents of \mathcal{E}'_k , as presented in Section 8.4. For instance, since $\{1, 2, 8\}$ is a superset of $\{1, 8\} \in \mathcal{E}'_2$, we have $\{1, 2, 8\} \in \mathcal{E}_3$, so removing $\{1, 2, 8\}$ from \mathbb{S}_{ULA} alters the difference coarray, as depicted later in Fig. 9.3(c) later. As another example, deleting $\{3, 5, 8\}$ from \mathbb{S}_{ULA} preserves the difference coarray, as illustrated later in Fig. 9.3(d). This observation is consistent with Fig. 9.2 since $\{3, 5, 8\}$ is not a superset of any elements in \mathcal{E}'_k for $k = 1, 2, 3$ and hence $\{3, 5, 8\} \notin \mathcal{E}_3$.

Theorem 9.3.1 also shows that *the elements at both ends of \mathbb{S}_{ULA} are more important than others*. It was reported in [5] that for the ULA with 6 elements ($\mathbb{S}_{\text{ULA}} = \{0, 1, 2, 3, 4, 5\}$), the elements at 0 and 5 are the most important ones while the elements 1, 2, 3, 4 are less important. On the other hand, as presented in Theorem 9.3.1, for $\mathbb{S}_{\text{ULA}} = \{0, 1, 2, 3, 4, 5\}$, *the elements 0 and 5 are essential while the elements 1, 2, 3, 4 are inessential*, which is in accordance with [5]. Our contribution here is to utilize the essentialness property as another notion of the importance of elements in arrays. Unlike the previous work [5], our approach depends purely on the array geometry, rather than other factors such as source directions and source powers.

Next, the closed-form expressions of the k -fragility for the ULA will be derived based on Theorem 9.3.1. The main focus would be F_1 , F_2 , and F_3 , for $N \geq 4$, $N \geq 7$, and $N \geq 10$, respectively. If $N \geq 4$, then $|\mathcal{E}'_1| = |\mathcal{E}_1| = 2$ so $F_1 = 2/N$. If $N \geq 7$, then due to Lemma 8.4.1, the cardinality of \mathcal{E}_2 can be computed as $|\mathcal{E}_2| = |\{\{0, n\}, \{n, N-1\}, \{0, N-1\}, \{1, N-2\} : 1 \leq n \leq N-2\}| = 2(N-1)$. Hence $F_2 = 2(N-1)/\binom{N}{2} = 4/N$. Finally, the 3-essential family for the ULA with $N \geq 10$ is given by

$$\begin{aligned} \mathcal{E}_3 = & \underbrace{\{\mathbb{A} \in \mathcal{S}_{3,\text{ULA}} : 0 \in \mathbb{A}\}}_{\mathcal{G}_1} \cup \underbrace{\{\mathbb{A} \in \mathcal{S}_{3,\text{ULA}} : N-1 \in \mathbb{A}\}}_{\mathcal{G}_2} \\ & \cup \underbrace{\{\mathbb{A} \in \mathcal{S}_{3,\text{ULA}} : \{1, N-2\} \subset \mathbb{A}\}}_{\mathcal{G}_3} \cup \mathcal{E}'_3, \end{aligned} \quad (9.23)$$

where $\mathcal{S}_{3,\text{ULA}} \triangleq \{\mathbb{A} \subseteq \mathbb{S}_{\text{ULA}} : |\mathbb{A}| = 3\}$ represents all the subarrays of size 3 over \mathbb{S}_{ULA} . Substituting $|\mathcal{G}_1| = |\mathcal{G}_2| = \binom{N-1}{2}$, $|\mathcal{G}_3| = |\mathcal{G}_1 \cap \mathcal{G}_2| = N-2$, $|\mathcal{G}_1 \cap \mathcal{G}_3| = |\mathcal{G}_2 \cap \mathcal{G}_3| = 1$, and $|\mathcal{G}_1 \cap \mathcal{E}'_3| = |\mathcal{G}_2 \cap \mathcal{E}'_3| = |\mathcal{G}_3 \cap \mathcal{E}'_3| = 0$, into (9.23) leads to $|\mathcal{E}_3| = (N-1)(N-2)$ so that fragility $F_3 = 6/N$. Summarizing, the k -fragility F_k for the ULA with N elements satisfies

$$\text{ULA:} \quad F_1 = \frac{2}{N}, \quad F_2 = \frac{4}{N}, \quad F_3 = \frac{6}{N}, \quad (9.24)$$

where these expressions are valid for $N \geq 4$, $N \geq 7$, and $N \geq 10$, respectively. For instance, for the ULA with $N = 16$ elements, (9.24) leads to $F_1 = 0.125$, $F_2 = 0.25$, and $F_3 = 0.375$, which are consistent with the numerical example in Fig. 8.8.

Failure probabilities. Finally, here are some remarks on the probability that the difference coarray changes, P_c , for ULA. Even though P_c has closed-form expressions associated with the fragility F_k , as in (8.28), it remains challenging to derive closed-form expressions of P_c for ULA, due to the lack of closed forms of \mathcal{E}'_k and F_k , for all k . Even so, P_c for the ULA can still be analyzed either numerically using (8.28), or analytically using the bounds of P_c , as in Theorem 8.5.1. For instance, as discussed in Section 8.5, if the probability of element failure p is sufficiently small, then P_c is approximately $|\mathcal{E}_1|p$. This approximation indicates that, for ULA with $N \geq 4$ elements, P_c has an asymptotic expression of $2p$. Namely, the probability that the difference coarray changes is around $2p$. This is the smallest among all possible array configurations with fixed N , due to Lemma 8.2.2.

Derivation of the Expressions in Theorem 9.3.1

Before deriving the expressions in Theorem 9.3.1, we first invoke Lemma 9.3.1 to describe the difference coarray after removing k physical sensors.

Lemma 9.3.1. Let $\mathbb{A} \subseteq \mathbb{S}_{\text{ULA}}$ satisfy $|\mathbb{A}| = k$. Assume that $\bar{\mathbb{S}} \triangleq \mathbb{S}_{\text{ULA}} \setminus \mathbb{A}$ and its difference coarray is denoted by $\bar{\mathbb{D}}$. If $N \geq 3k + 1$, then $\{0, \pm 1, \dots, \pm(N - k - 1)\} \subseteq \bar{\mathbb{D}}$.

Lemma 9.3.1 implies that, if N is sufficiently large, then even though k elements are removed from \mathbb{S}_{ULA} , the difference coarray $\bar{\mathbb{D}}$ still possesses a central ULA segment of at least $2(N - k - 1) + 1$ elements. The detailed proof of Lemma 9.3.1 will be given after Example 9.3.2:

Example 9.3.2. Fig. 9.3 demonstrates an example of Lemma 9.3.1. We consider the ULA with $N = 10$ elements and its difference coarray, as depicted in Fig. 9.3(a). In Figs. 9.3(b), (c), and (d), we remove $k = 3$ physical elements from \mathbb{S}_{ULA} and evaluate their difference coarrays. Regardless of the locations of the removed elements, all these difference coarrays possess a central ULA segment, whose size is at least $2(N - k - 1) + 1 = 13$, as claimed by Lemma 9.3.1.

Proof of Lemma 9.3.1. First let us consider several useful results for the proof [68]:

Definition 9.3.1. Let \mathbb{S} be an integer set. The discrete sequence $c(n)$ is defined as

$$c(n) = \begin{cases} 1, & \text{if } n \in \mathbb{S}, \\ 0, & \text{otherwise.} \end{cases} \quad (9.25)$$

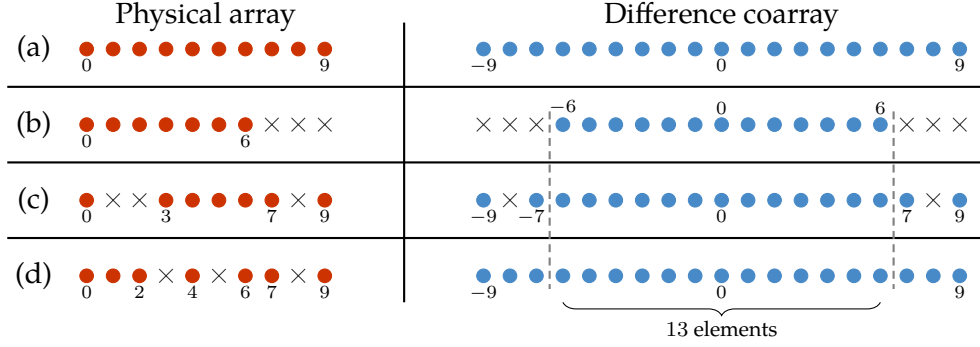


Figure 9.3: (a) The ULA with 10 physical elements \mathbb{S}_{ULA} and its difference coarray. The physical array (left) and the difference coarray (right) after removing (b) $\{7, 8, 9\}$, (c) $\{1, 2, 8\}$, and (d) $\{3, 5, 8\}$, from \mathbb{S}_{ULA} , respectively. Here bullets denote elements and crosses represent empty space. It can be observed that the difference coarrays of (b), (c), and (d) contain $\{0, \pm 1, \dots, \pm 6\}$.

Proposition 9.3.1. Let $c(n)$ and $w(m)$ be the discrete sequence and the weight function for \mathbb{S} , respectively. Then $w(m)$ satisfies

$$w(m) = \sum_{n=-\infty}^{\infty} c(n+m)c(n), \quad (9.26)$$

for any integer m .

Furthermore, the difference coarray can be expressed as the support of the weight function. Namely, $\mathbb{D} = \{m : w(m) \neq 0\}$.

Next it will be proved that $\{0, \pm 1, \pm 2, \dots, \pm(N-k-1)\} \subseteq \overline{\mathbb{D}}$. It suffices to consider the nonnegative part of the set, due to the symmetry of the difference coarray. Assume that there exists some $\hat{m} \in \{0, 1, 2, \dots, N-k-1\}$ such that $\hat{m} \notin \overline{\mathbb{D}}$. The discrete sequence and the weight function of $\overline{\mathbb{S}} \triangleq \mathbb{S}_{\text{ULA}} \setminus \mathbb{A}$ are denoted by $\bar{c}(n)$ and $\bar{w}(m)$, respectively. Since $\hat{m} \notin \overline{\mathbb{D}}$, we have $\bar{w}(\hat{m}) = 0$, implying that

$$\bar{c}(n+\hat{m})\bar{c}(n) = 0, \quad (9.27)$$

for all $n = 0, 1, \dots, N-\hat{m}-1$, due to (9.25) and (9.26). Eq. (9.27) indicates that, $n+\hat{m} \in \mathbb{A}$ or $n \in \mathbb{A}$. This condition implies

$$(\mathbb{A} - \hat{m}) \cup \mathbb{A} \supseteq \mathbb{O} \triangleq \{0, 1, \dots, N-\hat{m}-1\}. \quad (9.28)$$

Here the notation $\mathbb{A} \pm \hat{m} \triangleq \{a \pm \hat{m} : a \in \mathbb{A}\}$.

According to (9.28), the size of \mathbb{O} satisfies

$$\begin{aligned} |\mathbb{O}| &= |((\mathbb{A} - \hat{m}) \cup \mathbb{A}) \cap \mathbb{O}| = |((\mathbb{A} - \hat{m}) \cap \mathbb{O}) \cup (\mathbb{A} \cap \mathbb{O})| \\ &\leq |(\mathbb{A} - \hat{m}) \cap \mathbb{O}| + |\mathbb{A} \cap \mathbb{O}| = |\mathbb{A} \cap (\mathbb{O} + \hat{m})| + |\mathbb{A} \cap \mathbb{O}|, \end{aligned} \quad (9.29)$$

where the inequality is due to the union bound between sets. In what follows, (9.29) will be analyzed in detail. First, the set \mathbb{S}_{ULA} is partitioned into three subsets $\mathbb{L}_1, \mathbb{L}_2, \mathbb{L}_3$:

$$\mathbb{L}_1 = \{0, 1, \dots, P-1\}, \quad (9.30)$$

$$\mathbb{L}_2 = \{P, P+1, \dots, N-P-1\}, \quad (9.31)$$

$$\mathbb{L}_3 = \{N-P, N-P+1, \dots, N-1\}, \quad (9.32)$$

where $P \triangleq \min\{\widehat{m}, N-\widehat{m}\}$. We also define $\mathbb{A}_\ell \triangleq \mathbb{A} \cap \mathbb{L}_\ell$ and $k_\ell \triangleq |\mathbb{A}_\ell|$ for $\ell = 1, 2, 3$. It can be shown that

$$k = k_1 + k_2 + k_3, \quad 0 \leq k_\ell \leq \min\{k, |\mathbb{L}_\ell|\}, \quad (9.33)$$

for $\ell = 1, 2, 3$.

According to \widehat{m} , Eq. (9.29) can be analyzed in two cases:

1. If $\widehat{m} \leq N/2$, then we obtain $P = \widehat{m}$. The sets \mathbb{O} and $\mathbb{O} + \widehat{m}$ can be expressed as $\mathbb{O} = \mathbb{L}_1 \cup \mathbb{L}_2$ and $\mathbb{O} + \widehat{m} = \mathbb{L}_2 \cup \mathbb{L}_3$, respectively. Combining (9.29) and (9.33) leads to

$$N - \widehat{m} \leq (k_2 + k_3) + (k_1 + k_2) = k + k_2. \quad (9.34)$$

Now let us consider the upper bounds of $k + k_2$ for two cases of m . First, if $0 \leq \widehat{m} \leq N/3$, then using (9.33) and $N \geq 3k + 1$, we obtain $k + k_2 \leq 2k < 2k + \frac{2}{3} \leq \frac{2}{3}N \leq N - \widehat{m}$. Therefore $k + k_2 < N - \widehat{m}$, which contradicts (9.34). On the other hand, if $N/3 < \widehat{m} \leq N/2$, then we have $\widehat{m} > N/3 \geq k + \frac{1}{3}$ so $k - \widehat{m} < 0$. In addition, the size of \mathbb{L}_2 is given by $N - 2P = N - 2\widehat{m}$. In this case, we have $k + k_2 \leq k + |\mathbb{L}_2| = k + (N - 2\widehat{m}) = (N - \widehat{m}) + (k - \widehat{m}) < N - \widehat{m}$, disagreeing with (9.34).

2. If $N/2 < \widehat{m} \leq N - k - 1$, then $P = N - \widehat{m}$. In this case, we have $\mathbb{O} = \mathbb{L}_1$ and $\mathbb{O} + \widehat{m} = \mathbb{L}_3$. Hence (9.29) becomes

$$N - \widehat{m} \leq k_3 + k_1 = k - k_2. \quad (9.35)$$

However, the right-hand side of (9.35) satisfies $k - k_2 \leq k \leq N - \widehat{m} - 1$, due to (9.33) and $\widehat{m} \leq N - k - 1$. This result contradicts (9.35).

These arguments complete the proof of Lemma 9.3.1. \square

Next, the expressions in Theorem 9.3.1 will be derived. Here we will skip the expressions of \mathcal{E}'_k for $N \leq 3k$ and $k = 1, 2, 3$, since they can be readily verified by

enumerating all subarrays with size k . The main focus here would be the case of $N \geq 3k + 1$. In what follows, the sensor locations, the difference coarray, the discrete sequence (Definition 9.3.1), and the weight function after the removal of k elements will be denoted by $\bar{\mathbb{S}}$, $\bar{\mathbb{D}}$, $\bar{c}(n)$, and $\bar{w}(m)$, respectively. We will study the circumstances under which the difference coarray changes, namely $\bar{\mathbb{D}} \neq \mathbb{D}_{\text{ULA}}$, where \mathbb{D}_{ULA} is the difference coarray of \mathbb{S}_{ULA} .

1. \mathcal{E}'_1 for $N \geq 4$: Due to Lemma 9.3.1, the difference coarray $\bar{\mathbb{D}}$ contains $\{0, \pm 1, \pm 2, \dots, \pm(N-2)\}$ for $k = 1$. If $\bar{\mathbb{D}} \neq \mathbb{D}_{\text{ULA}}$, then $\bar{w}(N-1) = 0$. This implies

$$\bar{w}(N-1) = \bar{c}(N-1)\bar{c}(0) = 0, \quad (9.36)$$

due to Proposition 9.3.1. Eq. (9.36) shows that removing either 0 or $N-1$ leads to $\bar{\mathbb{D}} \neq \mathbb{D}_{\text{ULA}}$. Hence $\mathcal{E}'_1 = \{\{0\}, \{N-1\}\}$ for $N \geq 4$.

2. \mathcal{E}'_2 for $N \geq 7$: Lemma 9.3.1 indicates that it suffices to consider $\bar{w}(N-1) = 0$ and $\bar{w}(N-2) = 0$. Let \mathbb{A} be a subarray of size 2 over \mathbb{S}_{ULA} . First, assume that $\bar{w}(N-1) = 0$. The argument of (9.36) shows that $0 \in \mathbb{A}$ or $N-1 \in \mathbb{A}$. Therefore \mathbb{A} does not belong to \mathcal{E}'_2 . Second, if $\bar{w}(N-2) = 0$, then we obtain

$$\bar{w}(N-2) = \bar{c}(N-2)\bar{c}(0) + \bar{c}(N-1)\bar{c}(1) = 0. \quad (9.37)$$

There are four choices of \mathbb{A} satisfying (9.37): $\{0, 1\}$, $\{0, N-1\}$, $\{N-1, N-2\}$, and $\{1, N-2\}$. Since the first three subarrays contain either 0 or $N-1$, we have $\mathcal{E}'_2 = \{\{1, N-2\}\}$ for $N \geq 7$.

3. \mathcal{E}'_3 for $N \geq 10$: The arguments in \mathcal{E}'_2 indicates that, it suffices to consider $\bar{w}(N-3) = 0$ in this case. Hence we have

$$\bar{c}(N-3)\bar{c}(0) + \bar{c}(N-2)\bar{c}(1) + \bar{c}(N-1)\bar{c}(2) = 0.$$

Since the the elements in \mathcal{E}'_3 do not contain 0 or $N-1$, we have $\mathcal{E}'_3 = \{\{1, 2, N-3\}, \{2, N-3, N-2\}\}$, which proves Theorem 9.3.1. \square

9.4 Coprime Arrays

In this section, we will move on to coprime arrays, which have recently attracted considerable attention in sparse array signal processing [4], [19], [139], [186]. These arrays are defined as:

Definition 9.4.1. Let M and N be a coprime pair of positive integers. A coprime array $\mathbb{S}_{\text{coprime}}$ with parameters M and N can be defined as

$$\mathbb{S}_{\text{coprime}} = \{0\} \cup \mathbb{P}_1 \cup \mathbb{P}_2 \cup \{MN\} \cup \mathbb{P}_3, \quad (9.38)$$

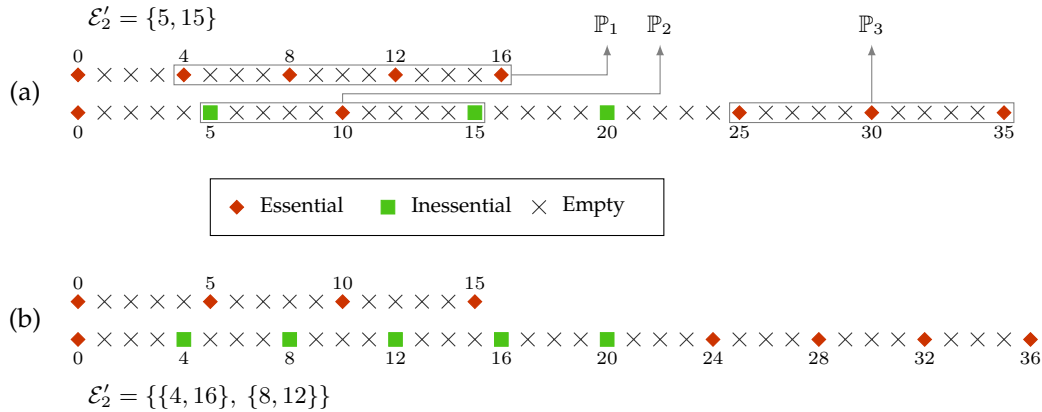


Figure 9.4: An illustration for the k -essential Sperner family of the coprime arrays with (a) $M = 4, N = 5$ and (b) $M = 5, N = 4$. In these figures, the coprime arrays are split into two sparse ULAs for clarity.

where the sets $\mathbb{P}_1, \mathbb{P}_2,$ and \mathbb{P}_3 are given by

$$\mathbb{P}_1 = \{p_1 M : 1 \leq p_1 \leq N - 1\}, \tag{9.39}$$

$$\mathbb{P}_2 = \{p_2 N : 1 \leq p_2 \leq M - 1\}, \tag{9.40}$$

$$\mathbb{P}_3 = \{p_3 N : M + 1 \leq p_3 \leq 2M - 1\}. \tag{9.41}$$

Note that Definition 9.4.1 is equivalent to (2.8). Here we use Definition 9.4.1 to facilitate the proof of Theorem 9.4.1. Coprime arrays are composed of two sparse ULAs. The first sparse ULA ($\{0\} \cup \mathbb{P}_1$) has N elements with interelement spacing M (in unit of half of the wavelength) while the second sparse ULA ($\{0\} \cup \mathbb{P}_2 \cup \{MN\} \cup \mathbb{P}_3$) owns $2M$ elements with separation N . It can be shown that the difference coarray of $\mathbb{S}_{\text{coprime}}$ has a central ULA segment $\mathbb{U}_{\text{coprime}} = \{0, \pm 1, \dots, \pm(MN + M - 1)\}$ and a hole at $MN + M$ [139], [186].

Example 9.4.1. Fig. 9.4(a) demonstrates the geometry of coprime arrays. For clarity, the first ULA with separation M is depicted on the top while on the bottom is shown the second ULA with separation N . The physical sensors are denoted by diamonds or rectangles and the empty space is marked by crosses. If $M = 4$ and $N = 5$, then we have $\mathbb{P}_1 = \{4, 8, 12, 16\}, \mathbb{P}_2 = \{5, 10, 15\},$ and $\mathbb{P}_3 = \{25, 30, 35\},$ which are also illustrated in Fig. 9.4(a).

In the following development, the robustness of coprime arrays will be investigated based on the general theory in the next chapter. To begin with, the closed-form expressions of \mathcal{E}'_k for coprime arrays will be presented in Theorem 9.4.1, whose proof can be found in Section 9.4.

Theorem 9.4.1. Let $\mathbb{S}_{\text{coprime}}$ be a coprime array with a coprime pair of integers M and N , as defined in Definition 9.4.1. Assume that $M, N \geq 2$. Then the k -essential Sperner family can be expressed as

$$\mathcal{E}'_1 = \begin{cases} \mathcal{A} \cup \mathcal{B}, & \text{if } M \text{ is odd,} \\ \mathcal{A} \cup \mathcal{B} \cup \{\{MN/2\}\}, & \text{if } M \text{ is even,} \end{cases} \quad (9.42)$$

$$\mathcal{E}'_2 = \begin{cases} \emptyset, & \text{if } M = 2, \\ \{\{N, 2N\}, \{2N, 3N\}\}, & \text{if } M = 3, \\ \mathcal{C}, & \text{otherwise,} \end{cases} \quad (9.43)$$

$$\mathcal{E}'_k = \emptyset, \quad 3 \leq k \leq |\mathbb{S}|, \quad (9.44)$$

where \mathcal{A} , \mathcal{B} , and \mathcal{C} are given by

$$\mathcal{A} \triangleq \{\{nM\} : 0 \leq n \leq N - 1\}, \quad (9.45)$$

$$\mathcal{B} \triangleq \{\{mN\} : M + 1 \leq m \leq 2M - 1\}, \quad (9.46)$$

$$\mathcal{C} \triangleq \{\{mN, (M - m)N\} : 1 \leq m \leq \lfloor (M - 1)/2 \rfloor\}. \quad (9.47)$$

Example 9.4.2. The implications of Theorem 9.4.1 are exemplified by Fig. 9.4, where the essential sensors (diamonds in Fig. 9.4), the inessential sensors (rectangles in Fig. 9.4), and \mathcal{E}'_2 , are enumerated. Here the coprime arrays have parameters (a) $M = 4, N = 5$ and (b) $M = 5, N = 4$. In Fig. 9.4(a), the essential elements 0, 4, 8, 12, 16 are associated with \mathcal{A} , as in (9.45), or $\{0\} \cup \mathbb{P}_1$, as in (9.39), while the elements 25, 30, 35 are related to \mathcal{B} in (9.46), or equivalently \mathbb{P}_3 in (9.41). Furthermore, in Fig. 9.4(a), the element $MN/2 = 10$ is also essential, which is consistent with (9.42). The sets in \mathcal{E}'_2 are also depicted in Fig. 9.4. For instance, in Fig. 9.4(b), both $\{8, 12\}$ and $\{4, 16\}$ belong to \mathcal{E}'_2 , as described in (9.43) and (9.47). Note that the elements in these sets are symmetric with respect to the location $MN/2 = 10$. Another interesting observation is that, among the inessential sensors in Fig. 9.4(b), some are related to \mathcal{E}'_2 , such as 4 and 8, but the inessential sensor $MN = 20$ does not belong to any elements in \mathcal{E}'_k for all k . In fact, if $M \geq 4$ and $N \geq 2$, it can be shown that MN does not belong to the elements in \mathcal{E}'_k for all k , due to Theorem 9.4.1.

Theorem 9.4.1 can be interpreted as a generalization of the thinned coprime array [144]. For sufficiently large M and N , it was shown in [144] that removing the elements at $(\lfloor M/2 \rfloor + 1)N, (\lfloor M/2 \rfloor + 2)N, \dots, MN$ in a coprime array preserves the difference coarray and the new array geometry is called the thinned coprime array. The above statement is equivalent to the condition that $\{(\lfloor M/2 \rfloor + 1)N, (\lfloor M/2 \rfloor + 2)N, \dots, MN\}$ is not $\lceil M/2 \rceil$ -essential with respect to $\mathbb{S}_{\text{coprime}}$. For instance, in Fig. 9.4(a), removing $\{15, 20\}$ from $\mathbb{S}_{\text{coprime}}$ does not alter the difference coarray, since

$\{15, 20\}$ is not 2-essential. Furthermore, Theorem 9.4.1 makes it possible to create other arrays than thinned coprime arrays but with the same difference coarray. For example, in Fig. 9.4(b), deleting either $\{8, 16, 20\}$, $\{4, 8, 20\}$, or $\{4, 12, 20\}$ from $\mathbb{S}_{\text{coprime}}$ does not alter the difference coarray, while none of them is identical to thinned coprime arrays.

The k -Fragility of Coprime Arrays

In the following development, closed-form expressions for the k -fragility of the coprime array will be derived. It is first assumed that M is an even number and $M \geq 4$. In this case, we have $|\mathcal{E}_1| = |\mathcal{E}'_1| = M + N$ so the fragility $F_1 = (N + M)/(N + 2M - 1)$. Next, due to Lemma 8.4.1, the 2-essential family \mathcal{E}_2 can be expressed as

$$\mathcal{E}_2 = \underbrace{\{\{n_1, n_2\} : \{n_1\} \in \mathcal{E}'_1, \{n_2\} \notin \mathcal{E}'_1, n_2 \in \mathbb{S}_{\text{coprime}}\}}_{\mathcal{H}_1} \cup \underbrace{\{\{n_1, n_2\} : \{n_1\}, \{n_2\} \in \mathcal{E}'_1\}}_{\mathcal{H}_2} \cup \mathcal{E}'_2.$$

Since \mathcal{H}_1 , \mathcal{H}_2 , and \mathcal{E}'_2 are disjoint, the size of \mathcal{E}_2 is given by $|\mathcal{E}_2| = |\mathcal{H}_1| + |\mathcal{H}_2| + |\mathcal{E}'_2| = (N + M)(M - 1) + \binom{N+M}{2} + (M/2 - 1)$ so that fragility F_2 becomes $F_2 = (3M^2 + 4MN - 2M + N^2 - 3N - 2)/((N + 2M - 1)(N + 2M - 2))$. Repeating similar arguments for odd M leads to these expressions

$$F_1 = \begin{cases} \frac{N+M-1}{N+2M-1}, & \text{if } M \text{ is odd,} \\ \frac{N+M}{N+2M-1}, & \text{if } M \text{ is even,} \end{cases} \quad (9.48)$$

$$F_2 = \begin{cases} \frac{3M^2+4MN-4M+N^2-3N+1}{(N+2M-1)(N+2M-2)}, & \text{if } M \text{ is odd,} \\ \frac{3M^2+4MN-2M+N^2-3N-2}{(N+2M-1)(N+2M-2)}, & \text{if } M \text{ is even,} \end{cases} \quad (9.49)$$

where $M \geq 4$.

As k increases, the closed-form expressions of F_k can be derived but the details become more involved. Here these expressions are omitted in this chapter. However, if k is sufficiently large, then F_k can still be characterized by the following proposition:

Proposition 9.4.1. For the coprime array with a coprime pair of integers $M \geq 4$ and $N \geq 2$, the k -fragility satisfies $F_k = 1$ for all $\lceil M/2 \rceil + 1 \leq k \leq N + 2M - 1$.

Proof. It follows from Item 3d in Section 9.4. □

For example, let $M = 4$ and $N = 9$. Using (9.48), (9.49), and Proposition 9.4.1, it can be shown that $F_1 = 0.8125$, $F_2 = 0.9833$, and $F_k = 1$ for all $3 \leq k \leq 16$.

The Probability that the Difference Coarray Changes

In this subsection, the closed-form expressions of P_c for the coprime array are characterized by the following theorem:

Theorem 9.4.2. Let $\mathbb{S}_{\text{coprime}}$ be the coprime array with a coprime pair of integers M, N , as in Definition 9.4.1. Assume that $M, N \geq 2$. Then the probability that the difference coarray changes is

$$P_c = \begin{cases} 1 - (1-p)^{|\mathcal{E}'_1|}(1-2p^2+p^3), & \text{if } M = 3, \\ 1 - (1-p)^{|\mathcal{E}'_1|}(1-p^2)^{|\mathcal{E}'_2|}, & \text{otherwise.} \end{cases} \quad (9.50)$$

Here \mathcal{E}'_1 and \mathcal{E}'_2 are the k -essential Sperner family of $\mathbb{S}_{\text{coprime}}$, whose expressions are given in Theorem 9.4.1.

Proof. According to the proof of Theorem 8.5.1, the probability P_c can be expressed as $1 - \Pr(\mathfrak{G}_1^c) + \Pr(\mathfrak{G}_1^c)\Pr(\mathfrak{G}_2)$, where \mathfrak{G}_1^c denotes the complement of the event \mathfrak{G}_1 . The events \mathfrak{G}_1 and \mathfrak{G}_2 are defined as

$$\mathfrak{G}_1 \triangleq \bigcup_{\mathbb{A}_1 \in \mathcal{E}'_1} \mathfrak{F}(\mathbb{A}_1), \quad \mathfrak{G}_2 \triangleq \bigcup_{k=2}^{|\mathbb{S}|} \bigcup_{\mathbb{A}_k \in \mathcal{E}'_k} \mathfrak{F}(\mathbb{A}_k). \quad (9.51)$$

Here $\mathfrak{F}(\mathbb{A}_k) \triangleq \cap_{n \in \mathbb{A}_k} (n \text{ fails})$ denotes the event in which all the elements in \mathbb{A}_k fail. It was proved in (8.34) that $\Pr(\mathfrak{G}_1^c) = (1-p)^{|\mathcal{E}'_1|}$ for any array geometry. Next we will simplify $\Pr(\mathfrak{G}_2)$. If $M = 2$, then $\Pr(\mathfrak{G}_2) = \Pr(\mathfrak{F}(\emptyset)) = 0$. If $M = 3$, then we obtain

$$\begin{aligned} \Pr(\mathfrak{G}_2) &= \Pr(\mathfrak{F}(\{N, 2N\}) \cup \mathfrak{F}(\{2N, 3N\})) \\ &= \Pr(\mathfrak{F}(\{N, 2N\})) + \Pr(\mathfrak{F}(\{2N, 3N\})) \\ &\quad - \Pr(\mathfrak{F}(\{N, 2N, 3N\})) \\ &= 2p^2 - p^3. \end{aligned} \quad (9.52)$$

If $M \geq 4$, then $\Pr(\mathfrak{G}_2)$ can be simplified as

$$\Pr(\mathfrak{G}_2) = 1 - \Pr(\mathfrak{G}_2^c) = 1 - \Pr\left(\bigcap_{\mathbb{A}_2 \in \mathcal{E}'_2} (\mathfrak{F}(\mathbb{A}_2))^c\right). \quad (9.53)$$

Due to (9.43), all the elements in \mathcal{E}'_2 are disjoint, so all the events $\mathfrak{F}(\mathbb{A}_2)$ are mutually independent. Hence (9.53) becomes

$$\begin{aligned} \Pr(\mathfrak{G}_2) &= 1 - \prod_{\mathbb{A}_2 \in \mathcal{E}'_2} \Pr((\mathfrak{F}(\mathbb{A}_2))^c) = 1 - \prod_{\mathbb{A}_2 \in \mathcal{E}'_2} (1-p^2) \\ &= 1 - (1-p^2)^{|\mathcal{E}'_2|}. \end{aligned} \quad (9.54)$$

Substituting (9.52), (9.54), and $\Pr(\mathfrak{G}_1^c) = (1-p)^{|\mathcal{E}'_1|}$, into $P_c = 1 - \Pr(\mathfrak{G}_1^c) + \Pr(\mathfrak{G}_1^c)\Pr(\mathfrak{G}_2)$ proves this theorem. \square

The closed-form expressions of P_c for MESA (9.3) and coprime arrays (9.50) can be validated by Monte-Carlo simulations, as in Fig. 8.12. It is also deduced from Fig. 8.12 that the smallest P_c is exhibited by the ULA, followed by the coprime array, and finally the nested array. This observation is also consistent with the conclusion drawn from the fragility F_k of these arrays.

Derivation of the Expressions in Theorem 9.4.1

Example 9.4.3. To begin with, let us demonstrate the main concept of the derivation. Fig. 9.5(a) shows the coprime array with $M = 7, N = 8$ and its nonnegative part of the difference coarray. Here the elements are depicted in dots while empty space is denoted by crosses. The elements 0, 7, 14, 21, 28, 35, 42, 49, 64, 72, 80, 88, 96, 104 can be shown to be essential (Lemma 8.2.2 and 9.4.2). Therefore, for the elements in \mathcal{E}'_k and $k \geq 2$, it suffices to consider the subarrays $\mathbb{A} \subseteq \{8, 16, 24, 32, 40, 48, 56\}$, as marked in Fig. 9.5(a). The remaining part of the derivation is to identify the constraints on \mathbb{A} such that $\overline{\mathbb{D}}$ (the difference coarray after the removal of \mathbb{A} from $\mathbb{S}_{\text{coprime}}$) is distinct from \mathbb{D} (the difference coarray of $\mathbb{S}_{\text{coprime}}$). To identify these constraints, we will state and prove three lemmas in this section (Lemmas 9.4.4 to 9.4.6). The brief implications of these lemmas are as follows

$$\begin{array}{ll} \text{Lemma 9.4.4:} & \boxed{|\mathbb{A}| \leq M - 2} \Rightarrow \boxed{\overline{\mathbb{D}}_1 = \mathbb{D}_1,} \\ \text{Lemma 9.4.5:} & \boxed{\mathbb{A} \text{ and } \mathbb{A}_R \text{ are disjoint}} \Leftrightarrow \boxed{\overline{\mathbb{D}}_3 = \mathbb{D}_3,} \\ \text{Lemma 9.4.6:} & \boxed{\overline{\mathbb{D}}_1 = \mathbb{D}_1 \text{ and } \overline{\mathbb{D}}_3 = \mathbb{D}_3} \Leftrightarrow \boxed{\overline{\mathbb{D}} = \mathbb{D},} \end{array}$$

where $\overline{\mathbb{D}}_1, \mathbb{D}_1, \overline{\mathbb{D}}_3, \mathbb{D}_3$, and \mathbb{A}_R will be defined shortly. These results can be applied to Fig. 9.5(b), where $\mathbb{A} = \{16, 32, 56\}$, $\mathbb{A}_R = \{0, 24, 40\}$, and $|\mathbb{A}| = 3$. It can be readily shown that $\overline{\mathbb{D}} = \mathbb{D}$ using Lemma 9.4.4 to 9.4.6 without actually computing $\overline{\mathbb{D}}$. As a result, \mathbb{A} does not belong to \mathcal{E}'_3 .

Next we will proceed to the rigorous derivation of the expressions in Theorem 9.4.1. In what follows, it is assumed that the coprime array, as defined in Definition 9.4.1, satisfies $M, N \geq 2$. The self difference of a set \mathbb{S} is denoted by $\text{SD}(\mathbb{S}) \triangleq \{n - n' : n, n' \in \mathbb{S}\}$ and the cross difference between \mathbb{S}_1 and \mathbb{S}_2 are given by $\text{CD}(\mathbb{S}_1, \mathbb{S}_2) \triangleq \{\pm(n_1 - n_2) : n_1 \in \mathbb{S}_1, n_2 \in \mathbb{S}_2\}$. The following lemmas are useful in proving Theorem 9.4.1:

Lemma 9.4.1. Assume that $n_1, n_2 \in \mathbb{S}_{\text{coprime}}$ and $1 \leq u \leq N - 1$ and $1 \leq v \leq M - 1$. Then $n_1 - n_2 = uM - vN$ if and only if the pair (n_1, n_2) is (uM, vN) or $((M - v)N, (N - u)M)$.

Proof. The proof consists of four cases of n_1 and n_2 :

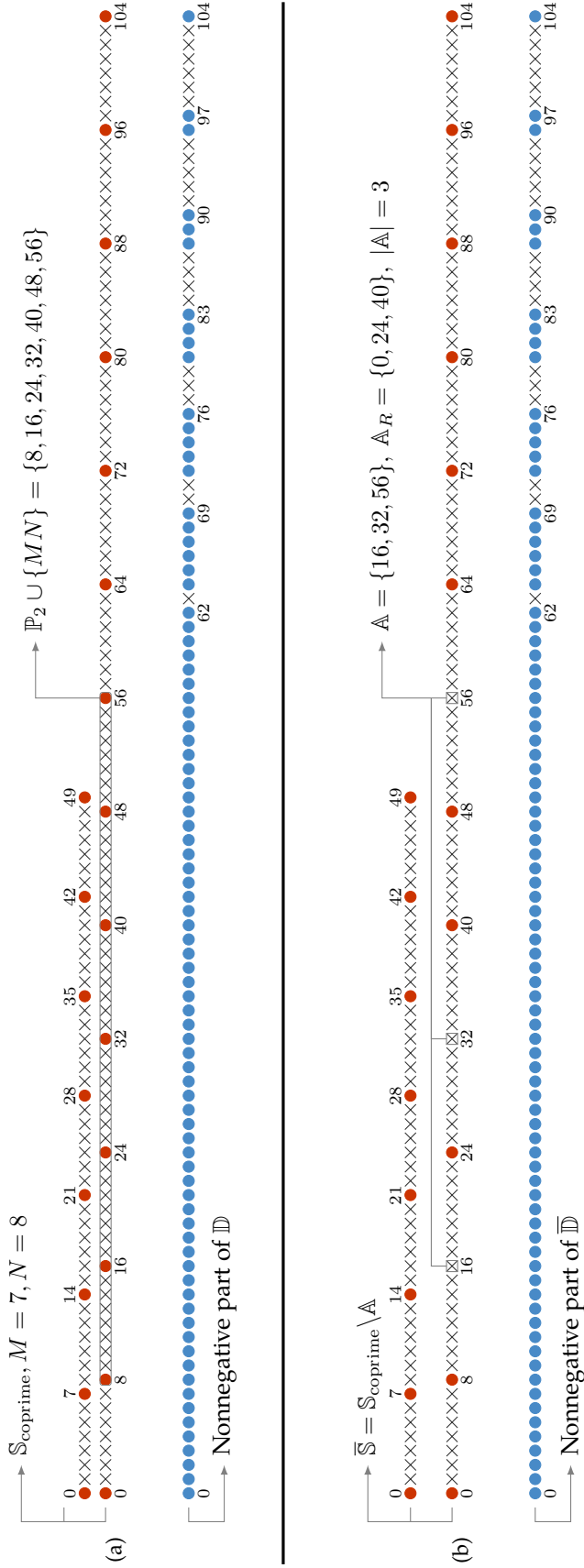


Figure 9.5: (a) the coprime array S_{coprime} with $M = 7, N = 8$ and the nonnegative part of the difference coarray \mathbb{D} . (b) The array \bar{S} , where the elements in $A = \{16, 32, 56\}$ are removed from S_{coprime} , and the nonnegative part of its difference coarray $\bar{\mathbb{D}}$.

1. $n_1, n_2 \in \{0\} \cup \mathbb{P}_1$: Let $n_1 = q_1M$ and $n_2 = q_2M$ for $0 \leq q_1, q_2 \leq N - 1$. The equation $n_1 - n_2 = uM - vN$ can be rearranged as $(u - q_1 + q_2)M = vN$. Since M and N are coprime, v is an integer multiple of M , which contradicts $1 \leq v \leq M - 1$.
2. $n_1, n_2 \in \mathbb{P}_2 \cup \{MN\} \cup \mathbb{P}_3$: Assume that $n_1 = q_1N$ and $n_2 = q_2N$ for $1 \leq q_1, q_2 \leq 2M - 1$. Then $n_1 - n_2 = uM - vN$ gives $(v + q_1 - q_2)N = uM$. Hence u is divisible by N , which disagrees with $1 \leq u \leq N - 1$.
3. $n_1 \in \{0\} \cup \mathbb{P}_1$ and $n_2 \in \mathbb{P}_2 \cup \{MN\} \cup \mathbb{P}_3$: Suppose $n_1 = q_1M$ and $n_2 = q_2N$ for $0 \leq q_1 \leq N - 1$ and $1 \leq q_2 \leq 2M - 1$. Rearranging $n_1 - n_2 = uM - vN$ leads to $(u - q_1)M = (v - q_2)N$. Since M and N are coprime and $-N + 2 \leq u - q_1 \leq N - 1$, we obtain $q_1 = u$ and $q_2 = v$. Hence $(n_1, n_2) = (uM, vN)$.
4. $n_1 \in \mathbb{P}_2 \cup \{MN\} \cup \mathbb{P}_3$ and $n_2 \in \{0\} \cup \mathbb{P}_1$: Consider $n_1 = q_1N$ and $n_2 = q_2M$ for $1 \leq q_1 \leq 2M - 1$ and $0 \leq q_2 \leq N - 1$. The equation $n_1 - n_2 = uM - vN$ can be rearranged as $(u + q_2)M = (v + q_1)N$. Then we obtain $u + q_2 = N$ and $v + q_1 = M$ because M and N are coprime and $1 \leq u + q_2 \leq 2N - 2$. Therefore $(n_1, n_2) = ((M - v)N, (N - u)M)$. \square

\square

Lemma 9.4.2. If $n \in \mathbb{P}_1$ or $n \in \mathbb{P}_3$, then n is essential with respect to $\mathbb{S}_{\text{coprime}}$.

Proof. Due to Lemma 8.2.1, it suffices to show that, if $n_1 = p_1M \in \mathbb{P}_1$ and $n_3 = p_3N \in \mathbb{P}_3$, then $w(n_1 - n_3) = 1$. Namely, (n_1, n_3) is the only sensor pair of $\mathbb{S}_{\text{coprime}}$ with difference $n_1 - n_3$.

Assume that there exists another pair $(s_1, s_2) \in \mathbb{S}_{\text{coprime}}^2$ such that $(s_1, s_2) \neq (n_1, n_3)$, and $s_1 - s_2 = n_1 - n_3$. According to (s_1, s_2) , we have the following cases:

1. $s_1, s_2 \in \{0\} \cup \mathbb{P}_1$: Assume that $s_1 = q_1M$ and $s_2 = q_2M$ for $0 \leq q_1, q_2 \leq N - 1$. The condition $s_1 - s_2 = n_1 - n_3$ can be rearranged as $(p_1 - q_1 + q_2)M = p_3N$. Since M and N are coprime, the parameter p_3 is an integer multiple of M , which contradicts (9.41).
2. $s_1, s_2 \in \mathbb{P}_2 \cup \{MN\} \cup \mathbb{P}_3$: Let $s_1 = q_1N$ and $s_2 = q_2N$ for $1 \leq q_1, q_2 \leq 2M - 1$. The condition $s_1 - s_2 = n_1 - n_3$ becomes $(p_3 + q_1 - q_2)N = p_1M$. Due to the coprimeness of M and N , the parameter p_1 is divisible by N , causing a contradiction with (9.39).
3. $s_1 \in \{0\} \cup \mathbb{P}_1$ and $s_2 \in \mathbb{P}_2 \cup \{MN\} \cup \mathbb{P}_3$: Suppose that $s_1 = q_1M$ and $s_2 = q_2N$ for $0 \leq q_1 \leq N - 1$ and $1 \leq q_2 \leq 2M - 1$. If $s_1 - s_2 = n_1 - n_3$, then

$(p_1 - q_1)M = (p_3 - q_2)N$. The coprimeness of M and N indicates that N divides $p_1 - q_1$. Since $-N + 2 \leq p_1 - q_1 \leq N - 1$, we have $p_1 = q_1$, $s_1 = n_1$, and $s_2 = n_3$, which contradicts $(s_1, s_2) \neq (n_1, n_3)$.

4. $s_1 \in \mathbb{P}_2 \cup \{MN\} \cup \mathbb{P}_3$ and $s_2 \in \{0\} \cup \mathbb{P}_1$: We assume that $s_1 = q_1N$ and $s_2 = q_2M$ for $1 \leq q_1 \leq 2M - 1$ and $0 \leq q_2 \leq N - 1$. The condition $s_1 - s_2 = n_1 - n_3$ becomes $(p_3 + q_1)N = (p_1 + q_2)M$. We have $p_1 + q_2 = N$ because M and N are coprime and $1 \leq p_1 + q_2 \leq 2N - 2$. Hence $p_3 + q_1 = M$, which contradicts the range of $p_3 + q_1$ ($M + 2 \leq p_3 + q_1 \leq 4M - 2$). \square

\square

Lemma 9.4.3. $\text{SD}(\{0\} \cup \mathbb{P}_1) \cup \text{CD}(\mathbb{P}_1, \{MN\}) = \text{SD}(\{0\} \cup \mathbb{P}_1)$.

Proof. The elements in $\text{CD}(\mathbb{P}_1, \{MN\})$ can be expressed as $\pm(MN - p_1M)$ for $1 \leq p_1 \leq N - 1$, which is equivalent to $\pm((N - p_1)M - 0)$. Since $1 \leq N - p_1 \leq N - 1$, we have $\pm(MN - p_1M) \in \text{SD}(\{0\} \cup \mathbb{P}_1)$. \square

Next we move on to the main argument. Due to Lemma 8.2.2 and 9.4.2, the family \mathcal{E}'_1 contains \mathcal{A} and \mathcal{B} . For the remaining elements in $\mathbb{S}_{\text{coprime}}$, it is assumed that $\mathbb{A} \subseteq \mathbb{P}_2 \cup \{MN\}$ and $|\mathbb{A}| = k$. Let $\overline{\mathbb{S}}$ be $\mathbb{S}_{\text{coprime}} \setminus \mathbb{A}$ and $\overline{\mathbb{D}}$ be the difference coarray of $\overline{\mathbb{S}}$. The sets $\overline{\mathbb{D}}_1$, $\overline{\mathbb{D}}_2$, and $\overline{\mathbb{D}}_3$ are defined as

$$\overline{\mathbb{D}}_1 \triangleq \text{SD}((\{0\} \cup \mathbb{P}_2 \cup \{MN\} \cup \mathbb{P}_3) \setminus \mathbb{A}), \quad (9.55)$$

$$\overline{\mathbb{D}}_2 \triangleq \text{CD}(\mathbb{P}_1, (\mathbb{P}_2 \cup \{MN\}) \setminus \mathbb{A}), \quad (9.56)$$

$$\overline{\mathbb{D}}_3 \triangleq \text{CD}(\mathbb{P}_1, \mathbb{P}_2 \setminus \mathbb{A}). \quad (9.57)$$

Furthermore, the sets $\mathbb{D}_1 \triangleq \text{SD}(\{0\} \cup \mathbb{P}_2 \cup \{MN\} \cup \mathbb{P}_3)$, $\mathbb{D}_2 \triangleq \text{CD}(\mathbb{P}_1, \mathbb{P}_2 \cup \{MN\})$, and $\mathbb{D}_3 \triangleq \text{CD}(\mathbb{P}_1, \mathbb{P}_2)$. Under these assumptions, $\overline{\mathbb{D}}$ can be expressed as

$$\begin{aligned} \overline{\mathbb{D}} &= \text{SD}(\{0\} \cup \mathbb{P}_1) \cup \text{SD}((\{0\} \cup \mathbb{P}_2 \cup \{MN\} \cup \mathbb{P}_3) \setminus \mathbb{A}) \\ &\quad \cup \text{CD}(\{0\} \cup \mathbb{P}_1, (\{0\} \cup \mathbb{P}_2 \cup \{MN\} \cup \mathbb{P}_3) \setminus \mathbb{A}) \end{aligned} \quad (9.58)$$

$$= \text{SD}(\{0\} \cup \mathbb{P}_1) \cup \overline{\mathbb{D}}_1 \cup \overline{\mathbb{D}}_2 \cup \text{CD}(\mathbb{P}_1, \mathbb{P}_3). \quad (9.59)$$

The term $\{0\}$ in the cross difference of (9.58) can be removed since $\text{CD}(\mathbb{B}, \{0\})$ is a subset of $\text{SD}(\{0\} \cup \mathbb{B})$ for any set \mathbb{B} . According to the relation between MN and \mathbb{A} , the set $\overline{\mathbb{D}}_2$ can be expressed as

$$\overline{\mathbb{D}}_2 = \begin{cases} \overline{\mathbb{D}}_3, & \text{if } MN \in \mathbb{A}, \\ \text{CD}(\mathbb{P}_1, \{MN\}) \cup \overline{\mathbb{D}}_3, & \text{if } MN \notin \mathbb{A}, \end{cases} \quad (9.60)$$

where $\overline{\mathbb{D}}_3$ is given by (9.57). Substituting (9.60) into (9.59) and using Lemma 9.4.3 result in

$$\overline{\mathbb{D}} = \text{SD}(\{0\} \cup \mathbb{P}_1) \cup \overline{\mathbb{D}}_1 \cup \overline{\mathbb{D}}_3 \cup \text{CD}(\mathbb{P}_1, \mathbb{P}_3). \quad (9.61)$$

The following lemmas characterize the difference coarray $\overline{\mathbb{D}}$ in terms of $\overline{\mathbb{D}}_1$ and $\overline{\mathbb{D}}_3$. Here \mathbb{D} is the difference coarray of the coprime array $\mathbb{S}_{\text{coprime}}$.

Lemma 9.4.4. Assume that $\mathbb{A} \subseteq \mathbb{P}_2 \cup \{MN\}$. If $|\mathbb{A}| = k \leq M - 2$, then $\overline{\mathbb{D}}_1 = \mathbb{D}_1$.

Proof. First, it can be shown that $\text{SD}(\{0\} \cup \mathbb{P}_3) = \mathbb{D}_1 \setminus \{\pm(M-1)N, \pm MN\}$. It suffices to show that $(M-1)N$ and MN belong to $\overline{\mathbb{D}}_1$ if $k \leq M - 2$. In this case, since $|(\mathbb{P}_2 \cup \{MN\}) \setminus \mathbb{A}| = M - k \geq 2$, there exists $n = qN \in (\mathbb{P}_2 \cup \{MN\}) \setminus \mathbb{A}$ such that $2 \leq q \leq M$. If $q = M$, then the differences $(M-1)N$ and MN reside in $\overline{\mathbb{D}}_1$ since $(M-1)N = (2M-1)N - MN$ and $MN = MN - 0$. If $2 \leq q \leq M-1$, then the differences $(M-1)N$ and MN live in $\overline{\mathbb{D}}_1$ since $(M-1)N = (M-1+q)N - qN$, $MN = (M+q)N - qN$, and $(M-1+q)N, (M+q)N \in \mathbb{P}_3$. \square

Lemma 9.4.5. Let $\mathbb{A} \subseteq \mathbb{P}_2 \cup \{MN\}$ and $\mathbb{A}_R \triangleq \{MN - a : a \in \mathbb{A}\}$. Then $\overline{\mathbb{D}}_3 = \mathbb{D}_3$ if and only if \mathbb{A} and \mathbb{A}_R are disjoint.

Proof. First, it is assumed that MN does not belong to \mathbb{A} . We have $\mathbb{D}_3 = \text{CD}(\mathbb{P}_1, \mathbb{P}_2) = \text{CD}(\mathbb{P}_1, \mathbb{P}_2 \setminus \mathbb{A}) \cup \text{CD}(\mathbb{P}_1, \mathbb{A})$. Therefore, the statement that $\overline{\mathbb{D}}_3 = \mathbb{D}_3$ is equivalent to $\text{CD}(\mathbb{P}_1, \mathbb{A}) \subseteq \overline{\mathbb{D}}_3$.

If \mathbb{A} and \mathbb{A}_R are disjoint, then for every $n \in \mathbb{A}$, the location $MN - n \in \mathbb{P}_2 \setminus \mathbb{A}$. Therefore $\text{CD}(\mathbb{P}_1, \mathbb{A}) \subseteq \text{CD}(\mathbb{P}_1, \mathbb{P}_2 \setminus \mathbb{A}) = \overline{\mathbb{D}}_3$. If \mathbb{A} and \mathbb{A}_R are not disjoint, then there exists $1 \leq v \leq M-1$ such that $\{vN, (M-v)N\} \subseteq \mathbb{A}$. As a result, $vN \notin \mathbb{P}_2 \setminus \mathbb{A}$ and $(M-v)N \notin \mathbb{P}_2 \setminus \mathbb{A}$. Due to Lemma 9.4.1, for some $1 \leq u \leq N-1$, the difference $uM - vN \in \mathbb{D}_3$ is related to the pair (uM, vN) or $((M-v)N, (N-u)M)$. These pairs cannot be found in the cross difference between \mathbb{P}_1 and $\mathbb{P}_2 \setminus \mathbb{A}$. Hence $\overline{\mathbb{D}}_3 \neq \mathbb{D}_3$.

Second, let us consider the case of $MN \in \mathbb{A}$. The set \mathbb{B} and \mathbb{B}_R are defined as $\mathbb{B} \triangleq \mathbb{A} \setminus \{MN\} \subseteq \mathbb{P}_2$ and $\mathbb{B}_R \triangleq \{MN - b : b \in \mathbb{B}\} \subseteq \mathbb{P}_2$, respectively. Due to the first part of the proof, we have $\overline{\mathbb{D}}_3 = \mathbb{D}_3$ if and only if \mathbb{B} and \mathbb{B}_R are disjoint. Since $0 \notin \mathbb{B}$ and $MN \notin \mathbb{B}_R$, \mathbb{B} and \mathbb{B}_R being disjoint is equivalent to \mathbb{A} and \mathbb{A}_R being disjoint, which completes the proof. \square

Lemma 9.4.6. $\overline{\mathbb{D}} = \mathbb{D}$ if and only if $\overline{\mathbb{D}}_1 = \mathbb{D}_1$ and $\overline{\mathbb{D}}_3 = \mathbb{D}_3$.

Proof. The sufficiency part of Lemma 9.4.6 is trivial using (9.61). The following shows the necessity part.

Let $m \in \mathbb{D}_1$ but $m \notin \overline{\mathbb{D}}_1$. We denote $m = rN$ for $-(2M - 1) \leq r \leq 2M - 1$. We will show that the union of $\text{SD}(\{0\} \cup \mathbb{P}_1)$, $\overline{\mathbb{D}}_3$, and $\text{CD}(\mathbb{P}_1, \mathbb{P}_3)$, does not contain m , implying that $\overline{\mathbb{D}} \neq \mathbb{D}$. If $m \in \text{SD}(\{0\} \cup \mathbb{P}_1)$, then there exists $-(N - 1) \leq s \leq N - 1$ such that $rN = sM$. Due to the coprimeness of M and N , the parameter s is an integer multiple of N , implying $s = 0$ and $m = 0$. But $0 \in \overline{\mathbb{D}}_1$, which contradicts $m \notin \overline{\mathbb{D}}_1$. If $m \in \overline{\mathbb{D}}_3$, then there exists a sensor pair in $\{0\} \cup \mathbb{P}_2 \cup \mathbb{P}_3$ (because $m \in \mathbb{D}_1$) whose difference is $uM - vN$ for $1 \leq u \leq N - 1$ and $1 \leq v \leq M - 1$ (since $m \in \overline{\mathbb{D}}_3 \subseteq \mathbb{D}_3$). This result contradicts Lemma 9.4.1. If $m \in \text{CD}(\mathbb{P}_1, \mathbb{P}_3)$, then there exist $1 \leq p_1 \leq N - 1$ and $M + 1 \leq p_3 \leq 2M - 1$ such that $rN = p_1M - p_3N$, implying $(r + p_3)N = p_1M$. Since M and N are coprime, we have that p_1 is divisible by N , which violates $1 \leq p_1 \leq N - 1$.

If $m \in \mathbb{D}_3$ but $m \notin \overline{\mathbb{D}}_3$, then m can be expressed as $uM - vN$ for $1 \leq u \leq N - 1$ and $1 \leq v \leq M - 1$. Lemma 9.4.1 indicates that, such difference can only be found in the cross difference between \mathbb{P}_1 and \mathbb{P}_2 . Therefore, m does not belong to the union of $\text{SD}(\{0\} \cup \mathbb{P}_1)$, $\overline{\mathbb{D}}_1$, and $\text{CD}(\mathbb{P}_1, \mathbb{P}_3)$. These arguments complete the proof. \square

Now let us consider how the subarray $\mathbb{A} \subseteq \mathbb{P}_2 \cup \{MN\}$ influences the difference coarray $\overline{\mathbb{D}}$. Based on the parameter M , we have the following cases:

1. $M = 2$: In this case, we have $\mathbb{A} \subseteq \mathbb{P}_2 \cup \{MN\} = \{N, 2N\}$. Due to Theorem 9.3.1, Lemma 9.4.5, and 9.4.6, it can be shown that $\overline{\mathbb{D}} \neq \mathbb{D}$ for $\mathbb{A} = \{N\}$ and $\overline{\mathbb{D}} = \mathbb{D}$ for $\mathbb{A} = \{2N\}$. Therefore, N is essential but $2N$ is inessential. If $\mathbb{A} = \{N, 2N\}$, then \mathbb{A} contains the essential element N , implying that $\mathbb{A} \notin \mathcal{E}'_2$. These arguments prove (9.42) to (9.44) for $M = 2$.
2. $M = 3$: This case leads to $\mathbb{A} \subseteq \mathbb{P}_2 \cup \{MN\} = \{N, 2N, 3N\}$. If $\mathbb{A} = \{N\}, \{2N\},$ or $\{3N\}$, then it can be shown that $\overline{\mathbb{D}} = \mathbb{D}$, due to Lemma 9.4.4 to 9.4.6. Hence these elements are inessential. If $\mathbb{A} = \{N, 2N\}$, then $\mathbb{A} = \mathbb{A}_R$, so $\overline{\mathbb{D}} \neq \mathbb{D}$, due to Lemma 9.4.5 and 9.4.6. Similarly, it can be shown that $\{2N, 3N\}$ is 2-essential, due to $\overline{\mathbb{D}}_1 \neq \mathbb{D}_1$, while $\{N, 3N\}$ is not 2-essential. If $\mathbb{A} = \{N, 2N, 3N\}$, then it is a superset of $\{N, 2N\}$, which is 2-essential. Therefore $\mathbb{A} \notin \mathcal{E}'_3$. As a result, we prove (9.42) to (9.44) for $M = 3$.
3. $M \geq 4$: According to the value of k , we have the following cases:
 - a) $k = 1$: Due to Lemma 9.4.4, we have $\overline{\mathbb{D}}_1 = \mathbb{D}_1$. Hence, based on Lemma 9.4.5 and 9.4.6, we have $\overline{\mathbb{D}} \neq \mathbb{D}$ if and only if \mathbb{A} and \mathbb{A}_R are not disjoint. For the essential sensors, since $|\mathbb{A}| = 1$, we have $\mathbb{A} = \mathbb{A}_R$, implying that $n = MN - n$ for some $n \in \mathbb{P}_2$. If M is an odd number, then n is not an integer and $n \notin \mathbb{P}_2$. If M is an even number, then this essential sensor becomes $n = MN/2$, which proves (9.42).

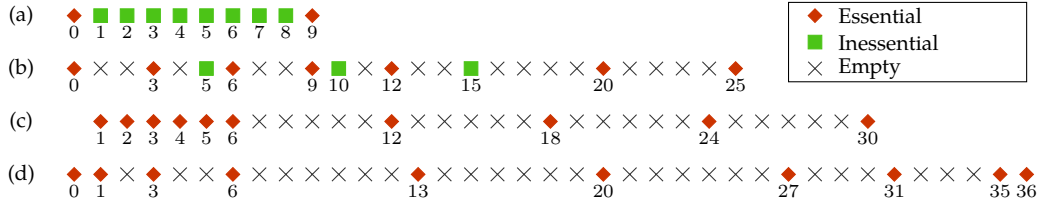


Figure 9.6: The array configurations for (a) ULA with 10 elements, (b) the coprime array with $M = 3, N = 5$, (c) the nested array with $N_1 = N_2 = 5$, and (d) the MRA with 10 elements.

- b) $k = 2$: Similar to the case of $M \geq 4$ and $k = 1$, we have $\overline{\mathbb{D}} \neq \mathbb{D}$ if and only if \mathbb{A} and \mathbb{A}_R are not disjoint, due to Lemma 9.4.4 to 9.4.6. This result means that, all the subarrays of the form $\{n, MN - n\}$ for $n \in \mathbb{P}_2$ belongs to \mathcal{E}'_2 , which proves (9.43).
- c) $3 \leq k \leq \lceil M/2 \rceil$: In this case, we have $k \leq \lceil M/2 \rceil \leq M - 2$, which implies $\overline{\mathbb{D}}_1 = \mathbb{D}_1$ due to Lemma 9.4.4. Next, according to the set \mathbb{A} , we have two cases. If \mathbb{A} and \mathbb{A}_R are disjoint, then $\overline{\mathbb{D}}_3 = \mathbb{D}_3$, due to Lemma 9.4.5. Therefore, $\overline{\mathbb{D}} = \mathbb{D}$ and $\mathbb{A} \notin \mathcal{E}'_k$. On the other hand, if \mathbb{A} and \mathbb{A}_R are not disjoint, then there exists $\{n, MN - n\} \subseteq \mathbb{A}$ for some $n \in \mathbb{P}_2$. Since $\{n, MN - n\} \in \mathcal{E}'_2$, we have $\mathbb{A} \notin \mathcal{E}'_k$. These arguments show that \mathcal{E}'_k is empty.
- d) $k \geq \lceil M/2 \rceil + 1$: For any choice of \mathbb{A} , it can be shown that there exists $n \in \mathbb{P}_2$ such that $\{n, MN - n\}$ is a subset of \mathbb{A} . Hence $\mathbb{A} \in \mathcal{E}_k$ but $\mathbb{A} \notin \mathcal{E}'_k$, implying that \mathcal{E}'_k is empty. All these arguments proves Theorem 9.4.1. \square

9.5 Numerical Examples

In what follows, we will study the estimation performance of arrays in the presence of random sensor failure, through numerical examples. Fig. 9.6 depicts (a) the ULA, (b) the coprime array with $M = 3, N = 5$, (c) the nested array with $N_1 = N_2 = 5$, and (d) the MRA. All these arrays have 10 elements. Here the essential sensors and the inessential sensors are denoted by diamonds and rectangles, respectively. It can be further shown that the difference coarrays are $\{0, \pm 1, \dots, \pm 9\}$ for the ULA, $\{0, \pm 1, \dots, \pm 17, \pm 19, \pm 20, \pm 22, \pm 25\}$ for the coprime array, $\{0, \pm 1, \dots, \pm 29\}$ for the nested array, and $\{0, \pm 1, \dots, \pm 36\}$ for the MRA. Hence, the largest size of the difference coarray is exhibited by the MRA ($|\mathbb{D}| = 73$), followed by the nested array ($|\mathbb{D}| = 59$), then the coprime array ($|\mathbb{D}| = 43$), and finally the ULA ($|\mathbb{D}| = 19$). On the other hand, based on Definition 8.3.1, the smallest fragility F_1 is given by the ULA ($F_1 = 0.2$, the most robust), followed by the coprime array ($F_1 = 0.7$), and finally the nested array and the MRA ($F_1 = 1$, the least robust).

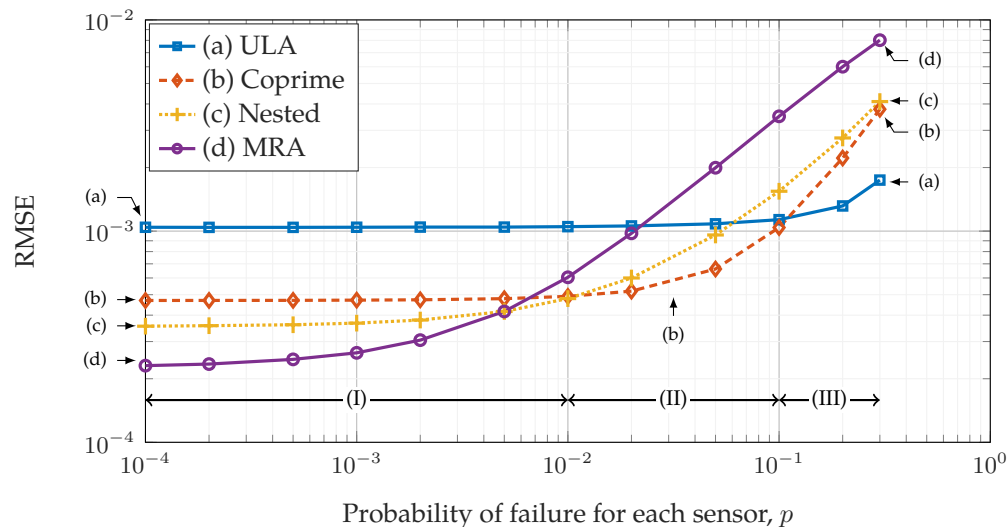


Figure 9.7: The dependence of RMSE on the element failure p with respect to the array configurations in Fig. 9.6. The number of snapshots is 100, SNR is 0dB, and the only one source has $\bar{\theta}_1 = 0.25$.

Fig. 9.7 plots the DOA estimation performance of these arrays as a function of the sensor failure rate p . Here the number of snapshots is 100 and the signal-to-noise ratio (SNR) is 0dB. There is one source ($D = 1$) at $\bar{\theta}_1 = 0.25$. In each run, each sensor fails independently with probability p and the array output is generated based on (1.5), from which coarray MUSIC [87] computes the estimated source direction $\hat{\theta}_i$. For all 10^6 Monte-Carlo runs, we only collect the instances that coarray MUSIC works, from which the root-mean-square error ($\text{RMSE} = (\sum_{i=1}^D (\bar{\theta}_i - \hat{\theta}_i)/D)^{1/2}$) is calculated and averaged.

According to the behavior of these arrays in terms of p , Fig. 9.7 can be divided into three regions: (I), (II), and (III). In Region (I), the best performance is enjoyed by the MRA, followed by the nested array, then the coprime array, and finally the ULA. This is because for sufficiently small p , all the sensors tend to be operational and the performance of coarray MUSIC is dominated by the size of the difference coarray [192]. Note that, as p goes to zero, the RMSE does not approach zero due to finite snapshots and 0dB SNR [192].

In Region (III), it can be deduced that the RMSE is in accordance with the robustness of these arrays. This is since for large p , it is very likely to have multiple faulty elements and the ULA has the least probability that the difference coarray changes. Another observation is that, empirically, for large p , the nested array has smaller RMSE than the MRA, even though they are both maximally economic. This is because the k -essentialness property only characterizes the integrity of the difference coarray, instead of the central ULA segment of the difference coarray. It is known

that the latter has significant influence on the applicability of coarray MUSIC [87], [192].

The last remark is on Region (II). It is observed in Fig. 9.6 that the coprime array does not have the largest difference coarray, nor does it have the smallest fragility F_1 , but it has the least RMSE in Region (II) of Fig. 9.7. This result shows the existence of sparse arrays that strike a balance between the size and the robustness of the difference coarray. Future research can be directed towards designing such array geometries, which work the best in Region (II).

9.6 Concluding Remarks

In this chapter, we studied the robustness of the difference coarrays for MRA, MHA, nested arrays, Cantor arrays, ULA, and coprime arrays, with respect to sensor failures, through the general theory presented in Chapter 8. The proposed closed-form expressions for the k -essential Sperner family not only indicate the importance of elements in these arrays, but also provide many insights into the reliability and the performance based on these arrays.

Future research will be directed towards designing novel sparse array geometries that strike a balance between performance and robustness. For instance, it could be possible to robustify a given array geometry by adding or redistributing the elements in the array.

CONCLUSIONS AND FUTURE DIRECTIONS

In this thesis, we presented several novel sparse arrays, such as super nested arrays (Chapters 3 and 4), half open box arrays, half open box arrays with two layers, and hourglass arrays (Chapter 5). These arrays not only have large hole-free difference coarrays, but also own reduced mutual coupling. Furthermore, we analyzed the performance of sparse arrays in terms of Cramér-Rao bounds (Chapter 6), generalized correlation subspace (Chapter 7), and the robustness (Chapters 8 and 9). Our theoretical analysis led to quite a few insights into the interplay between the sparse array geometry and its estimation performance.

Note that the presented topics are special cases of sparse sensing, and our results could be extended beyond array signal processing. For instance, similar concepts could be generalized to other research fields, such as *communications*, *medical imaging*, and *remote sensing*. In particular, the following list several future topics regarding sparse sensing, sparse sampling, and information inference:

1. *Sparse Arrays with Relaxed Assumptions*: The theory of the difference coarray assumes far-field, narrowband, uncorrelated, and point sources as well as uncorrelated, white, and equal-power noise. These assumptions are not necessarily true in applications such as radar, remote sensing, and communications [82]. Even so, this problem still falls into the category of *sparse sensing with of prior knowledge*, and hence, based on assumptions appropriate to the application, one may be able to devise novel sparse sampling and information inference algorithms.
2. *Non-Gaussian statistics*: The assumption of symmetric Gaussian distributions for the physical signals is known to be a poor fit for real data [118]. Non-Gaussian statistics, such as high-order statics [111] and complex elliptically symmetric distributions [118] have been studied to bridge the gap between theory and practice. It is of considerable interest to study how sparse sensing, sparse sampling, and information inference can be incorporated with non-Gaussian statistics. Sparse sampling schemes should remain robust even if the underlying distribution deviates from Gaussian distributions. Robust estimation of the information of interest in the face of such prior information is still a major challenge even today.

3. *Sparser than Sparse Samples – One-bit quantization*: By representing each sample with one bit (0 or 1), this technique has recently gained momentum in *massive MIMO systems, data converters, and array processing*, since 1) it offers low cost and low complexity in the implementation, 2) it reduces the overall volume of data significantly, and 3) it incurs only a moderate performance loss compared to the unquantized data. In this topic, we are interested in the *interplay between one-bit quantization and sparse sensing*. For instance, in the context of sparse arrays and DOA estimation, sparse arrays with one-bit quantizers are often found to be as good as ULAs with unquantized data, and found to resolve more sources than sensors [101], based on elegant theorems for the correlation of Gaussian data. Much remains to be done in the context of the novel sparse sampling patterns, information inference, and performance limits, for one-bit quantization.
4. *Other Forms of Nonlinearity*: Our previous work uses *linear* sparse sampling to acquire the data, from which the information of interest is inferred. For some applications in optical imaging and communications, only the *magnitude* of the samples is observable, due to physical limitations. It was demonstrated in [33] that the information of interest sometimes remains recoverable under this design constraint using *quadratic sampling*. In fact, this belongs to a broader family of *nonlinear sparse sampling*. In principle, nonlinear sparse samplers could handle other physical design constraints, achieve lower computational complexity, acquire smaller volume of data, or even lead to better estimation performance, compared to the linear case.
5. *Sparse Sampling Off the Grid*: The sparse sampling we have considered so far assumes a regular and uniform grid. This assumption might not hold in applications such as Internet of things, geological data analysis, magnetic resonance imaging, and remote sensing, where the data is collected irregularly. In these cases, sparse sampling can be mathematically reformulated as *choosing sample points from a predefined set S* . We will call this concept *gridless sparse sampling* or continuous sparse sensing [34]. For instance, $S = \{0, 1, 2, 3, \dots, N-1\}$ corresponds to sparse sampling from a uniform grid while $S = [0, 1]$ denotes the samples can be taken anywhere between 0 and 1 (gridless). As a generalization of the grid-based sparse sampling, gridless sparse sampling could achieve better estimation performance in the sense that, for the same number of samples, we have smaller estimation error. In the future, much remains to be explored in the context of novel gridless sparse sampling schemes, new information inference algorithms, and their performance analysis.

BIBLIOGRAPHY

- [1] Y. Abramovich, D. Gray, A. Gorokhov, and N. Spencer, "Positive-definite Toeplitz completion in DOA estimation for nonuniform linear antenna arrays—Part I: Fully augmentable arrays," *IEEE Trans. Signal Process.*, vol. 46, no. 9, pp. 2458–2471, Sep. 1998, ISSN: 1053-587X. DOI: 10.1109/78.709534.
- [2] Y. Abramovich, N. Spencer, and A. Gorokhov, "Positive-definite Toeplitz completion in DOA estimation for nonuniform linear antenna arrays—Part II: Partially augmentable arrays," *IEEE Trans. Signal Process.*, vol. 47, no. 6, pp. 1502–1521, Jun. 1999, ISSN: 1053-587X. DOI: 10.1109/78.765119.
- [3] K. Adhikari, J. R. Buck, and K. E. Wage, "Beamforming with extended coprime sensor arrays," in *Proc. IEEE Int. Conf. Acoust., Speech, and Sig. Proc.*, May 2013, pp. 4183–4186. DOI: 10.1109/ICASSP.2013.6638447.
- [4] K. Adhikari, J. R. Buck, and K. E. Wage, "Extending coprime sensor arrays to achieve the peak side lobe height of a full uniform linear array," *EURASIP J. Adv. Signal Process.*, vol. 2014, no. 1, 148, Sep. 2014. DOI: 10.1186/1687-6180-2014-148.
- [5] A. Alexiou and A. Manikas, "Investigation of array robustness to sensor failure," *Journal of the Franklin Institute*, vol. 342, no. 3, pp. 255–272, May 2005, ISSN: 0016-0032. DOI: 10.1016/j.jfranklin.2004.11.005.
- [6] J. G. Andrews, S. Buzzi, W. Choi, S. V. Hanly, A. Lozano, A. C. K. Soong, and J. C. Zhang, "What will 5G be?" *IEEE J. Sel. Areas Commun.*, vol. 32, no. 6, pp. 1065–1082, Jun. 2014, ISSN: 0733-8716. DOI: 10.1109/JSAC.2014.2328098.
- [7] D. D. Ariananda and G. Leus, "Compressive wideband power spectrum estimation," *IEEE Trans. Signal Process.*, vol. 60, no. 9, pp. 4775–4789, Sep. 2012, ISSN: 1053-587X. DOI: 10.1109/TSP.2012.2201153.
- [8] D. D. Ariananda and G. Leus, "Compressive joint angular-frequency power spectrum estimation," in *Proc. European Signal Proc. Conf.*, Marrakech, Morocco, Sep. 2013, pp. 1–5.
- [9] J. Aars, "Nouveau reseau pour l'observation radioastronomique de la brillance sur le soleil a 9350 mc/s," *Compt. Rend. Acad. Sci.*, vol. 240, pp. 942–945, Feb. 1955.
- [10] M. Atkinson, N. Santoro, and J. Urrutia, "Integer sets with distinct sums and differences and carrier frequency assignments for nonlinear repeaters," *IEEE Trans. Commun.*, vol. 34, no. 6, pp. 614–617, Jun. 1986, ISSN: 0090-6778. DOI: 10.1109/TCOM.1986.1096587.
- [11] C. A. Balanis, *Antenna theory: Analysis and design*, 4th. John Wiley & Sons, 2016, ISBN: 1118642066.
- [12] A. Barabell, "Improving the resolution performance of eigenstructure-based direction-finding algorithms," in *Proc. IEEE Int. Conf. Acoust., Speech, and Sig. Proc.*, vol. 8, Apr. 1983, pp. 336–339. DOI: 10.1109/ICASSP.1983.1172124.

- [13] A. J. Barabell, J. Capon, D. F. DeLong, J. R. Johnson, and K. D. Senne, "Performance comparison of superresolution array processing algorithms," MIT Lincoln Laboratory, Lexington, MA, Tech. Rep., 1984, revised 1998.
- [14] M. S. Bartlett, "Smoothing periodograms from time-series with continuous spectra," *Nature*, vol. 161, pp. 686–687, May 1948. doi: 10.1038/161686a0.
- [15] S. Bedrosian, "Nonuniform linear arrays: Graph-theoretic approach to minimum redundancy," *Proc. IEEE*, vol. 74, no. 7, pp. 1040–1043, Jul. 1986, issn: 0018-9219. doi: 10.1109/PROC.1986.13581.
- [16] B. N. Bhaskar, G. Tang, and B. Recht, "Atomic norm denoising with applications to line spectral estimation," *IEEE Trans. Signal Process.*, vol. 61, no. 23, pp. 5987–5999, Dec. 2013, issn: 1053-587X. doi: 10.1109/TSP.2013.2273443.
- [17] G. Bienvenu and L. Kopp, "Optimality of high resolution array processing using the eigensystem approach," *IEEE Trans. Acoust., Speech, Signal Process.*, vol. 31, no. 5, pp. 1235–1248, Oct. 1983, issn: 0096-3518. doi: 10.1109/TASSP.1983.1164185.
- [18] J. A. Bondy and U. Murty, *Graph theory with applications*. Elsevier Science Ltd/North-Holland, 1976, isbn: 0-444-19451-7.
- [19] E. BouDaher, Y. Jia, F. Ahmad, and M. G. Amin, "Multi-frequency co-prime arrays for high-resolution direction-of-arrival estimation," *IEEE Trans. Signal Process.*, vol. 63, no. 14, pp. 3797–3808, Jul. 2015, issn: 1053-587X. doi: 10.1109/TSP.2015.2432734.
- [20] E. BouDaher, F. Ahmad, M. G. Amin, and A. Hoorfar, "DOA estimation with co-prime arrays in the presence of mutual coupling," in *Proc. European Signal Proc. Conf.*, Nice, France, Sep. 2015, pp. 2830–2834. doi: 10.1109/eusipco.2015.7362901.
- [21] E. BouDaher, F. Ahmad, M. G. Amin, and A. Hoorfar, "Mutual coupling effect and compensation in non-uniform arrays for direction-of-arrival estimation," *Digit. Signal Process.*, vol. 61, pp. 3–14, Feb. 2017, Special Issue on Coprime Sampling and Arrays, issn: 1051-2004. doi: 10.1016/j.dsp.2016.06.005.
- [22] R. N. Bracewell, *Radio astronomy techniques*. Berlin: Springer, 1962, vol. 54, isbn: 978-3-662-39512-7. doi: 10.1007/978-3-662-39512-7.
- [23] R. N. Bracewell, "Optimum spacings for radio telescopes with unfilled apertures," *Nat. Acad. Sci. Nat. Res. Council., Publ.*, vol. 1408, pp. 243–244, 1966.
- [24] R. N. Bracewell, *The Fourier transform and its applications*, Third. McGraw-Hill, 2000, isbn: 9780073039381.
- [25] A. Camps, A. Cardama, and D. Infantès, "Synthesis of large low-redundancy linear arrays," *IEEE Trans. Antennas Propag.*, vol. 49, no. 12, pp. 1881–1883, Dec. 2001, issn: 0018-926X. doi: 10.1109/8.982474.
- [26] E. J. Candes and M. B. Wakin, "An introduction to compressive sampling," *IEEE Signal Process. Mag.*, vol. 25, no. 2, pp. 21–30, Mar. 2008, issn: 1053-5888. doi: 10.1109/MSP.2007.914731.

- [27] G. Cantor, "Über unendliche, lineare punktmannigfaltigkeiten v," *Mathematische Annalen*, vol. 21, pp. 545–591, 1883.
- [28] J. Capon, "High-resolution frequency-wavenumber spectrum analysis," *Proc. IEEE*, vol. 57, no. 8, pp. 1408–1418, Aug. 1969, ISSN: 0018-9219. DOI: 10.1109/PROC.1969.7278.
- [29] M. Carlin, G. Oliveri, and A. Massa, "On the robustness to element failures of linear ADS-thinned arrays," *IEEE Trans. Antennas Propag.*, vol. 59, no. 12, pp. 4849–4853, Dec. 2011, ISSN: 0018-926X. DOI: 10.1109/TAP.2011.2165510.
- [30] C. Chambers, T. Tozer, K. Sharman, and T. Durrani, "Temporal and spatial sampling influence on the estimates of superimposed narrowband signals: When less can mean more," *IEEE Trans. Signal Process.*, vol. 44, no. 12, pp. 3085–3098, Dec. 1996, ISSN: 1053-587X. DOI: 10.1109/78.553482.
- [31] H.-H. Chao and L. Vandenberghe, "Extensions of semidefinite programming methods for atomic decomposition," in *Proc. IEEE Int. Conf. Acoust., Speech, and Sig. Proc.*, Shanghai, China, Mar. 2016, pp. 4757–4761. DOI: 10.1109/ICASSP.2016.7472580.
- [32] C.-Y. Chen and P. P. Vaidyanathan, "MIMO radar space-time adaptive processing using prolate spheroidal wave functions," *IEEE Trans. Signal Process.*, vol. 56, no. 2, pp. 623–635, Feb. 2008, ISSN: 1053-587X. DOI: 10.1109/TSP.2007.907917.
- [33] Y. Chen, Y. Chi, and A. J. Goldsmith, "Exact and stable covariance estimation from quadratic sampling via convex programming," *IEEE Trans. Inf. Theory*, vol. 61, no. 7, pp. 4034–4059, Jul. 2015, ISSN: 0018-9448. DOI: 10.1109/TIT.2015.2429594.
- [34] S. P. Chepuri and G. Leus, "Continuous sensor placement," *IEEE Signal Process. Lett.*, vol. 22, no. 5, pp. 544–548, May 2015, ISSN: 1070-9908. DOI: 10.1109/LSP.2014.2363731.
- [35] F. R. K. Chung, *Spectral graph theory (cbms regional conference series in mathematics, no. 92)*. American Mathematical Society, 1996, ISBN: 978-0-8218-0315-8.
- [36] D. Coppersmith and S. Winograd, "Matrix multiplication via arithmetic progressions," *J. Symbolic Computation*, vol. 9, pp. 251–280, 1990. DOI: 10.1016/S0747-7171(08)80013-2.
- [37] H. Cramér, *Mathematical methods of statistics*. Princeton University Press, 1946, ISBN: 9780691005478.
- [38] J. Dai, D. Zhao, and X. Ji, "A sparse representation method for DOA estimation with unknown mutual coupling," *IEEE Antennas Wireless Propag. Lett.*, vol. 11, pp. 1210–1213, 2012, ISSN: 1536-1225. DOI: 10.1109/LAWP.2012.2223651.
- [39] I. Daubechies, "Time-frequency localization operators: A geometric phase space approach," *IEEE Trans. Inf. Theory*, vol. 34, no. 4, pp. 605–612, Jul. 1988, ISSN: 0018-9448. DOI: 10.1109/18.9761.

- [40] A. Dollas, W. Rankin, and D. McCracken, "A new algorithm for Golomb ruler derivation and proof of the 19 mark ruler," *IEEE Trans. Inf. Theory*, vol. 44, no. 1, pp. 379–382, Jan. 1998, issn: 0018-9448. doi: 10.1109/18.651068.
- [41] J. Dong, Q. Li, R. Jin, Y. Zhu, Q. Huang, and L. Gui, "A method for seeking low-redundancy large linear arrays in aperture synthesis microwave radiometers," *IEEE Trans. Antennas Propag.*, vol. 58, no. 6, pp. 1913–1921, Jun. 2010, issn: 0018-926X. doi: 10.1109/TAP.2010.2046846.
- [42] D. L. Donoho, "Compressed sensing," *IEEE Trans. Inf. Theory*, vol. 52, no. 4, pp. 1289–1306, Apr. 2006, issn: 0018-9448. doi: 10.1109/TIT.2006.871582.
- [43] C. Elachi and J. J. van Zyl, *Introduction to the physics and techniques of remote sensing*. Wiley-Interscience, 2007, isbn: 9780471475699. doi: 10.1002/0471783390.
- [44] K. Engel, *Sperner theory*, 1st ed. Cambridge University Press, 1997, 417 pp., isbn: 0521452066.
- [45] P. Erdős and I. S. Gál, "On the representation of $1, 2, \dots, N$ by differences," *Indagationes Mathematicae*, vol. 10, pp. 379–382, 1948.
- [46] K. Falconer, *Fractal geometry: Mathematical foundations and applications*, 2nd ed. Wiley, Jan. 28, 2005, isbn: 9780470848616. doi: 10.1002/0470013850.
- [47] J. Feder, *Fractals*. Springer, May 31, 1988, 310 pp., isbn: 0306428512. doi: 10.1007/978-1-4899-2124-6.
- [48] B. Friedlander, "A sensitivity analysis of the MUSIC algorithm," *IEEE Trans. Acoust., Speech, Signal Process.*, vol. 38, no. 10, pp. 1740–1751, Oct. 1990, issn: 0096-3518. doi: 10.1109/29.60105.
- [49] B. Friedlander and A. Weiss, "Direction finding in the presence of mutual coupling," *IEEE Trans. Antennas Propag.*, vol. 39, no. 3, pp. 273–284, Mar. 1991, issn: 0018-926X. doi: 10.1109/8.76322.
- [50] L. Godara, "Application of antenna arrays to mobile communications, Part II: Beam-forming and direction-of-arrival considerations," *Proc. IEEE*, vol. 85, no. 8, pp. 1195–1245, Aug. 1997, issn: 0018-9219. doi: 10.1109/5.622504.
- [51] C. R. Greene and R. C. Wood, "Sparse array performance," *J. Acoust. Soc. Am.*, vol. 63, no. 6, pp. 1866–1872, 1978. doi: 10.1121/1.381927.
- [52] J. R. Guerci, *Space-time adaptive processing for radar*. Artech House, 2003, isbn: 1580533779.
- [53] M. Haardt, F. Roemer, and G. Del Galdo, "Higher-order SVD-based subspace estimation to improve the parameter estimation accuracy in multidimensional harmonic retrieval problems," *IEEE Trans. Signal Process.*, vol. 56, no. 7, pp. 3198–3213, Jul. 2008. doi: 10.1109/TSP.2008.917929.
- [54] P. R. Halmos, *Measure theory*, 1st ed., ser. Graduate Texts in Mathematics. Springer-Verlag New York, 1950, vol. 18. doi: 10.1007/978-1-4684-9440-2.
- [55] K. Han and A. Nehorai, "Nested vector-sensor array processing via tensor modeling," *IEEE Trans. Signal Process.*, vol. 62, no. 10, pp. 2542–2553, May 2014. doi: 10.1109/TSP.2014.2314437.

- [56] R. A. Haubrich, "Array design," *Seismol. Soc. Am., Bull.*, vol. 58, no. 3, pp. 977–991, Jun. 1968.
- [57] S. Haykin, J. Reilly, V. Kezys, and E. Vertatschitsch, "Some aspects of array signal processing," *Proc. Inst. Electr. Eng. F–Radar Signal Process.*, vol. 139, no. 1, pp. 1–26, Feb. 1992, ISSN: 0956-375X. DOI: 10.1049/ip-f-2.1992.0001.
- [58] S. Haykin, *Array signal processing*. Englewood Cliffs, NJ, USA: Prentice-Hall, 1984, ISBN: 0130464821.
- [59] R. T. Hoctor and S. A. Kassam, "The unifying role of the coarray in aperture synthesis for coherent and incoherent imaging," *Proc. IEEE*, vol. 78, no. 4, pp. 735–752, Apr. 1990, ISSN: 0018-9219. DOI: 10.1109/5.54811.
- [60] R. A. Horn and C. R. Johnson, *Matrix analysis*. Cambridge, 1985, ISBN: 0521386322. DOI: 10.1017/cbo9780511810817.
- [61] P.-C. Hsiao, Y.-T. Lin, and S.-G. Chen, "An efficient searching algorithm for high DoF non-uniform linear antenna array with constrained spacing," in *2015 13th International Conference on Telecommunications (ConTEL)*, Jul. 2015, pp. 1–5. DOI: 10.1109/ConTEL.2015.7231200.
- [62] Y. Hua and T. K. Sarkar, "Matrix pencil method for estimating parameters of exponentially damped/undamped sinusoids in noise," *IEEE Trans. Acoust., Speech, Signal Process.*, vol. 38, no. 5, pp. 814–824, May 1990, ISSN: 0096-3518. DOI: 10.1109/29.56027.
- [63] H. T. Hui, "Decoupling methods for the mutual coupling effect in antenna arrays: A review," *Recent Patents on Engineering*, vol. 1, pp. 187–193, 2007. DOI: 10.2174/187221207780832200.
- [64] H. Hui, "Improved compensation for the mutual coupling effect in a dipole array for direction finding," *IEEE Trans. Antennas Propag.*, vol. 51, no. 9, pp. 2498–2503, Sep. 2003, ISSN: 0018-926X. DOI: 10.1109/TAP.2003.816303.
- [65] M. Ishiguro, "Minimum redundancy linear arrays for a large number of antennas," *Radio Science*, vol. 15, no. 6, pp. 1163–1170, 1980. DOI: 10.1029/RS015i006p01163.
- [66] M. Jansson, B. Goransson, and B. Ottersten, "A subspace method for direction of arrival estimation of uncorrelated emitter signals," *IEEE Trans. Signal Process.*, vol. 47, no. 4, pp. 945–956, Apr. 1999, ISSN: 1053-587X. DOI: 10.1109/78.752593.
- [67] T. Jiang, N. D. Sidiropoulos, and J. M. F. ten Berge, "Almost-sure identifiability of multidimensional harmonic retrieval," *IEEE Trans. Signal Process.*, vol. 49, no. 9, pp. 1849–1859, Sep. 2001, ISSN: 1053-587X. DOI: 10.1109/78.942615.
- [68] D. H. Johnson and D. E. Dudgeon, *Array signal processing: Concepts and techniques*. Addison Wesley Pub Co Inc, Feb. 11, 1993, 512 pp., ISBN: 0130485136.
- [69] S. M. Kay, *Fundamentals of statistical signal processing: Estimation theory*. Prentice Hall PTR, 1993, ISBN: 0133457117.

- [70] H. King, "Mutual impedance of unequal length antennas in echelon," *IRE Trans. Antennas Propag.*, vol. 5, no. 3, pp. 306–313, Jul. 1957, ISSN: 0096-1973. DOI: 10.1109/TAP.1957.1144509.
- [71] R. Klemm, *Space-time adaptive processing: Principles and applications*. IEEE Press, 1998, ISBN: 0852969465.
- [72] A. Kleyner and P. O'Connor, *Practical reliability engineering*. John Wiley and Sons Ltd, Jan. 6, 2012, 512 pp., ISBN: 978-0470979815. DOI: 10.1002/9781119961260.
- [73] A. Koochakzadeh and P. Pal, "Cramér-Rao bounds for underdetermined source localization," *IEEE Signal Process. Lett.*, vol. 23, no. 7, pp. 919–923, Jul. 2016, ISSN: 1070-9908. DOI: 10.1109/LSP.2016.2569504.
- [74] A. Koochakzadeh, H. Qiao, and P. Pal, "Compressive spectrum sensing with spectral priors for cognitive radar," in *2016 4th International Workshop on Compressed Sensing Theory and its Applications to Radar, Sonar and Remote Sensing (CoSeRa)*, Sep. 2016, pp. 100–104. DOI: 10.1109/CoSeRa.2016.7745708.
- [75] A. Koochakzadeh and P. Pal, "On the robustness of co-prime sampling," in *Proc. European Signal Proc. Conf.*, Aug. 2015, pp. 2825–2829. DOI: 10.1109/EUSIPCO.2015.7362900.
- [76] A. Koochakzadeh and P. Pal, "Sparse source localization in presence of co-array perturbations," in *2015 International Conference on Sampling Theory and Applications (SampTA)*, Washington D.C., USA, May 2015, pp. 563–567. DOI: 10.1109/SAMP.2015.7148954.
- [77] H. Krim and M. Viberg, "Two decades of array signal processing research: The parametric approach," *IEEE Signal Process. Mag.*, vol. 13, no. 4, pp. 67–94, Jul. 1996, ISSN: 1053-5888. DOI: 10.1109/79.526899.
- [78] R. Kumaresan and D. W. Tufts, "Estimating the angles of arrival of multiple plane waves," *IEEE Trans. Aerosp. Electron. Syst.*, vol. AES-19, no. 1, pp. 134–139, Jan. 1983, ISSN: 0018-9251. DOI: 10.1109/TAES.1983.309427.
- [79] A. Lam and D. Sarwate, "On optimum time-hopping patterns," *IEEE Trans. Commun.*, vol. 36, no. 3, pp. 380–382, Mar. 1988, ISSN: 0090-6778. DOI: 10.1109/26.1464.
- [80] E. G. Larsson, O. Edfors, F. Tufvesson, and T. L. Marzetta, "Massive MIMO for next generation wireless systems," *IEEE Commun. Mag.*, vol. 52, no. 2, pp. 186–195, Feb. 2014, ISSN: 0163-6804. DOI: 10.1109/MCOM.2014.6736761.
- [81] J. Leech, "On the representation of $1, 2, \dots, n$ by differences," *J. London Math. Soc.*, vol. s1-31, no. 2, pp. 160–169, 1956. DOI: 10.1112/jlms/s1-31.2.160.
- [82] J. Li and P. Stoica, *MIMO radar signal processing*. John Wiley & Sons Inc, Oct. 11, 2008, 448 pp., ISBN: 978-0-470-17898-0. DOI: 10.1002/9780470391488.
- [83] M. Lin and L. Yang, "Blind calibration and DOA estimation with uniform circular arrays in the presence of mutual coupling," *IEEE Antennas Wireless Propag. Lett.*, vol. 5, no. 1, pp. 315–318, Dec. 2006, ISSN: 1536-1225. DOI: 10.1109/LAWP.2006.878898.

- [84] D. Linebarger, I. Sudborough, and I. Tollis, "Difference bases and sparse sensor arrays," *IEEE Trans. Inf. Theory*, vol. 39, no. 2, pp. 716–721, Mar. 1993, issn: 0018-9448. doi: 10.1109/18.212309.
- [85] C.-L. Liu and P. P. Vaidyanathan, "Design of coprime DFT arrays and filter banks," in *Proc. IEEE Asil. Conf. on Sig., Sys., and Comp.*, Nov. 2014, pp. 455–459. doi: 10.1109/ACSSC.2014.7094484.
- [86] C.-L. Liu and P. P. Vaidyanathan, "Coprime arrays and samplers for space-time adaptive processing," in *Proc. IEEE Int. Conf. Acoust., Speech, and Sig. Proc.*, Brisbane, QLD, Australia, Apr. 2015, pp. 2364–2368. doi: 10.1109/ICASSP.2015.7178394.
- [87] C.-L. Liu and P. P. Vaidyanathan, "Remarks on the spatial smoothing step in coarray MUSIC," *IEEE Signal Process. Lett.*, vol. 22, no. 9, pp. 1438–1442, Sep. 2015. doi: 10.1109/LSP.2015.2409153,
- [88] C.-L. Liu and P. P. Vaidyanathan, "Tensor MUSIC in multidimensional sparse arrays," in *Proc. IEEE Asil. Conf. on Sig., Sys., and Comp.*, Nov. 2015, pp. 1783–1787. doi: 10.1109/ACSSC.2015.7421458.
- [89] C.-L. Liu and P. P. Vaidyanathan, "High order super nested arrays," in *Proc. IEEE Sensor Array and Multichannel Signal Process. Workshop*, Jul. 2016, pp. 1–5. doi: 10.1109/SAM.2016.7569621,
- [90] C.-L. Liu and P. P. Vaidyanathan, *Interactive interface for super nested arrays*, 2016. [Online]. Available: <http://systems.caltech.edu/dsp/students/clliu/SuperNested/SN.zip>.
- [91] C.-L. Liu and P. P. Vaidyanathan, "New Cramér-Rao bound expressions for coprime and other sparse arrays," in *Proc. IEEE Sensor Array and Multichannel Signal Process. Workshop*, Jul. 2016, pp. 1–5. doi: 10.1109/SAM.2016.7569620,
- [92] C.-L. Liu and P. P. Vaidyanathan, "Super nested arrays: Linear sparse arrays with reduced mutual coupling—Part I: Fundamentals," *IEEE Trans. Signal Process.*, vol. 64, no. 15, pp. 3997–4012, Aug. 2016, issn: 1053-587X. doi: 10.1109/TSP.2016.2558159,
- [93] C.-L. Liu and P. P. Vaidyanathan, "Super nested arrays: Linear sparse arrays with reduced mutual coupling—Part II: High-order extensions," *IEEE Trans. Signal Process.*, vol. 64, no. 16, pp. 4203–4217, Aug. 2016, issn: 1053-587X. doi: 10.1109/TSP.2016.2558167,
- [94] C.-L. Liu and P. P. Vaidyanathan, "Super nested arrays: Sparse arrays with less mutual coupling than nested arrays," in *Proc. IEEE Int. Conf. Acoust., Speech, and Sig. Proc.*, Shanghai, China, Mar. 2016, pp. 2976–2980. doi: 10.1109/ICASSP.2016.7472223,
- [95] C.-L. Liu and P. P. Vaidyanathan, "Two-dimensional sparse arrays with hole-free coarray and reduced mutual coupling," in *Proc. IEEE Asil. Conf. on Sig., Sys., and Comp.*, Nov. 2016, pp. 1508–1512. doi: 10.1109/ACSSC.2016.7869629,

- [96] C.-L. Liu and P. P. Vaidyanathan, "Correlation subspaces: Generalizations and connection to difference coarrays," *IEEE Trans. Signal Process.*, vol. 65, no. 19, pp. 5006–5020, Oct. 2017, ISSN: 1053-587X. DOI: 10.1109/TSP.2017.2721915,
- [97] C.-L. Liu and P. P. Vaidyanathan, "Cramér-Rao bounds for coprime and other sparse arrays, which find more sources than sensors," *Digit. Signal Process.*, vol. 61, pp. 43–61, Feb. 2017, Special Issue on Coprime Sampling and Arrays, ISSN: 1051-2004. DOI: 10.1016/j.dsp.2016.04.011,
- [98] C.-L. Liu and P. P. Vaidyanathan, "Hourglass arrays and other novel 2-D sparse arrays with reduced mutual coupling," *IEEE Trans. Signal Process.*, vol. 65, no. 13, pp. 3369–3383, Jul. 2017, ISSN: 1053-587X. DOI: 10.1109/TSP.2017.2690390,
- [99] C.-L. Liu and P. P. Vaidyanathan, *Interactive interface for hourglass arrays and other novel 2-d sparse arrays with reduced mutual coupling*, 2017. [Online]. Available: <http://systems.caltech.edu/dsp/students/clliu/Hourglass/Hourglass.zip>.
- [100] C.-L. Liu and P. P. Vaidyanathan, "Maximally economic sparse arrays and Cantor arrays," in *Proc. IEEE Int. Workshop on Comput. Advances in Multi-Sensor Adaptive Process.*, Dec. 2017, pp. 1–5. DOI: 10.1109/CAMSAP.2017.8313139,
- [101] C.-L. Liu and P. P. Vaidyanathan, "One-bit sparse array DOA estimation," in *Proc. IEEE Int. Conf. Acoust., Speech, and Sig. Proc.*, Mar. 2017, pp. 3126–3130. DOI: 10.1109/ICASSP.2017.7952732.
- [102] C.-L. Liu and P. P. Vaidyanathan, "The role of difference coarrays in correlation subspaces," in *Proc. IEEE Asil. Conf. on Sig., Sys., and Comp.*, Oct. 2017, pp. 1173–1177. DOI: 10.1109/ACSSC.2017.8335536,
- [103] C.-L. Liu and P. P. Vaidyanathan, "Robustness of coarrays of sparse arrays to sensor failures," in *Proc. IEEE Int. Conf. Acoust., Speech, and Sig. Proc.*, Apr. 2018,
- [104] C.-L. Liu, P. P. Vaidyanathan, and P. Pal, "Coprime coarray interpolation for DOA estimation via nuclear norm minimization," in *Proc. IEEE Int. Symp. Circuits and Syst.*, Montreal, Canada, May 2016, pp. 2639–2642. DOI: 10.1109/ISCAS.2016.7539135.
- [105] H. S. Lui and H. T. Hui, "Mutual coupling compensation for direction-of-arrival estimations using the receiving-mutual-impedance method," *International Journal of Antennas and Propagation*, vol. 2010, 2010, Article ID 373061. DOI: 10.1155/2010/373061.
- [106] H. Lütkepohl, *Handbook of matrices*. John Wiley & Sons, 1996, ISBN: 0471970158.
- [107] W.-K. Ma, T.-H. Hsieh, and C.-Y. Chi, "DOA estimation of quasi-stationary signals via Khatri-Rao subspace," in *Proc. IEEE Int. Conf. Acoust., Speech, and Sig. Proc.*, Taipei, Taiwan, Taiwan, Apr. 2009, pp. 2165–2168. DOI: 10.1109/ICASSP.2009.4960046.

- [108] W.-K. Ma, T.-H. Hsieh, and C.-Y. Chi, "DOA estimation of quasi-stationary signals with less sensors than sources and unknown spatial noise covariance: A Khatri-Rao subspace approach," *IEEE Trans. Signal Process.*, vol. 58, no. 4, pp. 2168–2180, Apr. 2010, ISSN: 1053-587X. DOI: 10.1109/TSP.2009.2034935.
- [109] A. Manikas, *Differential geometry in array processing*. Imperial College Press, 2004, ISBN: 186094423X.
- [110] D. G. Manolakis, V. K. Ingle, and S. M. Kogon, *Statistical and adaptive signal processing: Spectral estimation, signal modeling, adaptive filtering, and array processing*. Artech House, 2005, ISBN: 1580536107.
- [111] J. M. Mendel, "Tutorial on higher-order statistics (spectra) in signal processing and system theory: Theoretical results and some applications," *Proc. IEEE*, vol. 79, no. 3, pp. 278–305, Mar. 1991, ISSN: 0018-9219. DOI: 10.1109/5.75086.
- [112] K. V. Mishra, M. Cho, A. Kruger, and W. Xu, "Spectral super-resolution with prior knowledge," *IEEE Trans. Signal Process.*, vol. 63, no. 20, pp. 5342–5357, Oct. 2015, ISSN: 1053-587X. DOI: 10.1109/TSP.2015.2452223.
- [113] A. T. Moffet, "Minimum-redundancy linear arrays," *IEEE Trans. Antennas Propag.*, vol. AP-16, no. 2, pp. 172–175, Mar. 1968. DOI: 10.1109/TAP.1968.1139138.
- [114] M. Muma, Y. Cheng, F. Roemer, M. Haardt, and A. M. Zoubir, "Robust source number enumeration for r -dimensional arrays in case of brief sensor failures," in *Proc. IEEE Int. Conf. Acoust., Speech, and Sig. Proc.*, Kyoto, Japan, Mar. 2012, pp. 3709–3712. DOI: 10.1109/ICASSP.2012.6288722.
- [115] A. Myers, *Complex system reliability*. Springer-Verlag GmbH, Nov. 11, 2010, ISBN: 9781849964135. DOI: 10.1007/978-1-84996-414-2.
- [116] D. Nion and N. Sidiropoulos, "Tensor algebra and multidimensional harmonic retrieval in signal processing for MIMO radar," *IEEE Trans. Signal Process.*, vol. 58, no. 11, pp. 5693–5705, Nov. 2010. DOI: 10.1109/TSP.2010.2058802.
- [117] G. Oliveri, P. Rocca, and A. Massa, "Reliable diagnosis of large linear arrays—A Bayesian compressive sensing approach," *IEEE Trans. Antennas Propag.*, vol. 60, no. 10, pp. 4627–4636, Oct. 2012, ISSN: 0018-926X. DOI: 10.1109/TAP.2012.2207344.
- [118] E. Ollila, D. E. Tyler, V. Koivunen, and H. V. Poor, "Complex elliptically symmetric distributions: Survey, new results and applications," *IEEE Trans. Signal Process.*, vol. 60, no. 11, pp. 5597–5625, Nov. 2012, ISSN: 1053-587X. DOI: 10.1109/TSP.2012.2212433.
- [119] P. Pal and P. P. Vaidyanathan, "Correlation-aware techniques for sparse support recovery," in *Proc. IEEE Statist. Signal Process. (SSP) Workshop*, Aug. 2012, pp. 53–56. DOI: 10.1109/SSP.2012.6319753.

- [120] P. Pal and P. P. Vaidyanathan, "Multiple level nested array: An efficient geometry for $2q$ th order cumulant based array processing," *IEEE Trans. Signal Process.*, vol. 60, no. 3, pp. 1253–1269, Mar. 2012, ISSN: 1053-587X. DOI: 10.1109/TSP.2011.2178410.
- [121] P. Pal and P. P. Vaidyanathan, "Nested arrays in two dimensions, Part I: Geometrical considerations," *IEEE Trans. Signal Process.*, vol. 60, no. 9, pp. 4694–4705, Sep. 2012, ISSN: 1053-587X. DOI: 10.1109/TSP.2012.2203814.
- [122] P. Pal and P. P. Vaidyanathan, "Nested arrays in two dimensions, Part II: Application in two dimensional array processing," *IEEE Trans. Signal Process.*, vol. 60, no. 9, pp. 4706–4718, Sep. 2012, ISSN: 1053-587X. DOI: 10.1109/TSP.2012.2203815.
- [123] P. Pal and P. P. Vaidyanathan, "A grid-less approach to underdetermined direction of arrival estimation via low rank matrix denoising," *IEEE Signal Process. Lett.*, vol. 21, no. 6, pp. 737–741, Jun. 2014, ISSN: 1070-9908. DOI: 10.1109/LSP.2014.2314175.
- [124] P. Pal and P. P. Vaidyanathan, "Nested arrays: A novel approach to array processing with enhanced degrees of freedom," *IEEE Trans. Signal Process.*, vol. 58, no. 8, pp. 4167–4181, Aug. 2010. DOI: 10.1109/TSP.2010.2049264.
- [125] P. Pal and P. P. Vaidyanathan, "Coprime sampling and the MUSIC algorithm," in *Proc. IEEE Dig. Signal Process. Signal Process. Educ. Workshop*, Sedona, AZ, USA, Jan. 2011, pp. 289–294. DOI: 10.1109/DSP-SPE.2011.5739227.
- [126] P. Pal and P. P. Vaidyanathan, "Gridless methods for underdetermined source estimation," in *Proc. IEEE Asil. Conf. on Sig., Sys., and Comp.*, Nov. 2014, pp. 111–115. DOI: 10.1109/ACSSC.2014.7094408.
- [127] P. Pal and P. P. Vaidyanathan, "Pushing the limits of sparse support recovery using correlation information," *IEEE Trans. Signal Process.*, vol. 63, no. 3, pp. 711–726, Feb. 2015, ISSN: 1053-587X. DOI: 10.1109/TSP.2014.2385033.
- [128] V. Y. Pan and Z. Q. Chen, "The complexity of the matrix eigenproblem," in *the thirty-first annual ACM symposium on Theory of computing*, 1999, pp. 507–516. DOI: 10.1145/301250.301389.
- [129] K. Pasala, "Mutual coupling effects and their reduction in wideband direction of arrival estimation," *IEEE Trans. Aerosp. Electron. Syst.*, vol. 30, no. 4, pp. 1116–1122, Oct. 1994, ISSN: 0018-9251. DOI: 10.1109/7.328785.
- [130] D. Pearson, S. Pillai, and Y. Lee, "An algorithm for near-optimal placement of sensor elements," *IEEE Trans. Inf. Theory*, vol. 36, no. 6, pp. 1280–1284, Nov. 1990, ISSN: 0018-9448. DOI: 10.1109/18.59928.
- [131] D. B. Percival and A. T. Walden, *Spectral analysis for physical applications*. Cambridge University Press, 1993. DOI: 10.1017/CB09780511622762.
- [132] S. Pillai, Y. Bar-Ness, and F. Haber, "A new approach to array geometry for improved spatial spectrum estimation," *Proc. IEEE*, vol. 73, no. 10, pp. 1522–1524, Oct. 1985, ISSN: 0018-9219. DOI: 10.1109/PROC.1985.13324.

- [133] S. Pillai and F. Haber, "Statistical analysis of a high resolution spatial spectrum estimator utilizing an augmented covariance matrix," *IEEE Trans. Acoust., Speech, Signal Process.*, vol. ASSP-35, no. 11, pp. 1517–1523, Nov. 1987, issn: 0096-3518. doi: 10.1109/TASSP.1987.1165068.
- [134] V. F. Pisarenko, "The retrieval of harmonics from a covariance function," *Geophys. J. R. astr. Soc.*, vol. 33, pp. 347–366, 1973. doi: 10.1111/j.1365-246X.1973.tb03424.x.
- [135] B. Porat and B. Friedlander, "Analysis of the asymptotic relative efficiency of the MUSIC algorithm," *IEEE Trans. Acoust., Speech, Signal Process.*, vol. 36, no. 4, pp. 532–544, Apr. 1988, issn: 0096-3518. doi: 10.1109/29.1557.
- [136] C. Puente-Baliarda and R. Pous, "Fractal design of multiband and low side-lobe arrays," *IEEE Trans. Antennas Propag.*, vol. 44, no. 5, pp. 730–739, May 1996, issn: 0018-926X. doi: 10.1109/8.496259.
- [137] H. Qiao and P. Pal, "Unified analysis of co-array interpolation for direction-of-arrival estimation," in *Proc. IEEE Int. Conf. Acoust., Speech, and Sig. Proc.*, New Orleans, LA, USA, Mar. 2017, pp. 3056–3060. doi: 10.1109/ICASSP.2017.7952718.
- [138] S. Qin, Y. D. Zhang, M. G. Amin, and F. Gini, "Frequency diverse coprime arrays with coprime frequency offsets for multitarget localization," *IEEE J. Sel. Topics Signal Process.*, vol. 11, no. 2, pp. 321–335, Mar. 2017, issn: 1932-4553. doi: 10.1109/JSTSP.2016.2627184.
- [139] S. Qin, Y. D. Zhang, and M. G. Amin, "Generalized coprime array configurations for direction-of-arrival estimation," *IEEE Trans. Signal Process.*, vol. 63, no. 6, pp. 1377–1390, Mar. 2015, issn: 1053-587X. doi: 10.1109/TSP.2015.2393838.
- [140] S. Qin, Y. Zhang, and M. Amin, "Generalized coprime array configurations," in *Proc. IEEE Sensor Array and Multichannel Signal Process. Workshop*, Jun. 2014, pp. 529–532. doi: 10.1109/SAM.2014.6882459.
- [141] M. Rahmani and G. K. Atia, "A subspace method for array covariance matrix estimation," in *Proc. IEEE Sensor Array and Multichannel Signal Process. Workshop*, Rio de Janeiro, Brazil, Jul. 2016, pp. 1–5. doi: 10.1109/SAM.2016.7569686.
- [142] C. R. Rao, "Information and the accuracy attainable in the estimation of statistical parameters," *Bulletin of the Calcutta Mathematical Society*, vol. 37, pp. 81–89, 1945.
- [143] Rappaport, S. Sun, R. Mayzus, H. Zhao, Y. Azar, K. Wang, G. N. Wong, J. K. Schulz, M. Samimi, and F. Gutierrez, "Millimeter wave mobile communications for 5G cellular: It will work!" *IEEE Access*, vol. 1, pp. 335–349, 2013, issn: 2169-3536. doi: 10.1109/ACCESS.2013.2260813.
- [144] A. Raza, W. Liu, and Q. Shen, "Thinned coprime arrays for DOA estimation," in *Proc. European Signal Proc. Conf.*, Kos island, Greece, Aug. 2017, pp. 395–399. doi: 10.23919/EUSIPCO.2017.8081236.

- [145] L. Rédei and A. Rényi, "On the representation of $1, 2, \dots, N$ by differences," *Recueil Mathématique*, T. 61, 1948.
- [146] J. Robinson and A. Bernstein, "A class of binary recurrent codes with limited error propagation," *IEEE Trans. Inf. Theory*, vol. 13, no. 1, pp. 106–113, Jan. 1967, ISSN: 0018-9448. DOI: 10.1109/TIT.1967.1053951.
- [147] R. Roy and T. Kailath, "ESPRIT-estimation of signal parameters via rotational invariance techniques," *IEEE Trans. Acoust., Speech, Signal Process.*, vol. 37, no. 7, pp. 984–995, Jul. 1989, ISSN: 0096-3518. DOI: 10.1109/29.32276.
- [148] M. Rubsamen and A. Gershman, "Sparse array design for azimuthal direction-of-arrival estimation," *IEEE Trans. Signal Process.*, vol. 59, no. 12, pp. 5957–5969, Dec. 2011, ISSN: 1053-587X. DOI: 10.1109/TSP.2011.2168222.
- [149] C. Ruf, "Numerical annealing of low-redundancy linear arrays," *IEEE Trans. Antennas Propag.*, vol. 41, no. 1, pp. 85–90, Jan. 1993, ISSN: 0018-926X. DOI: 10.1109/8.210119.
- [150] R. Schmidt, "Multiple emitter location and signal parameter estimation," *IEEE Trans. Antennas Propag.*, vol. 34, no. 3, pp. 276–280, Mar. 1986, ISSN: 0018-926X. DOI: 10.1109/TAP.1986.1143830.
- [151] F. Sellone and A. Serra, "A novel online mutual coupling compensation algorithm for uniform and linear arrays," *IEEE Trans. Signal Process.*, vol. 55, no. 2, pp. 560–573, Feb. 2007, ISSN: 1053-587X. DOI: 10.1109/TSP.2006.885732.
- [152] T.-J. Shan, M. Wax, and T. Kailath, "On spatial smoothing for direction-of-arrival estimation of coherent signals," *IEEE Trans. Acoust., Speech, Signal Process.*, vol. 33, no. 4, pp. 806–811, Aug. 1985, ISSN: 0096-3518. DOI: 10.1109/TASSP.1985.1164649.
- [153] Q. Shen, W. Liu, W. Cui, and S. Wu, "Extension of co-prime arrays based on the fourth-order difference co-array concept," *IEEE Signal Process. Lett.*, vol. 23, no. 5, pp. 615–619, May 2016, ISSN: 1070-9908. DOI: 10.1109/LSP.2016.2539324.
- [154] Q. Shen, W. Liu, W. Cui, and S. Wu, "Extension of nested arrays with the fourth-order difference co-array enhancement," in *Proc. IEEE Int. Conf. Acoust., Speech, and Sig. Proc.*, Shanghai, China, Mar. 2016. DOI: 10.1109/icassp.2016.7472226.
- [155] F. J. Simons and D. V. Wang, "Spatiospectral concentration in the Cartesian plane," *GEM - International Journal on Geomathematics*, vol. 2, no. 1, pp. 1–36, 2011, ISSN: 1869-2680. DOI: 10.1007/s13137-011-0016-z.
- [156] J. Singer, "A theorem in finite projective geometry and some applications to number theory," *Trans. Amer. Math. Soc.*, vol. 43, pp. 377–385, 1938. DOI: 10.1090/S0002-9947-1938-1501951-4.
- [157] M. I. Skolnik, *Introduction to radar systems*, 3rd ed. McGraw Hill, 2001, ISBN: 978-0072881387.

- [158] D. Slepian, "Prolate spheroidal wave functions, Fourier analysis, and uncertainty – V: The discrete case," *The Bell System Technical Journal*, vol. 57, no. 5, pp. 1371–1430, May 1978, ISSN: 0005-8580. DOI: 10.1002/j.1538-7305.1978.tb02104.x.
- [159] H. J. S. Smith, "On the integration of discontinuous functions," *Proceedings of the London Mathematical Society*, 1st ser., vol. 6, pp. 140–153, 1874. DOI: 10.1112/plms/s1-6.1.140.
- [160] E. Sperner, "Ein satz über untermengen einer endlichen menge," *Mathematische Zeitschrift*, vol. 27, no. 1, pp. 544–548, Dec. 1928, ISSN: 1432-1823. DOI: 10.1007/BF01171114.
- [161] P. Stoica, P. Babu, and J. Li, "SPICE: A sparse covariance-based estimation method for array processing," *IEEE Trans. Signal Process.*, vol. 59, no. 2, pp. 629–638, Feb. 2011, ISSN: 1053-587X. DOI: 10.1109/TSP.2010.2090525.
- [162] P. Stoica and K. C. Sharman, "Maximum likelihood methods for direction-of-arrival estimation," *IEEE Trans. Acoust., Speech, Signal Process.*, vol. 38, no. 7, pp. 1132–1143, Jul. 1990, ISSN: 0096-3518. DOI: 10.1109/29.57542.
- [163] P. Stoica and P. Babu, "SPICE and LIKES: Two hyperparameter-free methods for sparse-parameter estimation," *Signal Process.*, vol. 92, pp. 1580–1590, 2012. DOI: 10.1016/j.sigpro.2011.11.010.
- [164] P. Stoica, E. G. Larsson, and A. B. Gershman, "The stochastic CRB for array processing: A textbook derivation," *IEEE Signal Process. Lett.*, vol. 8, no. 5, pp. 148–150, May 2001, ISSN: 1070-9908. DOI: 10.1109/97.917699.
- [165] P. Stoica and R. Moses, *Spectral analysis of signals*. Upper Saddle River, New Jersey: Upper Saddle River, NJ, USA: Prentice-Hall, 2005, ISBN: 0-13-113956-8.
- [166] P. Stoica and A. Nehorai, "MUSIC, maximum likelihood, and Cramer-Rao bound," *IEEE Trans. Acoust., Speech, Signal Process.*, vol. 37, no. 5, pp. 720–741, May 1989, ISSN: 0096-3518. DOI: 10.1109/29.17564.
- [167] P. Stoica and A. Nehorai, "Performance study of conditional and unconditional direction-of-arrival estimation," *IEEE Trans. Acoust., Speech, Signal Process.*, vol. 38, no. 10, pp. 1783–1795, Oct. 1990, ISSN: 0096-3518. DOI: 10.1109/29.60109.
- [168] P. Stoica, D. Zachariah, and J. Li, "Weighted SPICE: A unifying approach for hyperparameter-free sparse estimation," *Digit. Signal Process.*, vol. 33, pp. 1–12, Oct. 2014. DOI: 10.1016/j.dsp.2014.06.010.
- [169] V. Strassen, "Gaussian elimination is not optimal," *Numer. Math.*, vol. 13, pp. 354–356, 1969. DOI: 10.1007/BF02165411.
- [170] P. Suetens, *Fundamentals of medical imaging*. Cambridge University Press, 2009, ISBN: 0521519152. DOI: 10.1017/CB09780511596803.
- [171] T. Svantesson, "Direction finding in the presence of mutual coupling," Master's thesis, Chalmers Univ. Technology, 1999.

- [172] T. Svantesson, "Modeling and estimation of mutual coupling in a uniform linear array of dipoles," in *Proc. IEEE Int. Conf. Acoust., Speech, and Sig. Proc.*, vol. 5, 1999, pp. 2961–2964. DOI: 10.1109/ICASSP.1999.761384.
- [173] T. Svantesson, "Mutual coupling compensation using subspace fitting," in *Proc. IEEE Sensor Array and Multichannel Signal Process. Workshop*, 2000, pp. 494–498. DOI: 10.1109/SAM.2000.878058.
- [174] M. B. Sverdlik, *Optimal discrete signals*. Moscow, Russia: Sovietsckoe Radio, 1975.
- [175] Z. Tan, Y. Eldar, and A. Nehorai, "Direction of arrival estimation using coprime arrays: A super resolution viewpoint," *IEEE Trans. Signal Process.*, vol. 62, no. 21, pp. 5565–5576, Nov. 2014, ISSN: 1053-587X. DOI: 10.1109/TSP.2014.2354316.
- [176] Z. Tan and A. Nehorai, "Sparse direction of arrival estimation using coprime arrays with off-grid targets," *IEEE Signal Process. Lett.*, vol. 21, no. 1, pp. 26–29, Jan. 2014, ISSN: 1070-9908. DOI: 10.1109/LSP.2013.2289740.
- [177] H. Taylor and S. W. Golomb, "Rulers, Part I," Univ. Southern Calif., Los Angeles, Tech. Rep. 85-05-01, 1985.
- [178] D. J. Thomson, "Spectrum estimation and harmonic analysis," *Proc. IEEE*, vol. 70, no. 9, pp. 1055–1096, Sep. 1982, ISSN: 0018-9219. DOI: 10.1109/PROC.1982.12433.
- [179] T. E. Tuncer, T. K. Yasar, and B. Friedlander, "Direction of arrival estimation for nonuniform linear arrays by using array interpolation," *Radio Science*, vol. 42, no. 4, Aug. 2007, ISSN: 1944-799X. DOI: 10.1029/2007RS003641.
- [180] T. E. Tuncer and B. Friedlander, *Classical and modern direction-of-arrival estimation*. Academic Press, 2009, ISBN: 9780123745248.
- [181] P. P. Vaidyanathan, *Multirate systems and filter banks*. Pearson Prentice Hall, 1993, ISBN: 0136057187.
- [182] P. P. Vaidyanathan and T. Nguyen, "Eigenfilters: A new approach to least-squares FIR filter design and applications including Nyquist filters," *IEEE Trans. Circuits Syst.*, vol. 34, no. 1, pp. 11–23, Jan. 1987, ISSN: 0098-4094. DOI: 10.1109/TCS.1987.1086033.
- [183] P. P. Vaidyanathan and P. Pal, "Theory of sparse coprime sensing in multiple dimensions," *IEEE Trans. Signal Process.*, vol. 59, no. 8, pp. 3592–3608, Aug. 2011, ISSN: 1053-587X. DOI: 10.1109/TSP.2011.2135348.
- [184] P. P. Vaidyanathan and P. Pal, "Direct-MUSIC on sparse arrays," in *2012 International Conference on Signal Processing and Communications (SPCOM)*, Jul. 2012, pp. 1–5. DOI: 10.1109/SPCOM.2012.6289992.
- [185] P. P. Vaidyanathan and P. Pal, "Why does direct-MUSIC on sparse-arrays work?" In *Proc. IEEE Asil. Conf. on Sig., Sys., and Comp.*, Nov. 2013, pp. 2007–2011. DOI: 10.1109/ACSSC.2013.6810658.

- [186] P. P. Vaidyanathan and P. Pal, "Sparse sensing with co-prime samplers and arrays," *IEEE Trans. Signal Process.*, vol. 59, no. 2, pp. 573–586, Feb. 2011, ISSN: 1053-587X. DOI: 10.1109/TSP.2010.2089682.
- [187] P. P. Vaidyanathan, S.-M. Phoong, and Y.-P. Lin, *Signal processing and optimization for transceiver systems*. Cambridge, 2010, ISBN: 0521760798. DOI: 10.1017/cbo9781139042741.
- [188] H. L. Van Trees, *Optimum array processing: Part IV of detection, estimation, and modulation theory*. Hoboken, NJ, USA: Wiley, 2002. DOI: 10.1002/0471221104.
- [189] A. J. van der Veen, M. C. Vanderveen, and A. Paulraj, "Joint angle and delay estimation using shift-invariance techniques," *IEEE Trans. Signal Process.*, vol. 46, no. 2, pp. 405–418, Feb. 1998, ISSN: 1053-587X. DOI: 10.1109/78.655425.
- [190] E. Vertatschitsch and S. Haykin, "Nonredundant arrays," *Proc. IEEE*, vol. 74, no. 1, pp. 217–217, Jan. 1986, ISSN: 0018-9219. DOI: 10.1109/PROC.1986.13435.
- [191] S. Vigneshwaran, N. Sundararajan, and P. Saratchandran, "Direction of arrival (DoA) estimation under array sensor failures using a minimal resource allocation neural network," *IEEE Trans. Antennas Propag.*, vol. 55, no. 2, pp. 334–343, Feb. 2007, ISSN: 0018-926X. DOI: 10.1109/TAP.2006.889794.
- [192] M. Wang and A. Nehorai, "Coarrays, MUSIC, and the Cramér-Rao bound," *IEEE Trans. Signal Process.*, vol. 65, no. 4, pp. 933–946, Feb. 2017, ISSN: 1053-587X. DOI: 10.1109/TSP.2016.2626255.
- [193] M. Wang, Z. Zhang, and A. Nehorai, "Direction finding using sparse linear arrays with missing data," in *Proc. IEEE Int. Conf. Acoust., Speech, and Sig. Proc.*, New Orleans, LA, USA, Mar. 2017, pp. 3066–3070. DOI: 10.1109/ICASSP.2017.7952720.
- [194] D. H. Werner and S. Ganguly, "An overview of fractal antenna engineering research," *IEEE Antennas Propag. Mag.*, vol. 45, no. 1, pp. 38–57, Feb. 2003, ISSN: 1045-9243. DOI: 10.1109/MAP.2003.1189650.
- [195] D. H. Werner, R. L. Haupt, and P. L. Werner, "Fractal antenna engineering: The theory and design of fractal antenna arrays," *IEEE Antennas Propag. Mag.*, vol. 41, no. 5, pp. 37–58, Oct. 1999, ISSN: 1045-9243. DOI: 10.1109/74.801513.
- [196] P. Wirfalt, G. Bouleux, M. Jansson, and P. Stoica, "Optimal prior knowledge-based direction of arrival estimation," *IET Signal Processing*, vol. 6, no. 8, pp. 731–742, Oct. 2012, ISSN: 1751-9675. DOI: 10.1049/iet-spr.2011.0453.
- [197] M. Yang, A. Haimovich, B. Chen, and X. Yuan, "A new array geometry for DOA estimation with enhanced degrees of freedom," in *Proc. IEEE Int. Conf. Acoust., Speech, and Sig. Proc.*, Shanghai, China, Mar. 2016. DOI: 10.1109/icassp.2016.7472236.
- [198] Z. Yang and L. Xie, "On gridless sparse methods for line spectral estimation from complete and incomplete data," *IEEE Trans. Signal Process.*, vol. 63, no. 12, pp. 3139–3153, Jun. 2015, ISSN: 1053-587X. DOI: 10.1109/TSP.2015.2420541.

- [199] Z. Ye, J. Dai, X. Xu, and X. Wu, "DOA estimation for uniform linear array with mutual coupling," *IEEE Trans. Aerosp. Electron. Syst.*, vol. 45, no. 1, pp. 280–288, Jan. 2009, ISSN: 0018-9251. DOI: 10.1109/TAES.2009.4805279.
- [200] Y. D. Zhang, M. G. Amin, and B. Himed, "Sparsity-based DOA estimation using co-prime arrays," in *Proc. IEEE Int. Conf. Acoust., Speech, and Sig. Proc.*, May 2013, pp. 3967–3971. DOI: 10.1109/ICASSP.2013.6638403.
- [201] Y. D. Zhang, S. Qin, and M. G. Amin, "DOA estimation exploiting coprime arrays with sparse sensor spacing," in *Proc. IEEE Int. Conf. Acoust., Speech, and Sig. Proc.*, May 2014, pp. 2267–2271. DOI: 10.1109/ICASSP.2014.6854003.
- [202] C. Zhu, W. Q. Wang, H. Chen, and H. C. So, "Impaired sensor diagnosis, beamforming, and DOA estimation with difference co-array processing," *IEEE Sensors J.*, vol. 15, no. 7, pp. 3773–3780, Jul. 2015, ISSN: 1530-437X. DOI: 10.1109/JSEN.2015.2399510.
- [203] M. D. Zoltowski, M. Haardt, and C. P. Mathews, "Closed-form 2-D angle estimation with rectangular arrays in element space or beamspace via unitary ESPRIT," *IEEE Trans. Signal Process.*, vol. 44, no. 2, pp. 316–328, Feb. 1996, ISSN: 1053-587X. DOI: 10.1109/78.485927.